PRACTICAL ROCK ENGINEERING

Evert Hoek

PRACTICAL ROCK ENGINEERING

1. Preface

These notes were originally prepared during the period of 1987 to 1993 for graduate courses in rock engineering in the Department of Civil Engineering at the University of Toronto, where I was a Professor of Rock Engineering. From time to time, these notes were added to and updated, but they have remained in their original form for the past thirty years.

In 1996, the software company, RocScience Inc., was established for the development and marketing of geotechnical software for both educational purposes and for use in the design and analysis of civil and mining projects. These notes, with the title of Practical Rock Engineering, were placed online as one of the components of the RocScience website and they have always been freely accessible to anyone wishing to use them.

In 2020, I retired from all my consulting and academic activities and started the process of assembling material for a complete update and rewrite of these notes. In 2022 and 2023 I prepared several new chapters and re-wrote several of the original chapters to incorporate advances and practical applications in the field.

The original notes were prepared as a series of completely self-contained chapters each with its own page numbering and references. This proved to be a very effective presentation since the users could access a volume dealing with a particular topic of immediate interest to them. Wherever possible, case histories are included to illustrate the basic topics presented in the notes.

These notes are not a formal text and have not been, and will not be, published in any other format.

Evert Hoek
102-3200 Capilano Crescent
North Vancouver, British Columbia
Canada V7R 4H7

ehoek@mailas.com

Evert Hoek

Evert Hoek was born in 1933 in Southern Rhodesia, now Zimbabwe, Africa. He graduated in mechanical engineering from the University of Cape Town with a B.Sc. in 1955 and an M.Sc. in 1957.

He became involved in rock mechanics in 1958 when he was employed by the South African Council for Scientific and Industrial Research and worked on problems of rock fracture in very deep level gold mines. He was awarded a Ph.D. in 1965 by the University of Cape Town for his research on brittle rock failure.

In 1966, he was appointed Reader and, in 1970, Professor of Rock Mechanics in the Royal School of Mines at the Imperial College of Science and Technology in London. He was responsible for establishing an inter-departmental group for teaching and research in rock mechanics.

In 1974, he was awarded a Doctor of Science (Engineering) degree by the University of London based on his published works and research record. He ran two major research projects, sponsored by several international mining companies, that provided practical training for graduate students. These research projects also resulted in the publication of two books: *Rock Slope Engineering* (with J.W. Bray) in 1971 and *Underground Excavations in Rock* (with E.T. Brown) in 1980.

In 1975, he moved to Vancouver in Canada as a Principal in Golder Associates, an international geotechnical consulting organization. During his twelve years with Golder Associates he worked as a consultant on major civil and mining projects more than twenty countries around the world.

In 1987, he returned to academia as a Professor of Rock Engineering in the Department of Civil Engineering in the University of Toronto. Here he was involved in another industry sponsored research project which resulted in the publication of a book entitled *Support of Underground Excavations in Hard Rock* (with P.K. Kaiser and W.F. Bawden) in 1995. During this time, he continued to work as a member of consulting boards and panels of experts on several international projects.

In 1993, he returned to Vancouver to devote his full time to consulting as an independent specialist, working exclusively on consulting and review boards and on panels of experts on civil and mining projects around the world. He has maintained his research interests and has continued to write papers with friends and colleagues associated with these consulting projects. He retired from these activities in 2018.

His contributions to rock engineering have been recognized by the award of an honorary D.Sc. in Engineering from the University of Waterloo in 1994, an honorary D.Eng. in Engineering from the University of Toronto in 2004, an Honorary Doctorate from the Polytechnic University of Catalonia in Spain in 2019 and by his election as a Fellow of the Royal Academy of Engineering (UK) in 1982, a Fellow of the Canadian Academy of Engineering in 2001 and as an International Member of the US National Academy of Engineering in 2006.

He has also received many awards and presented several named lectures including the Consolidated Goldfields Gold Medal, UK (1970), the AIME Rock Mechanics Award, US (1975), the E. Burwell Award from the Geological Society of America (1979), the Sir Julius Werhner Memorial Lecture, UK (1982), the Rankine Lecture, British Geotechnical Society (1983), the Gold Medal of the Institution of Mining and Metallurgy, UK (1985), the Müller Award, International Society of Rock Mechanics (1991), the William Smith Medal, Geological Society, UK (1993), the Glossop Lecture, Geological Society, UK (1998), and the Terzaghi Lecturer, American Society of Civil Engineers (2000).

Rock engineering before computers

The contents of the chapters in Practical Rock Engineering have all been written during the past thirty years during which almost all our problem solutions utilize the power of modern computers. These were not available until the early 1980s and it is interesting to consider how stress analysis problems were dealt with during the early years of the development of rock mechanics and rock engineering. My own experience dates from 1957 when I started using the techniques which were then available for the solution of rock mechanics problems. Some of these techniques are discussed very briefly in the following pages.

I graduated with a degree in mechanical engineering from the University of Cape Town in 1955. I continued to a Master of Science degree, graduating in 1957, with research into the stress distribution in threaded connections (bolts and nuts) using three-dimensional photoelastic techniques. In those days all investigations into the stresses in mechanical components were done on physical models. Stresses were measured by means of strain gauges, bonded onto the models at appropriate locations, or by using two- and three-dimensional photoelastic models.

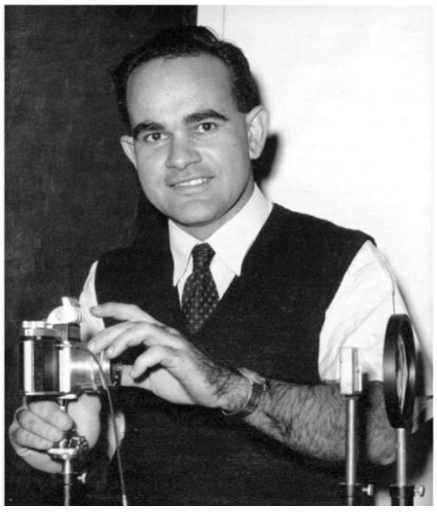

Figure 1: Evert Hoek working on a Photoelastic model, shown in Figure 2, in the Department of Mechanical Engineeriing in the University of Cape Town, in 1957.

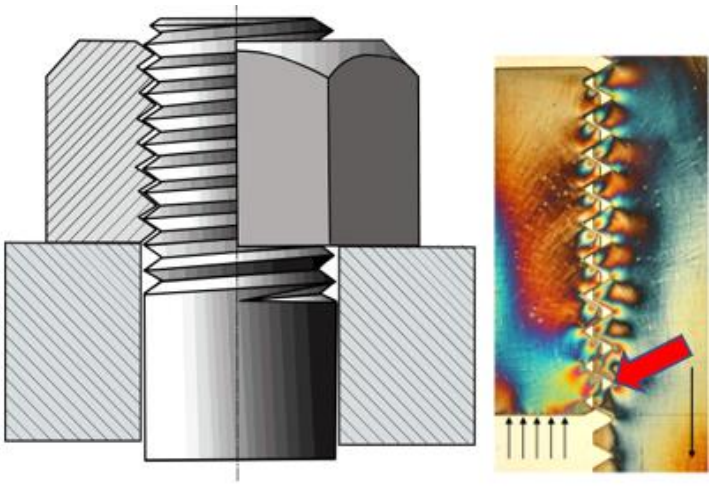

Figure 2: A sectioned bolt and nut and a slice cut from a three-dimensional epoxy resin model. The stress pattern, made visible by viewing the model in polarized light, was "frozen" into the resin by heating the loaded model to 150ºC and then cooling it slowly to room temperature. This model revealed that the highest stresses, shown by the red arrow, occurred in the first supported thread of the bolt, where the stress is about five times that of the stress in the bolt shank.

In 1958, I applied for a position with the National Mechanical Engineering Research Institute of the South African Council for Scientific and Industrial Research (CSIR), located in the city of Pretoria. It turned out that I was lucky since a giant photoelastic polariscope, shown in Figure 3, had been constructed at this Institute. The designer of this instrument had resigned shortly before my application was received. Since none of the remaining staff knew how to operate this machine, or very much about photoelastic analysis, I was appointed as a research engineer, responsible for stress analysis and strength of materials projects.

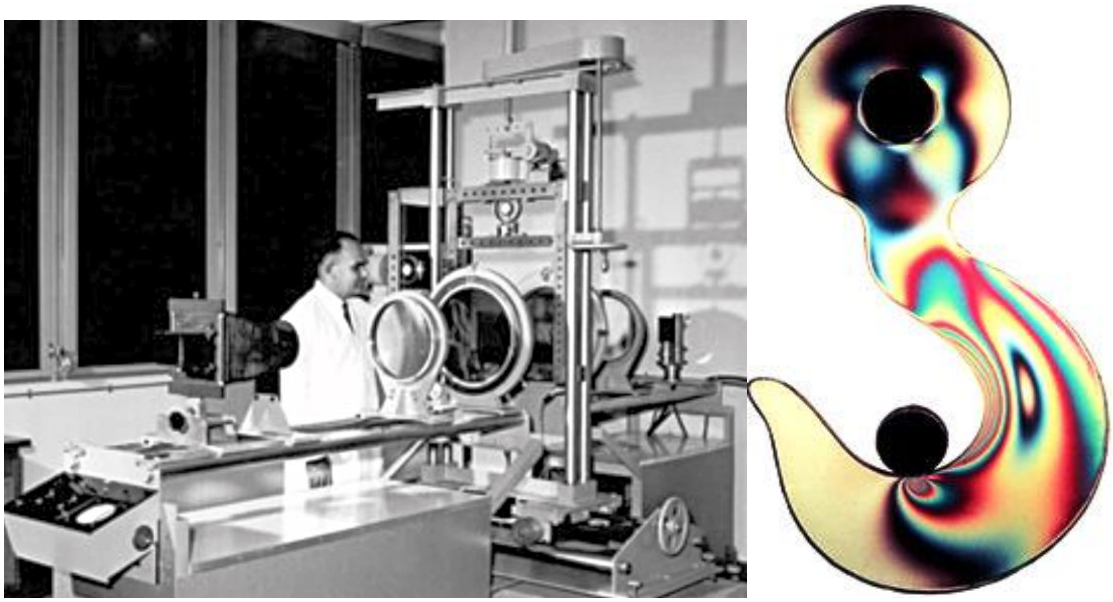

Figure 3: A large photoelastic polariscope and a photoelastic pattern in a loaded crane hook. Photographed in 1958 at the National Mechanical Engineering Research Institute in South Africa.

In addition to its work on mechanical engineering components, the CSIR also had a small rock mechanics department in which work on the measurement of in situ stresses in deep level gold mines was being carried out. I worked with this department on brittle fracture problems in the rock in these mines (Hoek, 1965). At mining depths of up to 3 km below surface, the high stress levels cause extensive fracturing in the rock, and, in some cases, these fractures took the form of very violent and dangerous rock bursts. I became a member of a team of researchers, from various universities and research organizations in South Africa, who were attempting to understand and to devise methods for minimizing the danger of rockbursts (Cook et al, 1966).

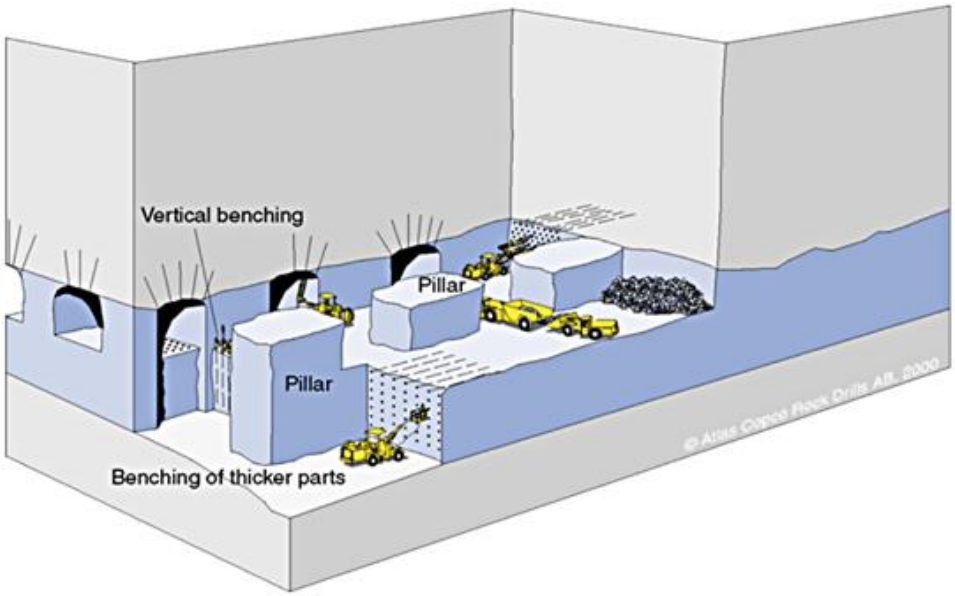

Figure 4: Simplified layout of a room and pillar mine (Image from Atlas Copco Rock Drills AB).

The Coalbrook mine collapse was the worst mining disaster in the history of South Africa. It occurred in the Coalbrook coal mine of Clydesdale Colliery on 21 January 1960, when approximately 900 pillars caved in, almost 180 metres underground. About 1,000 miners were in the mine at the time and 437 died because of the collapse.

Following the disaster, the South African government established the Coal Mines Research Controlling Council to improve coal mine safety and to research pillar strength. It was supported by the Council for Scientific and Industrial Research and the Chamber of Mines Research Organization.

I was involved in the determination of the stress distribution and strength of coal mine pillars as part of the research program established after the Coalbrook disaster. This program existed for several years and resulted in the publication of several papers and guidelines for coal pillar design and the general safety of underground mines. The layout of an underground room and pillar mine is illustrated in Figure 4.

The three-dimensional photoelastic models used to study the stress distribution in the rock forming and surrounding pillars were constructed from blocks of epoxy resin, created by heating the component mix to 150ºC to induce the chemical reaction, followed by slow cooling to ensure that these blocks were free from locked-in stresses. The rooms between the pillars were machined from one of the two blocks used in each model. These blocks were then glued together with an epoxy adhesive to form the complete three-dimensional model. The model was loaded uniformly to simulate the gravitational load due to the weight of the overlying rock and, while still under load, the model was heated in an oven to a temperature of 150ºC and then cooled at 1.5ºC per hour until the temperature had fallen to below 70ºC. This process “froze” the three-dimensional stress field into the epoxy resin model which could then be cut into slices, approximately 3 mm thick, to allow the resulting photoelastic pattern to be viewed in polarized light.

A typical photoelastic image in one of these slices is reproduced in Figure 5. The colour fringes, illustrated below, represent the contours of principal stress difference ($\sigma_1 - \sigma_3$) in the model. To separate the principal stresses, an electrical analog model was used as illustrated in Figure 6. This model uses the voltage distribution in a sheet of uniformly conducting material to represent the distribution of the principal stress sum ($\sigma_1 + \sigma_3$). These two stress distribution patterns permit separation of the individual principal stresses σ_1 and σ_3 throughout the model.

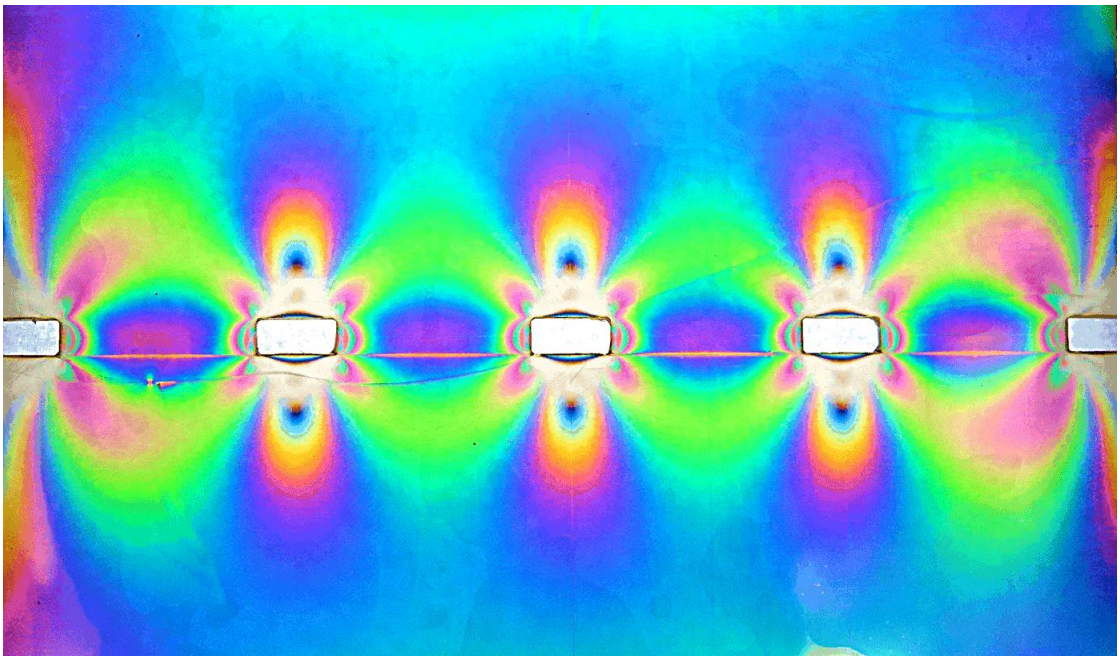

Figure 5: Photoelastic pattern in a slice from a three-dimensional frozen stress model representing a room and pillar coal mine. The fringes define the distribution of the principal stress difference ($\sigma_1 - \sigma_3$) in the model.

Figure 6: An electrical analog model in which the distribution of voltage in a sheet of uniformly conducting material defines the distribution of the principal stress sum ($\sigma_1 + \sigma_3$) in the model.

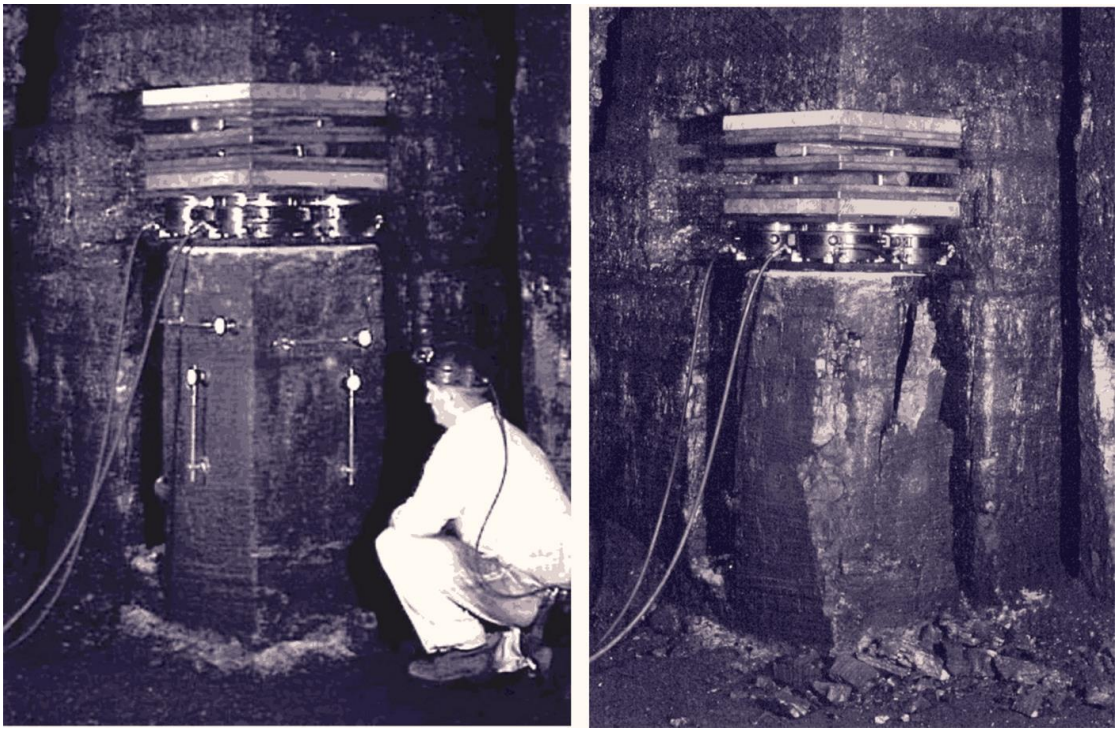

Figure 7: Uniaxial compressive strength test on a specimen cut from the corner of a coal pillar in an underground room and pillar mine.

The design of pillars in a room and pillar mine requires a knowledge of both the stresses in the pillar and the strength of the rock mass forming the pillars. I was involved in designing and managing the first phase of a program to determine the strength of large specimens of coal in-situ. Testing of these specimens is illustrated in Figure 7. After my departure from the CSIR in 1966, this project was continued under the direction of Dr. Z.T. Bieniawski (Bieniawski and Van Zyl, 1975).

One of the most sophisticated pieces of equipment that I designed and operated in the CSIR was a biaxial loading frame for the application of uniform biaxial stresses to the boundaries of 15 cm square glass or rock plates. These stresses, which could be different in vertical and horizontal directions, were applied to induce failure in the material surrounding excavations of various shapes. A photoelastic fringe pattern in a glass plate model pattern surrounding a circular tunnel, with vertical cracks in the roof and floor, is illustrated in the lower left-hand photograph in Figure 8. The photograph in the lower right-hand side of this figure illustrates tensile roof and floor vertical cracks, as well as notches resulting from spalling in the sidewalls in a rock plate model. Both models were loaded with vertical stresses of six times the horizontal stresses, which were typical stress ratios in many deep level gold mines in South Africa.

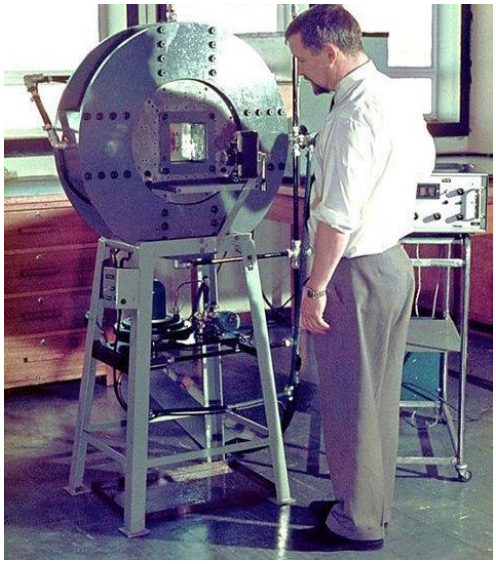

Model loading frame for 10 cm square glass or rock models.

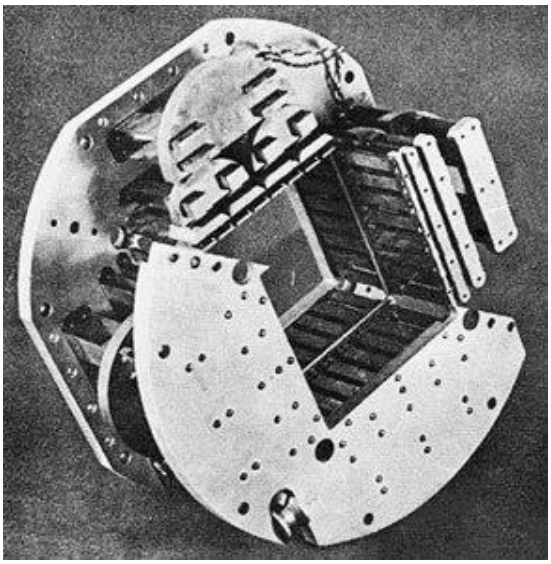

Load distribution system to apply uniformly distributed loads on the model boundaries.

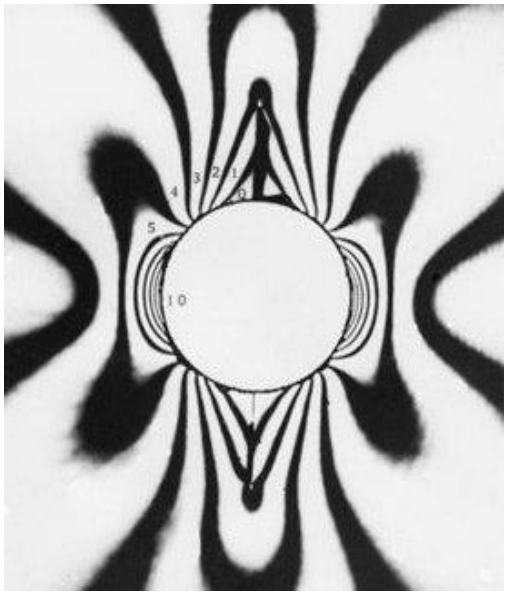

Photoelastic fringe pattern of principal stress differences in a glass plate model.

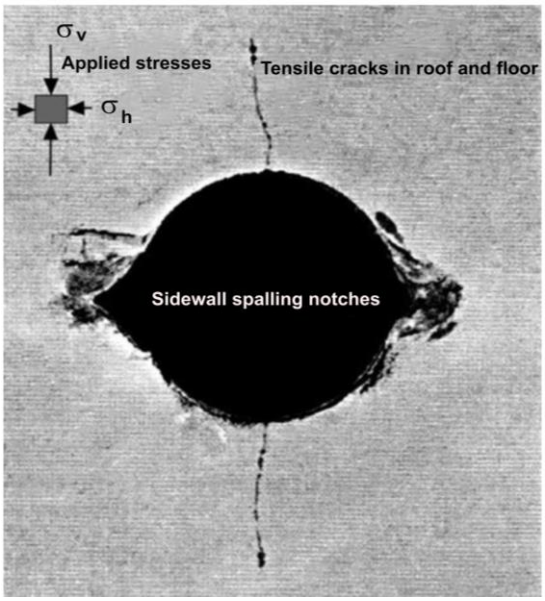

Vertical tension cracks and sidewall spalls induced in a stressed rock plate model.

Figure 8: Biaxial stress modelling to induce failure in glass and rock plate models.

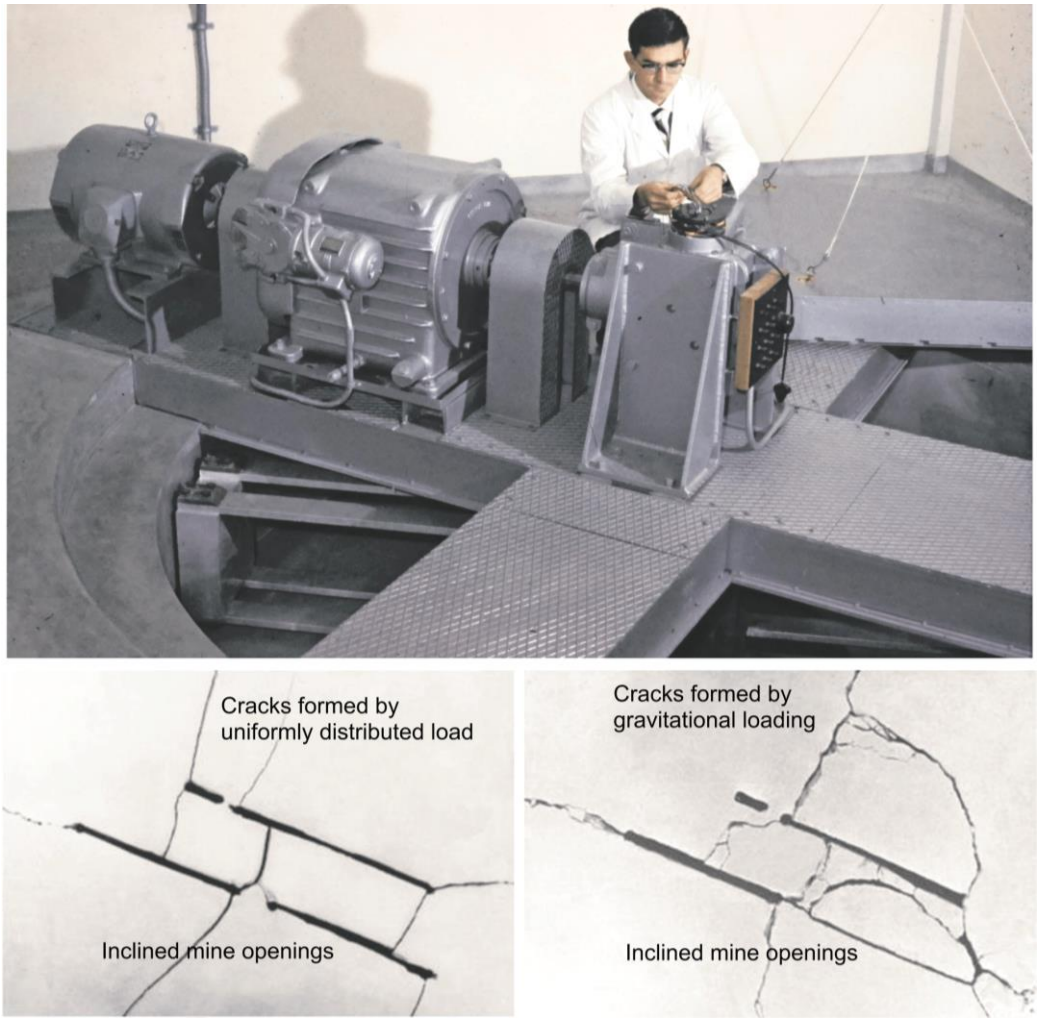

Figure 9: A three metre diameter centrifuge capable of accelerating models to 1000 times the normal gravitational acceleration.

In 1963, I designed the centrifuge, illustrated in Figure 9, to apply high gravitational loading to mine models. The photograph in the lower left-hand side shows cracks developed in a plaster mine model loaded with uniformly distributed vertical stresses. The lower right-hand photograph shows cracks in a similar model in which gravitational loading was simulated in the centrifuge. It will be seen that the crack patterns are quite different, with the gravitationally loaded model giving roof failures and collapse which are much closer to reality than the uniformly loaded model.

The rapid development of computers, in the early 1960s, resulted in the availability of numerical models to which a wide variety of loads, including gravitation loading, could be applied. Numerical modelling soon rendered many of the traditional physical models obsolete. The centrifuge shown above was only used for a few tests before being moth-balled.

In 1966, I was appointed to the academic staff of the Imperial College of Science and Technology, one of the colleges of the London University in England. I worked in the Royal School of Mines, but I had close associations with the Departments of Civil Engineering and Geology. The Department of Civil Engineering had a strong soil mechanics division, and the Department of Geology had a division of engineering geology. The purpose of my appointment was to establish a division of rock mechanics in the Royal School of Mines to offer introductory and graduate courses as well as research opportunities in this field.

My arrival at Imperial College in 1966 coincided with the creation of the post-graduate Centre for Computing and Automation. This centre incorporated work in computing by the Department of Mathematics which, in the early 1950s, had built a digital relay computer named the Imperial College Computing Engine. My post-graduate students had access to this new computing centre and were soon preparing their own punched cards and delivering stacks of these cards to the computing centre; returning the next day to receive the results. While this was a clumsy and time-consuming process, it played a critical role in the development of the powerful programs that we take for granted today. One of the first papers published on this work was by Peter Cundall (Cundall, 1971).

Figure 10: A model used to study slope failure in rock jointed rock masses.

This shift to numerical analysis also resulted in the decline of the use of physical models such as photoelasticity since problems could be analysed numerically in a fraction of the time and with a significantly higher level of accuracy. However, physical models, such as that illustrated in Figure 10, still played an important role in helping to understand some of the failure mechanisms in jointed rock masses. In this model, designed by Nick Barton (Barton, 1973) for his work on jointed rock masses, small pre-cast plaster blocks, representing the intact rock, were set in place on a large horizontal glass plate. Once the assembly of the model had been completed, a second parallel glass plate was added to keep the blocks in place. The frame was then rotated into the vertical position, thereby activating the gravitation load on each block. The resulting slope failures were important components in the development of our understanding of rock mass behaviour.

Another important development at Imperial College was the design of compact and robust testing equipment that could be used on the site of a construction project or in a site laboratory.

One of these tools is a triaxial test cell, illustrated in Figure 11, which is very compact and portable, but which can produce excellent results when used in a reliable compression testing machine. The design details of this cell were published by Hoek and Franklin (1968). These cells have been manufactured and used all over the world. A detailed discussion of the use of this cell, and the analysis of the results in terms of the Hoek-Brown failure criterion is presented in Hoek and Brown, 1980. A summary of some of the test results is presented in Figure 12.

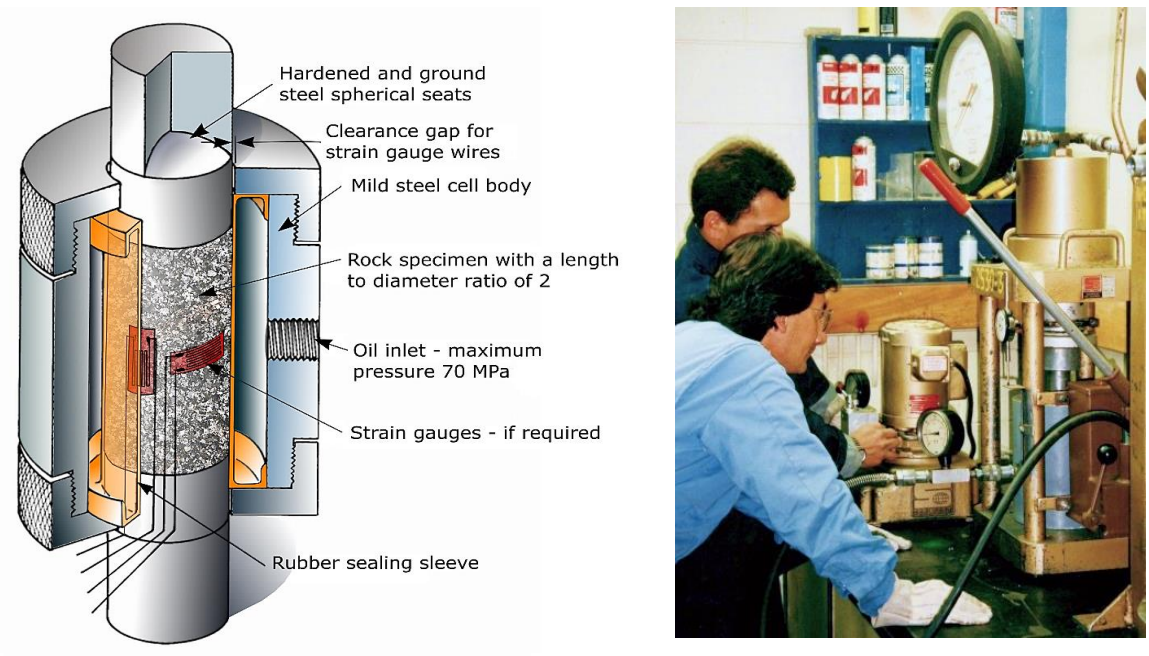

Figure 11: Triaxial testing call designed by Hoek and Franklin at Imperial College.

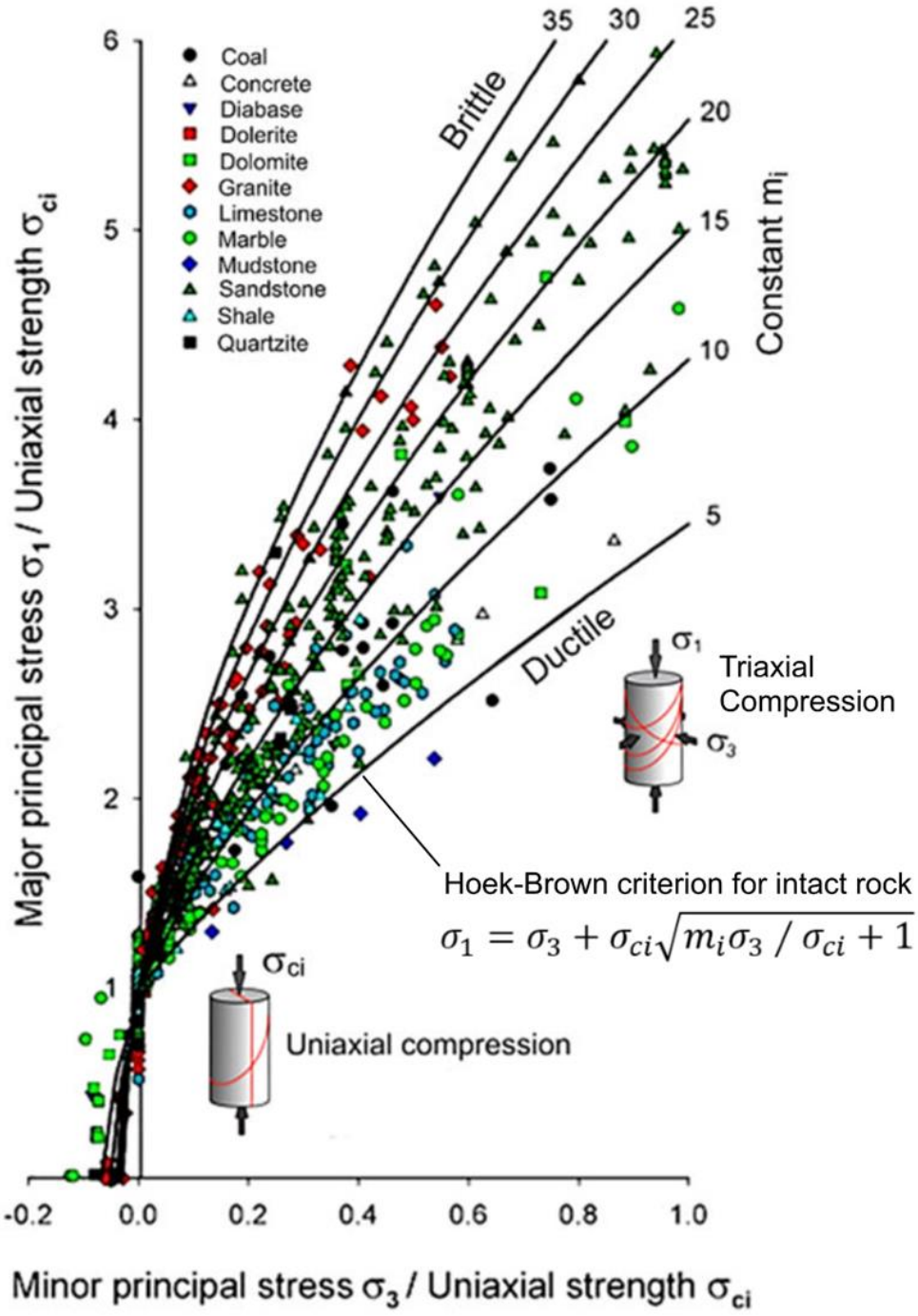

Figure 12: Plot of typical triaxial test results on intact rock specimens with an interpretation of these results in terms of the Hoek-Brown failure criterion.

References

Barton, N. (1973). Review of a new shear strength criterion for rock joints. *Engineering Geology*, 8, pages 287-332.

Bieniawski, Z.T. and Van Zyl, H.W. L. (1975). The significance of in situ tests on large rock specimens. *Int. J. Rock Mech. Min. Sci. Geomech. Abstr.* 12(4), pages101-113.

Cook, N.G.W., Hoek, E., Pretorius, J.P.G., Ortlepp, W.D. and Salamon, M.D.G. (1966). Rock mechanics applied to the study of rockbursts. *J. S. Afr. Inst. Min. Metall.* 66, pages 436-528.

Cundall, P. (1971): A Computer Model for Simulating Progressive, Large-Scale Movements in Blocky Rock Systems, *Proceedings International Symposium on Rock Fractures*, Nancy, France, Paper II-8.

Hoek, E. (1965). Rock fracture under static stress conditions. National Mechanical Engineering Research Institute, CSIR, Pretoria, South Africa, *Report MEG 385*.

Hoek, E. and Franklin J.A, (1968). Simple Triaxial Cell for Field or Laboratory Testing of Rock. *Trans. Institution of Mining and Metallurgy*. A22-26.

Hoek, E. and Brown, E.T. (1980), *Underground Excavations in Rock*, The Institution of Mining and Metallurgy, London.

2. What is Rock Engineering?

Introduction

Rock Engineering deals with the use of rock and rock masses as engineering materials. It utilizes all the techniques used in mechanical, civil, and mining engineering for designing structures in steel and concrete, but it incorporates the special strength and deformation characteristics of intact rock and fractured rock masses as well as the uncertainties associated with in situ and induced stresses in rock masses.

Structures have been built on, or in, rock for centuries as shown in the photograph reproduced in Figure 1. The basic design principles have been understood for a very long time. Rock engineering is merely a formal expression of some of these principles and it is only during the past few decades that the theory and practice in this subject have come together in the discipline that we know today.

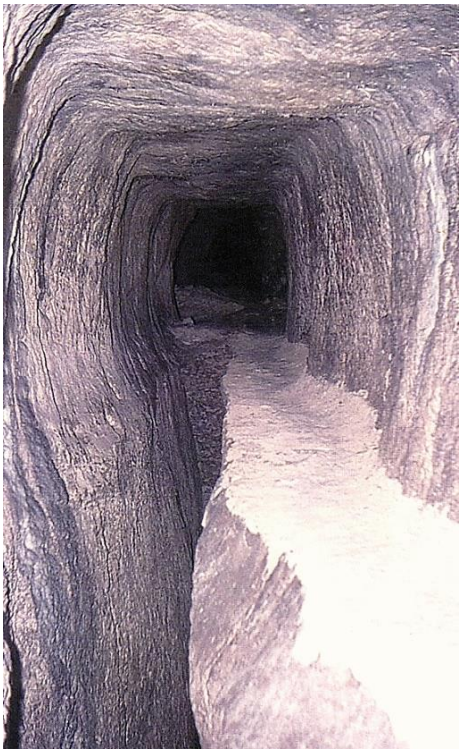

Figure 1: The 1036 m long Eupalinos water supply tunnel was built more than 2,500 years ago on the Greek island of Samos. This is the first known tunnel in rock to have been built from two portals with the two drives meeting in the middle.

This photograph was provided by Professor Paul Marinos of the National Technical University of Athens.

In December 1959, the foundation of the Malpasset concrete arch dam in France failed during first filling because of excessive water pressure in a fault upstream of the dam wall (Figure 2). The resulting flood killed about 450 people. In October 1963, about 2500 people in the Italian town of Longarone were killed because of a landslide-generated wave which overtopped the Vajont Dam.

Figure 2: Remains of the Malpasset Dam as seen today. Photograph provided by Dr Mark Diederichs, 2003.

These two disasters had a major impact on rock engineering. In 1960, a room and pillar coal mine at Coalbrook, South Africa, collapsed with the loss of 432 lives. This event was responsible for the initiation of an intensive research programme which resulted in significant advances in the methods used for designing coal pillars (Salamon and Munro, 1967).

These failures in the early 1960s confirmed the warning by Terzaghi (1936) who, in discussing slopes in the Panama Canal excavations wrote, 'The catastrophic descent of the slopes of the deepest cut of the Panama Canal issued a warning that we were overstepping the limits of our ability to predict the consequences of our actions ....'.

The development of rock engineering as a recognizable engineering discipline dates from about the period in which the major failures, discussed above, occurred. I consider myself extremely fortunate to have been involved in the subject since 1958. I have been in positions that required extensive travel, which have brought me into personal contact with most of the persons with whom the development of modern rock engineering is associated.

Using rock as an engineering material

Many civil and mining structures are built in, or on, rock masses, which like steel and concrete, must be treated as engineering materials. Information on the properties of the rock masses and estimates of the stresses acting on the rock are required to design foundations, tunnels, large underground caverns, underground mines, highway slopes and open pit mines. This information is assembled from geological observations and measurements in the field, laboratory testing on diamond drilled core and specimens, measurements of in situ stresses and other properties which may be required in specific cases. Because of wide variations of these observations and measurements, the use of some form of reliability analysis is generally required by the designer to determine the support necessary to stabilize tunnels, calculate the permitted loading of foundations and estimate the safe angles for excavated slopes.

Failure of a tunnel in a weak rock mass at a depth of 1000 m below surface.

Failure of the toe of a slope in jointed rock mass.

Rockfall danger in a steep slope in massive rock.

Brittle spalling failure in a mine excavation in very strong intact rock at 3000 m below surface.

Shallow slope failure in a jointed rock mass in a large open pit mine.

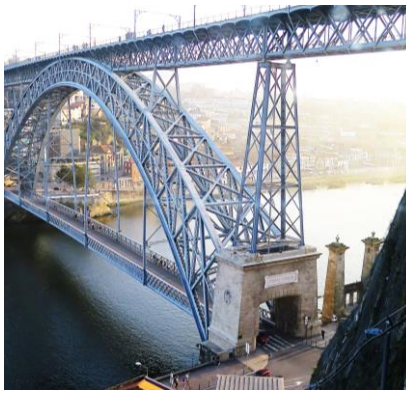

Stable bridge foundation on massive rock.

Figure 3: Examples of the types of problems that are encountered by rock engineers.

Typical problems encountered by rock engineers in the field are illustrated in Figure 3. These involve failure of rock or rock masses at different scales and under different loading conditions which may be simple vertical gravity loads due to the self-weight of loose blocks in slopes or foundations of dams. On the other hand, in the case of underground excavations, failure may be induced by in situ stresses in the rock mass surrounding tunnels, mining excavations or large underground caverns.

Intact rock strength

A starting point in understanding the engineering properties of rock masses is a discussion of the strength and deformation properties of intact rock. Figure 4 illustrates a tray of intact rock core obtained by diamond drilling into a rock mass in which a foundation, slope or tunnel is to be excavated. Also included in this figure is an illustration of a triaxial cell in which intact rock specimens can be subjected to a range of triaxial stresses, with deformation of the intact rock being measured by means of strain gauges. Core drilling, specimen preparation and testing procedures, and the interpretation of the results, are described in detail in the chapter on intact rock in these notes.

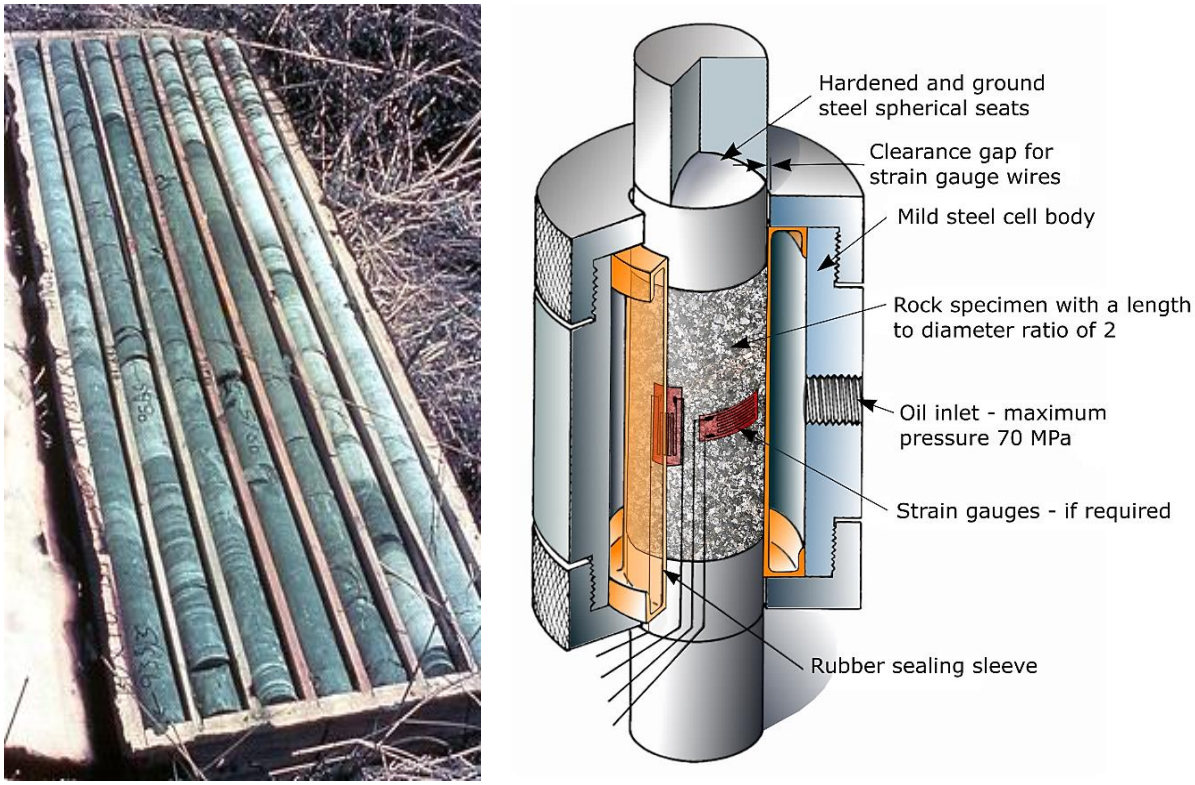

Figure 4: Intact rock specimens recovered by diamond drilling in an in-situ rock mass and a triaxial cell for testing core samples to determine their strength and deformation characteristics.

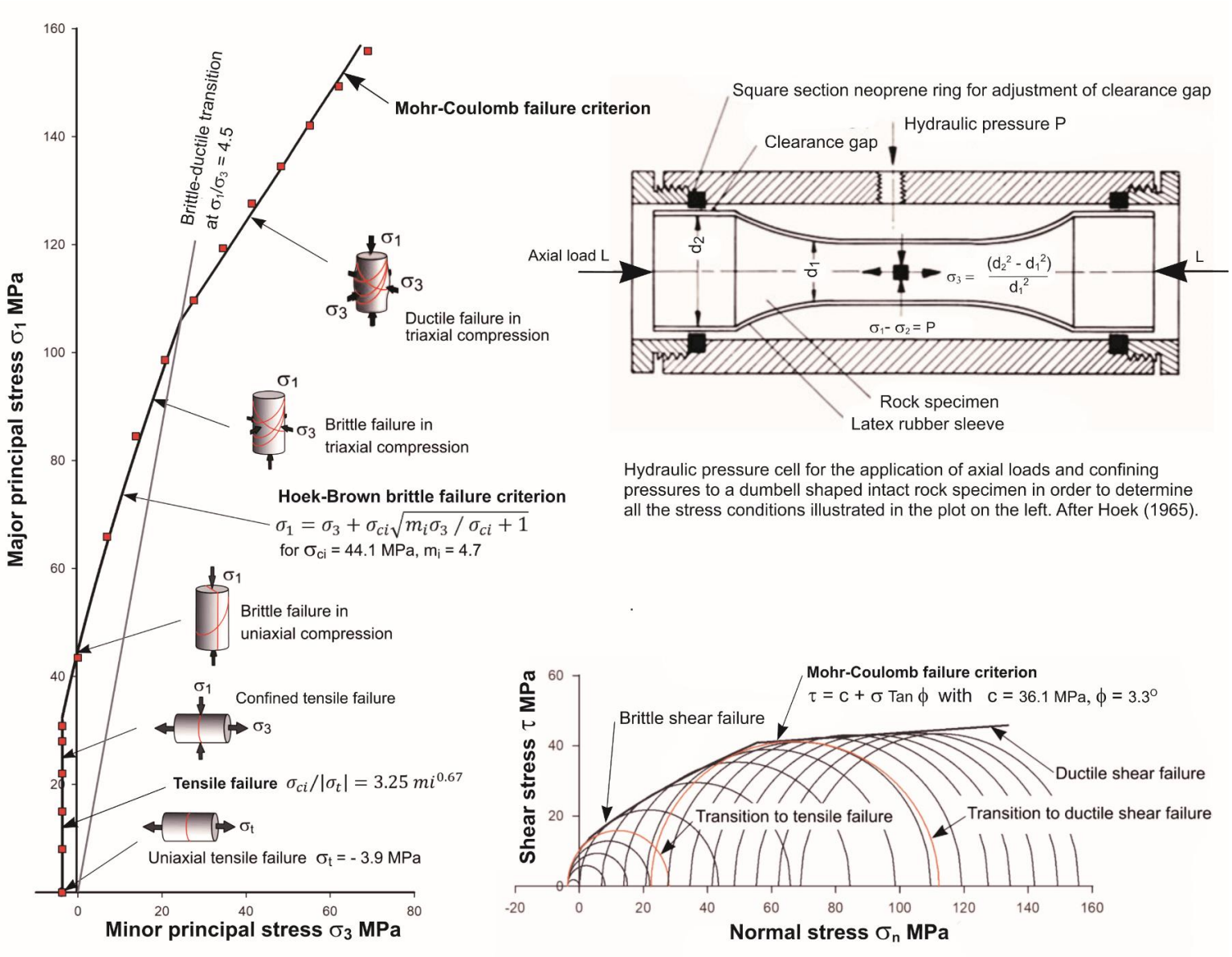

Figure 5: An interpretation of the results of triaxial tests on intact rock specimens.

Figure 5 presents the results of triaxial compression tests on samples of Wombeyan Marble by Paterson (1958) and tensile tests on Carrara marble by Ramsey and Chester (2004). The plot indicates that the tensile tests fall along a well-defined tension cut-off. Brittle failure of the intact rock is represented by the Hoek-Brown failure criterion which defines brittle shear failure in the stress regime between tensile failure and ductile failure at higher stress levels. For these marbles, a transition to ductile failure occurs at the ratio of $\sigma_1/\sigma_3 = 4.5$ and this ductile failure is defined by the linear Mohr-Coulomb criterion which is generally used to define failure in soils.

Figure 6 shows that the relationships presented in Figure 5 apply to most rock types of interest in rock engineering.

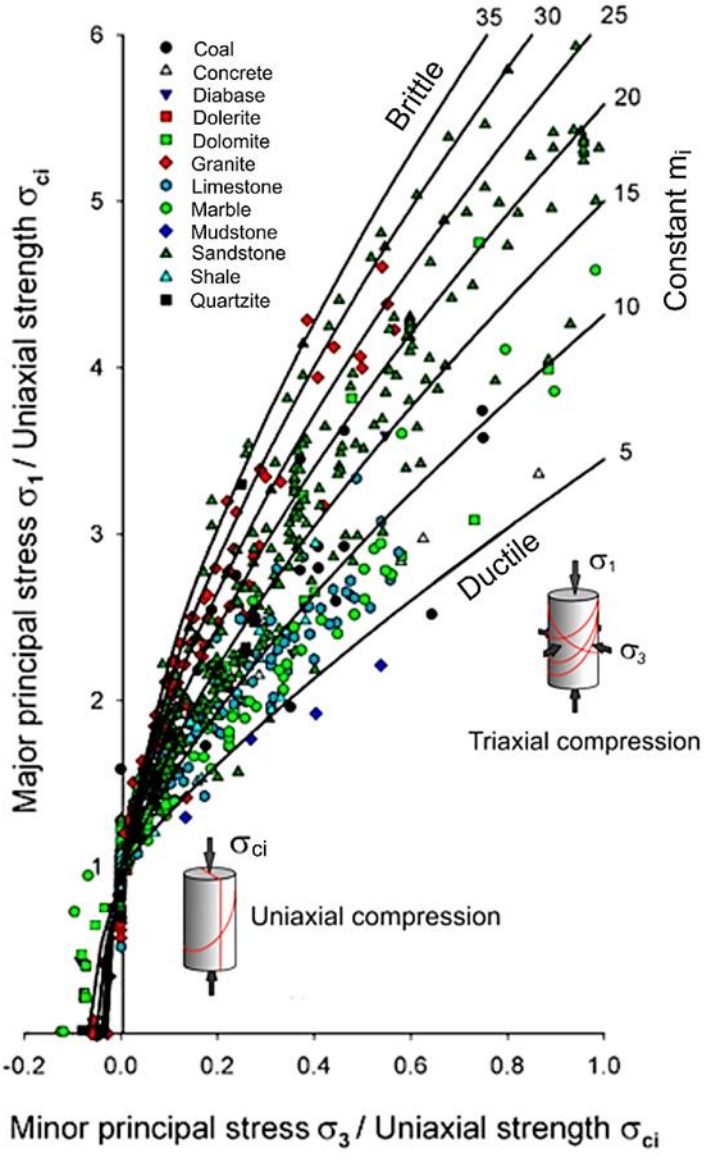

Figure 6: Plot of triaxial and tensile test data for a wide range of intact rock samples, illustrating that relationships presented in Figure 4 apply to most rock types.

Jointed rock masses

While the behaviour of intact rock is of fundamental importance in rock engineering, an even more important topic, in practical applications in the field, is the behaviour of jointed rock masses, such as those illustrated in Figures 7 and 8. The discontinuities in these illustrations are bedding planes, joints, shear zones and faults resulting from deformations in the rock mass during formation and subsequent movements of the overall rock mass due to movements in the earth's crust. In hard rock masses these discontinuities tend to occur in families of planes, some of which extend for significant distances through the rock mass, as can be seen in Figure 7.

As shown in Figure 7, the spacing of the discontinuities, relative to the size of the structure under construction, is important in determining the mode of overall rock mass failure. The tunnel on the left has widely spaced bedding planes and joints and the failures in the rock mass surrounding the tunnel involve large blocks falling due to their own weight. The highway cutting on the right, created by careful blasting, has a stable vertical slope of interlocking blocks formed by predominantly horizontal and vertical discontinuities. This type of rock mass can be dealt with as a homogeneous material when the spacing between the discontinuities is small compared to the dimensions of the rock mass under consideration.

Figure 7: A tunnel excavated through rock with widely spaced intersecting discontinuities and a slope cut into a blocky rock mass by careful blasting during the construction of a highway.

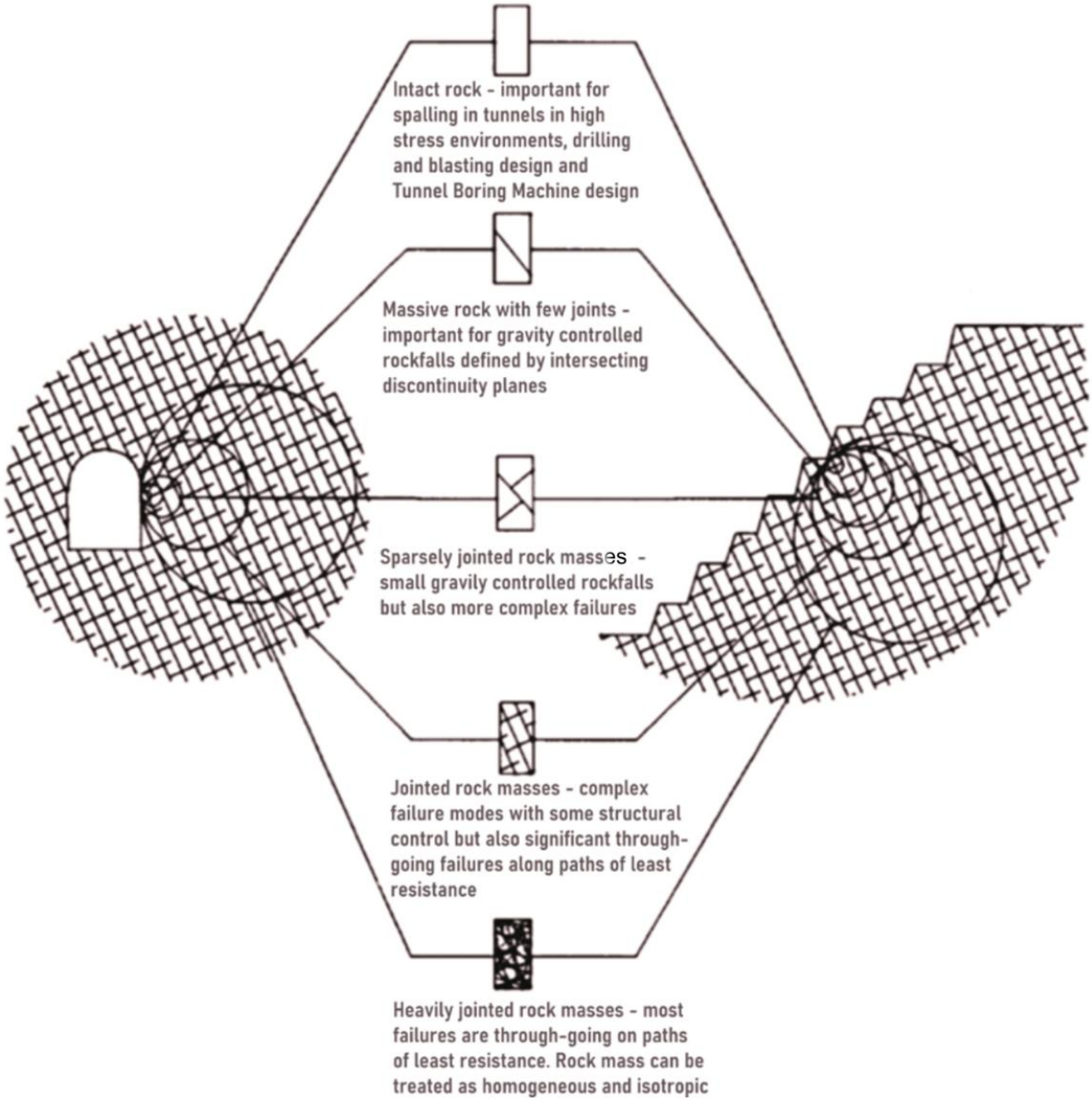

Figure 8: The influence of scale on jointed rock masses.

In addition to the location and orientation of the discontinuities in a rock mass, the shear strength of the discontinuity surfaces is important in any analysis of the failure process in a jointed rock mass, discussed in detail in a later chapter in these notes.

Figure 9 illustrates the basic principles of a shear test and a photograph of small shear test machine that can be used in the field, if necessary, for shear tests on joint surfaces in diamond drill core samples.

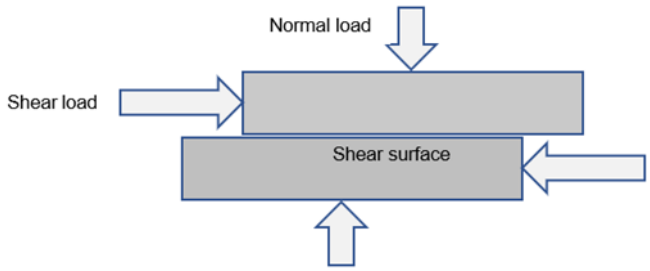

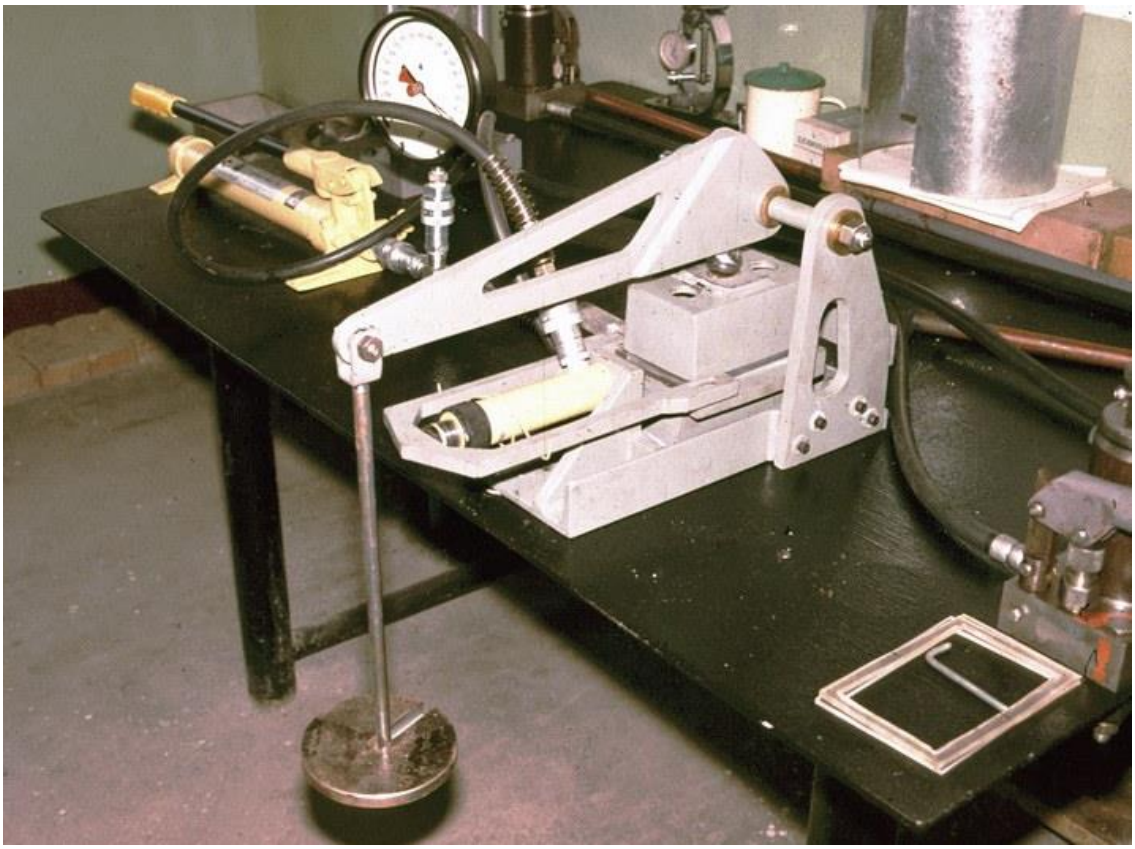

Figure 9: Diagrammatic illustration of a shear test and a simple shear machine for testing discontinuities in core samples.

The strength of a jointed rock mass can be described by the Hoek-Brown failure criterion defined by $\sigma_1 = \sigma_3 + \sigma_{ci}(m_i\sigma_3/\sigma_{ci} + s)^{0.5}$ (Hoek and Brown, 2019). This is the same equation used for calculating the intact rock strength but, for rock masses, the values of the constants m_i and s both decrease to account for the strength reduction due to the presence of discontinuities.

Relationship between rock mass strength and in situ stress in tunnels

Figure 10 is a plot of tunnel strain, defined by the ratio of tunnel closure to diameter, for a range of rocks with an increasing ratio of rock mass strength to the in-situ stress in the surrounding rock mass. This plot was published by Hoek and Marinos (2000). It was derived by running analyses to calculate tunnel strain for several thousand cases of tunnels of different diameters, different rock mass properties and different depths below surface. Theoretical solutions by Duncan Fama (1993) and Carranza-Torres and Fairhurst (1999) were used to calculate the strains for these cases. The behaviour of all the tunnel analysed follows a clearly defined pattern, which is adequately predicted by means of the equation $\varepsilon = 0.2\ (\sigma_{cm}/p_0)^{-2}$ included in the figure. Several illustrations of tunnel squeezing are also included in the figure.

Examples of the conditions that can be encountered in mining tunnels in rock masses, with a range of properties and in situ stresses, are given in Figure 10. Depending upon the stress distribution in the rock mass, shallow spalling of the rock in the walls of the tunnel can occur at a relatively shallow depth. This spalling propagates a limited distance into the rock and stabilizes relatively quickly. With an increase in depth, the spalling can become more severe and significant support, in the form of wire mesh and rockbolts, is usually required to stabilize the tunnel walls. At greater depths, violent shear failure or rockbursting of the rock mass surrounding the tunnel, can occur. This can be very dangerous and is difficult to control by the installation of support. The only mitigating factor is that, once the energy of the burst has been released, the rock mass stabilizes. This means that, in some cases it may be possible to install flexible support, such as steel ribs, which will keep the broken material in place until repairs can be made.

The presence of geological discontinuities, such as faults, shear zones and joints, results in a deterioration of the rock mass strength and deformation characteristics. This causes a decrease in the stability of the rock mass surrounding the tunnel. Combining the influence of both depth below surface and rock mass quality results in a severe reduction of tunnel stability. The photograph at the top of Figure 10 illustrates severe squeezing in the Yacambú-Quibor Tunnel in Venezuela, mined in weak graphitic phyllite at a depth of up to 1270 m below surface (Hoek and Guevara, 2009).

A long tunnel may pass through a variety of rock types and in situ stress conditions, with the result that more than one type of instability may be encountered. Recognition of which types of instability are likely to occur and what types of mining methods and support systems will be most effective is critical in the very early stages of route selection and planning. It is probably at this stage of a tunnelling project that an experienced consultant, with many years of practical experience, can provide the most useful input to a project.

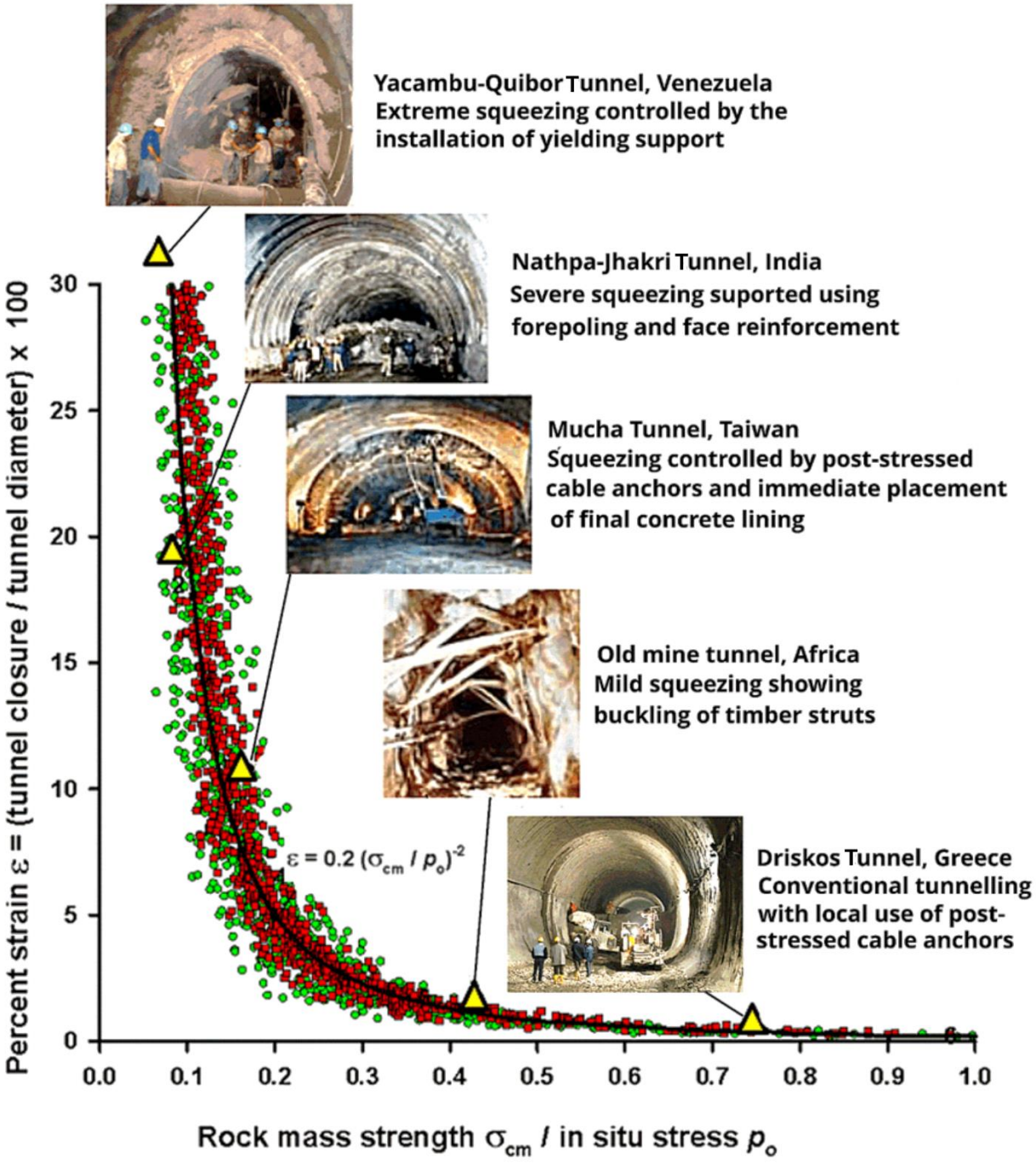

Figure 10: Approximate relationship between tunnel strain and the ratio of rock mass strength to the in-situ stress magnitude, together with comments on geotechnical issues and support solutions associated with different strain levels. Note that the plot is for unsupported tunnels.

Driskos Tunnel on the Egnatia Highway in Greece

To demonstrate the processes described above, an example involving one of the tunnels on the Egnatia Highway in Greece is presented in the following discussion. This highway runs for 680 km across Northern Greece. It meets all the requirements set out by the European Union for highways forming part of the Trans-European Highway Network. The highway includes 72 two-lane tunnels, with an internal diameter of 11 m and a total length of approximately 100 km. Fifty interchanges and 1,650 bridges, with a total length of about 64 km, are also included in the highway, which was completed in 2009. The Driskos Tunnel was excavated through a range of different rock types, the weakest of which was sheared flysch like that illustrated in the centre of the photograph in Figure 11.

Figure 11: Appearance of sheared flysch in a surface outcrop along the Egnatia Highway.

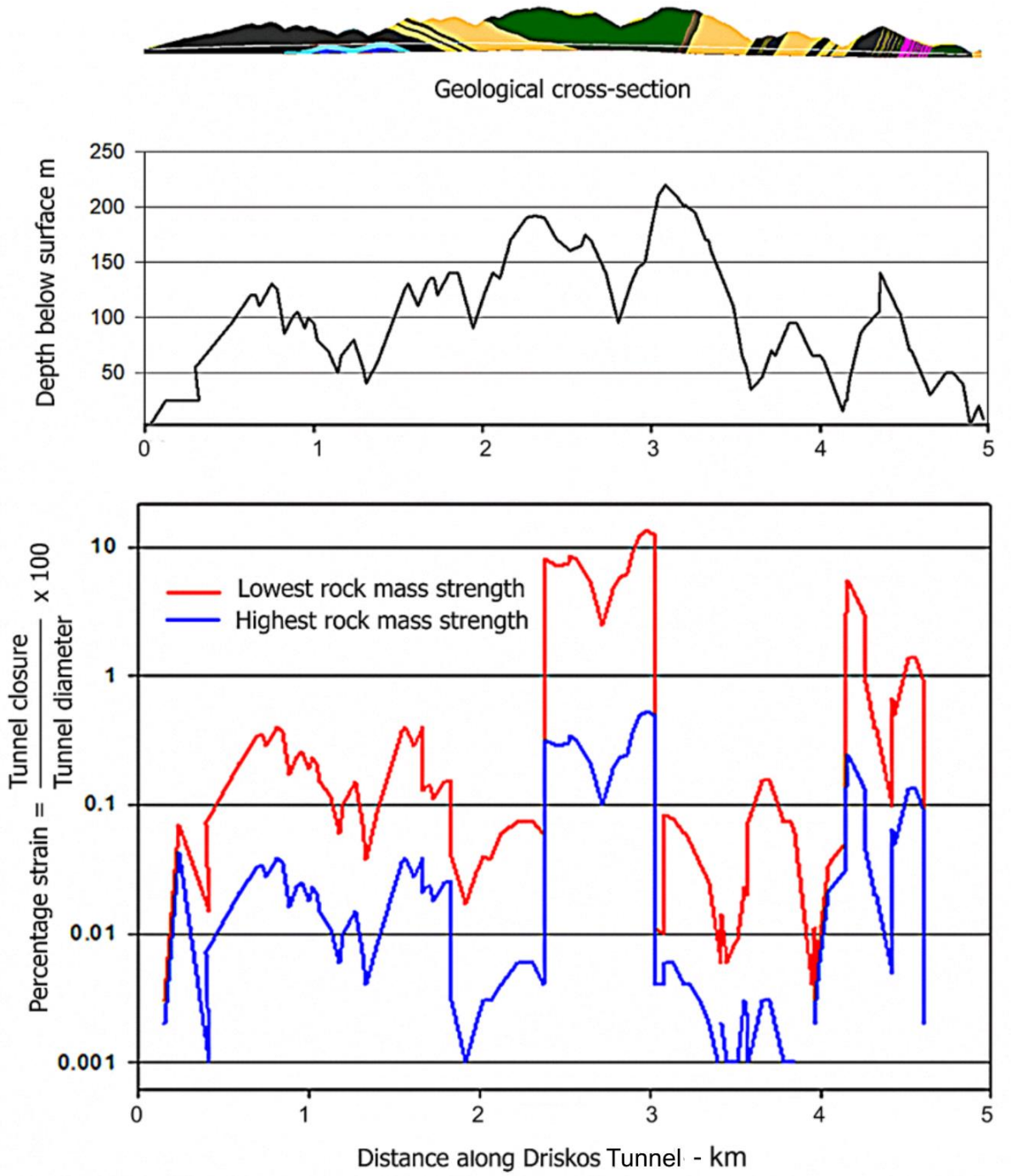

Figure 12: Results of an analysis of tunnel closure of the Driskos Tunnel, based on the stresses induced by the depth of the tunnel and the estimated rock mass strength of rock masses along the tunnel.

Figure 12 presents the results of an analysis of potential squeezing in the unsupported Driskos Tunnel, indicating that strains of approximately 10% were anticipated between distances of 2.3 km and 3 km, in poor quality flysch at depths between 100 and 200 m below surface. As shown in Figure 10, minor squeezing of the tunnel could be anticipated at this depth.

To check on the adequacy of conventional support systems to stabilize this tunnel, the analysis was re-run with a uniform support pressure of 1 MPa. This is typical of the support pressures that can be generated in a 12 m span tunnel with rockbolts, lattice girders or steel sets used in combination with shotcrete lining (Hoek, 1999). The results of this analysis suggested that the strains in the tunnel would be reduced by approximately 50% which suggested that stabilization of the tunnel by means of relatively conventional support measures would be entirely feasible.

Figure 13 shows that minor squeezing did occur as predicted and that it was necessary to supplement the support locally by the installation of patterns of 10 m long post-stressed cables. The tunnel was excavated successfully, and shown in Figure 14, with a shotcrete layer to complete the temporary support system. A final concrete lining was placed after completion of the excavation, using the components illustrated in Figure 15.

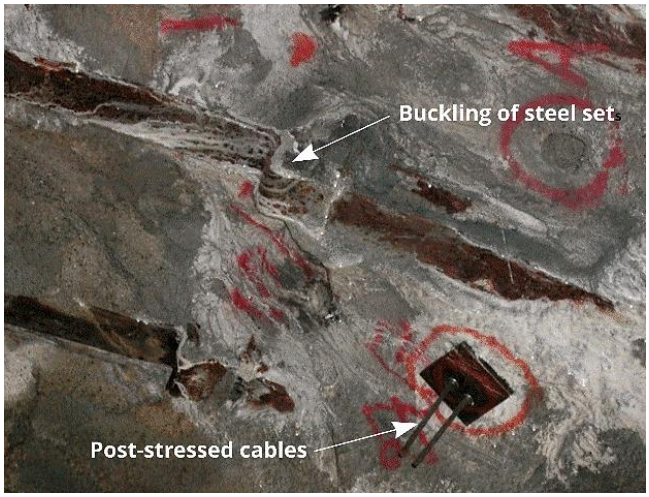

Figure 13: Deformation of steel sets because of mild squeezing in the Driskos Tunnel at the location predicted in Figure 12. Post-stressed cables of 10 m length were used to supplement local support.

Figure 14: Driskos Tunnel being advanced by top-heading and bench drill and blast methods. A 20 cm thick shotcrete lining was added to the steel sets and rockbolts to provide support pending the installation of the final concrete lining.

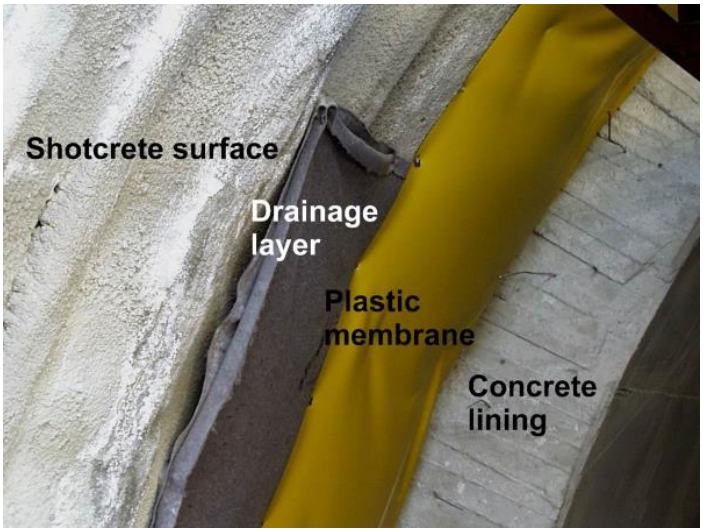

Figure 15: Details of placement of the final concrete lining.

Decision making in Rock Engineering

The example of the Driskos Tunnel presented above shows that, even in the case of the excavation of a relatively simple tunnel, several decisions must be made by the designer and the contractor to ensure that the tunnel can be constructed safely. It is necessary to ensure that enough information is available to make these decisions at appropriate times during the design and construction process. This requires careful planning at the start of the project.

Table 1 presents a summary of the steps involved in the design and construction of a typical rock engineering project such as a tunnel, a dam or bridge foundation, a rock slope in an open pit mine or a highway. Each project is unique, and details of the steps outlined must be chosen and refined to meet the requirements, constraints, and budgets for each case. Figure 16 is a simplified presentation of the increase in confidence in the design for each of the steps presented in Table 1. The general aim in this process is to minimize the risk of failure to the lowest possible level, given the inherent uncertainties associated with the properties and behaviour of naturally occurring rock masses. While strenuous efforts have, and continue to be, made to improve the techniques and tools for predicting rock mass properties and their behaviour when used as engineering material in civil and mining engineering structures, it is highly improbable that we will be able to reach the level of confidence associated with the use of man-made materials such as steel or concrete.

The examples presented in the following pages of this document are intended to present actual projects in order to demonstrate some of the methods used to arrive at practical, economical and safe solutions to projects in which rock and rock masses are used as engineering materials.

Table 1: Steps involved in the design and construction of a rock engineering project.

Step	Examples	Processes
Definition of problem	Mine layout, tunnel route selection, open pit mine layout, large underground cavern configuration, foundation specifications	Creation of preliminary geological model, walk-over surveys, preliminary assessment of anticipated problems
Pre-feasibility study	Definition of investigations and studies required for design of slopes, tunnels, foundations, and other components. Analysis of functional and budgetary requirements and constraints.	Drafting of project layout and alternative solutions, if available. Drilling of exploration boreholes at critical locations, description and classification of rock outcrops
Feasibility study	Execution of defined investigations and studies, including creation of detailed geological maps and cross-sections, diamond drilling for rock samples, laboratory testing of intact rock and discontinuities, detailed classification of rock and rock mass to estimate rock mass properties, collection of groundwater data to create groundwater model. Detailed analyses, using empirical and numerical tools, of critical project details to establish ranges of practical and cost-effective methodologies and designs.	Interpretation and analysis of information collected, refinement of project layout options and selection, construction sequences, contractual details. In some cases, access roads, accommodation for designers and contractors, construction of pilot or access tunnels and installation of drainage systems can be carried out in an initial contract, followed up by construction of project components in the final design and construction stage.
Final design	Use of pilot tunnels or trail excavations to confirm predicted rock mass behaviour. Detailed analyses of defined problems by experienced engineers and geologists, using most sophisticated tools available, to finalize choices and sequencing of excavation methods, temporary and final support designs, drainage and ventilation measures. Ongoing monitoring, back-analyses and evaluation of stability issues and deformations of completed project components.	Construction and completion of the project which may involve refinement of design and construction components, based on observed and measured behaviour and re-analysis of refined estimates of rock mass properties, in situ and induced stresses, groundwater and drainage conditions and, in some cases, the performance of excavation and support methodologies.

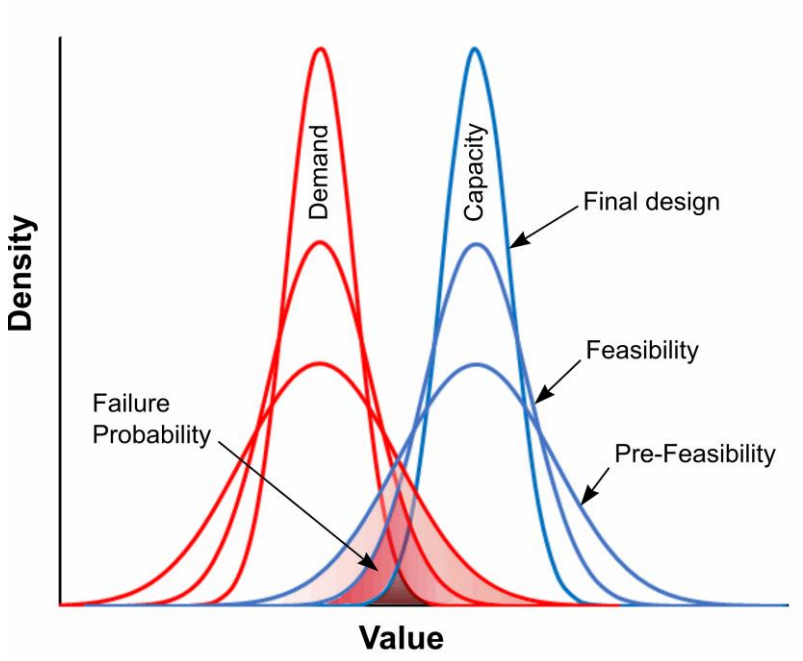

Figure 16: Reliability of the design at different stages of investigation, design, and construction. (Hoek, 1991, 1993).

A set of hypothetical distribution curves representing the degree of uncertainty, associated with available information on shear strength parameters and disturbing stresses for different stages in the design of a rock or soil structure, was illustrated in Figure 10. The factor of safety is defined as A/B where A is the mean of the distribution of shear strength values and B is the mean of the distribution of driving stresses. For this discussion, the same distribution has been assumed for all three stages illustrated.

During preliminary design studies, the amount of information available is usually very limited. Estimates of the shear strength of the rock or soil are generally based upon the judgement of an experienced engineer or geologist which may be supplemented, in some cases, by estimates based upon rock mass classifications or simple index tests. Similarly, the disturbing forces are not known with very much certainty since the location of the critical failure surface will not have been well defined and the magnitude of externally applied loads may not have been established. In the case of dam design, the magnitude of the probable maximum flood, which is usually based upon probabilistic analysis, frequently remains poorly defined until very late in the design process.

For this case, the range of both available shear strength and disturbing stresses, which must be considered, is large. If too low a factor of safety is used, there may be a significant probability of failure, represented by the section where the distribution curves overlap in Figure 16. To minimise this failure probability, a high value for the factor of safety is sometimes used. For example, in the 1977 edition of the US Bureau of Reclamation Engineering Monograph on Design Criteria for Concrete Arch and Gravity Dams, a factor of safety of 3.0 is recommended for normal loading conditions when …'only limited information is available on the strength parameters'. This value can be reduced to 2.0 when the strength parameters are … 'determined by testing of core samples from a field investigation program or by past experience'.

During detailed design studies, the amount of information available is usually significantly greater than in the preliminary design stage discussed above. A comprehensive program of site investigations and laboratory or in situ shear strength tests will normally have been carried out and the external loads acting on the structure will have been better defined. In addition, studies of the groundwater flow and pressure distributions in the rock mass, together with modifications of these distributions by grouting and drainage, will usually have been carried out. Consequently, the ranges of shear strength and driving stress values, which must be considered in the design, are smaller and the distribution curves are more tightly constrained.

Changes in the size and scope of projects involving rock engineering

In the past fifty years, there have been dramatic changes in the type and scale of civil and mining engineering projects involving the use of rock masses as the principal construction material. Tunnels have become significantly longer and deeper, foundations larger and more complex and excavated open pit mine slopes with heights more than one kilometre, have become relatively common. To deal with these changes, improvements have been made in design methodologies for existing problems involving deformation driven tunnel failures, rockfalls, groundwater control and time dependent deformations in materials such as evaporites.

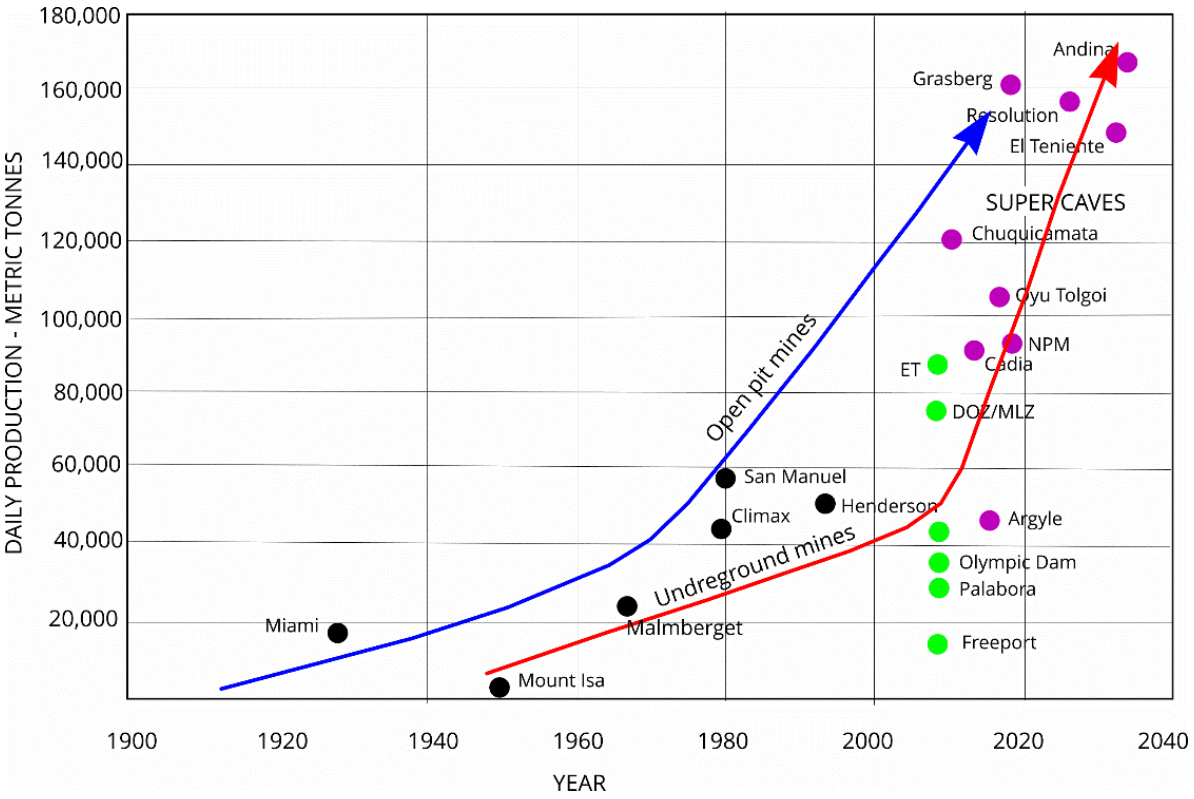

Figure 17: Changes in the production rate of open pit and underground mines (after Brown (2004) and Eberhardt (2019)).

An example of the rapid changes in open pit and underground mines is presented in Figure 17, which shows changes in the daily production rates during the 1970s in open pit mining and in the period from 2000 onward for underground mines. The locations of some of the mines, included in Figure 17, are shown in Figure 18.

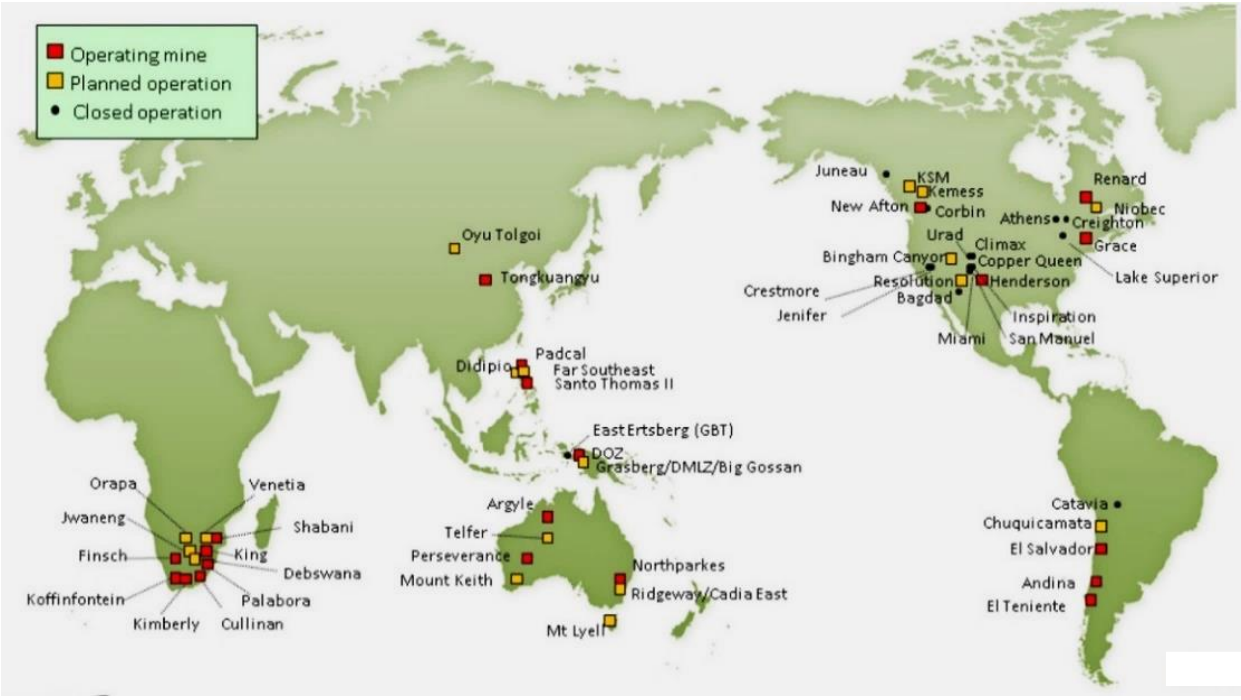

Figure 18: Major open pit and underground mines around the world, after Woo et al (2013).

The development of very large open pit mines, such as the Chuquicamata Copper Mine in Chile illustrated in Figure 19, became feasible because of an improved understanding and experience in the behaviour of rock masses and improvements in equipment and methodologies used in excavation.

Hoek and Martin (2014) have described a detailed stability analysis of the east wall of the Chuquicamata Mine. This is a good illustration of the application of many of the most advanced theoretical tools available to the solution of a very practical problem involving the stability of a conveyor transfer station located in the rock mass behind the slope. Most of the crushed ore mined in the pit passed through this transfer station on its way to the processing plant, making its stability a critical factor in the overall operation of the mine.

Figure 19: The Chuquicamata open pit mine in Chile in 2013. Before conversion to an underground block caving operation in approximately 2019, the pit was 4 km long, 3 km wide and 1 km deep.

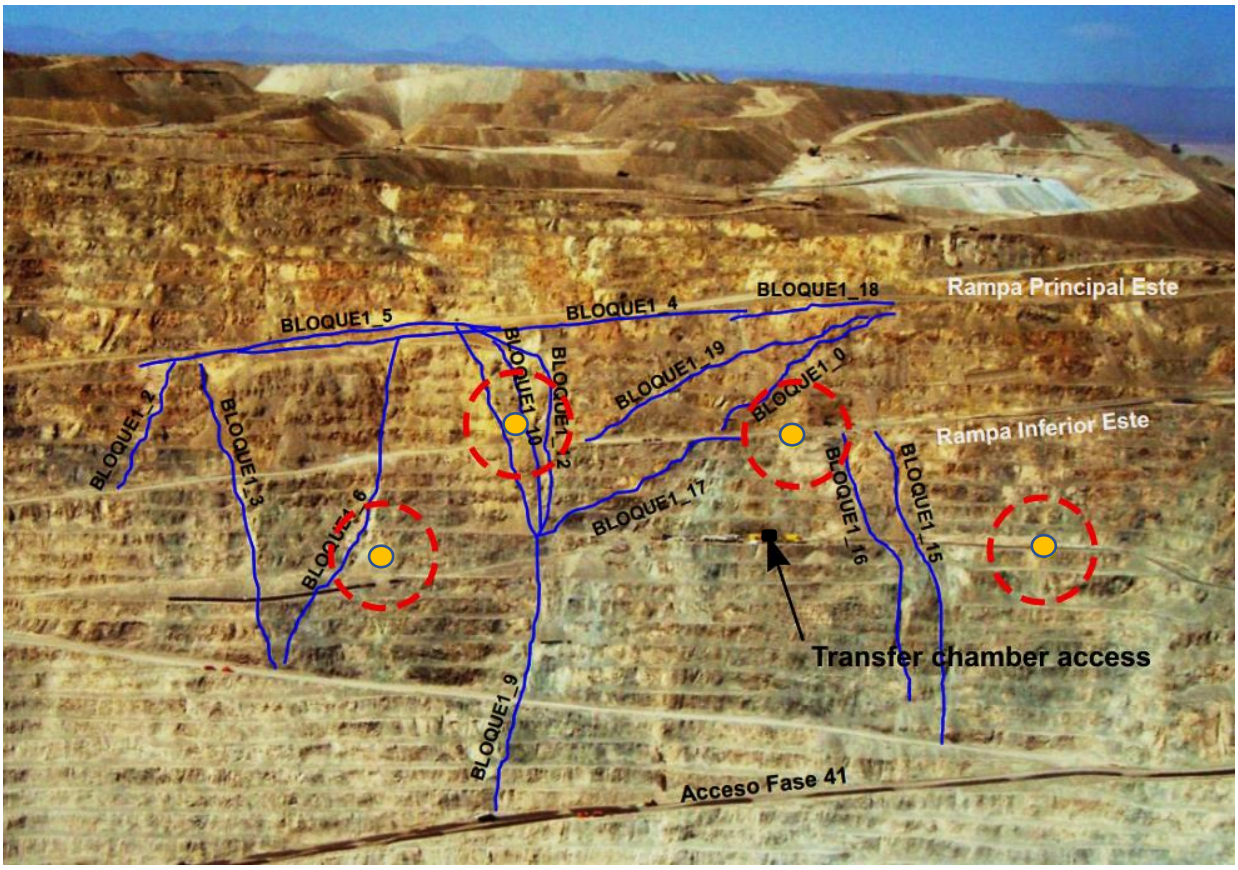

Figure 20: View of the Chuquicamata Mine east face showing locations of the conveyor transfer chamber, major structural features and optical targets for distance measurement (yellow spots circled in red).

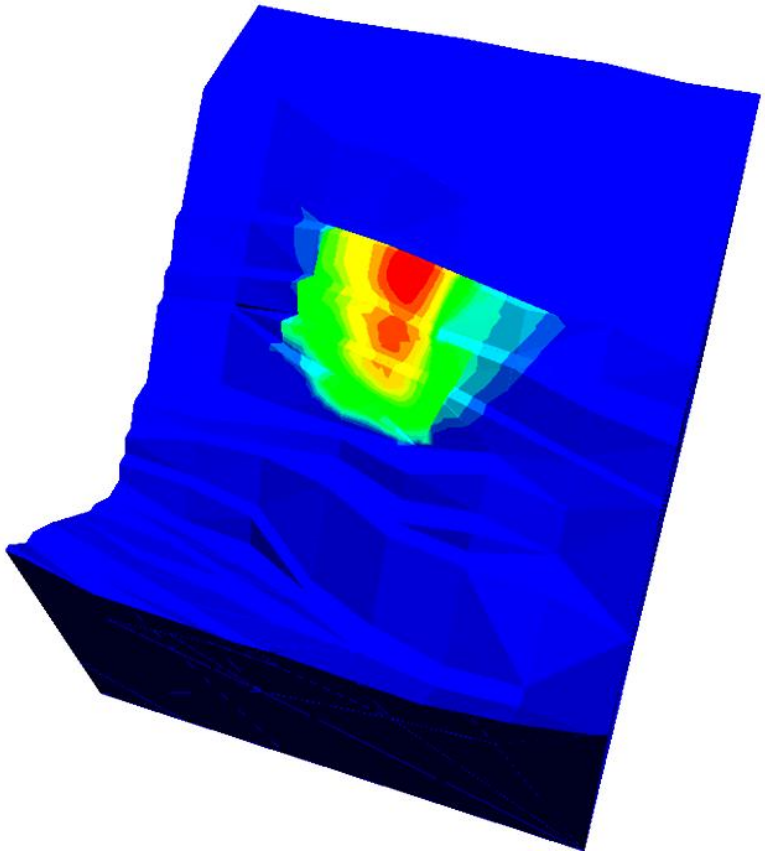

Figure 21: Displacement contours in the east face generated in a 3DEC model. The colours, from blue to red, show increasing displacement in the rock mass.

Figure 20 illustrates the East Wall and the location of the entrance to the underground conveyor transfer station. A detailed 3DEC[1] analysis was carried out, by Pedro Varona of Itasca and Felipe Duran of Chuquicamata, in 2012/13 assuming that the overall rock mass could be treated as homogeneous, using the rock mass properties based on the Hoek-Brown criterion and the Geological Strength Index (Hoek and Brown, 2019), with super-imposed major discontinuities (shown in blue). The yellow dots are locations of some of the 1000 laser distance measurement targets that surround the open pit. An underground conveyor transfer chamber is located behind the potentially unstable wedge, defined by the coloured contours in the centre of the east face in Figure 21.

There are many other examples, in both open pit and underground mining, where practical decisions have been made based on sound rock engineering principles. Some of these decisions have incorporated detailed analytical studies, but most of them are made based on practical rock engineering experience acquired from years of empirical observation and cautious trial and error development.

[1] A three-dimensional discrete element numerical model in which individual elements, defined by intersecting structural features in the rock mass, can be incorporated (Itasca, 2002).

Underground mining is an unknown world to many of us. An excellent introduction to different methods used to mine ore can be found in Brady and Brown's book, Rock Mechanics for Underground Mining (Brady and Brown, 2004). Well-illustrated Chapters 12 and 15 on underground mining methods and longwall and caving methods, respectively, are particularly useful in helping the reader to distinguish between a huge array of complex ore recovery methods.

As shown in Figure 17, a spectacular step change around 2010 resulted from advances in block-caving technology. This is a very old mining technique, originally developed in the underground coal mines in the United Kingdom (Sainsbury, 2012), involving undercutting an orebody and allowing it to cave, in a controlled manner, into draw points where the coal or ore is collected. The principal features of a caving operation are illustrated in Figure 22 while details of the support required to stabilize draw-points are given in Figure 23. The most used approach for estimating caveability, developed by Laubscher (Diering and Laubscher 1987, Laubscher 1990, 1994, 2000) is based on a compilation of caving case histories – largely derived from low strength, kimberlitic deposits in South Africa.

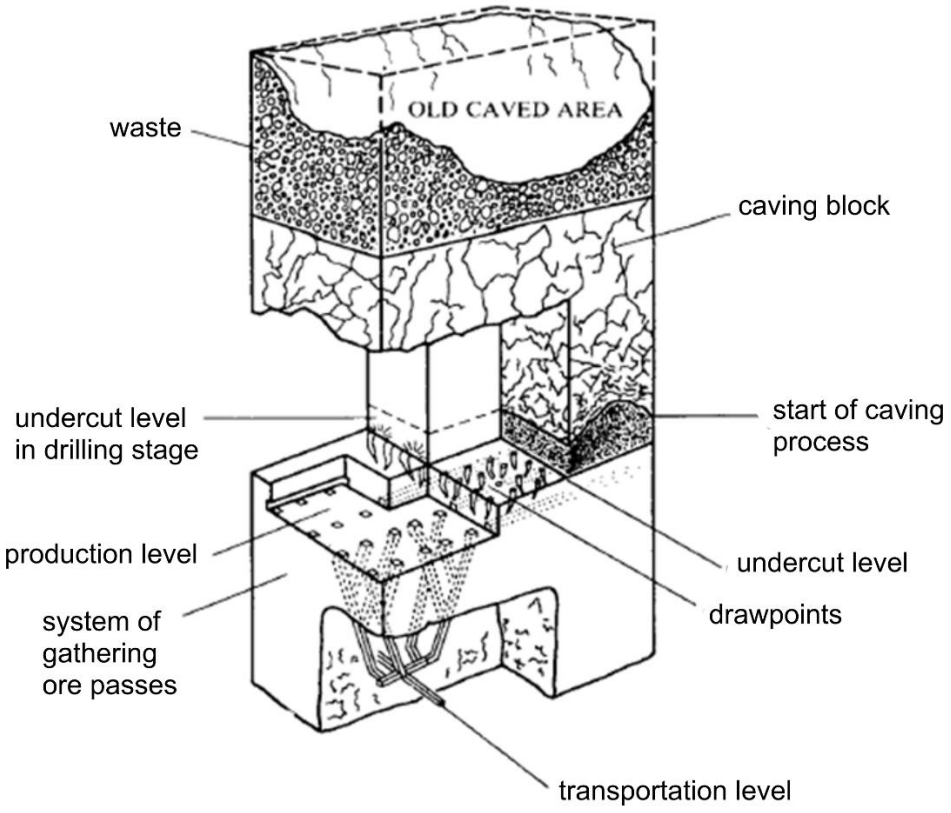

Figure 22: Principal features of a caving operation (Borquez, 1981).

Figure 23: Placement of grouted bars to pre-reinforce a draw-point in a large, mechanised mine. The shaded area is blasted last, after the reinforcement has been installed from the draw-point and the trough drive (after Hoek and Brown, 1980).

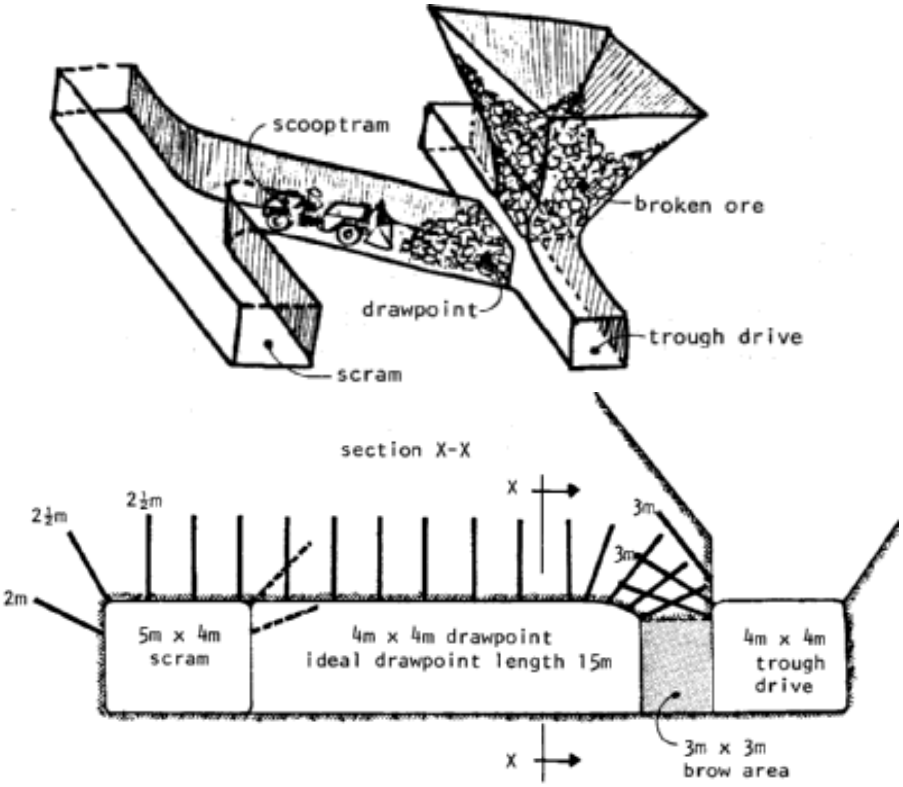

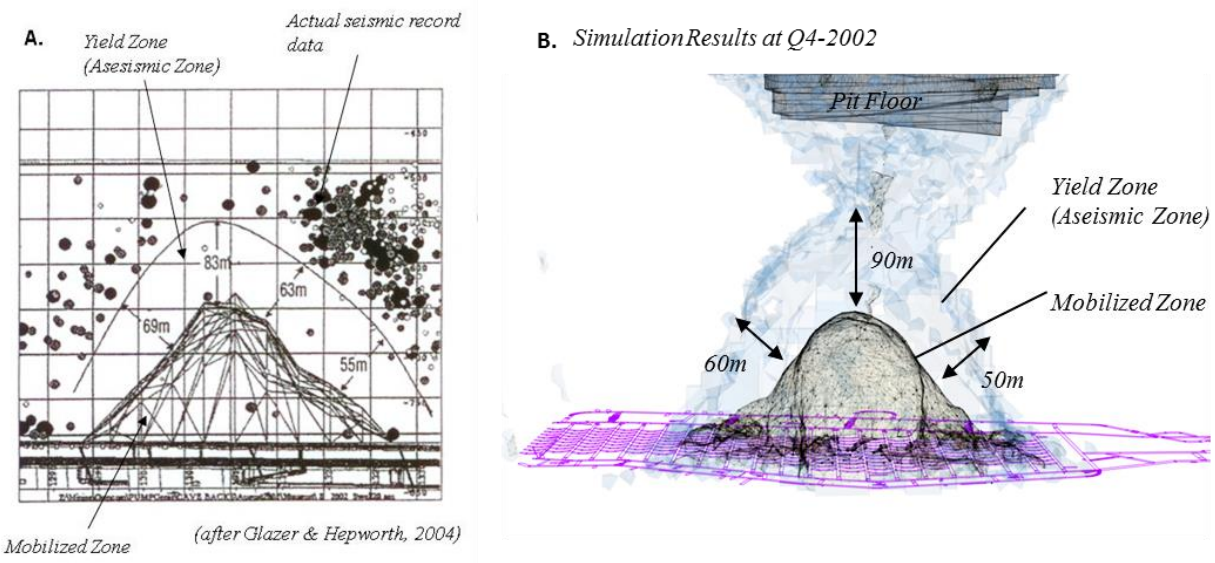

Figure 24: Observed seismic activity at the Palabora Mine during cave initiation and propagation (A) observed mobilized, yield and seismogenic zones during production (after Glazer and Hepworth, 2004); (B) numerical prediction of mobilized and yield zones during production at the Palabora Mine (after Sainsbury, 2012).

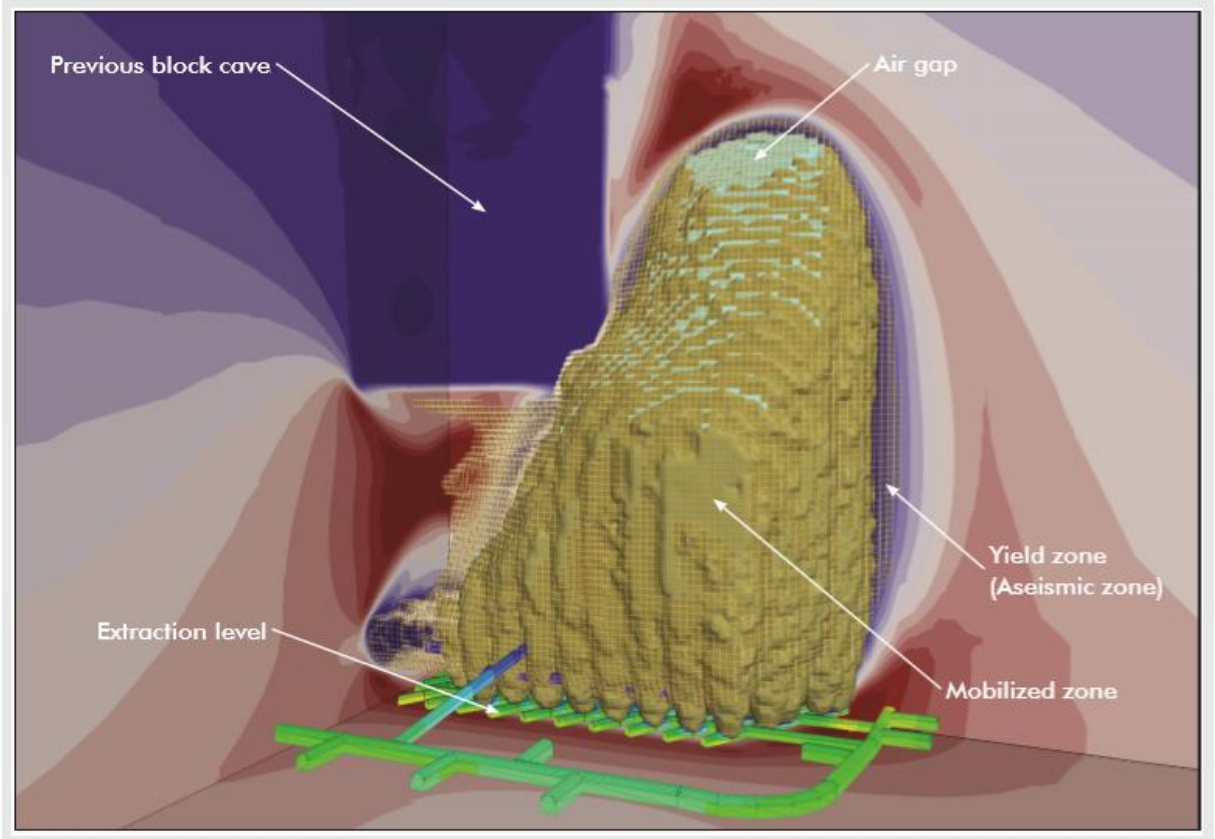

Figure 25: Coupled FLAC3D/REBOP block cave model indicating the predicted flow and yield (blasted/swell) zones and the formation of air gaps after 20 months of production at New Afton Mine, NewGold, Inc. Contours of the maximum principal stress are shown along octant cut-planes (blue for lower stress and red for higher stress). Image provided by Itasca Consulting Group, Inc**.,** with permission from NewGold, Inc.

Most of the mines designated "super caves" in Figure 17 are block caving operations. Control of the progressive caving and the movement of the broken rock, which is critical in maintaining a stable progressive mining operation, has benefitted greatly from the development of three-dimensional discrete element numerical tools. These methods, collectively named Synthetic Rock Mass Modelling tools, are generally accepted as the current state-ot-the-art in anisotropic rock mass behaviour analysis. An excellent discussion of this technology, with several case histories, can be found in a PhD thesis by Bre-Anne Sainsbury (2012). General discussion on caving by Lorig et al., 1995, Laubscher, 2000, Cundall, 2008, Sainsbury et al, 2008, and Mas Ivers et al, 2011, provide important background material on this topic. Several specific cases are discussed by Sainsbury and Lorig, 2005, Fuentes and Villegas, 2014 and Flores and Catalan, 2019.

Examples of the application of three-dimensional numerical analysis to the prediction of block caving in the Palabora Mine in South Africa and the New Afton Mine in British Columbia, Canada, are presented in Figures 24 and 25 respectively.

Examples to illustrate the design principals used in rock engineering

Figure 26 shows a circular tunnel advancing through a rock mass in which in situ stresses exist due to the weight of the overlying rock mass and the lateral constraints provided by the surrounding rock mass. For the sake of simplicity, the three orthogonal principal stresses are shown as perpendicular and parallel to the tunnel axis. In fact, these stresses may be inclined at any direction; their magnitudes are dependent upon the tectonic history of the rock mass in which the tunnel is being driven.

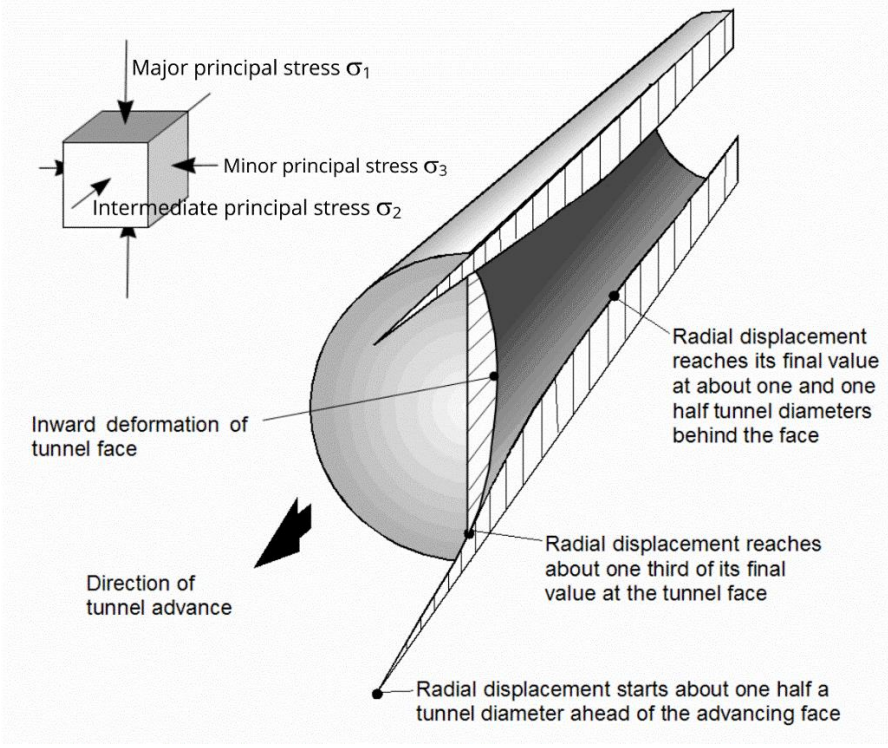

Figure 26: Advance of a circular tunnel through a stressed rock mass.

The boundary displacements, shown in Figure 26, result from the stresses induced in the rock mass surrounding the tunnel which, in turn, depend upon the depth below surface and the tectonically induced lateral stresses.

In situ stresses, expressed in terms of the vertical stress and the ratio k of horizontal to vertical stress, are plotted in Figure 27, reported by Brady and Brown (2004), based on 900 determinations of the pre-mining in situ state of stress at numerous locations of mining, civil and petroleum projects around the world. The line in the left-hand plot in Figure 27 is calculated on the basis that the vertical stress is a product of the depth below surface and the unit weight of the rock mass, assumed to be 0.027 MN/m^3. While the measured data are scattered around this line, the plotted line can be considered a reasonable average relationship between vertical in situ stress and depth below surface.

The right-hand plot in Figure 27 shows that the ratio of horizontal to vertical stress varies widely at shallow depth, with k > 6 having been reliably reported in some locations. With increasing depth, the variability decreases and the upper bound tends towards unity. A probable explanation for this is that the rock mass is not able to sustain shear stresses at great depth due to time-dependent viscoplastic flow, resulting from progressive failure of defects.

Brady and Brown (2004) also discuss the highly variable stress distribution which can be anticipated in jointed and fractured rock masses and quote several cases in which the state of stress is related to the locally dominant geological structure. They conclude that the viscoplastic flow, discussed above, together with the influence of geological structures, means that the virgin stress state in a rock mass is not amenable to calculation by any known method, but must be determined experimentally.

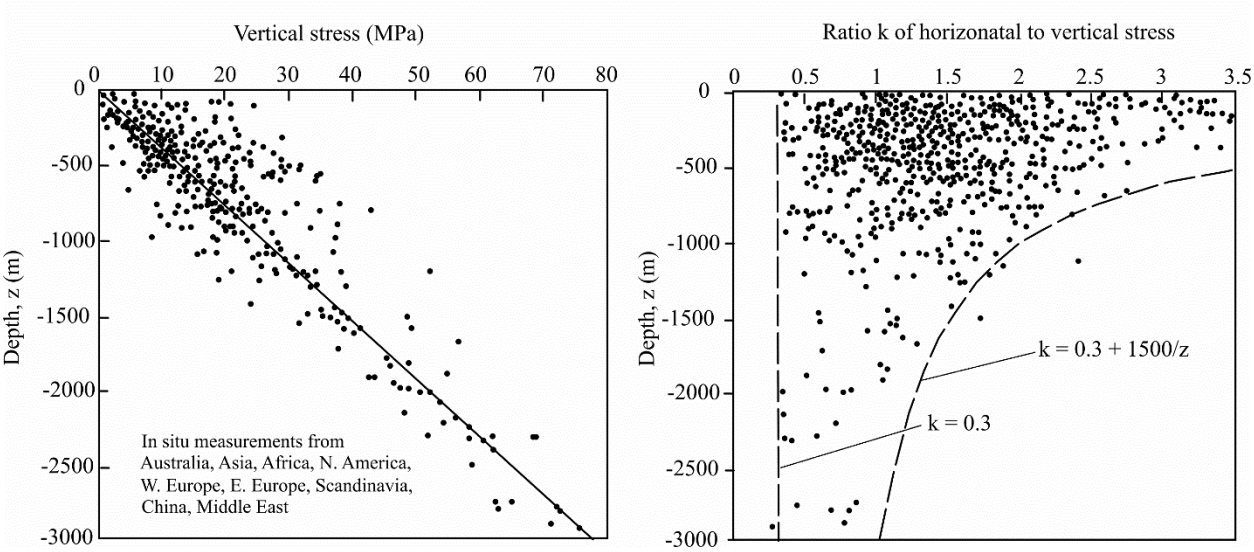

Figure 27: Variation of in situ vertical stress and the ratio of horizontal to vertical stress (k) with depth below surface (after Brady and Brown, 2004).

Measurement of these in situ stresses has been, and remains, an ongoing challenge in rock engineering (Leeman and Hayes,1966, Worotnicki and Walton, 1976). Fortunately, recent advances by Mills (1997), Mills and Puller (2017) have resulted in instrumentation that can be used to measure the three-dimensional in situ stress state at depths of up to 1 km below surface in competent rocks. In weak rocks such stress measurements are practically impossible, and stresses must be estimated based on engineering geology reasoning.

From a design perspective, before the commencement of any excavation, the most practical approach is to use all stress measurement information that is available, including that from adjacent projects, to make an estimate of the range of possible values of in situ stresses that could be encountered. The proposed excavation, such as a tunnel or an underground cavern, is then analysed for a variety of possible in situ stress regimes to determine whether conceptual designs can be created that would accommodate any stress conditions within the range considered.

Figure 28 shows that, when excavating tunnels or shafts in competent rocks at significant depths below surface, spalling failure of the rock in the excavation perimeter can occur at a depth (H) defined by a combination of the uniaxial compressive strength (UCS) of the rock and the ratio of horizontal to vertical stresses (k). For example, as shown by the red dot in Figure 28, an intact rock with a UCS value of 150 MPa will spall at a depth of H = 500 m when the ratio of horizontal to vertical stress is k = 2.

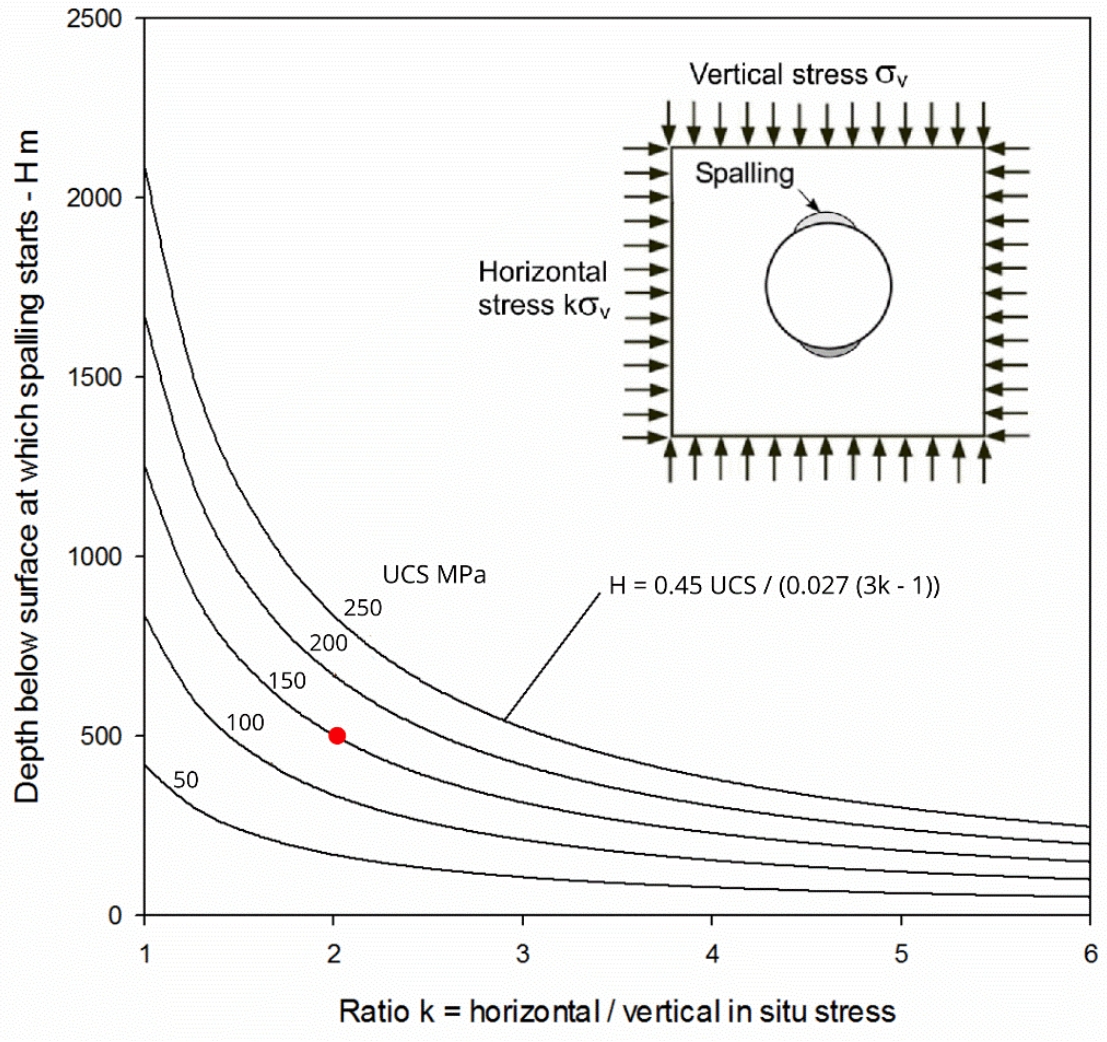

Figure 28: Approximate depth at which spalling occurs in a circular tunnel in intact rock.

Spalls, of the type and size illustrated in Figure 29 do not pose a significant threat since they propagate a limited distance, depending upon the strength of the rock and the in-situ stresses, and then stabilize. Small rockfalls can be contained by a layer of wire mesh supported by a pattern of rockbolts. A final lining consisting of a layer of shotcrete is generally adequate in such cases. The approximate depth of the spalls in a circular tunnel of a shaft can be estimated from the plot reproduced in Figure 30, in which the maximum boundary stress σ_{max} is calculated by simple elastic theory.

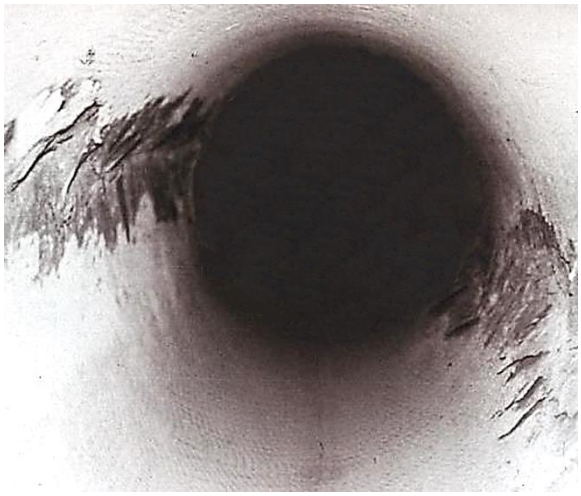

Figure 29: Spalling in the walls of a bored vertical shaft in competent rock at a depth approximately 600 m below surface.

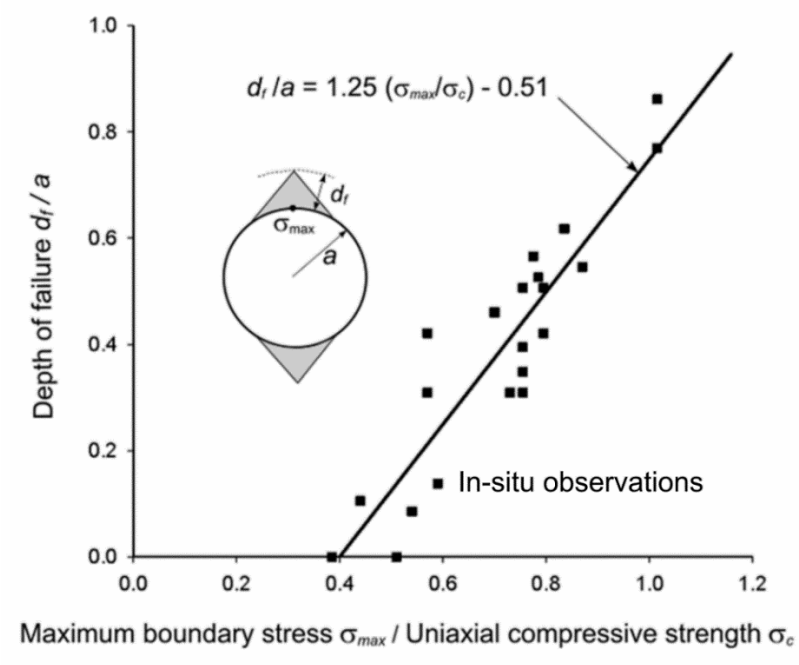

Figure 30: Estimated depth of spalls in a circular tunnel based on field measurement of spalls in competent rock.

When the maximum boundary stress σ_{max} exceeds the uniaxial compressive strength σ_c, in Figure 30, the potential exists for the spalling to occur with a violent release of energy. This phenomenon is known as rockbursting, which can result very dangerous working conditions in the excavation. Figure 31 illustrates the damage due to a severe rockburst in hard rock in a deep level gold mine in South Africa in about 1955.

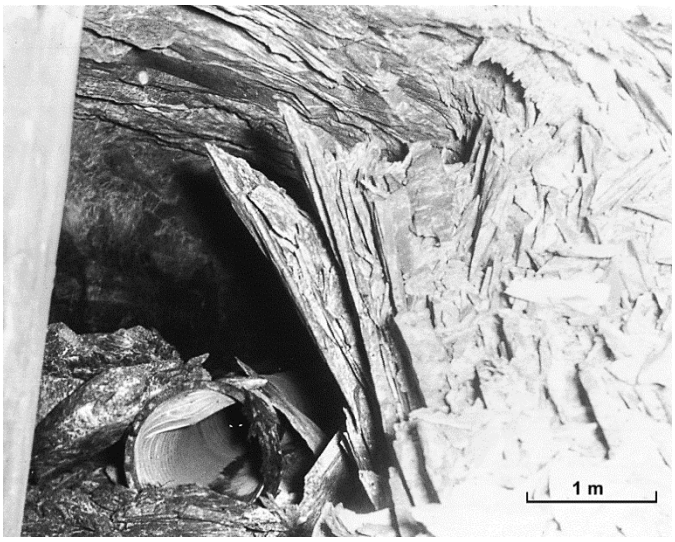

Figure 31: Damage due to a rockburst in a deep level gold mine in South Africa. Photograph from the files of the late Professor Alastair Black of the Royal School of Mines in London.

The problems of spalling and rockbursting in very deep level mines has been familiar to miners for many years. In 1942, Morrison prepared a report on the rockburst situation in the Ontario mines in Canada. Cook et al (1966) published a paper on rock mechanics applied to the study of rockbursts, in deep level gold mines in South Africa, which discussed extensive research into this problem dating back to the 1950s.

References

Borquez, G.V. 1981. Sequence of the analysis of a block caving method. *Design and Operation of Caving and Sublevel Stoping Mines* (ed. D. R. Stewart), pp, 283–297. Soc. Min. Engrs, AIME: New York.

Brady, B.H.G. and Brown, E.T. 2004. *Rock Mechanics for Underground Mining.* New York, Kluwer Academic Publishers. p. 628.

Brown, E.T. 2007. *Block caving geomechanics.* 2nd. ed. Brisbane, Australia. Julius Kruttschnitt Mineral Research Centre. p. 696.

Carranza-Torres, C. and Fairhurst, C. 1999. General formulation of the elasto-plastic response of openings in rock using the Hoek-Brown failure criterion. *International Journal of Rock Mechanics and Mining Sciences*. 36 (6), 777-809.

Cook, N.G.W., Hoek, E., Pretorius, J.P.G., Ortlepp, W.D. and Salamon, M.D.G. 1966. Rock mechanics applied to the study of rockbursts. *J. S. Afr. Inst. Min. Metall.* **66,** 436-528.

Cundall, P. 2008. Recent advances in numerical modelling for large-scale mining projects, *ACG News*. 30, 1-7 (June 2008).

Duncan-Fama, M.E, 1993, Numerical modelling of yield zones in weak rocks. In *Comprehensive Rock Engineering*, (ed. J.A. Hudson.) Vol. 2, 49-75. Pergamon, Oxford.

Duplancic, P. and Brady, B.H. 1999. Characterization of caving mechanisms by analysis of seismicity and rock stress, *Proceedings 9th International Congress on Rock Mechanics (*Paris) Vol. 2, pp. 1049–1053. Balkema, Rotterdam.

Feng, XT. 2017. *Rockburst: Mechanisms, monitoring, warning and mitigation.* Elsevier.

Flores, G. and Catalan, A. 2019. A transition from a large open pit into a novel "macroblock variant" block caving geometry at Chuquicamata Mine, Codelco, Chile. *Journal of Rock Mechanics and Geotechnical Engineering*, **11**, 549-561.

Fuentes, S. and Villegas, F. 2014. Block caving using macro blocks. In Castro, R, editor, Caving 2014, proceedings of the 3rd international symposium on block caving and sublevel caving. Santiago, Chile. pp. 211-216.

Hoek, E. and Marinos, P., 2000, Predicting tunnel squeezing problems in weak heterogeneous rock masses. *Tunnels and Tunnelling International*. Part 1 - November 2000, Part 2 - December 2002.

Hoek, E. 1999. Support for very weak rock associated with faults and shear zones. In rock support and reinforcement practice in mining. (Villaescusa, E., Windsor, C.R. and Thompson, A.G. eds.). Rotterdam: Balkema. pp. 19-32.

Hoek, E. and Brown, E.T. 1980. *Underground Excavations in Rock*. London: Instn Min. Metall. 527 pages.

Hoek, E. and Guevara, R. 2009. Overcoming squeezing in the Yacambú-Quibor Tunnel, Venezuela. *Rock Mechanics and Rock Engineering*, Vol. 42, No. 2, 389 – 418.

Hoek, E. and Brown, E.T. 2019. The Hoek-Brown failure criterion and GSI – 2018 edition. *Journal of Rock Mechanics and Geotechnical Engineering*, **11**, 445-463.

Kaiser, P.K., McCreath, D.R. and Tannant, D.D. 1996. *Canadian Rockburst Support Handbook.* Geomechanics Research Centre.

Laubscher, D.H. 1994. Cave mining – the state of the art. *Journal of the South African Institute of Mining and Metallurgy*, October 1994, pp. 279-293.

Laubscher, D.H. (2000) *Block Caving Manual*. Prepared for International Caving Study. JKMRC and Itasca Consulting Group, Brisbane.

Leeman, E.R. and Hayes, D.J. 1966. A technique for determining the complete state of stress in rock using a single borehole. *Proc. 1st Cong. Int. Soc. Rock Mech, Lisbon* **2** , 17-24.

Lorig, L., Board, M., Potyondy, D. and Coetzee, M. 1995. Numerical modelling of caving using continuum and micro-mechanical models. CAMI'95:*3rd Canadian Conference on Computer Applications in the Mineral Industry*. Montreal, Quebec, Canada, October 22-25, 1995, pp. 416-425.

Mas Ivars, D., Pierce, M., Darcel, C., Reyes-Montes, J., Potyondy, D., Young, P. and Cundall, P,, 2011. The synthetic rock mass approach for jointed rock mass modelling. *International Journal of Rock Mechanics & Mining Sciences* 48 (2011) 219–244.

Mills, K.W. 1997. In situ stress measurements using the ANZI stress cell. *Proc. International Symposium on Rock Stress*. Editors K. Sugawara and Y. Obara. Balkema, Rotterdam, 149-154.

Mills, K.W. and Puller, J. 2017. Development of the ANZI cell for three dimensional in situ stress determinations in deep exploration boreholes. *Proceedings of the 17th Coal Opperators Conference*, University of Wollongong, February 2017, 138-148.

Morrison, R.G.K. 1942. Report on the rockburst situation in Ontario mines. *Trans. Can. Inst. Min. Metall.* **45**.

Paterson, M.S, 1958. Experimental deformation and faulting in Wombeyan marble. *GSA Bulletin 69* (4): 465–476.

Pierce, M., Cundall, P., Potyondy, D. and Mas Ivars, D. 2007. A synthetic rock mass model for jointed rock, In Rock Mechanics: Meeting Society's Challenges and Demands, *Proc. 1st Canada-U.S. Rock Mechanics Symposium* Vol. 1, pp. 341-349.

Ramsey J. and Chester F. 2004. Hybrid fracture and the transition from extension fracture to shear fracture, *Nature, 428,* 63-66.

Sainsbury, B. 2012. A model for cave propagation and subsidence assessment in jointed rock masses. *PhD thesis,* University of New South Wales, Australia.

Sainsbury, D. and Lorig, L. 2005. Caving Induced Subsidence at the Abandoned Grace Mine. *ICG Report to Arcadia Land Company*.

Sainsbury, B., Pierce, M. and Mas Ivars, D. 2008. Analysis of Caving Behaviour Using a Synthetic Rock Mass - Ubiquitous Joint Rock Mass Modelling Technique, In *Proceedings of the 1st Southern Hemisphere International Rock Mechanics Symposium,* 16–19 September 2009, Perth, Australia, Australian Centre for Geomechanics, Vol. 1 – Mining and Civil, pp. 243–254.

Salamon, M.D.G. and Munro, A.H. 1967. A study of the strength of coal pillars. *J. S. Afr. Inst. Min. Metall.* **65** , 55- 67.

Stacey, TR and Ortlepp, WD. 2018. Rockburst mechanisms and tunnel support in rockburst conditions. *Geomechanics 93 – Strata Mechanics.* Taylor and Francis.

Terzaghi, K. 1936. Presidential Address. *Proc. 1st Int. Conf. for Soil Mechanics and Foundations Engineering, Cambridge, Mass*. **1** , 22-3.

Terzaghi, R. and Voight, B. 1979. Karl Terzaghi on rockslides: the perspective of a half-century. In *Rockslides and Avalanches* (ed. B. Voight), Part 2, 111-131. New York: Elsevier.

Vyazmensky, A., Stead, D., Elmo, D. and Moss, A. 2010. Numerical Analysis of Block Caving-Induced Instability in Large Open Pit Slopes: A Finite Element / Discrete Element Approach. *Rock Mechanics and Rock Engineering Journal.* Volume 43, Number 1 / February (2010), 21 - 39. TOP 5 - 2011/2012.

Worotnicki, G. and Walton, R.J. 1976. Triaxial 'hollow inclusion' gauges for determination of rock stresses in situ. *Proc symp. ISRM on Investigation of Stress in Rock, Sydney*. Supplement 1-8. Sydney, Australia: Instn Engrs.

3. Intact rock strength

Introduction

A starting point for a discussion on the mechanical properties of rock and rock masses is the following statement by Palmström (1995): "A rock mass is a material quite different from other structural materials used in civil engineering. It is heterogeneous and quite often discontinuous, but it is one of the materials in the earth's crust, which is most used in man's construction."

Geologists describe, classify and name rocks based on their mode of origin, colour, texture, fabric, and history rather than based on their strength or other mechanical characteristics. Often multiple rock units are then grouped together into formations based on lithology or age relationships. Classically, formation boundaries in bedded sedimentary units are stratigraphically delineated by specific depositional time horizons. Such divisions are often more complex in igneous and metamorphic terrains. Geologists commonly also subdivide rock names based on an abundance of a particular type of mineral within the rock or based on fabric pervasiveness, degree of metamorphism or alteration.

It is typical for geologists to define three main types of rocks – igneous, sedimentary, and metamorphic, based on their general mode of origin – igneous rocks being derived directly from the cooling of molten magma; sedimentary rocks being generally derived from deposited accumulations of reworked older debris and metamorphic rocks created through significant pressure and temperature change to other rocks. A summary of these different rock types is given in Table 1 in Appendix 1, which also includes a more detailed discussion on the definitions.

Practical and reliable methods for collecting, preparing, and testing samples of intact rock subjected to triaxial compressive and tensile loading to failure are described in Appendix 2 to this chapter. The aim in this appendix is to describe methods and equipment that can be used in both the laboratory and in the field to generate reliable information that can be incorporated into the interpretation of rock and rock mass behaviour models. Wherever possible, the simplest equipment that can be used to provide reliable basic information has been chosen to present a practical introduction to students and graduates entering the field of rock engineering for the first time and to geologists, engineering geologists and engineers already working in the field. Undoubtedly, those involved in research into more detailed aspects of rock and rock mass behaviour may need to use more sophisticated equipment and techniques, which are not discussed in this chapter.

The mechanical behaviour of intact rock samples when subjected to stress is the principal topic of discussion in this chapter. High quality testing of intact rock samples has been going on for at least the past seventy years. This has been prompted by the need to understand rock deformation and failure processes related to applications involving the use of rock as an engineering material in tunnels, mining excavations, slopes, and foundations. It is strongly recommended that laboratory testing of intact rock, as described in this chapter, should be a required component of any project involving the design and construction of significant tunnels, shafts, caverns, slopes, or foundations in rock.

The basic mechanics of rock failure are discussed, with particular attention to the determination of the tensile strength of intact rock. Two tables dealing with textural and origin-based classification and with average values of intact rock modulus, uniaxial compressive strength and the Hoek-Brown m_i constant have been included in the text. These tables are to assist readers who may need to understand some of the issues discussed and who may have difficulty in finding reliable classifications and engineering properties of typical rocks in available literature.

Triaxial confining stresses for intact rock testing

In the context of this discussion, the stresses to which intact rock can be subjected are those associated with the construction of slopes, tunnels, caverns and foundations in rock and rock masses. Failure of the intact rock is one of the critical components which define the failure on rock masses in any of these structures. The highest excavated slopes are typically those in large open pit mines in which pit depths are currently limited to about 1000 m which means that the vertical gravitational stress is approximately 27 MPa at the base of the pit. Deep level underground mines are currently approaching 4000 m in depth, and this means that vertical gravitational stresses of about 100 MPa need to be considered in relation to intact rock strength.

The intact uniaxial compressive strength of rock ranges from about 25 to 50 MPa for sedimentary rock such as claystone, chalk and siltstone and 200 to 400 MPa for igneous rocks such as basalt, diabase and dolerite. These strengths may increase by factors of 3 to 5 with confinement. Hence, in designing triaxial test equipment for a rock mechanics laboratory to cover the full range of stresses which maybe encountered in mining, axial stresses of up to 1000 MPa and confining pressures of up to 50 MPa are required. For 50 mm diameter core samples, this means that a testing machine or loading frame with a capacity of 250 tons should be considered for a rock mechanics laboratory.

The confining stresses used to establish the strength of intact rock should consider the confining stresses anticipated in the problem being analyzed. For example, in the 1000 m high pit slope wall slope failures are relatively shallow and confining stresses in the failed region are much less than the vertical stress at the bottom of the pit. In an underground mine, confining stresses are increased by the extraction of ore. Because the failure of intact rock discussed in this chapter is analyzed using an empirical criterion, the Hoek-Brown parameters should be determined at confining stresses that are appropriate for the problem being analyzed.

Selection of samples for determining Hoek-Brown criterion for intact rock

Note that this chapter deals with establishing the strength for isotropic homogeneous intact rock specimens only. Laboratory strength results for intact specimens may be significantly affected by the presence of defects such as veins, fractures and inclusions. Such strength results for defected samples when grouped with results from intact rock samples can produce a wide scatter in strength results often resulting in bi-modal strength distributions. Bewick et al (2015) and Bewick et al (2019) provides guidance on grouping the failure mode observed in samples containing defects and separating those groups for analysis. It is essential that results from defected samples are not included when establishing the

Hoek-Brown criterion for isotropic homogeneous intact rock. Figure 1 illustrates the selection of isotropic intact samples from a diamond drill core, chosen to eliminate the impact of defects.

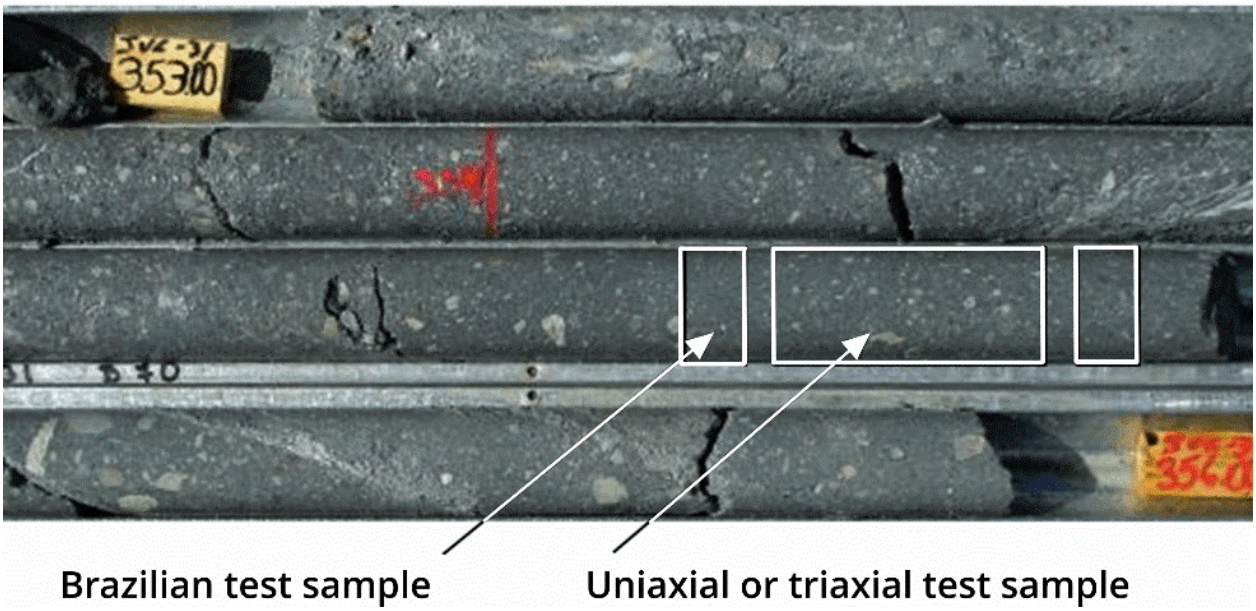

Figure 1: Selection of isotropic intact samples of diamond drill core for testing.

The Hoek-Brown failure criterion

Hoek and Brown (1980) describe the development of the Hoek-Brown failure criterion as a trial-and-error process using Griffith (1924) theory as a starting point. They were seeking an empirical relationship that fitted observed failure conditions for brittle rock subjected to compressive stresses, such as the shear failures illustrated in Figure 2. The equation chosen to represent the failure of intact rock was:

$$\sigma_1 = \sigma_3 + \sigma_c \sqrt{m_i \frac{\sigma_3}{\sigma_c} + 1} \qquad (1)$$

where σ_c is the uniaxial compressive strength of the material and m_i is a material constant which defines the brittleness of intact rock.

The general solution for a Mohr envelope was published by Balmer (1952). Hoek et al (2002) published a solution which expresses the normal and shear stresses in terms of the corresponding principal stresses as follows:

$$\sigma = \frac{(\sigma_1+\sigma_3)}{2} - \frac{(\sigma_1-\sigma_3)}{2} \cdot \frac{\partial\sigma_1/\partial\sigma_3-1}{\partial\sigma_1/\partial\sigma_3+1} \quad (2)$$

$$\tau = (\sigma_1 - \sigma_3)\frac{\sqrt{\partial\sigma_1/\partial\sigma_3}}{\partial\sigma_1/\partial\sigma_3+1} \quad (3)$$

$$\frac{\partial\sigma_1}{\partial\sigma_3} = 1 + \frac{m_i\sigma_c}{2\sqrt{m_i\sigma_3/\sigma_c+1}} \quad (4)$$

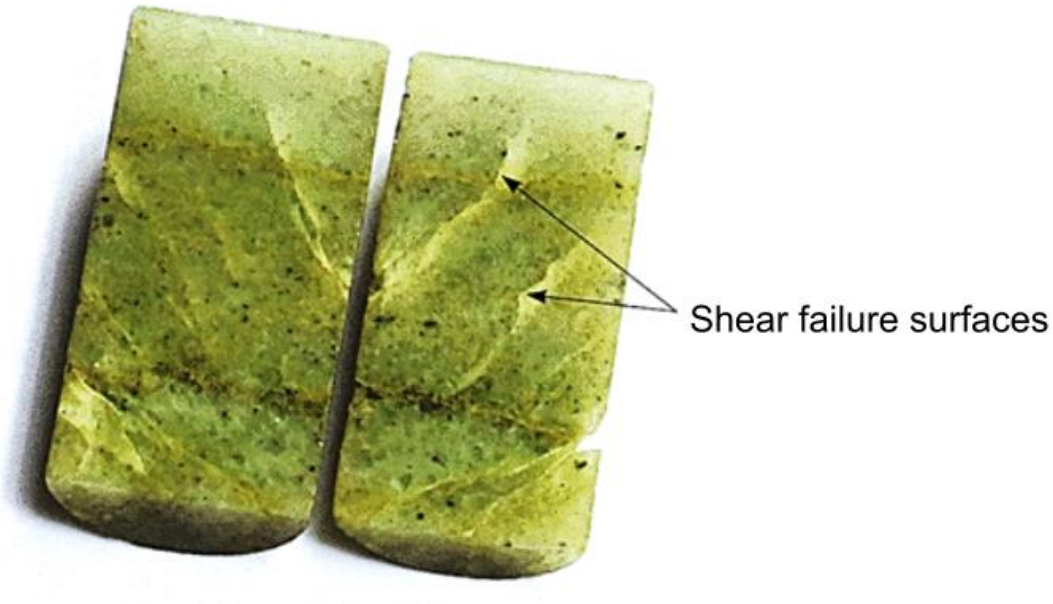

Figure 2: Fine grained granite triaxial test specimen with shear failure surfaces. This specimen was cut into two pieces after removal from a triaxial cell. It had been loaded to about 80% of the failure stresses, so that the shear failures had developed, but the specimen had not failed. Tested by Evert Hoek in 1965.

Figure 3 presents an example of a triaxial test program carried out by Schwartz in 1964 as part of a research effort in the USA to investigate the mechanisms of earthquake generation. High quality testing was carried out at several universities and research institutes and a summary of this work can be found in Judd (1964). It is clear, from Figure 3, that the triaxial test data reported by Schwartz is the result of high-quality testing and the careful selection of the acceptable data points. Only a single point is presented for each confining pressure, including the uniaxial compressive strength, resulting in very simple fitting of the Hoek Brown criterion.

It is also clear, from the data presented by Schwartz, that there is a sharp distinction between the shear failure process, to which the Hoek-Brown criterion applies, and the ductile failure process, which is adequately described by the linear Mohr-Coulomb criterion. The brittle-ductile transition for this data set is defined by $\sigma_1/\sigma_3 = 4.5$, as shown in Figure 3.

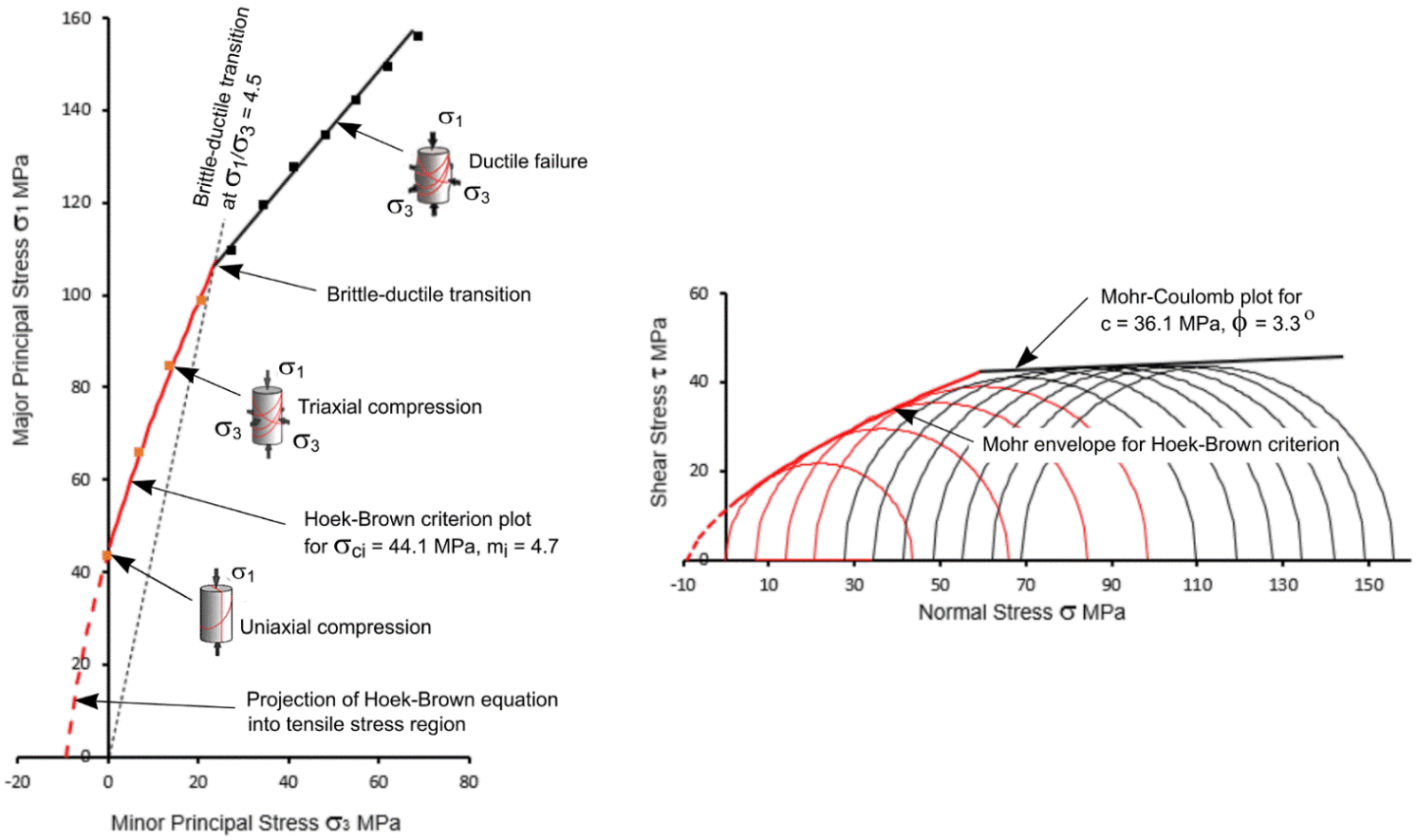

Figure 3: Analysis of triaxial test results on Indiana Limestone by Schwartz (1964). The Hoek-Brown criterion is only applicable to the range, plotted as a red line, between the uniaxial compressive stress ($\sigma_3 = 0$, $\sigma_1 = 43.45$) and the brittle-ductile transition at $\sigma_1/\sigma_3 = 4.5$

One of the main problems with compressive strength testing is the unreliability of the uniaxial test which is carried out with zero applied confining pressure. This occurs at the transition between compressive shear failure and tensile splitting failure of the intact rock. Chakraborty et al (2019) describe the various failure modes that are observed in uniaxial testing, and these are illustrated in Figure 4. The Hoek-Brown criterion is only applicable to shear failure, and it is important, when interpreting the results of triaxial tests, to attempt to remove the results of tests exhibiting other types of failure from the data base.

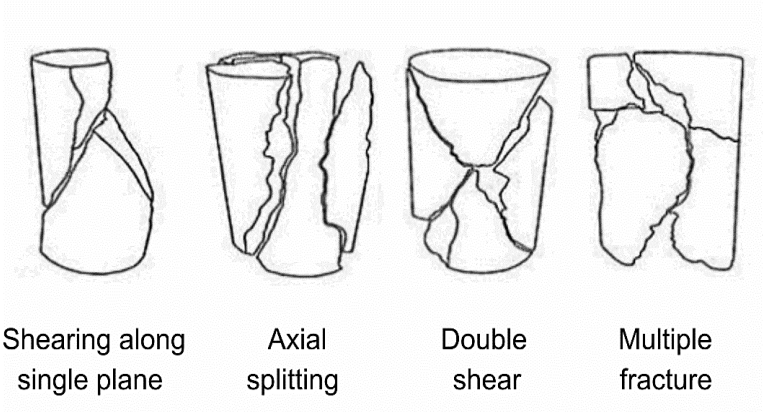

Figure 4: Shear failure, axial splitting and more complex failure modes observed in uniaxial compression testing. Adapted from Chakraborty et al (2019).

Mogi (1966), Byerlee (1968), Scholtz (1968), Evans et al (2013), Hu et al (2018) and many others have all researched the transition from brittle to ductile failure in intact rock and have written about this topic. In general, the transition occurs in the range $3 < \sigma_1/\sigma_3 < 5$ and this range is adequately accurate for most rock engineering design purposes. Where greater precision is required, it is prudent to carry out a test program of the type illustrated in Figure 3.

During the early years in the development of the current triaxial testing methodology, most of the tests were performed by, or under, the supervision of the developers of the equipment as described by Schwartz (1964), Brace (1964), Murrell (1965), and Hoek and Franklin (1968). This meant that the results of non-acceptable failure modes could be deleted based on direct examination of the specimens. In subsequent years, most testing was carried out in commercial laboratories, and it became more difficult to determine and remove those tests which did not exhibit pure shear failure along a single plane. Consequently, it is necessary to establish a methodology to minimize errors resulting from the inclusion of inappropriate data.

A triaxial testing program for intact rock should include a minimum of 3, but preferably 5 triaxial tests, in addition to the uniaxial compressive tests. Ideally, several tests should be carried out at each confining pressure or minor principal stress σ_3 value, as shown in Figure 4. Typically, a greater number of uniaxial test results will be available than the triaxial results and, to carry out a meaningful statistical analysis, a normal distribution curve for each confining pressure should be constructed. The mean and standard deviations of these distribution can then be used as input in the curve fitting process required to determine the uniaxial compressive strength and the value of the Hoek-Brown constant m_i

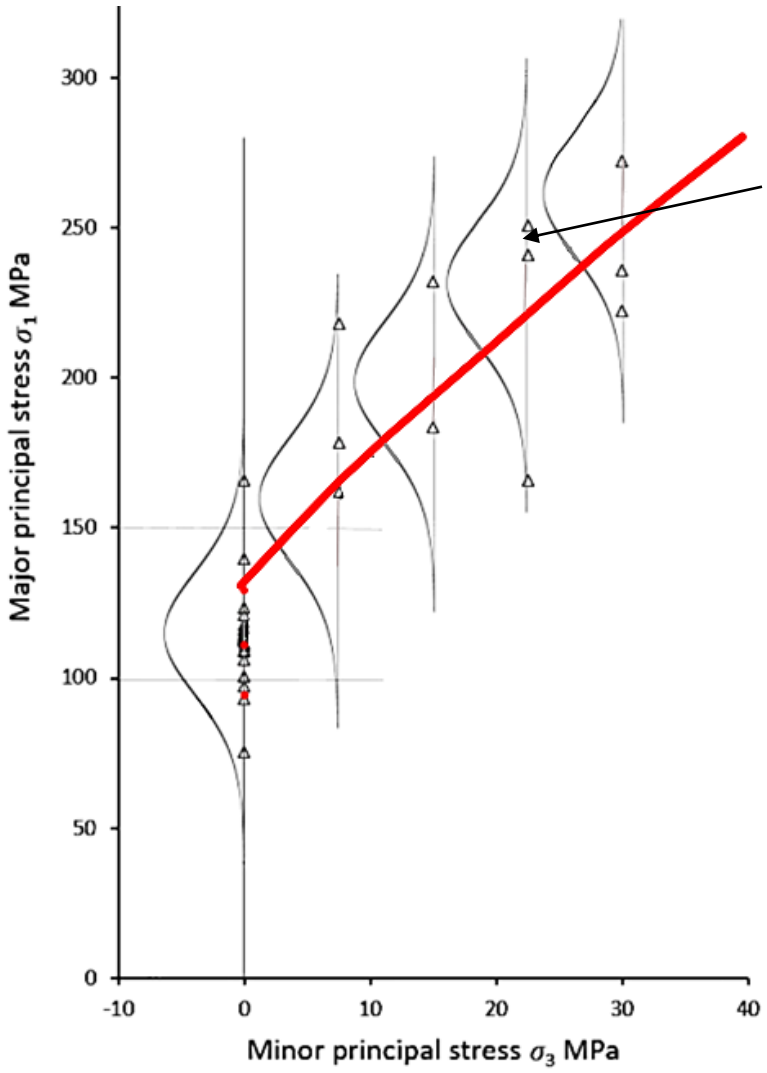

Regression analysis with major principal stresses for each confining pressure defined by a normal distribution. The mean values and standard deviations for each confining pressure are listed below and a regression analysis, gives Hoek-Brown values of σ_{ci} = 130.4 MPa and m_i = 8.1.

σ_3	σ_1
0	115.3
0	116.3
0	117.8
7.5	162.3
7.5	178.5
7.5	218
15	183.6
15	196.8
15	232.1
22.5	165.8
22.5	240.7
22.5	250.9
30	222.3
30	235.7
30	272.4

Figure 4: Analysis of uniaxial and triaxial tests on Coburg Limestone,

Tensile strength of intact rock

Perras and Diederichs (2014) wrote: "Despite the importance of tensile capacity in controlling many failure processes, tensile strength determination is often overlooked in engineering practice due to difficulties with obtaining reliable results". They went on to say: "To date direct tensile testing is regarded as the most valid method for determining the true tensile strength of rock since there are minimal outside influences when the test is completed properly, (Hoek 1964)". Brace (1964) described the best shape for direct tensile specimens to be the "dog bone shape".

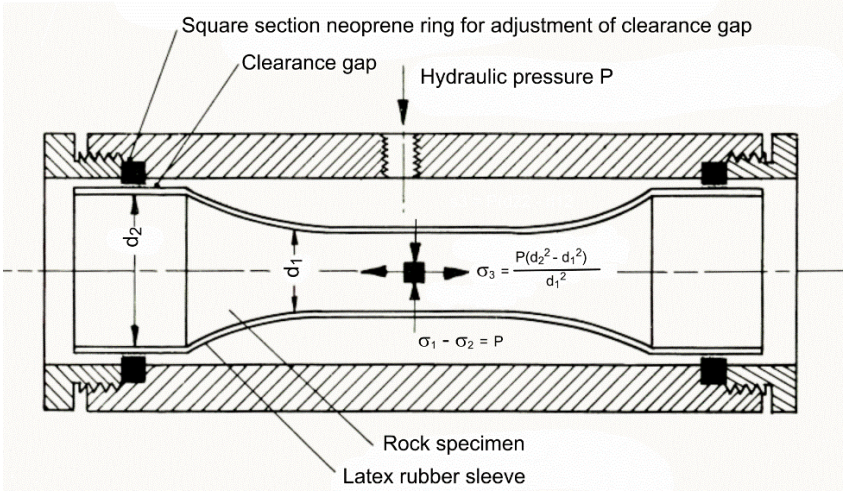

Figure 5: Dogbone specimen used for the determination of the tensile strength of intact rock from Hoek (1965).

Hoek (1965) used the apparatus illustrated in Figure 5 to determine the tensile strength of intact rock. The design of this equipment was based on that used by Brace (1964) in all his triaxial tests on intact rock. The uniformity of the stresses induced in the central section of the dogbone specimen is illustrated in Figure 6 which shows the results of an axisymmetric finite element analysis of the stresses induced by the application of a confining pressure of 10 MPa.

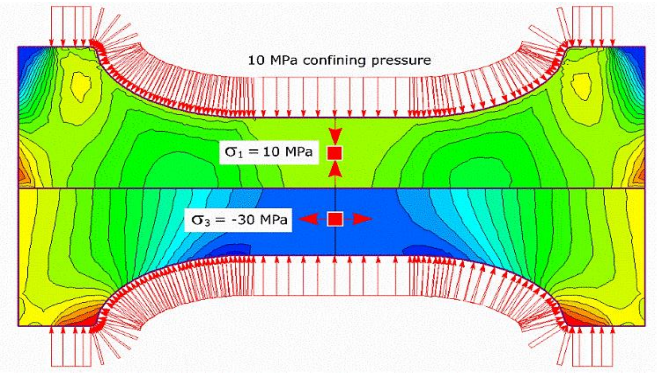

Figure 6: Analysis of stresses induced in the test section of a dog-bone shaped specimen subjected to lateral confining pressure, with no axial load applied. The ends of the specimen illustrated are twice the diameter of the central test section.

Ramsey and Chester (2004) and Bobich (2005) investigated the tensile behaviour of Carrara marble in a series of experiments in which they used dogbone shaped specimens like that shown in Figure 7. The results obtained by Ramsey and Chester are well defined by Fairhurst's generalization of Griffith's theory of brittle failure (Fairhurst, 1964). A detailed plot of Ramsey and Chester's test results is given in Figure 8, together with the values of the stresses measured in their experiments.

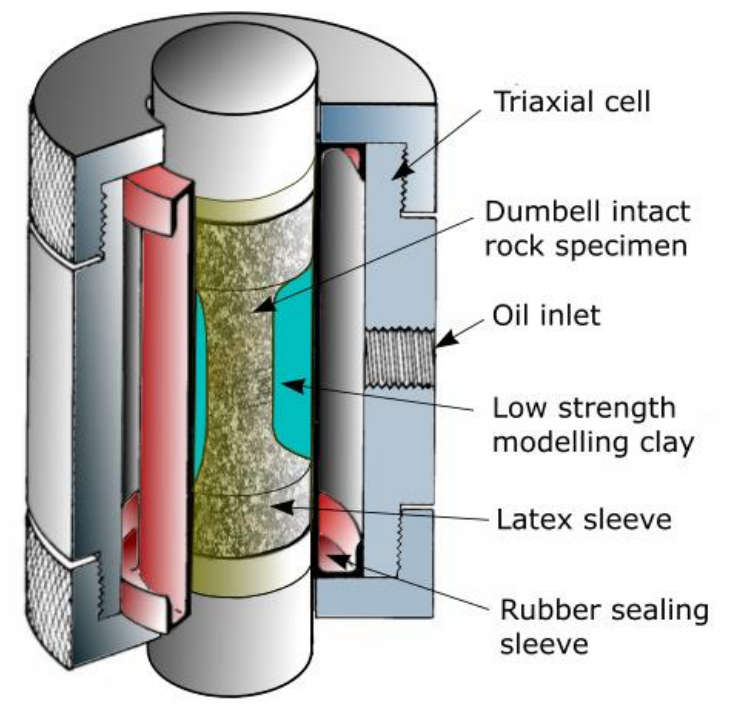

Figure 7: Equipment for confined tensile testing of dog-bone shaped intact rock specimens (based on method used by Ramsey and Chester, 2004). Deformation of the modelling clay, surrounding the reduced section of the specimen, applies a uniform confining pressure. The pressure acting on the enlarged ends induces a tensile stress in the reduced section as shown in Figure 5.

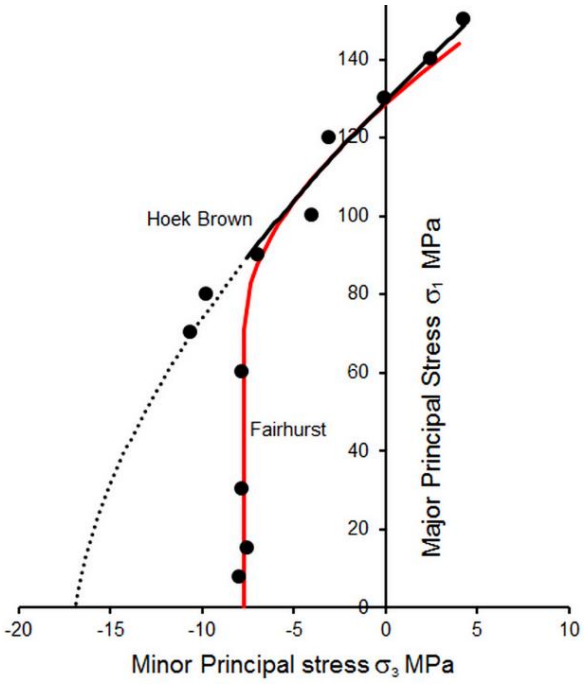

σ_3 MPa	σ_1 MPa	
-7.9	7.5	
-7.5	15.0	TENSILE FAILURE
-7.8	30.0	
-7.8	60.0	
-10.6	70.0	
-9.8	80.0	
-6.9	90.0	TRANSITION FAILURE
-4.0	100.0	
-3.0	120.0	
0.0	130.0	
2.5	140.0	SHEAR FAILURE
4.3	150.0	

Figure 8: Results of confined tensile tests on Carrara marble by Ramsey and Chester (2004) showing both the Hoek-Brown and Generalized Fairhurst Griffith Theory (in red) fitted plots.

Fairhurst's generalization of Griffith's Theory of brittle failure is expressed in terms of the ratio of compressive to tensile strength $\sigma_{ci}/|\sigma_t|$, where σ_{ci} is the unconfined compressive strength determined by regression analysis of triaxial data for $\sigma_3 \geq 0$.

Defining $w = \sqrt{\frac{\sigma_{ci}}{|\sigma_t|} + 1}$, $A = 2(w-1)^2$, $B = \left(\frac{w-1}{2}\right)^2 - 1$

If $\sigma_1/\sigma_3 \leq -w(w-2)$, tensile failure occurs when $\sigma_3 \leq \sigma_t$
If $\sigma_1/\sigma_3 \geq -w(w-2)$, transition between tensile and shear failure occurs when

$$\sigma_1 = \frac{1}{2}\left((2\sigma_3 - A\sigma_t) + \sqrt{(A\sigma_t - 2\sigma_3)^2 - 4(\sigma_3^2 + A\sigma_t\sigma_3 + 2AB\sigma_t^2)}\right) \quad (2)$$

The equivalent relationship for shear and normal stresses is

$$\tau^2 = |\sigma_t|(|\sigma_t| + \sigma_n)(w-1)^2 \quad (3)$$

As shown in Figure 8, only two low confinement triaxial compressive test values are included in the results obtained by Ramsey and Chester. These do not permit an extrapolation of the Hoek-Brown failure curve to higher confinement values as shown in Figure 9. However, by normalizing the results of Ramsey and Chester's tests, as well as triaxial test results on Carrara marble by Franklin and Hoek (1970), it is possible to arrive at the approximate composite curve in Figure 9.

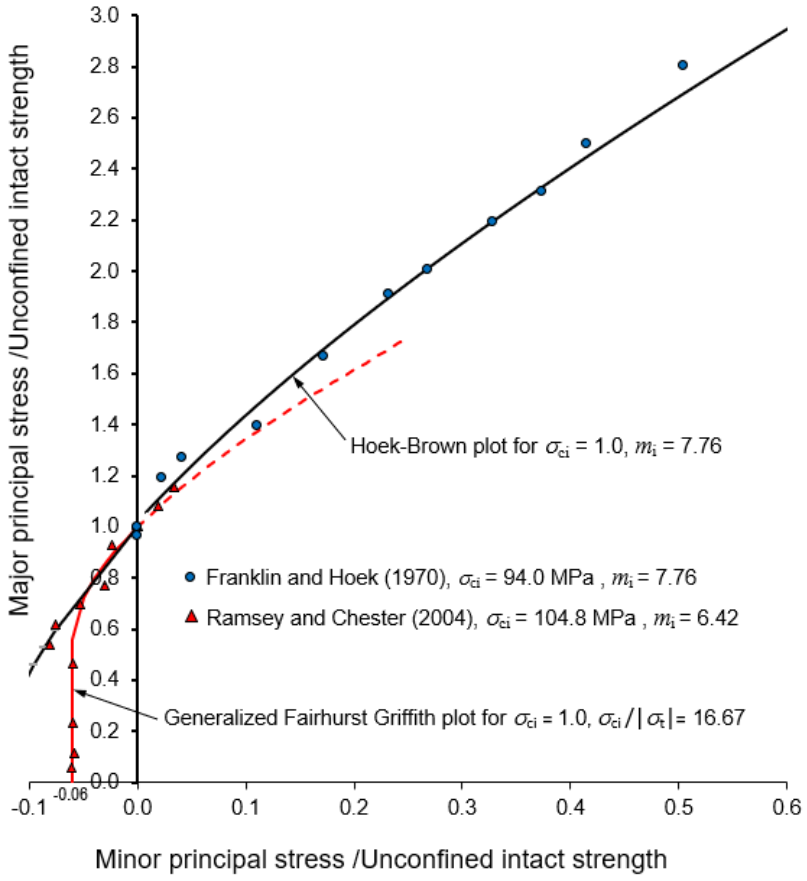

Figure 9: Transition from the Generalized Fairhurst Griffith theory to the Hoek-Brown failure criterion.

To generalize the plot shown in Figure 9, an Excel spreadsheet was prepared[1] in which a Griffith plot, tangential to the Hoek Brown plot for a chosen value of mi, was created. A series of tensile strengths defined by several Griffith plots were then used to plot the mi versus $\sigma_{ci}/|\sigma_t|$ curve presented in Figure 10. Reliable published values of the $\sigma_{ci}/|\sigma_t|$ ratios for a variety of rocks, included in the same plot, confirm the validity of the equation included in Figure 10.

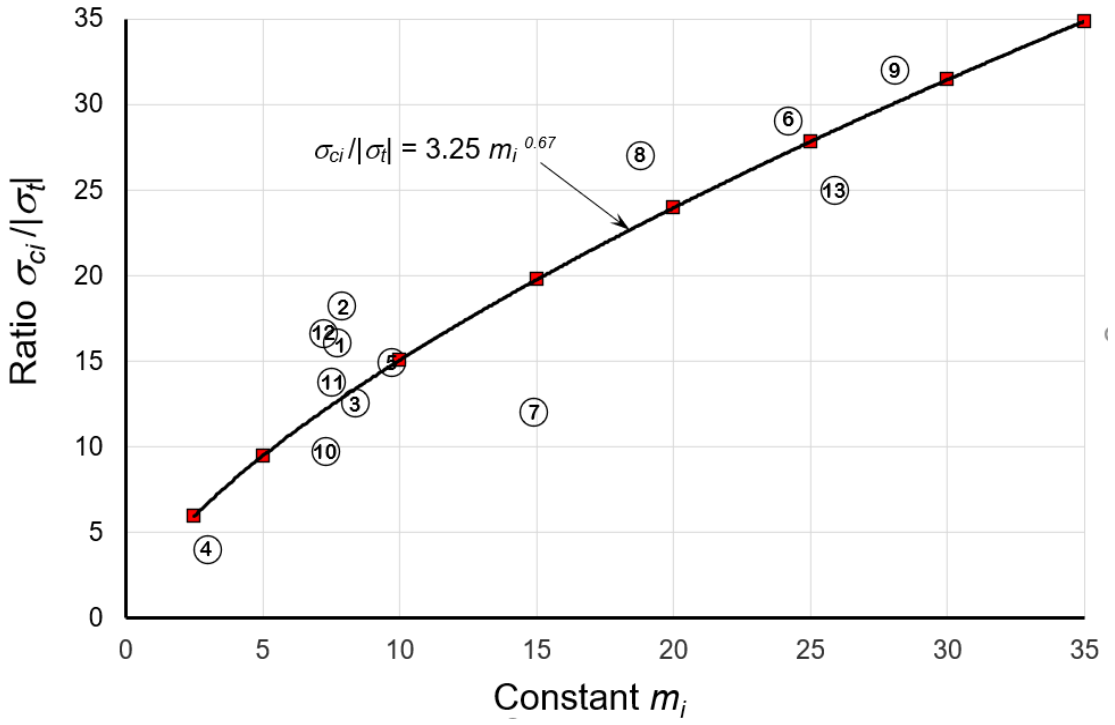

Point	Rock	σci MPa	σt MPa	m_i	σci/|σt|	Reference
1	Gosford Sandstone	72.4	-4.5	7.7	16.1	Brace (1964)
2	Webtuck Dolomite	121.4	-6.64	7.9	18.2	Brace (1964)
3	Blair Dolomite	473.9	-37	8.37	12.54	Brace (1964)
4	Longmaxi Shale	22	-5.5	3	4	Lan et al (2019)
5	Berea Sandstone	102	-6.4	9.7	14.9	Bobich (2005)
7	Witwatersrand Quartzite	226.6	-18.6	14.9	12	Hoek (1965)
6	Bowral Trachyte	200	-7.6	24.2	29	Brace (1964)
8	South African Aplite	600.4	-22.2	18.8	27	Hoek (1965)
9	Lac du Bonnet Granite	224	-7	28.1	32	Martin (1997)
10	Westerly Granite	225	-23.2	7.28	9.7	Brace (1963)
11	Marble	111	-8.07	7.5	13.8	Ros and Eichinger (1928)
12	Carrara Marble	104	-7.7	7.2	16.6	Hoek and Martin (2014)
13	Pottsville sandstone	75.1	-3	25.9	25	Schwartz (1964)

Figure 10: Plot illustrating fitted Hoek-Brown plots for triaxial tests for a range of mi values with the tension cut-off as a function of the mi constant.

[1] This analysis was performed by Dr Connor Langford.

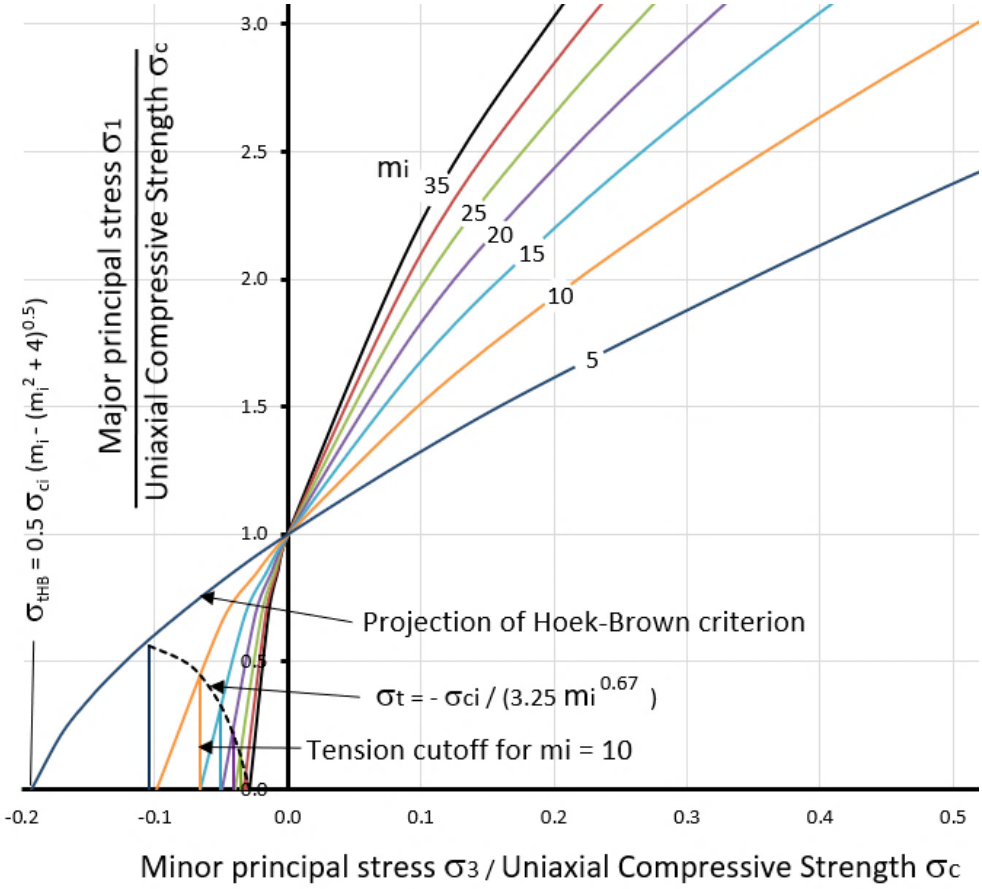

Figure 11: Plot of tension cut-off values for a range of Hoek-Brown curves.

Hoek and Brown (1980) suggested that the tensile strength of intact rock could be estimated from the intercept of the Hoek-Brown curve and the minimum principal stress axis, as shown in Figure 11. This value is defined by the equation:

$$\sigma_{tHB} = 0.5\sigma_{Ci}\left(m_i - \sqrt{m_i^2 + 4}\right) \tag{4}$$

Experimental results, such as those presented in Figures 10 and 11 show that this suggestion was incorrect and that the actual tensile strength σ_t can be calculated more realistically from the empirical, equation numbered, 5, shown below and included in Figures 10 and 11:

$$\sigma_t = -\sigma_{ci} / (0.325\, m_i{}^{0.67}) \tag{5}$$

Equation 5 was derived from a curve fitting analysis of the data on 13 rock types, listed in Figure 10. These results are considered to be the most reliable currently available and it is probable that, as more results of this type become available, the constants in Equation 5 and, perhaps, the form of the equation itself will change. Hence, this equation should be regarded as the best interim solution available rather than a final solution.

Brazilian tests for estimating tensile strength

Relatively few laboratories have access to the full range of equipment required to determine the tensile strength of intact rock dogbone specimens, as described in Figures 5 and 7. Consequently, estimates are frequently made by using a test known as the Brazilian test, in which a disc of intact rock is loaded across its diameter, as shown in Figures11.

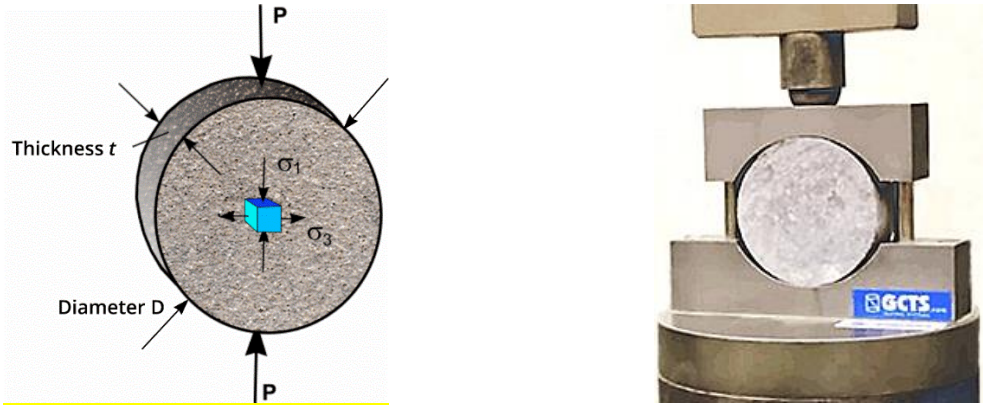

Figure 11: A Brazilian tensile test in which a disc of intact rock, cut from a diamond drilled core, is subjected to a load P across its diameter. As shown on the left, the disc has a diameter D, a thickness *t*, typically one-half the diameter. The Brazilian tensile strength (BTS) is calculated from equation 6, presented below. The photograph on the right illustrates a Brazilian test setup in the University of Alberta, Civil and Environmental Engineering, School of Mining and Petroleum Engineering.

$$\sigma_t = -2P/\pi Dt \qquad (6)$$

The tensile strength σ_t is estimated from Equation 6 when the applied load P is high enough to induce tensile splitting along the vertical diameter. Perras and Diederichs (2014) show, in Figure 12, that estimates of the ratio of direct tensile tests (DTS) to Brazilian tensile test (BTS) estimates are widely distributed.

Differences between tests on metamorphic, sedimentary, and igneous rocks overlap to the extent that they are not particularly useful in providing clear and reliable guidelines on DTS/BTS values for each of the three categories.

However, Perras and Diederichs suggest that DTS/BTS ratios of 0.86, 0.82 and 0.70 for metamorphic, sedimentary, and igneous rocks provide approximate estimates of the DTS from BTS test results. Figure 13 shows an alternative interpretation, provided by Carter (2021), in which the ratio of DTS/BTS is plotted against the Hoek-Brown constant m_i, giving a similar wide scatter or results but indicating a trend for less variation for rocks with high m_i values.

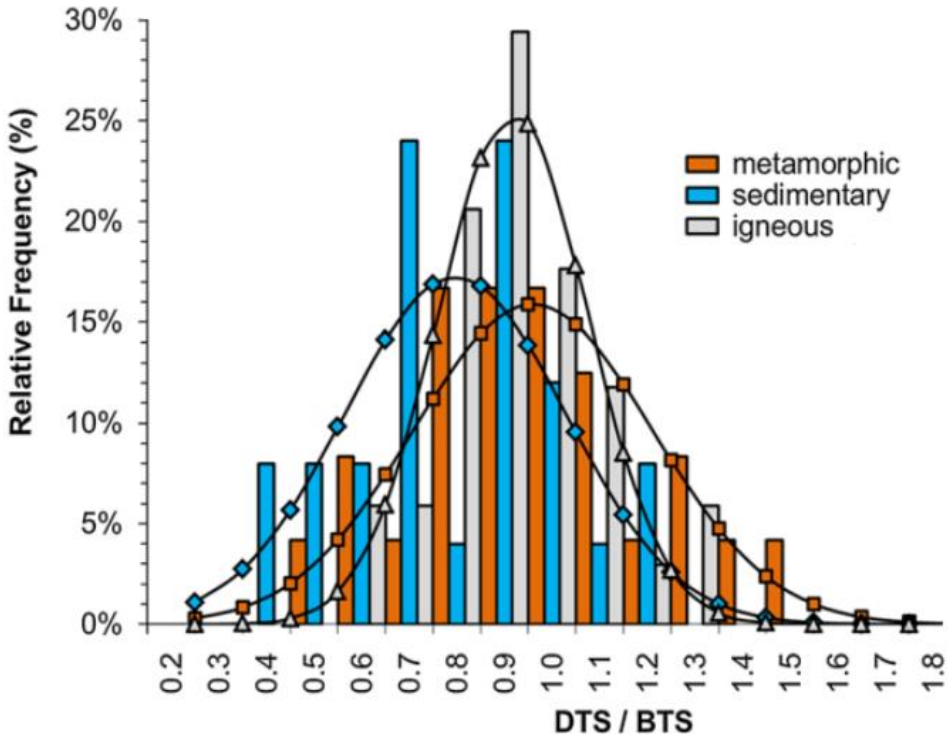

Figure 12: Histogram of the ratio between DTS and BTS for the main rock types.

Brittle shear and tensile failure predicted by the Hoek-Brown criterion

For application in the analysis of practical rock engineering problems, such as tensile failure and spalling in tunnels, it is necessary to simplify the Hoek-Brown failure criterion to the maximum extent possible. Maintaining the accuracy and reliability of the criterion is essential in this simplification process. Figure 14 presents such a simplification in which the Hoek-Brown criterion for brittle shear failure is combined with the criterion for tensile failure, summarized in Equation 5 and Figures 9 and 10.

Throughout this chapter it has been emphasized that the Hoek-Brown criterion is only valid for the brittle shear failure of rock, as shown in Figures 2. However, Figure 8 shows that a backward projection of the curve generated by Equation 1 is very close to the curve generated by the Fairhurst generalized Griffith plot (Equation 2) for the region between the uniaxial compressive strength and the tensile cutoff, defined by Equation 5. Consequently, in developing the simplified plot presented in Figure 14, it has been assumed that an acceptably small error will be generated by the backward projection of the Hoek-Brown curve to link the uniaxial compressive strength to the tensile cutoff, defined by Equation 5.

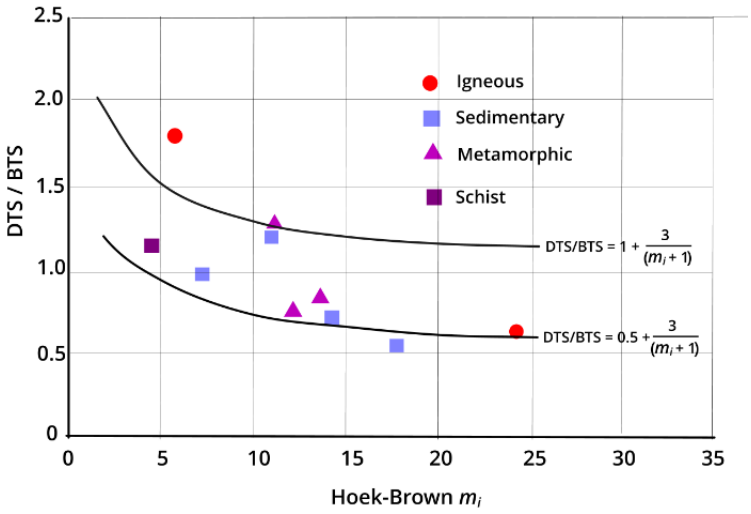

Figure 13: Ratio of DTS/BTS for different m_i values. After Carter (2021).

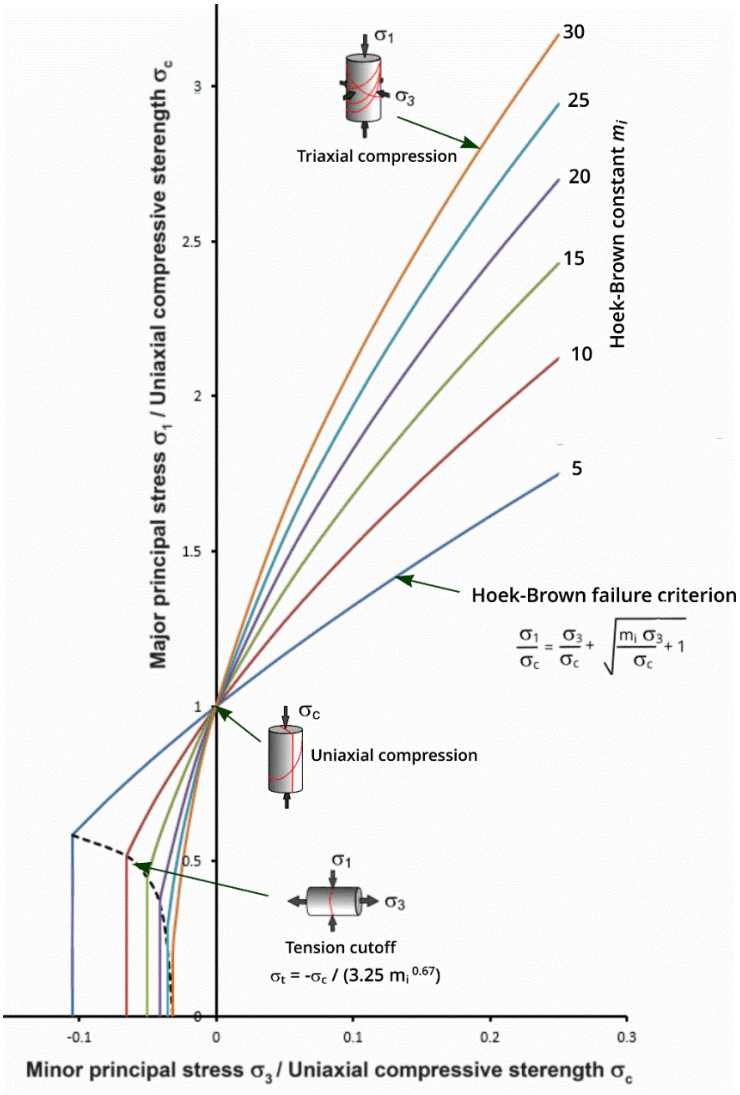

Figure 14: Dimensionless Hoek-Brown criterion plot, with tension cut-off.

Variability of Strength, Stiffness and Hoek-Brown m_i with rock type composition

In the preceding sections variability in intact strength over the range from tensile through shear to ductile failure in compression have been examined. An additional useful measure for characterizing rock types is stiffness, defined in this context by intact Young's Modulus, E_i, the measured tangent to the slope of the stress-strain curve at 50% strain to failure. However, natural rock types are seldom uniform and homogeneous and wide ranges in measured values of these key governing parameters will be determined if a comprehensive laboratory testing program is undertaken. As an example, Figure 15 shows the distribution curves obtained from high quality uniaxial compressive tests on intact samples from the rock mass in which the tunnels and caverns were excavated for the Ingula Pumped Storage Project in South Africa.

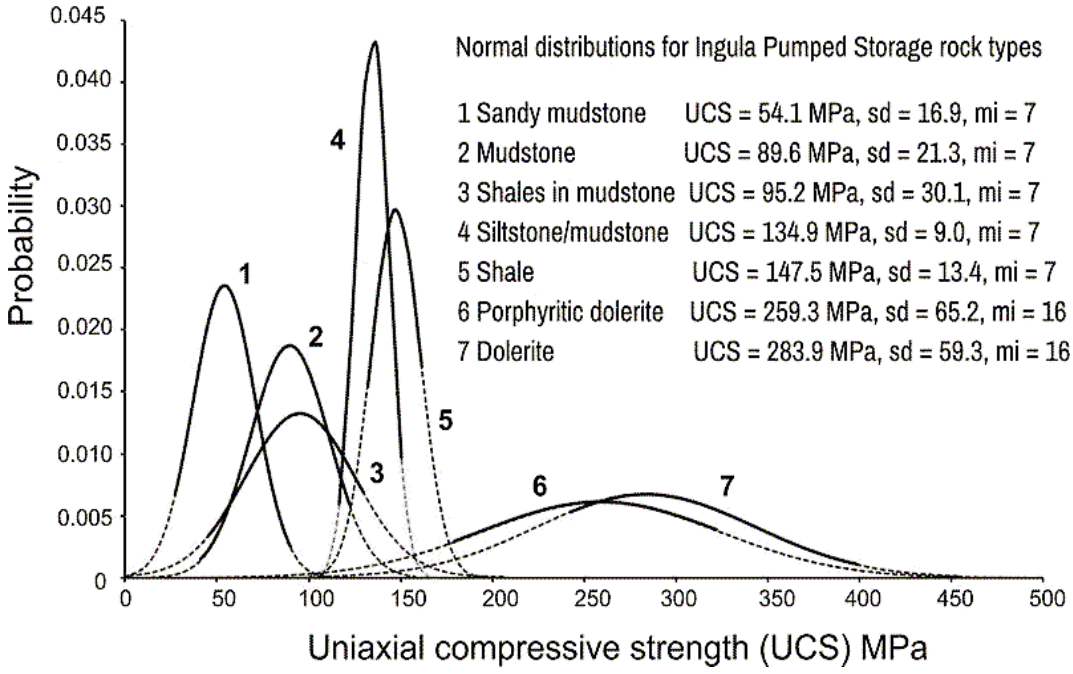

Figure 15: Results of uniaxial compressive strength tests on 7 rock types from the site of the Ingula Pumped Storage Project in South Africa, carried out in the laboratory of the rock mechanics division of the Council for Scientific and Industrial Research. Keyter et al. (2008).

Figure 16 defines each of the 42 rocktypes, derived from Hoek (1999) and Hoek and Diederichs (2006), providing typical ranges the intact modulus E_i, the uniaxial compressive strength σ_{ci} and the Hoek-Brown constant m_i. The rocktypes are subdivided not just by their igneous, sedimentary, or metamorphic origins, but also with respect to their typical texture, or range of textures. This is an important point to note, as both compositional variability as well as origin and geological age control rocktype competence and, hence, all key geo-mechanical parameters.

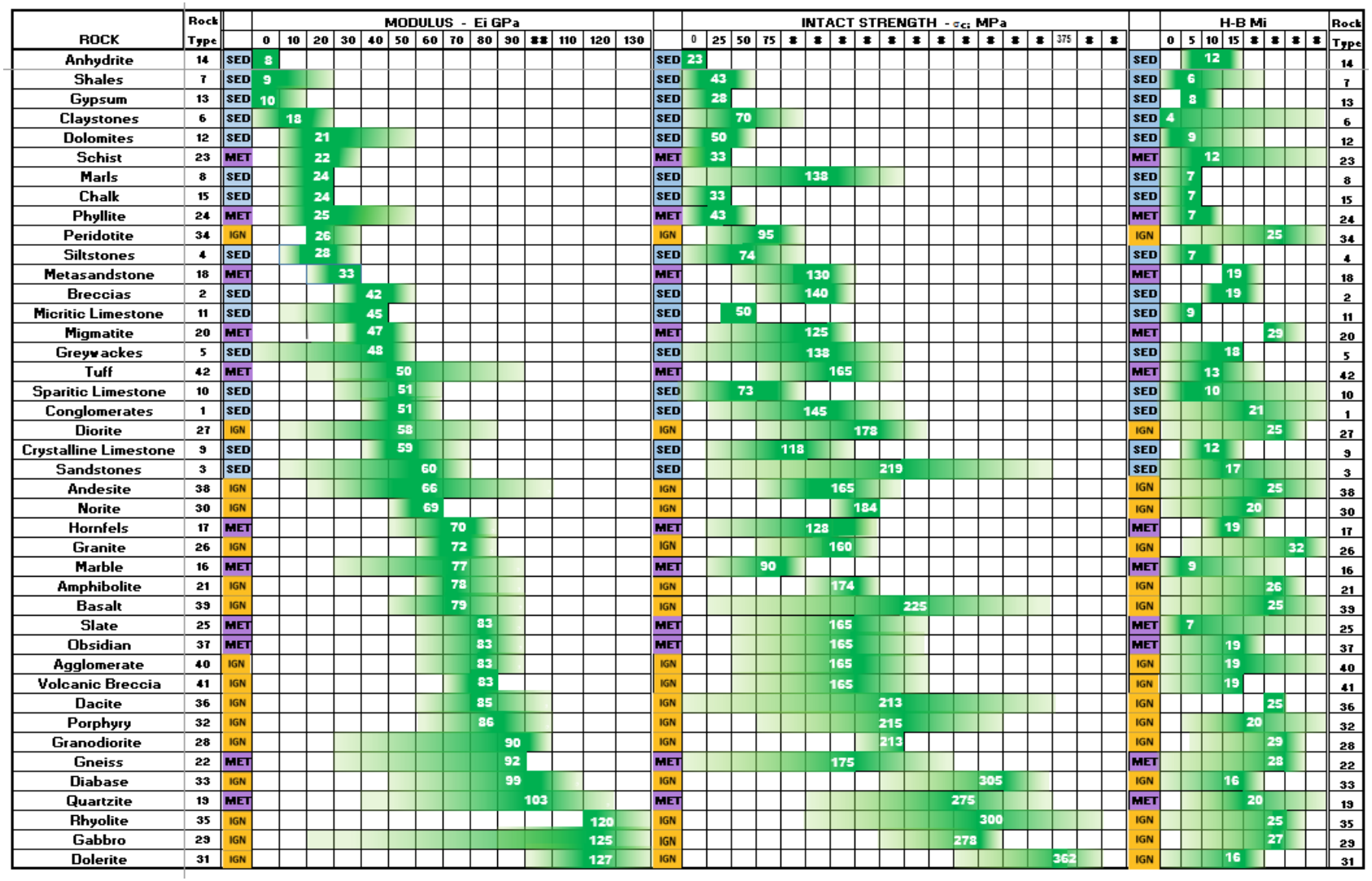

Figure 16: Average values of intact rock modulus Ei, uniaxial compressive strength σci and Hoek-Brown constant mi for various rock types, sorted in terms of increasing rock stiffness. Plot updated from Carter and Marinos, 2020.

Plotting m_i values versus strength σ_{ci} or plotting m_i values versus modulus ratio E_i/σ_{ci} yields plots that show little correlation with rocktype characteristics or mode of origin, as discussed in detail in Carter and Marinos, 2020. The most promising inter-relationships are seen when the 42 rocktypes are sorted by modulus E_i rather than either of the other key parameters, σ_{ci} and m_i, as shown in Figure 16. It is also clear that ranking the rock types by modulus, rather than strength or m_i, sorts the rock types appropriately by origin – the sedimentary rocks almost all showing low stiffness as compared with the igneous rocks at the other end of the stiffness scale, with the metamorphic rocks quite logically distributed right across the spectrum.

Figure 16 is a particularly useful tool during early design stages on a project, when the potential location of a foundation, slope, tunnel, or large underground excavation is being considered, before any detailed core drilling or field mapping has been carried out.

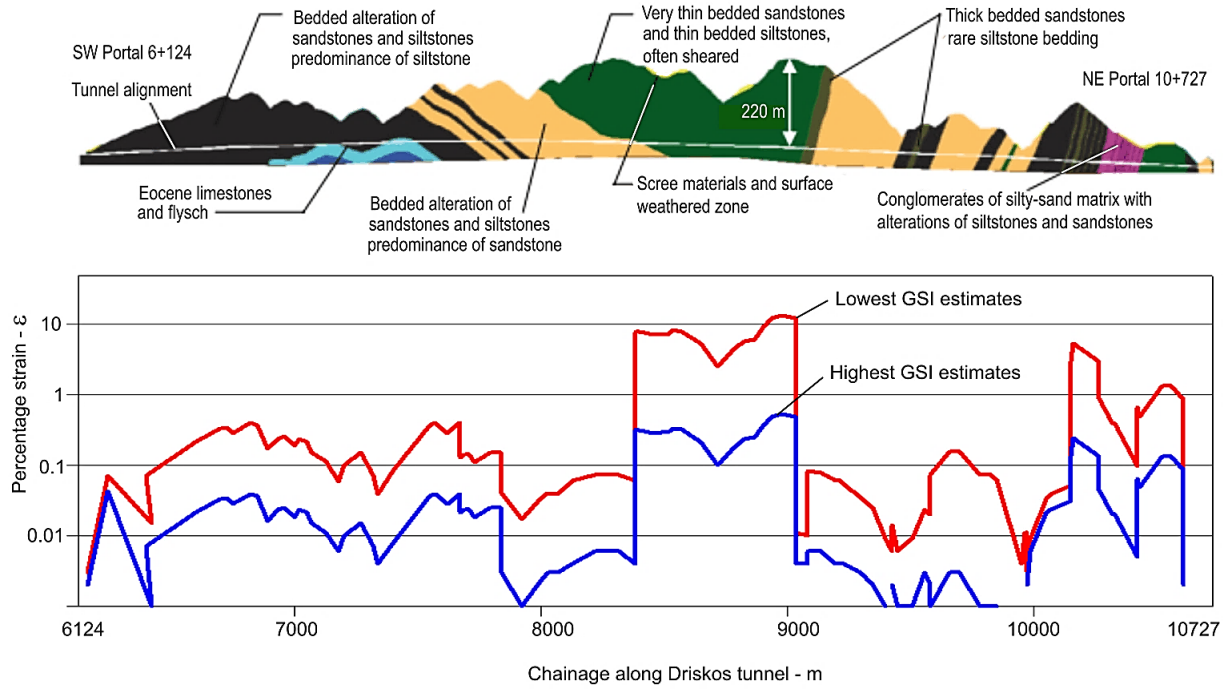

Figure 17: Prediction of potential deformations in the Driskos Tunnel on the Egnatia Highway in Northern Greece. (Percentage strain = (tunnel closure/tunnel diameter) x 100)).

Figure 17 shows the preliminary analysis carried out on the Driskos Tunnel in the Egnatia Highway in Greece. Based on a vey general description of the geology of the potential site, approximate values for the Deformation Modulus, the Uniaxial Compressive Strength, and the Hoek-Brown constant m_i were estimated. Together with the Geological Strength Index (GSI), described in the chapter on rock mass properties, an approximate analysis of the stability and deformation characteristics of the tunnel was carried out. This indicated percentage strains (ratio of tunnel closure to tunnel diameter) of up to 10% in sandstones and siltstones, at a depth of 220 m, in the central portion of the tunnel. Such strains were encountered, during the construction of the tunnel, and these were controlled by the placement of tensioned and grouted multi-strand steel cables before the installation of the final concrete lining.

Acknowledgements

Dr Connor Langford has contributed to the analyses presented in Figures 9 and 11 and Dr Trevor Carter and Dr Vasillis Marinos have contributed to the rock type classifications, plotted in Figures 1 and 16. The assistance of these friends is gratefully acknowledged.

APPENDIX 1: Definition of Sedimentary, Igneous and Metamorphic Rocks

Sedimentary rocks can be considered as being of two types, clastic and non-clastic, as defined in Table 1. The clastic sedimentary rocks typically consist of mineral grains that can vary in size from clays to boulders and at each grain size can also vary significantly in angularity from rounded (sometimes with a high degree of sphericity) to blocky and angular with little rounding, all dependent on degree of comminution involved in their deposition. Like soils, grain size is the predominant divider of rock names within the clastic suite, (ref Table 1, which lists 8 naming divisions, with calcareous mudstone (marl) units included in this suite, although some would argue they should be in the non-clastic grouping). In clastic rocks, individual grains are not always interlocking; rather, mostly they are bonded together by some form of inter-granular matrix cement. Bedding, lamination, and other sedimentation structures in these rocks may create significant anisotropy, with interbedded sequences of alternating argillaceous and arenaceous rocks being the most strongly anisotropic. Some of the more argillaceous rocks, commonly called mudrocks, are susceptible to slaking and in some cases swelling. This group of rocks creates many problems and challenges in rock construction. The non-clastic sedimentary rocks by contrast are formed by various types of chemical precipitation processes that can create rocks that vary in composition from cemented aggregates of bio-organism skeletal fabrics through to almost amorphous crystalline or cryptocrystalline rocks that have interlocked crystal assemblages, similar in many ways to igneous rock crystal geometries. Table 1 gives a guide to further subdivisions of these non-clastic rock types.

Igneous rocks are of two quite different types – *intrusive* – meaning they were injected into the overlying rock units, but formed at depth, only being exposed near surface long after they had solidified; and *extrusive/pyroclastic* – meaning they became exposed on the surface of the earth during their original formation – either as flowing lavas or as ash or other hot ejectamenta derived from a volcanic eruption. Table 1 further divides the intrusive rocks into plutonic and hyperbyssal – reflecting depth of original formation. Both types of rock units tend to be massive and strong with individual crystals essentially welded together as part of their original formation. However, geologists further divide the *intrusive* rocks depending on the mineralogical mix of the original magma, identifying plutonic rocks as either light or dark coloured, but with a typical range of crystal sizes dependent again on the parent mineralogy and the original cooling history. Table 1 outlines the broad subdivisions, with hypabyssal rocks typically always dark.

Mostly, these rocktypes, irrespective of grain size, show complex interlock between crystals, resulting in minor directional differences in mechanical properties. Therefore, good quality aggregates can usually be made from many of these rocktypes and rock engineering construction problems related to *intrusive* rocks in their intact state tend to be minor.

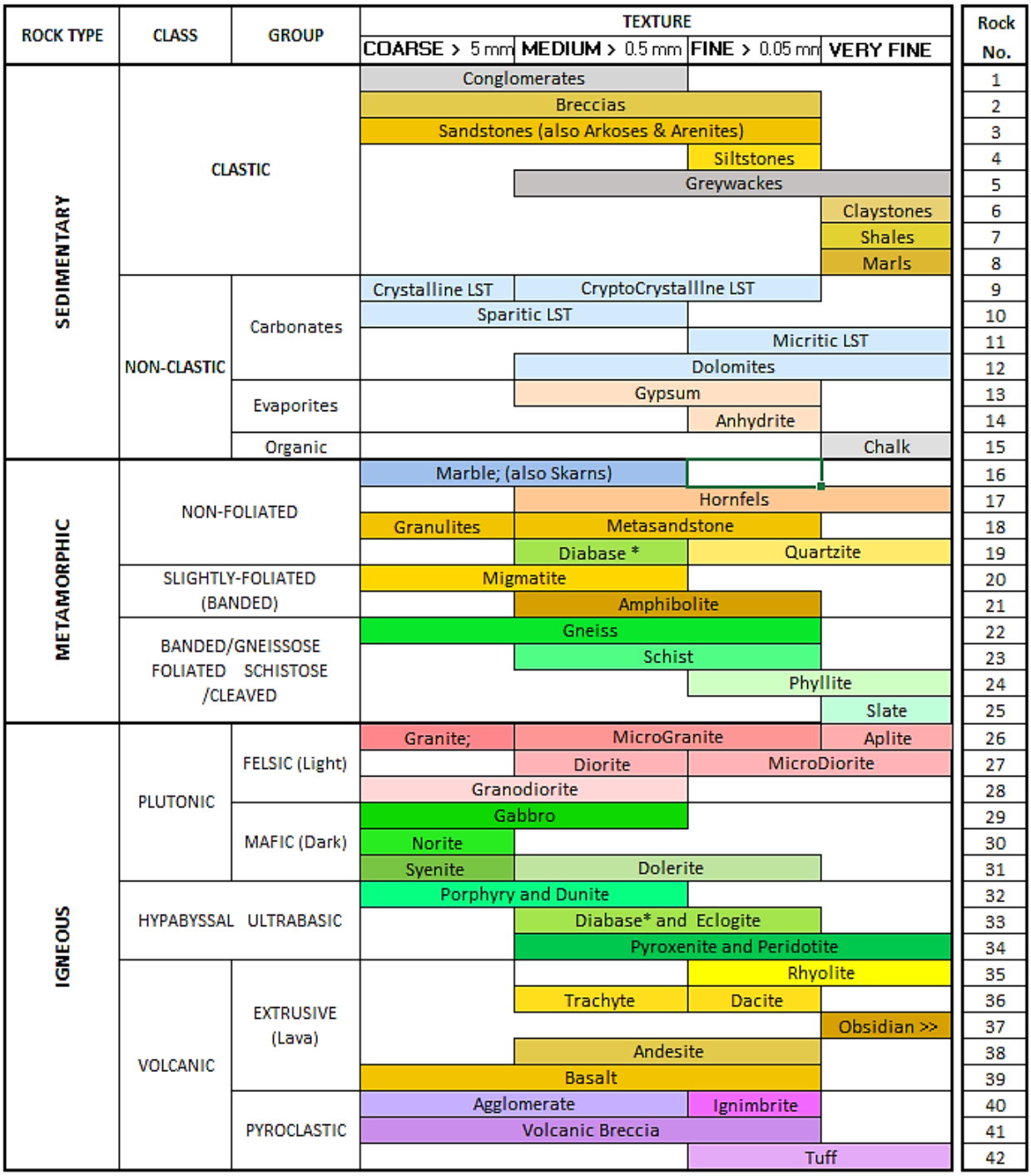

*Diabase = Dolerite per N.American nomenclature; = Metamorphosed Dolerite (European nomenclature)

Table 1: Textural and origin-based classification of common rock types (Plot courtesy of Dr. Trevor Carter, 2021).

Geologically young (eg. Tertiary to Cretaceous < 100my) *extrusive* igneous rocks, by contrast, can be extremely problematic, as almost all, including even the most competent units may contain deleterious mineralogy, which, with weathering, can break down sometimes to swelling clays. The most problematic young extrusive rocks are the gassy lavas – mainly these occur just amongst the andesites, while almost all the pyroclastics can be troublesome, especially the tuffaceous (ash, scoria, etc.) rock units, except sometimes when welded. The volcaniclastic group of rocks are amongst the most problematic of all. These rock types, which originated as pyroclastic origin deposits that ended up falling into water and then being deposited as sediments, under the same processes as the sedimentary rocks, can look like sedimentary rock and exhibit all the same characteristics, but contain deleterious mineralogy and, hence, exhibit inferior engineering properties compared with their normal pure sedimentary counterparts. Great care must therefore be taken when constructing in, or on, any of these types of volcanic rock units. Such construction difficulties may not be such a problem in geologically much older rocks of the same names – such as might occur in the Cambrian or Archean, 600-6000 million years as with induration and even light metamorphism many of these problematic characters become much less prevalent or may even be completely absent.

Metamorphic rocks are so named because they have been changed from their original character by pressure or temperature, or both. This results in many different fabrics, which is what geologists typically use as the primary descriptor when naming a metamorphic rock. The second descriptor is mineralogy, as certain suites of minerals are only found in certain specific pressure and temperature ranges. The full suite of metamorphic rock types listed in Table 1 can be found in areas of *Regional Metamorphism* but may not always be present when dealing with areas of *Contact Metamorphism* (such as may occur around an igneous intrusion, or an ore emplacement zone, due to baking of the country rock), as quite commonly seen around many deposits being exploited by both surface and underground mining. Both processes can create a wide range of different metamorphic rock fabrics depending on the original starting rocktype. It is surprising how many of the world's rocks are metamorphosed to some degree. Layered gneisses and schists of various geological ages, right back to the Archean are extremely common worldwide, as they generally represent the metamorphosed equivalents of original arenaceous and argillaceous clastic sedimentary rock units. Shales, (ie., fissile mudstones), which are also common worldwide, are typically grouped in with the sedimentary rock units (ref. Table 1), but really should be included as metamorphic rocks as they are essentially the product of very low-grade pressure (consolidation) metamorphism. By contrast hornfels and granulite metamorphic rocks, which are less widespread can be quite amorphous and exhibit quite good engineering properties compared with the more foliated metamorphic rock types, notably the schists. Taken overall, metamorphic rocks can show as wide as, or wider, range in structure and composition and properties as the sedimentary rocks. Some of the highest-grade metamorphic processes result in near melting and annealing occurring, thus generating rocks of high competence and high intact rock strength, devoid of any of anisotropy common amongst all the other metamorphic rocks of lower grade. At lower grades preferred orientation of platy (sheet) minerals results in considerable directional differences in mechanical properties. Micaceous and chloritic schists are amongst the most anisotropic from the viewpoint of strength and stiffness contrasts, while slates are not mineralogically as variable as schists, yet exhibit an extreme fabric anisotropy created by pressure induced cleavage throughout the rock.

APPENDIX 2: Diamond core sampling, storage, and preparation

Figure A1 illustrates a compact drill rig, suitable for use on surface and in relatively small sized tunnels. There are many variations of this type of drill and, with correct set up and operating procedures, they produce high quality core which is suitable for testing to determine the strength and deformation properties of the intact rock.

Typically, the core size chosen for geotechnical testing is 47.6 mm in diameter and is designated as NQ core. However, a wide range of core sizes is available to researchers with other requirements. In general, it is advisable to consult a geotechnical engineer or specialist contractor on setting up a site investigation program since costly mistakes can occur if such a program is not well planned and executed.

Once the core has been recovered, geotechnical logging and storage of the core are critical requirements. Figure A2 shows a series of cores recovered from an exploration site for a large open pit copper mine on a site with no surface exposure of the potential orebody. Hence, all information on both the mineral content and the geotechnical properties of the orebody, and the surrounding rock, had to be determined from the core.

Figure A1: A compact diamond drill rig that can be used for drilling from surface or in a tunnel.

Figure A2: Diamond drilled core, for both mineral exploration and geotechnical properties, laid out for logging.

Figure A3: A storage facility for diamond drilled core for geotechnical investigations.

A very well-designed storage facility for diamond drilled core is illustrated in Figure A3. The core is stored in closed core boxes which, in turn, are stored on numbered shelves in the storage sheds. Hence, the core is protected from exposure and yet, is easy to access when required for inspection.

In contrast, inappropriate core storage is illustrated in Figures A4 and A5. Given the high cost of the diamond drilling process and the potential loss of valuable information, treatment of core in this manner is unacceptable.

Figure A4: Inappropriate core storage in a tropical environment.

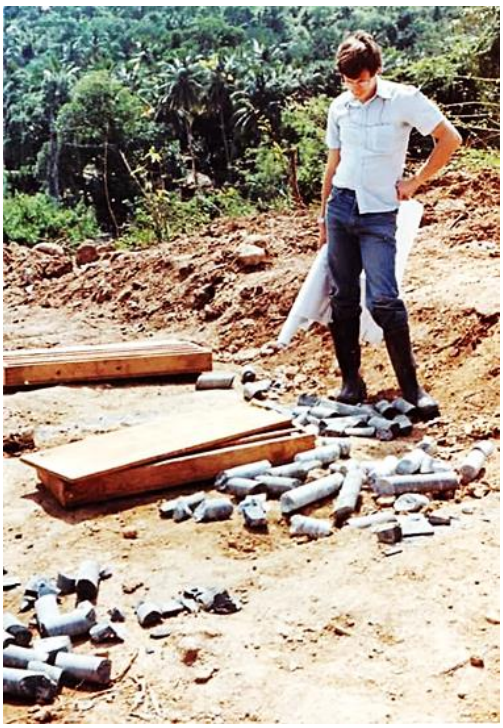

Figure A5: Security is essential to prevent tampering and vandalism of core storage facilities.

In some situations, such as that illustrated in Figure A6, unusual steps may have to be taken to recover reliable geotechnical information. In this case, the site investigations were being carried out for the design of a large underground cavern in a hydro-electric project. The rock mass in which the cavern was excavated consisted of a sedimentary series of inter-bedded sandstone, siltstone, and shale. As shown on the right of the photograph, the siltstone and shale deteriorated quickly due to changes in moisture content when it was removed from its in situ environment. This required that geotechnical testing of the core had to be carried out as soon as possible after drilling, preferably on site. It also necessitated a change in the basic design of the cavern support system in that shotcrete had to be applied to exposed rock surfaces, as soon as possible after excavation, to prevent deterioration and loss of strength of the rock forming the cavern walls.

Figure A6: Diamond drilled core samples through a sedimentary sequence consisting of inter-bedded sandstone, siltstone and shale. Freshly drilled core is shown on the left while, on the right, is core that has been stored in a core shed for six months. Deterioration of the mudstone and shale in the centre of the core box is due to changes in moisture content.

The next stage in the geotechnical investigation process is to prepare the core specimens for testing to determine the strength and deformation characteristics of the intact rock. This involves cutting specimens from the core and preparing these specimens for loading in the equipment to be described in the following pages. Typically, the length of each specimen should be a minimum of twice its diameter. The American Institute of Mining, Metallurgical, and Petroleum Engineers and the International Society for Rock Mechanics and Rock Engineering recommend a length to diameter ratio of 2.5 to 3 for the testing of core samples. Both ends of the specimen should be perpendicular to the core axis and perfectly flat.

All the steps required for the preparation of the specimens to meet these requirements can be performed using a conventional metal cutting and turning lathe, as illustrated in Figures A7 to A12. The most important addition to the lathe is a toolpost grinder on which a range of diamond-impregnated steel cutting tools can be attached.

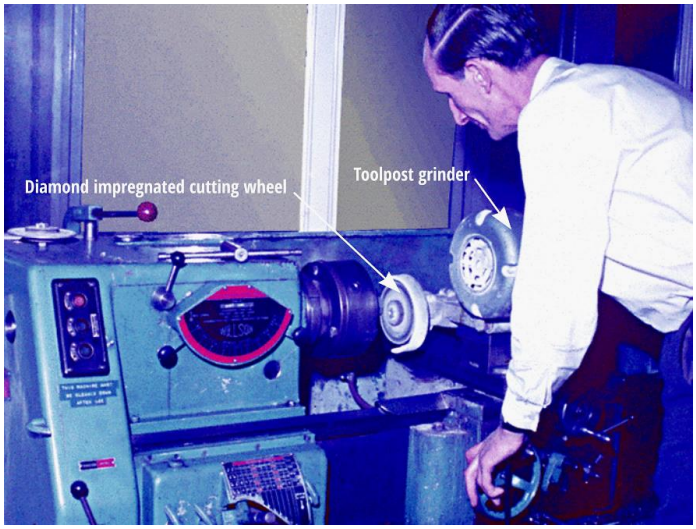

Figure A7: A lathe, equipped with a toolpost grinder mounted on the cross slide, can be used to perform all the preparations required for testing diamond drilled core samples of intact rock.

Figure A8: Cutting through a core specimen using a diamond impregnated steel cutting disc, mounted on a toolpost grinder as shown in Figure 7. Water can generally be used for cooling but, for sensitive soft rock, air should be used.

Figure A9: Cutting the dimple off the end of a core specimen by running the diamond impregnated cutting blade across the centre of the core.

Figure A10: Where necessary, the final trimming of the ends of the core specimen can be done by running the diamond impregnated surface of a cup-shaped grinding wheel across the centre of the specimen.

Figure A11: Rock core end flatness tester.

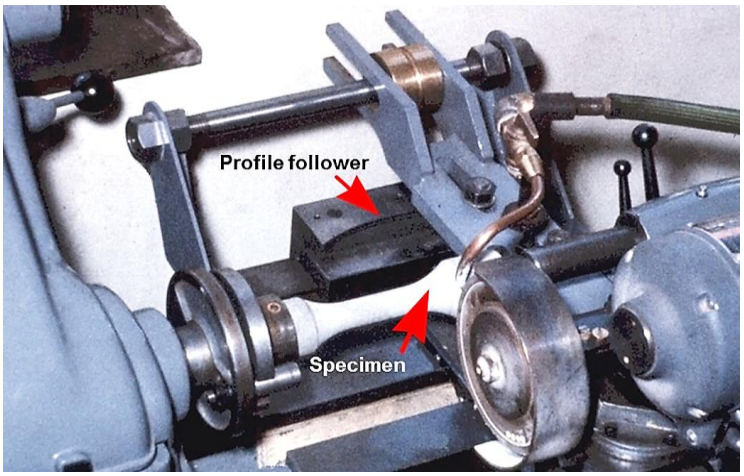

Figure A12: Preparation of a dog-bone shaped specimen for confined tensile testing can be done by using a profile follower which guides the diamond blade mounted on a toolpost grinder to form the required shape.

In addition to the preparation of cylindrical core specimens with flat ends, as described above, the lathe can also be used to machine dog-bone or dumb-bell shaped specimens such as that illustrated in Figure A12. In this case, one end of the diamond drilled core is mounted in the lathe chuck while the other end is held in a cup which rotates in a roller bearing attached to the tailstock of the lathe. The toolpost grinder is guided to cut the recessed shape in the core by a profile follower such as that illustrated in Figure A12. Specimens of this shape are used for confined tensile testing, as described in a section of this chapter.

Triaxial testing of intact rock specimens

Triaxial compression testing of the flat ended core specimens, prepared as described above, can be carried out in a triaxial cell such as that illustrated in Figure A13. Details of the design and construction for this cell can be found in papers by Hoek and Franklin (1968) and Franklin and Hoek (1970). Testing machines used to apply the axial loads to the specimens range from relatively simple equipment, such as that illustrated in Figure A14, to more sophisticated equipment such as that shown in Figures A15 and A16. Careful preparation of the specimens and the testing procedures can ensure that the results obtained using any of the equipment illustrated will meet the highest standards required for practical applications in rock engineering.

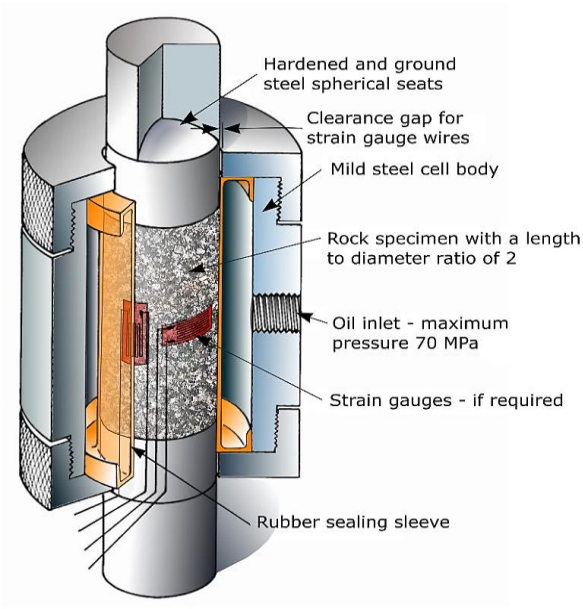

Figure A13: Cut-away view of a triaxial cell for subjecting laterally confined specimens to axial loading.

Figure A14: A small field laboratory on a large open pit mine project. High quality uniaxial and triaxial testing can be carried out in such a laboratory.

Figure A15: Controls Group semi-automatic equipment for uniaxial and triaxial testing of rock specimens with limited data acquisition capability.

Figure A16: Controls Group equipment for triaxial testing of rock specimens with full data acquisition capability.

References

Arshadnejad, S. 2018. Determination of "*mi*" in the Hoek-Brown failure criterion of rock. *Mining Science*. 25, 111-17.

Balmer, G. 1952. A general analytic solution for Mohr's envelope. Paper POR1952-5. *ASTM Proceedings* 1952, 52. 1260-1271.

Bewick, R. P., Amann, F., Kaiser, P. K., & Martin, C. D. (2015). Interpretation of UCS Test Results for Engineering Design. Proceedings 13th International Congress of Rock Mechanics - ISRM Congress 2015, Montreal, pp 1-14.

Bewick, R. P., Kaiser, P. K., & Amann, F. (2019). Strength of massive to moderately jointed hard rock masses. Journal of Rock Mechanics and Geotechnical Engineering, 11, 562-575.

Bobich, J.K. 2005. Experimental analysis of the extension to shear fracture transition in Berea sandstone. *MS thesis*. Texas A & M University.

Brace, W.F., 1964. Brittle fracture of rocks. *In State of Stress in the Earth's Crust*. W.R. Judd (ed.), New York: Elsevier, 111-174.

Byerlee, J.D., 1968. Brittle-Ductile transition in rocks. *Journal of Geophysical Research*. 73, 14.

Carter, T.G., and Marinos, V. 2020. Putting geological focus back into rock engineering design. *Rock Mech Rock Eng* Vol. 53(10):4487–4508.

Carter, T.G., 2021. Towards Improved Definition of the Hoek-Brown Constant mi for Numerical Modelling, *Paper RICAB84, Rocscience International Conference 2021*, 20-21.

Carranza-Torres, C.T. and Corkum, B. 2002. Hoek-Brown Failure Criterion— 2002 Edition. *Proceedings of the 5th North American Rock Mechanics Symposium*, Toronto, July 2002, 267-273.

Chakraborty, S., Bisal, R., Palaniappon, S.,K. and Pal, S.K. 2019. Failure modes in rock under uniaxial compression tests: an experimental approach. *Journal of Advances in Geotechnical Engineering*, Vol. 2, No. 3.

Evans, B., Fredrich, J.T. and Wong, T-F. 2013. The Brittle-Ductile Transition in Rocks: Recent Experimental and Theoretical Progress, in *The Brittle-Ductile Transition in Rocks: The Heard Volume*, Editors: A. G. Duba, W. B. Durham , J. W. Handin , H. F. Wang, American Geophysical Union. 1-20.

Fairhurst C. 1964. On the validity of the "Brazilian" test for brittle materials. *International Journal of Rock Mechanics and Mining Sciences.* 4, 535-46.

Franklin, J.A. and Hoek, E. 1970. Developments in triaxial testing equipment. *Rock Mech*. **2**, 223-228.

Griffith, A.A. 1924. The theory of rupture, *Proc. Int. Congr. Appl. Mech*. 56-63.

Hoek, E. 1964. Fracture of anisotropic rock. *Journal of the South African Institute of Mining and Metallurgy* 64, 10, 501-518.

Hoek, E. 1965. Rock fracture under static stress conditions. *CSIR Report MEG. 1965*. p. 383.

Hoek E. & Franklin J.A, 1968. Simple Triaxial Cell for Field or Laboratory Testing of Rock. *Trans. Inst. Min. Metall*. A22-26.

Hoek, E., and Brown, E.T. 1980. *Underground excavations in rock*. London: Instn Min. Metall.

Hoek, E., and Brown, E.T. 1980. Empirical strength criterion for rock masses. *J. Geotech. Engng Div*., ASCE,106 (GT9),1013-1035.

Hoek, E., and Brown, E.T. 2019. The Hoek-Brown failure criterion and GSI – 2018 edition. *Journal of Rock Mechanics and Geotechnical Engineering.* 11, 3, 445-463.

Hoek, E. 1999. Putting numbers to geology – an engineer's point of view. *Quarterly Journal of Engineering Geology*, 32, 1, 1-19.

Hoek, E., Carranza-Torres, C. and Corkum, B. 2002. Hoek-Brown criterion – 2002 edition. In *5th North American Rock Mechanics Symposium.* Toronto, 7-10 July 2002. Eds. R. Hammah et al. 267-73. Toronto, University of Toronto Press.

Hoek, E. and Diederichs, M.S. 2006. Empirical Estimation of Rock Mass Modulus. I*nternational Journal of Rock Mechanics and Mining Sciences*, 43, 203-215.

Hu, K., Zhu, Q.Z, Chen, L, Shao, J.F. and Liu, J. 2018. A micromechanics-based elastoplastic damage model for rocks with a brittle–ductile transition in mechanical response, *Rock Mechanics and Rock Engineering*, 51, 6, 1729–1737.

Keyter, G.J., Ridgeway, M. and Varley, P.M. 2008. Rock Engineering aspects of the Ingula Powerhouse caverns. *Proc. 6th International Symposium on Ground Support in Mining and Civil Engineering Construction.* SAIMM, 309-445.

Judd, W. R. 1964. Proc. Intnl. Conf. on the State of Stress in the Earth's Crust. Santa Monica, ed. W. R. Judd. Elsevier Publishing Co., New York, 1964.

Mogi, K., 1966. Pressure dependence of rock strength and transition from brittle ductile flow, *Bull. Earthquake Res. Inst.* Tokyo Univ. 215-232.

Murrell, SAF, 1965. The effect of triaxial stress systems on the strength of rocks at atmospheric temperatures, *Geophysical Journal International*, 3, 3, 231-281.

Palmström, A., 1995. RMi – a rock mass characterization system for rock engineering purposes. *PhD* thesis, Oslo University, Norway, 400 pages.

Perras, M.A. and Diederichs, M.S. 2014. A Review of the Tensile Strength of Rock. Concepts and Testing, Geotechnical and Geological Engineering. 32(2), 525-546.

Ramsey, J. and Chester, F. 2004. Hybrid fracture and the transition from extension fracture to shear fracture, *Nature, 428*, 63-66.

Scholz, C.H., 1968. Microfracturing and the inelastic deformation of rock in compression, *Journal of Geophysical Research*, 73, 4, 1417–1432.

Schwartz, A. E., 1964. Failure of rock in triaxial shear. *Proc. 6th Rock Mechanics Symposium.* Rolla, Missouri. 109-135.

4. Shear strength of discontinuities

Introduction

All rock masses contain discontinuities such as bedding planes, joints, shear zones and faults. The failure of these rock masses involves failure of both the rock blocks, defined by intersecting discontinuities, and failure of the discontinuities. Failure of the individual intact rock blocks was discussed in the previous chapter on intact rock strength. This chapter is devoted to a discussion on the behaviour of the discontinuities.

Shear strength of planar surfaces

Assume that several samples of a rock are obtained for shear testing. Each sample contains a through-going bedding plane that is cemented; in other words, a tensile force would have to be applied to the two halves of the specimen to separate them. The bedding plane is planar, having no surface irregularities or undulations. As illustrated in Figure 1, in a shear test each specimen is subjected to a stress σ_n normal to the bedding plane and the shear stress τ required to cause a displacement δ.

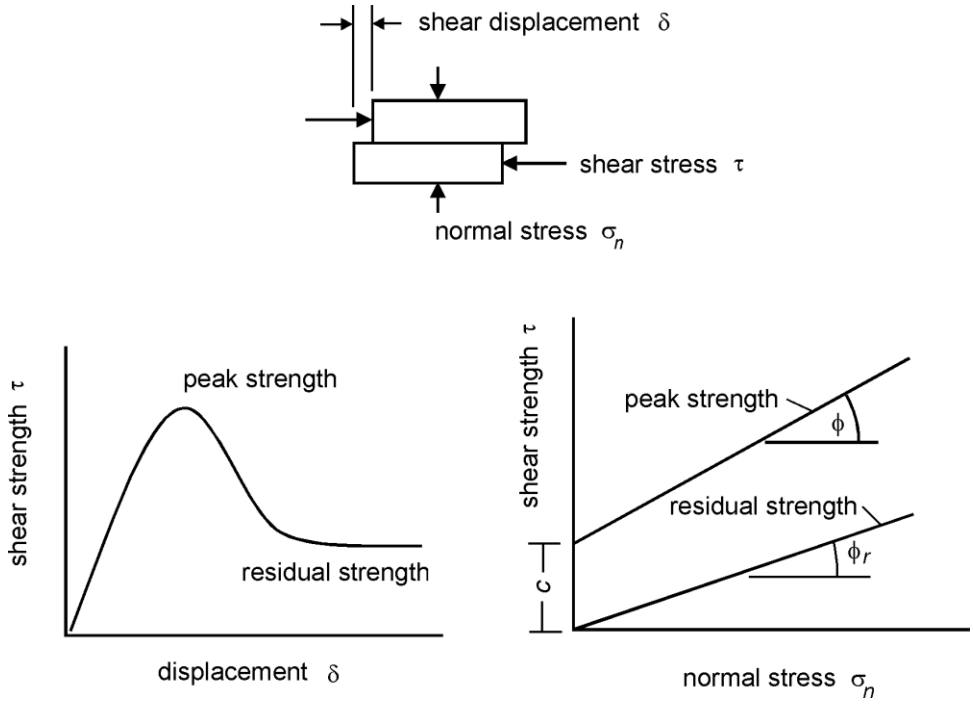

Figure 1: Shear testing of discontinuities.

The shear stress will increase rapidly until the peak strength is reached. This corresponds to the sum of the strength of the cementing material bonding the two halves of the bedding plane together and the frictional resistance of the matching surfaces. As the displacement continues, the shear stress will fall to some residual value that will then remain constant, even for large shear displacements. This residual strength depends on the frictional properties of the discontinuity surface.

Plotting the peak and residual shear strengths for different normal stresses results in the two lines illustrated in Figure 1. For planar discontinuity surfaces the experimental points will generally fall along straight lines. The peak strength line has a slope of ϕ and an intercept of c on the shear strength axis. The residual strength line has a slope of ϕ_r.

The relationship between the peak shear strength τ_p and the normal stress σ_n can be represented by the Mohr-Coulomb equation:

$$\tau_p = c + \sigma_n \tan\phi \qquad (1)$$

where c is the cohesive strength of the cemented surface and
ϕ is the angle of friction.

In the case of the residual strength, the cohesion c has dropped to zero and the relationship between ϕ_r and σ_n can be represented by:

$$\tau_r = \sigma_n \tan\phi_r \qquad (2)$$

where τ_r is the residual shear strength and
ϕ_r is the residual angle of friction.

A typical shear testing machine, which can be used to determine the friction angle ϕ is illustrated in Figures 2 and 3. This is a very simple machine. The use of a mechanical lever arm ensures that the normal load on the specimen remains constant throughout the test. This is an important practical consideration since it is difficult to maintain a constant normal load in hydraulically or pneumatically controlled systems which makes it difficult to interpret test data. Note it is important that, in setting up the specimen, great care must be taken to ensure that the shear surface is aligned accurately to avoid the need for an additional angle correction.

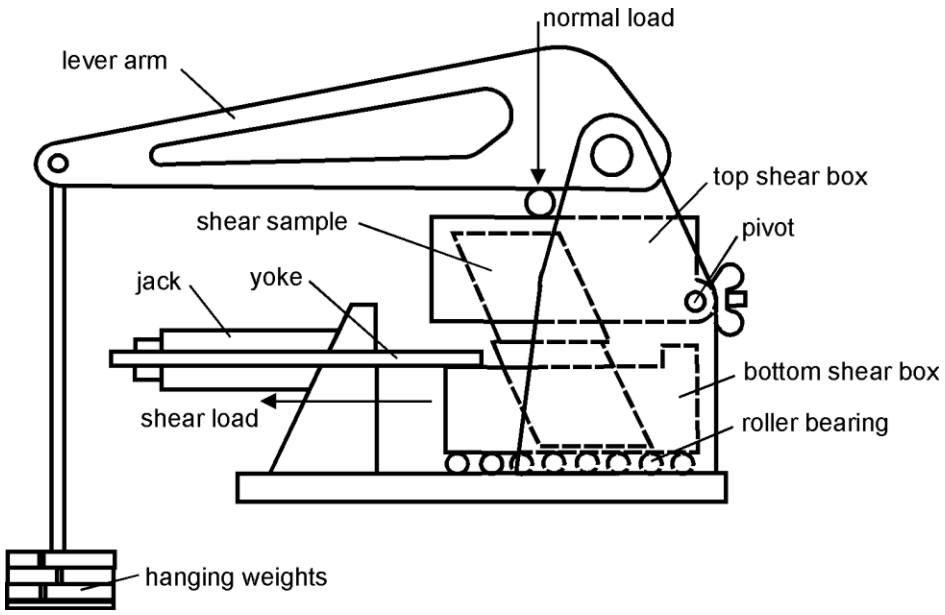

Figure 2: Diagrammatic section through shear machine used by Hencher and Richards (1982).

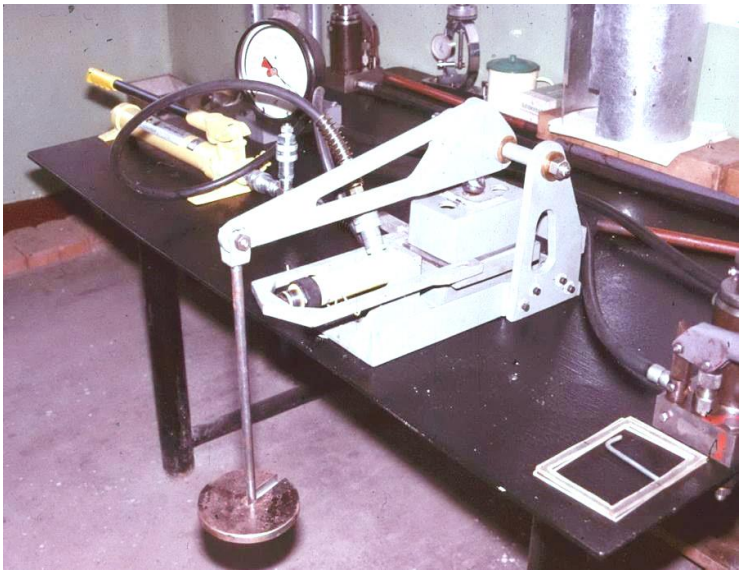

Figure 3: Shear machine of the type used by Hencher and Richards (1982) for measurement of the shear strength of sheet joints in Hong Kong granite.

Most shear strength determinations today are carried out by determining the basic friction angle, as described above, and then making corrections for surface roughness as discussed in the following sections of this chapter. In the past, there was more emphasis on testing full scale discontinuity surfaces, either in the laboratory, or in the field.

There are a significant number of papers in the literature of the 1960s and 1970s describing large and elaborate in situ shear tests, many of which were carried out to determine the shear strength of weak layers in dam foundations. However, the high cost of these tests together with the difficulty of interpreting the results, has resulted in a decline in the use of these large-scale tests. They are seldom seen today.

The author's opinion is that it makes both economical and practical sense to carry out a number of small scale laboratory shear tests, using equipment such as that illustrated in Figures 2 and 3, to determine the basic friction angle. The roughness component, which is then added to this basic friction angle to give the effective friction angle, is a number which is site specific and scale dependent and is best obtained by visual estimates in the field. Practical techniques for making these roughness angle estimates are described below.

Shear strength of rough surfaces

A natural discontinuity surface in hard rock is never as smooth as a sawn or ground surface of the type used for determining the basic friction angle. The undulations and asperities on a natural joint surface have a significant influence on its shear behaviour. Generally, this surface roughness increases the shear strength of the surface. This strength increase is extremely important in terms of the stability of excavations in rock.

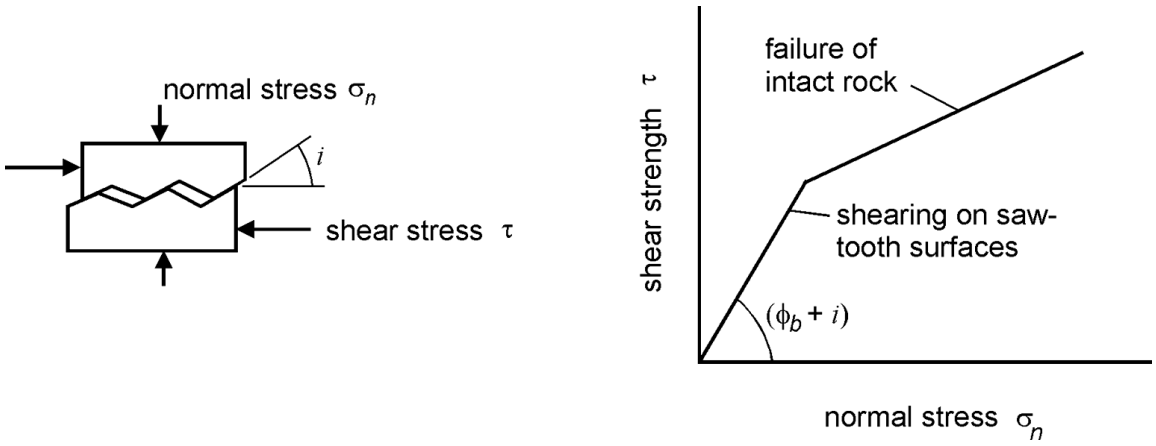

Figure 4: Patton's experiment on the shear strength of saw-tooth specimens.

Patton (1966) demonstrated this influence by means of an experiment in which he carried out shear tests on 'saw-tooth' specimens such as the one illustrated in Figure 4. Shear displacement in these specimens occurs because of the surfaces moving up the inclined faces, causing dilation (an increase in volume) of the specimen.

The shear strength of Patton's saw-tooth specimens can be represented by:

$$\tau = \sigma_n \tan(\phi_b + i) \tag{3}$$

where ϕ_b is the basic friction angle of the surface and
i is the angle of the saw-tooth face.

Equation (3) is valid at low normal stresses where shear displacement is due to sliding along the inclined surfaces. At higher normal stresses, the strength of the intact material will be exceeded, and the teeth will tend to break off, resulting in a shear strength behaviour which is more closely related to the intact material strength.

Barton's estimate of shear strength

While Patton's approach has the merit of being very simple, it does not reflect the reality that changes in shear strength, with increasing normal stress, is gradual rather than abrupt. Barton and Choubey (1977) studied the behaviour of natural rock joints and carried out direct shear test results on 130 samples of variably weathered rock joints. They proposed that equation 3 could be re-written as:

$$\tau = \sigma_n \tan\left(\phi_r + JRC \log_{10}\left(\frac{JCS}{\sigma_n}\right)\right) \tag{4}$$

Where ϕ_r is the residual friction angle
JRC is the joint roughness coefficient and
JCS is the joint wall compressive strength.

Barton and Choubey suggest that the residual friction angle ϕ_r can be estimated from

$$\phi_r = (\phi_b - 20) + 20(r / R) \tag{5}$$

where r is the Schmidt hammer rebound number for wet and weathered fracture surfaces and R is the Schmidt rebound number on dry unweathered sawn surfaces.

Equations 4 and 5 have become part of the Barton-Bandis criterion for rock joint strength and deformability (Barton and Bandis, 1990).

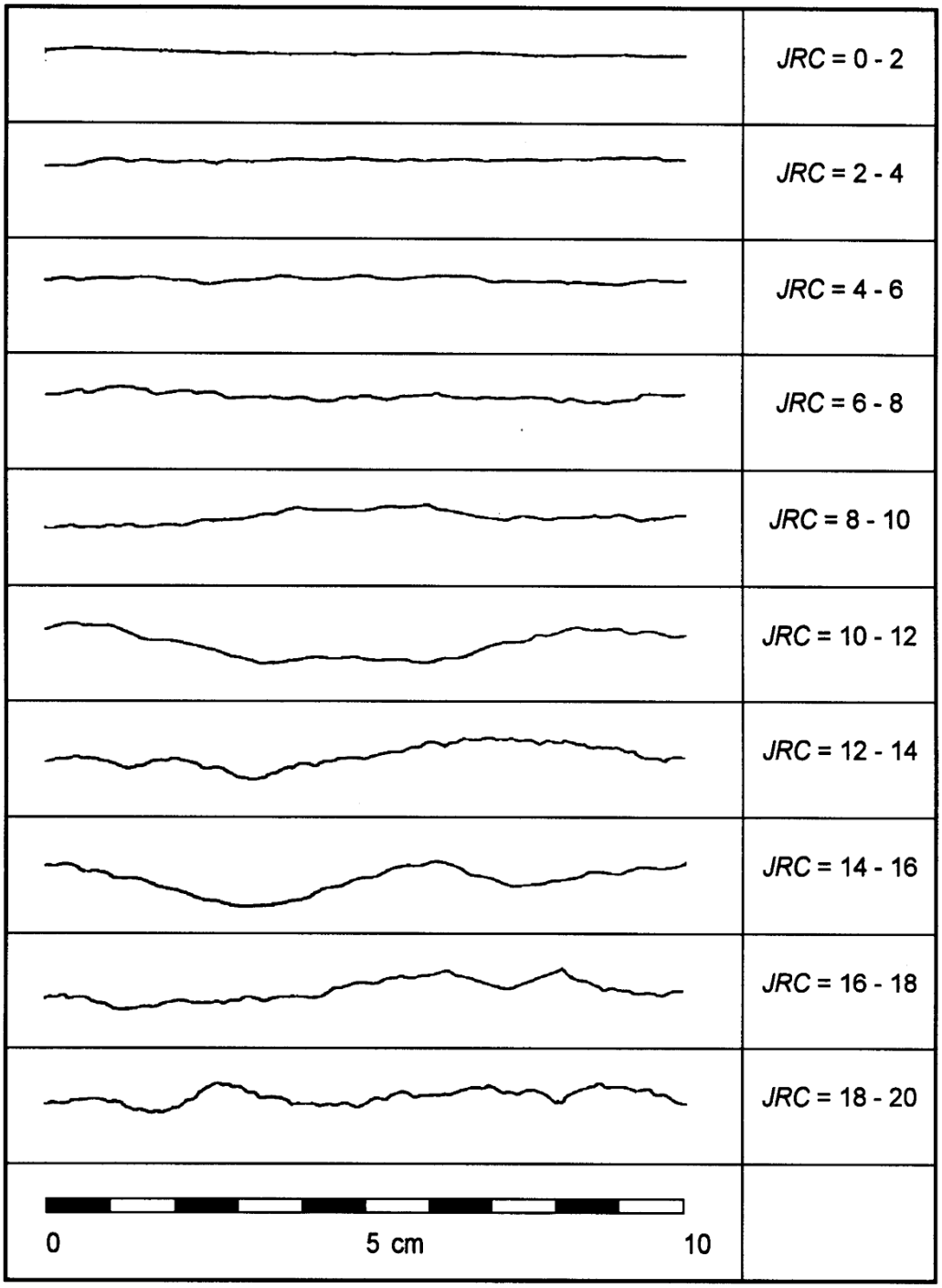

Figure 5: Roughness profiles and corresponding *JRC* values (After Barton and Choubey, 1977).

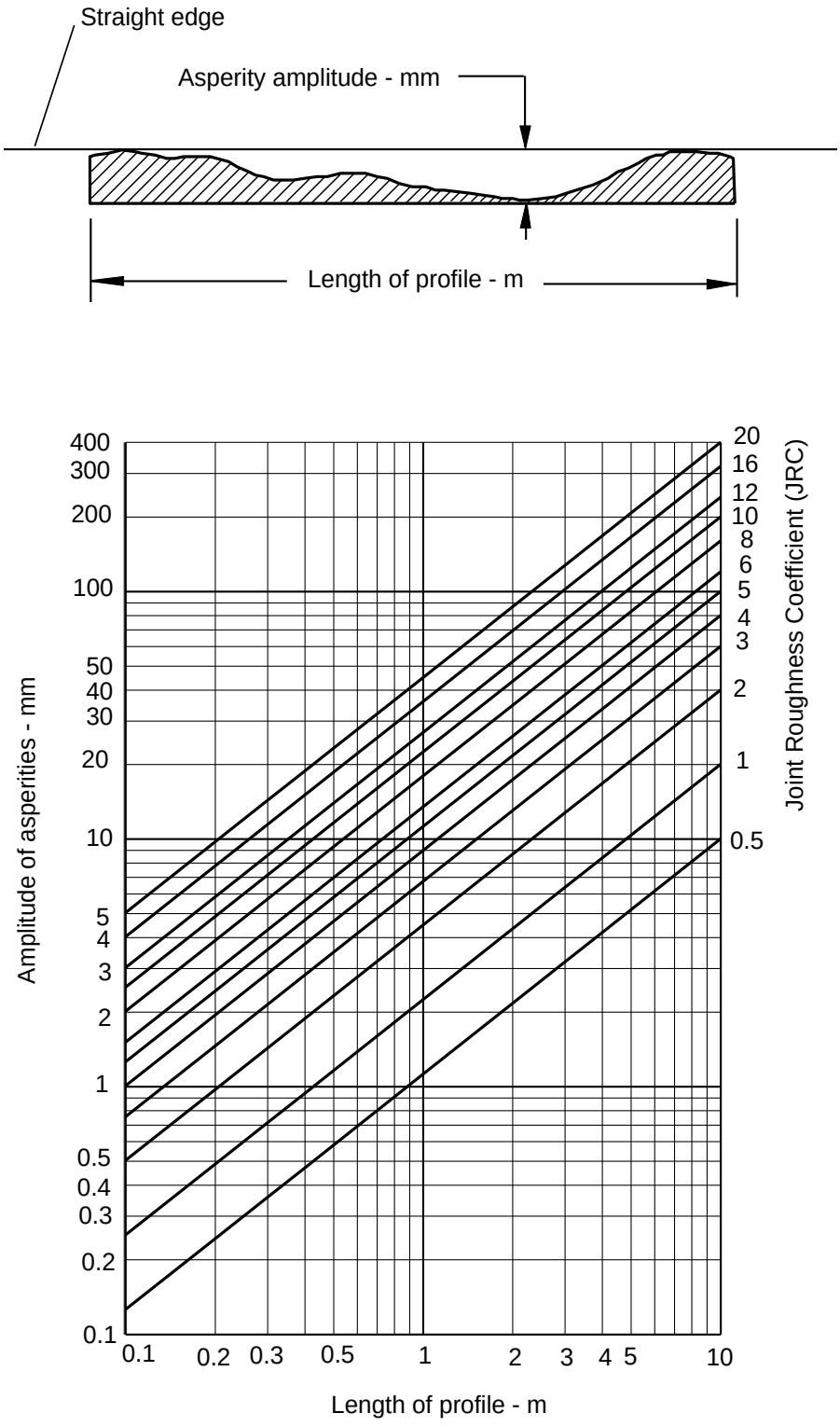

Figure 6: Alternative method for estimating *JRC* from measurements of surface roughness amplitude from a straight edge (Barton 1982).

Field estimates of *JRC*

The joint roughness coefficient *JRC* is a number that can be estimated by comparing the appearance of a discontinuity surface with standard profiles published by Barton and others. One of the most useful of these profile sets was published by Barton and Choubey (1977) which is reproduced in Figure 5.

The appearance of the discontinuity surface of the sample is compared visually with the profiles shown in Figure 5. The *JRC* value corresponding to the profile which most closely matches that of the discontinuity surface is chosen. In the case of small-scale laboratory specimens, the scale of the surface roughness will be approximately the same as that of the profiles illustrated. However, in the field the length of the surface of interest may be several metres or even tens of metres and the *JRC* value must be estimated for the full-scale surface.

An alternative method for estimating *JRC*, proposed by Barton (1982), is presented in Figure 6.

Influence of scale on *JRC* and *JCS*

Based on extensive testing of joints, joint replicas, and a review of literature, Barton and Bandis (1982) proposed a scale correction for *JRC* defined by the following relationship:

$$JRC_n = JRC_o \left(\frac{L_n}{L_o} \right)^{-0.02\,JRC_o} \tag{6}$$

where JRC_o, and L_o (length) refer to 100 mm laboratory scale samples and JRC_n, and L_n refer to in situ block sizes.

Because of the greater possibility of weaknesses in a large surface, it is likely that the average joint wall compressive strength (*JCS*) decreases with increasing scale. Barton and Bandis (1982) proposed the scale corrections for *JCS* defined by the following relationship:

$$JCS_n = JCS_o \left(\frac{L_n}{L_o} \right)^{-0.03\,JRC_o} \tag{7}$$

where JCS_o and L_o (length) refer to 100 mm laboratory scale samples and JCS_n and L_n refer to in situ block sizes.

Shear strength of filled discontinuities

The discussion presented in the previous sections has dealt with the shear strength of discontinuities in which rock wall contact occurs over the entire length of the surface under consideration. For planar surfaces, such as bedding planes in sedimentary rock, a thin clay coating will result in a significant shear strength reduction. For a rough or undulating joint, the filling thickness must be greater than the amplitude of the undulations before the shear strength is reduced to that of the filling material.

A comprehensive review of the shear strength of filled discontinuities was prepared by Barton (1974). A summary of the shear strengths of typical discontinuity fillings, based on Barton's review, is given in Table 1.

Table 1: Shear strength of filled discontinuities and filling materials (After Barton 1974).

Rock	Description	Peak c' (MPa)	Peak ϕ°	Residual c' (MPa)	Residual ϕ°
Basalt	Clayey basaltic breccia, wide variation from clay to basalt content	0.24	42		
Bentonite	Bentonite seam in chalk Thin layers Triaxial tests	0.015 0.09-0.12 0.06-0.1	7.5 12-17 9-13		
Bentonitic shale	Triaxial tests Direct shear tests	0-0.27	8.5-29	0.03	8.5
Clays	Over-consolidated, slips, joints and minor shears	0-0.18	12-18.5	0-0.003	10.5-16
Clay shale	Triaxial tests Stratification surfaces	0.06	32	0	19-25
Coal-measure rocks	Clay mylonite seams, 10 to 25 mm	0.012	16	0	11-11.5
Dolomite	Altered shale bed, ±150 mm thick	0.04	1(5)	0.02	17

Diorite granodiorite porphyry	Clay gouge (2% clay, PI = 17%)	0	26.5		
Granite	Clay filled faults Sandy loam fault filling Tectonic shear zone schistose and broken granites, disintegrated rock, and gouge	0-0.1 0.05 0.24	24-45 40 42		
Greywacke	1-2 mm clay in bedding planes			0	21
Limestone	6 mm clay layer 10-20 mm clay fillings <1 mm clay filling	0.1 0.05-0.2	13-14 17-21	0	13
Limestone, Marl, Lignites	Interbedded lignite layers Lignite/marl contact	0.08 0.1	38 10		
Limestone	Marlaceous joints, 20 mm thick	0	25	0	15-24
Lignite	Layer between lignite and clay	0.014-.03	15-17.5		
Montmorillonite Bentonite clay	80 mm seams of bentonite (montmorillonite) clay in chalk	0.36 0.016-.02	14 7.5-11.5	0.08	11
Schists, quartzites siliceous schists	100-15- mm thick clay filling Stratification, thin clay Stratification, thick clay	0.03-0.08 0.61-0.74 0.38	32 41 31		
Slates	Finely laminated and altered	0.05	33		
Quartz / kaolin / pyrolusite	Remoulded triaxial tests	0.042-.09	36-38		

Where a significant thickness of clay or gouge fillings occurs in rock masses and where the shear strength of the filled discontinuities is likely to play an important role in the stability of the rock mass, it is strongly recommended that samples of the filling be sent to a soil mechanics laboratory for testing.

Influence of water pressure

When water pressure is present in a rock mass, the surfaces of the discontinuities are forced apart and the normal stress σ_n is reduced. Under steady state conditions, where there is sufficient time for the water pressures in the rock mass to reach equilibrium, the reduced normal stress is defined by $\sigma_n' = (\sigma_n - u)$, where u is the water pressure. The reduced normal stress σ_n' is usually called the effective normal stress, which can be used in place of the normal stress term σ_n in all the equations presented above.

Instantaneous cohesion and friction

Due to the historical development of the subject of rock mechanics, many of the analyses, used to calculate factors of safety against sliding, are expressed in terms of the Mohr-Coulomb cohesion (c) and friction angle (ϕ), defined in Equation 1. Since the 1970s it has been recognised that the relationship between shear strength and normal stress is more accurately represented by a non-linear relationship such as that proposed by Barton and Bandis (1990). However, because this relationship is not expressed in terms of c and ϕ, it is necessary to devise some means for estimating the equivalent cohesive strengths and angles of friction from relationships such as those proposed by Barton and Bandis.

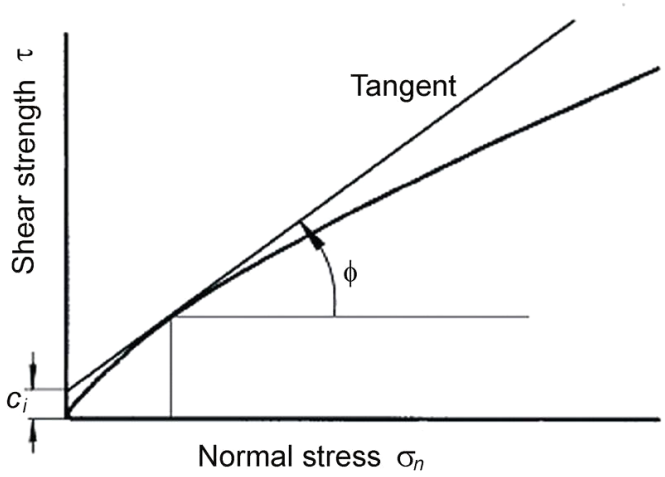

Figure 7: Definition of instantaneous cohesion c_i and the instantaneous friction angle ϕ_i for a non-linear failure criterion.

Figure 7 gives definitions of the *instantaneous cohesion* c_i and the *instantaneous friction* angle ϕ_i for a normal stress of σ_n. These quantities are given by the intercept and the inclination, respectively, of the tangent to the non-linear relationship between shear strength and normal stress. These quantities may be used for stability analyses in which the Mohr-Coulomb failure criterion (Equation 1) is applied, provided that the normal stress σ_n is reasonably close to the value used to define the tangent point.

Note that equation 4 is not valid for $\sigma_n = 0$ and it ceases to have any practical meaning for $\phi_r + JRC \log_{10}(JCS / \sigma_n) > 70°$. This limit can be used to determine a minimum value for σ_n. An upper limit for σ_n is given by σ_n = JCS.

In a typical practical application, a spreadsheet program can be used to solve equation 4 and to calculate the instantaneous cohesion and friction values for a range of normal stress values. In this spreadsheet the instantaneous friction angle ϕ_i, for a normal stress of σ_n, can be calculated from the relationship:

$$\phi_i = \arctan\left(\frac{\partial\tau}{\partial\sigma_n}\right) \tag{8}$$

$$\frac{\partial\tau}{\partial\sigma_n} = \tan\left(JRC\log_{10}\frac{JCS}{\sigma_n} + \phi_r\right) - \frac{\pi JRC}{180\ln 10}\left[\tan^2\left(JRC\log_{10}\frac{JCS}{\sigma_n} + \phi_r\right) + 1\right] \tag{9}$$

The instantaneous cohesion c_i is calculated from:

$$c_i = \tau - \sigma_n \tan\phi_i \tag{10}$$

In choosing the values of c_i and ϕ_i for use in a particular application, the average normal stress σ_n acting on the discontinuity planes should be estimated and used to determine the appropriate row in the spreadsheet. For many practical problems in the field, a single average value of σ_n will suffice but, where critical stability problems are being considered, this selection should be made for each important discontinuity surface.

References

Barton, N.R 1982. Modelling rock joint behaviour from in situ block tests: *Implications for Nuclear Waste Repository Design*. ONWI 308. Prepared by Tera Tek, Inc. for Office of Nuclear Waste Isolation, Battelle Memorial Institute, Columbus, Ohio.

Barton, N.R. 1974. *A review of the shear strength of filled discontinuities in rock.* Norwegian Geotech. Inst. Publ. No. 105. Oslo: Norwegian Geotech. Inst.

Barton, N.R. 1976. The shear strength of rock and rock joints. *Int. J. Mech. Min. Sci. & Geomech. Abstr*. **13**(10), 1-24.

Barton, N.R. and Bandis, S.C. 1982. Effects of block size on the shear behaviour of jointed rock. *23rd U.S. symp. on rock mechanics*, Berkeley, 739-760.

Barton, N.R. and Bandis, S.C. 1990. Review of predictive capabilities of JRC-JCS model in engineering practice. In *Rock joints, proc. int. symp. on rock joints,* Loen, Norway, (editors N. Barton and O. Stephansson), 603-610. Rotterdam: Balkema.

Barton, N.R. and Choubey, V. 1977. The shear strength of rock joints in theory and practice. *Rock Mech.* **10**(1-2), 1-54.

Hencher, S.R. & Richards, L.R. (1982). The basic frictional resistance of sheeting joints in Hong Kong granite *Hong Kong Engineer*, Feb., 21-25.

Patton, F.D. 1966. Multiple modes of shear failure in rock. *Proc. 1st congr. Int. Soc. Rock Mech.*, Lisbon **1**, 509-513.

```

# 5. Rock mass properties

## Introduction

Reliable estimates of the strength and deformation characteristics of rock masses are required for almost any form of analysis used for the design of slopes, foundations, and underground excavations. Hoek and Brown (1980a, 1980b) proposed a method for obtaining estimates of the strength of jointed rock masses, based upon an assessment of the interlocking of rock blocks and the condition of the surfaces between these blocks. This method was modified over the years to meet the needs of users who were applying it to problems that were not considered when the original criterion was developed (Hoek 1983, and Hoek and Brown 1988). The application of the method to very poor-quality rock masses required further changes (Hoek, Wood, and Shah 1992) and, eventually, the development of a new classification called the Geological Strength Index (Hoek, Kaiser and Bawden 1995, Hoek 1994, Hoek and Brown 1997, Hoek, Marinos and Benissi, 1998, Marinos and Hoek, 2001) was developed. A major revision was carried out in 2002 to smooth out the curves, necessary for the application of the criterion in numerical models, and to update the methods for estimating Mohr Coulomb parameters (Hoek, Carranza-Torres and Corkum, 2002). A related modification for estimating the deformation modulus of rock masses was made by Hoek and Diederichs (2006). The most recent and probably final version of the criterion was published by Hoek and Brown (2019).

This chapter presents the Hoek-Brown criterion in a form that has been found to be practical in the field and provide the most reliable set of results to use as input for the methods of analysis in current use in rock engineering.

## Generalised Hoek-Brown criterion

The Generalised Hoek-Brown failure criterion for jointed rock masses is defined by:

$$\sigma_1' = \sigma_3' + \sigma_{ci}\left(m_b\frac{\sigma_3'}{\sigma_{ci}} + s\right)^a \qquad (1)$$

where $\sigma_1'$ and $\sigma_3'$ are the maximum and minimum effective principal stresses at failure, $m_b$ is the value of the Hoek-Brown constant *m* for the rock mass, *s* and *a* are constants which depend upon the rock mass characteristics, and $\sigma_{ci}$ is the uniaxial compressive strength of the intact rock pieces.
```

```

Normal and shear stresses are related to principal stresses by the equations originally published by Balmer (1952).

$$\sigma_n' = \frac{\sigma_1' + \sigma_3'}{2} - \frac{\sigma_1' - \sigma_3'}{2} \cdot \frac{d\sigma_1'/d\sigma_3' - 1}{d\sigma_1'/d\sigma_3' + 1} \tag{2}$$

$$\tau = (\sigma_1' - \sigma_3') \frac{\sqrt{d\sigma_1'/d\sigma_3'}}{d\sigma_1'/d\sigma_3' + 1} \tag{3}$$

$$where \;\; d\sigma_1'/d\sigma_3' = 1 + am_b(m_b\sigma_3'/\sigma_{ci} + s)^{a-1} \tag{4}$$

To use the Hoek-Brown criterion for estimating the strength and deformability of jointed rock masses, three properties of the rock mass must be estimated. These are:

- uniaxial compressive strength $\sigma_{ci}$ of the intact rock pieces,
- value of the Hoek-Brown constant $m_i$ for these intact rock pieces, and
- value of the Geological Strength Index GSI for the rock mass.

Figure 1 presents a summary of estimates of the uniaxial compressive strength of rock and comments on the estimation of these values in the field. Figure 2 presents a more comprehensive summary of values of deformation modulus, uniaxial compressive strength, and the Hoek-Brown constant $m_i$ for intact rock specimens. These summaries can be used as a starting point in the estimation of rock mass strengths.

Anisotropic and foliated rocks such as slates, schists and phyllites, the behaviour of which is dominated by closely spaced planes of weakness, cleavage or schistosity, present difficulties in the determination of the uniaxial compressive strengths.

Salcedo (1983) has published the results of a set of directional uniaxial compressive tests on a graphitic phyllite from Venezuela. These results showed that the uniaxial compressive strength of this material varies by a factor of about 5, depending upon the direction of loading.

In deciding upon the value of $\sigma_{ci}$ for foliated rocks, a decision must be made on whether to use the highest or the lowest uniaxial compressive strength obtained from tests. Mineral composition, grain size, grade of metamorphism and tectonic history all play a role in determining the characteristics of the rock mass. The author cannot offer any detailed guidance on the choice of $\sigma_{ci}$, but insight into the role of schistosity in rock masses can be obtained by considering the case of the Yacambú-Quibor tunnel in Venezuela.
```

```

| Grade* | Term | Uniaxial Comp. Strength (MPa) | Point Load Index (MPa) | Field estimate of strength | Examples |
|---|---|---|---|---|---|
| R6 | Extremely Strong | > 250 | >10 | Specimen can only be chipped with a geological hammer | Fresh basalt, chert, diabase, gneiss, granite, quartzite |
| R5 | Very strong | 100 - 250 | 4 - 10 | Specimen requires many blows of a geological hammer to fracture it | Amphibolite, sandstone, basalt, gabbro, gneiss, granodiorite, limestone, marble, rhyolite, tuff |
| R4 | Strong | 50 - 100 | 2 - 4 | Specimen requires more than one blow of a geological hammer to fracture it | Limestone, marble, phyllite, sandstone, schist, shale |
| R3 | Medium strong | 25 - 50 | 1 - 2 | Cannot be scraped or peeled using a pocketknife, specimen can be fractured with a single blow from a geological hammer | Claystone, coal, concrete, schist, shale, siltstone |
| R2 | Weak | 5 - 25 | ** | Can be peeled with a pocketknife with difficulty, shallow indentation made by firm blow with point of a geological hammer | Chalk, rocksalt, potash |
| R1 | Very weak | 1 - 5 | ** | Crumbles under firm blows with point of a geological hammer, can be peeled by a pocketknife | Highly weathered or altered rock |
| R0 | Extremely weak | 0.25 - 1 | ** | Indented by thumbnail | Stiff fault gouge |

* Grade according to Brown (1981).
** Point load tests on rocks with a uniaxial compressive strength below 25 MPa are likely to yield highly ambiguous results.

Figure 1: estimates of uniaxial compressive strength.
```

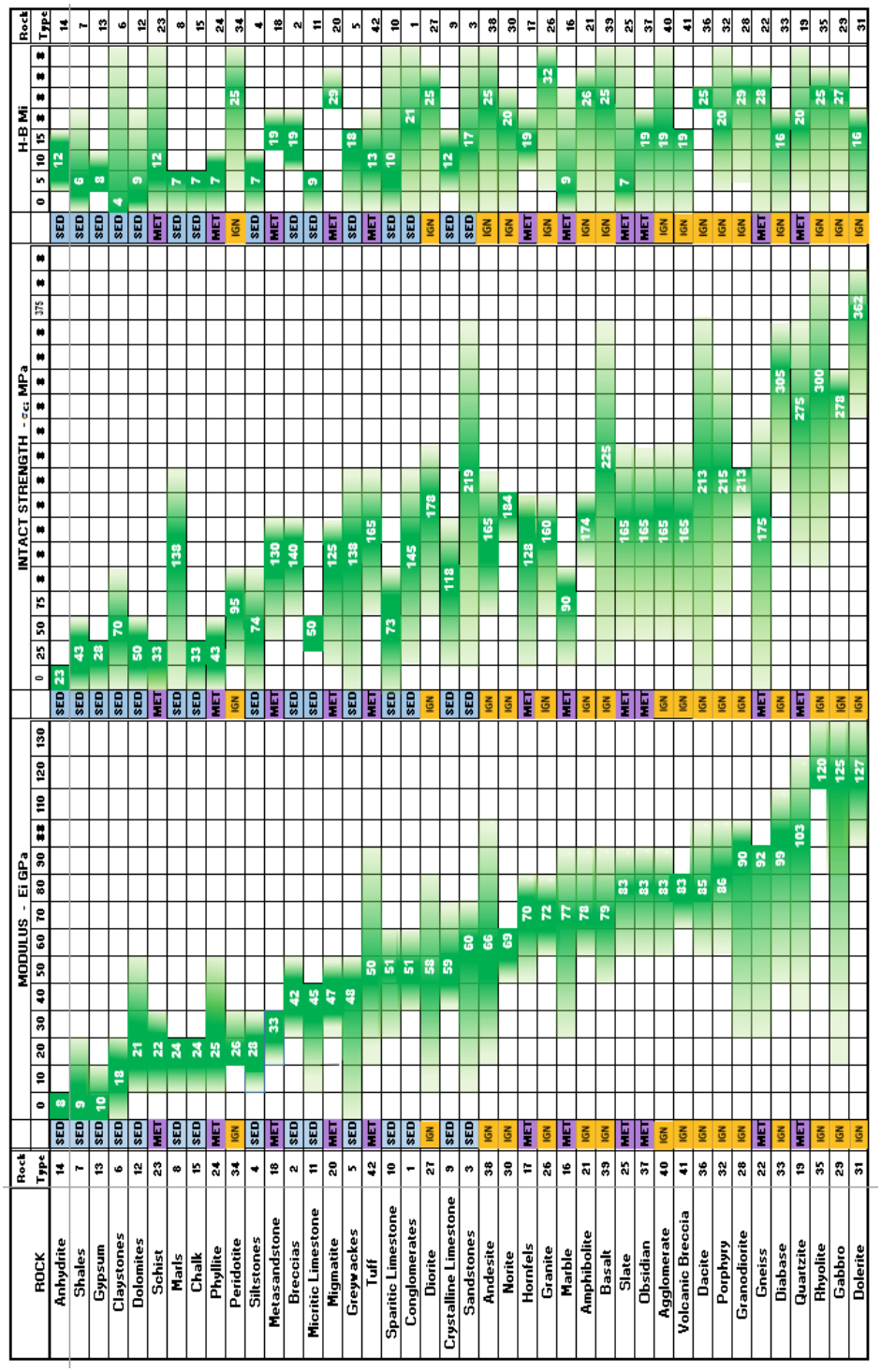

Figure 2: Average values of intact rock modulus *Ei*, uniaxial compressive strength σ_{ci} and Hoek-Brown constant m_i for various rock types, sorted in terms of increasing rock stiffness. From Chapter on Intact Rock Strength.

```

Figure 3: Yacambú-Quibor graphitic phyllite in the tunnel face.

The Yacambú-Quibor tunnel, discussed in a later chapter, was excavated in graphitic phyllite at depths of up to 1200 m in the Andes Mountains in Venezuela. The appearance of the rock mass at the tunnel face is shown in Figure 3. Back analysis of the behaviour of this material suggests that an appropriate value for $\sigma_{ci}$ is approximately 50 MPa. In other words, on the scale of the 5.5 m diameter tunnel, the rock mass properties are "averaged" and there is no sign of anisotropic behaviour in the deformations measured in the tunnel.

**Influence of sample size**

The influence of sample size upon rock strength has been widely discussed in geotechnical literature and it is generally assumed that there is a significant reduction in strength with increasing sample size. Based upon an analysis of published data, Hoek and Brown (1980a) have suggested that the uniaxial compressive strength $\sigma_{cd}$ of a rock specimen with a diameter of d mm is related to the uniaxial compressive strength $\sigma_{c50}$ of a 50 mm diameter sample by the following relationship:

$$\sigma_{cd} = \sigma_{c50} \left(\frac{50}{d}\right)^{0.18} \quad (5)$$

This relationship, together with the data upon which it was based, is shown in Figure 4.
```

```

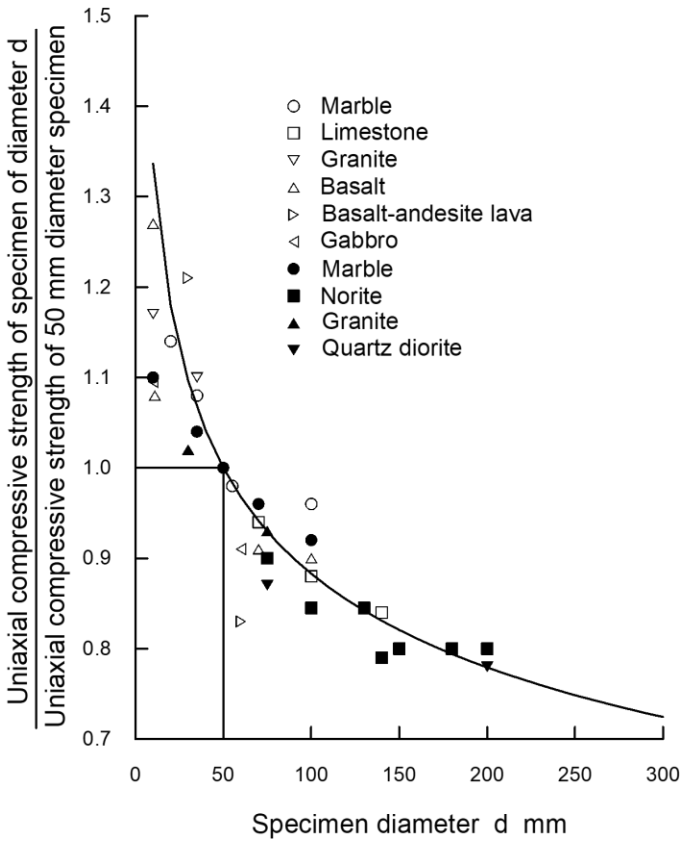


Figure 4: Influence of specimen size on the strength of intact rock. Hoek and Brown (1980a).

It is suggested that the reduction in strength is due to the greater opportunity for failure through and around grains, the 'building blocks' of the intact rock, as more and more of these grains are included in the test sample. Eventually, when a sufficiently large number of grains are included in the sample, the strength reaches a constant value.

The Hoek-Brown failure criterion, which assumes isotropic rock and rock mass behaviour, should only be applied to those rock masses in which many closely spaced discontinuities exist, such that isotropic behaviour involving failure on discontinuities can be assumed. When the structure being analysed is large and the block size small in comparison, the rock mass can be treated as a Hoek-Brown material.

Where the block size is of the same order as that of the structure being analysed, or when one of the discontinuity sets is significantly weaker than the others, the Hoek-Brown criterion should not be used. In these cases, the stability of the structure should be analysed by considering failure mechanisms involving the sliding or rotation of blocks and wedges defined by intersecting structural features.
```

```

It is reasonable to extend this argument to suggest that, when dealing with large scale rock masses, the strength will reach a constant value when the size of individual rock pieces is small in relation to the overall size of the structure being considered. This suggestion is embodied in Figure 5 which shows the transition from an isotropic intact rock specimen, through a highly anisotropic rock mass in which failure is controlled by one or two discontinuities, to an isotropic heavily jointed rock mass.

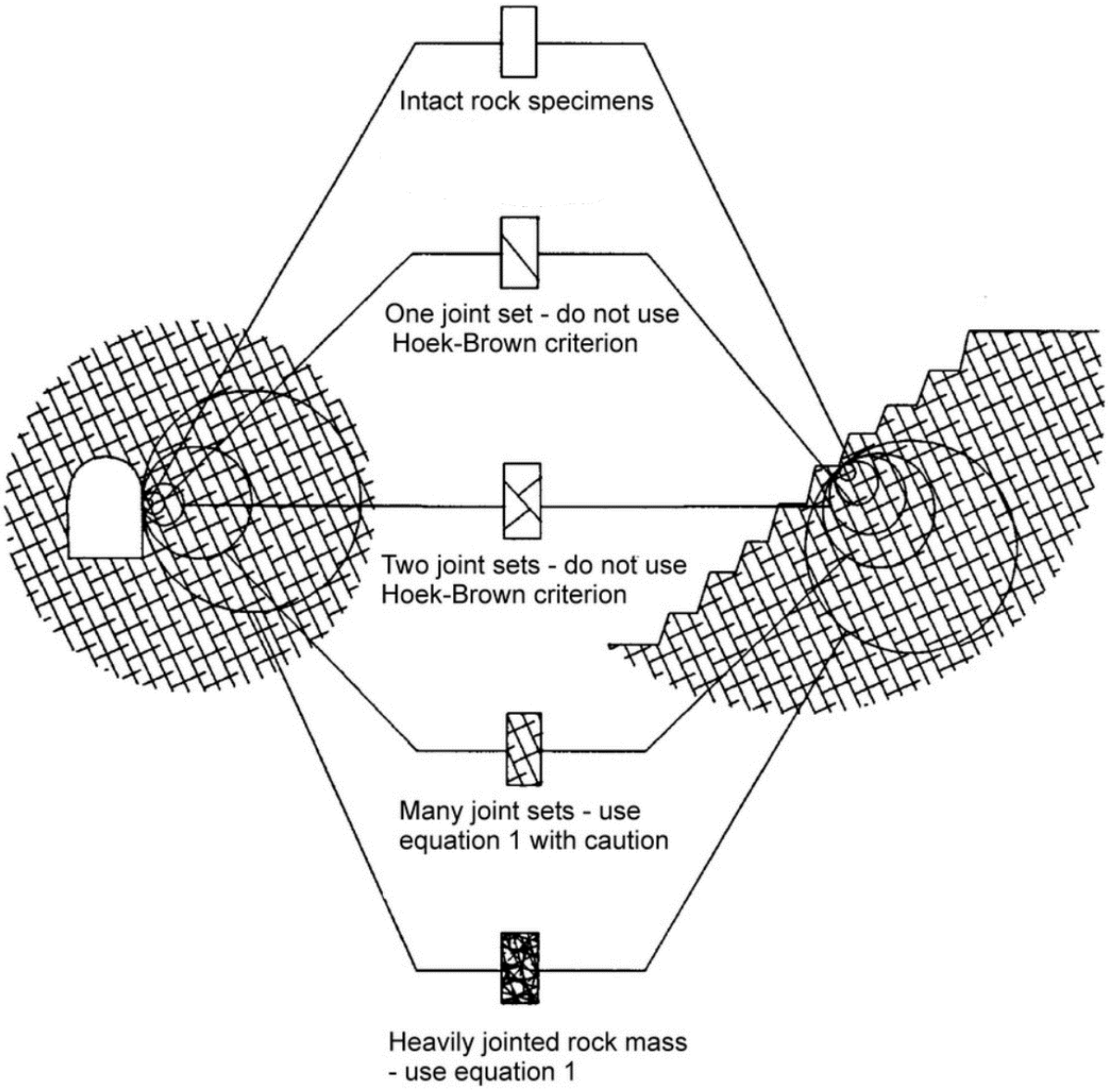


Figure 5: Idealised diagram showing the transition from intact to a heavily jointed rock mass with increasing sample size.
```

```

## Geological Strength Index

The strength of a jointed rock mass depends on the properties of the intact rock pieces and the freedom of these pieces to slide and rotate under different stress conditions. This freedom depends on the geometrical shape of the intact rock pieces as well as the condition of the surfaces separating the pieces. Angular rock pieces with clean, rough discontinuity surfaces will result in a much stronger rock mass than one which contains rounded particles surrounded by weathered and altered material.

The Geological Strength Index (GSI), introduced by Hoek (1994) and Hoek, Kaiser and Bawden (1995) provides a number which, when combined with the intact rock properties, can be used for estimating the reduction in rock mass strength for different geological conditions. This system is presented in Figure 6, for blocky rock masses, and Figure 7 for heterogeneous rock masses such as flysch. Figure 7 has also been extended to deal with molassic rocks (Hoek et al, 2006) and ophiolites (Marinos et al, 2005).

Before the introduction of the GSI system in 1994, the application of the Hoek-Brown criterion in the field was based on a correlation with the 1976 version of Bieniawski's Rock Mass Rating (RMR), with the Groundwater Rating set to 10 (dry) and the Adjustment for Joint Orientation set to 0 (very favourable) (Bieniawski, 1976). If the 1989 version of RMR (Bieniawski, 1989) is used, then the Groundwater Rating is set to 15 and the Adjustment for Joint Orientation set to zero.

During the early years the value of GSI was estimated directly from RMR. However, this correlation has proved to be unreliable, particularly for poor quality rock masses and for rocks with lithological peculiarities that cannot be accommodated in the RMR classification. Consequently, it is recommended that GSI should be estimated directly by means of the charts presented in Figures 6 and 7 and not from the RMR classification.

Experience shows that most geologists and engineering geologists are comfortable with the descriptive and largely qualitative nature of the GSI tables and generally have little difficulty in arriving at an estimated value. On the other hand, many engineers feel the need for a more quantitative system in which they can "measure" some physical dimension. Conversely, these engineers have little difficulty understanding the importance of the intact rock strength $\sigma_{ci}$ and its incorporation in the assessment of the rock mass properties.

Many geologists tend to confuse intact and rock mass strength and consistently underestimate the intact strength.

An additional practical question is whether borehole cores can be used to estimate the GSI value behind the visible faces. Borehole cores are the best source of data at depth, but it must be recognized that it is necessary to extrapolate the one-dimensional information provided by core to the three-dimensional rock mass. However, this is a common problem in borehole investigation and most experienced engineering geologists are comfortable with this extrapolation process. Multiple boreholes and inclined boreholes are of great help in the interpretation of rock mass characteristics at depth.
```

```

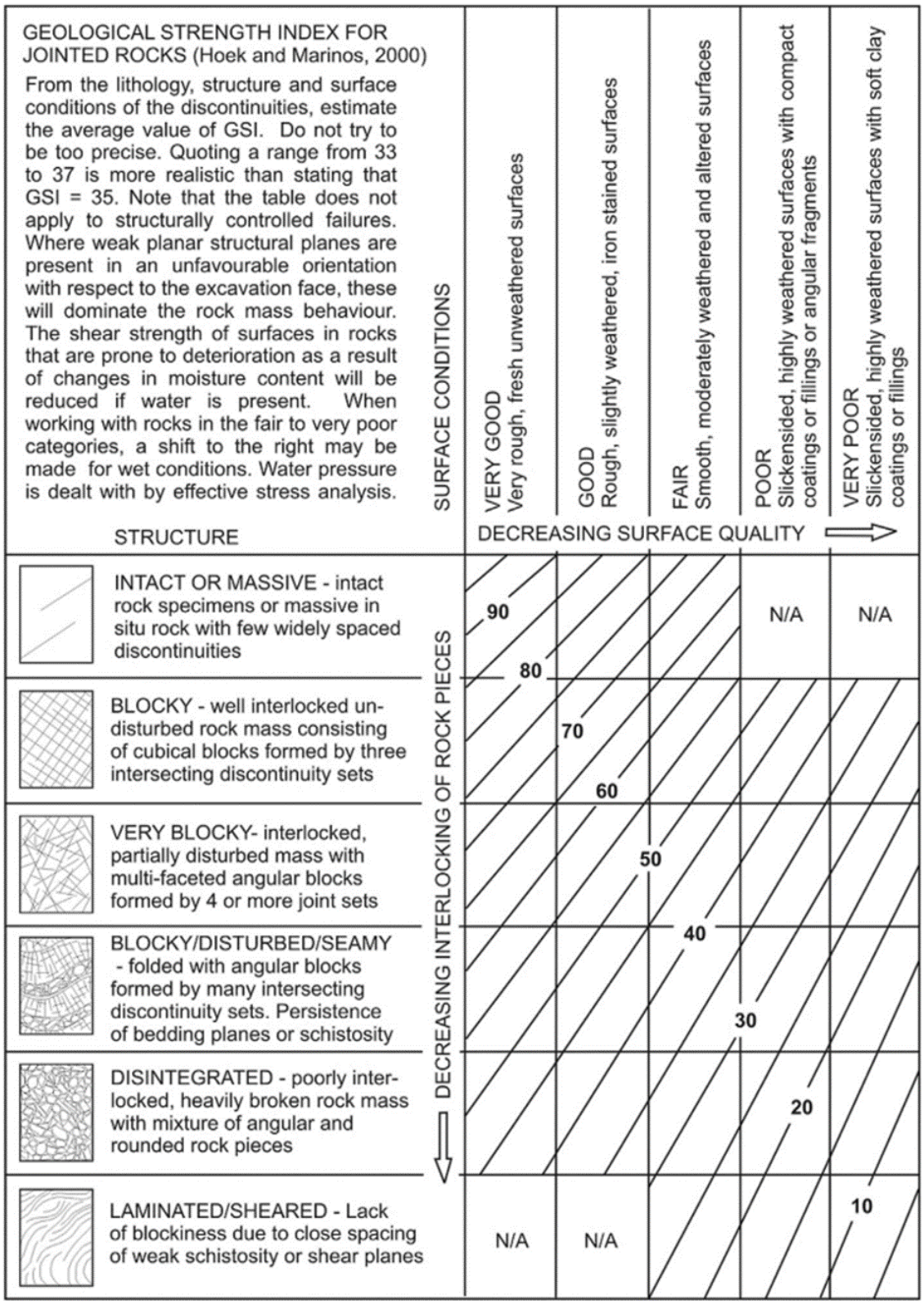


Figure 6: Characterisation of blocky rock masses based on interlocking and joint conditions.
```

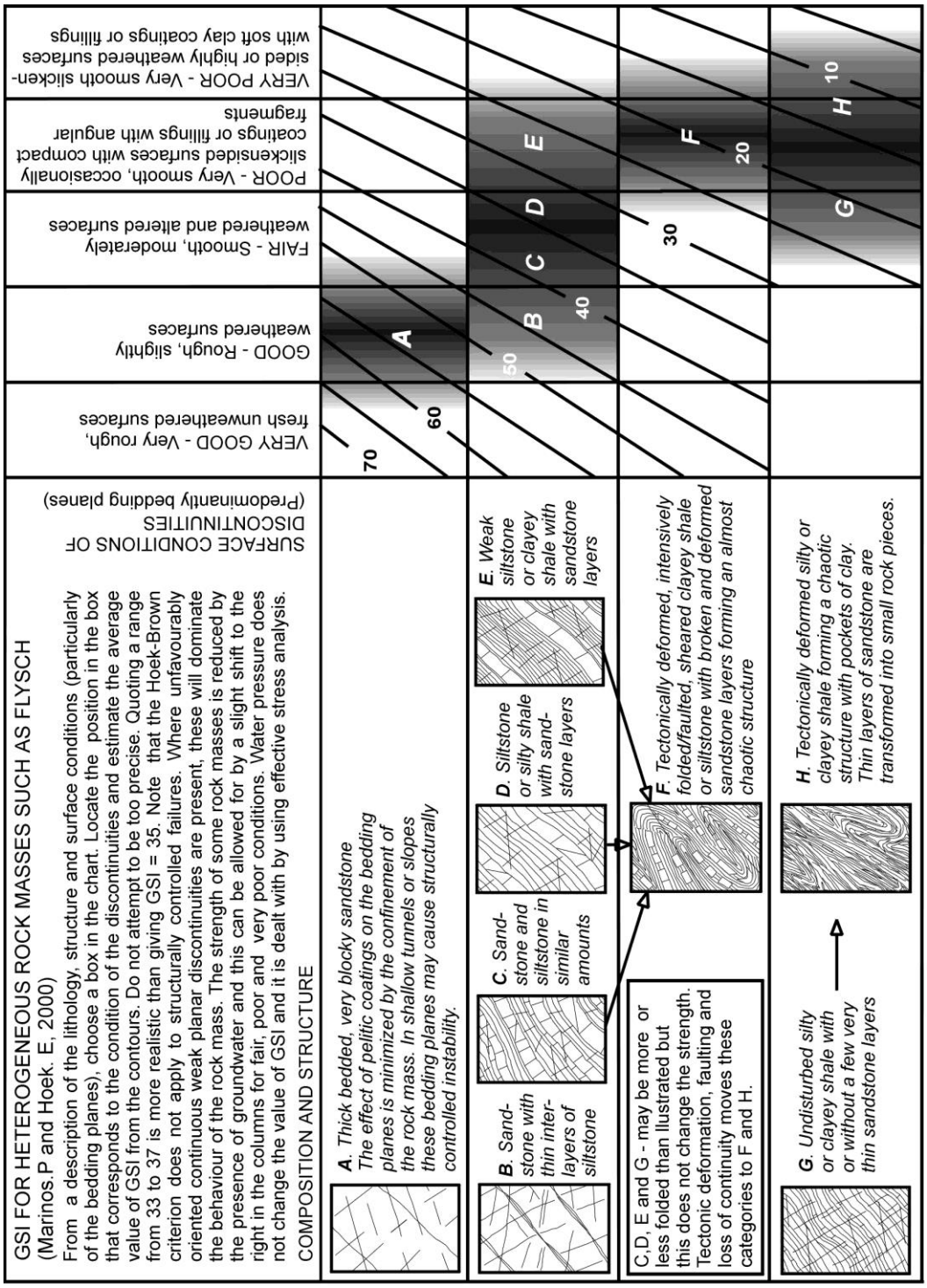

Figure 7: Estimate of Geological Strength Index GSI for heterogeneous rock masses, such as flysch. (After Marinos and Hoek, 2001).

```

The most important decision to be made in using the GSI system is whether it should be used. If the discontinuity spacing is large compared with the dimensions of the tunnel or slope under consideration then, as shown in Figure 5, the GSI tables and the Hoek-Brown criterion should not be used, and the discontinuities should be treated individually. Where the discontinuity spacing is small compared with the size of the structure (bottom of Figure 5) then the GSI tables can be used with confidence.

One of the practical problems that arises when assessing the value of GSI in the field is related to blast damage. As illustrated in Figure 8, there is a considerable difference in the appearance of a rock face which has been excavated by controlled blasting and a face which has been damaged by bulk blasting. Wherever possible, the undamaged face should be used to estimate the value of GSI since the overall aim is to determine the properties of the undisturbed rock mass.

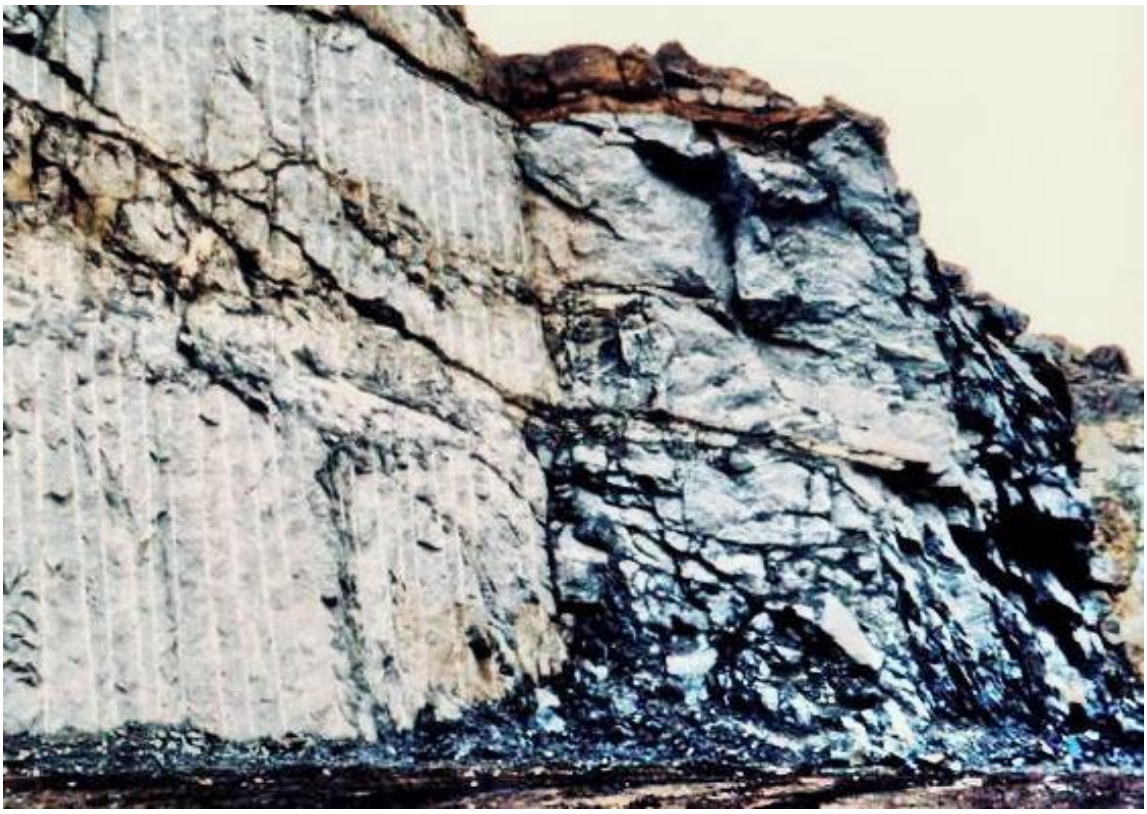

Figure 8: Comparison between the results achieved using controlled blasting (on the left) and normal bulk blasting for a surface excavation in gneiss.
```

```

The influence of blast damage on the near surface rock mass properties has been considered in the 2002 version of the Hoek-Brown criterion (Hoek, Carranza-Torres and Corkum (2002)).

$$m_b = m_i \, exp\left(\frac{GSI-100}{28-14D}\right) \tag{6}$$

$$s = exp\left(\frac{GSI-100}{9-3D}\right) \tag{7}$$

$$a = \frac{1}{2} + \frac{1}{6}\left(e^{-GSI/15} - e^{-20/3}\right) \tag{8}$$

D is a factor which depends upon the degree of disturbance due to blast damage and stress relaxation. It varies from 0 for undisturbed in situ rock masses to 1 for very disturbed rock masses. Guidelines for the selection of D are presented in Figure 9.

Note that the factor D applies only to the blast damaged zone. It should not be applied to the entire rock mass. For example, in tunnels the blast damage is generally limited to a 1 to 2 m thick zone around the tunnel, and this should be incorporated into numerical models as a different and weaker material than the surrounding rock mass. Applying the blast damage factor D to the entire rock mass is inappropriate and can result in misleading and unnecessarily pessimistic results.

The uniaxial compressive strength of the rock mass is obtained by setting $\sigma_3' = 0$ in equation 1, giving:

$$\sigma_c = \sigma_{ci} . s^a \tag{9}$$

and the tensile strength of the rock mass is:

$$\sigma_t = -\frac{s\sigma_{ci}}{m_b} \tag{10}$$

Equation 15, on page 16, is obtained by setting $\sigma_1' = \sigma_3' = \sigma_t$ in equation 1. This represents a condition of biaxial tension. Hoek (1983) showed that, for brittle materials, the uniaxial tensile strength is equal to the biaxial tensile strength.
```

```

| Appearance of rock | Description of rock mass | Suggested D value |
|---|---|---|
|  | Excellent quality-controlled blasting or excavation by Tunnel Boring Machine results in minimal disturbance to the confined rock mass surrounding a tunnel. | D = 0 |
|  | Mechanical or hand excavation in poor quality rock masses (no blasting) results in minimal disturbance to the surrounding rock mass. Where squeezing problems result in significant floor heave, disturbance can be severe unless a temporary invert, as shown in the photograph, is placed. | Mechanical excavation<br>D = 0<br>No invert<br>D = 0.5 |
|  | Very poor-quality blasting in a hard rock tunnel results in severe local damage, extending 2 or 3 m, in the surrounding rock mass. | D = 0.8 |
|  | Small scale blasting in civil engineering slopes results in modest rock mass damage, particularly if controlled blasting is used as shown on the left-hand side of the photograph. However, stress relief results in some disturbance. | D = 0.7<br>Good blasting<br>D = 1.0<br>Poor blasting |
|  | Very large open pit mine slopes suffer significant disturbance due to heavy production blasting and also due to stress relief from overburden removal.<br>In some softer rocks excavation can be carried out by ripping and dozing and the degree of damage to the slopes is less. | D = 1.0<br>Production blasting<br>D = 0.7 |

```

Figure 9: Guidelines for estimating the disturbance factor D.

```

Note that the "switch" at GSI = 25 for the coefficients *s* and *a* (Hoek and Brown, 1997) has been eliminated in equations 9 and 10, giving a smooth continuous transition for the entire range of GSI values. The numerical values of *s* and *a*, given by these equations, are remarkably close to those given by the previous equations and it is not necessary for readers to revisit and make corrections to old calculations.

**Mohr-Coulomb parameters**

Since many geotechnical software programs are written in terms of the Mohr-Coulomb failure criterion, it is sometimes necessary to determine equivalent angles of friction and cohesive strengths for each rock mass and stress range. This is done by fitting an average linear relationship to the curve generated by solving equation 1 for a range of minor principal stress values defined by $\sigma_t < \sigma_3 < \sigma_{3max}$, as illustrated in Figure 10. The fitting process involves balancing the areas above and below the Mohr-Coulomb plot. This results in the following equations for the angle of friction $\varphi'$ and cohesive strength $c'$ :

$$\varphi' = sin^{-1}\left[\frac{6am_b(s+m_b\sigma'_{3n})^{a-1}}{2(1+a)(2+a)+6am_b(s+m_b\sigma'_{3n})^{a-1}}\right] \quad (11)$$

$$c' = \frac{\sigma_{ci}[(1+2a)s+(1-a)m_b\sigma'_{3n}](s+m_b\sigma'_{3n})^{a-1}}{(1+a)(2+a)\sqrt{1+(6am_b(s+m_b\sigma'_{3n})^{a-1})/((1+a)(2+a))}} \quad (12)$$

where $\sigma_{3n} = \sigma'_{3max}/\sigma_{ci}$

Note that the value of $\sigma'_{3max}$, the upper limit of confining stress over which the relationship between the Hoek-Brown and the Mohr-Coulomb criteria is considered, must be determined for each individual case. Guidelines for selecting these values for slopes as well as shallow and deep tunnels are presented later.

The Mohr-Coulomb shear strength $\tau$, for a given normal stress $\sigma$, is found by substitution of these values of $c'$ and $\varphi'$ into the equation:

$$\tau = c' + \sigma\, tan\, \varphi' \quad (13)$$

The equivalent plot, in terms o the major and minor principal stresses, is defined by:

$$\sigma'_1 = \frac{2c'\, cos\, \varphi'}{1-sin\, \varphi'} + \frac{1+sin\, \varphi'}{1-sin\, \varphi'}\sigma'_3 \quad (14)$$
```

```

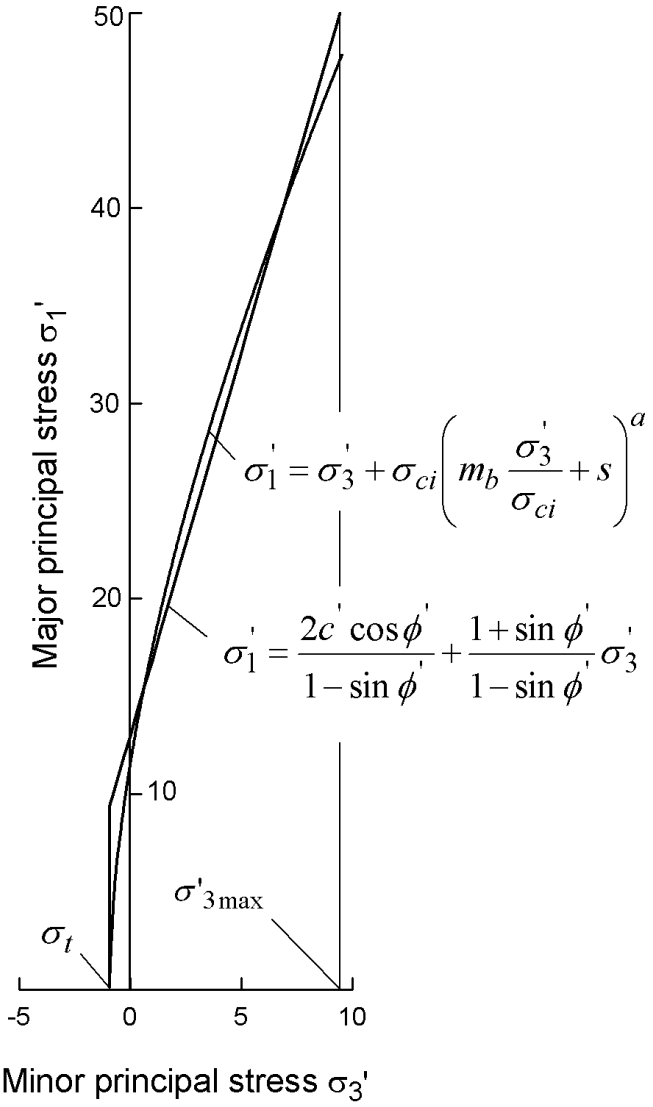


Figure 10: Relationships between major and minor principal stresses for Hoek-Brown and the equivalent Mohr-Coulomb criteria.

**Rock mass strength**

The uniaxial compressive strength of the rock mass $\sigma_c$ is given by equation 9. Failure initiates at the boundary of an excavation when $\sigma_c$ is exceeded by the stress induced on that boundary. The failure propagates from this initiation point into a biaxial stress field and it eventually stabilizes when the local strength, defined by equation 1, is higher than the induced stresses $\sigma_1'$ and $\sigma_3'$. Most numerical models can follow this process of fracture propagation and this level of detailed analysis is very important when considering the stability of excavations in rock and when designing support systems.
```

```

However, there are times when it is useful to consider the overall behaviour of a rock mass rather than the detailed failure propagation process described above. For example, when considering the strength of a pillar, it is useful to have an estimate of the overall strength of the pillar rather than a detailed evaluation of the extent of fracture propagation in the pillar. This leads to the concept of a global "rock mass strength" and Hoek and Brown (1997) proposed that this could be estimated from the Mohr-Coulomb relationship:

$$\sigma'_{cm} = \frac{2c' \cos \varphi'}{1 - \sin \varphi'} \tag{15}$$

with $c'$ and $\varphi'$ determined for the stress range $\sigma_t < \sigma'_3 < \sigma_{ci}/4$ giving

$$\sigma'_{cm} = \sigma_{ci} \cdot \frac{(m_b + 4s - a(m_b - 8s))(m_b/4 + s)^{a-1}}{2(1+a)(2+a)} \tag{16}$$

**Determination of $\sigma'_{3max}$**

The issue of determining the appropriate value of $\sigma'_{3max}$ for use in equations 11 and 12 depends upon the specific application. Two cases will be investigated:

***Tunnels*** – where the value of $\sigma'_{3max}$ is that which gives equivalent characteristic curves for the two failure criteria for deep tunnels or equivalent subsidence profiles for shallow tunnels.

***Slopes*** – here the calculated factor of safety and the shape and location of the failure surface must be equivalent.

For the case of deep tunnels, solutions for both the Generalized Hoek-Brown and the Mohr-Coulomb criteria have been used to generate hundreds of solutions and to find the value of $\sigma'_{3max}$ that gives equivalent characteristic curves. For shallow tunnels, where the depth below surface is less than 3 tunnel diameters, comparative numerical studies of the extent of failure and the magnitude of surface subsidence gave an identical relationship to that obtained for deep tunnels if caving to surface is avoided.

The results of the studies for deep tunnels are plotted in Figure 11 and the fitted equation for both shallow and deep tunnels is:

$$\frac{\sigma'_{3max}}{\sigma'_{cm}} = 0.47 \left( \frac{\sigma'_{cm}}{\gamma H} \right)^{-0.94} \tag{17}$$

where $\sigma'_{cm}$ is the rock mass strength, defined by equation 21, $\gamma$ is the unit weight of the rock mass and H is the depth of the tunnel below surface. In cases where the horizontal stress is higher than the vertical stress, the horizontal stress value should be used in place of $\gamma H$.
```

```

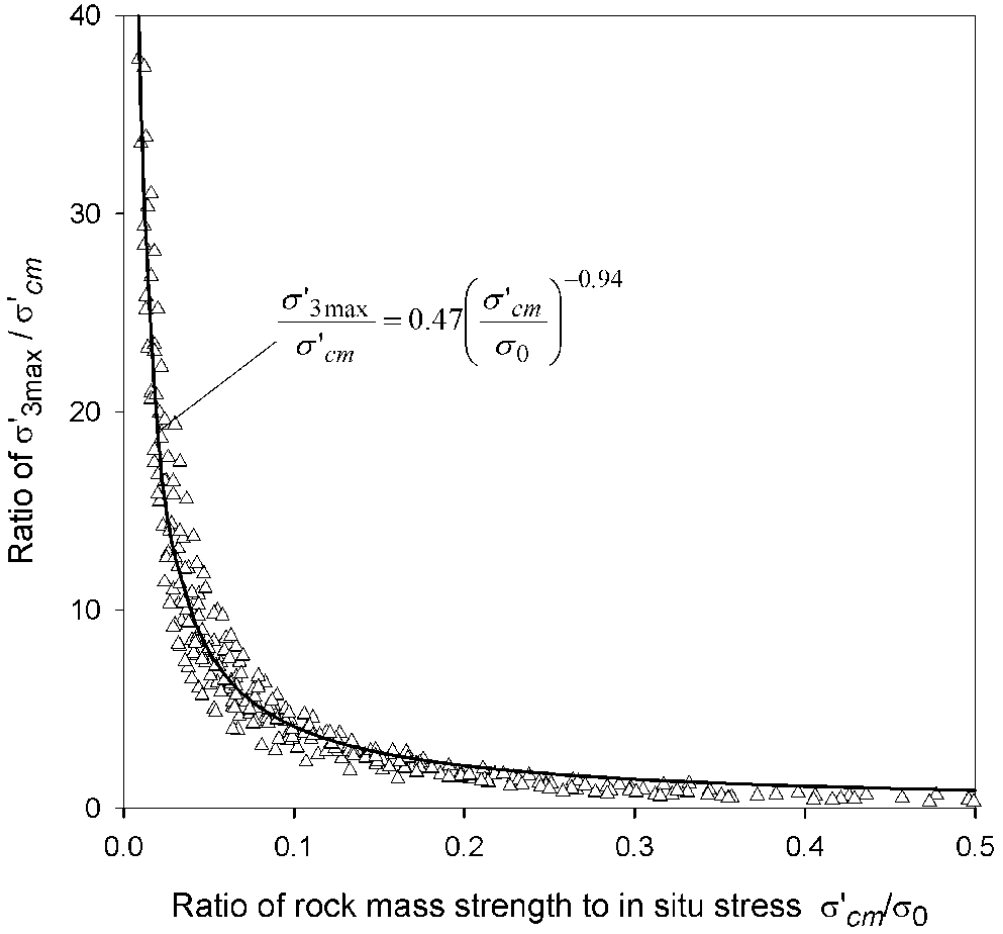


Figure 11: Relationship for the calculation of $\sigma'_{3max}$ for equivalent Mohr-Coulomb and Hoek-Brown parameters for tunnels.

Equation 17 applies to all underground excavations, which are surrounded by a zone of failure that does not extend to surface. For studies of problems such as block caving in mines, it is recommended that no attempt should be made to relate the Hoek-Brown and Mohr-Coulomb parameters and that the determination of material properties and subsequent analysis should be based on only one of these criteria.

Similar studies for slopes, using Bishop's circular failure analysis for a wide range of slope geometries and rock mass properties, gave:

$$\frac{\sigma'_{3max}}{\sigma'_{cm}} = 0.72\left(\frac{\sigma'_{cm}}{\gamma H}\right)^{-0.91} \qquad (18)$$

Where *H* is the height of the slope.
```

```

**Deformation modulus**

Hoek and Diederichs (2006) re-examined existing empirical methods for estimating rock mass deformation modulus and concluded that none of these methods provided reliable estimates over the entire range of rock mass conditions encountered. Large errors were found for very poor rock masses and, at the other end of the spectrum, for massive strong rock masses. Fortunately, a new set of reliable measured data from China and Taiwan was available for analyses and it was found that the equation which gave the best fit to this data is a sigmoid function having the form:

$$y = c + \frac{a}{1+e^{-((x-x_0)/b)}} \tag{19}$$

Using commercial curve fitting software, Equation 19 was fitted to the Chinese and Taiwanese data and the constants a and b in the fitted equation were then replaced by expressions incorporating GSI and the disturbance factor D. These were adjusted to give the equivalent average curve and the upper and lower bounds into which > 90% of the data points fitted. Note that the constant a = 100 000 in Equation 20 is a scaling factor which is not directly related to the physical properties of the rock mass.

The following best-fit equation was derived:

$$E_{rm}(MPa) = 100000 \left(\frac{1-D/2}{1+e^{((75+25D-GSI)/11)}}\right) \tag{20}$$

The rock mass deformation modulus data from China and Taiwan includes information on the geology as well as the uniaxial compressive strength ($\sigma_{ci}$) of the intact rock. This information permits a more detailed analysis in which the ratio of mass to intact modulus ($E_{rm}/E_i$) can be included. Using the modulus ratio MR proposed by Deere (1968) (modified by the authors based in part on this data set and on additional correlations from Palmstrom and Singh (2001)), it is possible to estimate the intact modulus from:

$$E_i = MR \cdot \sigma_{ci} \tag{21}$$

This relationship is useful when no direct values of the intact modulus ($E_i$) are available or where completely undisturbed sampling for measurement of $E_i$ is difficult. A detailed analysis of the Chinese and Taiwanese data, using Equation (21) to estimate $E_i$ resulted in the following equation:

$$E_{rm} = E_i \left(0.02 + \frac{1-D/2}{1+e^{((60+15D-GSI)/11)}}\right) \tag{22}$$

This equation incorporates a finite value for the parameter c (Equation 19) to account for the modulus of broken rock (transported rock, aggregate or soil) described by GSI = 0. This equation is plotted against the average normalized field data from China and Taiwan in Figure 12.
```

```

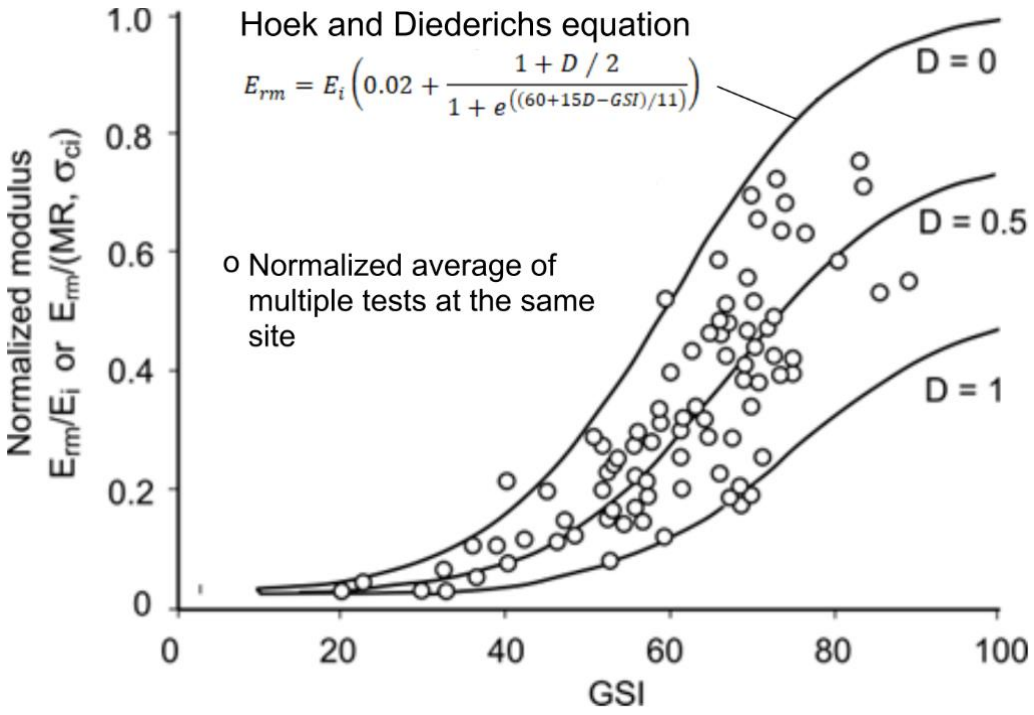


Figure 12: Plot of normalized in situ rock mass deformation modulus from China and Taiwan against Hoek and Diederichs Equation (22). Each data point represents the average of multiple tests at the same site in the same rock mass.

Figure 13, based on the modulus ratio (MR) values proposed by Deere (1968) can be used for calculating the intact rock modulus $E_i$. In general, measured values of $E_i$ are seldom available and, even when they are, their reliability is suspect because of specimen damage. This specimen damage has a greater impact on modulus than on strength and, hence, the intact rock strength, when available, can usually be considered more reliable for use in equation (21).

**Post-failure behaviour**

When using numerical models to study the progressive failure of rock masses, estimates of the post-peak or post-failure characteristics of the rock mass are required. In some of these models, the Hoek-Brown failure criterion is treated as a yield criterion and the analysis is carried out using plasticity theory. No definite rules for dealing with this problem can be given but based upon experience in numerical analysis of a variety of practical problems, the post-failure characteristics, illustrated in Figure 14, are suggested as a starting point.
```

```

| | Class | Group | Texture | | | |
|---|---|---|---|---|---|---|
| | | | Coarse | Medium | Fine | Very fine |
| SEDIMENTARY | Clastic | | Conglomerates 300-400<br>Breccias 230-350 | Sandstones 200-350 | Siltstones 350-400<br>Greywackes 350 | Claystones 200-300<br>Shales 150-250 *<br>Marls 150-200 |
| | Non-Clastic | Carbonates | Crystalline Limestone 400-600 | Sparitic Limestones 600-800 | Micritic Limestones 800-1000 | Dolomites 350-500 |
| | | Evaporites | | Gypsum (350)** | Anhydrite (350)** | |
| | | Organic | | | | Chalk 1000+ |
| METAMORPHIC | Non Foliated | | Marble 700-1000 | Hornfels 400-700<br>Metasandstone 200-300 | Quartzites 300-450 | |
| | Slightly foliated | | Migmatite 350-400 | Amphibolites 400-500 | Gneiss 300-750* | |
| | Foliated* | | | Schists 250-1100* | Phyllites /Mica Schist 300-800* | Slates 400-600* |
| IGNEOUS | Plutonic | Light | Granite+ 300-550<br>Granodiorite+ 400-450 | Diorite+ 300-350 | | |
| | | Dark | Gabbro 400-500<br>Norite 350-400 | Dolerite 300-400 | | |
| | Hypabyssal | | Porphyries (400)** | | Diabase 300-350 | Peridotite 250-300 |
| | Volcanic | Lava | | Rhyolite 300-500<br>Andesite 300-500 | Dacite 350-450<br>Basalt 250-450 | |
| | | Pyroclastic | Agglomerate 400-600 | Volcanic breccia (500) ** | Tuff 200-400 | |

* Highly anisotropic rocks: the value of MR will be significantly different if normal strain and/or loading occurs parallel (high MR) or perpendicular (low MR) to a weakness plane. Uniaxial test loading direction should be equivalent to field application.
+ Felsic Granitoids: Coarse Grained or Altered (high MR), fined grained (low MR).
** No data available, estimated on the basis of geological logic.
```

Figure 13: Guidelines for the selection of modulus ratio (MR) values in Equation (21) - based on Deere (1968) and Palmstrom and Singh (2001).

```

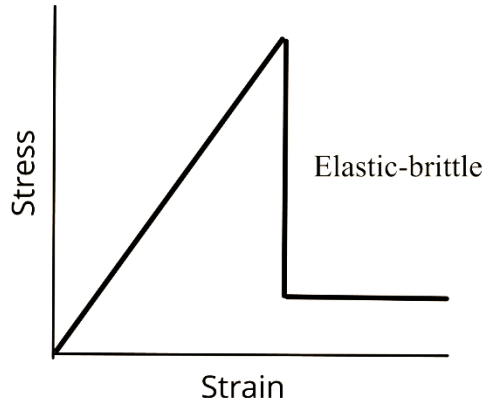


a) Very good quality hard rock mass

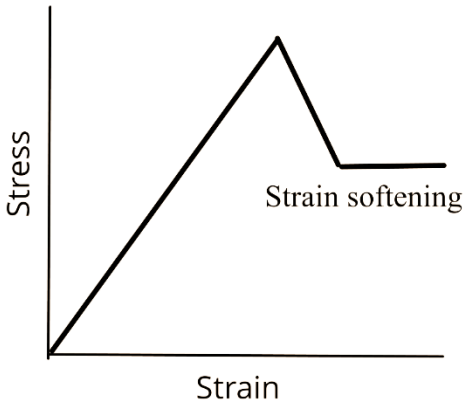


b) Average quality hard rock mass

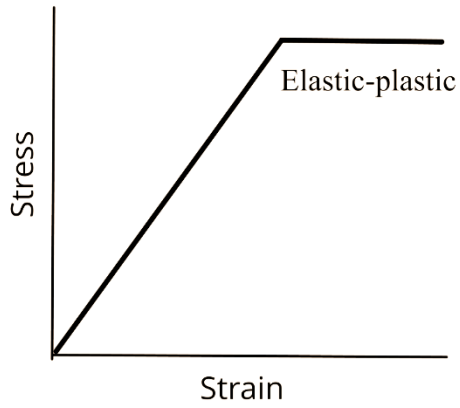


c) Poor quality hard rock mass

Figure 14: Suggested post failure characteristics for different quality rock masses.
```

```

## Reliability of rock mass strength estimates

The techniques described in the preceding sections of this chapter can be used to estimate the strength and deformation characteristics of isotropic jointed rock masses. When applying this procedure to rock engineering design problems, most users consider only the 'average' or mean properties. In fact, all these properties exhibit a distribution about the mean, even under the most ideal conditions, and these distributions can have a significant impact upon the design calculations.

In the text that follows, a slope stability calculation and a tunnel support design calculation are carried out to evaluate the influence of these distributions. In each case the strength and deformation characteristics of the rock mass are estimated by means of the Hoek-Brown procedure, assuming that the three input parameters are defined by normal distributions.

## Input parameters

Figure 15 has been used to estimate the value of GSI from field observations of the block size, shape and discontinuity surface conditions. Included in this figure is a cross-hatched circle representing the 90% confidence limits of a GSI value of 25 ± 5 (equivalent to a standard deviation of approximately 2.5). This represents the range of values that an experienced geologist would assign to a rock mass described as BLOCKY/DISTURBED or DISINTEGRATED and POOR. Typically, rocks such as flysch, schist and some phyllites may fall within this range of rock mass descriptions.

In the author's experience, some geologists go to extraordinary lengths to try to determine an 'exact' value of GSI. Geology does not lend itself to such precision and it is simply not realistic to assign a single value. A range of values, such as that illustrated in Figure 15 is more appropriate. In fact, in some complex geological environments, the range indicated by the cross-hatched circle may be too optimistic.

The two laboratory properties required for the application of the Hoek-Brown criterion are the uniaxial compressive strength of the intact rock ($\sigma_{ci}$) and the intact rock material constant $m_i$. Ideally these two parameters should be determined by triaxial tests on carefully prepared specimens as described by Hoek and Brown (1997).

The standard deviations assigned to these three distributions are based upon the author's experience of geotechnical programs for major civil and mining projects where adequate funds are available for high quality investigations. For preliminary field investigations or 'low budget' projects, it is prudent to assume larger standard deviations for the input parameters.

It is assumed that all three input parameters (GSI, $\sigma_{ci}$ and $m_i$) can be represented by normal distributions as illustrated in Figure 16.
```

```

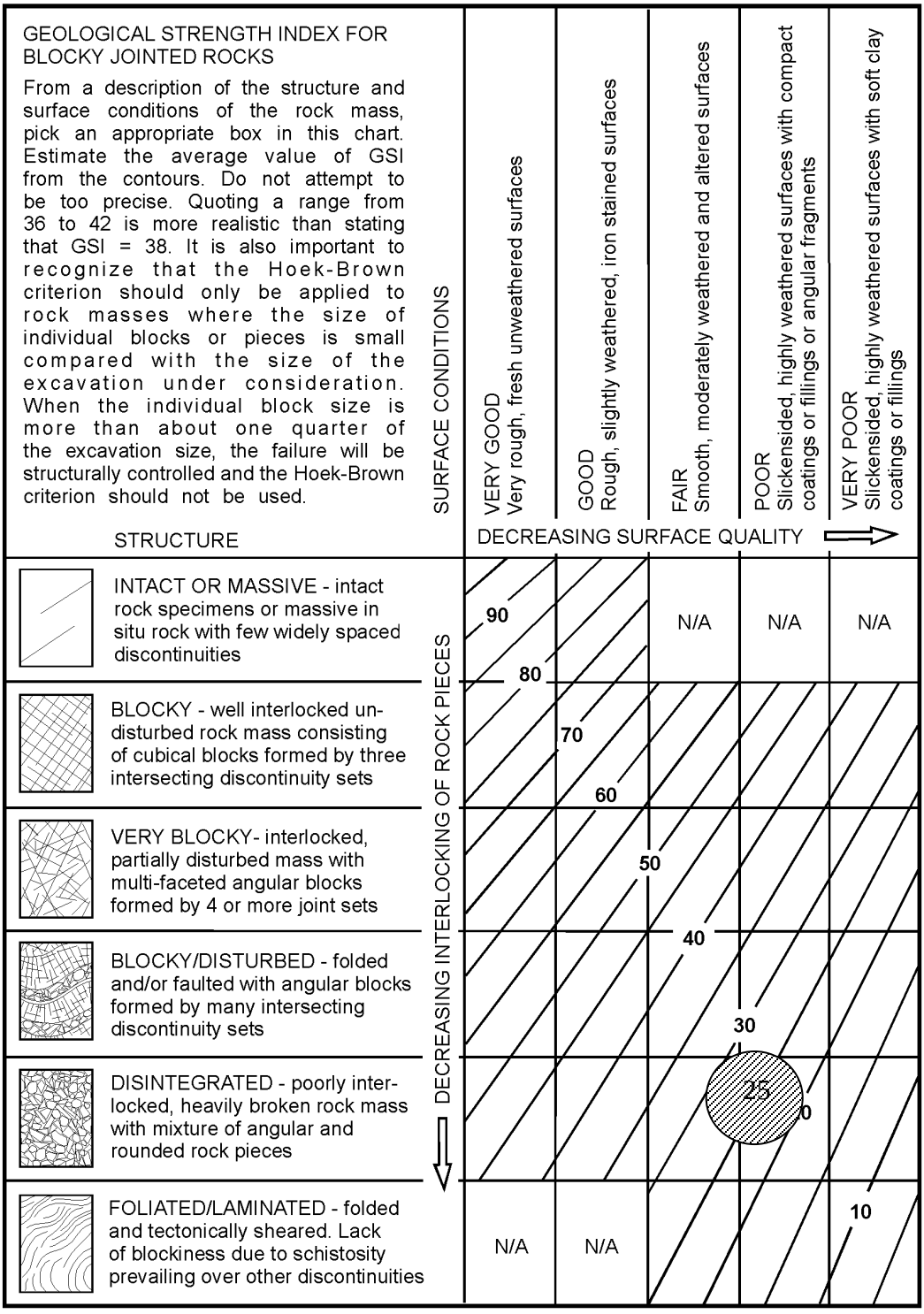


Figure 15: Estimate of Geological Strength Index GSI based on geological descriptions.
```

```

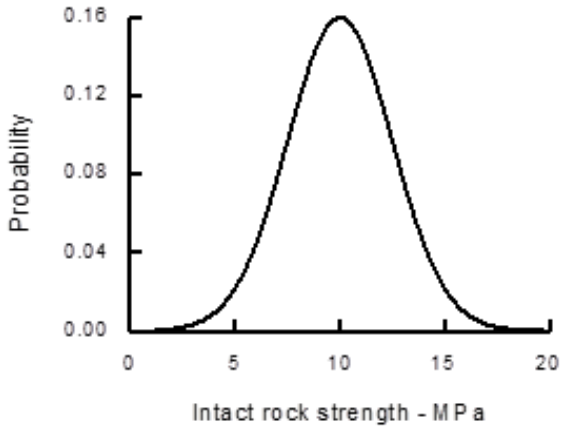


$\sigma_{ci}$ - Mean 10 MPa, Stdev 2.5 MPa

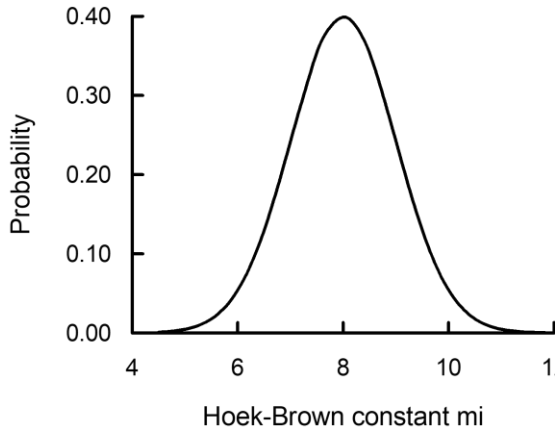


$m_i$ – Mean 8, Stdev 1

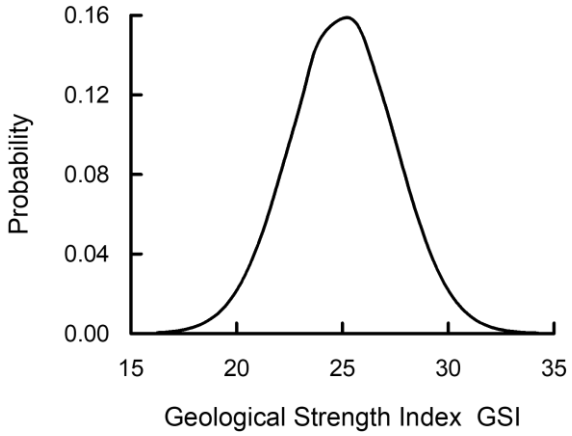


*GSI* – Mean 25, Stdev 2.5

Figure 16: Assumed normal distributions for input parameters.

Note that where software programs will accept input in terms of the Hoek-Brown criterion directly, it is preferable to use this input rather than estimates of Mohr Coulomb parameters c and ϕ given by equations 11 and 12 on page 14. This eliminates the uncertainty associated with estimating equivalent Mohr-Coulomb parameters, as described above, and allows the program to compute the conditions for failure at each point directly from the curvilinear Hoek-Brown relationship. In addition, the input parameters for the Hoek-Brown criterion ($m_i$, s, and a) are independent variables and can be treated as such in any probabilistic analysis. On the other hand, the Mohr Coulomb c and ϕ parameters are correlated, which results in an additional complication in probabilistic analyses.
```

```

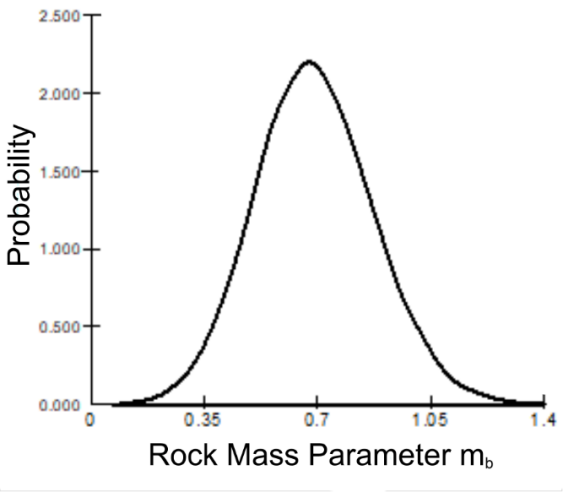


$m_b$ - Mean 0.689, Stdev 0.183

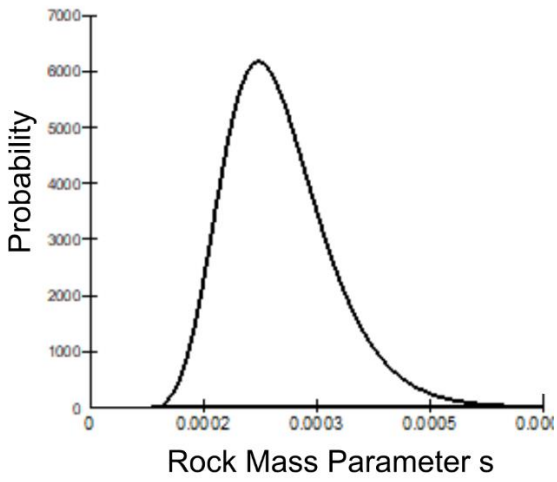


*s* – Mean 0.00025, Stdev 0.00007

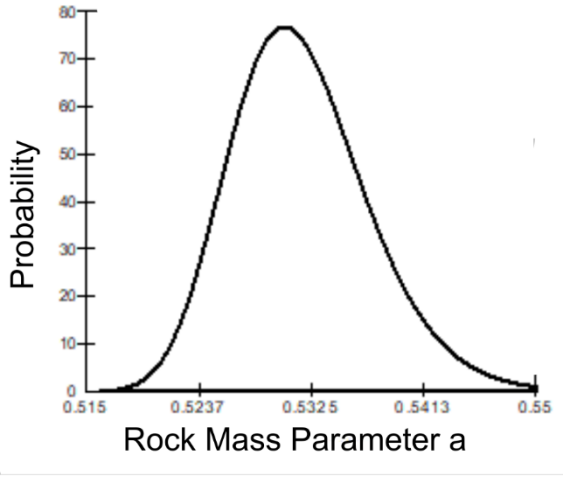


*a* – Mean 0.532, Stdev 0.00535

Figure 17: Calculated distributions for rock mass parameters.

Based on the three normal distributions for GSI, $\sigma_{ci}$ and $m_i$ given in Figure 16, distributions for the rock mass parameters $m_b$, s and a can be determined by a variety of methods. One of the simplest is to use a Monte Carlo simulation in which the distributions given in Figure 12 are used as input for equations 6, 7 and 8 to determine distributions for mi, s and a. The results of such an analysis, using the Excel add-in @RISK (available from www.palisade.com), are given in Figure 17.
```

```

**Slope stability calculation**

To assess the impact of the variation in rock mass parameters, illustrated in Figures 16 and 17, a calculation of the factor of safety for a homogeneous slope was carried out using Bishop's circular failure analysis in the program SLIDE (available from www.rocscience.com). The geometry of the slope and the phreatic surface are shown in Figure 18. The probabilistic option offered by the program was used and the rock mass properties were input as follows:

| Property | Distribution | Mean | Std. dev. | Min* | Max* |
|---|---|---|---|---|---|
| $m_b$ | Normal | 0.6894 | 0.1832 | 0.0086 | 1.44 |
| $s$ | Lognormal | 0.0002498 | 0.0000707 | 0.0000886 | 0.000704 |
| $a$ | Normal | 0.5317 | 0.00535 | 0.5171 | 0.5579 |
| $\sigma_{ci}$ | Normal | 10000 kPa | 2500 kPa | 1000 kPa | 20000 kPa |
| Unit weight γ | | 23 kN/m$^3$ | | | |

* Note that, in SLIDE, these values are input as relative proportions of the mean value and not as the absolute values shown here.

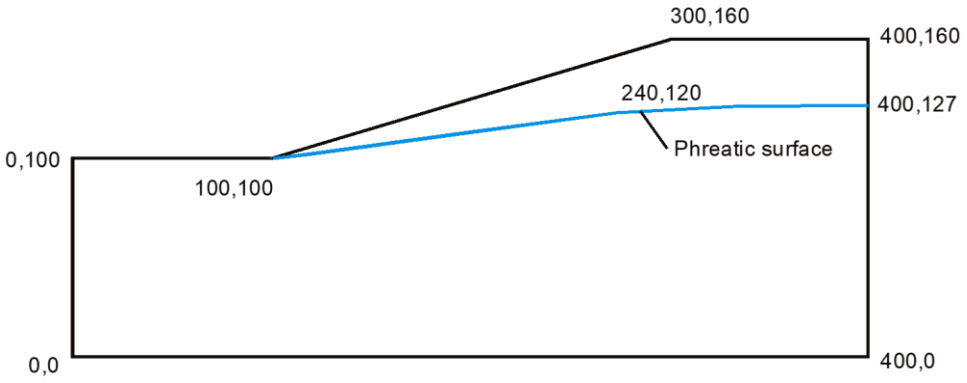


Figure 18: Slope and phreatic surface geometry for a homogeneous slope**.**

The distribution of the calculated factor of safety is shown in Figure 19 and it was found that this is best represented by a beta distribution with a mean value of 2.998, a standard deviation of 0.385, a minimum value of 1.207 and a maximum value of 4.107. There is zero probability of failure for this slope as indicated by the minimum factor of safety of 1.207. All critical failure surface exit at the toe of the slope.
```

```

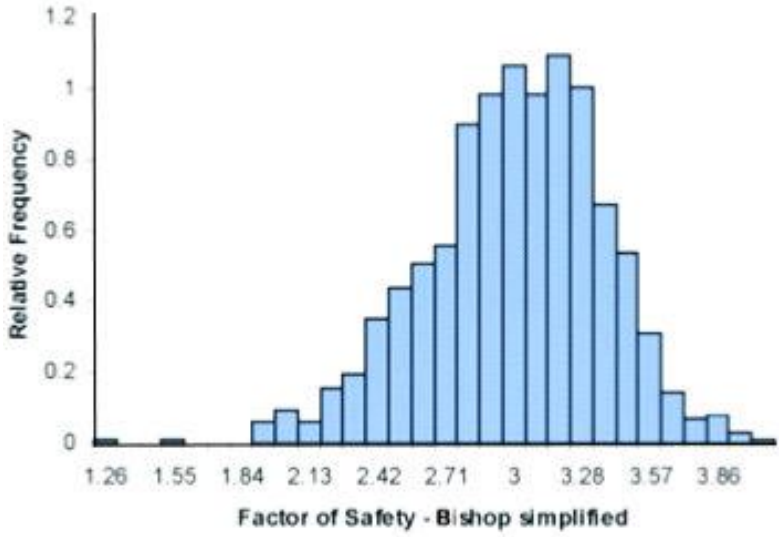


Figure 19: Distribution of factors of safety for the slope shown in Figure 18 from a probabilistic analysis using the program SLIDE.

Consider a circular tunnel, illustrated in Figure 20, with a radius $r_o$ in a stress field in which the horizontal and vertical stresses are both $p_o$. If the stresses are high enough, a 'plastic' zone of damaged rock of radius $r_p$ surrounds the tunnel. A uniform support pressure $p_i$ is provided around the perimeter of the tunnel.

A probabilistic analysis of the behaviour of this tunnel was carried out using the program RocSupport (available from www.rocscience.com) with the following input parameters:

| Property | Distribution | Mean | Std. dev. | Min* | Max* |
|---|---|---|---|---|---|
| Tunnel radius $r_o$ | | 5 m | | | |
| In situ stress $p_o$ | | 2.5 MPa | | | |
| $m_b$ | Normal | 0.6894 | 0.1832 | 0.0086 | 1.44 |
| $s$ | Lognormal | 0.0002498 | 0.0000707 | 0.0000886 | 0.000704 |
| $a$ | Normal | 0.5317 | 0.00535 | 0.5171 | 0.5579 |
| $\sigma_{ci}$ | Normal | 10 MPa | 2.5 MPa | 1 MPa | 20 MPa |
| $E$ | | 1050 MPa | | | |

* Note that, in RocSupport, these values are input as values relative to the mean value and not as the absolute values shown above.
```

```

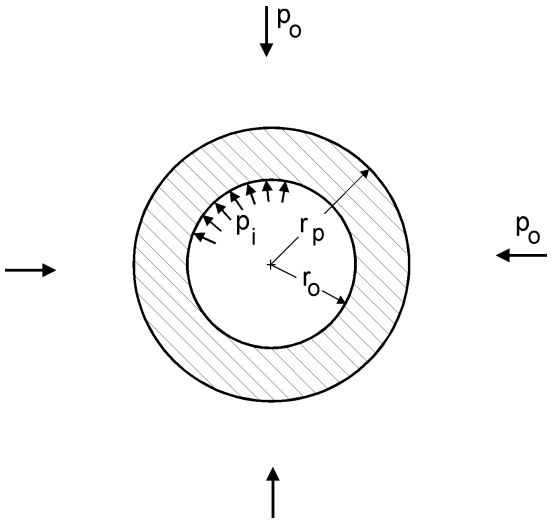


Figure 20: Development of a plastic zone around a circular tunnel in a hydrostatic stress field.

The resulting characteristic curve or support interaction diagram is presented in Figure 21. This diagram shown the tunnel wall displacements induced by progressive failure of the rock mass surrounding the tunnel as the face advances. The support is provided by a 5 cm shotcrete layer with 15 cm wide flange steel ribs spaced 1 m apart. The support is assumed to be installed 2 m behind the face after a wall displacement of 25 mm or a tunnel convergence of 50 mm has occurred. At this stage the shotcrete is assigned a 3-day compressive strength of 11 MPa.

The Factor of Safety of the support system is defined by the ratio of support capacity to demand as defined in Figure 21. The capacity of the shotcrete and steel set support is 0.4 MPa and it can accommodate a tunnel convergence of approximately 30 mm. As can be seen from Figure 21, the mobilised support pressure at equilibrium (where the characteristic curve and the support reaction curves cross) is approximately 0.15 MPa. This gives a first deterministic estimate of the Factor of Safety as 2.7.

The probabilistic analysis of the factor of safety yields the histogram shown in Figure 22. A Beta distribution is found to give the best fit to this histogram and the mean Factor of Safety is 2.73, the standard deviation is 0.46, the minimum is 2.23 and the maximum is 9.57.

This analysis assumes that the tunnel is circular, the rock mass is homogeneous and isotropic, the in-situ stresses are equal in all directions and the support is placed as a closed circular ring. These assumptions are seldom valid for actual tunnelling conditions and hence the analysis described above should only be used as a first rough approximation in design. Where the analysis indicates that tunnel stability is likely to be a problem, it is essential that a more detailed numerical analysis, considering actual tunnel geometry and rock mass conditions, should be carried out.
```

```

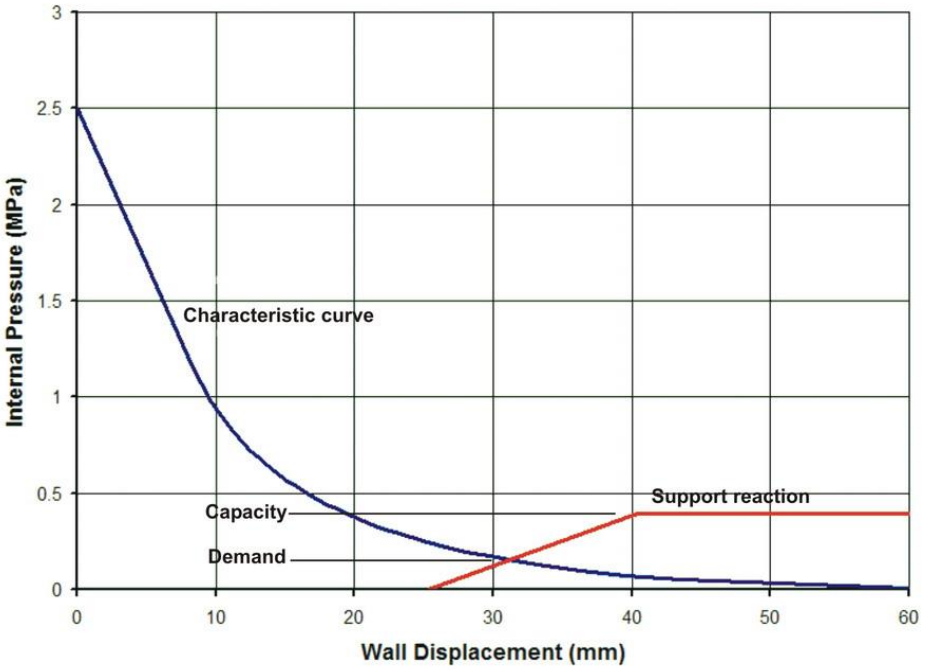


Figure 21: Rock support interaction diagram for a 10 m diameter tunnel subjected to a uniform in situ stress of 2.5 MPa.

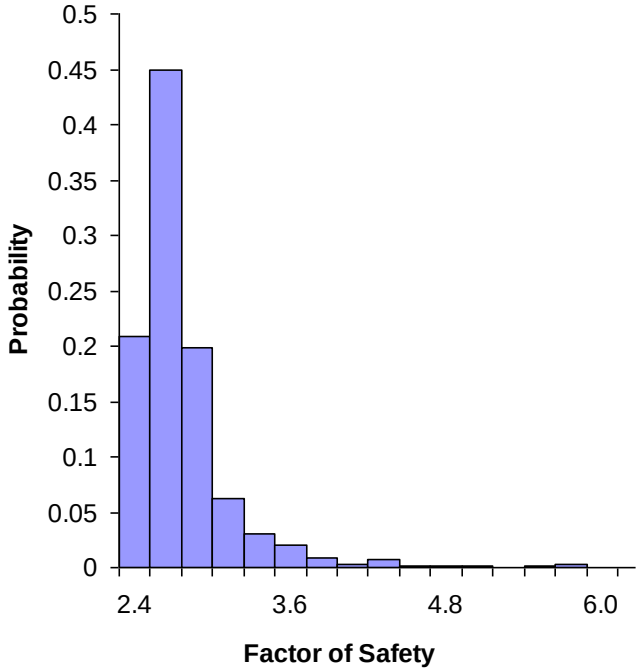


Figure 22: Distribution of the Factor of Safety for the tunnel discussed above.
```

```

## Conclusions

The uncertainty associated with estimating the properties of in situ rock masses has a significant impact or the design of slopes and excavations in rock. The examples that have been explored in this section show that, even when using the 'best' estimates currently available, the ranges of calculated factors of safety are uncomfortably large. These ranges become alarmingly large when poor site investigation techniques and inadequate laboratory procedures are used.

Given the inherent difficulty of assigning reliable numerical values to rock mass characteristics, it is unlikely that 'accurate' methods for estimating rock mass properties will be developed in the foreseeable future. Consequently, the user of the Hoek-Brown procedure or of any other equivalent procedure for estimating rock mass properties should not assume that the calculations produce unique reliable numbers. The simple techniques described in this section can be used to explore the possible range of values and the impact of these variations on engineering design.

## Practical examples of rock mass property estimates

The following examples are presented to illustrate the range of rock mass properties that can be encountered in the field and to give the reader some insight of how the estimation of rock mass properties was tackled in several actual projects.

### *Massive weak rock*

Karzulovic and Diaz (1994) have described the results of a program of triaxial tests on a cemented breccia known as Braden Breccia from the El Teniente mine in Chile. To design underground openings in this rock, attempts were made to classify the rock mass in accordance with Bieniawski's RMR system. However, as illustrated in Figure 23, this rock mass has very few discontinuities and so assigning realistic numbers to terms depending upon joint spacing and condition proved to be very difficult. Finally, it was decided to treat the rock mass as a weak but homogeneous 'almost intact' rock, like a weak concrete, and to determine its properties by means of triaxial tests on large diameter specimens.

A series of triaxial tests was carried out on 100 mm diameter core samples, illustrated in Figure 24. The results of these tests were analysed by means of the regression analysis using the program RocLab. Back analysis of the behaviour of underground openings in this rock indicate that the in-situ GSI value is approximately 75. From RocLab the following parameters were obtained:
```

```

| | | | | | |
|---|---|---|---|---|---|
| Intact rock strength | $\sigma_{ci}$ | 51 MPa | Hoek-Brown constant | $m_b$ | 6.675 |
| Hoek-Brown constant | $m_i$ | 16.3 | Hoek-Brown constant | $s$ | 0.062 |
| Geological Strength Index | *GSI* | 75 | Hoek-Brown constant | $a$ | 0.501 |
| | | | Deformation modulus | $E_m$ | 15000 MPa |

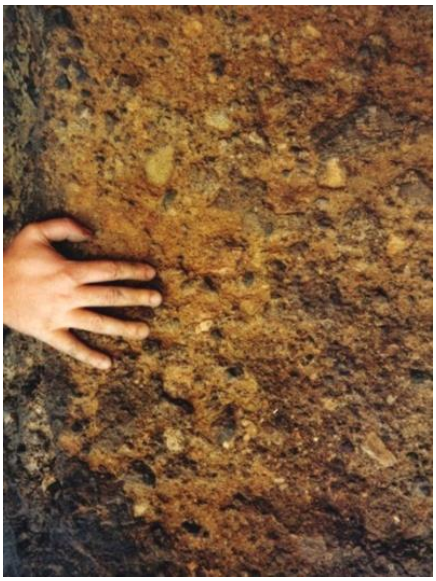

Figure 23: Braden Breccia at El Teniente Mine in Chile. This rock is a cemented breccia with practically no joints. It was dealt with in a manner like weak concrete and tests were carried out on 100 mm diameter specimens illustrated in Figure 24.

Figure 24. 100 mm diameter by 200 mm long specimens of Braden Breccia from the El Teniente mine in Chile.
```

```

***Massive strong rock masses***

The Rio Grande Pumped Storage Project in Argentina includes a large underground powerhouse, a surge control complex and a 6 km long tailrace tunnel. The rock mass surrounding these excavations is massive gneiss with very few joints. A typical core from this rock mass is illustrated in Figure 25. The appearance of the rock at the surface was illustrated earlier in Figure 8, which shows a cutting for the dam spillway.

Figure 25: Excellent quality core with very few discontinuities from the massive gneiss of the Rio Grande project in Argentina.

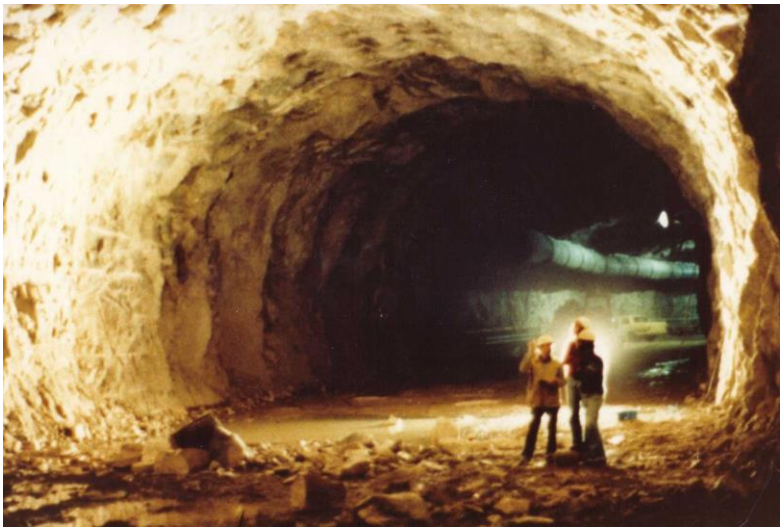

Figure 26: Top heading of the 12 m span, 18 m high tailrace tunnel for the Rio Grande Pumped Storage Project.
```

```

The rock mass can be described as BLOCKY/VERY GOOD and the GSI value, from Figure 6, is 75. Typical characteristics for the rock mass are as follows:

| | | | | | |
|---|---|---|---|---|---|
| Intact rock strength | $\sigma_{ci}$ | 110 MPa | Hoek-Brown constant | $m_b$ | 11.46 |
| Hoek-Brown constant | $m_i$ | 28 | Hoek-Brown constant | $s$ | 0.062 |
| Geological Strength Index | *GSI* | 75 | Constant | $a$ | 0.501 |
| | | | Deformation modulus | $E_m$ | 45000 MPa |

Figure 26 illustrates the 8 m high 12 m span top heading for the tailrace tunnel. The final tunnel height of 18 m was achieved by blasting two 5 m high benches. The top heading was excavated by full-face drill and blast and, because of the excellent quality of the rock mass and the tight control on blasting quality, most of the top heading did not require any support.

Details of this project are to be found in Moretto et al (1993). Hammett and Hoek (1981) have described the design of the support system for the 25 m span underground powerhouse in which a few structurally controlled wedges were identified and stabilised during excavation. This cavern has performed for more than 40 years without stability problems.

***Average quality rock mass***

The partially excavated powerhouse cavern in the Nathpa Jhakri Hydroelectric project in Himachel Pradesh, India, is illustrated in Figure 26. The rock is a jointed quartz mica schist, which has been extensively evaluated by the Geological Survey of India as described by Jalote et al (1996). An average GSI value of 65 was chosen to estimate the rock mass properties which were used for the cavern support design. Additional support, installed on the instructions of the engineers, was placed in weaker rock zones.

The assumed rock mass properties are as follows:

| | | | | | |
|---|---|---|---|---|---|
| Intact rock strength | $\sigma_{ci}$ | 30 MPa | Hoek-Brown constant | $m_b$ | 4.3 |
| Hoek-Brown constant | $m_i$ | 15 | Hoek-Brown constant | $s$ | 0.02 |
| Geological Strength Index | *GSI* | 65 | Constant | $a$ | 0.5 |
| | | | Deformation modulus | $E_m$ | 10000 MPa |
```

```

Two- and three-dimensional stress analyses of the nine stages used to excavate the cavern were carried out to determine the extent of potential rock mass failure and to provide guidance in the design of the support system. An isometric view of one of the three-dimensional models is given in Figure 27.

Figure 26: Partially completed 20 m span, 42.5 m high underground powerhouse cavern of the Nathpa Jhakri Hydroelectric Project in Himachel Pradesh, India. The cavern is approximately 300 m below the surface.

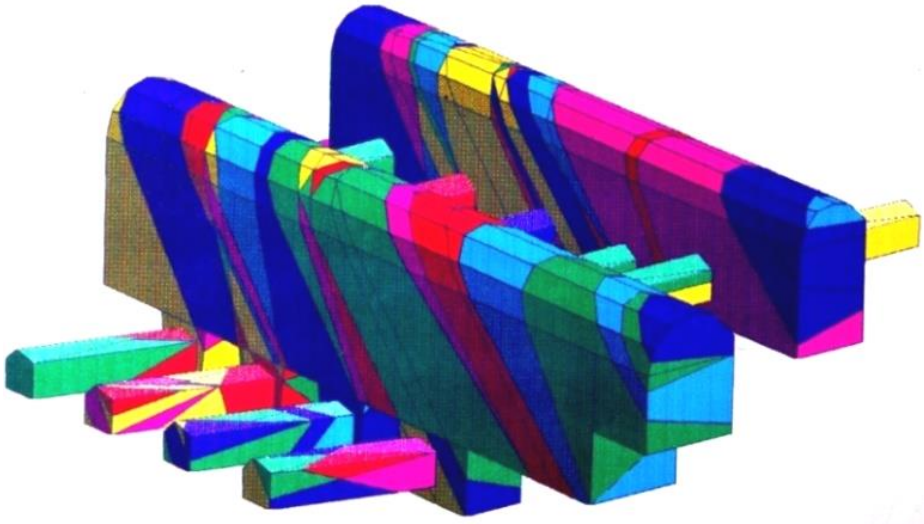

Figure 27: Isometric view of the 3DEC model of the underground powerhouse cavern and the transformer gallery of the Nathpa Jhakri Hydroelectric Project, analysed by Dr. B. Dasgupta.
```

```

The support for the powerhouse cavern consists of rockbolts and mesh reinforced shotcrete. Alternating 6 and 8 m long 32 mm diameter bolts on 1 x 1 m and 1.5 x 1.5 m centres are used in the arch. Alternating 9 and 7.5 m long 32 mm diameter bolts were used in the upper and lower sidewalls with alternating 9 and 11 m long 32 mm rockbolts in the centre of the sidewalls, all at a grid spacing of 1.5 m. Shotcrete consists of two 50 mm thick layers of plain shotcrete with an interbedded layer of weldmesh. The support provided by the shotcrete was not included in the support design analysis, which relies upon the rockbolts to provide all the support required.

In the headrace tunnel, some zones of sheared quartz mica schist were encountered, which resulted in large displacements as illustrated in Figure 28 This is a common problem in hard rock tunnelling where the excavation sequence and support system have been designed for 'average' rock mass conditions. Unless very rapid changes in the length of blast rounds and the installed support are made when an abrupt change to poor rock conditions occurs, for example when a fault is encountered, problems with controlling tunnel deformation can arise.

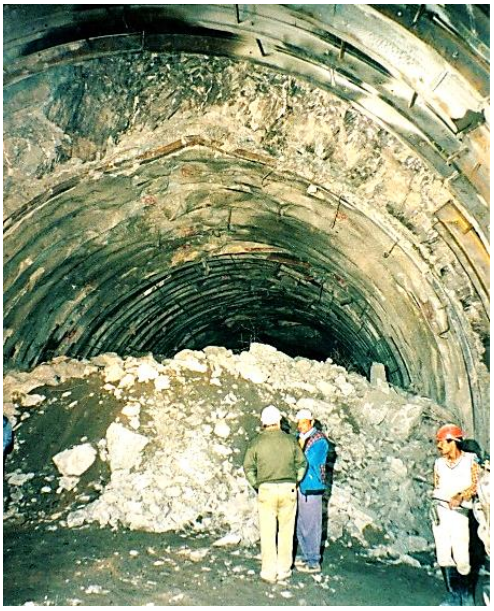

Figure 28: Large displacements in the top heading of the headrace tunnel of the Nathpa Jhakri Hydroelectric project. Displacements are the result of deteriorating rock mass quality when tunnelling through a fault zone.

The only effective way to anticipate this type of problem is to probe ahead of the advancing face. Typically, a long probe hole is percussion drilled during a maintenance shift and the penetration rate, return water flow and chippings are constantly monitored during drilling. Where significant problems are indicated by this percussion drilling, one or two diamond-drilled holes may be required to investigate these problems in more detail. In some special cases, the use of a pilot tunnel may be more effective in that it permits the ground properties to be defined more accurately than is possible with probe hole drilling. In addition, pilot tunnels allow pre-drainage and pre-reinforcement of the rock ahead of the development of the full excavation profile.
```

```

***Poor quality rock mass at shallow depth***

Kavvadas et al (1996) have described some of the geotechnical issues associated with the construction of 18 km of tunnels and the 21 underground stations of the Athens Metro. These excavations are all shallow with typical depths to tunnel crown of between 15 and 20 m. The principal problem is one of surface subsidence rather than failure of the rock mass surrounding the openings.

The rock mass is locally known as Athenian schist which is a term used to describe a sequence of Upper Cretaceous flysch-type sediments including thinly bedded clayey and calcareous sandstones, siltstones (greywackes), slates, shales, and limestones. During the Eocene, the Athenian schist formations were subjected to intense folding and thrusting. Later extensive faulting caused extensional fracturing and widespread weathering and alteration of the deposits.

The GSI values range from approximately 15 to 45. The higher values correspond to the intercalated layers of sandstones and limestones, which can be described as BLOCKY/DISTURBED and POOR (Figure 6). The completely decomposed schist can be described as DISINTEGRATED and VERY POOR and has GSI values ranging from 15 to 20. Rock mass properties for the completely decomposed schist, using a GSI value of 20, are as follows:

| | | | | | |
|---|---|---|---|---|---|
| Intact rock strength - MPa | $\sigma_{ci}$ | 5-10 | Hoek-Brown constant | $m_b$ | 0.55 |
| Hoek-Brown constant | $m_i$ | 9.6 | Hoek-Brown constant | $s$ | 0.0001 |
| Geological Strength Index | *GSI* | 20 | Hoek-Brown constant | $a$ | 0.544 |
| | | | Deformation modulus | $E_m$ | 600 MPa |

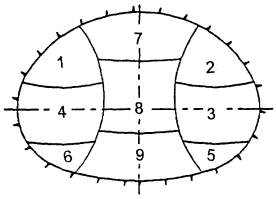


Figure 29: Twin side drift and central pillar excavation method. Temporary support consists of double wire mesh reinforced 250 - 300 mm thick shotcrete shells with embedded lattice girders or HEB 160 steel sets at 0.75 - 1 m spacing.

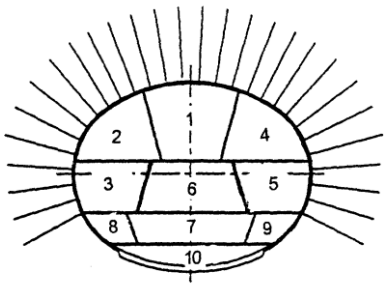


Figure 30: Top heading and bench method of excavation. Temporary support consists of a 200 mm thick shotcrete shell with 4 and 6 m long untensioned grouted rockbolts at 1.0 - 1.5 m spacing.
```

```

The Academia, Syntagma, Omonia and Olympion stations were constructed using the New Austrian Tunnelling Method twin side drift and central pillar method as illustrated in Figure 29. The more conventional top heading and bench method, illustrated in Figure 30, was used for the excavation of the Ambelokipi station. These stations are all 16.5 m wide and 12.7 m high. The appearance of the rock mass in one of the Olympion station side drift excavations is illustrated in Figure 31.

Figure 31: Appearance of the very poor-quality Athenian Schist at the face of the side heading illustrated in Figure 29.

Numerical analyses of the two excavation methods showed that the twin side drift method resulted in slightly less rock mass failure in the crown of the excavation. However, the final surface displacements induced by the two excavation methods were practically identical.

Maximum vertical displacements of the surface above the centreline of the Omonia station amounted to 51 mm. Of this, 28 mm occurred during the excavation of the side drifts, 14 mm during the removal of the central pillar and a further 9 mm occurred as a time dependent settlement after completion of the excavation. According to Kavvadas et al (1996), this time dependent settlement is due to the dissipation of excess pore water pressures which were built up during excavation. In the case of the Omonia station, the excavation of recesses towards the eastern end of the station, after completion of the station excavation, added a further 10 to 12 mm of vertical surface displacement at this end of the station.

***Poor quality rock mass under high stress***

The Yacambú Quibor tunnel in Venezuela is one of the most difficult tunnels in the world. This 25 km long water supply tunnel, through the Andes, is being excavated in sandstones and phyllites at depths of up to 1200 m below surface. The graphitic phyllite is a very poor-quality rock and gives rise to serious squeezing problems which, without adequate support, result in complete closure of the tunnel. A full-face tunnel-boring machine was destroyed in 1979 when trapped by squeezing ground conditions.

The graphitic phyllite has an average unconfined compressive strength of about 50 MPa and the estimated GSI value is about 25 (see Figures 2 and 3). Typical rock mass properties are as follows:
```

```

| | | | | | |
|---|---|---|---|---|---|
| Intact rock strength MPa | σci | 50 | Hoek-Brown constant | $m_b$ | 0.481 |
| Hoek-Brown constant | mi | 10 | Hoek-Brown constant | $s$ | 0.0002 |
| Geological Strength Index | GSI | 25 | Hoek-Brown constant | $a$ | 0.53 |
| | | | Deformation modulus MPa | $E_m$ | 1000 |

Various support methods were used on this tunnel and only one will be considered here. This was a trial section of tunnel, at a depth of approximately 600 m, constructed in 1989. The support of the 5.5 m span tunnel was by means of a complete ring of 5 m long, 32 mm diameter untensioned grouted dowels with a 200 mm thick shell of reinforced shotcrete. This support system proved to be very effective but was later abandoned in favour of yielding steel sets (steel sets with sliding joints) because of construction schedule considerations. In fact, at a depth of 1200 m below surface (2004-2006) it is doubtful if the rockbolts would have been effective because of the very large deformations that could only be accommodated by steel sets with sliding joints.

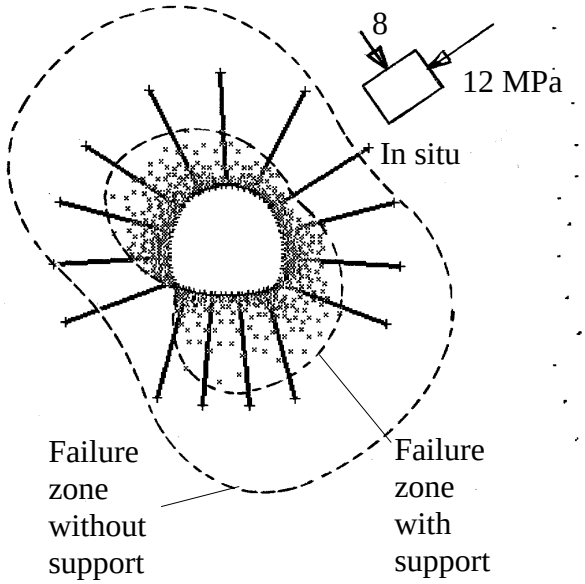


Figure 33: Results of a numerical analysis of the failure of the rock mass surrounding the Yacambu-Quibor tunnel when excavated in graphitic phyllite at a depth of approximately 600 m below surface.

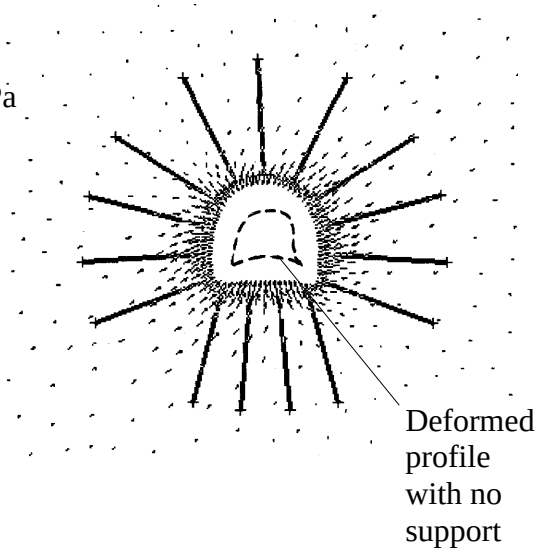


Figure 34: Displacements in the rock mass surrounding the Yacambu-Quibor tunnel. The maximum calculated displacement is 258 mm with no support and 106 mm with support.
```

```

Examples of the results of a typical numerical stress analysis of this trial section, carried out using the program PHASE2, are given in Figures 33 and 34. Figure 33 shows the extent of failure, with and without support, while Figure 34 shows the displacements in the rock mass surrounding the tunnel. Note that the criteria used to judge the effectiveness of the support design are that the zone of failure surrounding the tunnel should lie within the envelope of the rockbolt support, the rockbolts should not be stressed to failure and the displacements should be of reasonable magnitude and should be uniformly distributed around the tunnel. All these objectives were achieved by the support system described earlier.

***Slope stability considerations***

When dealing with slope stability problems in rock masses, great care must be taken in attempting to apply the Hoek-Brown failure criterion, particularly for small, steep slopes. As illustrated in Figure 35, even rock masses that appear to be good candidates for the application of the criterion can suffer shallow structurally controlled failures under the very low stress conditions which exist in such slopes.

Figure 35: Structurally controlled failure in the face of a steep bench in a heavily jointed rock mass.
```

```

As a rule, when designing slopes in rock, the initial approach should always be to search for potential failures controlled by adverse structural conditions. These may take the form of planar failures on outward dipping features, wedge failures on intersecting features, toppling failures on inward dipping failures or complex failure modes involving all these processes. Only when the potential for structurally controlled failures has been eliminated, should consideration be given to treating the rock mass as an isotropic material as required by the Hoek-Brown failure criterion.

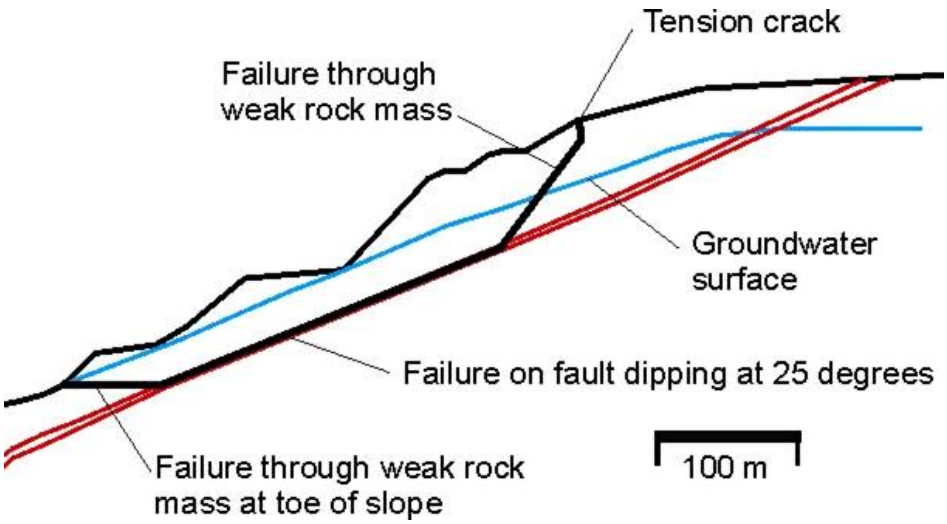


Figure 36: Complex slope failure controlled by an outward dipping basal fault and circular failure through the poor-quality rock mass overlying the toe of the slope.

Figure 36 illustrates a case in which the base of a slope failure is defined by an outward dipping fault that does not daylight at the toe of the slope. Circular failure through the poor-quality rock mass overlying the fault allows failure of the toe of the slope. Analysis of this problem was carried out by assigning the rock mass at the toe properties that had been determined by application of the Hoek-Brown criterion. A search for the critical failure surface was carried out utilising the program SLIDE which allows complex failure surfaces to be analysed and which includes facilities for the input of the Hoek-Brown failure criterion.
```

```

## References


Balmer, G. 1952. A general analytical solution for Mohr's envelope. *Am. Soc. Test. Mat*. 52, 1260-1271.

Bieniawski, Z.T. 1976. Rock mass classification in rock engineering. *In Exploration for rock engineering*, proc. of the symp., (ed. Z.T. Bieniawski) 1, 97-106. Cape Town: Balkema.

Bieniawski, Z.T. 1989. *Engineering rock mass classifications*. New York: Wiley.

Deere D.U. 1968. Chapter 1: Geological considerations. In *Rock Mechanics in Engineering Practice* (eds. Stagg K.G. and Zienkiewicz, O.C.), 1-20. London: John Wiley and Sons.

Franklin, J.A. and Hoek, E. 1970. Developments in triaxial testing equipment. *Rock Mech*. 2, 223-228. Berlin: Springer-Verlag.

Hammett, R.D. and Hoek, E. 1981. Design of large underground caverns for hydro-electric projects, with reference to structurally controlled failure mechanisms. *Proc. American Soc. Civil Engrs. Int. Conf. on recent developments in geotechnical engineering for hydro projects*. 192-206. New York: ASCE

Hoek, E. 1983. Strength of jointed rock masses, 23rd. Rankine Lecture. *Géotechnique* 33(3), 187-223.

Hoek, E. 1994. Strength of rock and rock masses, *ISRM News Journal*, 2(2), 4-16.

Hoek, E. and Brown, E.T. 1980a. *Underground excavations in rock*. London: Instn Min. Metall.

Hoek, E. and Brown, E.T. 1980b. Empirical strength criterion for rock masses. J. *Geotech. Engng Div., ASCE* 106(GT9), 1013-1035.

Hoek, E. and Brown, E.T. 1988. The Hoek-Brown failure criterion - a 1988 update. In Rock engineering for underground excavations, *proc. 15th Canadian rock mech. symp.,* (ed. J.C. Curran), 31-38. Toronto: Dept. Civ. Eng University of Toronto.

Hoek, E., Marinos, P. and Benissi, M. 1998. Applicability of the Geological Strength Index (GSI) classification for very weak and sheared rock masses. The case of the Athens Schist Formation. *Bull. Engng. Geol. Env*. 57(2), 151-160.

Hoek, E. and Brown, E.T. 1997. Practical estimates or rock mass strength. *Int. J. Rock Mech. Mining Sci. & Geomech. Abstr*. 34(8), 1165-1186.

Hoek, E., Kaiser, P.K. and Bawden. W.F. 1995. *Support of underground excavations in hard rock*. Rotterdam: Balkema.

Hoek, E., Wood, D. and Shah, S. 1992. A modified Hoek-Brown criterion for jointed rock masses. *Proc. rock characterization, symp. Int. Soc. Rock Mech*.: Eurock '92, (ed. J.A. Hudson), 209-214. London: Brit. Geol. Soc.
```

```

Hoek E, Carranza-Torres CT, Corkum B. Hoek-Brown failure criterion-2002 edition. In: *Proceedings of the 5th North American Rock Mechanics Symp*., Toronto, Canada, 2002: 1: 267–73.

Hoek, E., Marinos, P., Marinos, V. 2005. Characterization and engineering properties of tectonically undisturbed but lithologically varied sedimentary rock masses. *Int. J. Rock Mech. Min. Sci.*, 42/2, 277-285.

Hoek, E and Diederichs, M. 2006. Empirical estimates of rock mass modulus. *Int. J Rock Mech. Min. Sci.*, 43, 203–215.

Hoek, E. and Brown, E.T. 2019. The Hoek-Brown criterion and GSI -2018 edition. *Journal of Rock Mechanics and Geotechnical Engineering*. 2019; 6(3): 445-463.

Karzulovic A. and Díaz, A.1994. Evaluación de las Propiedades Geomacánicas de la Brecha Braden en Mina El Teniente. *Proc. IV Congreso Sudamericano de Mecanica de Rocas*, Santiago 1, 39-47.

Kavvadas M., Hewison L.R., Lastaratos P.G., Seferoglou, C. and Michalis, I. 1996.Experience in the construction of the Athens Metro. *Proc. Int. symp. geotechnical aspects of underground construction in soft ground*. (Eds Mair R.J. and Taylor R.N.), 277-282. London: City University.

Jalote, P.M., Kumar A. and Kumar V. 1996. Geotechniques applied in the design of the machine hall cavern, Nathpa Jhakri Hydel Project, N.W. Himalaya, *India. J. Engng Geol*. (India) XXV(1-4), 181-192.

Marinos, P, and Hoek, E. 2001. Estimating the geotechnical properties of heterogeneous rock masses such as flysch. *Bull. Engng Geol. & the Environment (IAEG)*, 60, 85-92.

Marinos, P., Hoek, E., Marinos, V. 2006. Variability of the engineering properties of rock masses quantified by the geological strength index: the case of ophiolites with special emphasis on tunnelling. *Bull. Eng. Geol. Env*., 65/2, 129-142.

Moretto O., Sarra Pistone R.E. and Del Rio J.C. 1993. A case history in Argentina - Rock mechanics for underground works in the pumping storage development of Rio Grande No 1. In *Comprehensive Rock Engineering*. (Ed. Hudson, J.A.) 5, 159-192. Oxford: Pergamon.

Palmstrom A. and Singh R. 2001.The deformation modulus of rock masses: comparisons between in situ tests and indirect estimates. *Tunnelling and Underground Space Technology*. 16: 115-131.

Salcedo D.A.1983. Macizos Rocosos: Caracterización, Resistencia al Corte y Mecanismos de Rotura. *Proc. 25 Aniversario Conferencia Soc. Venezolana de Mecánica del Suelo e Ingeniería de Fundaciones*, Caracas. 143-172.
```

6. In situ and induced stresses

Introduction

Rock at depth is subjected to stresses resulting from the weight of the overlying strata and from locked in stresses of tectonic origin. When an opening is excavated in this rock, the stress field is locally disrupted, and a new set of stresses are induced in the rock surrounding the opening. Knowledge of the magnitudes and directions of these in situ and induced stresses is an essential component of underground excavation design since, in many cases, the strength of the rock is exceeded, and the resulting instability can have serious consequences on the behaviour of the excavations.

This chapter deals with the question of in situ stresses and with the stress changes that are induced when tunnels or caverns are excavated in stressed rock. Problems, associated with failure of the rock around underground openings and with the design of support for these openings, will be dealt with in later chapters.

The presentation which follows is intended to cover only those topics which are essential for the reader to know about when dealing with the analysis of stress induced instability and the design of support to stabilise the rock under these conditions.

In situ stresses

Consider an element of rock at a depth of 1,000 m below the surface. The weight of the vertical column of rock resting on this element is the product of the depth and the unit weight of the overlying rock mass (typically about 2.7 tonnes/m^3 or 0.027 MN/m^3). Hence, the vertical stress on the element is 2,700 tonnes/m^2 or 27 MPa. This stress is estimated from the simple relationship:

$$\sigma_v = \gamma z \qquad (1)$$

where σ_v is the vertical stress
γ is the unit weight of the overlying rock and
z is the depth below surface.

Measurements of vertical stress at various mining and civil engineering sites around the world confirm that this relationship is valid although, as illustrated in Figure 1, there is a significant amount of scatter in the measurements.

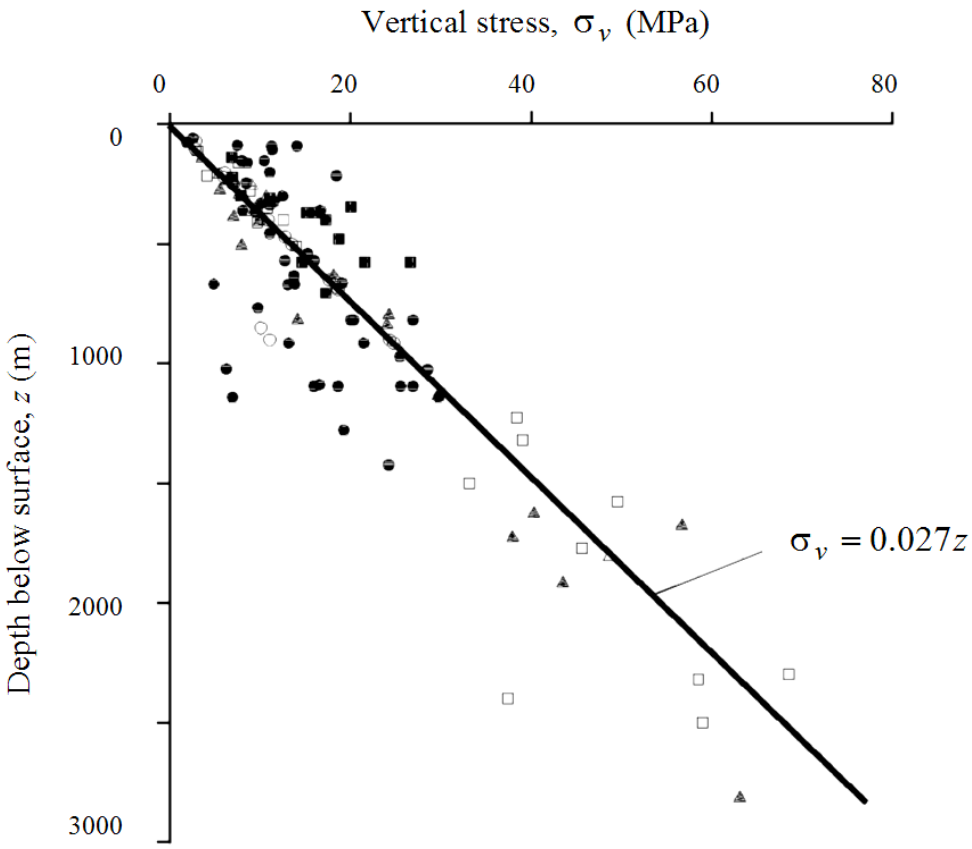

Figure 1: Vertical stress measurements from mining and civil engineering projects around the world (Brown and Hoek 1978).

The horizontal stresses acting on an element of rock at a depth z below the surface are much more difficult to estimate than the vertical stresses. Normally, the ratio of the average horizontal stress to the vertical stress is denoted by the letter k such that:

$$\sigma_h = k\sigma_v = k\,\gamma\,z \qquad (2)$$

Terzaghi and Richart (1952) suggested that, for a gravitationally loaded rock mass in which no lateral strain was permitted during formation of the overlying strata, the value of k is independent of depth and is given by $k = \nu/(1-\nu)$, where ν is the Poisson's ratio of the rock mass. This relationship was widely used in the early days of rock mechanics but as discussed below, it proved to be inaccurate and is seldom used today.

Measurements of horizontal stresses at civil and mining sites around the world show that the ratio k tends to be high at shallow depth and that it decreases with increasing depth (Brown and Hoek, 1978, Herget, 1988). To understand the reason for these horizontal stress variations, it is necessary to consider the problem on a much larger scale than that of a single site.

Sheorey (1994) developed an elasto-static thermal stress model of the earth. This model considers curvature of the crust and variation of elastic constants, density and thermal expansion coefficients through the crust and mantle. A detailed discussion on Sheorey's model is beyond the scope of this chapter, but he did provide a simplified equation which can be used for estimating the horizontal to vertical stress ratio *k*. This equation is:

$$k = 0.25 + 7E_h\left(0.001 + \frac{1}{z}\right) \qquad (3)$$

where z (m) is the depth below surface and E_h (GPa) is the average deformation modulus of the upper part of the earth's crust measured in a horizontal direction. This direction of measurement is important, particularly in layered sedimentary rocks, in which the deformation modulus may vary in different directions.

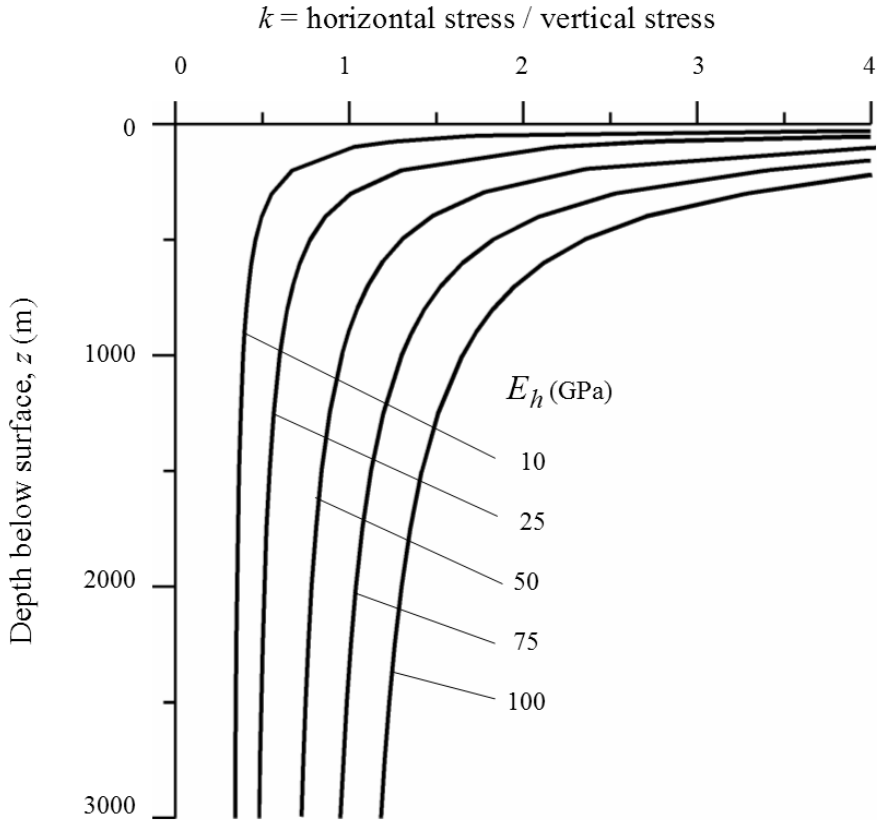

Figure 2: Ratio of horizontal to vertical stress for different deformation moduli based upon Sheorey's equation (Sheorey, 1994).

A plot of this equation is given in Figure 2 for a range of deformation moduli. The curves relating *k* with depth below surface *z* are like those published by Brown and Hoek (1978), Herget (1988) and others for measured in situ stresses. Hence, equation 3 is considered to provide a reasonable basis for estimating the value of *k*.

Sheorey's work does not explain the occurrence of measured vertical stresses that are higher than the calculated overburden pressure, the presence of very high horizontal stresses at some locations or why the two horizontal stresses are seldom equal. These differences are probably due to local topographic and geological features that cannot be accommodated in a large-scale model such as that proposed by Sheorey.

Where sensitivity studies have shown that the in-situ stresses are likely to have a significant influence on the behaviour of underground openings, it is recommended that the in-situ stresses should be measured. Suggestions for setting up a stress measuring programme are discussed later in this chapter.

The World stress map

The World Stress Map project, completed in July 1992, involved over 30 scientists from 18 countries and was carried out under the auspices of the International Lithosphere Project (Zoback, 1992). The aim of the project was to compile a global database of contemporary tectonic stress data. The World Stress Map (WSM) is now maintained and has been extended by the Geophysical Institute of Karlsruhe University as a research project of the Heidelberg Academy of Sciences and Humanities. The 2005 version of the map contains approximately 16,000 data sets and various versions of the map for the World, Europe, America, Africa, Asia and Australia can be downloaded from the Internet. The WSM is an open-access database that can be accessed at www.world-stress-map.org (Reinecker et al, 2005). The 2005 World Stress Map is reproduced in Figure 3 while a stress map for the Mediterranean is reproduced in Figure 4. These figures can be updated from www.world-stress-map.org.

The stress maps display the orientations of the maximum horizontal compressive stress. The length of the stress symbols represents the data quality, with A being the best quality. Quality A data are assumed to record the orientation of the maximum horizontal compressive stress to within 10°-15°, quality B data to within 15°-20°, and quality C data to within 25°. Quality D data are considered to give questionable tectonic stress orientations.

The 1992 version of the World Stress Map was derived mainly from geological observations on earthquake focal mechanisms, volcanic alignments, and fault slip interpretations. Less than 5% of the data was based upon hydraulic fracturing or overcoring measurements of the type commonly used in mining and civil engineering projects. In contrast, the 2005 version of the map includes a significantly greater number of observations from borehole breakouts, hydraulic fracturing, overcoring and borehole slotting.

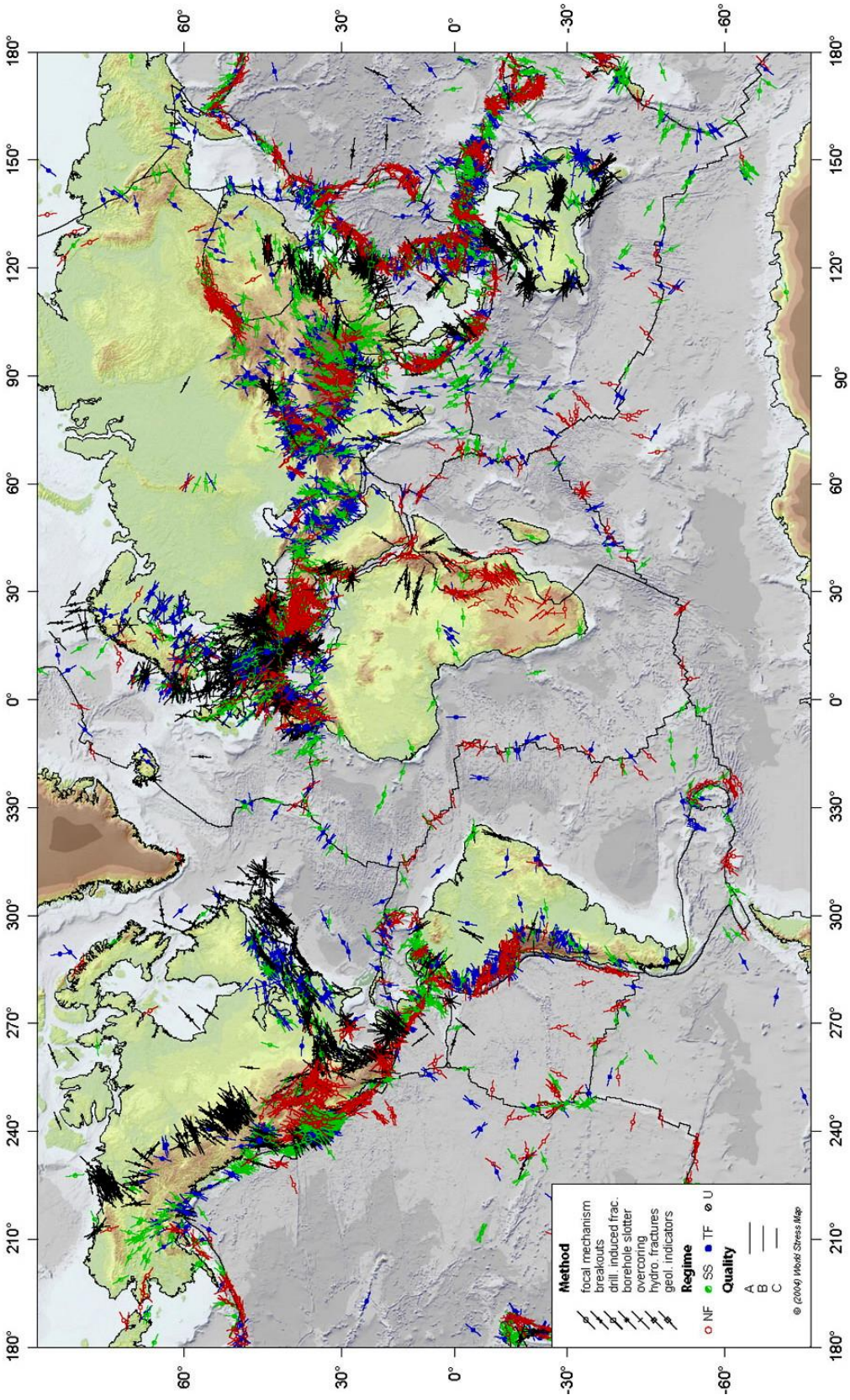

Figure 3: World stress map giving orientations of the maximum horizontal compressive stress.

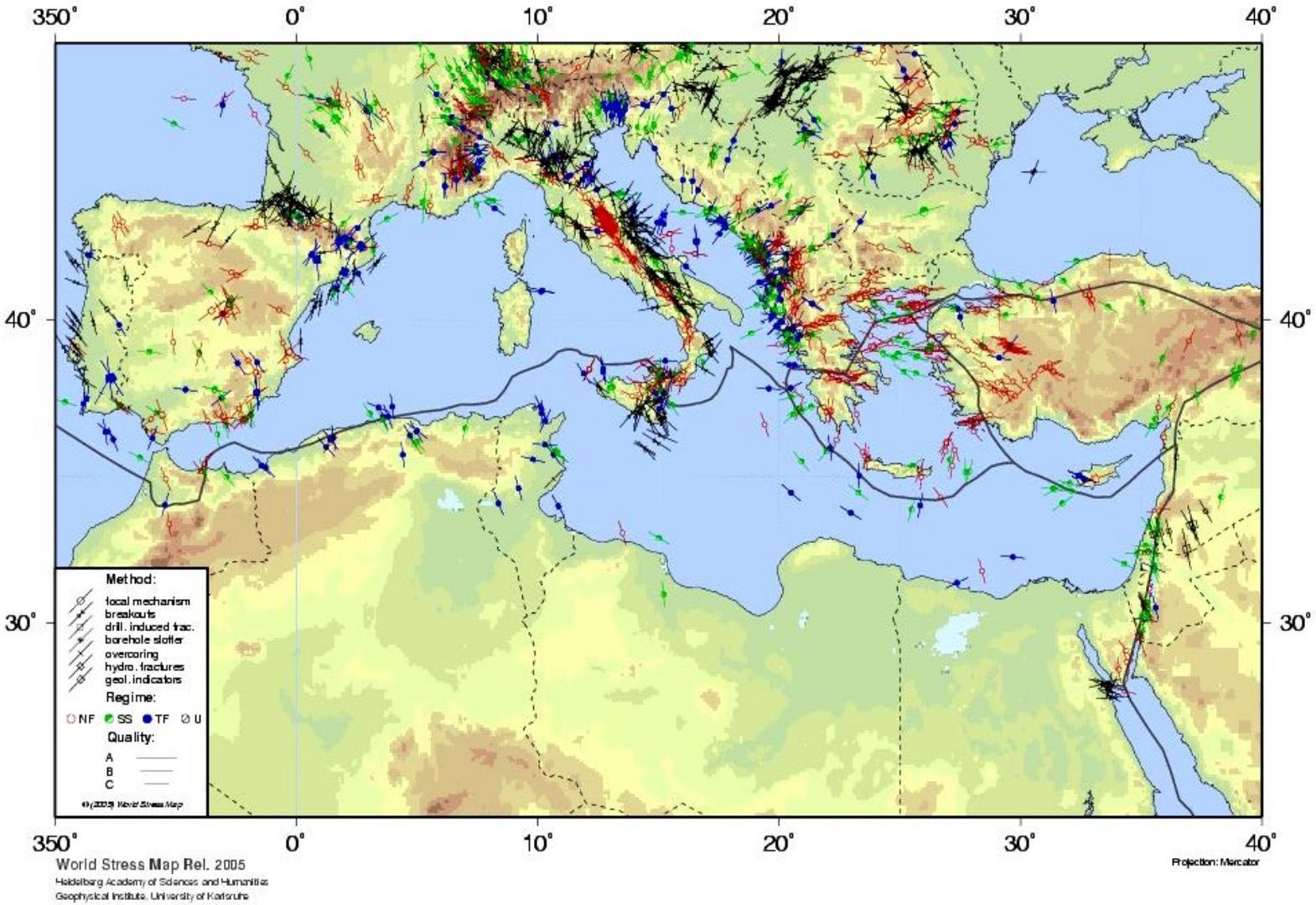

Figure 4: Stress map of the Mediterranean giving orientations of the maximum horizontal compressive stress.

In discussing hydraulic fracturing and overcoring stress measurements, Zoback (1992) has the following comments:

> 'Detailed hydraulic fracturing testing in a number of boreholes beginning very close to surface (10-20 m depth) has revealed marked changes in stress orientations and relative magnitudes with depth in the upper few hundred metres, possibly related to effects of nearby topography or a high degree of near surface fracturing.
>
> Included in the category of 'overcoring' stress measurements are a variety of stress or strain relief measurement techniques. These techniques involve a three-dimensional measurement of the strain relief in a body of rock when isolated from the surrounding rock volume; the three-dimensional stress tensor can subsequently be calculated with a knowledge of the complete compliance tensor of the rock. There are two primary drawbacks with this technique which restricts its usefulness as a tectonic stress indicator: measurements must be made near a free surface, and strain relief is determined over very small areas (a few square millimetres to square centimetres). Furthermore, near surface measurements (by far the most common) have been shown to be subject to effects of local topography, rock anisotropy, and natural fracturing (Engelder and Sbar, 1984). In addition, many of these measurements have been made for specific engineering applications (for example, dam site evaluation, mining work), places where topography, fracturing or nearby excavations could strongly perturb the regional stress field.'

Obviously, from a global or even a regional scale, the type of engineering stress measurements carried out in a mine or on a civil engineering site are not considered to be very reliable. Conversely, the World Stress Map versions presented in Figures 3 and 4 can only be used to give first order estimates of the stress directions which are likely to be encountered on a specific site. Since both stress directions and stress magnitudes are critically important in the design of underground excavations, it follows that a stress measuring program may be required in any major underground mining or civil engineering project.

Developing a stress measuring programme

Consider the example of a tunnel to be excavated at a depth of 1,000 m below surface in a hard rock environment. The depth of the tunnel is such that it is probable that in situ and induced stresses will be an important consideration in the design of the excavation. Typical steps that could be followed in the analysis of this problem are:

1. The World Stress Map for the area under consideration will give a good first indication of the possible complexity of the regional stress field and possible directions for the maximum horizontal compressive stress.

2. During preliminary design, the information presented in equations 1 and 3 can be used to obtain a first rough estimate of the vertical and average horizontal stress in the vicinity of the tunnel. For a depth of 1,000 m, these equations give the vertical stress σ_v = 27 MPa, the ratio k = 1.3 (for E_h = 75 GPa) and hence the average horizontal stress σ_h= 35.1 MPa. A preliminary analysis of the stresses induced around the proposed tunnel shows that

these induced stresses are likely to exceed the strength of the rock and that the question of stress measurement must be considered in more detail. Note that for many openings in strong rock at shallow depth, stress problems may not be significant, and the analysis need not proceed any further.

For this case, stress problems are important. A typical next step would be to search the literature to determine whether the results of in situ stress measurement programmes are available for mines or civil engineering projects within a radius of about 50 km of the site. With luck, a few stress measurement results will be available for the region in which the tunnel is located, and these results can be used to refine the analysis discussed above.

If the results of the analysis of induced stresses in the rock surrounding the proposed tunnel indicate that significant zones of rock failure are likely to develop, and that support costs are likely to be high, it is probably justifiable to set up a stress measurement project on the site. These measurements can be carried out in deep boreholes from the surface, using hydraulic fracturing techniques, or from underground access using overcoring methods. The choice of the method and the number of measurements to be carried out depends upon the urgency of the problem, the availability of underground access and the costs involved in the project. Note that very few project organisations have access to the equipment required to carry out a stress measurement project and, rather than purchase this equipment, it may be worth bringing in an organisation which has the equipment which specialises in such measurements.

3. Where regional tectonic features such as major faults are likely to be encountered, the in-situ stresses in the vicinity of the feature may be rotated with respect to the regional stress field. The stresses may be significantly different in magnitude from the values estimated from the general trends described above. These differences can be very important in the design of the openings and in the selection of support and, where it is suspected that this is likely to be the case, in situ stress measurements become an essential component of the overall design process.
4.

Analysis of induced stresses

When an underground opening is excavated into a stressed rock mass, the stresses in the vicinity of the new opening are re-distributed. Consider the example of the stresses induced in the rock surrounding a horizontal circular tunnel as illustrated in Figure 5, showing a vertical slice normal to the tunnel axis.

Before the tunnel is excavated, the in-situ stresses σ_v, σ_{h1} and σ_{h2} are uniformly distributed in the slice of rock under consideration. After removal of the rock from within the tunnel, the stresses in the immediate vicinity of the tunnel are changed and new stresses are induced. Three principal stresses σ_1, σ_2 and σ_3 acting on a typical element of rock are shown in Figure 5.

The convention used in rock engineering is that *compressive* stresses are always *positive,* and the three principal stresses are numbered such that σ_1 is the largest compressive stress and σ_3 is the smallest compressive stress or the largest tensile stress of the three.

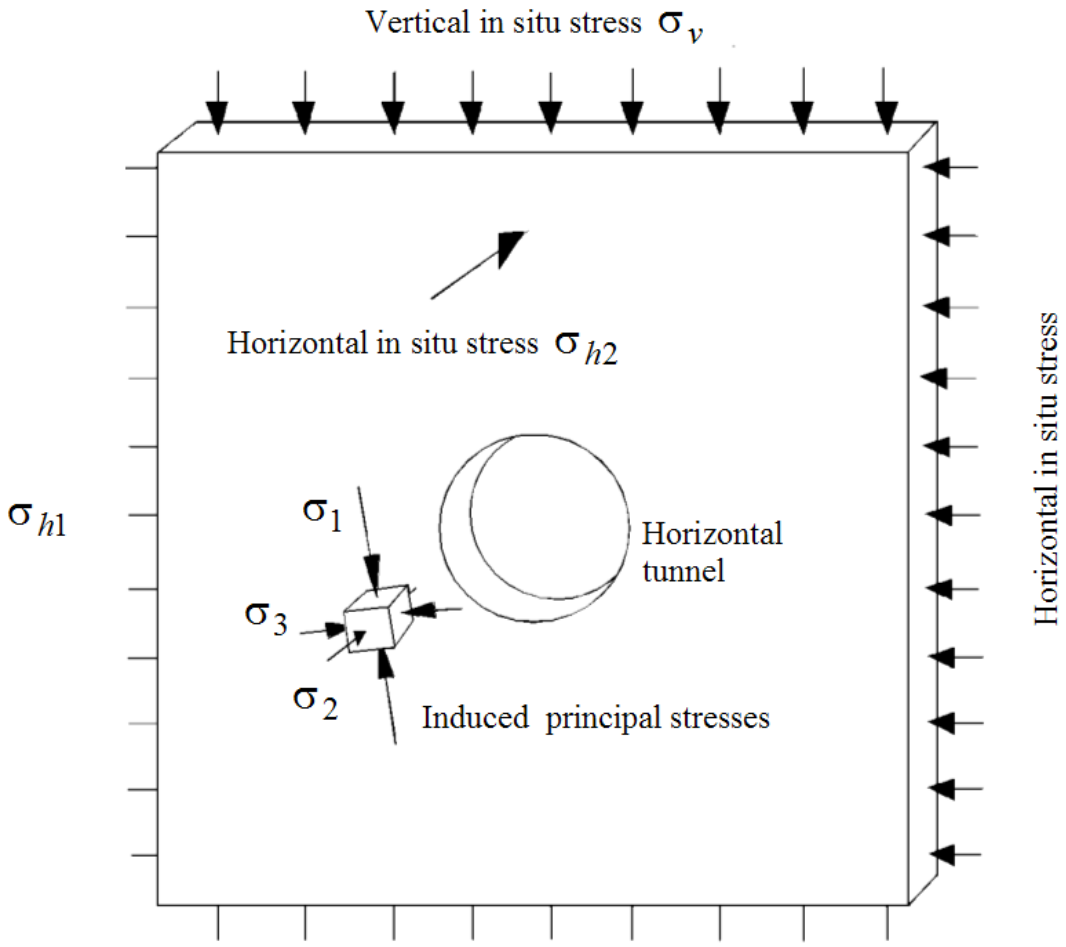

Figure 5: Illustration of principal stresses induced in an element of rock close to a horizontal tunnel subjected to a vertical in situ stress σ_v, a horizontal in situ stress σ_{h1} in a plane normal to the tunnel axis and a horizontal in situ stress σ_{h2} parallel to the tunnel axis.

The three principal stresses are mutually perpendicular, but they may be inclined to the direction of the applied in situ stress. This is evident in Figure 6 which shows the directions of the stresses in the rock surrounding a horizontal tunnel subjected to a horizontal in situ stress σ_{h1} equal to three times the vertical in situ stress σ_v. The longer bars in this figure represent the directions of the maximum principal stress σ_1, while the shorter bars give the directions of the minimum principal stress σ_3 at each element considered. In this particular case, σ_2 is coaxial with the in situ stress σ_{h2}, but the other principal stresses σ_1 and σ_3 are inclined to σ_{h1} and σ_v in the immediate vicinity of the tunnel.

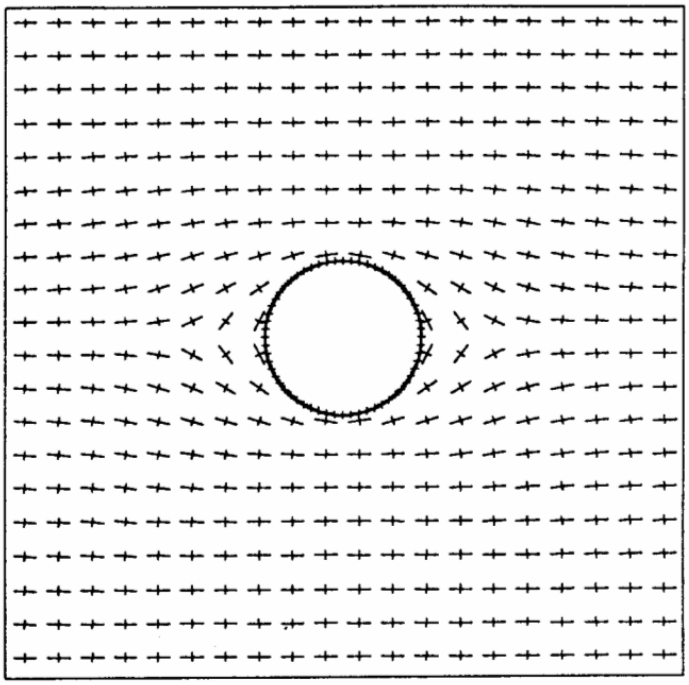

Figure 6: Principal stress directions in the rock surrounding a horizontal tunnel subjected to a horizontal in situ stress σ_{h1} equal to $3\sigma_v$, where σ_v is the vertical in situ stress.

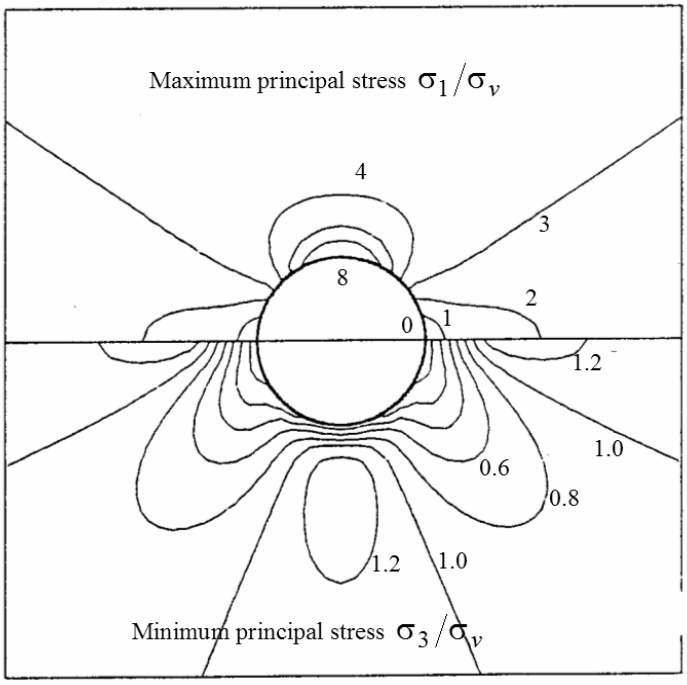

Figure 7: Contours of maximum and minimum principal stress magnitudes in the rock surrounding a horizontal tunnel subjected to a vertical in situ stress of σ_v and a horizontal in situ stress of $3\sigma_v$.

Contours of the magnitudes of the maximum principal stress σ_1 and the minimum principal stress σ_3 are given in Figure 7. This figure shows that the redistribution of stresses is concentrated in the rock close to the tunnel and that, at a distance approximately three times the radius from the centre of the hole, the disturbance to the in-situ stress field is negligible.

An analytical solution for the stress distribution in a stressed elastic plate containing a circular hole was published by Kirsch (1898) which formed the basis for many early studies of rock behaviour around tunnels and shafts. Following along the path pioneered by Kirsch, researchers such as Love (1927), Muskhelishvili (1953) and Savin (1961) published solutions for excavations of various shapes in elastic plates. A useful summary of these solutions and their application in rock mechanics was published by Brown in an introduction to a volume entitled *Analytical and Computational Methods in Engineering Rock Mechanics* (1987).

Closed form solutions still possess great value for the conceptual understanding of behaviour and for the testing and calibration of numerical models. For design purposes, however, these models are restricted to very simple geometries and material models. They are of limited practical value. Fortunately, with the development of computers, many powerful programs that provide numerical solutions to these problems are now readily available. A brief review of some of these numerical solutions is given below.

Numerical methods of stress analysis

Most underground excavations are irregular in shape and are frequently grouped close to other excavations. These groups of excavations can form a set of complex three-dimensional shapes. In addition, because of the presence of geological features such as faults and dykes, the rock properties are seldom uniform within the rock volume of interest. Consequently, closed form solutions are of limited value in calculating the stresses, displacements, and failure of the rock mass surrounding underground excavations. Several computer-based numerical methods have been developed over the past few decades which provide the means for obtaining approximate solutions to these problems.

Numerical methods for the analysis of stress driven problems in rock mechanics can be divided into two classes:

- *Boundary discretization methods*, in which only the boundary of the excavation is divided into elements and the interior of the rock mass is represented mathematically as an infinite continuum. These methods are normally restricted to elastic analyses.
- *Domain discretization methods*, in which the interior of the rock mass is divided into geometrically simple elements each with assumed properties. The collective behaviour and interaction of these simplified elements model the more complex overall behaviour of the rock mass. In other words, domain methods allow consideration of more complex material models than boundary methods. *Finite element* and *finite difference* methods are domain techniques which treat the rock mass as a continuum. The *distinct element* method is also a domain method which models each individual block of rock as a unique element.

These two classes of analysis can be combined in the form of *hybrid models* to maximise the advantages and minimise the disadvantages of each method.

It is possible to make some general observations about the two types of approaches discussed above. In domain methods, a significant amount of effort is required to create the mesh that is used to divide the rock mass into elements. In the case of complex models, such as those containing multiple openings, meshing can become extremely difficult. In contrast, boundary methods require only that the excavation boundary be discretized, and the surrounding rock mass is treated as an infinite continuum. Since fewer elements are required in the boundary method, the demand on computer memory and on the skill and experience of the user is reduced. The availability of highly optimised mesh-generators in many domain models has narrowed this difference to the point where most users of domain programs would be unaware of the mesh generation problems discussed above and the choice of models can be based on other considerations.

In the case of domain methods, the outer boundaries of the model must be placed sufficiently far away from the excavations in order that errors, arising from the interaction between these outer boundaries and the excavations, are reduced to an acceptable minimum. On the other hand, since boundary methods treat the rock mass as an infinite continuum, the far field conditions need only be specified as stresses acting on the entire rock mass and no outer boundaries are required. The main strength of boundary methods lies in the simplicity achieved by representing the rock mass as a continuum of infinite extent. It is this representation, however, that makes it difficult to incorporate variable material properties and discontinuities such as joints and faults. While techniques have been developed to allow some boundary element modelling of variable rock properties, these types of problems are more conveniently modelled by domain methods.

Before selecting the appropriate modelling technique for types of problems, it is necessary to understand the basic components of each technique.

Boundary Element Method

The boundary element method derives its name from the fact that only the boundaries of the problem geometry are divided into elements. In other words, only the excavation surfaces, the free surface for shallow problems, joint surfaces where joints are considered explicitly and material interfaces for multi-material problems are divided into elements. In fact, several types of boundary element models are collectively referred to as ‘the boundary element method’ (Crouch and Starfield, 1983). These models may be grouped as follows:

Indirect (Fictitious Stress) method, so named because the first step in the solution is to find a set of fictitious stresses that satisfy prescribed boundary conditions. These stresses are then used in the calculation of actual stresses and displacements in the rock mass.

Direct method, so named because the displacements are solved directly for the specified boundary conditions.

Displacement Discontinuity method, so named because the solution is based on the superposition of the fundamental solution of an elongated slit in an elastic continuum and shearing and normal displacements in the direction of the slit.

The differences between the first two methods are not apparent to the program user. The direct method has certain advantages in terms of program development, as will be discussed later in the section on Hybrid approaches.

The fact that a boundary element model extends 'to infinity' can also be a disadvantage. For example, a heterogeneous rock mass consists of regions of finite, not infinite, extent. Special techniques must be used to handle these situations. Joints are modelled explicitly in the boundary element method using the displacement discontinuity approach, but this can result in a considerable increase in computational effort. Numerical convergence is often found to be a problem for models incorporating many joints. For these reasons, problems, requiring explicit consideration of several joints and/or sophisticated modelling of joint constitutive behaviour, are often better handled by one of the domain methods such as finite elements.

A widely used application of displacement discontinuity boundary elements is in the modelling of tabular ore bodies. Here, the entire ore seam is represented as a 'discontinuity' which is initially filled with ore. Mining is simulated by reduction of the ore stiffness to zero in those areas where mining has occurred. The resulting stress redistribution to the surrounding pillars may be examined (Salamon, 1974, von Kimmelmann et al., 1984).

Finite element and finite difference methods

In practice, the finite element method is usually indistinguishable from the finite difference method; thus, they will be treated here as one and the same. For the boundary element method, it was seen that conditions on a domain boundary could be related to the state at *all* points throughout the remaining rock, even to infinity. In comparison, the finite element method relates the conditions at a few points within the rock (nodal points) to the state within a finite closed region formed by these points (the element). In the finite element method, the physical problem is modelled numerically by dividing the entire problem region into elements.

The finite element method is well suited to solving problems involving heterogeneous or non-linear material properties, since each element explicitly models the response of its contained material. However, finite elements are not well suited to modelling infinite boundaries, such as occur in underground excavation problems. One technique for handling infinite boundaries is to discretize beyond the zone of influence of the excavation and to apply appropriate boundary conditions to the outer edges. Another approach has been to develop elements for which one edge extends to infinity i.e., so-called 'infinity' finite elements. In practice, efficient pre- and post-processors allow the user to perform parametric analyses and assess the influence of approximated far-field boundary conditions. The time required for this process is negligible compared to the total analysis time.

Joints can be represented explicitly using specific 'joint elements'. Different techniques have been proposed for handling such elements, but no single technique has found universal favour.

Joint interfaces may be modelled, using quite general constitutive relations, though possibly at increased computational expense depending on the solution technique.

Once the model has been divided into elements, material properties have been assigned and loads have been prescribed, some technique must be used to redistribute any unbalanced loads and thus determine the solution to the new equilibrium state. Available solution techniques can be broadly divided into two classes - implicit and explicit. Implicit techniques assemble systems of linear equations that are then solved using standard matrix reduction techniques. Any material non-linearity is accounted for by modifying stiffness coefficients (secant approach) and/or by adjusting prescribed variables (initial stress or initial strain approach). These changes are made in an iterative manner such that all constitutive and equilibrium equations are satisfied for the given load state.

The response of a non-linear system generally depends upon the sequence of loading. Thus, it is necessary that the load path modelled be representative of the actual load path experienced by the body. This is achieved by breaking the total applied load into load increments, each increment being sufficiently small, so that solution convergence for the increment is achieved after only a few iterations. However, as the system being modelled becomes increasingly non-linear and the load increment represents an ever-smaller portion of the total load, the incremental solution technique becomes like modelling the quasi-dynamic behaviour of the body, as it responds to gradual application of the total load.

To overcome this, a ‘dynamic relaxation’ solution technique was proposed (Otter et al., 1966) and first applied to geomechanics modelling by Cundall (1971). In this technique no matrices are formed. Rather, the solution proceeds explicitly - unbalanced forces, acting at a material integration point, result in acceleration of the mass associated with the point; applying Newton's law of motion expressed as a difference equation yields incremental displacements, applying the appropriate constitutive relation produces the new set of forces, and so on marching in time, for each material integration point in the model. This solution technique has the advantage that both geometric and material non-linearities are accommodated, with relatively little additional computational effort as compared to a corresponding linear analysis, and computational expense increases only linearly with the number of elements used. A further practical advantage lies in the fact that numerical divergence usually results in the model predicting obviously anomalous physical behaviour. Thus, even relatively inexperienced users may recognise numerical divergence.

Most commercially available finite element packages use implicit (i.e., matrix) solution techniques. For linear problems and problems of moderate non-linearity, implicit techniques tend to perform faster than explicit solution techniques. However, as the degree of non-linearity of the system increases, imposed loads must be applied in smaller increments which implies a greater number of matrix re-formations and reductions and hence, increased computational expense. Therefore, highly non-linear problems are best handled by packages using an explicit solution technique.

Distinct Element Method

In ground conditions conventionally described as blocky (i.e., where the spacing of the joints is of the same order of magnitude as the excavation dimensions), intersecting joints form wedges of rock that may be regarded as rigid bodies. That is, these individual pieces of rock may be free to rotate and translate, and the deformation that takes place at block contacts may be significantly greater than the deformation of the intact rock. Hence, individual wedges may be considered rigid. For such conditions it is usually necessary to model many joints explicitly. However, the behaviour of such systems is so highly non-linear, that even a jointed finite element code, employing an explicit solution technique, may perform relatively inefficiently.

An alternative modelling approach is to develop data structures that represent the blocky nature of the system being analysed. Each block is considered a unique free body that may interact at contact locations with surrounding blocks. Contacts may be represented by the overlaps of adjacent blocks, thereby avoiding the necessity of unique joint elements. This has the added advantage that arbitrarily large relative displacements at the contact may occur, a situation not generally tractable in finite element codes.

Due to the high degree of non-linearity of the systems being modelled, explicit solution techniques are favoured for distinct element codes. As is the case for finite element codes employing explicit solution techniques, this permits very general constitutive modelling of joint behaviour with little increase in computational effort and results in computation time being only linearly dependent on the number of elements used. The use of explicit solution techniques places fewer demands on the skills and experience than the use of codes employing implicit solution techniques.

Although the distinct element method has been used most extensively in academic environments to date, it is finding its way into the offices of consultants, planners, and designers. Further experience in the application of this powerful modelling tool to practical design situations and subsequent documentation of these case histories is required, so that an understanding may be developed of where, when, and how the distinct element method is best applied.

Hybrid approaches

The objective of a hybrid method is to combine the above methods to eliminate undesirable characteristics while retaining as many advantages as possible. For example, in modelling an underground excavation, most non-linearity will occur close to the excavation boundary, while the rock mass at some distance will behave in an elastic fashion. Thus, the near-field rock mass might be modelled, using a distinct element or finite element method, which is then linked at its outer limits to a boundary element model, so that the far-field boundary conditions are modelled exactly. In such an approach, the direct boundary element technique is favoured as it results in increased programming and solution efficiency.

Lorig and Brady (1984) used a hybrid model consisting of a discrete element model for the near field and a boundary element model for the far field in a rock mass surrounding a circular tunnel.

Two-dimensional and three-dimensional models

A two-dimensional model, such as that illustrated in Figure 5, can be used for the analysis of stresses and displacements in the rock surrounding a tunnel, shaft, or borehole, where the length of the opening is much larger than its cross-sectional dimensions. The stresses and displacements in a plane, normal to the axis of the opening, are not influenced by the ends of the opening, provided that these ends are far enough away.

On the other hand, an underground powerhouse or crusher chamber has a much more equi-dimensional shape, and the effect of the end walls cannot be neglected. In this case, it is much more appropriate to carry out a three-dimensional analysis of the stresses and displacements in the surrounding rock mass. Unfortunately, this switch from two to three dimensions is not as simple as it sounds and there are relatively few good three-dimensional numerical models, which are suitable for routine stress analysis work in a typical engineering design office.

EXAMINE3D (www.rocscience.com) is a three-dimensional boundary element program that provides a starting point for an analysis of a problem in which the three-dimensional geometry of the openings is important. Such three-dimensional analyses provide clear indications of stress concentrations and of the influence of three-dimensional geometry. In many cases, it is possible

to simplify the problem to two-dimensions by considering the stresses on critical sections identified in the three-dimensional model.

More sophisticated three-dimensional finite element models such as FLAC3D (www.itascacg.com) are available, but the definition of the input parameters and interpretation of the results of these models would stretch the capabilities of all but the most experienced modellers. It is probably best to leave this type of modelling in the hands of these specialists.

It is recommended that, where the problem being considered is obviously three-dimensional, a preliminary elastic analysis be carried out by means of one of the three-dimensional boundary element programs. The results can then be used to decide whether further three-dimensional analyses are required or whether appropriate two-dimensional sections can be modelled using a program such as PHASE2 (www.rocscience.com), a powerful but user-friendly finite element program that generally meets the needs of most underground excavation design projects.

Examples of two-dimensional stress analysis

A boundary element program called EXAMINE2D is available from www.rocscience.com. While this program is limited to elastic analyses it can provide a very useful introduction for those who are not familiar with the numerical stress analysis methods described above. The following examples demonstrate the use of this program to explore some common problems in tunnelling.

Tunnel shape

Most contractors like a simple horseshoe shape for tunnels since this gives a wide flat floor for the equipment used during construction. For relatively shallow tunnels in good quality rock this is an appropriate tunnel shape and there are many hundreds of kilometres of horseshoe shaped tunnels all over the world.

In poor quality rock masses or in tunnels at great depth, the simple horseshoe shape is not a good choice because of the high stress concentrations at the corners where the sidewalls meet the floor or invert. In some cases, failures initiating at these corners can lead to severe floor heave and even to failure of the entire tunnel perimeter as shown in Figure 8.

The stress distribution in the rock mass surrounding the tunnel can be improved by modifying the horseshoe shape as shown in Figure 9. In some cases, this can eliminate or minimise the types of failure shown in Figure 8 while, in other cases, it may be necessary to use a circular tunnel profile.

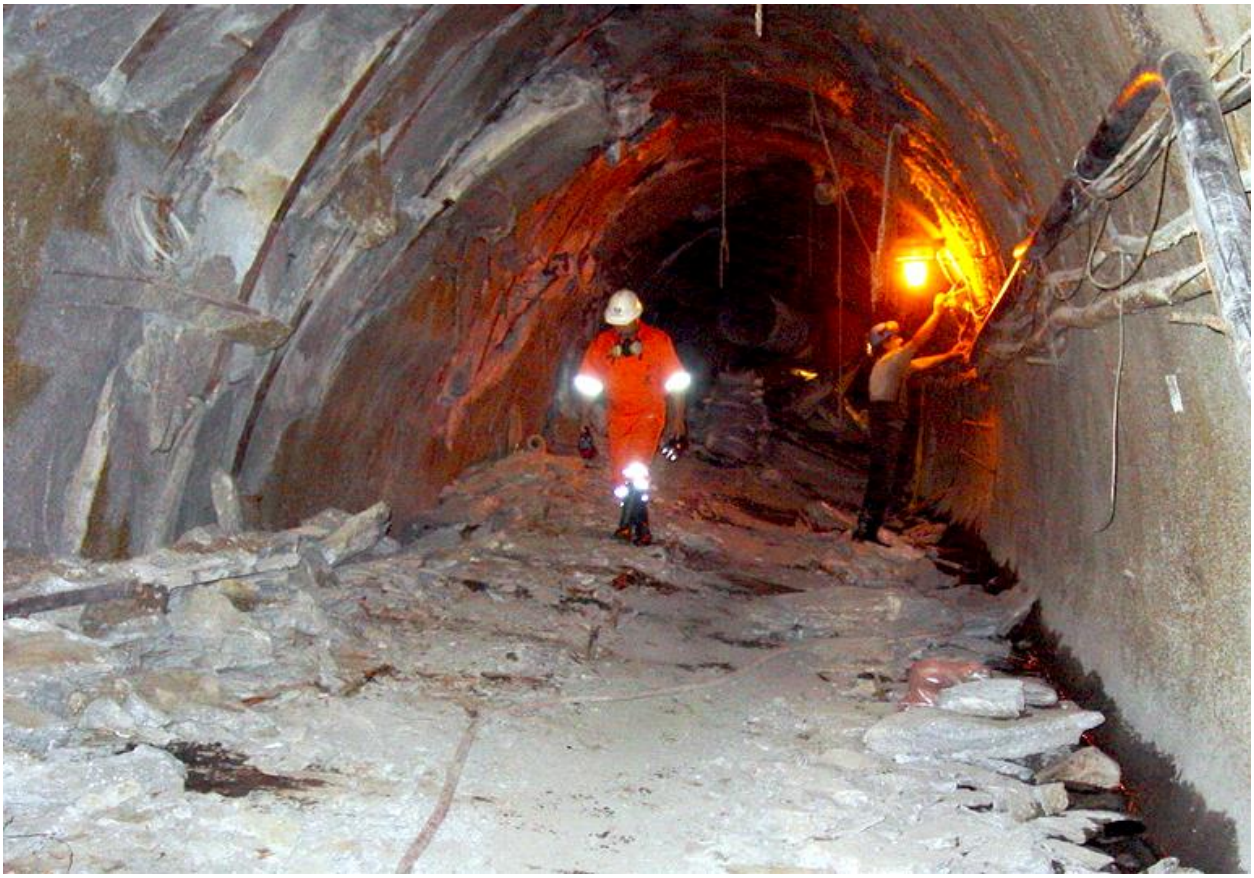

Figure 8: Failure of the lining in a horseshoe-shaped tunnel in a highly stressed poor quality rock mass. This failure initiated at the corners where the invert meets the sidewalls.

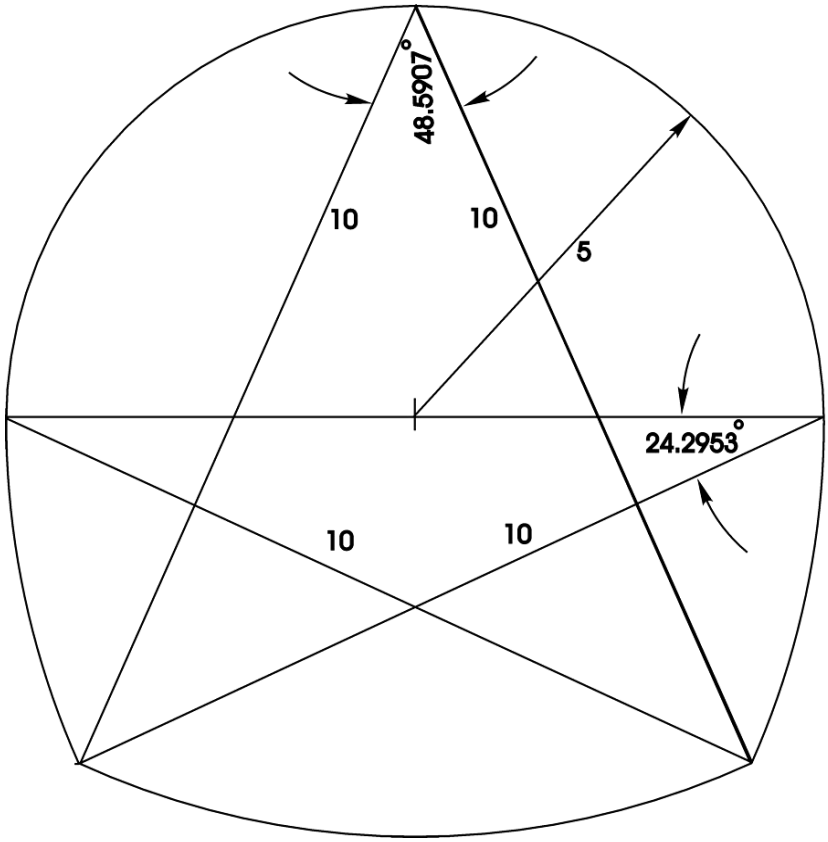

Figure 9: Dimensions of a 10 m span modified horseshoe tunnel shape designed to overcome some of the problems illustrated in Figure 8.

The application of the program EXAMINE2D to compare three tunnel shapes is illustrated in Figure 10. Typical "average" in situ stresses and rock mass properties were used in this analysis and the three figures compare Strength Factor contours and deformed excavation profiles (exaggerated) for the three tunnel shapes.

The flat floor of the horseshoe tunnel (top figure) allows upward displacement or heaving of the floor. The sharp corners at the junction between the floor and the tunnel sidewalls create high stress concentrations and generate large bending moments in any lining installed in the tunnel. Failure of the floor generally initiates at these corners as illustrated in Figure 8.

Floor heave is reduced significantly by the concave curvature of the floor of the modified horseshoe shape (middle figure). In marginal cases these modifications to the horseshoe shape may be sufficient to prevent or at least minimise the type of damage illustrated in Figure 8. However, in severe cases, a circular tunnel profile is invariably the best choice, as shown by the smooth Strength Factor contours and the deformed tunnel boundary shape in the bottom figure in Figure 10.

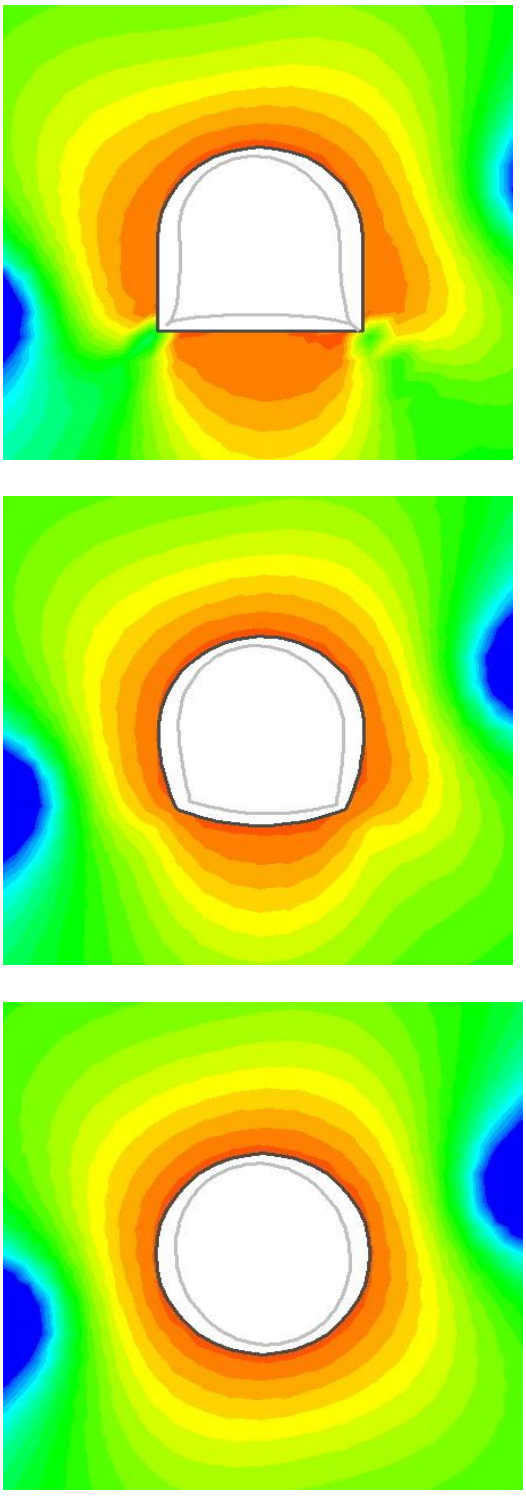

In situ stresses:

Major principal stress σ_1 = 10 MPa
Minor principal stress σ_3 = 7 MPa
Intermediate principal stress σ_2 = 9 MPa
Inclination of major principal stress to the horizontal axis = 15º

Rock mass properties:

Friction angle ϕ = 35º
Cohesion c = 1 MPa
Tensile strength = zero
Deformation modulus E = 4600 MPa

Figure 10: Comparison of three tunnel excavation profiles using EXAMINE2D. The contours are for the Strength Factor defined by the ratio of rock mass strength to the induced stress at each point. The deformed boundary profile (exaggerated) is shown inside each excavation.

Large underground caverns

A typical underground complex in a hydroelectric project has a powerhouse with a span of 20 to 25 m and a height of 40 to 50 m. Four to six turbine-generator sets are housed in this cavern and a cutaway sketch through one of these sets is shown in Figure 11.

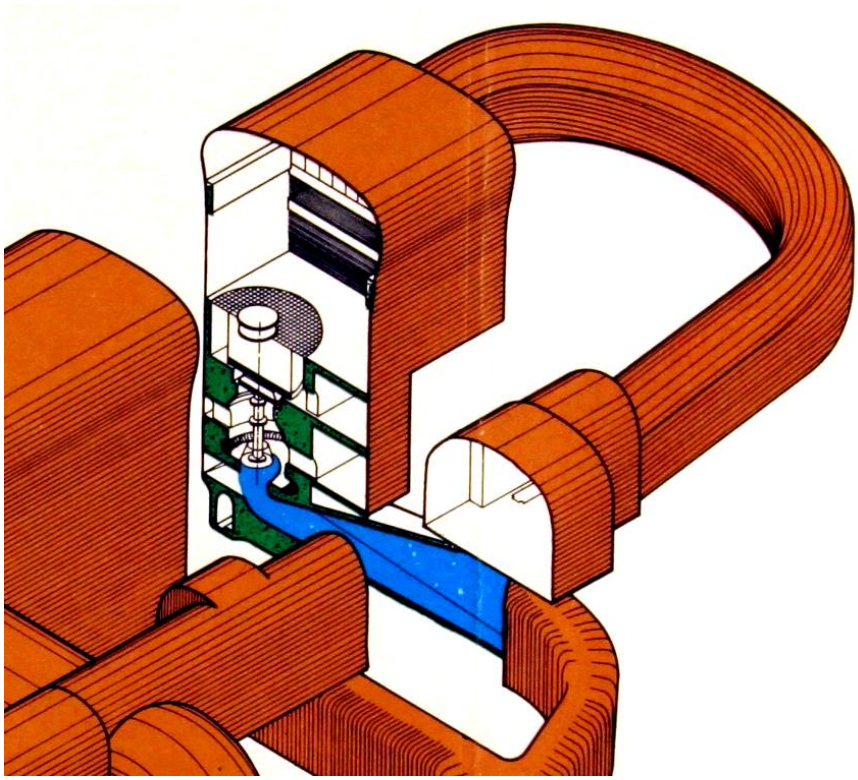

Figure 11: Cutaway sketch of the layout of an underground powerhouse cavern and a parallel transformer gallery.

Transformers are frequently housed in a chamber or gallery parallel to the powerhouse. Ideally these two caverns should be as close as possible to minimise the length of the busbars connecting the generators and transformers. This must be balanced against the size, and hence, the stability of the pillar between the caverns. The relative locations and distances between the caverns are explored in the series of EXAMINE2D models shown in Figure 12, using the same in situ stresses and rock mass properties as listed in Figure 10.

A closer examination of the deformations induced in the rock mass by the excavation of the underground powerhouse and transformer gallery, in Figure 13, shows that the smaller of the two excavations is drawn towards the larger cavern and its profile is distorted in this process. This distortion can be reduced by relocating the transformer gallery and by increasing the spacing between the galleries as has been done in Figure 12.

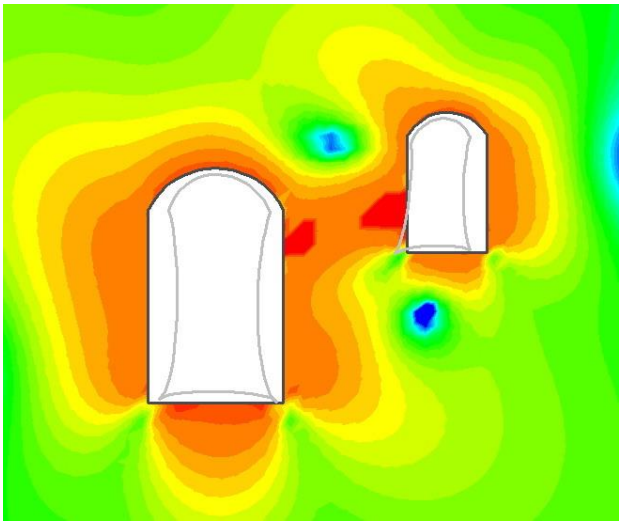

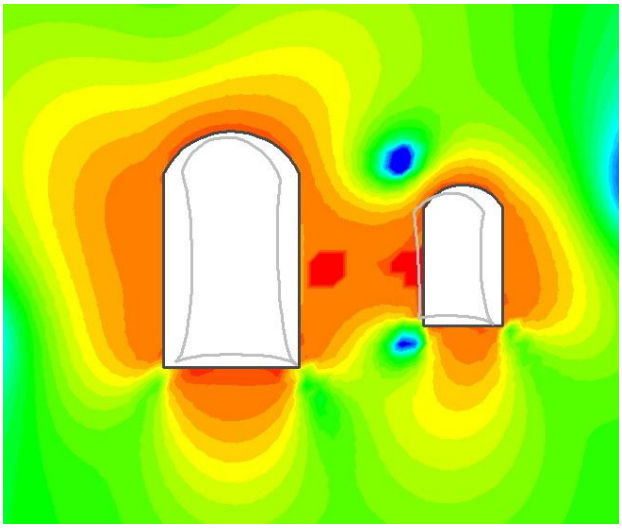

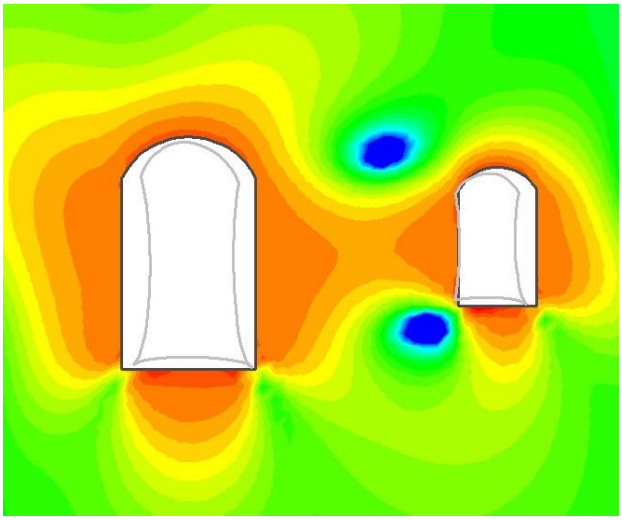

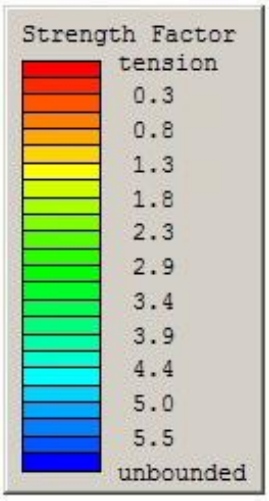

In situ stresses:

Major principal stress σ_1 = 10 MPa

Minor principal stress σ_3 = 7 MPa

Intermediate stress σ_2 = 9 MPa

Inclination of major principal stress to the horizontal axis = 15º

Rock mass properties:

Friction angle ϕ = 35º

Cohesion c = 1 MPa

Tensile strength = zero

Deformation modulus E = 4600 MPa

Figure 12: Comparison of three underground powerhouse and transformer gallery layouts, using EXAMINE2D. The contours are for the Strength Factor defined by the ratio of rock mass strength to the induced stress at each point. The deformed boundary profile (exaggerated) is shown inside each excavation.

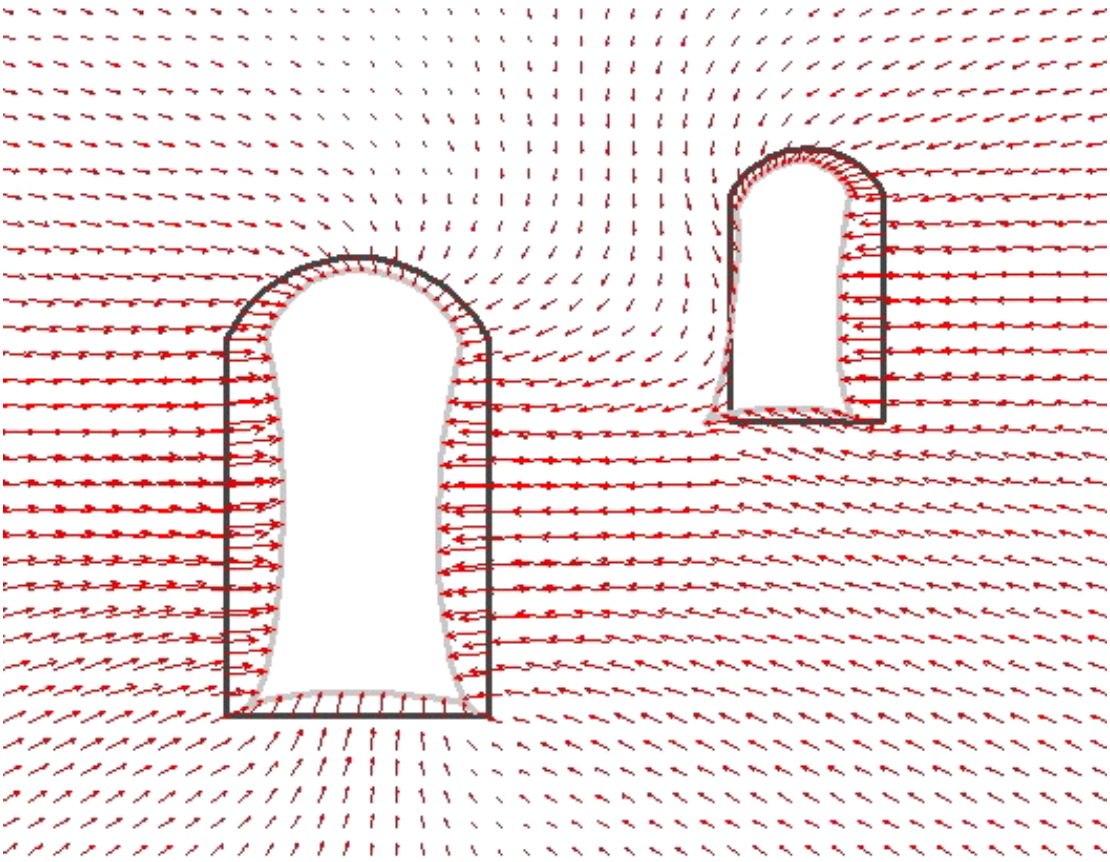

Figure 13: Displacement vectors and deformed excavation shapes for the underground powerhouse and transformer gallery.

Where the combination of rock mass strength and in situ stresses is likely to cause overstressing around the caverns and in the pillar, a good rule of thumb is that the distance between the two caverns should be approximately equal to the height of the larger cavern.

The interested reader is encouraged to download the program EXAMINE2D and use it to explore the problem, such as those illustrated in Figures 10 and 12, for themselves.

References

Brown, E.T. 1987. Introduction. *Analytical and computational methods in engineering rock mechanics*, (ed. E.T. Brown), 1-31. London: Allen and Unwin.

Brown, E.T. and Hoek, E. 1978. Trends in relationships between measured rock in situ stresses and depth. *Int. J. Rock Mech. Min. Sci. & Geomech. Abstr.* **15**, pp.211-215.

Crouch, S.L. and Starfield, A.M. 1983. *Boundary element methods in solid mechanics*. London: Allen and Unwin.

Cundall, P.A. 1971. A computer model for simulating progressive large-scale movements in blocky rock systems. *Rock Fracture , Proc. symp. ISRM, Nancy* **1,** Paper 2-8.

Engelder, T. and Sbar, M.L. 1984. Near-surface in situ stress: introduction. *J. Geophys. Res*. **89**, pp.9321-9322. Princeton, NJ: Princeton University Press.

Herget, G. 1988. *Stresses in rock.* Rotterdam: Balkema.

Hoek, E., Carranza – Torres, C. and Corkum, B., 2002. Hoek - Brown failure criterion – *2002 edition*. In *Proceedings of NARMS-TAC 2002*, Toronto (eds. Bawden,R.W., Curran, J., Telesnicki, M) pp. 267-273. Download from www.rocscience.com.

Kirsch, G., 1898. Die theorie der elastizitat und die bedurfnisse der festigkeitslehre. *Veit. Deit. Ing.* **42** (28), 797-807.

Lorig, L.J. and Brady, B.H.G. 1984. A hybrid computational scheme for excavation and support design in jointed rock media. In *Design and performance of underground excavations*, (eds E.T. Brown and J.A. Hudson), 105-112. London: Brit. Geotech. Soc.

Love, A.E.H. 1927. A treatise on the mathematical theory of elasticity. New York: Dover.

Muskhelishvili, N.I. 1953. *Some basic problems of the mathematical theory of elasticity*. 4th edition, translated by J.R.M. Radok. Gronigen: Noordhoff.

Otter, J.R.H., Cassell, A.C. and Hobbs, R.E. 1966. Dynamic relaxation. *Proc. Instn Civ. Engrs* **35**, 633-665.

Reinecker, J., Heidbach, O., Tingay, M., Sperner, B., & Müller, B. 2005: The release 2005 of the World Stress Map (available online at www.world-stress-map.org).

Salamon, M.D.G. 1974. Rock mechanics of underground excavations. In Advances *in rock mechanics, Proc. 3rd Cong.ISRM., Denver* **1B,** 951-1009. Washington, DC: National Academy of Sciences

Savin, G.N. 1961. *Stress concentrations around holes.* London: Pergamon.

Sheory, P.R. 1994. A theory for in situ stresses in isotropic and transversely isotropic rock. *Int. J. Rock Mech. Min. Sci. & Geomech. Abstr*. **31**(1), 23-34.

Terzaghi, K. and Richart, F.E. 1952. Stresses in rock about cavities. *Geotechnique* **3**, 57-90.

von Kimmelmann, M.R., Hyde, B. and Madgwick, R.J. 1984. The use of computer applications at BCL Limited in planning pillar extraction and the design of mine layouts. In *Design and performance of underground excavations*, (eds E.T. Brown and J.A. Hudson), 53-64. London: Brit. Geotech. Soc.

Zoback, M. L. 1992. First- and second-order patterns of stress in the lithosphere: the World Stress Map Project. *J. Geophys. Res*. **97**(B8), 11761-11782.

11. When is a design acceptable

Introduction

When is a design in rock engineering acceptable? The aim of the following text[1] is to demonstrate that there are no simple universal rules for acceptability. There are no standard factors of safety which can be used to guarantee that a rock structure will be safe and that it will perform adequately. Each design is unique, and the acceptability of the structure must be considered in terms of the set of circumstances, rock types, design loads and end use for which it is intended. The responsibility of geotechnical engineers is to find a safe and economical solution which is compatible with all the constraints which apply to the project. Such a solution should be based upon engineering judgement guided by practical and theoretical studies such as stability or deformation analyses when these are applicable.

Tables 1 to 4 summarise some of the typical problems, critical parameters, analysis methods and acceptability criteria which apply to several different rock engineering structures. These examples have been drawn from my own consulting experience and I make no claims that this is a complete list, nor do I expect readers to agree with all the items which I have included under the various headings. The purpose of presenting these tables is to demonstrate the diversity of problems and criteria which must be considered and to emphasise the dangers of attempting to use standard factors of safety or other acceptability criteria.

Numerical analysis of slopes, foundations, caverns, and other engineering structures is a critical component of a design. However, these analyses must be supported by sound field investigations, to provide reliable input parameters, and by observations during construction, to determine the adequacy and accuracy of the input information for such analyses. For small projects it may be possible for a single geotechnical engineer or engineering geologist to perform all the required tasks for an adequate design. For large project such as the design of open pit mine slopes, large underground caverns in hydroelectric projects or long tunnels through a variety of rock units, it is essential that a team of engineers and geologists should be available to carry out the required data collection and design analyses.

To amplify some of the items included in Tables 1 to 4, several case histories are discussed in terms of the factors which were considered and the acceptability criteria which were used.

[1]Based upon the text of the Müller lecture presented at the 7th Congress of the International Society for Rock Mechanics held in Aachen, Germany, in September 1991.

Table 1 : Typical problems, critical parameters, methods of analysis and acceptability criteria for slopes.

STRUCTURE	TYPICAL PROBLEMS	CRITICAL PARAMETERS	ANALYSIS METHODS	ACCEPTABILITY CRITERIA
 Landslides.	Complex failure along a circular or near circular failure surface involving sliding on faults and other structural features as well as failure of intact materials.	• Presence of regional faults. • Shear strength of materials along failure surface. • Groundwater distribution in slope, particularly in response to rainfall or to submergence of slope toe. • Potential earthquake loading.	Limit equilibrium methods which allow for non-circular failure surfaces can be used to estimate changes in factor of safety as a result of drainage or slope profile changes. Numerical methods such as finite element or discrete element analysis can be used to investigate failure mechanisms and history of slope displacement.	Absolute value of factor of safety has little meaning but rate of change of factor of safety can be used to judge effectiveness of remedial measures. Long term monitoring of surface and subsurface displacements in slope is the only practical means of evaluating slope behaviour and effectiveness of remedial action.
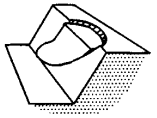 Soil or heavily jointed rock slopes.	Circular failure along a spoon-shaped surface through soil or heavily jointed rock masses.	• Height and angle of slope face. • Shear strength of materials along failure surface. • Groundwater distribution in slope. • Potential surcharge or earthquake loading.	Two-dimensional limit equilibrium methods which include automatic searching for the critical failure surface are used for parametric studies of factor of safety. Probability analyses, three-dimensional limit equilibrium analyses or numerical stress analyses are occasionally used to investigate unusual slope problems.	Factor of safety > 1.3 for "temporary" slopes with minimal risk of damage. Factor of safety > 1.5 for "permanent" slopes with significant risk of damage. Where displacements are critical, numerical analyses of slope deformation may be required and higher factors of safety will generally apply in these cases.
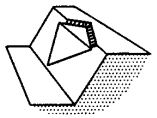 Jointed rock slopes.	Planar or wedge sliding on one structural feature or along the line of intersection of two structural features.	• Slope height, angle and orientation. • Dip and strike of structural features. • Groundwater distribution in slope. • Potential earthquake loading. • Sequence of excavation and support installation.	Limit equilibrium analyses which determine three-dimensional sliding modes are used for parametric studies on factor of safety. Failure probability analyses, based upon distribution of structural orientations and shear strengths, are useful for some applications.	Factor of safety > 1.3 for "temporary" slopes with minimal risk of damage. Factor of safety > 1.5 for "permanent" slopes with significant risk of damage. Probability of failure of 10 to 15% may be acceptable for open pit mine slopes where cost of clean up is less than cost of stabilization.
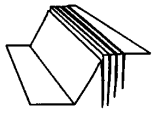 Vertically jointed rock slopes .	Toppling of columns separated from the rock mass by steeply dipping structural features which are parallel or nearly parallel to the slope face.	• Slope height, angle and orientation. • Dip and strike of structural features. • Groundwater distribution in slope. • Potential earthquake loading.	Crude limit equilibrium analyses of simplified block models are useful for estimating potential for toppling and sliding. Discrete element models of simplified slope geometry can be used for exploring toppling failure mechanisms.	No generally acceptable criterion for toppling failure is available although potential for toppling is usually obvious. Monitoring of slope displacements is the only practical means of determining slope behaviour and effectiveness of remedial measures.
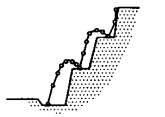 Loose boulders on rock slopes.	Sliding, rolling, falling and bouncing of loose rocks and boulders on the slope.	• Geometry of slope. • Presence of loose boulders. • Coefficients of restitution of materials forming slope. • Presence of structures to arrest falling and bouncing rocks.	Calculation of trajectories of falling or bouncing rocks based upon velocity changes at each impact is generally adequate. Monte Carlo analyses of many trajectories based upon variation of slope geometry and surface properties give useful information on distribution of fallen rocks.	Location of fallen rock or distribution of a large number of fallen rocks will give an indication of the magnitude of the potential rockfall problem and of the effectiveness of remedial measures such as draped mesh, catch fences and ditches at the toe of the slope.

Table 2 : Typical problems, critical parameters, methods of analysis and acceptability criteria for dams and foundations.

STRUCTURE	TYPICAL PROBLEMS	CRITICAL PARAMETERS	ANALYSIS METHODS	ACCEPTABILITY CRITERIA
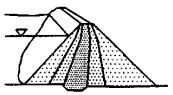 Zoned fill dams.	Circular or near-circular failure of dam, particularly during rapid drawdown. Foundation failure on weak seams. Piping and erosion of core.	• Presence of weak or permeable zones in foundation. • Shear strength, durability, gradation and placement of dam construction materials, particularly filters. • Effectiveness of grout curtain and drainage system. • Stability of reservoir slopes.	Seepage analyses are required to determine water pressure and velocity distribution through dam and abutments. Limit equilibrium methods should be used for parametric studies of stability. Numerical methods can be used to investigate dynamic response of dam during earthquakes.	**Safety factor >1.5 for full pool with steady state seepage; >1.3 for end of construction with no reservoir loading and undissipated foundation porewater pressures; >1.2 for probable maximum flood with steady state seepage and >1.0 for full pool with steady state seepage and maximum credible horizontal psuedo-static seismic loading.**
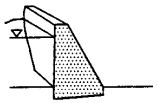 Gravity dams.	Shear failure of interface between concrete and rock or of foundation rock. Tension crack formation at heel of dam. Leakage through foundation and abutments.	• Presence of weak or permeable zones in rock mass. • Shear strength of interface between concrete and rock. • Shear strength of rock mass. • Effectiveness of grout curtain and drainage system. • Stability of reservoir slopes.	Parametric studies using limit equilibrium methods should be used to investigate sliding on the interface between concrete and rock and sliding on weak seams in the foundation. A large number of trial failure surfaces are required unless a non-circular failure analysis with automatic detection of critical failure surfaces is available.	**Safety factor against foundation failure should exceed 1.5 for normal full pool operating conditions provided that conservative shear strength values are used ($c' \approx 0$).** **Safety factor > 1.3 for probable mximum food (PMF).** **Safety factor > 1 for extreme loading - maximum credible earthquake and PMF.**
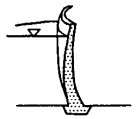 Arch dams.	Shear failure in foundation or abutments. Cracking of arch due to differential settlements of foundation. Leakage through foundations or abutments.	• Presence of weak, deformable or permeable zones in rock mass. • Orientation, inclination and shear strength of structural features. • Effectiveness of grout curtain and drainage system. • Stability of reservoir slopes.	Limit equilibrium methods are used for parametric studies of three-dimensional sliding modes in the foundation and abutments, including the influence of water pressures and reinforcement. Three-dimensional numerical analyses are required to determine stresses and displacements in the concrete arch.	**Safety factor against foundation failure >1.5 for normal full pool operating conditions and >1.3 for probable maximum flood conditions provided that conservative shear strength values are used ($c' \approx 0$).** **Stresses and deformations in concrete arch should be within allowable working levels defined in concrete specifications.**
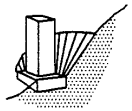 Foundations on rock slopes.	Slope failure resulting from excessive foundation loading. Differential settlement due to anisotropic deformation properties of foundation rocks.	• Orientation, inclination and shear strength of structural features in rock mass forming foundation. • Presence of inclined layers with significantly different deformation properties. • Groundwater distribution in slope.	Limit equilibrium analyses of potential planar or wedge failures in the foundation or in adjacent slopes are used for parametric studies of factor of safety. Numerical analyses can be used to determine foundation deformation, particularly for anisotropic rock masses.	Factor of safety against sliding of any potential foundation wedges or blocks should exceed 1.5 for normal operating conditions. Differential settlement should be within limits specified by structural engineers.
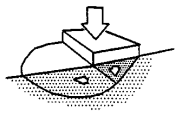 Foundations on soft rock or soil.	Bearing capacity failure resulting from shear failure of soils or weak rocks underlying foundation slab.	• Shear strength of soil or jointed rock materials. • Groundwater distribution in soil or rock foundation. • Foundation loading conditions and potential for earthquake loading.	Limit equilibrium analyses using inclined slices and non-circular failure surfaces are used for parametric studies of factor of safety. Numerical analyses may be required to determine deformations, particularly for anisotropic foundation materials.	**Bearing capacity failure should not be permitted for normal loading conditions.** **Differential settlement should be within limits specified by structural engineers.**

Table 3 : Typical problems, critical parameters, methods of analysis and acceptability criteria for underground civil engineering excavations.

STRUCTURE	TYPICAL PROBLEMS	CRITICAL PARAMETERS	ANALYSIS METHODS	ACCEPTABILITY CRITERIA
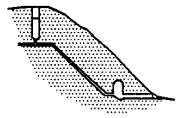 Pressure tunnels in hydro-power projects.	Excessive leakage from unlined or concrete lined tunnels. Rupture or buckling of steel lining due to rock deformation or external pressure.	• Ratio of maximum hydraulic pressure in tunnel to minimum principal stress in the surrounding rock. • Length of steel lining and effectiveness of grouting. • Groundwater levels in the rock mass.	Determination of minimum cover depths along pressure tunnel route from accurate topographic maps. Stress analyses of sections along and across tunnel axis. Comparison between minimum principal stresses and maximum dynamic hydraulic pressure to determine steel lining lengths.	Steel lining is required where the minimum principal stress in the rock is less than 1.3 times the maximum static head for typical hydroelectric operations or 1.15 for operations with very low dynamic pressures. Hydraulic pressure testing in boreholes at the calculated ends of the steel lining is essential to check the design assumptions.
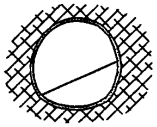 Soft rock tunnels.	Rock failure where strength is exceeded by induced stresses. Swelling, squeezing or excessive closure if support is inadequate.	• Strength of rock mass and of individual structural features. • Swelling potential, particularly of sedimentary rocks. • Excavation method and sequence. • Capacity and installation sequence of support systems.	Stress analyses using numerical methods to determine extent of failure zones and probable displacements in the rock mass. Rock-support interaction analyses using closed-form or numerical methods to determine capacity and installation sequence for support and to estimate displacements in the rock mass.	Capacity of installed support should be sufficient to stabilize the rock mass and to limit closure to an acceptable level. Tunnelling machines and internal structures must be designed for closure of the tunnel as a result of swelling or time-dependent deformation. Monitoring of deformations is an important aspect of construction control.
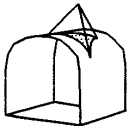 Shallow tunnels in jointed rock.	Gravity driven falling or sliding wedges or blocks defined by intersecting structural features. Unravelling of inadequately supported surface material.	• Orientation, inclination and shear strength of structural features in the rock mass. • Shape and orientation of excavation. • Quality of drilling and blasting during excavation. • Capacity and installation sequence of support systems.	Spherical projection techniques or analytical methods are used for the determination and visualization of all potential wedges in the rock mass surrounding the tunnel. Limit equilibrium analyses of critical wedges are used for parametric studies on the mode of failure, factor of safety and support requirements.	Factor of safety, including the effects of reinforcement, should exceed 1.5 for sliding and 2.0 for falling wedges and blocks. Support installation sequence is critical and wedges or blocks should be identified and supported before they are fully exposed by excavation. Displacement monitoring is of little value.
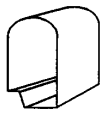 Large caverns in jointed rock.	Gravity driven falling or sliding wedges or tensile and shear failure of rock mass, depending upon spacing of structural features and magnitude of in situ stresses.	• Shape and orientation of cavern in relation to orientation, inclination and shear strength of structural features in the rock mass. • In situ stresses in the rock mass. • Excavation and support sequence and quality of drilling and blasting.	Spherical projection techniques or analytical methods are used for the determination and visualization of all potential wedges in the rock mass. Stresses and displacements induced by each stage of cavern excavation are determined by numerical analyses and are used to estimate support requirements for the cavern roof and walls.	An acceptable design is achieved when numerical models indicate that the extent of failure has been controlled by installed support, that the support is not overstressed and that the displacements in the rock mass stabilize. Monitoring of displacements is essential to confirm design predictions.
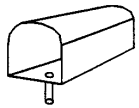 Underground nuclear waste disposal.	Stress and/or thermally induced spalling of the rock surrounding the excavations resulting in increased permeability and higher probability of radioactive leakage.	• Orientation, inclination, permeability and shear strength of structural features in the rock mass. • In situ and thermal stresses in the rock surrounding the excavations. • Groundwater distribution in the rock mass.	Numerical analyses are used to calculate stresses and displacements induced by excavation and by thermal loading from waste canisters. Groundwater flow patterns and velocities, particularly through blast damaged zones, fissures in the rock and shaft seals are calculated using numerical methods.	An acceptable design requires extremely low rates of groundwater movement through the waste canister containment area in order to limit transport of radioactive material. Shafts, tunnels and canister holes must remain stable for approximately 50 years to permit retrieval of waste if necessary.

Table 4 : Typical problems, critical parameters, methods of analysis and acceptability criteria for underground hard rock mining excavations.

STRUCTURE	TYPICAL PROBLEMS	CRITICAL PARAMETERS	ANALYSIS METHODS	ACCEPTABILITY CRITERIA
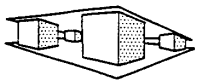 Pillars.	Progressive spalling and slabbing of the rock mass leading to eventual pillar collapse or rockbursting.	• Strength of the rock mass forming the pillars. • Presence of unfavourably oriented structural features. • Pillar geometry, particularly width to height ratio. • Overall mine geometry including extraction ratio.	For horizontally bedded deposits, pillar strength from empirical relationships based upon width to height ratios and average pillar stress based on tributary area calculations are compared to give a factor of safety. For more complex mining geometry, numerical analyses including progressive pillar failure may be required.	Factor of safety for simple pillar layouts in horizontally bedded deposits should exceed 1.6 for "permanent" pillars. In cases where progressive failure of complex pillar layouts is modelled, individual pillar failures can be tolerated provided that they do not initiate "domino" failure of adjacent pillars.
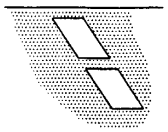 Crown pillars.	Caving of surface crown pillars for which the ratio of pillar depth to stope span is inadequate. Rockbursting or gradual spalling of overstressed internal crown pillars.	• Strength of the rock mass forming the pillars. • Depth of weathering and presence of steeply dipping structural features in the case of surface crown pillars. • In situ stress levels and geometry of internal crown pillars.	Rock mass classification and limit equilibrium analyses can give useful guidance on surface crown pillar dimensions for different rock masses. Numerical analyses, including discrete element studies, can give approximate stress levels and indications of zones of potential failure.	Surface crown pillar depth to span ratio should be large enough to ensure very low probability of failure. Internal crown pillars may require extensive support to ensure stability during mining of adjacent stopes. Careful planning of mining sequence may be necessary to avoid high stress levels and rockburst problems.
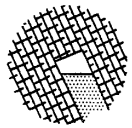 Cut and fill stopes.	Falls of structurally defined wedges and blocks from stope backs and hanging walls. Stress induced failures and rockbursting in high stress environments.	• Orientation, inclination and shear strength of structural features in the rock mass. • In situ stresses in the rock mass. • Shape and orientation of stope. • Quality, placement and drainage of fill.	Numerical analyses of stresses and displacements for each excavation stage will give some indication of potential problems. Some of the more sophisticated numerical models will permit inclusion of the support provided by fill or the reinforcement of the rock by means of grouted cables.	Local instability should be controlled by the installation of rockbolts or grouted cables to improve safety and to minimize dilution. Overall stability is controlled by the geometry and excavation sequence of the stopes and the quality and sequence of filling. Acceptable mining conditions are achieved when all the ore is recovered safely.
 Non-entry stopes.	Ore dilution resulting from rockfalls from stope back and walls. Rockbursting or progressive failure induced by high stresses in pillars between stopes.	• Quality and strength of the rock. • In situ and induced stresses in the rock surrounding the excavations. • Quality of drilling and blasting in excavation of the stope.	Some empirical rules, based on rock mass classification, are available for estimating safe stope dimensions. Numerical analyses of stope layout and mining sequence, using three-dimensional analyses for complex orebody shapes, will provide indications of potential problems and estimates of support requirements.	A design of this type can be considered acceptable when safe and low cost recovery of a large proportion of the orebody has been achieved. Rockfalls in shafts and haulages are an unacceptable safety hazard and pattern support may be required. In high stress environments, local destressing may be used to reduce rockbursting.
 Drawpoints and orepasses.	Local rock mass failure resulting from abrasion and wear of poorly supported drawpoints or orepasses. In extreme cases this may lead to loss of stopes or orepasses.	• Quality and strength of the rock. • In situ and induced stresses and stress changes in the rock surrounding the excavations. • Selection and installation sequence of support.	Limit equilibrium or numerical analyses are not particularly useful since the processes of wear and abrasion are not included in these models. Empirical designs based upon previous experience or trial and error methods are generally used.	The shape of the opening should be maintained for the design life of the drawpoint or orepass. Loss of control can result in serious dilution of the ore or abandonment of the excavation. Wear resistant flexible reinforcement such as grouted cables, installed during excavation of the opening, may be successful in controlling instability.

Landslides in reservoirs

The presence of unstable slopes in reservoirs is a major concern for the designers of dams for hydroelectric and irrigation projects. The Vajont failure in 1963 alerted the engineering community of the danger of underestimating the potential for the mobilisation of existing landslides because of submergence of the slide toe during impounding of the reservoir.

During the construction of the Mica and Revelstoke dams on the Columbia River in British Columbia, Canada, several potential slides were investigated. Two of these, the Downie Slide, a 1.4 billion cubic metre ancient rockslide, and Dutchman's Ridge, a 115 million cubic metre potential rockslide, were given special attention because of the serious consequences which could have resulted from failure of these slides (Imrie, 1983, Lewis and Moore, 1989, Imrie, Moore and Enegren, 1992).

The Downie Slide and Dutchman's Ridge are in steep, narrow, V-shaped sections of the Columbia River valley which has been subjected to several episodes of glaciation. The bedrock at these sites consists mainly of Pre-Cambrian para-gneisses and schists within, or, on the fringe of the Shuswap Metamorphic Complex. In both cases, the potential slide planes, determined by diamond drilling and slope displacement monitoring, are relatively flat-lying, outward-dipping tectonic faults or shears which daylight in the base of the river valley.

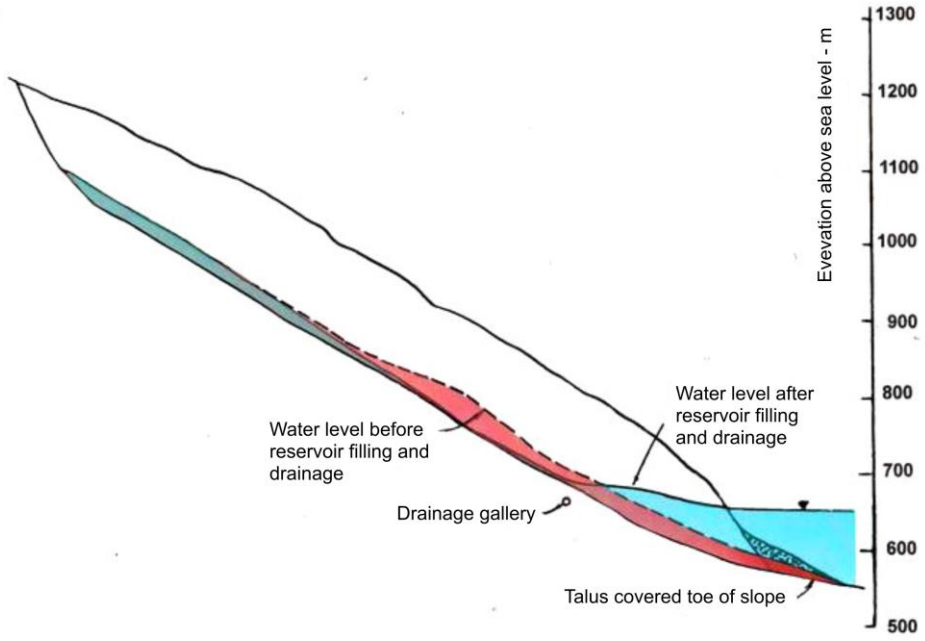

Figure 1: Section through Dutchman's Ridge showing potential slide surface and water levels before and after drainage.

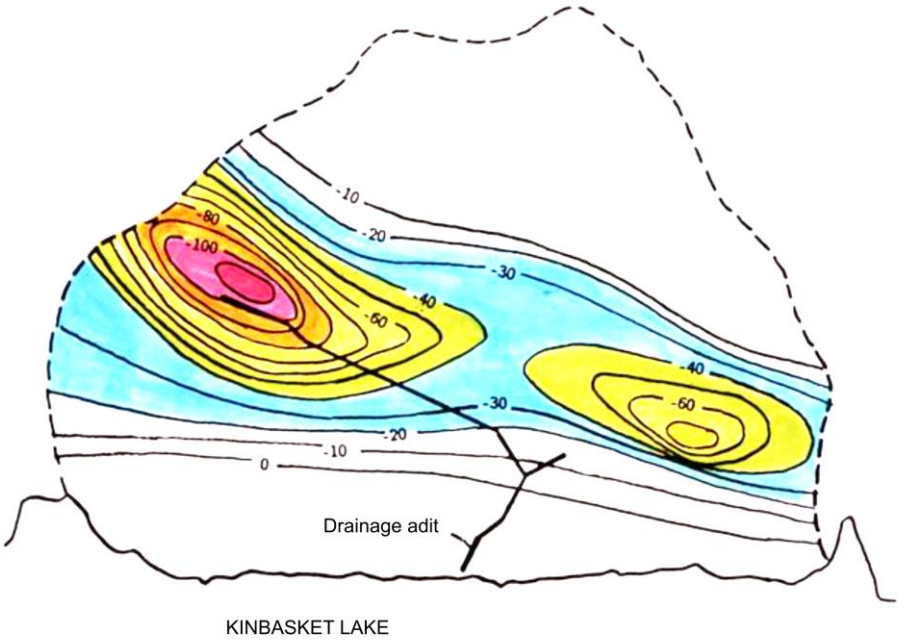

Figure 2: Contours of water level reduction (in metres) due to the implementation of drainage in Dutchman's Ridge.

A section through Dutchman's Ridge is given in Figure 1 which shows the water levels in the slope before reservoir filling and after reservoir filling and the construction of the drainage system. Figure 2 shows contours of reduction in water levels because of the installation of the drainage system which consisted of 872 m of adit and 12,000 m of drain hole drilling. Note that the drawdown area on the right-hand side of the potential slide was achieved by long boreholes from the end of the drainage adit branch.

Based on thorough investigation and monitoring programs, British Columbia Hydro and Power Authority (BC Hydro) decided that remedial measures had to be taken to improve the stability of both the Downie Slide and Dutchman's Ridge. These remedial measures consisted of drainage adits extending within and/or behind the failure surfaces and supplemented by drain holes drilled from chambers excavated along the adits. Work on the Downie Slide was carried out in the period 1977 to 1982 (which included a three-year observation period) and work on Dutchman's Ridge was carried out from 1986 to 1988.

Comparative studies of the stability of the slope section shown in Figure 1, based upon a factor of safety of 1.00 for the slope after reservoir filling, but before implementation of the drainage system, gave a factor of safety of 1.06 for the drained slope. This 6% improvement in factor of safety may not seem very significant to the designer of small-scale rock and soil slopes, but it was considered acceptable in this case for several reasons:

1. The factor of safety of 1.00 calculated for the undrained slope is based upon 'back-analyses' of observed slope behaviour. Provided that the same method of analysis and shear strength parameters are used for the stability analysis of the same slope with different groundwater conditions, the ratio of the factors of safety is a very reliable indicator of the change in slope stability, even if the absolute values of the factor of safety are not accurate. Consequently, the degree of uncertainty, which must be allowed in slope designs, where no back-analyses have been performed, can be minimized and a lower factor of safety accepted.
2. The groundwater levels in the slope were reduced by drainage to lower than the pre-reservoir conditions. The stability of the slope is at least as good, if not better than, these pre-reservoir conditions. This slope is considered to have withstood several significant earthquakes during the 10,000 years since the last episode of glaciation which is responsible for the present valley shape.
3. Possibly the most significant indicator of an improvement in stability, for both the Downie Slide and Dutchman's Ridge, has been a significant reduction in the rate of down-slope movement which has been monitored for the past 25 years. In the case of the Downie Slide, this movement has practically ceased. At Dutchman's Ridge, the movements are significantly lower, and it is anticipated that they will stabilize when the drainage system has been in operation for a few more years.

Deformation of rock slopes

In a slope in which the rock is jointed but, where there are no significant discontinuities dipping out of the slope, which could cause sliding, deformation and failure of the slope is controlled by a complex process of block rotation, tilting, and sliding. In an extreme case, where the rock mass consists of near vertical joints separating columns of massive rock, toppling movement and failure may occur.

Figure 3 is a section through part of the power tunnel for the Wahleach Hydroelectric Project in British Columbia, Canada. A break in the steel lining in this power tunnel occurred in January 1989. It is thought that this break was caused by a slow down-slope gravitational movement caused by block rotations (toppling) within a near-surface zone of loosened jointed rock.

The Wahleach Project is located 120 km east of Vancouver and power is generated from 620 m of head between Wahleach Lake and a surface powerhouse located adjacent to the Fraser River. Water flows through a 3500 m long, three metre diameter unlined upper tunnel, a rock trap, a 600 m long, two metre diameter concrete encased steel-lined shaft inclined at 48° to the horizontal, a 300 m long lower tunnel and a 485 m long surface penstock to the powerhouse.

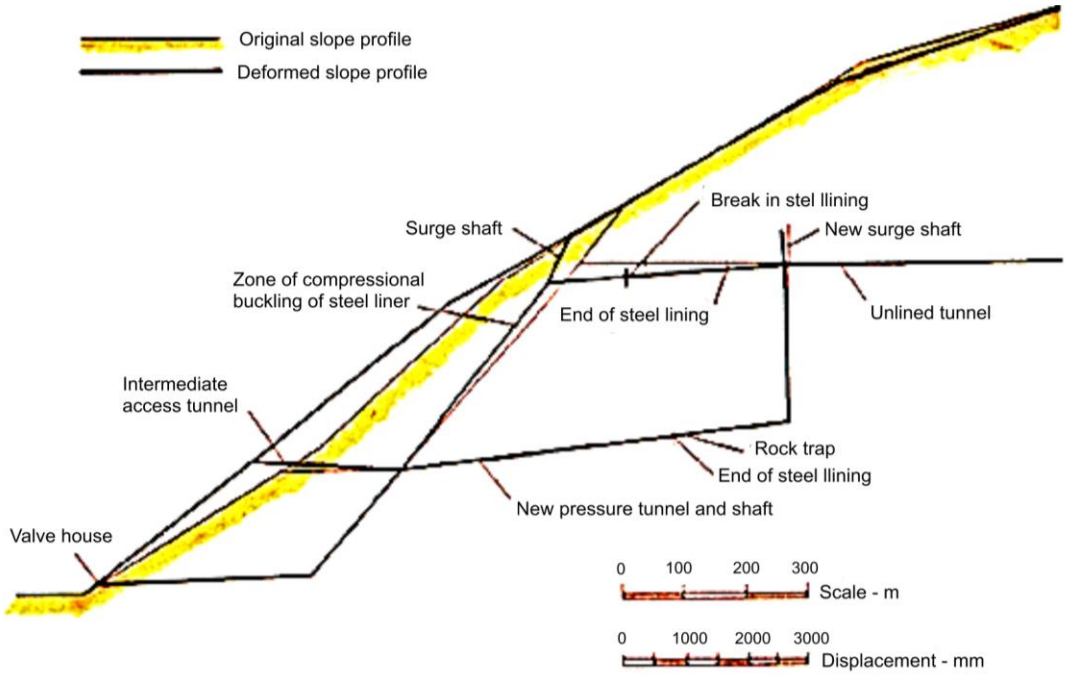

Figure 3: Cross-section through a section of the Wahleach Power Tunnel showing the original tunnel alignment and the location of the replacement conduit.

The tunnels were excavated mainly in granodiorite which varies from highly fractured and moderately weathered in the upper portions of the slope, to moderately fractured and fresh in both the lower portions of the slope and below the highly fractured mass. Two main joint sets occur in the rock mass, one set striking parallel to the slope and the other perpendicular to it. Both dip very steeply. Average joint spacings range from 0.5 to 1 m. A few joints occur sub-parallel to the ground surface. These joints are well developed in the ground surface adjacent to the inclined shaft. Thorough investigations failed to reveal any significant shear zones or faults conducive to sliding.

The toe of the slope is buried beneath colluvial and fan deposits from two creeks which have incised the Fraser Valley slope to form the prominence in which the inclined shaft was excavated. This prominence is crossed by several linear troughs which trend along the ground surface contours and are evidence of previous down-slope movement of the prominence. Mature trees growing in these troughs indicate a history of movement of at least several hundred years (Moore, Imrie and Baker, 1991).

The water conduit operated without incident between the initial filling in 1952 and May 1981 when leakage was first noted from the upper access adit located near the intersection of the inclined shaft and the upper tunnel (see Figure 3). This leakage stopped when two drainpipes, embedded in the concrete backfill beneath the steel lining,

were plugged at their upstream ends. Large holes had been eroded in these drainage pipes where they were not encased in concrete and it was concluded that this corrosion was responsible for the leakage. This conclusion appeared to be valid until 25 January 1989 when a much larger water flow occurred.

Investigations in the dewatered tunnel revealed a 150 mm wide circumferential tension crack in the steel lining of the upper tunnel, about 55 m upstream from its intersection with the inclined shaft. In addition, eight compressional buckle zones were found in the steel lining of the upper portion of the inclined shaft. Subsequent investigations revealed that approximately 20 million cubic metres of rock are involved in down-slope creep which, during 1989-90, amounted to several centimetres per year and which appears to be ongoing. This down-slope creep appears to be related to a process of block rotation rather than to any deep-seated sliding as was the case at both the Downie Slide and Dutchman's Ridge.

While discrete element models may give some indication of the overall mechanics of this type of slope deformation, there is no way in which a factor of safety, equivalent to that for sliding failure, can be calculated. Consequently, in deciding upon the remedial measures to be implemented, other factors must be taken into consideration.

After a thorough study by the BC Hydro and their consultants, it was decided to construct a replacement conduit consisting of an unlined shaft and tunnel section and a steel-lined section where the rock cover is insufficient to contain the internal pressure in the tunnel. This replacement conduit, illustrated in Figure 3, will remove the steel lined portions of the system from zones in which large displacements are likely to occur in the future. This in turn will minimise the risk of a rupture of the steel lining which would inject high pressure water into the slope. It was agreed that such high-pressure water leakage could be a cause for instability of the overall slope. Further studies are being undertaken to determine whether additional drainage is required to provide further safeguards.

Careful measurements of the displacements in the inclined shaft, the length of the steel lining cans as compared with the original specified lengths and the opening of the tensile crack in the upper portion of the steel lined tunnel, provided an overall picture of the displacements in the rock mass. These observed displacements were compared with displacement patterns computed by means of several numerical studies using both continuum and discrete element models and the results of these studies were used in deciding upon the location of the replacement conduit.

In addition to the construction of this replacement conduit to re-route the water away from the upper and potentially unstable part of the slope, a comprehensive displacement and water pressure monitoring system has been installed and is being monitored by BC Hydro (Baker, 1991, Tatchell, 1991).

Structural failures in rock masses

In slopes, foundations and shallow underground excavations in hard rock, failure is frequently controlled by the presence of discontinuities such as faults, shear zones, bedding planes and joints. The intersection of these structural features can release blocks or wedges which can fall or slide from the surface of the excavation. Failure of the intact rock is seldom a problem in these cases where deformation and failure are caused by sliding along individual discontinuity surfaces or along lines of intersection of surfaces. Separation of planes and rotation of blocks and wedges can also play a role in the deformation and failure process.

An analysis of the stability of these excavations depends primarily upon a correct interpretation of the structural geological conditions in the rock mass followed by a study of the blocks and wedges which can be released by the creation of the excavation. Identification and visualisation of these blocks and wedges is by far the most important part of this analysis. Analysis of the stability of the blocks and wedges, and of the reinforcing forces required to stabilize them, is a relatively simple process once this identification has been carried out.

The Río Grande Pumped Storage Project is in the Province of Córdoba in the Republic of Argentina. Four reversible pump-turbines operating at an average head of 170 m give the project a total installed capacity of 750 MW. These turbines are installed in a 25 m span, 50 m high, 105 m long cavern at an average depth of 160 m.

The rock in which the underground excavations are situated is a massive tonalitic gneiss of excellent quality (Amos et al, 1981). The gneiss has an average uniaxial compressive strength of 140 MPa. The maximum principal stress, determined by overcoring tests, is 9.4 MPa and is almost horizontal and oriented approximately normal to the cavern axis. In massive rocks, this 15:1 ratio of uniaxial strength to maximum principal stress is unlikely to result in any significant failure in the rock. This was confirmed by numerical stress analyses (Moretto, 1982). The principal type of instability which had to be dealt with in the underground excavations was that of potentially unstable blocks and wedges defined by intersecting structural features (Hammett and Hoek, 1981). In one section of the cavern, the axis of which is oriented in the direction 158-338, four joint sets were mapped and were found to have the following dip/dip direction values:

Table 5. Dip and dip direction values for joints in one location in the Río Grande cavern

N.	Dip	Dip dir.	Comments
1	50	131	infrequently occurring joints
2	85	264	shear joint set
3	70	226	shear joint set
4	50	345	tension joint set

Figure 4 is a perspective view of the Río Grande power cavern showing typical wedges which can be formed in the roof, sidewalls, bench, and floor by joint sets 2, 3 and 4. These figures represent the maximum possible sizes of wedges which can be formed. During construction, the sizes of the wedges were scaled down in accordance with average joint trace lengths measured in the excavation faces. In Figure 4 it is evident that the roof and the two sidewall wedges were potentially unstable and that they needed to be stabilised. This stabilisation was achieved by the placement of tensioned and grouted rockbolts which were installed at each stage of the cavern excavation. Decisions on the number, length, and capacity of the rockbolts were made by on-site geotechnical staff using limit equilibrium calculations based upon the volume of the wedges defined by the measured trace lengths. For those wedges which involved sliding on one plane or along the line of intersection of two planes, rockbolts were installed across these planes to bring the sliding factor of safety of the wedge up to 1.5. For wedges which were free to fall from the roof, a factor of safety of 2 was used. This factor was calculated as the ratio of the total capacity of the bolts to the weight of the wedge and was intended to account for uncertainties associated with the bolt installation.

The floor wedge was of no significance while the wedges in the bench at the base of the upstream wall were stabilised by dowels placed in grout-filled vertical holes before excavation of the lower benches.

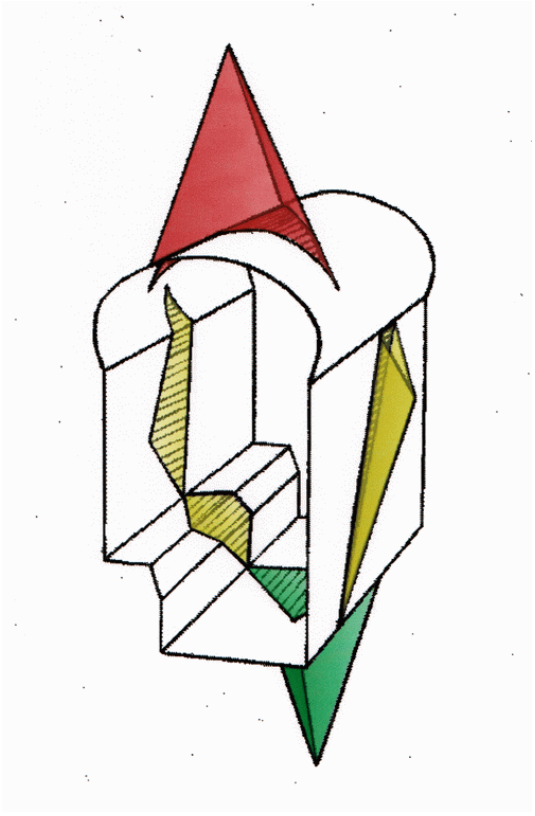

Figure 4: Perspective view of Río Grande power cavern showing potentially unstable wedges in the roof, sidewalls, bench, and floor.

Early recognition of the potential instability problems, identification and visualization of the wedges which could be released and the installation of support at each stage of excavation, before the wedge bases were fully exposed, resulted in a very effective stabilisation program. Apart from a minimal amount of mesh and shotcrete applied to areas of intense jointing, no other support was used in the power cavern which has operated without any signs of instability since its completion in 1982.

Excavations in weak rock

In contrast to the structurally controlled failures in strong rock discussed in the previous section, there are many cases where tunnels and caverns are excavated in rock masses which are weak because of intense jointing or because the rock material itself has a low strength. Rocks such as shales, mudstones, siltstones, phyllites and tuffs are typical weak rocks in which even moderate in situ stresses are likely to induce failure in the rock surrounding underground excavations.

Progressive failure of this type, which can occur in the rock surrounding an underground excavation in a weak rock mass, is a difficult analytical problem and there are no simple numerical models nor factor of safety calculations which can be used to define acceptable limits to this failure process. Judgement on the adequacy of a support design must be based upon an evaluation of a number of factors such as the magnitude and distribution of deformations in the rock and the stresses induced in support elements such as grouted cables, steel sets or concrete linings. This design process is illustrated by means of an example.

The Mingtan pumped storage project is in the central region of the island of Taiwan and utilizes the 400 m head difference between the Sun Moon Lake and the Shuili River to generate up to 1600 MW at times of peak demand. The power cavern is 22 m wide, 46 m high and 158 m long and a parallel transformer hall is 13 m wide, 20 m high and 17 m long. The caverns are 45 m apart and are located at a depth of 30 m below surface in the steep left bank of the Shuili River (Liu, Cheng, and Chang, 1988).

The rock mass consists of weathered, interbedded sandstones, siltstones and shales dipping at about 35° to the horizontal. The Rock Mass Ratings (RMR) (Bieniawski, 1974) and Tunnelling Quality Index Q (Barton, Lien and Lunde, 1974) and approximate shear strength values for the various components of the rock mass are given in Table 6 below.

Table 6. Rock mass classifications and approximate friction angles ϕ and cohesive strengths c for the rock mass in which the Mingtan power cavern is excavated

Rock type	RMR	Q	degrees	c' MPa
Jointed sandstone	63-75	12-39	50	1.0
Bedded sandstone	56-60	7-31	45	0.8
Faults or shears	10-33	0.1-1.1	30-40	0.15-0.3

Weak beds of siltstone, up to 2 m thick, appear to have caused a concentration of shear movements during tectonic activity so that fault zones have developed parallel to the bedding. The common feature observed for all these faults is the presence of continuous clay filling with a thickness varying from a few mm to 200 mm. The cavern axis is intentionally oriented at right angles to the strike of these faults.

The measured in situ stresses in the rock mass surrounding the cavern are approximately:

Maximum principal stress (horizontal) = 10.9 MPa

Minimum principal stress (vertical) = 7.5 MPa

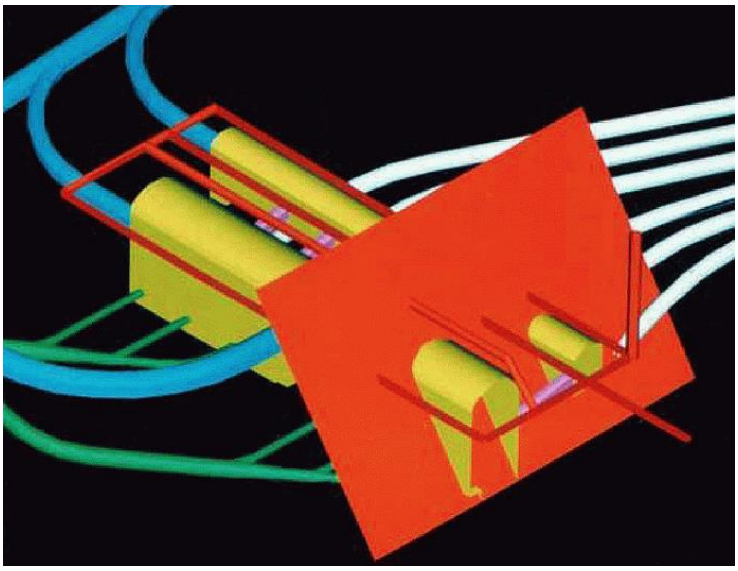

Figure 5: Orientation of the underground excavations in relation to the faults in the bedded sandstone surrounding the power cavern and transformer hall of the Mingtan Project. The red plane indicates the dip and strike of the faults.

Bedding faults of significant thickness, which were intersected in the roof of the cavern, were treated by using high pressure water jets to remove the clay and then filling the cavities with non shrink cementitious mortar (Cheng, 1987, Moy and Hoek, 1989). This was followed by the installation of 50 tonne capacity untensioned grouted cables from a

drainage gallery 10 m above the cavern roof to create a pre-reinforced rock mass above the cavern. All this work was carried out from construction adits before the main contract for the cavern excavation commenced.

The initial design of the reinforcing cables was based upon experience and precedent practice. Figures 6 and 7 give the lengths of rockbolts and cables in the roof and sidewalls of some typical large powerhouse caverns in weak rock masses. Plotted on the same graphs are empirical relationships suggested by Barton (1989) for bolt and cable lengths for underground powerhouses.

During benching down in the cavern, 112 tonne capacity tensioned and grouted cables were installed on a 3 m x 3 m grid in the sidewalls. The final layout of the cables in the rock surrounding the power cavern and the transformer hall is illustrated in Figure 8. Five metre long grouted rockbolts were installed as required at the centre of the squares formed by the cable face plates A 50 mm layer of steel fibre reinforced microsilica shotcrete was applied within 5 to 10 m of the face. This shotcrete was later built up to a thickness of 150 mm on the roof and upper sidewalls and 50 mm on the lower sidewalls where it would eventually be incorporated into the concrete foundations.

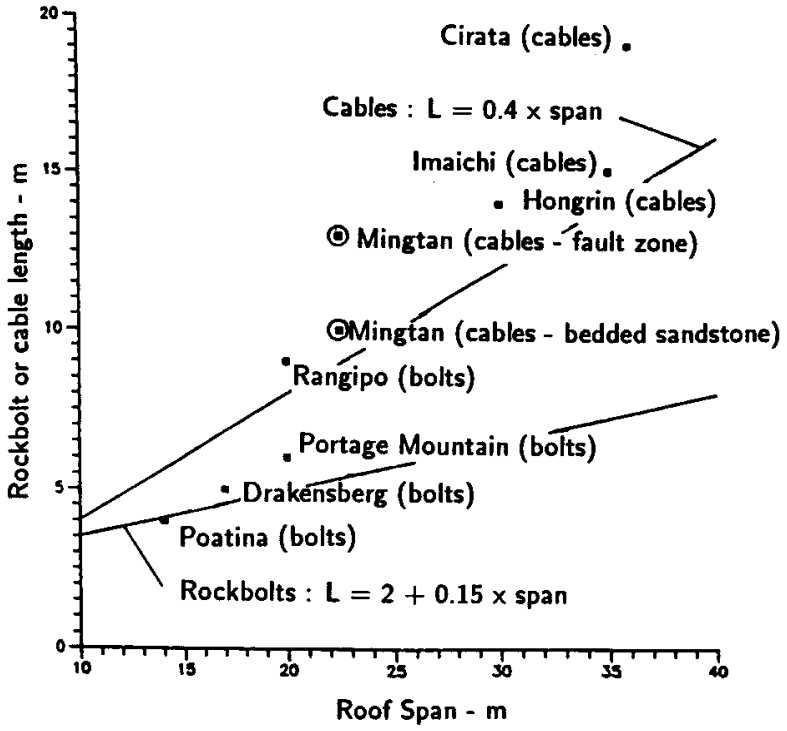

Figure 6: Lengths of rockbolts and cables used for roof support in some large caverns in weak rock. Equations defining trend lines were suggested by Barton (1989).

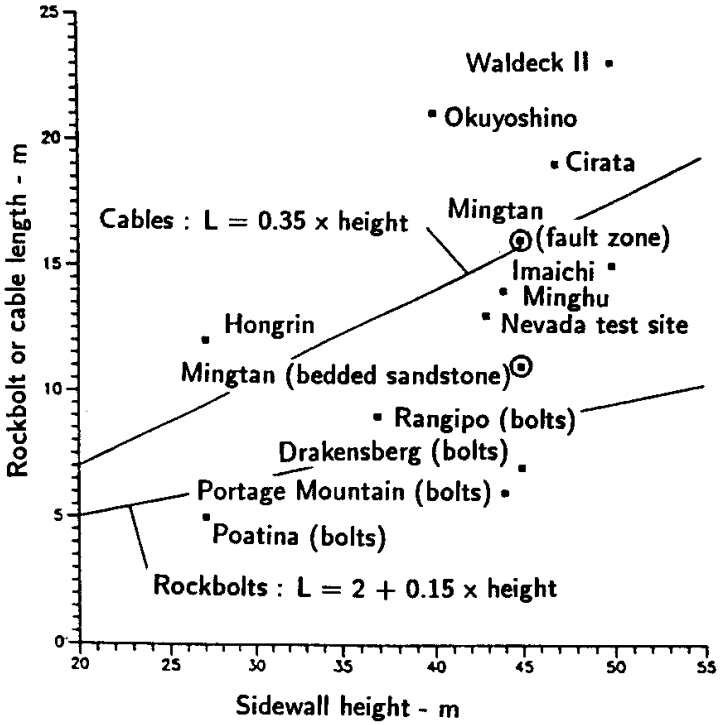

Figure 7: Lengths of rockbolts and cables used for sidewall support in some large caverns in weak rock. Equations defining trend lines were suggested by Barton (1989).

A key element in the decision making process on the adequacy of the support system was a monitoring and analysis process which involved the following steps:

1. Displacements in the rock surrounding the excavations monitored by means of convergence arrays and extensometers, some of which had been installed from construction galleries before excavation of the caverns commenced.

2. Numerical modelling of each excavation stage using non-linear multiple-material models. The material properties used in the models of the early excavation stages were adjusted to obtain the best match between predicted and measured displacements.

3. Prediction of displacements and support loads during future excavation stages and adjustment of support capacity, installation and pre-tensioning to control displacements and cable loads.

4. Measurement of displacements and cable loads (using load cells on selected cables which had been de-bonded) and comparison between measured and predicted displacements and cable loads.

5. Installation of additional cables or adjustment of cable loads to control unusual displacements or support loads.

The aim of this program was to maintain as uniform a displacement pattern around the excavations as possible and to keep the loads on the cables at less than 45% of their yield load. The intermediate rockbolts and the shotcrete were not accounted for in the numerical modelling since it was assumed that their role was confined to supporting the rock immediately adjacent to the excavations and that the overall stability was controlled by the 10 to 15 m long grouted cables.

Figure 8 shows the combination of materials used in analysing one section of the cavern, assuming that the bedding faults could be represented by horizontal layers in the two-dimensional model. To match the measured and predicted displacements in the rock mass, it was found that a 2.5 m thick zone of softened and weakened material had to be wrapped around the excavations to account for blast damaged material (achieving good blasting results was difficult in this interbedded rock).

In Figure 9, the predicted and measured displacements along six extensometers installed in the power cavern sidewalls are compared. The overall agreement is acceptable. Maximum sidewall displacements were of the order of 100 mm at the mid-height of the upstream wall, adjacent to one of the major faults. Elsewhere, displacements were of the order to 25 to 46 mm.

Figure 10 shows the results of monitoring at seven stations along the axis of the power cavern. Before excavation of the cavern commenced, extensometers were installed at each of these stations from a drainage gallery above the roof arch and from construction galleries as shown in the upper part of Figure 10. In addition, load cells were installed on cables adjacent to some of the extensometers.

Rapid responses were recorded in all extensometers and load cells as the top heading passed underneath them. Further responses occurred as the haunches of the cavern arch were excavated and as the first bench was removed. As can be seen from the plots, after this rapid response to the initial excavation stages, the displacements and cable loads became stable and showed very little tendency to increase with time. The difference in the magnitudes of the displacements and cable loads at different stations can be related to the proximity of the monitoring instruments to faults in the rock above the cavern arch.

The rapid load acceptance and the modest loading of the cables together with the control of the displacements in the rock mass were the goals of the support design. Measurements obtained from the extensometers and cable load cells indicate that these goals have been met.

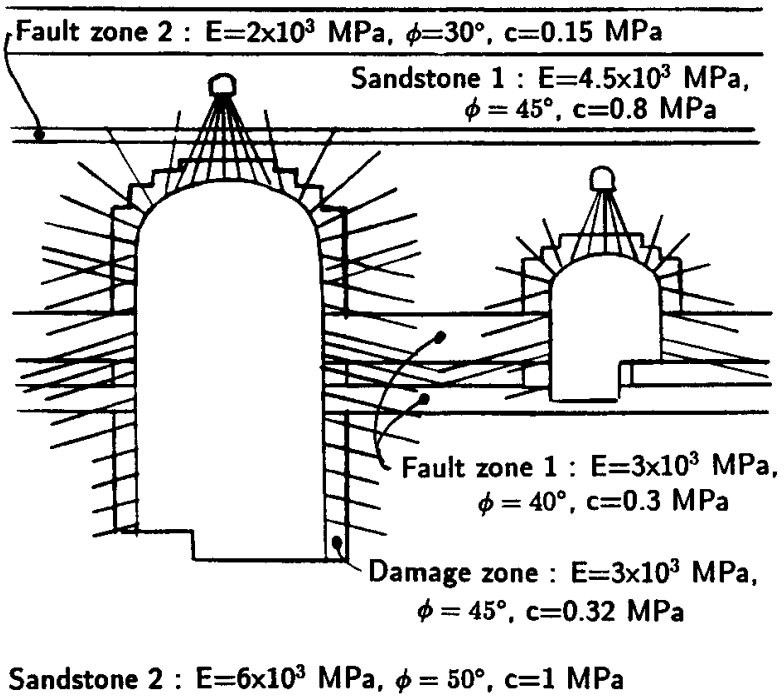

Figure 8: Layout of cables used to support the rock surrounding the power cavern and the transformer hall in the Mingtan pumped storage project. The location and properties of the rock units represent those used in the numerical analysis of failure, deformation, and cable loading in a typical vertical section.

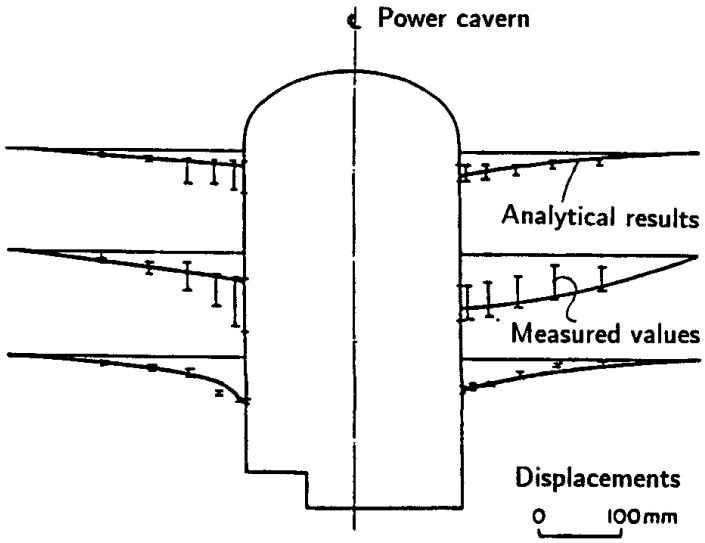

Figure 9: Comparison between calculated and measured displacements along six extensometers installed in the sidewalls of the Mingtan power cavern.

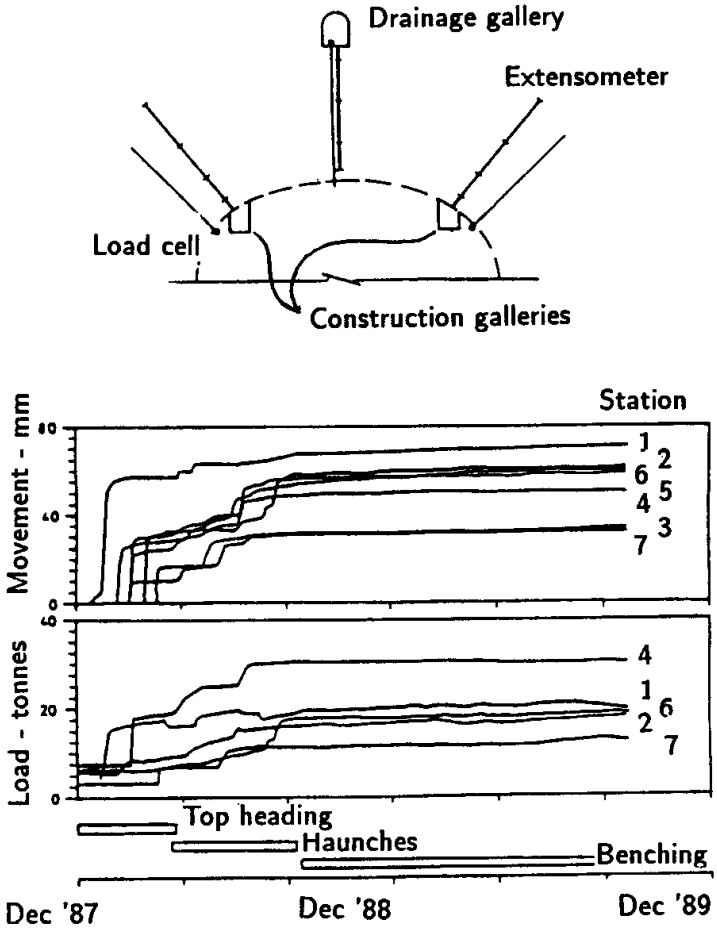

Figure 10: Surface displacements and cable loads measured at seven stations along the power cavern axis.

Factor of safety

The four case histories, discussed in previous sections, have been presented to demonstrate that a variety of criteria must be considered in deciding upon the adequacy of a rock structure to perform its design objectives. This is true for any design in rock since the performance of each structure will be uniquely dependent upon the set of rock conditions, design loads and intended end use.

In one group of structures, traditional designs have been based upon a `factor of safety' against sliding. These structures, which include gravity and fill dams as well as rock and soil slopes, all involve the potential for sliding along well-defined failure surfaces. The factor of safety is defined as the factor by which the shear strength parameters may be

reduced to bring the slope (or dam foundation) into a state of limiting equilibrium (Morgenstern, 1991). The numerical value of the factor of safety chosen for a particular design depends upon the level of confidence which the designer has in the shear strength parameters, the groundwater pressures, the location of the critical failure surface and the magnitude of the external driving forces acting upon the structure.

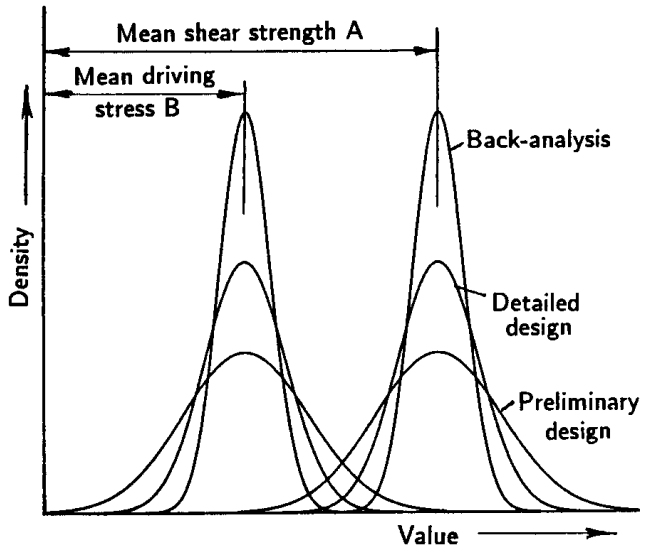

Figure 11: Hypothetical distribution curves representing the degree of uncertainty associated with information on driving stresses and shear strengths at different stages in the design of a structure such as a dam foundation.

Figure 11 illustrates a set of hypothetical distribution curves representing the degree of uncertainty associated with available information on shear strength parameters and disturbing stresses for different stages in the design of a rock or soil structure. The factor of safety is defined as A/B where A is the mean of the distribution of shear strength values and B is the mean of the distribution of driving stresses. For this discussion, the same factor of safety has been assumed for all three cases illustrated.

During preliminary design studies, the amount of information available is usually very limited. Estimates of the shear strength of the rock or soil are generally based upon the judgement of an experienced engineer or geologist which may be supplemented, in some cases, by estimates based upon rock mass classifications or simple index tests. Similarly, the disturbing forces are not known with very much certainty since the location of the critical failure surface will not have been well defined and the magnitude of externally applied loads may not have been established. In the case of dam design, the magnitude of the probable maximum flood, which is usually based upon probabilistic analysis, frequently remains ill defined until very late in the design process.

For this case, the range of both available shear strength and disturbing stresses, which must be considered, is large. If too low a factor of safety is used, there may be a significant probability of failure, represented by the section where the distribution curves overlap in Figure 11. To minimise this failure probability, a high value for the factor of safety is sometimes used. For example, in the 1977 edition of the US Bureau of Reclamation Engineering Monograph on Design Criteria for Concrete Arch and Gravity Dams, a factor of safety of 3.0 is recommended for normal loading conditions when 'only limited information is available on the strength parameters'. This value can be reduced to 2.0 when the strength parameters are 'determined by testing of core samples from a field investigation program or by past experience'.

During detailed design studies, the amount of information available is usually significantly greater than in the preliminary design stage discussed above. A comprehensive program of site investigations and laboratory, or in situ shear strength tests, will normally have been carried out and the external loads acting on the structure will have been better defined. In addition, studies of the groundwater flow and pressure distributions in the rock mass, together with modifications of these distributions by grouting and drainage, will usually have been carried out. Consequently, the ranges of shear strength and driving stress values, which must be considered in the design, are smaller and the distribution curves are more tightly constrained.

The case histories of the Downie Slide and Dutchman's Ridge, discussed earlier, are good examples of designs based upon back-analyses. In both cases, very extensive site investigations and displacement monitoring had established the location of the critical failure surfaces with a high degree of certainty. Careful monitoring of the groundwater in the slopes (256 piezometer measuring points were installed in Dutchman's Ridge) had defined the water pressures in the slopes and their fluctuations over several years. Some shear testing on fault material recovered from cores was carried out but, more importantly, the mobilized shear strength along the potential failure surfaces was calculated by back-analysis, assuming a factor of safety of 1.00 for existing conditions.
Figure 11 illustrates the hypothetical distribution curves for the range of values for shear strength and driving stresses for the case of a structure in which an existing failure has been carefully back analysed. Depending upon the degree of care which has been taken with this back-analysis, these curves will be very tightly constrained, and a low factor of safety can be used for the design of the remedial works.

This discussion illustrates the point that different factors of safety may be appropriate for different stages in the design of a rock structure. This difference is primarily dependent upon the level of confidence which the designer has in the values of shear strength to be included in the analysis. Hence, a critical question which arises in all these cases is the determination or estimation of the shear strength along the potential sliding surface. In a paper on the strength of rockfill materials, Marachi, Chan and Seed (1972) summarize this problem as follows: 'No stability analysis, regardless of how intricate and

theoretically exact it may be, can be useful for design if an incorrect estimation of the shearing strength of the construction material has been made'.

Except in simple cases involving homogeneous soils or planar continuous weak seams, determination of the shear strength along potential sliding surfaces is a notoriously difficult problem. This is particularly true of the determination of the cohesive component, *c'*, of the commonly used Mohr-Coulomb failure criterion. Laboratory test specimens tend to be too small to give representative results while in situ tests are difficult and expensive and, unless carried out with very great care, are liable to give unreliable results.

Table 7: Factors of safety for different loading in the design of earth and rockfill dams.

Loading condition	S.F.	Remarks
End of construction porewater pressures in the dam and undissipated porewater pressures in the foundation. No reservoir loading.	1.3	
Reservoir at full supply level with steady state seepage in the dam and undissipated end-of-construction porewater pressures in the foundation.	1.3	Possibly the most critical (even if rare) condition.
Reservoir at full supply level with steady state seepage.	1.5	Critical to design.
Reservoir at probable maximum flood level with steady state seepage conditions.	1.2	
Rapid reservoir drawdown from full supply level to minimum supply level	1.3	Not significant in design. Failures very rare and, if they occur, usually shallow.

For failure surfaces which involve sliding on rough or undulating rock surfaces such as joints or bedding planes, the methodology proposed by Barton (1976) is appropriate for estimating the overall shear strength of the potential sliding surface. This involves adding a measured or estimated roughness component to the basic frictional strength which can be determined on sawn and polished laboratory shear test specimens.

For heavily jointed rock masses in which there are no dominant weakness zones such as faults or shear zones, a crude estimate of the shear strength of the rock mass can be obtained by means of the use of rock mass classification systems as proposed by Hoek and Brown (1988).

In all cases, a greater reliance can be placed upon the frictional component, ϕ, of the Mohr-Coulomb shear strength equation and extreme care must be taken in the estimation of the cohesive strength, *c*'. Where no reliable estimates of this value are available from carefully conducted shear tests or from back-analysis of existing failures, it is prudent to assume a cohesive strength of zero for any stability analysis involving structures such as dam foundations.

In the design of fill and gravity dams there is a tendency to move away from the high factors of safety of 2 or 3 which have been used in the past, if care is taken in choosing sensible conservative shear strength parameters, particularly for continuous weak seams in the foundations. An example of the range of factors of safety which can be used in the design of earth or rockfill dams is given in Table 7.

Probabilistic analyses

The uncertainty associated with the properties of geotechnical materials and the great care which must be taken in selecting appropriate values for analyses has prompted several authors to suggest that the traditional deterministic methods of slope stability analyses should be replaced by probabilistic methods (Priest and Brown, 1983, McMahon, 1975, Vanmarcke, 1980, Morriss and Stoter, 1983, Read and Lye, 1983).

One branch of rock mechanics in which probabilistic analyses have been accepted for many years is that of the design of open pit mine slopes. This is because open pit planners are familiar with the concepts of risk analysis applied to ore grade and metal price fluctuations. Probabilistic methods are used in estimating the economic viability of various options in developing an open pit mine and so it is a small step to incorporate the probability of a geotechnical failure into the overall risk assessment of the mine. The mine planner has the choice of reducing the probability of failure by the installation of reinforcement, reducing the angle of the slope, or accepting that failure will occur and providing for extra equipment which may be needed to clean up the failure. Since the mine is usually owned and operated by a single company and access to the mine benches is restricted to trained personnel, accepting a risk of failure, and dealing with the consequences on a routine basis is a viable option.
On the other hand, the emotional impact of suggesting to the public that there is a finite risk of failure attached to a dam design is such that it is difficult to suggest the replacement of the standard factor of safety design approach with one which explicitly states a probability of failure or a coefficient of reliability. The current perception is that the factor of safety is more meaningful than the probability of failure. Even if this were not so, there is still the problem of deciding what probability of failure is acceptable for a rock structure to which the public has access.

Despite these difficulties, there does appear to be a slow but steady trend in society to accept the concepts of risk analysis more readily than has been the case in the past. The geotechnical community has an obligation to take note of these developments and to

encourage the teaching and practical use of probabilistic as well as deterministic techniques with the aim of removing the cloak of mystery which surrounds the use of these methods.

Fortunately, there is a compromise solution which is a form of risk analysis used intuitively by most experienced engineers. This is a parametric analysis in which a wide range of possibilities are considered in a conventional deterministic analysis to gain a 'feel' for the sensitivity of the design. Hence, the factor of safety for a slope would be calculated for both fully drained and fully saturated groundwater conditions, for a range of friction angles and cohesive strengths covering the full spectrum which could be anticipated for the geological conditions existing on the site, for external forces ranging from zero to the maximum possible for that slope. The availability of user-friendly microcomputer software for most forms of limit equilibrium analysis means that these parametric studies can be carried out quickly and easily for most designs.

References

Amos, A.J., Granero Hernandez, A. and Rocca, R.J. 1981. Problemas de meteorizacion del geneis en la Presa Principal del complejo hidroeléctrico Río Grande I. *Proc. VIII Cong. Geol. Arg. Actas* **2,** 123-135.

Baker, D.G. 1991. Wahleach power tunnel monitoring. *Proc. 3rd Int. Symp. on Field Measurements in Geomechanics,* Oslo, Norway.

Barton, N.R. 1976. The shear strength of rock and rock joints. *Int. J. Rock Mech. Min. Sci. & Geomech. Abstr.* **13,** 1-24.

Barton, N.R. 1989. Cavern design for Hong Kong rocks. *Proc. Rock Cavern Seminar - Hong Kong* (eds A.W. Malone and P.G.D. Whiteside), 179-202. London: Instn Min. Metall.

Barton, N.R. 1976. The shear strength of rock and rock joints. *Int. J. Mech. Min. Sci. & Geomech. Abstr*. **13**(10), 1-24.

Barton, N.R., Lien, R. and Lunde, J. 1974. Engineering classification of rock masses for the design of tunnel support. *Rock Mech.* **6**(4), 189-239.

Bieniawski, Z.T. 1974. Estimating the strength of rock materials. *J. S. African Inst. Min. Metall* . **74** (8), 312-320.

Bieniawski, Z.T. 1974. Geomechanics classification of rock masses and its application in tunnelling. In *Advances in Rock Mechanics,* **2**, part A:27-32. Washington, D.C.: Nat. Acad. of Sciences.

Cheng, Y. 1987. New development in seam treatment of Feitsui arch dam foundation. *Proc. 6th Cong. ISRM, Montreal*, 319-326.

Hammett, R.D. and Hoek, E. 1981. Design of large underground caverns for hydroelectric projects, with reference to structurally controlled failure mechanisms. *Proc. American Soc. Civil Engrs. Int. Conf. on Recent Developments in Geotechnical Engineering for Hydro Projects.* 192-206. New York: ASCE.

Hoek, E. and Brown, E.T. 1988. The Hoek-Brown failure criterion - a 1988 update. *Proc. 15th Canadian Rock Mech. Symp*. (ed. J.H. Curran), 31-38. Toronto: Civil Engineering Dept., University of Toronto.

Imrie, A.S. 1983. Taming the Downie Slide. *Canadian Geographic* **103**.

Imrie, A.S., Moore, D.P. and Enegren, E.G. 1992. Performance and maintenance of the drainage system at Downie Slide. *Proc. 6th Int. Symp. on Landslides,* Christchurch, New Zealand.

Lewis, M.R. and Moore, D.P. 1989. Construction of the Downie Slide and Dutchman's Ridge drainage adits. *Canadian Tunnelling* (ed. Z. Eisenstein), 163-172. Vancouver: Bi-Tech.

Liu, S.C., Cheng, Y., and Chang, C.T. 1988. Design of the Mingtan cavern. *Proc .symp. ISRM. on Rock Mech. and Power Plants, Madrid*, 199-208.

Marachi, N.D., Chan, C.K. and Seed, H.B. 1972. Evaluation of properties of rockfill materials. *J. Soil Mechs. Fdns. Div. ASCE* **98** (SM4), 95-114.

McMahon, B.K. 1975. Probability of failure and expected volume of failure in high rock slopes. *Proc. 2nd Aust.-New Zealand Conf. on Geomech., Brisbane*.

Moore, D.P., Imrie, A.S. and Baker, D.G. 1991. Rockslide risk reduction using monitoring. *Proc. Can. Dam Safety Assn. Annual Meeting,* Whistler, British Columbia.

Moretto, O. 1982. Mecánica de rocas en el complejo hidroeléectrico Río Grande No. 1. *Proc. Primer. Cong. Sudamericano de Mecánica de Rocas, Bogotá, Colombia*.

Morgenstern, N.R. 1991. Limitations of stability analysis in geo-technical practice. *Geotecnia* **61**: 5-19.

Morriss, P. and Stoter, H.J. 1983. Open-cut slope design using probabilistic methods. *Proc. 5th. Cong. ISRM., Melbourne* **1** , C107-C113. Rotterdam: Balkema.

Moy, D. and Hoek, E. 1989. Progress with the excavation and support of the Mingtan power cavern roof. *Proc. Rock Cavern Seminar - Hong Kong* (eds. A.W. Malone and P.G.D. Whiteside), 235-245. London: Instn Min. Metall.

Priest, S.D. and Brown, E.T. 1983. Probabilistic stability analysis of variable rock slopes. *Trans. Inst. Min. Metall.*(Sect. A*)* **92**: 1-12.

Read, J.R.L. and Lye, G.N. 1983. Pit slope design methods, Bougainville Copper Limited open cut. *Proc. 5th Cong. ISRM., Melbourne,* C93-C98. Rotterdam: Balkema.

Tatchell, G.E. 1991. Automatic data acquisition systems for monitoring dams and landslides. *Proc. 3rd Int. symp. on Field Measurements in Geomechanics*, Oslo, Norway.

Vanmarcke, E.H. 1980. Probabilistic analysis of earth slopes. *Engineering Geology* **16**: 29-50.

8. Structurally controlled instability

Introduction

In tunnels excavated in jointed rock masses at relatively shallow depth, the most common types of failure are those involving wedges falling from the roof or sliding out of the sidewalls of the openings. These wedges are formed by intersecting structural features, such as bedding planes and joints, which separate the rock mass into discrete but interlocked pieces. When a free face is created by the excavation of the opening, the restraint from the surrounding rock is removed. One or more of these wedges can fall or slide from the surface if the bounding planes are continuous or rock bridges along the discontinuities are broken.

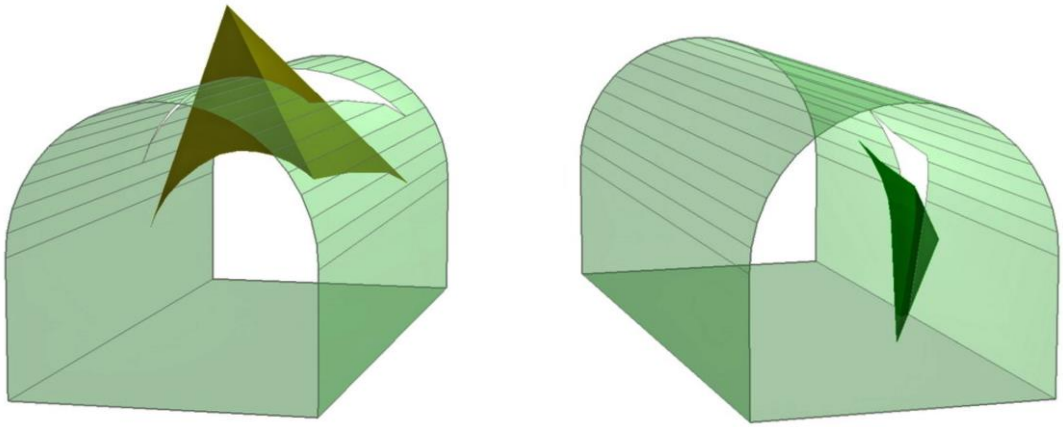

Roof fall Sidewall wedge

Unless steps are taken to support these loose wedges, the stability of the back and walls of the opening may deteriorate rapidly. Each wedge, which is allowed to fall or slide, will cause a reduction in the restraint and the interlocking of the rock mass and this, in turn, will allow other wedges to fall. This failure process will continue until natural arching in the rock mass prevents further unravelling or until the opening is full of fallen material.

The steps which are required to deal with this problem are:

1. determination of average dip and dip direction of significant discontinuity sets
2. identification of potential wedges which can slide or fall from the back or walls
3. calculation of the factor of safety of these wedges, depending upon the mode of failure
4. calculation of the amount of reinforcement required to bring the factor of safety of individual wedges up to an acceptable level.

Identification of potential wedges

The size and shape of potential wedges in the rock mass surrounding an opening depends upon the size, shape, and orientation of the opening and upon the orientation of the significant discontinuity sets. The three-dimensional geometry of the problem necessitates a set of relatively tedious calculations. While these can be performed by hand, it is far more efficient to utilise one of the computer programs which are available. One such RocScience program, called UNWEDGE, was developed specifically for use in underground hard rock mining and is utilised in the following discussion.

Consider a rock mass in which three strongly developed joint sets occur. The average dips and dip directions of these sets, shown as great circles in Figure 1, are as follows:

Joint set	*dip°*	*dip direction°*
J1	70 ± 5	036 ± 12
J2	85 ±8	144 ± 10
J3	55 ± 6	262 ± 15

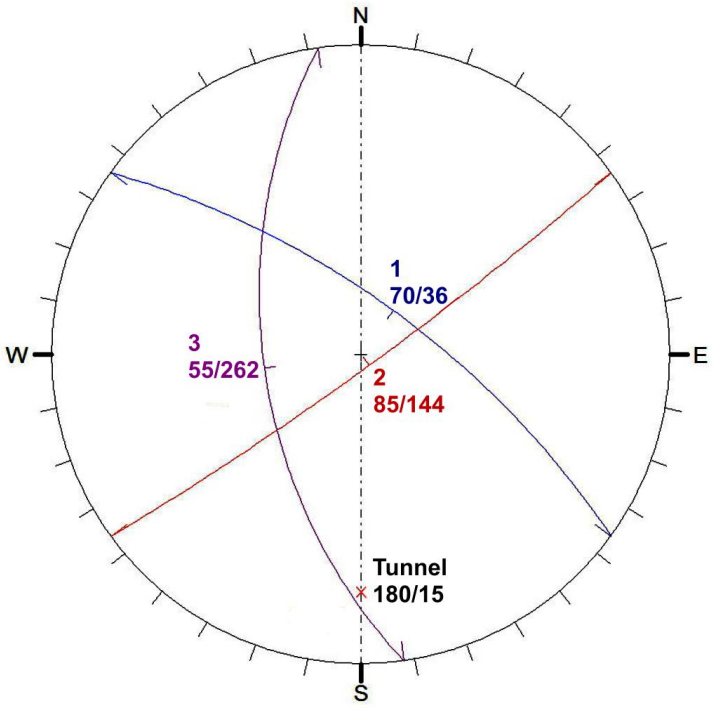

Figure 1: An equal area lower hemisphere plot of great circles representing the average dip and dip directions of three discontinuity sets in a rock mass. Also shown, as a chain dotted line, is the trend of the axis of a tunnel excavated in this rock mass. The tunnel plunge is marked with a red cross.

It is assumed that all these discontinuities are planar and continuous and that the shear strength of the surfaces can be represented by a friction angle $\phi = 30°$ and a cohesive strength of zero. These shear strength properties are very conservative estimates, but they provide a reasonable starting point for most analyses of this type.

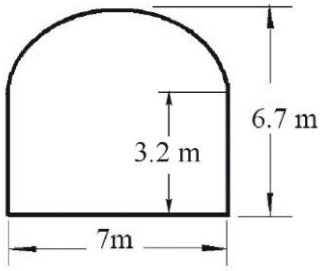

Tunnel section

A tunnel is to be excavated in this rock mass and the cross-section of the ramp is given in the sketch. The axis of the tunnel is inclined at 15° to the horizontal or, to use the terminology associated with structural geology analysis, the tunnel axis plunges at 15°. In the portion of the tunnel under consideration in this example, the axis runs due north-south, or the trend of the axis is 180°.

The tunnel axis is shown as a chain dotted line in the stereonet in Figure 1. The trend of the axis is shown as 0°, measured clockwise from north. The plunge of the axis is 15° wich is shown as a cross on the chain dotted line representing the axis. The angle is measured inwards from the perimeter of the stereonet since this perimeter represents a horizontal reference plane.

The three structural discontinuity sets, represented by the great circles plotted in Figure 1, are entered into the program UNWEDGE, together with the cross-section of the tunnel and the plunge and trend of the tunnel axis. The program then determines the location and dimensions of the largest wedges which can be formed in the roof, floor and sidewalls of the excavation as shown in Figure 2.

The maximum number of simple tetrahedral wedges which can be formed by three discontinuities in the rock mass surrounding a circular tunnel is six. In the case of a square or rectangular tunnel this number is reduced to four. For the tunnel under consideration in this example, four wedges are formed.

Note that these wedges are the largest which can be formed for the given geometrical conditions. The calculation used to determine these wedges assumes that the discontinuities are ubiquitous; in other words, they can occur anywhere in the rock mass. The joints, bedding planes and other structural features included in the analysis are also assumed to be planar and continuous. These conditions mean that the analysis will always find the largest possible wedges which can form. This result can generally be considered conservative since the size of wedges, formed in actual rock masses, will be limited by the persistence and the spacing of the structural features. The program UNWEDGE allows wedges to be scaled down to more realistic sizes if it is considered that maximum wedges are unlikely to form.

Details of the four wedges illustrated in Figure 2 are given in the following table:

Wedge	Weight - tonnes	Failure mode	Factor of Safety
Roof wedge	44.2	Falls	0
Right side wedge	5.2	Slides on J1/J2	0.36
Left side wedge	3.6	Slides on J3	0.40
Floor wedge	182	Stable	∞

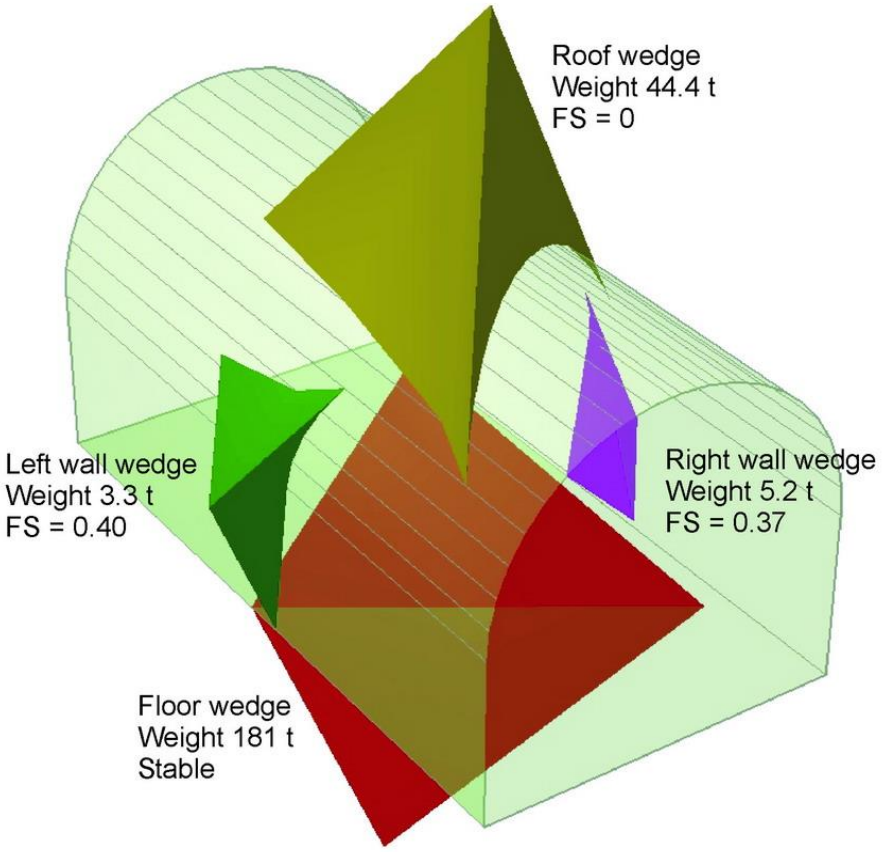

Figure 2: Wedges formed in the roof, floor and sidewalls of a ramp excavated in a jointed rock mass, in which the average dip and dip direction of three dominant structural features are defined by the great circles plotted in Figure 1.

The roof wedge will fall because of gravity loading and, because of its shape, there is no restraint from the three bounding discontinuities. This means that the factor of safety of

the wedge, once it is released by excavation of the ramp opening, is zero. In some cases, sliding on one plane or along the line of intersection of two planes may occur in a roof wedge and this will result in a finite value for the factor of safety.

The two sidewall wedges are 'cousin' images of one another in that they are approximately the same shape but disposed differently in space. The factors of safety are different since, as shown in the table, sliding occurs on different surfaces in the two cases.

The floor wedge is completely stable and requires no further consideration.

Influence of in situ stress

The program UNWEDGE can consider in situ stresses in the rock mass surrounding the opening. For the example under consideration, the influence of in situ stresses can be illustrated by the following example:

Stress	Magnitude	Plunge	Trend
Vertical stress σ_1	30 t/m^2	90º	030º
Intermediate stress σ_2	21 t/m^2	0º	030º
Minor stress σ_3	15 t/m^2	0º	120º

Wedge	Factor of Safety with no in situ stress	Factor of Safety with applied in situ stress
Roof wedge	0	1.23
Right side wedge	0.36	0.70
Side wedge 2	0.40	0.68
Floor wedge	∞	∞

The difference in the calculated factors of safety, with and without in situ stresses, show that the clamping forces acting on the wedges can have a significant influence on their stability. The roof wedge is stable with the in-situ stresses applied, but completely unstable when released. This large difference suggests a tendency for sudden failure when the in-situ stresses are diminished for any reason and is a warning sign that care must be taken in terms of the excavation and support installation sequence.

Since it is very difficult to predict the in-situ stresses precisely and to determine how these stresses can change with excavation of the tunnel or of adjacent tunnels or openings, many tunnel designers consider that it is prudent to design the tunnel support on the basis that there are no in situ stresses. This ensures that, for almost all cases, the support design will be conservative.

In rare cases the in-situ stresses can result in a reduction of the factor of safety of sidewall wedges which may be forced out of their sockets. These cases are rare enough that, generally, they can be ignored for support design purposes.

Support to control wedge failure

A characteristic feature of wedge failures in blocky rock is that very little movement occurs in the rock mass before failure of the wedge. In the case of a roof wedge that falls, failure can occur as soon as the base of the wedge is fully exposed by excavation of the opening. For sidewall wedges, sliding of a few millimetres along one plane or the line of intersection of two planes is generally sufficient to overcome the peak strength of these surfaces. This dictates that movement along the surfaces must be minimised. Consequently, the support system must provide a 'stiff' response to movement. This means that mechanically anchored rockbolts need to be tensioned while fully grouted rockbolts or other continuously coupled devices can be left untensioned provided that they are installed before any movement has taken place i.e. before the wedge perimeter has been fully exposed.

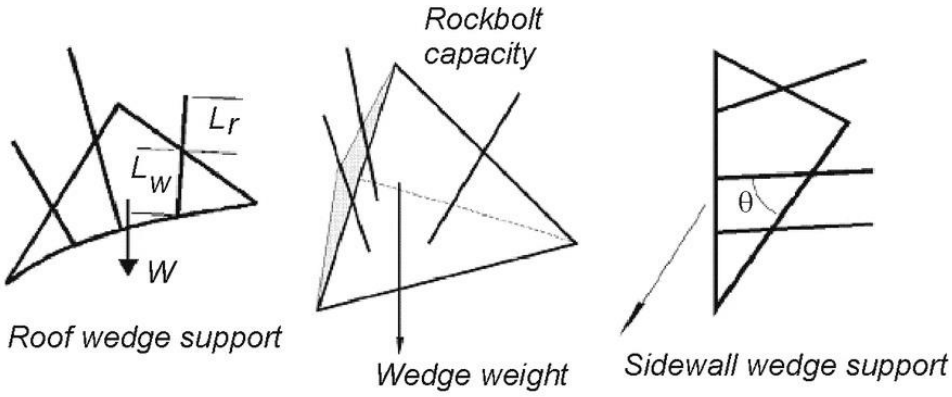

Figure 3: Rockbolt support mechanisms for wedges in the roof and sidewalls of tunnels

Rock bolting wedges

For roof wedges, the total force which should be applied by the reinforcement, should be sufficient to support the full dead weight of the wedge, plus an allowance for errors and poor-quality installation. Hence, for the roof wedge illustrated in Figure 3; the total tension applied to the rock bolts or cables should be 1.3 to 1.5 × W, giving factors of safety of 1.3 to 1.5. The lower factor of safety would be acceptable in a temporary mine access opening, such as a drilling drive, while the higher factor of safety would be used in a more permanent access opening such as a highway tunnel.

When the wedge is clearly identifiable, some attempt should be made to distribute the support elements uniformly about the wedge centroid. This will prevent any rotations which can reduce the factor of safety.

In selecting the rock bolts or cable bolts to be used, attention must be paid to the length and location of these bolts. For grouted cable bolts, the length Lw through the wedge and the length Lr in the rock behind the wedge should both be sufficient to ensure that adequate anchorage is available, as shown in Figure 3. In the case of correctly grouted bolts or cables, these lengths should generally be a minimum of about one metre. Where there is uncertainty about the quality of the grout, longer anchorage lengths should be used. When mechanically anchored bolts with face plates are used, the lengths should be sufficient to ensure that enough rock is available to distribute the loads from these attachments. These conditions are automatically checked in the program UNWEDGE.

In the case of sidewall wedges, the bolts or cables can be placed in such a way that the shear strength of the sliding surfaces is increased. As illustrated in Figure 3; this means that more bolts or cables are placed to cross the sliding planes than across the separation planes. Where possible, these bolts or cables should be inclined so that the angle θ is between 15° and 30° since this inclination will induce the highest shear resistance along the sliding surfaces.

The program UNWEDGE includes several options for designing support for underground excavations. These include pattern bolting, from a selected drilling position or placed normal to the excavation surface; and spot bolting, in which the location and length of the bolts are decided by the user for each installation. Mechanically anchored bolts with face plates or fully grouted bolts or cables can be selected to provide support. In addition, a layer of shotcrete can be applied to the excavation surface.

In most cases it is not practical to identify individual wedges in a tunnel perimeter and the general approach is to design a rockbolt pattern that will take care of all potential wedges. In the example under consideration, the maximum wedge sizes have been identified as shown in Figure 2, and it has been decided that in situ stresses will not be included in the stability analysis. Consequently, the wedges and their associated factors of safety shown in Figure 2 can be regarded as the most conservative estimate.

Figure 4 shows a typical pattern of 3 m long mechanically anchored 10 tonne capacity rockbolts on a 1.5 x 1.5 m grid. This pattern produces factors of safety of 1.40 for the roof wedge, 3.77 for the right sidewall wedge and 4.77 for the left sidewall wedge.

Shotcrete support for wedges

Shotcrete can be used for additional support of wedges in blocky ground and can be very effective if applied correctly. This is because the base of a typical wedge has a large perimeter and, hence, even for a relatively thin layer of shotcrete, a significant cross-sectional area of the material must be punched through before the wedge can fail.

In the example under consideration, the application of a 10 cm thick shotcrete with a shear strength of 200 t/m^2 to the roof of the tunnel will increase the factor of safety from 1.40 (for the rockbolted case) to 8.5. Note that this only applies to fully cured (28 day) shotcrete and that the factor of safety increase given by the application of shotcrete cannot be relied on for short term stability. It is recommended that only the rockbolts be considered for immediate support after excavation and that the shotcrete only be considered for the long-term factor of safety.

It is important to ensure that the shotcrete is well bonded to the rock surface in order to prevent a reduction in support capacity by peeling-off of the shotcrete layer. Good adhesion to the rock is achieved by washing the rock surface, using water only as feed to the shotcrete machine, before the shotcrete is applied.

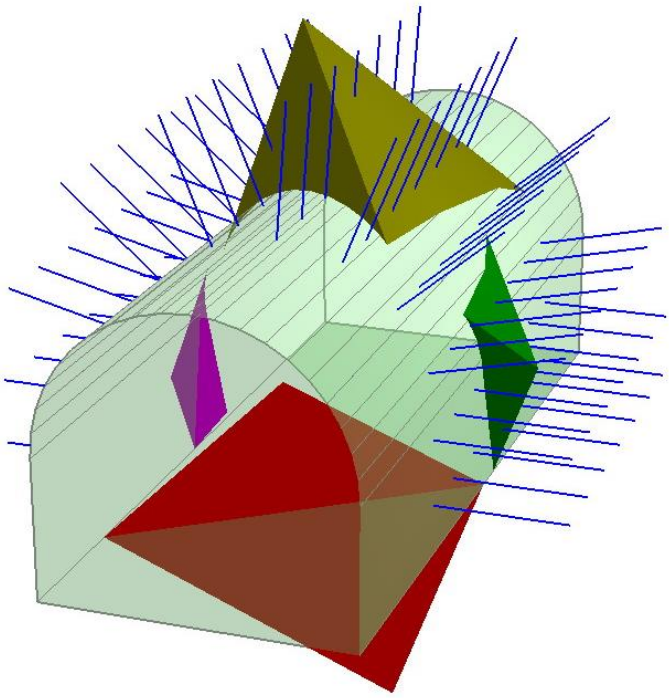

Figure 4: Rock bolting pattern to stabilize the roof and sidewall wedges in the tunnel example discussed earlier.

Figure 5: Ravelling of small wedges in a closely jointed rock mass. Shotcrete can provide effective support in such rock masses.

The ideal application for shotcrete is in closely jointed rock masses such as that illustrated in Figure 5. In such cases wedge failure would occur as a progressive process, starting with smaller wedges exposed at the excavation surface and gradually working its way back into the rock mass. In these circumstances, shotcrete provides very effective support and deserves to be much more widely used than is currently the case. The addition of wire mesh, such as that illustrated in Figure 6, is also effective for supporting blocky rock.

Figure 6: Wire mesh, used in conjunction with steel sets and/or rockbolts, is very effective for the support of blocky rock, particularly in tunnelling using a TBM, as shown in this figure. It also provides effective reinforcement for the shotcrete layer.

Consideration of excavation sequence

As has been emphasised several times in this chapter, wedges tend to fall or slide as soon as they are fully exposed in an excavated face. Consequently, they require immediate support to ensure stability. Placing this support is an important practical question to be addressed when working in blocky ground which is prone to wedge failure.

When the structural geology of the rock mass is reasonably well understood, the program UNWEDGE can be used to investigate potential wedge sizes and locations. A support pattern, which will secure these wedges, can then be designed and rockbolts can be installed as excavation progresses.

When dealing with larger excavations such as caverns, underground crusher chambers or shaft stations, the problem of sequential support installation is a little simpler, since these excavations are usually excavated in stages. Typically, in an underground crusher chamber, the excavation is started with a top heading which is then slashed out before the remainder of the cavern is excavated by benching, as illustrated below.

The margin sketch shows a large opening excavated in four stages with rock bolts or cables installed at each stage to support wedges, which are progressively exposed in the roof and sidewalls of the excavation. The length, orientation and spacing of the bolts or cables are chosen to ensure that each wedge is adequately supported before it is fully exposed in the excavation surface.

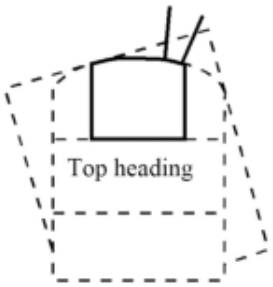

When dealing with large excavations of this type, the structural geology of the surrounding rock mass will have been defined from core drilling or access adits and a reasonable projection of potential wedges will be available. These projections can be confirmed by additional mapping as each stage of the excavation is completed. The program UNWEDGE provides an effective tool for exploring the size and shape of potential wedges and the support required to stabilise them.

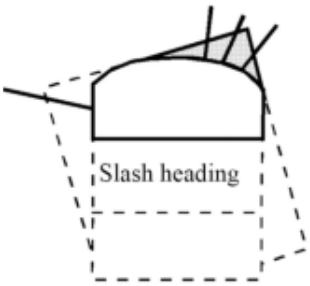

The margin sketch shows a support design which is based upon the largest possible wedges which can occur in the roof and walls of the excavation. These wedges can sometimes form in rock masses with very persistent discontinuity surfaces such as bedding planes in layered sedimentary rocks. In many metamorphic or igneous rocks, the discontinuity surfaces are not continuous and the size of the wedges that can form is limited by the persistence of these surfaces.

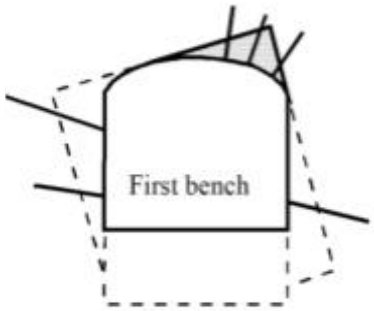

The program UNWEDGE provides several options for sizing wedges. One of the most measured lengths in structural mapping is the length of a joint trace on an excavation surface and one of the sizing options is based upon this trace length. The surface area of the base of the wedge, the volume of the wedge and the apex height of the wedge are all calculated by the program and all these values can be edited by the user to set a scale for the wedge. This scaling option is very important when using the program interactively for designing support for large openings, where the maximum wedge sizes become obvious as the excavation progresses.

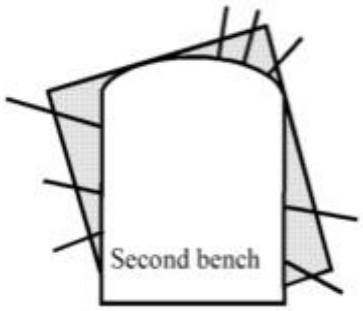

Application of probability theory

The program UNWEDGE has been designed for the analysis of a single wedge defined by three intersecting discontinuities. The "Combination Analyzer" in the program UNWEDGE can be used to sort through all possible joint combinations in a large discontinuity population to select the three joints which define most critical wedges.

Early attempts have been made by several authors, including Tyler et al (1991) and Hatzor and Goodman (1992), to apply probability theory to these problems with some promising results. The analyses developed, thus far, are not easy to use and cannot be considered as design tools. However, these studies have shown the way for future development of such tools. It is anticipated that powerful and user-friendly methods of probabilistic analysis will be available within a few years.

References

Hatzor, Y. and Goodman, R.E. 1992. Application of block theory and the critical key block concept in tunnelling; two case histories. *In Proc. Int. Soc. Rock Mech. conf. on fractured and jointed rock masses*, Lake Tahoe, California, 632-639.

Tyler, D.B., Trueman, R.T. and Pine, R.J. 1991. Rockbolt support design using a probabilistic method of key block analysis. In *Rock mechanics as a multidisciplinary science*, (ed. J.C. Roegiers), 1037-1047. Rotterdam: Balkema.

Tyler, D.B., Trueman, R. and Pine, R.J. 1991. Rockbolt support design using a probabilistic method of key block analysis. *Proc. 32nd U.S. Symp. Rock Mechanics*, Norman, Oklahoma, 1037-47.

9. Factor of safety and probability of failure

Introduction

How does one assess the acceptability of an engineering design? Relying on judgement alone can lead to one of the two extremes illustrated in Figure 1. The first case is economically unacceptable while the example illustrated in the drawing on the right violates all normal safety standards.

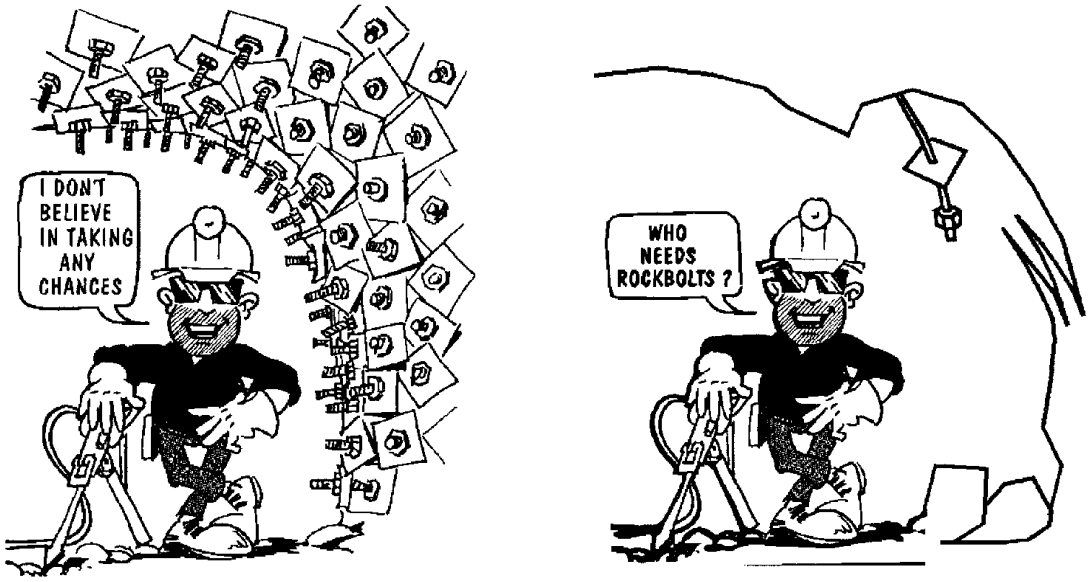

Figure 1: Rock bolting alternatives involving individual judgement. (Drawings from a brochure on rockfalls published by the Department of Mines of Western Australia.)

Sensitivity studies

The classical approach used in designing engineering structures is to consider the relationship between the capacity C (strength or resisting force) of the element and the demand D (stress or disturbing force). The Factor of Safety of the structure is defined as F = C/D. Failure is assumed to occur when F is less than unity.

Rather than base an engineering design decision on a single calculated factor of safety, an approach which is frequently used to give a more rational assessment of the risks associated with a particular design, is to carry out a sensitivity study. This involves a series of calculations in which each significant parameter is varied systematically over its maximum credible range to determine its influence upon the factor of safety. This is a useful means of exploring a range of possibilities and reaching practical decisions on some difficult problems. On the following pages this idea of sensitivity studies will be extended to the use of probability theory, and it will be shown that, even with very limited field data, useful information can be obtained from an analysis of probability of failure.

An introduction to probability theory

A complete discussion on probability theory exceeds the scope of these notes. The techniques discussed on the following pages are intended to introduce the reader to the subject and to give an indication of the power of these techniques in engineering decision making. A more detailed treatment of this subject will be found in a book by Harr (1987) entitled, 'Reliability-based design in civil engineering'. A paper on geotechnical applications of probability theory entitled 'Evaluating calculated risk in geotechnical engineering', was published by Whitman (1984). It is recommended reading for anyone with a serious interest in this subject. Pine (1992), Tyler et al (1991), Hatzor and Goodman (1993) and Carter (1992) have published papers on the application of probability theory to the analysis of problems encountered in underground mining and civil engineering.

Many geotechnical engineers regard the subject of probability theory with doubt and suspicion. At least part of the reason for this mistrust is associated with the language which has been adopted by those who specialise in the field of probability theory and risk assessment. The following definitions are given to dispel some of the mystery which tends to surround this subject.

Random variables: Parameters such as the angle of friction of rock joints, the uniaxial compressive strength of rock specimens, the inclination and orientation of discontinuities in a rock mass and the measured in situ stresses in the rock surrounding an opening do not have a single fixed value but may several values. There is no way of predicting exactly what the value of one of these parameters will be at any given location. Hence, these parameters are described as random variables.

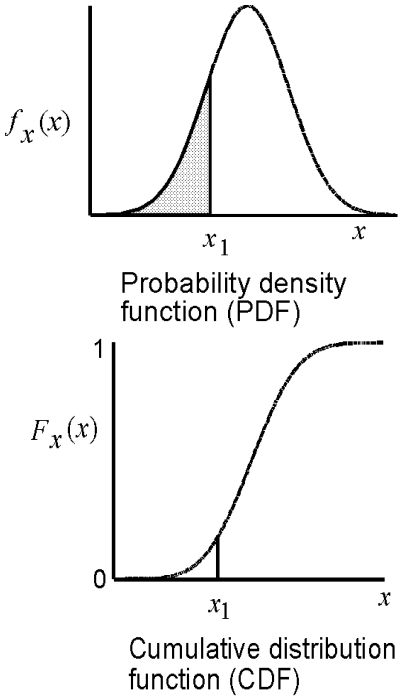

Probability distribution: A probability density function (PDF) describes the relative likelihood that a random variable will assume a particular value. A typical probability density function is illustrated opposite. In this case the random variable is continuously distributed (i.e., it can take on all possible values). The area under the PDF is always unity.

An alternative way of presenting the same information is in the form of a cumulative distribution function (CDF), which gives the probability that the variable will have a value less than or equal to the selected value. The CDF is the integral of the corresponding probability density function, i.e., the ordinate at x_1 on the cumulative distribution is the area under the probability density function to the left of x_1. Note the fx(x) is used for the ordinate of a PDF while Fx(x) is used for a CDF.

One of the most common graphical representations of a probability distribution is a histogram in which the fraction of all observations falling within a specified interval is plotted as a bar above that interval.

Data analysis: For many applications it is not necessary to use all the information contained in a distribution function and quantities summarised only by the dominant features of the distribution may be adequate.

The sample mean or expected value or first moment indicates the centre of gravity of a probability distribution. A typical application would be the analysis of a set of results $x_1, x_2, ..., x_n$ from uniaxial strength tests carried out in the laboratory. Assuming that there are *n* individual test values x_i, the mean $\bar{x}$ is given by:

$$\bar{x} = \frac{1}{n} \sum_{i=1}^{n} x_i \qquad (1)$$

The sample variance s^2 *or the second moment* of the mean of a distribution is defined as the mean of the square of the difference between the value of xi and the mean value $\bar{x}$.

Hence:

$$s^2 = \frac{1}{n-1}\sum_{i=1}^{n}(x_i - \bar{x})^2 \qquad (2)$$

Note that, theoretically, the denominator for calculation of variance of samples should be *n*, not (*n* - 1). However, for a finite number of samples, it can be shown that the correction factor *n*/(*n*-1), known as Bessel's correction, gives a better estimate. For practical purposes the correction is only necessary when the sample size is less than 30.

The *standard deviation s* is given by the positive square root of the variance s^2. In the case of the commonly used normal distribution, about 68% of the test values will fall within an interval defined by the *mean* ± *one standard deviation* while approximately 95% of all the test results will fall within the range defined by the *mean* ± two *standard deviations*. A small standard deviation will indicate a tightly clustered data set while a large standard deviation will be found for a data set in which there is a large scatter about the mean.

The *coefficient of variation* (COV) is the ratio of the standard deviation to the mean, i.e., COV = $s/\bar{x}$. COV is dimensionless and it is a particularly useful measure of uncertainty. A small uncertainty would typically be represented by a COV = 0.05 while considerable uncertainty would be indicated by a COV = 0.25.

Normal distribution: The *normal* or *Gaussian* distribution is the most common type of probability distribution function, and the distributions of many random variables conform to this distribution. It is generally used for probabilistic studies in geotechnical engineering unless there are good reasons for selecting a different distribution. Typically, variables which arise as a sum of several random effects, none of which dominate the total, are normally distributed.

The problem of defining a normal distribution is to estimate the values of the governing parameters which are the true mean (μ) and true standard deviation (σ). Generally, the best estimates for these values are given by the sample mean and standard deviation, determined from several tests or observations. Hence, from equations 1 and 2:

$$\mu = \bar{x} \qquad (3)$$

$$\sigma = s \qquad (4)$$

It is important to recognise that equations 3 and 4 give the most probable values of μ and σ and not necessarily the true values.

Obviously, it is desirable to include as many samples as possible in any set of observations but, in geotechnical engineering, there are serious practical and financial limitations to the amount of data which can be collected. Consequently, it is often necessary to make estimates based on judgement, experience or from comparisons with results published by others. These difficulties are often used as an excuse for not using probabilistic tools in geotechnical engineering, but as will be shown later in this chapter, useful results can still be obtained from very limited data.

Having estimated the mean μ and standard deviation σ, the probability density function for a normal distribution is defined by:

$$f_x(x) = \frac{\exp\left[-\frac{1}{2}\left(\frac{x-\mu}{\sigma}\right)^2\right]}{\sigma\sqrt{2\pi}} \qquad (5)$$

for $-\infty \leq x \leq \infty$.

As will be seen later, this range of $-\infty \leq x \leq \infty$ can cause problems when a normal distribution is used as a basis for a Monte Carlo analysis in which the entire range of values is randomly sampled. This can give rise to a few very small numbers (sometimes negative) and very large numbers which, in certain analyses, can cause numerical instability. To overcome this problem, the normal distribution is sometimes truncated so that only values falling within a specified range are considered valid.

There is no closed form solution for the cumulative distribution function (CDF) which must by found by numerical integration.

Other distributions: In addition to the commonly used normal distribution there are several alternative distributions which are used in probability analyses. Some of the most useful are:

Beta distributions (Harr, 1987) are very versatile distributions which can be used to replace almost any of the common distributions, and which do not suffer from the extreme value problems discussed above because the domain (range) is bounded by specified values.

Exponential distributions are sometimes used to define events such as the occurrence of earthquakes or rockbursts or quantities such as the length of joints in a rock mass.

Lognormal distributions are useful when considering processes such as the crushing of aggregates in which the final particle size results from several collisions of particles of many sizes moving in different directions with different velocities. Such multiplicative

mechanisms tend to result in variables which are lognormally distributed as opposed to the normally distributed variables resulting from additive mechanisms.

Weibul distributions are used to represent the lifetime of devices in reliability studies or the outcome of tests such as point load tests on rock core in which a few very high values may occur.

It is no longer necessary for the person starting out in the field of probability theory to know and understand the mathematics involved in all these probability distributions since commercially available software programs can be used to carry out many of the computations automatically. Note that the author is not advocating the blind use of 'black-box' software and the reader should exercise extreme caution is using such software without trying to understand what the software is doing. However, there is no point in writing reports by hand if one is prepared to spend the time learning how to use a good word-processor correctly and the same applies to mathematical software.

One of the most useful software packages for probability analysis is a Microsoft Excel add-in program called @RISK[1] which can be used for risk evaluations using the techniques described below.

Sampling techniques: Consider a problem in which the factor of safety depends upon several random variables such as the cohesive strength *c*, the angle of friction ϕ and the acceleration α due to earthquakes or large blasts. Assuming that the values of these variables are distributed about their means in a manner which can be described by one of the continuous distribution functions such as the normal distribution described earlier, the problem is how to use this information to determine the distribution of factor of safety values and the probability of failure.

The Monte Carlo method uses random or pseudo-random numbers to sample from probability distributions and, if sufficiently large numbers of samples are generated and used in a calculation such as that for a factor of safety, a distribution of values for the product will be generated. The term 'Monte Carlo' is believed to have been introduced as a code word to describe this hit-and-miss technique used during secret work on the development of the atomic bomb during World War II (Harr 1987). Today, Monte Carlo techniques can be applied to a wide variety of problems involving random behaviour and several algorithms are available for generating random Monte Carlo samples from different types of input probability distributions. With highly optimised software programs such as @RISK, problems involving relatively large samples can be run efficiently on most desktop or portable computers.

[1] @RISK is available from www.palisade.com.

The *Latin Hypercube* sampling technique (Imam et al, 1980, Startzman and Watterbarger, 1985) is a relatively recent development which gives comparable results to the Monte Carlo technique but with fewer samples. The method is based upon stratified sampling with random selection within each stratum. Typically, an analysis using 1000 samples obtained by the Latin Hypercube technique will produce comparable results to an analysis using 5000 samples obtained using the Monte Carlo method. Both techniques are incorporated in the program @RISK.

Note that both the Monte Carlo and the Latin Hypercube techniques require that the distribution of all the input variables should either be known or that they be assumed. When no information on the distribution is available it is usual to assume a normal or a truncated normal distribution.

The *Generalised Point Estimate Method*, developed by Rosenbleuth (1981) and discussed in detail by Harr (1987), can be used for rapid calculation of the mean and standard deviation of a quantity such as a factor of safety which depends upon random behaviour of input variables. Hoek (1989) discussed the application of this technique to the analysis of surface crown pillar stability while Pine (1992) has applied this technique to the analysis of slope stability and other mining problems.

To calculate a quantity such as a factor of safety, two-point estimates are made at one standard deviation on either side of the mean ($\mu \pm \sigma$) from each distribution representing a random variable. The factor of safety is calculated for every possible combination of point estimates, producing 2^n solutions where n is the number of random variables involved. The mean and the standard deviation of the factor of safety are then calculated from these 2^n solutions.

While this technique does not provide a full distribution of the output variable, as do the Monte Carlo and Latin Hypercube methods, it is very simple to use for problems with relatively few random variables and is useful when general trends are being investigated. When the probability distribution function for the output variable is known, for example, from previous Monte Carlo analyses, the mean and standard deviation values can be used to calculate the complete output distribution.

Some of the techniques described above have been incorporated into specialized commercial software packages and one of these called RocPlane[2] was used to analyse the Sau Mau Ping slope.

[2] Available from www.rocscience.com

Probability of failure

In the case of a rock slope problem, illustrated below, the input parameters and assumed distributions for the calculation of the factor of safety of the overall slope with a tension crack are as follows:

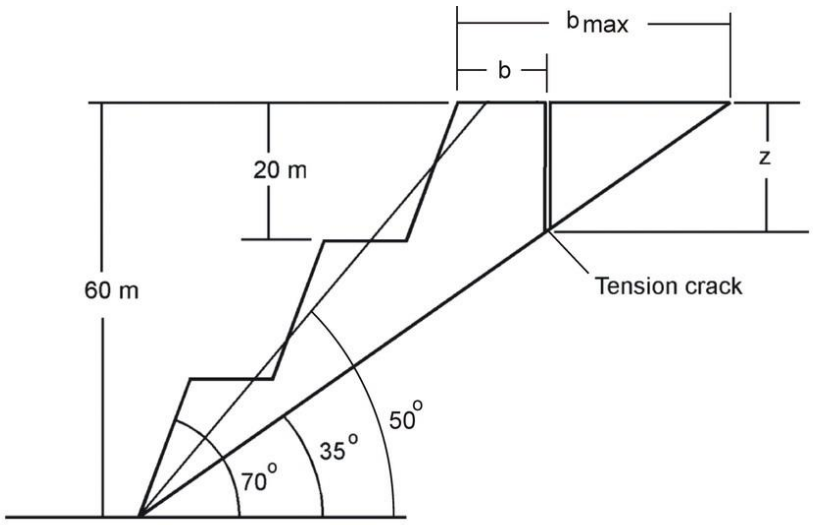

1. Fixed dimensions:

Overall slope height	H = 60 m
Overall slope angle	ψ_f = 50°
Failure plane angle	ψ_p = 35°
Upper slope inclination	horizontal
Bench width $b_{max} = H(\cot \psi_p - \text{Cot } \psi_f)$	b_{max} = 35.34 m
Unit weight of rock	γ_r = 2.6 tonnes/m^3
Unit weight of water	γ_w = 1.0 tonnes/m^3

2. Random variables	*Mean values*	*Standard deviation*	*Distribution*
Friction angle on joint surface	ϕ = 35°	± 5	Normal
Cohesive strength of joint surface	c = 10 tonnes/m^2	± 2	Normal
Depth of tension crack	z = 14 m	± 3	Normal
Distance from crest to tension crack	b = 15.3 m	± 4	Normal
Depth of water in tension crack	z_w = z/2	min = 0, max = z	Exponential
Ratio of horizontal earthquake to gravitational acceleration	α = 0.08	min = 0, max = 2α	Exponential

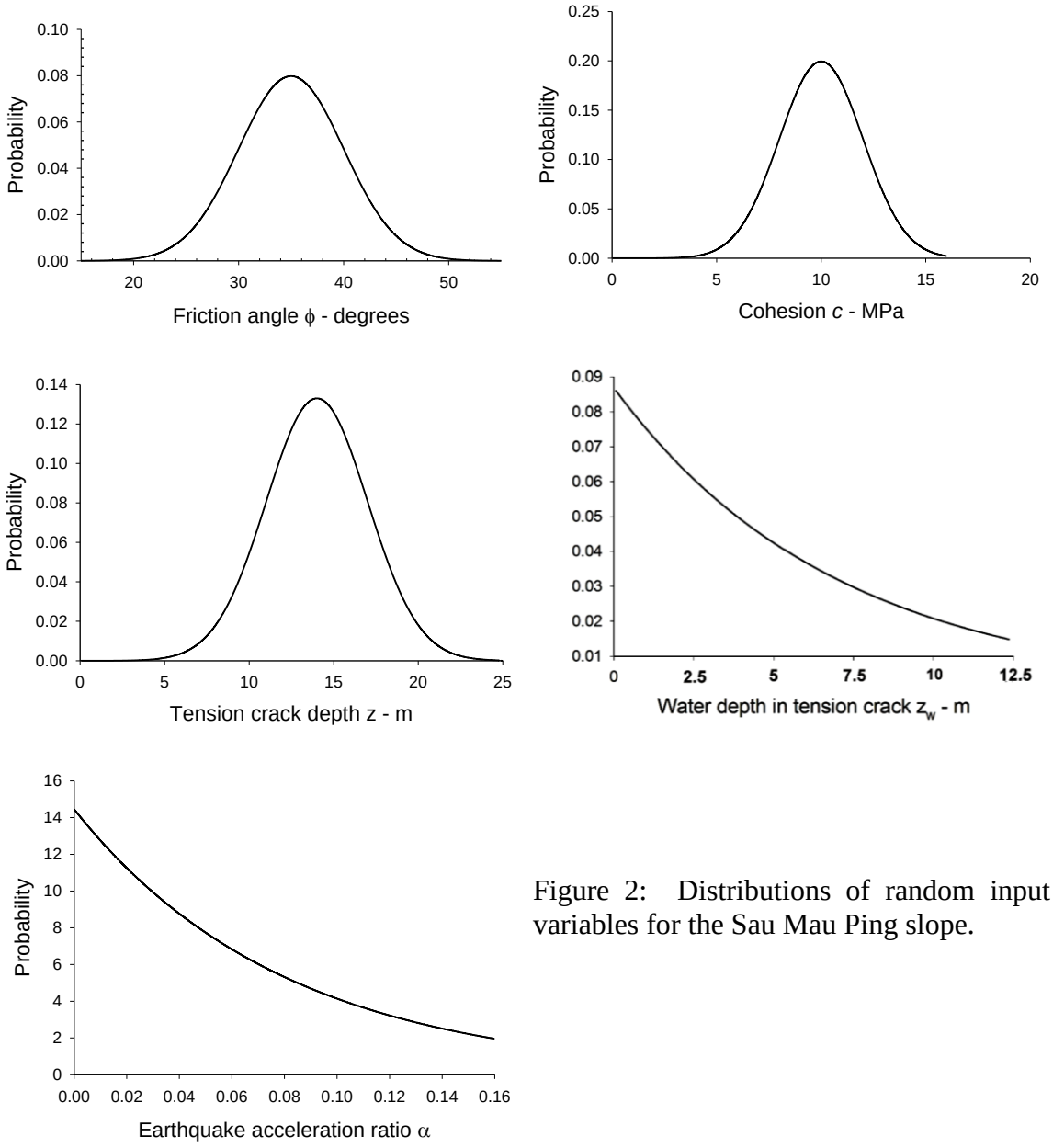

Figure 2: Distributions of random input variables for the Sau Mau Ping slope.

Figure 2 illustrates the plots of the probability distribution functions of the random input variables. It is worth discussing each of the plots in detail to demonstrate the reasoning behind the choice of the probability distribution functions.

Friction angle ϕ - A truncated normal distribution has been assumed for this variable. The mean is assumed to be 35° which is typical for the relatively rough surfaces of discontinuities in rock masses. The standard deviation of 5° implies that about 68% of the friction angle values defined by the distribution will lie between 30° and 40°. The normal distribution is truncated by a minimum value of 15° and a maximum value of 70° which have been arbitrarily chosen as the extreme values represented by a smooth slickensided surface and a fresh, rough tension fracture.

Cohesive strength c - Again using a typical range of shear strength values, a value of 10 tonnes/m^2 has been chosen as the mean cohesive strength and the standard deviation has been set at 2 tonnes/m^2. To allow for the wide range of possible cohesive strengths the minimum and maximum values used to truncate the normal distribution are 0 and 25 tonnes/m^2 respectively. Those with experience in the interpretation of laboratory shear strength test results may argue that the friction angle ϕ and the cohesive strength *c* are not independent variables as has been assumed in this analysis. This is because the cohesive strength generally drops as the friction angle rises and vice versa. The program @RISK allows the user to define variables as dependent but, for the sake of simplicity, the friction angle ϕ and the cohesive strength *c* have been kept independent for this analysis.

Distance of tension crack behind face b – The RocScience program, RocPlane, uses the horizontal distance *b* of the tension crack behind the slope crest as input in place of the tension crack depth *z* because *b* can be measured in the field and because it is not influenced by the inclination of the upper slope. Hoek and Bray (1974) give the value of b as $b = H\left(\sqrt{\cot\psi_f \tan\psi_p} - \cot\psi_f\right)$ with the limits as $0 < b < H\left(\cot\psi_p - \cot\psi_f\right)$.

Tension crack depth z – The tension crack depth z has a value of 14 m for the assumed conditions shown for this slope. A truncated normal distribution is assumed to define the possible range of tension crack depths and the standard deviation has been arbitrarily chosen at 3 m. The minimum tension crack depth is zero, but a value of 0.1 m has been chosen to avoid possible numerical problems. The maximum tension crack depth is given by $z = H(1 - \tan\psi_p / \tan\psi_f)$ = 24.75 m which occurs when the vertical tension crack is located at the crest of the slope.

Water depth z_w in tension crack - The water which would fill the tension crack in this slope would come from direct surface run-off during heavy rains. In Hong Kong the heaviest rains occur during typhoons and it is likely that the tension crack would be filled completely during such events. The probability of occurrence of typhoons has been

defined by a truncated exponential distribution where the mean water depth is assumed to be one half of the tension crack depth. The maximum water depth cannot exceed the tension crack depth *z* and, as defined by the exponential distribution, this value would occur very rarely. The minimum water depth is zero during dry conditions which is assumed to be a frequent occurrence.

Ratio of horizontal earthquake acceleration to gravitational acceleration α - The frequent occurrence of earthquakes of different magnitudes can be estimated by means of an exponential distribution which suggests that large earthquakes are very rare while small ones are very common. In this case, a 'design' horizontal acceleration of 0.08g has been assumed. In other words, this level of acceleration could be anticipated at least once during the operating life of a civil engineering structure. A rough rule of thumb suggests that the 'maximum credible' acceleration is approximately twice the 'design' value. Based upon these very crude guidelines, the distribution of values of α used in these calculations was defined by a truncated exponential distribution with a mean value of α = 0.08, a maximum of 0.16 and a minimum of 0.

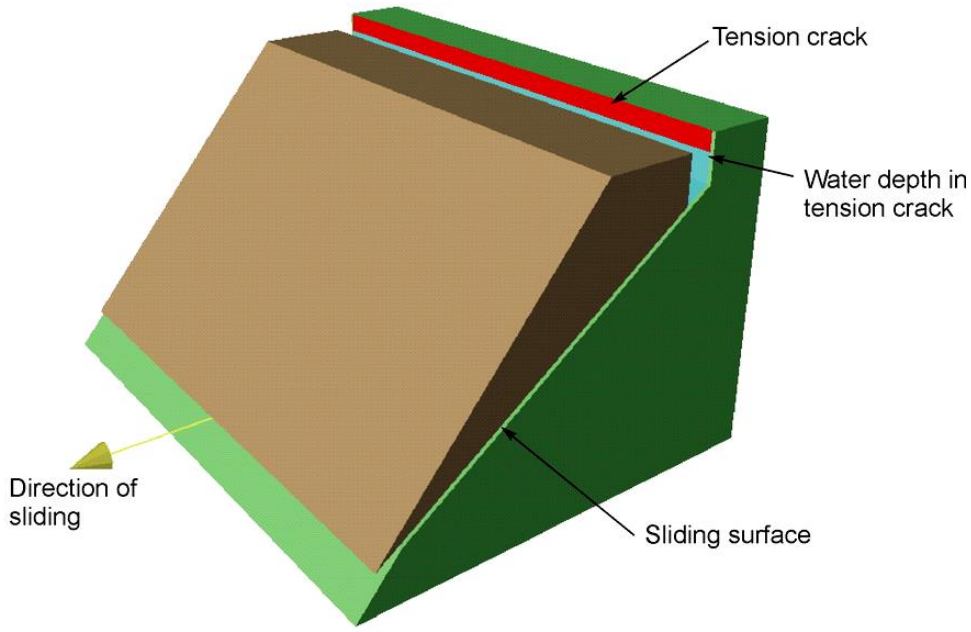

Figure 3: RocPlane model of the defined slope.

Using the distributions shown in Figure 2, the RocPlane model shown in Figure 3 was used, with Latin Hypercube sampling, to carry out 5,000 iterations on the factor of safety. The resulting probability distribution is plotted in Figure 4. This histogram gives a mean

factor of safety of 1.34 with a standard deviation of 0.23, a minimum of 0.61 and a maximum of 2.33. The best fit distribution is a beta distribution with the same mean, standard deviation, minimum and maximum.

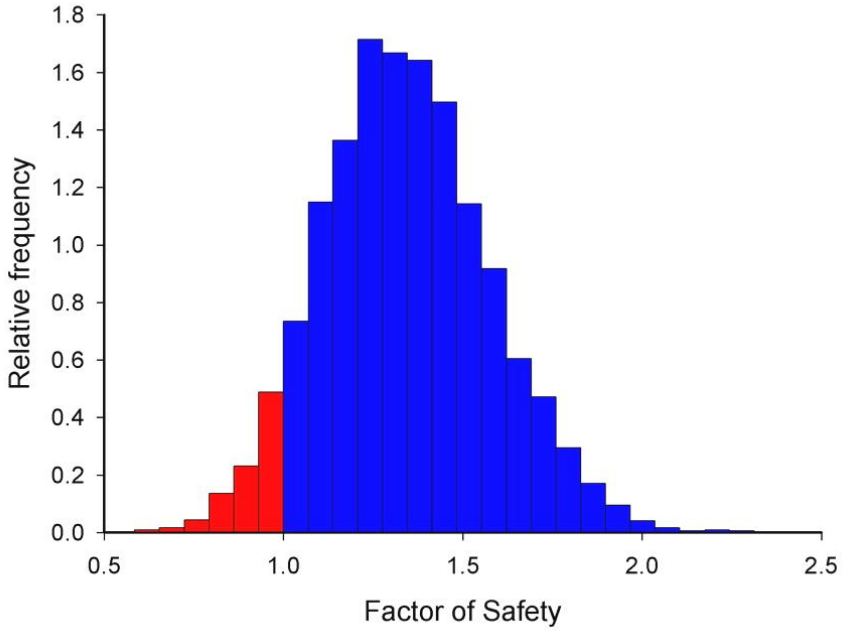

Figure 4: Distribution of the factor of safety for the rock slope computed by means of the program RocPlane.

The calculated *probability of failure* is found to be 6.4% and is given by the ratio of the area under the distribution curve for F<1 (shown in red in Figure 4) divided by the total area under the distribution curve. This means that, for the combination of slope geometry, shear strength, water pressure and earthquake acceleration parameters assumed, 64 out of 1000 similar slopes could be expected to fail at some time during the life of the slope. Alternatively, a length of 64 m could be expected to fail in every 1000 m of slope.

This is a reasonable risk of failure for short term conditions and a risk of this magnitude may be acceptable in an open pit mine, with limited access fot trained miners, and even on a rural road. However, in the long term, this probability of failure is not acceptable for a densely populated region. In considering remedial measures to improve the long-term stability of the slope, the effectiveness of these measures could be evaluated using the same probabilistic techniques as described above.

Acknowledgements

The author wishes to express his thanks to Dr. Eugenio Casteli, Mr. Damiano Giordano and Dr. Bak Kong Low for bringing to his attention several errors in the original Monte Carlo analysis. These errors have been corrected in this revision on the notes.

References

Carter, T.G. 1992. A new approach to surface crown pillar design. *Proc. 16th. Canadian Rock Mechanics Symp., Sudbury,* 75-83.

Carter, T.G. 1992. Prediction and uncertainties in geological engineering and rock mass characterization assessments. *Proc. 4th. int. rock mechanics and rock engineering conf.*, Torino. Paper 1.

Harr, M.E. 1987. *Reliability-based design in civil engineering*. New York: McGraw-Hill.

Hatzor, Y. and Goodman. R.E. 1993. Determination of the 'design block' for tunnel supports in highly jointed rock. In *Comprehensive Rock Engineering, Principles, Practice and Projects.* (ed. J.A. Houson) **2,** 263-292. Oxford: Pergamon.

Hoek, E. and Bray, J.W. 1974. *Rock Slope Engineering.* London: Instn Min. Metall.

Hoek, E. 1989. A limit equilibrium analysis of surface crown pillar stability. In *Surface crown pillar evaluation for active and abandoned metal mines,* (ed. M.C. Betourney), 3-13. Ottawa: Dept. Energy, Mines & Resources Canada.

Iman, R.L., Davenport, J.M. and Zeigler, D.K. 1980. *Latin Hypercube sampling (A progam user's guide).* Technical Report SAND79-1473. Albuquerque, New Mexico: Sandia Laboratories.

Pine, R.J. 1992. Risk analysis design applications in mining geomechanics. *Trans. Instn Min. Metall.* (Sect.A) **101,** 149-158.

Rosenbleuth, E. 1981. Two-point estimates in probabilities. *J. Appl. Math. Modelling* **5**, October, 329-335.

Startzman, R.A. and Wattenbarger, R.A. 1985. An improved computation procedure for risk analysis problems with unusual probability functions. *Proc. symp. Soc. Petrolm Engrs hydrocarbon economics and evaluation,* Dallas.

Tyler, D.B., Trueman, R.T. and Pine, R.J. 1991. Rockbolt support design using a probabilistic method of key block analysis. In *Rock mechanics as a multidisciplinary science,* (ed. J.C. Roegiers), 1037-1047. Rotterdam: Balkema.

Whitman. R.V. 1984. Evaluating calculated risk in geotechnical engineering. *J. Geotech. Engng, ASCE* **110 (**2), 145-186.

10. A slope stability problem in Hong Kong

Introduction

In the early 1970s a series of landslides occurred in Hong Kong as a result of exceptionally heavy rains. These slides caused some loss of life and a significant amount of property damage. Consequently, an extensive review was carried out on the stability of soil and rock slopes in the Territory.

During this review, a rock slope on Sau Mau Ping Road in Kowloon was identified as being potentially unstable. The stability of this particular slope was critical because it was located immediately across the road from two blocks of apartments, each housing approximately 5,000 people.

Figure 1 gives a general view down Sau Mau Ping Road, showing the steep rock slopes on the left and the apartment blocks on the right.

The concern was that a major rock slide could cross the road and damage the apartment blocks. In order to decide upon whether or not the residents of the two apartment blocks should be evacuated, the two questions which required an immediate response were:

What was the factor of safety of the slope under normal conditions and under conditions which could occur during an earthquake or during exceptionally heavy rains associated with a typhoon?

What factor of safety could be considered acceptable for long term conditions and what steps would be required in order to achieve this factor of safety?

Description of problem

The rock mass, in which the slope adjacent to the Sau Mau Ping Road was cut, is unweathered granite with exfoliation or sheet joints similar to those illustrated in Figure 2. These joints are parallel to the surface of the granite and the spacing between successive joints increases with increasing distance into the rock mass. Undercutting of these sheet joints can cause a rock slide such as that illustrated in Figure 3.

During excavation of the original slopes for the Sau Mau Ping Road, a small rock slide was induced by blasting. The surface on which this failure occurred is illustrated in Figure 4. Blasting, such as that used in civil construction in an urban environment, does not impose very large loads on rock slopes and it can be assumed that the factor of safety of the slope was close to unity.

Figure 1: A view down Sau Mau Ping Road in Kowloon showing apartment blocks across the road from the steep rock slopes.

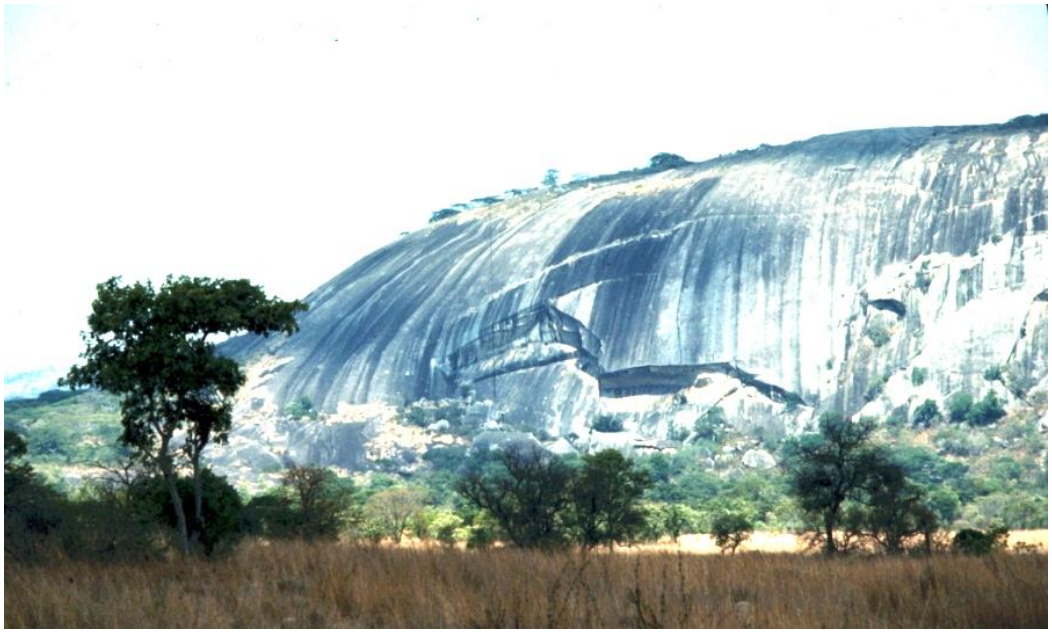

Figure 2: Sheet jointing in granite. These features, sometimes referred to as ‘onion skin’ joints, are the result of exfoliation processes during cooling of the granite.

Figure 3: A rockslide on a road caused by the undercutting of sheet joints in a granite slope. In hard rocks such as granite, failure can occur very suddenly if the factor of safety of the slope is close to 1. A rise in groundwater levels during a heavy storm or ice jacking in winter may be sufficient to induce failure.

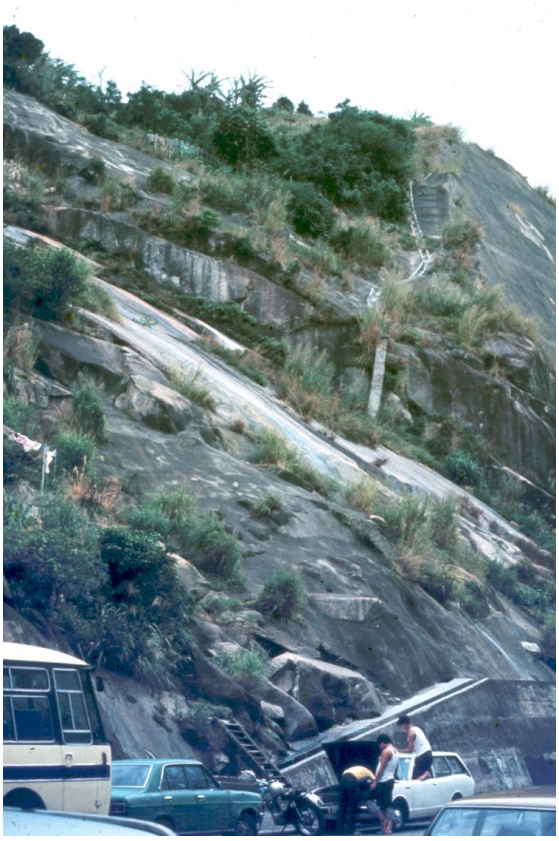

Figure 4: The failure surface defined by a sheet joint surface on which a small slide occurred during blasting of the original cut slope for the Sau Mau Ping Road. The potentially unstable slope discussed is visible in the background.

The potentially unstable slope under consideration is visible in the background of this photograph. It is obvious from this photograph that the sheet joint surface continues under the potentially unstable slope. Hence, from the evidence of the small-scale failure, it can be deduced that the factor of safety of the slope in question is not very high.

The geometry of the slope is illustrated in Figure 5 which shows a 60 m high slope with three 20 m high benches. The overall slope angle is 50° and the individual bench faces are inclined at 70° to the horizontal. An exfoliation joint surface dips at 35° and undercuts the slope as shown in the figure. The slope face strikes parallel to the underlying exfoliation surface, and hence, the slope can be analysed by means of a two-dimensional model.

Tension cracks are frequently observed behind the crest of slopes which have a factor of safety of less than about 1.2. These cracks are dangerous in that they allow water to enter the slope at a particularly critical location. Unfortunately, in the case of the Sau Mau Ping slope, recently cultivated market gardens located on the top of the slope made it impossible to determine whether or not such tension cracks were present and hence it was decided to carry out two sets of analyses - one with and one without tension cracks. These analyses were carried out for both the overall slope and for individual benches.

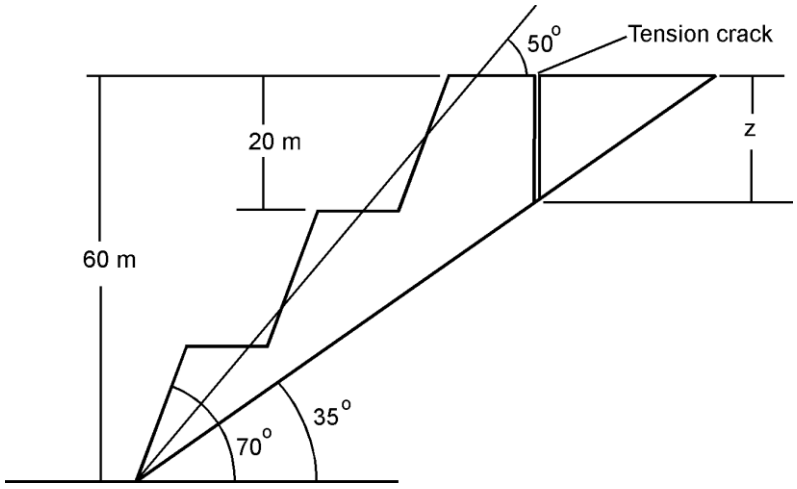

Figure 5: Geometry assumed for the two-dimensional analysis of the Sau Mau Ping Road slope.

Limit equilibrium models

At the time of this investigation, no rock mechanics facilities existed in Hong Kong and no diamond drilling or laboratory testing had ever been carried out on the granitic rocks in which this slope had been excavated. Consequently, the problem was tackled on the basis of a crude form of risk analysis, using simple analytical models to predict the

response of the slope to a range of possible conditions. The two models are defined in Figure 6 and Figure 7.

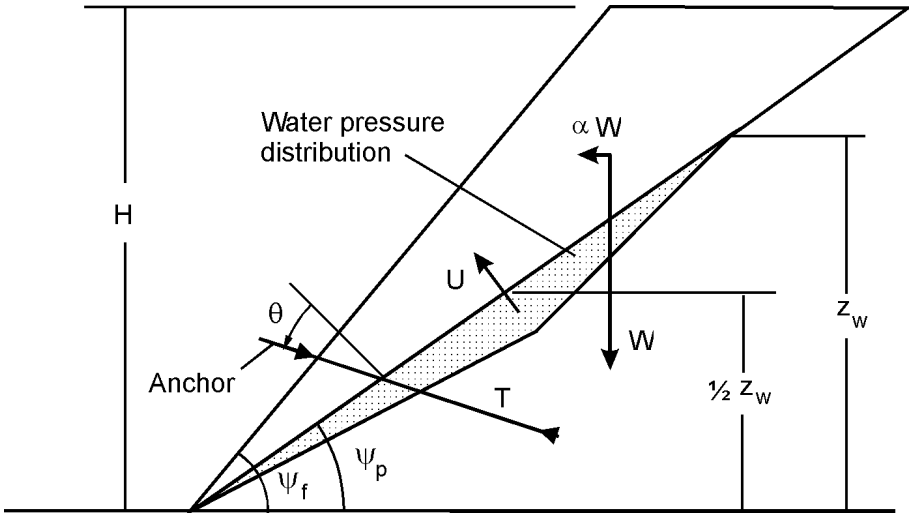

$$F = \frac{cA + \left(W(\cos\psi_p - \alpha\sin\psi_p) - U + T\cos\theta\right)\tan\phi}{W(\sin\psi_p + \alpha\cos\psi_p) - T\sin\theta} \tag{1}$$

where

$$A = \frac{H}{\sin\psi_p} \tag{2}$$

$$W = \frac{\gamma_r H^2}{2}(\cot\psi_p - \cot\psi_f) \tag{3}$$

$$U = \frac{\gamma_w H_w^2}{4\sin\psi_p} \tag{4}$$

Figure 6: Factor of Safety calculation for a slope with no tension crack.

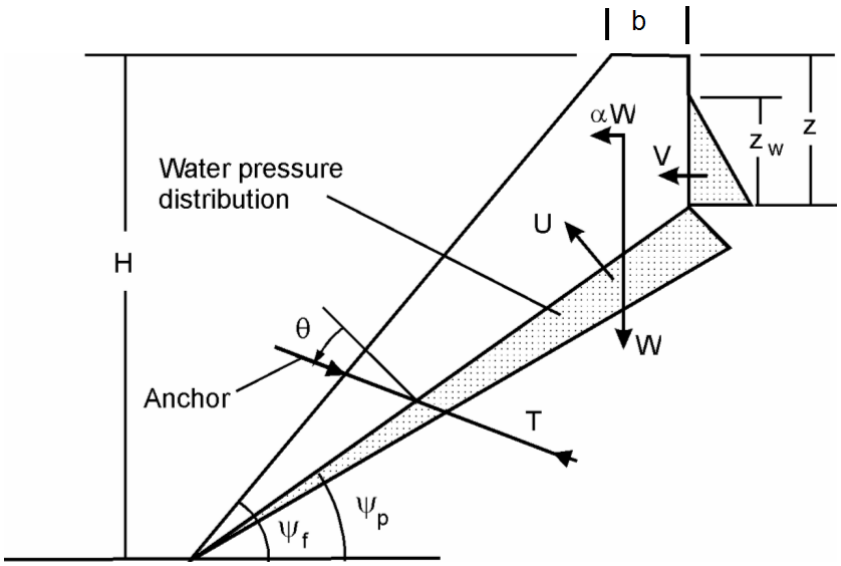

$$F = \frac{cA + \left(W(\cos\psi_p - \alpha\sin\psi_p) - U - V\sin\psi_p + T\cos\theta\right)\tan\phi}{W(\sin\psi_p + \alpha\, con\psi_p) + V\cos\psi_p - T\sin\theta} \tag{5}$$

where

$$z = H\left(1 - \sqrt{\cot\psi_f \tan\psi_p}\right) \tag{6}$$

$$b = H\left(\sqrt{\cot\psi_f \cdot \cot\psi_p} - \cot\psi_f\right) \tag{7}$$

$$A = \frac{H - z}{\sin\psi_p} \tag{8}$$

$$W = \frac{\gamma_r H^2}{2}\left(\left(1 - \left(\frac{z}{H}\right)^2\right)\cot\psi_p - \cot\psi_f\right) \tag{9}$$

$$U = \frac{\gamma_w z_w A}{2} \tag{10}$$

$$V = \frac{\gamma_w z_w^2}{2} \tag{11}$$

Figure 7: Factor of Safety calculation for a slope with a water-filled tension crack.

The Symbols and dimensions used in these models are as follows:

Symbol	Parameter	Dimensions
F	Factor of safety against sliding along sheet joint	Calculated
H	Height of the overall slope or of each bench	60 m or 20 m respectively
ψf	Angle of slope face, measured from horizontal	50°
ψp	Angle of failure surface, measured from horizontal	35°
b	Distance of tension crack behind crest	Calculated (m)
z	Depth of tension crack	Calculated (m)
zw	Depth of water in tension crack or on failure surface	Variable (m)
α	Horizontal earthquake acceleration	0.08 g (proportion of g)
γr	Unit weight of rock	0.027 MN/m3
γw	Unit weight of water	0.01 MN/m3
W	Weight of rock wedge resting on failure surface	Calculated (MN)
A	Base area of wedge	Calculated (m2)
U	Uplift force due to water pressure on failure surface	Calculated (MN)
V	Horizontal force due to water in tension crack	Calculated (MN)
c	Cohesive strength along sliding surface	Variable (MN/m2)
ϕ	Friction angle of sliding surface	Variable (degrees)
T	Force applied by anchor system (if present)	Specified (MN)
θ	Inclination of anchor, anti-clockwise from normal	Specified (degrees)

Note that this is a two-dimensional analysis, and these dimensions refer to a 1-metre-thick slice through the slope. It is also important to recognise that this analysis considers only force equilibrium and assumes that all forces pass through the centroid of the wedge. In other words, moment equilibrium is not considered in this analysis. While this is a simplification of the actual situation depicted in Figure 6 and Figure 7, the errors introduced are not considered to be significant, given the uncertainty of the other input data used in these analyses.

In Figure 7 the depth z of the tension crack is calculated by equation 6. This equation is obtained by minimising equation 5 with respect to the tension crack depth z (Hoek and Bray, 1974). This minimisation is carried out for a dry slope and the accuracy of equation 6 decreases as the water depth in the tension crack increases. However, for the purposes of this analysis, the estimate given by equation 6 is considered acceptable.

Estimates of shear strength

One of the most critical steps in any limit equilibrium analysis is the determination or the estimation of the shear strength parameters (c and ϕ) for the surface along which it is anticipated that sliding will take place. In the case of this slope on Sau Mau Ping Road, no information on shear strength was available at the time of the initial studies and so estimates had to be made based on published information for similar rocks.

Hoek and Bray (1974) published a plot, reproduced in Figure 8, of cohesive strengths and friction angles for rocks and soils, based upon the results of published back analysis of slope failures. Superimposed on this plot is an elliptical zone which encompasses the estimated range of shear strength for sheet joints in unweathered granite. In choosing this range it was considered that the friction angle ϕ probably ranges from 30° for very smooth planar surfaces to 45° for rough or partly cemented surfaces. The cohesive strength c is more difficult to estimate and the range of 0.05 to 0.2 MPa was chosen on the basis of the results of back-analyses of slope failures, plotted in Figure 8.

Some readers may be surprised that a cohesive strength has been assumed for joint surfaces which obviously have no tensile strength or 'stickiness' as would be found in a clayey soil. In fact, this assumed cohesive strength is defined by the intercept, on the shear strength axis, of a tangent to a curvilinear Mohr envelope. This curvature is the result of the interlocking of asperities on the matching surfaces of the joints and the increase in shear strength given by this interlocking plays a crucial role in the stability of slopes such as that under consideration in this chapter.

Estimate of earthquake acceleration

Hong Kong is not considered a highly seismic region, but relatively minor earthquakes are not unknown in the region. Consequently, it was felt that some allowance should be made for the possible influence of earthquake loading on the stability of the Sau Mau Ping slope.

The traditional method of incorporating the acceleration induced by earthquakes or large blasts in slope stability analyses is to add an outward force αW to the forces acting on the slope (see Figure 6 and Figure 7), where α is the acceleration as a proportion of g, the acceleration due to gravity. This 'pseudo-static' form of analysis is known to be very conservative but, in the case of the Sau Mau Ping slope, this conservatism was not considered to be out of place.

In discussion with local engineers and geologists, the consensus opinion was that the horizontal acceleration which could be induced by a 10-year return period earthquake in the region would be approximately 0.08 g. This value was used in all the sensitivity analyses discussed in the following sections.

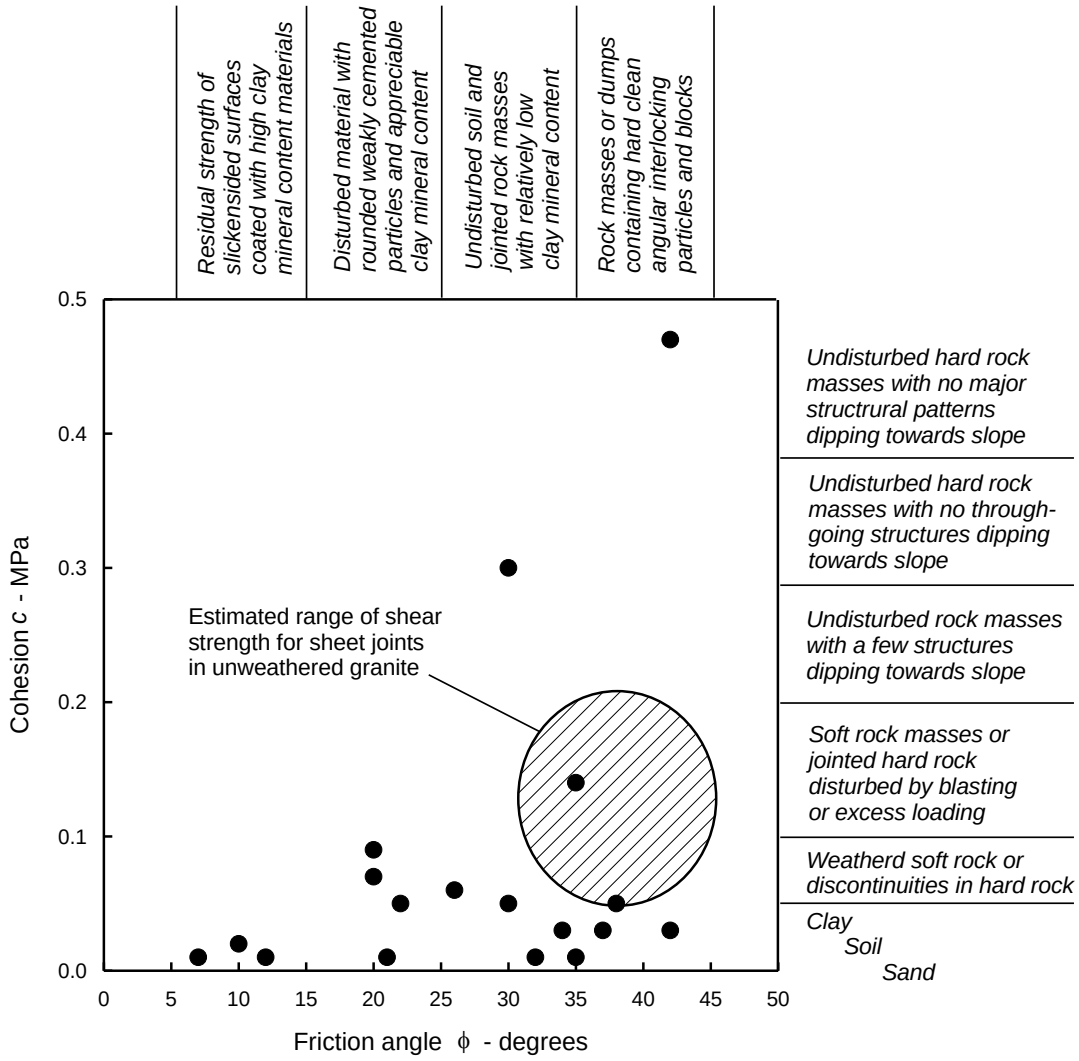

Figure 8: Relationship between friction angles and cohesive strengths mobilised at failure of slopes in various materials. The plotted points were obtained from published information from the back analysis of slope failures. (After Hoek and Bray 1974).

Analysis of mobilised shear strength

One method for assessing the stability of slopes is to calculate the shear strength that would be mobilised at failure and to compare this strength with the shear strength which is available along the failure surface. In the case of the Sau Mau Ping slope, this was done by substituting F = 1 in equations 1 and 5 and solving for the cohesive strength c and the friction angle ϕ. The results of this analysis are plotted in Figure 9. The estimated range of available shear strength (from Figure 8) is also shown on this plot.

Figure 9 shows that only two of the cases analysed result in conditions where the shear strength mobilised at failure falls within the estimated range of available shear strength. These two cases are designated 2 and 4 and they are for fully saturated slopes, with and without tension cracks.

Decision on short-term stability of the Sau Mau Ping slope

From the results of the sensitivity study described above, it was concluded that instability of this particular slope could occur if the slope was fully saturated and subjected to earthquake loading. Typhoons occur several times every year in Hong Kong and the intensity of precipitation during these events is certainly sufficient to saturate the slopes. As discussed earlier, minor earthquakes do occur in the region, but they are not very frequent. Consequently, the chance of simultaneous saturation and earthquake loading was considered to be small and it was concluded that there was no serious short-term threat of instability of the Sau Mau Ping Slope.

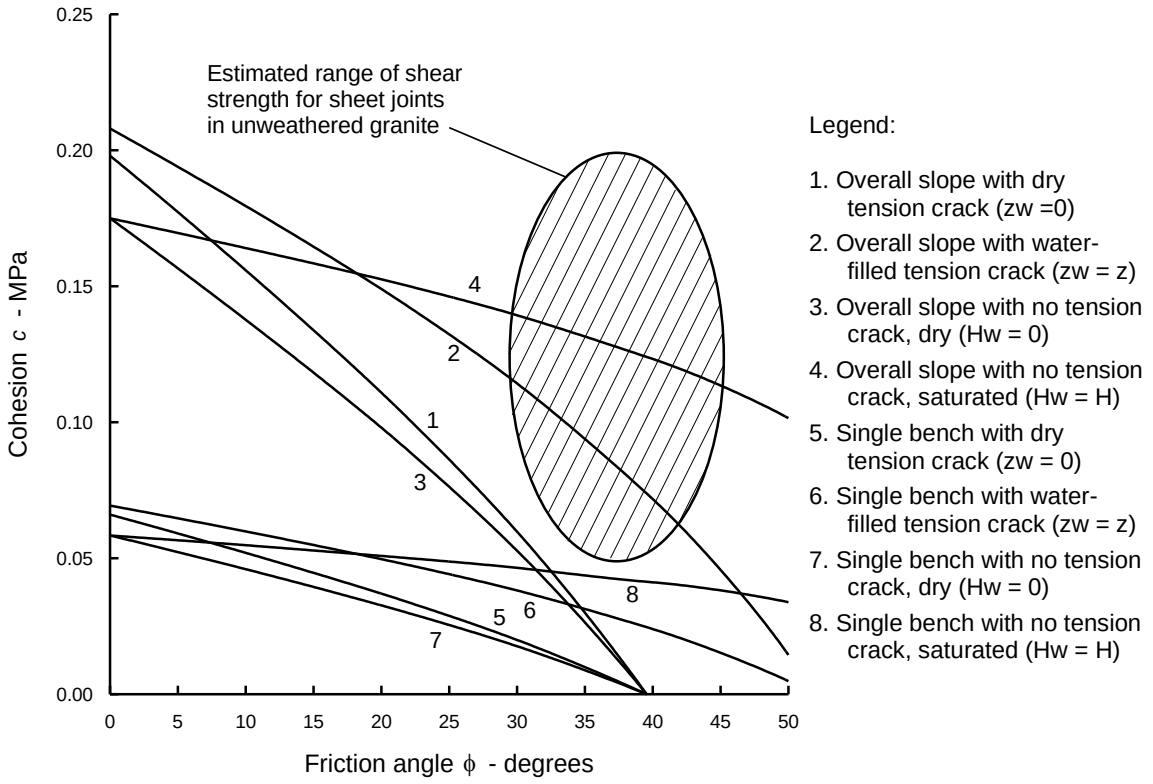

Figure 9: Comparison of the shear strength mobilised by failure under various conditions with the estimated shear strength available on sheet joints in unweathered granite.

In discussion with the highway authorities in Hong Kong, the following decisions were made:

- No evacuation of the residents of the two apartment blocks, located across the street from the slope in question, would be carried out.
- Horizontal drainage holes would be drilled into the slope face to penetrate the potential failure surface to reduce uplift pressures in the slope.
- Piezometers would be installed in holes drilled from the top of the slope. These piezometers would be measured regularly during periods of significant rainfall and the road would be closed to traffic if water rose to levels decided by the engineers responsible for the project.
- An investigation would be carried out into the most effective remedial measures to stabilise the slope for the long-term.

Figure 10 shows the drilling of the horizontal drain holes into the slope face and Figure 11 shows the drilling of the vertical holes into which the piezometers were installed. These piezometers were monitored for the next few years, while preparations for the final stabilisation of the slope were made. The road was closed to traffic on two occasions when water levels were dangerously high.

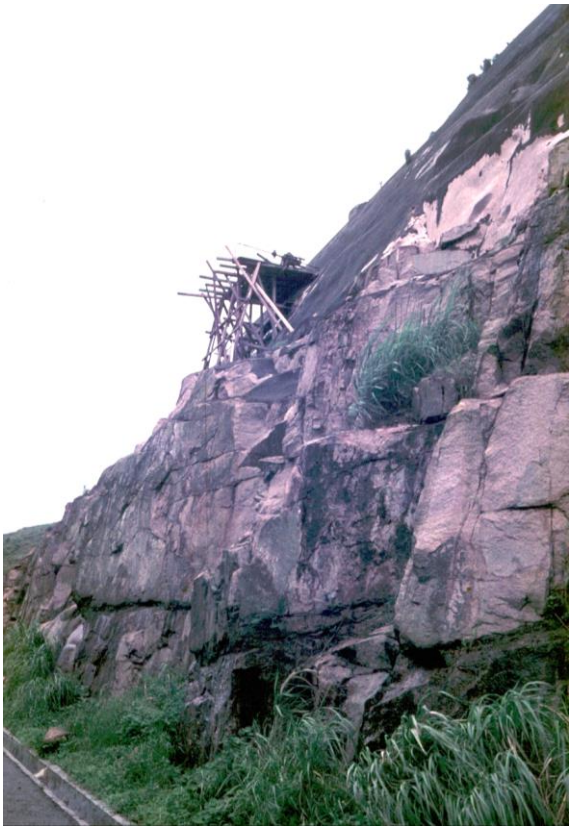

Figure 10: Drilling horizontal drain holes into the face of one of the benches of the Sau Mau Ping slope.

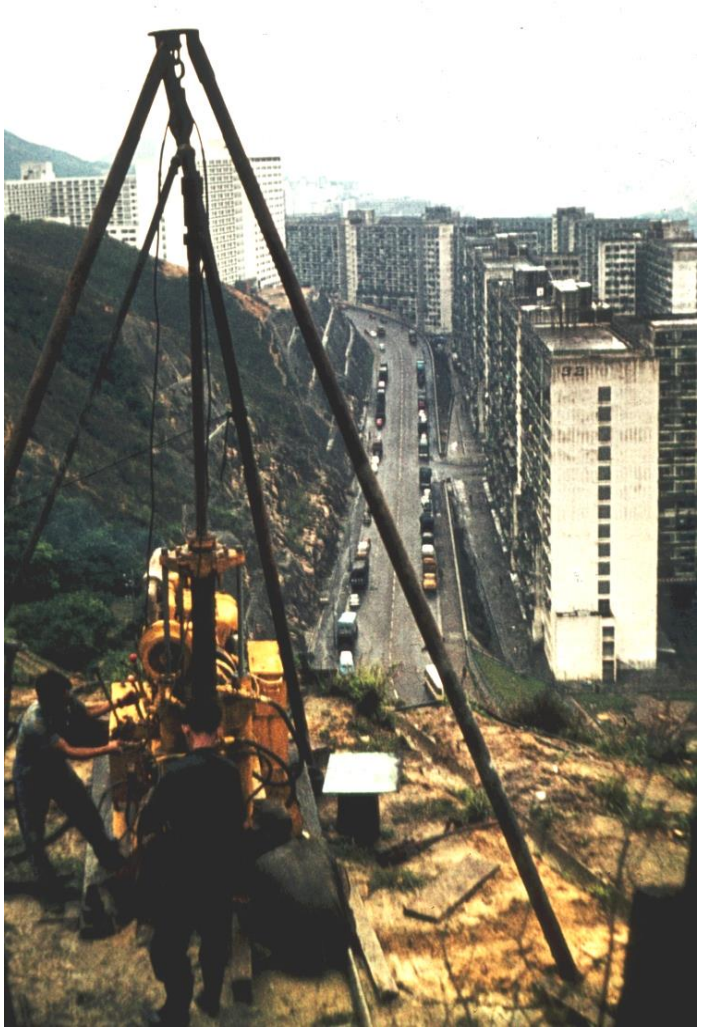

Figure 11: Drilling vertical diamond core holes into the Sau Mau Ping slope. These holes were used for geotechnical investigation purposes and for the installation of piezometers in the rock mass.

Evaluation of long-term remedial measures

While the short-term threat of instability was small, the longer-term stability of the slope was considered to be unacceptable. A study was carried out to evaluate various options for stabilising the slope. It was agreed that a factor of safety of 1.5 was required to meet long term requirements. The following alternatives were considered:

1. Reducing the height of the slope
2. Reducing the angle of the slope face
3. Drainage of the slope
4. Reinforcement of the slope.

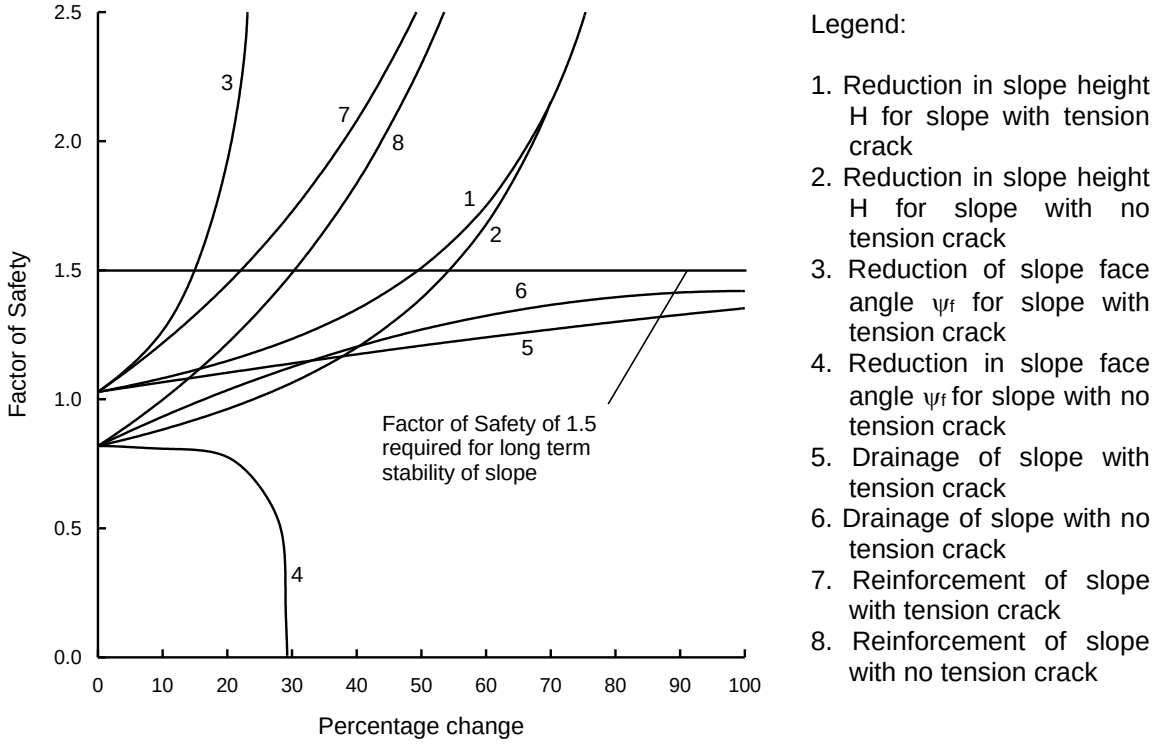

Figure 12: Evaluation of remedial options to increase the stability of the slope.

The limit equilibrium models defined in Figure 6 and Figure 7 were used for this evaluation. The results are plotted in Figure 12.

In calculating the factors of safety shown in this figure, the shear strength was maintained constant and was defined by c = 0.10 MPa and ϕ = 35°. Similarly, an earthquake acceleration of α = 0.08 g was used for all the analyses. The percentage change refers to the ratios of slope height, slope angle and water depth to the original dimensions defined in Figure 5.

In the case of the reinforcement options, the percentage change refers to the ratio of anchor force T to the weight of the wedges (24.8 MN for the slope with the tension crack and 28.6 MN for the slope with no tension crack). The anchor inclination was kept constant at $\theta = \phi$ = 35°. This anchor inclination gives the minimum anchor load for a dry slope. It can be determined by minimising equations 1 or 5 with respect to θ.

The curves presented in Figure 12 show clearly that some remedial measures are much more effective than others and that it is worth examining each of the options in turn.

Curves 1 (slope with tension crack) and 2 (slope without tension crack) show that reduction of the slope height is not an effective solution to the problem. In order to achieve the required factor of safety of 1.5, the slope height would have to be reduced by 50%. If this solution were to be adopted, it would be more practical to excavate the entire slope since most of the volume of the rock to be excavated is contained in the upper half of the slope.

Curve 3 (slope with tension crack) shows that reduction of the slope angle is a very effective remedial measure. The required factor of safety of 1.5 is achieved for a reduction of less than 25% of the slope angle. In other words, a reduction of the overall slope face angle from 50° to 37.5° would achieve the desired result. This finding is generally true that a reduction in the face angle of a slope is usually an effective remedial step. In the case of slopes under construction, using a flatter slope is always one of the prime choices for achieving greater stability.

Curve 4 (slope without tension crack) is an anomaly. It demonstrates that calculations can sometimes produce nonsense. The reduction in factor of safety shown by this curve is a result of the reduction in the weight of the sliding block as the face angle is reduced. Since the water pressure on the sliding surface remains constant, the effective stress acting on the sliding surface decreases, and hence, the frictional component of the resisting forces decreases. When a very thin sliver of rock remains, the water pressure will float it off the slope. The problem with this analysis lies in the assumption that the block is completely impermeable and that the water remains trapped beneath the failure surface. In fact, the block would break up long before it floated and hence the water pressure acting on the failure plane would be dissipated.

Curves 5 and 6 show that drainage is not a very effective option for either of the slope models considered. In neither case is a factor of safety of 1.5 achieved. This is something of a surprise since drainage is usually one of the most effective and economical remedial measures. The reasons for the poor performance of drainage in this case is due to the combination of the geometry of the slope and the shear strength of the failure surface.

Curves 7 and 8 show that, for both slope models considered, slope reinforcement by means of rockbolts or cables can be an effective remedial measure. The anchor force required for a factor of safety of 1.5 would be about 100 tonnes per metre of slope length for the slope with no tension crack.

Final decision on long term remedial works

The two most attractive options for long term remedial works on this slope are reinforcement by means of cables or bolts or reduction of the slope face angle. The first option was finally rejected because of the high cost and because of the uncertainty about the long-term corrosion resistance of reinforcement which could be placed in the slope.

This latter concern may not have been justified, but considering the very poor quality of some of the construction in Hong Kong at the time of this study, it was decided that the risk was not worth taking.

The option finally chosen was to reduce the slope face angle down to 35° by excavating the entire block resting on the failure surface, and hence, removing the problem entirely. Since good quality aggregate is always required in Hong Kong, it was decided to work this slope face as a quarry. It took several years to organise this activity and, during this time, the water levels in the slope were monitored by means of piezometers. Although the road was closed twice during this period, no major problems occurred, and the slope was finally excavated back to the failure plane.

References

Hoek E. and Bray, J.W. 1974. *Rock Slope Engineering.* London: Instn Min. Metall.

11. Rock slopes in civil and mining engineering

Introduction

Free-standing unsupported rock slopes are important components of open pit mines, large excavations for building foundations, highway cuts in mountainous terrain large and mountain slopes in which landslides can occur. Installation of support or reinforcement in these slopes is uneconomical. Their safety depends upon the inherent strength of the rock masses in which they are excavated or in which they were created by mountain building processes. Hence, the "design" of the slopes is limited to the recognition of weak features, such as through-going joints and faults, the understanding and control of groundwater pressures in the slope and the control of blasting and mechanical excavation methods used in creating the slopes.

Hoek, Read, Karzulovic and Chen, (2000) presented a comprehensive review of the state of the art of the design of these slopes with an emphasis on open pit slopes. Their paper provided much of the discussion in the following text.

The geological model

In an open pit mine a great deal of effort is devoted to defining a reliable geological model in order to locate and quantify the ore reserves. Consequently, the refinement of these models to include features, such as the distribution of weak features like joints which can cause slope instability, is both logical and feasible. This is not the case for slopes for foundations and highways where the profile of the slopes in the excavation is of fundamental importance and where detailed geological investigations are generally limited to those locations which show signs of potential instability. Similarly, in the case of landslides, detailed investigations are only undertaken when there is a history of slope instability.

Rock slope failures are geological events controlled by natural physical processes. Geological-geotechnical models that can be used to understand and analyse these processes must include structural data as well as information on lithology, mineralization and alteration, weathering, hydrogeology and rock mass characteristics such as joint persistence and the condition of the joints. The most important information is the structural data which should include information on major structures and on structural domains. This information must be sufficiently detailed that meaningful structural trends can be derived and used as input for analytical models.

Routinely, these models are stored and manipulated electronically. The availability of a number of computer geological models is an important aspect of modern rock slope design. Packages such as Minex-Horizon, Vulcan and Minescape provide three-dimensional solid modelling systems which permit the construction and visualization of comprehensive models that can include geological and structural geology information, ore grade distributions, groundwater distributions and a variety of geotechnical details. The construction of these models is itself a useful exercise since it highlights deficiencies in the database and forces the user to consider the inter-relationships between the various types of information displayed in the model.

These modelling systems are already fully operational and are used routinely by most large- scale open pit mining operations. However, they are very seldom used in civil engineering projects which is a serious deficiency that I hope to see remedied in the years to come. Under development are interfaces which will allow a direct transfer from these three-dimensional models to other types of limit equilibrium and numerical models used for slope design.

Geological and geotechnical data collection

The tools and techniques for geological data collection are well developed and have been widely used by the mining and civil engineering industries. The definition of what information to collect and the efficient use of the collected data is another matter. There is a fundamental need to collect good quality geological data in the form of original and site lithological, structural and hydrological information, detailed core logs and photographs that can be interpreted by an engineering geologist at any time. Currently, there are a few standards for data collection. The type and quality of information gathered depends very much upon the personal opinion and preferences of the individuals or organizations carrying out the work. Disadvantages of this approach are that the reasons for collecting the data become unclear and it becomes difficult to maintain continuity when staff or organizational changes occur.

The current state of practice includes a variety of rock mass classification schemes, some of which have been specifically adapted for rock slope engineering (Haines and Terbrugge, 1991, Romana, 1995, Chen, 1995). Unfortunately, the use of these classification systems is highly questionable since most of them were developed for the confined conditions that apply in the rock masses surrounding underground excavations, which have been found to produce unreliable results in the low confining stress conditions in slopes. The use of classification systems, in which the properties of the rock mass are characterized by a single number, also tends to produce a false sense of security. At best, it may be possible to define ranges of values of these rock mass quality indices. These ranges may be used to delineate zones that can be used to complement all the other geological, hydrogeological and geotechnical information. Where classification systems are used, the need to understand their limiting assumptions, and to calibrate them to the regional and local site conditions, is emphasized.

Rock slope failures are geological events controlled by natural physical processes. Geological – geotechnical models that can be used to understand and to analyze these processes must include structural data as well as information on lithology, mineralization and alteration, weathering, hydrogeology, and rock mass characteristics such as joint, persistence, and the condition of joints. The most important information is the structural data which should include information on major structures and structural domains. This information must be sufficiently detailed that meaningful statistical trends can be derived and used as input for analytical models.

The input of the results of the geological data collection process into a geological model should preferably be carried out by an engineering geologist. Deficiencies and anomalies in the data become obvious during this model construction process which provide useful guidance to the development of future site investigation programmes.

The role of major structures

No one questions the role of major geological discontinuities such as lithological boundaries, bedding planes, or faults in controlling the stability of large slopes. Clearly, it is essential that the data gathering process embraces the development of regional and local geological models, which include these major structures, and that on-going mapping of these structures as they are exposed in the slopes, be used as a means of continually updating the geological model.

From a practical point of view, the role of second order structures, such as joints, is more of a problem. Their importance in controlling the behaviour of the rock mass is clearly recognized but, because of the large number of such features, a question that arises is - how much data should be collected and how should it be used in the design of rock slopes?

The current state of practice tends to separate slope designs into two distinct categories. The first of these categories is for those designs that can be dealt with in terms of kinematically possible structurally controlled failures. For example, failures that involve wedges, sliding along the line of intersection of two intersecting faults can be analyzed using limits equilibrium models. This type of failure is commonly seen in slopes of up to 20 or 30 m high in hard, jointed rock masses. The design of such slopes can sometimes be based upon analysis of simple wedge failures.

The second category is that which includes non-structurally controlled failures in which some or all the failure surfaces pass through the rock mass which has been weakened by the presence of joints or other second order structural features. An assumption commonly made is that the second order structural features are randomly or chaotically distributed and the rock mass strength can be defined by a simple failure criterion which is ‘smeared’ or ‘average’ non-directional strength properties that are assigned to the rock mass. This approach is frequently used for the analysis of the overall stability of large slopes where it is believed that no obvious failure mode presents itself.

Specialists in slope stability recognize that there are two categories described above which are inadequate. Figures 1 and 2 illustrate the difficulties.

Figure 1: Slope failure in which some structural control by faults is evident at the top of the failure, but where the mechanisms involved in the low part of the failure are unclear.

Figure 2: A large scale slope failure in an open pit mine.

Figure 2 is an approximately 350 m high mine slope failure. The rock mass within the failed material is altered and closely jointed. There is evidence of faults at the back of a failure, but what triggered the failure? Was it the faults at the back of the failure or was it a non-structurally control failure where most of the failure surface passes through an altered rock mass which has been weakened further by the presence of joints or other second order structural features? Can the failure be analyzed and the slope redesigned?

Figure 3 illustrates a joint map of the foundation for the Three Gorges Dam, published by Wang, Chen and Jia, (1998) and Chen (1999). This map was generated by Monte Carlo analysis using probability density functions for the joint dip, strike, spacing and trace length (Priest and Samaniego, 1983). The map was then used in stability analysis of this 60 m high slope by searching for joint and rock bridge combinations that result in minimum shear strength along potential failure surfaces. A similar process was used to investigate the seepage and drainage processes in the rock mass by considering the conductivity of the joint fabric.

Sainsbury and Sainsbury (2013) reported on three-dimensional slope stability models, developed in Australia, for the analysis of complex failures in jointed rock masses. Their papers are highly recommended reading for anyone seeking a deeper understanding of these analyses.

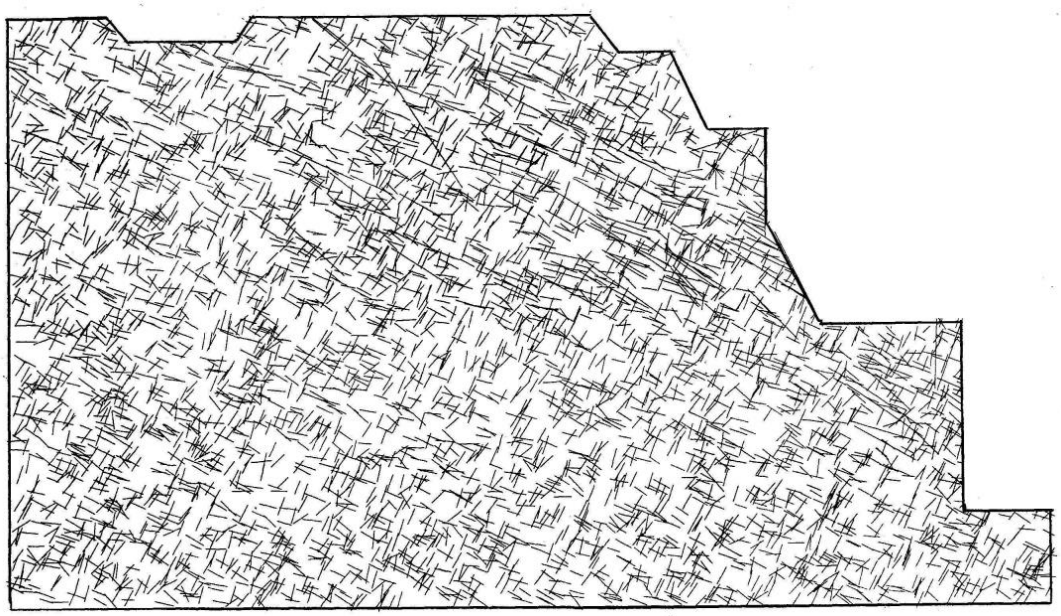

Figure 3: Joint map for the rock mass forming the foundation of the Three Gorges Dam in China.

Determination of rock mass properties

The determination of rock mass strength is a significant challenge in current rock slope design practice. Even in terms of the state-or-the-art, there are many unanswered questions and many opinions on how this task should be performed in the low stress environment that is characteristic of rock slopes, particularly where weak/altered rocks are present.

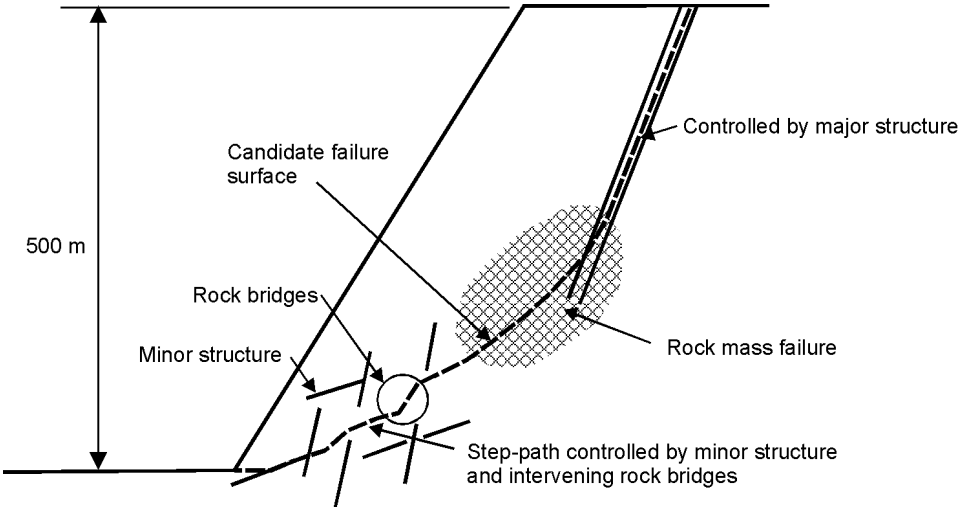

Figure 4: Candidate failure surface involving a number of different shear failure mechanisms.

In terms of the state of practice, most slope designers use some form of 'smeared' failure criterion to estimate the shear strength properties of the rock in the blocks or domains defined by major structural features such as faults. The Hoek-Brown failure criterion is commonly used for estimating the properties of these 'homogeneous and isotropic' rock masses. An alternative is to estimate mass shear strength value

from the component parts along a given candidate failure surface, shown in Figure 4. For the failure surface illustrated, the component shear strengths could be obtained from (i), direct shear tests of samples taken from the fault that defines the upper part of the surface (ii), the Hoek-Brown failure criterion, for the central part of the failure and for the rock bridges in the step-path surface at the toe of the slope and (iii), either direct shear tests of samples taken from the joints or by applying a method such as the Barton-Bandis shear failure criterion to the joints forming the step-path surface at the toe of the slope.

One of the problems that impedes progress on these questions is the lack of current research in rock slope stability and rock mass properties. Changes in priorities of university research and research funding means that there are very few research centres or individual researchers working in this area. It is not clear where suitably qualified researchers can be found and how such research on open pit stability would be funded.

Impact of alteration

In open pit mining, copper porphyry deposits are associated with a zone of altered rock as a result of the ore emplacement process. In some areas this alteration is relatively mild and does not have a major impact on rock mass strength. On the other hand, in most of the open pit mines associated with the South American Andes, the orebodies are surrounded by a halo of strongly altered rock. The impact on rock mass strength and slope stability is significant

Results of tests at the Chuquicamata Mine in Chile suggest that potassic alteration has the least influence on rock strength, chloritic alteration has a significant impact and quartz-sericitic and argillic alteration have a major impact. These strength reductions are illustrated in Figure 5.

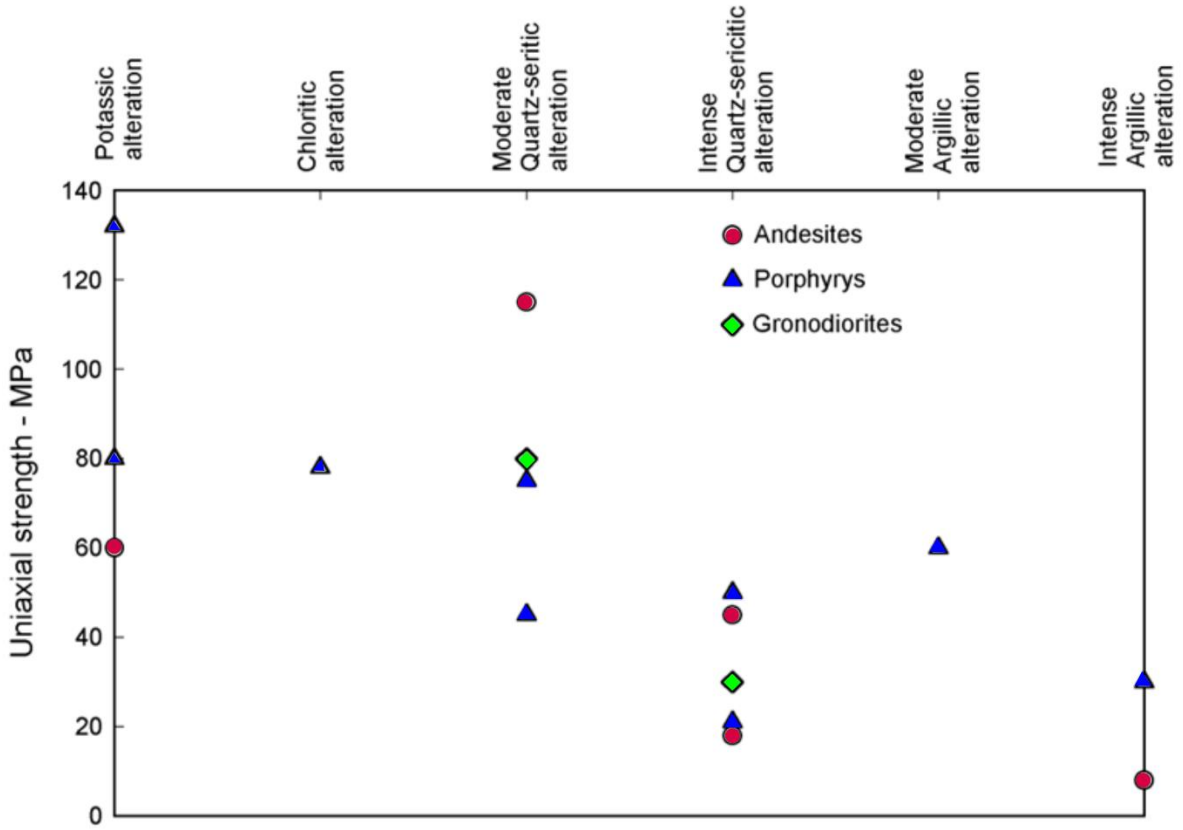

Figure 5: Relationship between intact rock strength and degree of alteration.

Role of groundwater

The presence of groundwater in a rock slope is a critical factor in any assessment of the stability of that slope. Water pressure, acting within discontinuities in the rock mass, reduces effective stresses with a consequent reduction of shear strength. Depressurisation using horizontal or vertical wells or drainage galleries is a powerful tool in controlling slope behaviour.

The technology and tools for groundwater pressure, flow evaluation and control are well developed. It is considered that no further research into this area is required. While it is difficult to maintain piezometers and drains during the excavation of a slope, this is often used as an excuse for not maintaining adequate control or monitoring of groundwater conditions. It is also important that water from horizontal drains should be collected and piped or pumped to a disposal area away from active slope stability problem areas.

As for the geological and geotechnical models discussed earlier, the development of a good groundwater model is an important component in the rational design of large slopes. It is important that resources be provided to ensure that sufficient information is collected to permit the construction of such a model.

On the question of drainage versus depressurisation, it is water pressure that creates slope stability problems and, provided that these water pressures are reduced, it is not necessary for a 'drainage' hole or well to produce large water flows. This is a common misconception which leads operators to abandon 'drains' that do not appear to be working because they do not produce much water. The judgement should be based upon the response of piezometers, which reflect water pressure change, rather than on volume flow. Sub-horizontal drainage holes can be very effective in hard rock slopes provided that they are long enough to depressurise the rock mass in the vicinity of potential failure surfaces. In large rock slopes, holes of 200 to 300 m in length may be required to achieve this goal.

Drainage galleries can have an important function, not only because of the depressurisation that can result from their construction, but also because of the valuable geological information that can be collected from locations that are not normally accessible. Typical drainage gallery construction costs are in the range of US$ 1500 per meter which can sometimes give an overall depressurisation scheme that is comparable in cost to one based upon horizontal holes and/or vertical pumped wells. More serious consideration has to be given to galleries for slope depressurisation than is currently the case in practice.

An example of the use of depressurisation to control slope instability is illustrated in Figure 6. This shows a section through a potential landslide in a hillside known as Dutchman's Ridge, immediately upstream of the Mica Dam on the Columbia River in British Columbia, Canada. This 700 m high 155 million ton potential slide was recognised during site investigation work for the Mica Dam, constructed in the 1960s. However, it was decided that no remedial action would be taken at that time but that the slope would be monitored by means of electro-optical distance measurements from stable observation posts across the valley. Movements averaging approximately 1 cm per year were measured over a 20 year period and, during a re-evaluation of dam safety in the early 1980s, it was decided that some form of stabilisation was required in order to reduce the downward movement of the slope. A detailed geological and geotechnical investigation established that the slide mass was moving on a basal fault surface, dipping parallel to the slope and it was concluded that depressurisation was the only feasible stabilisation option. The aim of the depressurisation programme was to reduce the water levels in the slope to approximately the equivalent of the levels that existed before the slope toe was submerged by impoundment of the reservoir. It was argued that the original slope had been stable for approximately 10,000 years since the last ice age and that it had withstood several large earthquakes known to have occurred in this area of British Columbia. Hence, it was felt that restoring the groundwater conditions to the pre-reservoir conditions would also restore the stability of slope.

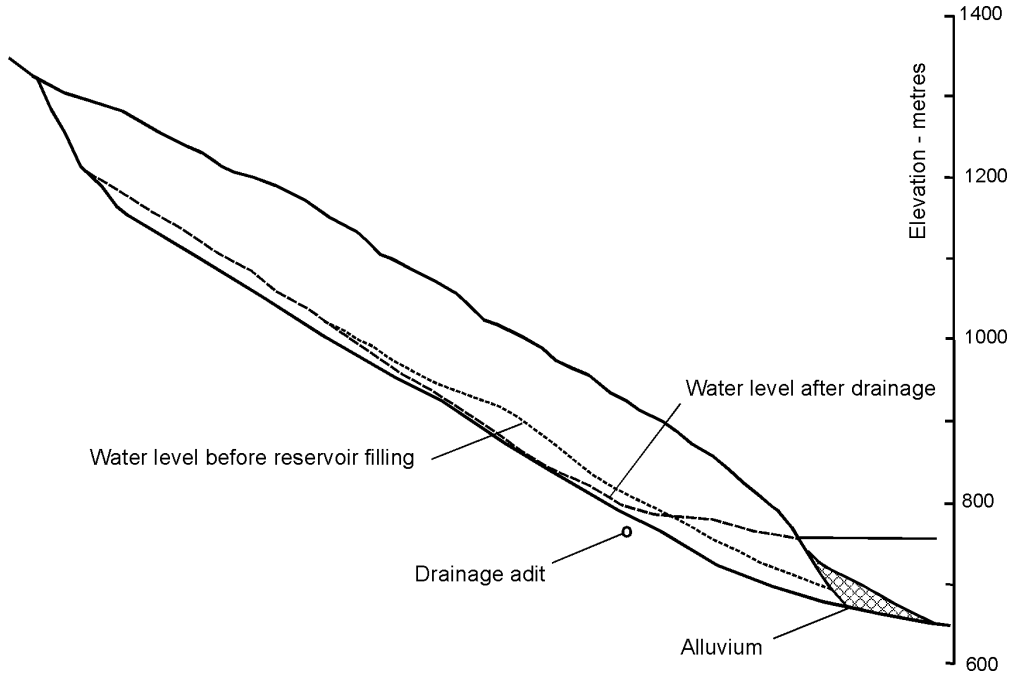

Figure 6: Section through Dutchman's Ridge slide showing the location of the drainage gallery and the phreatic surfaces before impoundment of the reservoir and after impoundment and drainage.

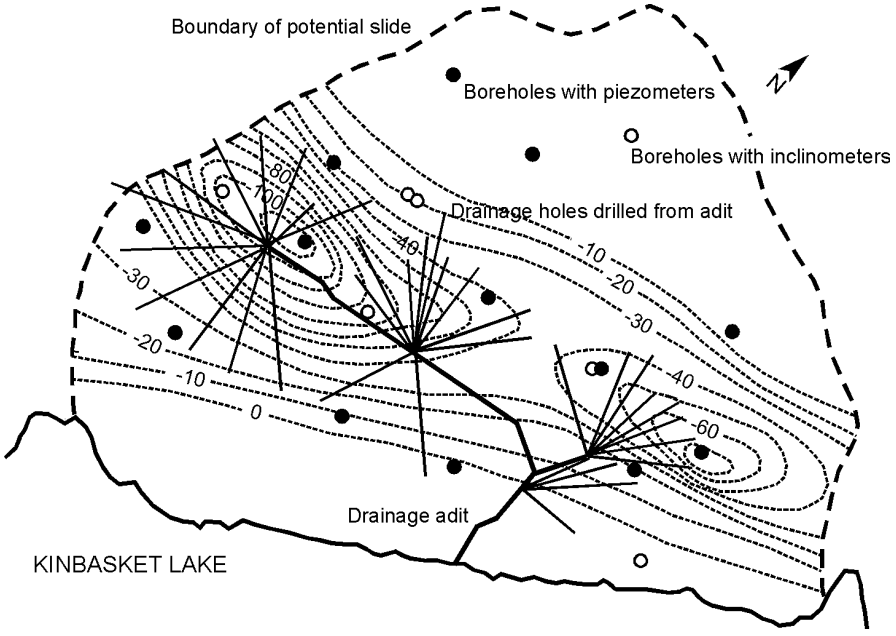

Figure 7: Extent of potential slide with layout of drainage gallery and drain holes drilled from underground. Contours indicate the drawdown of the groundwater levels achieved by the drainage.

Figure 7 shows the layout of the drainage gallery and the boreholes drilled from underground to target zones of high groundwater pressures. These zones had been determined from an array of 256 piezometer measuring points in the rock mass. The reduction in groundwater levels is also illustrated by means of the contours included in Figure 7.

Although analysis of the slope, using two- and three-dimensional limit equilibrium methods, indicated that the factor of safety was only increased approximately 6% by the depressurisation programme, measurement of displacements indicated that these had been reduced to negligible levels and the slope stabilisation program was judged to have been successful.

Figure 8: Collection of water from the boreholes drilled from the Downie Slide drainage gallery.

A similar depressurisation programme was used to stabilise the Downie Slide on the Columbia River, between the Mica and the Revelstoke Dams. The effectiveness of the underground drainage holes drilled from the Downie drainage gallery is illustrated in Figure 8. In both the Dutchman's Ridge and Downie cases, the drainage galleries have required routine maintenance but the drain holes have continued flowing and have kept the groundwater levels under control for the past 30 or more years.

In situ rock stress

It is well known that rock noses or slopes that are convex in plan are less stable than concave slopes. This is generally because of the lack of confinement in convex slopes and the beneficial effects of confinement in concave slopes. These observations provide practical evidence that lateral stresses, in the rock in which slopes are excavated, can have an important influence on slope stability.

In the current state of practice in rock slope design, these lateral stresses are usually ignored or are dealt with in a very simplistic manner. In fact, all limit equilibrium models are based upon gravity loading only and lateral stresses are excluded from any slope stability analysis that uses these models. Numerical models can incorporate lateral stresses, but most analyses, using these models, are based upon a very simple approximation in which the horizontal stress applied to the model is some proportion of the vertical stress.

Measurement of the in-situ stress field in the vicinity of large slopes is seldom carried out, in spite of the fact that such measurements are entirely feasible. This is because the in situ stress field is generally considered to be of minor significance. This assumption may be adequate for small slopes but it needs to be questioned for the design of very large slopes. Lorig (1999), based on the results of numerical analysis, suggests that in situ stresses have no significant effect on the safety factor. However, they do have an influence on deformations, and if the slope is composed of materials that weaken as a result of deformation, then the in-situ stress can have a very important effect in reducing strength and thereby affecting slope stability.

Before embarking on a programme of in situ stress measurement for any specific site, it is probably worth carrying out a parametric study using a three-dimensional model, such as FLAC3D, to determine whether variations in horizontal in situ stresses have a significant impact upon the stresses induced in the near-surface rock in which slope failures could occur. In cases in which lateral stresses in potential failure zones show a large variation, serious consideration would have to be given to a field programme to measure the in-situ stress field.

Blast damage

In the case of large production blasts in open pit mines, blast damage can extend many tens of meters into the rock mass behind the slope face. This blast damage is due to rock fracture and joint opening as a result of the dynamic stresses induced by the blast. In addition, penetration of gas pressure from the blast can open existing discontinuities for considerable distances from the face. This damage causes loosening of the rock mass with a consequent reduction in strength.

Control of the amount of explosive detonated per delay and pre-splitting, smooth-blasting or buffer blasting are methods commonly used to minimise blast damage and, where done correctly on a routine basis, certainly are effective. However, a certain amount of blast damage is inevitable. It is usually necessary to work towards a compromise between effective fragmentation of the rock mass, for easy digging, and leaving the remaining rock face as undamaged as possible. Figure 9 shows the damage to open pit mine benches as a result of uncontrolled large tonnage production blasting. In contrast, the lack of damage to the final walls of the same mine as a result of pre-split blasting and control of the adjacent production blasts is illustrated in Figure 10.

Figure 9: Bench faces created by normal production blasting.

Figure 10: Benches created by pre-split blasting.

One of the consequences of blast damage is that the appearance of the rock mass exposed in the bench faces is not representative of the undisturbed rock mass through which a potential surface may develop. Since most geotechnical mapping is carried out on these bench faces, the shear strength of joints and the overall strength of the rock mass, estimated on the basis of this mapping, may be unrealistically low. Therefore, it is important that observations on diamond drill core and exposures in underground excavations should be incorporated in the evaluation of rock mass strength. This is a largely qualitative process since none of the methods currently used to estimate joint shear strength or rock mass strength incorporate realistic corrections for blast damage.

Slope management

Slope failures, such as that of Mount Toc in the reservoir impounded by the Vajont Dam in Italy, have resulted in major loss of life and destruction of the project. As illustrated in Figure 2, slope failures in the open pit mines, where access is generally restricted, may not result in loss of life, but they certainly have the potential to disrupt the mining operation.

Many 'slope failures' are more subtle than the simple cases just described. For example, the gradual deformation of a slope, even when the movement is of the order of 4 m per year, as is the case on the West Wall of the Chuquicamata open pit copper mine in Chile (Figure 11), are not considered as 'failures', but rather are regarded as 'problems' that must be managed. This is in contrast to civil engineering practice where slope deformations, such as those shown in Figure 11, would certainly be considered as 'failures.'

One of the threats in open pit mining and civil engineering is the potential for the gradual deformation of a large slope to develop into a fast-moving catastrophic slide, as was the case in the Vajont failure. This is a very poorly understood process. There are few reliable documented case histories, but the process must be considered as a potential threat where large deforming slopes occur. Numerical modelling of these slopes for possible combinations of structural and rock mass failure and comparison of the results of these models with observations and measurements of actual slope behaviour is probably the best hope that we have of understanding this problem.

In any open pit mine, a variety of slope instabilities may be present at various locations in the mine at any time. The successful management of these features is the art of good open pit mining. The absence of any failures is a sign of over-conservative slope design, and hence, inefficient mine management.

Figure 11: Large deformations in the West wall of the Chuquicamata Open Pit Mine in Chile.

It is, therefore, an absolute requirement that engineering geologists, geotechnical engineers and mine planners work together all the time to ensure that (i), the appropriate data is collected (ii), the appropriate analyses are carried out (iii), the slope designs are clearly conveyed to and understood by the mine planners and operators, and (iv), well-conceived slope monitoring programmes are established to monitor the service performance of the slopes throughout the life of the mine. Contingency plans must also be drawn up to deal with the inevitable surprises that will occur from time to time.

Large rock slopes in civil engineering projects can also suffer ongoing displacements, as illustrated in the example of the Dutchman's Ridge and the Downie Slide discussed earlier. These movements are generally much smaller than those observed in open pit mines but the consequences of slope failure are such that the same requirements for data collection, analysis, interpretation and slope monitoring exist.

A slope design is based upon the best possible evaluations of the rock types and characteristics, the structural geology and the groundwater conditions in the slope. Even the best slope designs require some averaging all of information and local variations in geology or groundwater conditions will not always be incorporated into the design. These local variations can have a significant impact on slope stability and, depending upon the location of this instability, these may have important consequences for the performance of the slope. For example, local failure of benches adjacent to a haul road in an open pit mine can have a major impact on the performance of the mine even if the overall slopes are stable.

Advance warning of these slope instability problems is very important and monitoring of slope movement has proved to be the most reliable method for the detection of slope instability. The more accurate this measurement, the earlier the developing problem can be detected.

Tools for slope displacement monitoring are well developed and are used routinely on most large open pit mines and in many civil engineering projects in which large slopes exist or are being excavated. These are generally based upon observations on numerous targets placed at carefully selected locations on the benches of the mine. Electro-optical distance measuring (EDM) equipment and, more recently, Global Positioning by Satellite (GPS) systems are used to monitor the relative positions of these targets on a daily basis. High quality EDM or GPS systems can give an accuracy of less than one centimetre over measuring distances of a kilometre or more. This order of measurement accuracy is generally sufficient to give advance warning of most slope stability problems.

The use of down-hole inclinometers and extensometers tends to be restricted to local slope instability problems. Maintaining this equipment for any length of time in a deforming operating slope is very difficult, and hence, this type of equipment tends not be used for large-scale slope deformation or failure studies. This picture may be changed if equipment to be installed in the west wall of the Chuquicamata open pit mine proves to be successful. Developed by the CSIRO in Australia, this equipment consists of self-contained battery-operated devices that can be located precisely in space by radio signal triangulation. The anticipated accuracy of these devices is in the order of millimetres and the design life of about five years. Installed in boreholes at depths of up to 150 m, these devices will be able to track the movement of the rock mass behind the slope. This information is very important in the development of an understanding of how some of these large slopes deform.

Simple visual observation by geologists and geotechnical engineers is a tool that is frequently ignored. The development of tension cracks, the appearance of bench faces and the presence of rocks that have fallen from steep faces are all important signs of slope behaviour. If these are observed routinely and recorded systematically, a 'feel' for the behaviour of the slopes can be gradually developed. This is important information that can be taken into account when signs of significant slope instability appear and when discussions on remedial measures and contingency planning take place.

One of the tools that has been tried unsuccessfully on a number of mines is microseismic monitoring. Background noise from truck and shovel operations, blasting and regional seismic activity tends to mask any measurements of the microseismic noise generated by moving slopes.

Limit equilibrium and numerical modelling of slopes

The design of any slope must involve some form of analysis in which the disturbing forces, due to gravity and water pressure, are compared to the available strength of the rock mass. Traditionally these analyses have been carried out by means of limit equilibrium models but, more recently, numerical models have been used for this purpose.

Limit equilibrium models fall into two main categories: models that deal with structurally controlled planar or wedge slides and models that deal with circular or near circular failure surfaces in 'homogeneous' materials. Many of these models have been available for more than 40 years and can be considered reliable slope design tools.

As illustrated in Figure 4, failure of large rock slopes may involve the combination of several different failure mechanisms. This type is failure cannot be modelled by means of the simple 'homogeneous' material models described above and it is necessary to utilise non-circular failure models of the type originally proposed by Sarma (1979).

Significant improvements to Sarma's original analysis were made by Donald and Giam (1989) and later by Chen (1995), Donald and Chen (1997) and Chen (1999). Many of these advances have been incorporated into commercially available slope stability software and an example is given in Figure 12. This example involves a complex failure surface in an open pit mine slope in which several fault zones and rock types occur. Based upon the orientation of structural features, directional strength properties have been assigned to each of the rock types and the most critical failure surface is generated from an automatic search process. Numerical modelling of slope deformation behaviour is now a routine activity on many large open pit mines. Programs such as FLAC and UDEC[1] are generally used for such modelling and these codes do not require any further development to meet the needs of slope modelling. Using these codes correctly is not a

[1] Details available from www.itascacg.com

trivial process and mines embarking on a numerical modelling programme should anticipate a learning process of at least a year, even with expert help from consultants. Obtaining realistic input information for these models and interpreting the results produced are the most difficult aspect of numerical modelling in the context of large-scale slopes.

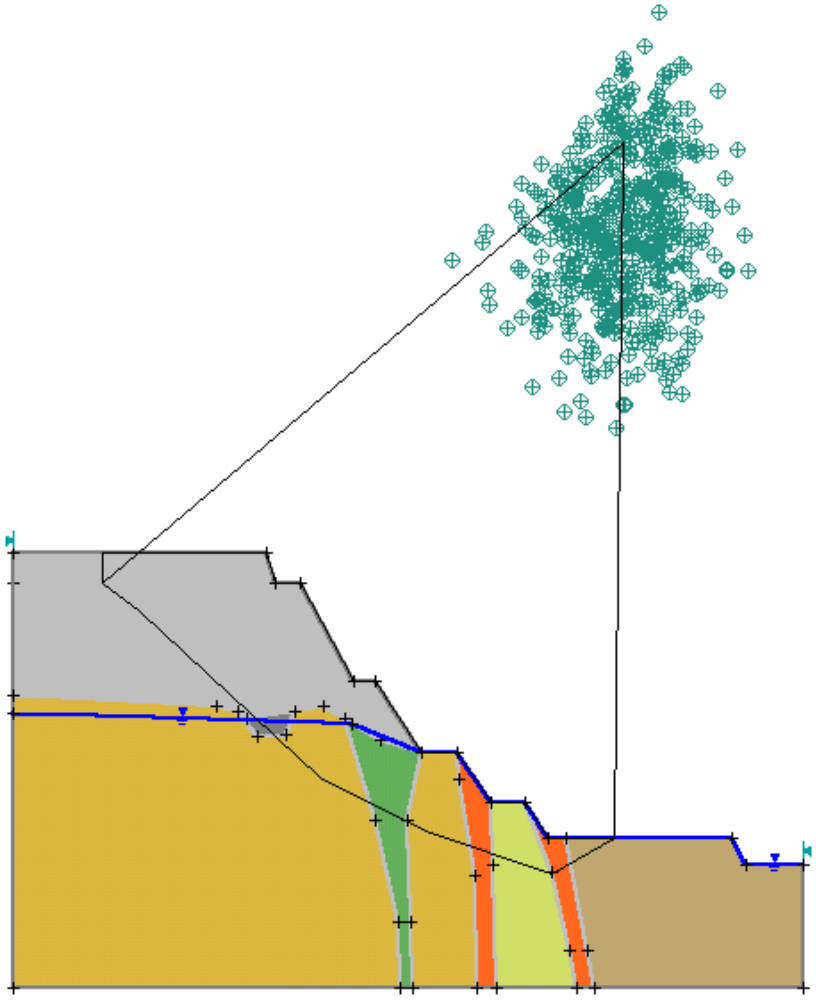

Figure 12: Non-circular failure surface in a rock slope composed of several different rock types separated by fault zones. The factor of safety for the critical failure surface indicated is 2.42. This analysis was performed by means of the program Slide2 [2].

In practice, both limit equilibrium and numerical modelling tools are used together to generate a range of possible solutions for the range of input parameters that exist for a particular site. While this may be frustrating for mine management and mine planners in that the geotechnical department does not appear to be capable of producing a single definitive design, it is far more realistic to look at the results of a parametric study than to rely on a single analysis.

[2] Details available from www.rocscience.com

The advantage of these numerical models over the limit equilibrium models described earlier is that they can be used to model progressive failure and displacement as opposed to a simple factor of safety. This makes them much more useful in managing ongoing slope displacements such as the case illustrated in Figure 11. These numerical models can also be used to determine the factor of safety of a slope in which a number of failure mechanisms can exist simultaneously or where the mechanism of failure may change as progressive failure occurs. Figures 13 and 14 illustrate this procedure which has been described by Dawson, Roth and Drescher (1999).

The Itasca UDEC model is set up to incorporate all the rock types, faults and joint systems as well as groundwater conditions within the slope. The strength of all the rock units, faults and joint systems is then decreased progressively by dividing them by a 'strength reduction factor'. The displacement of a target on the slope is monitored during this strength reduction process and, as shown in Figure 14, a sudden increase in displacement indicates that failure of the slope has started. The factor of safety of the slope is equivalent to the strength reduction factor at which failure starts. Factors of safety calculated in this way have been found to coincide very closely with those determined by limit equilibrium analyses in cases where limit equilibrium analyses are known to give reliable results.

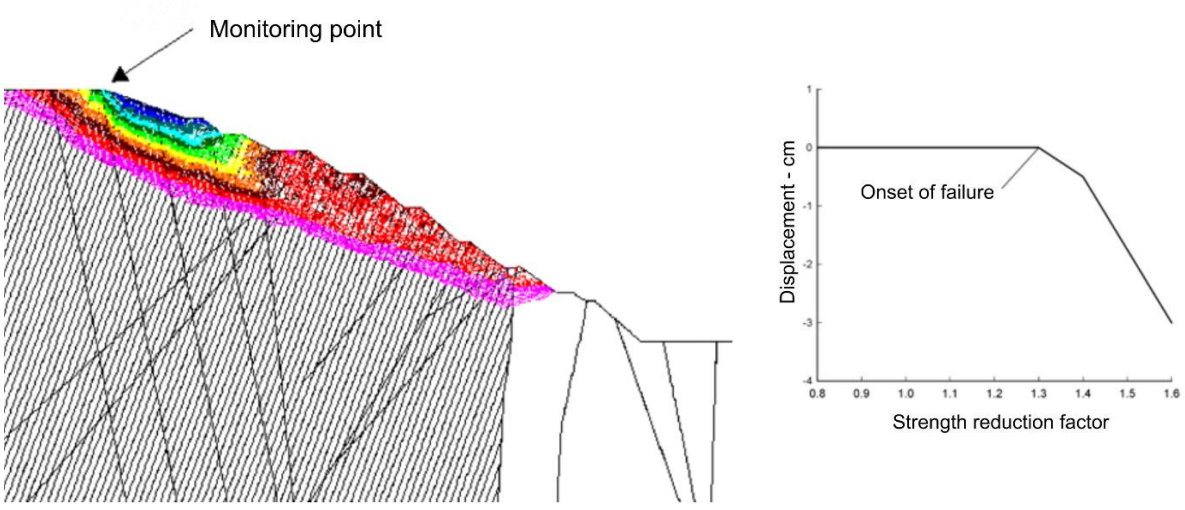

Figure 13: UDEC model of Chuquicamata West Wall showing displacement velocity contours and strength reduction factor.

References

Chen, Z. Y. (1995). "Recent developments in slope stability analysis". *Proc. 8th Int. Congress on Rock Mechanics*, Tokyo. Vol. 3, pp. 1041-1048.

Dawson, E. M., Roth, W. H. and Drescher, A. (1999). "Slope stability analysis by strength reduction". *Geotechnique*, Vol. 49, No.6, pp. 835-840.

Donald, I. and Chen, Z. Y. (1997). "Slope stability analysis by an upper bound plasticity method". *Canadian Geotechnical Journal*, December, Vol. 34, pp. 853-862.

Donald, I.B. and Giam, P.S.K. (1989). "Improved comprehensive limit equilibrium stability analysis". *Monash University Civil Engineering Research Report No. 1/1989.*

Haines, A. and Terbrugge, P. J. (1991). "Preliminary slope estimation of rock slope stability using rock mass classification systems". *Proc. 7th Int. Congress Rock Mechanics,* ISRM, Aachen, Vol. 2, pp. 887-892.

Hoek, E., Read, J., Karzulovic, A. and Chen, Z.Y. (2000). Rock slopes in civil and mining engineering. *Proc. International Conference on Geotechnical and Geological Engineering 2000,* 19-24 November, 2000, Melbourne.

Lorig, L. (1999). "Lessons learned from slope stability studies". *FLAC and Numerical Modeling in Geomechanics,* Detournay & Hart (eds).

Priest, S.D. and Samaniego, J.A. (1983). "A model for the analysis of discontinuity characteristics in two dimensions". *Proc. 5th ISRM Congress,* Melbourne. pp. 199-207.

Sainsbury, D.P. and Sainsbury, B. (2013) Three-dimensional analysis of pit slope stability in anisotropic rock masses, in P.M. Dight (ed.), Slope Stability 2013. Proceedings of the 2013 Symposium on Slope Stability Analysis. Mastuyama., pp. 31-48.

Wang. X, Chen, Z. and Jia, Z. (1998). "Joint mapping and its applications". Unpublished Report, China Institute of Water Resources and Hydropower Research.

12. Rock mass classification

Introduction

During the feasibility and preliminary design stages of a project, when very little detailed information is available on the rock mass and its stress and hydrologic characteristics, the use of a rock mass classification scheme can be of considerable benefit. At its simplest, this may involve using the classification scheme as a checklist to ensure that all relevant information has been considered. At the other end of the spectrum, one or more rock mass classification schemes can be used to build up a picture of the composition and characteristics of a rock mass to provide initial estimates of support requirements, and to provide estimates of the strength and deformation properties of the rock mass.

It is important to understand the limitations of rock mass classification schemes (Palmstrom and Broch, 2006) and that their use does not (and cannot) replace some of the more elaborate design procedures. However, the use of these design procedures requires access to relatively detailed information on in situ stresses, rock mass properties and planned excavation sequence, none of which may be available at an early stage in the project. As this information becomes available, the use of the rock mass classification schemes should be updated and used in conjunction with site specific analyses.

Engineering rock mass classification

Rock mass classification schemes have been developing for over 100 years since Ritter (1879) attempted to formalise an empirical approach to tunnel design, in particular for determining support requirements. While the classification schemes are appropriate for their original application, especially if used within the bounds of the case histories from which they were developed, considerable caution must be exercised in applying rock mass classifications to other rock engineering problems.

Summaries of some important classification systems are presented in this chapter, and although every attempt has been made to present all of the pertinent data from the original texts, there are numerous notes and comments which cannot be included. The interested reader should make every effort to read the cited references for a full appreciation of the use, applicability and limitations of each system.

Most of the multi-parameter classification schemes (Wickham et al (1972) Bieniawski (1973, 1989) and Barton et al (1974)) were developed from civil engineering case histories in which all of the components of the engineering geological character of the rock mass were included. In underground hard rock mining, however, especially at deep levels, rock mass weathering and the influence of water usually are not significant and may be ignored. Different classification systems place different emphases on the various parameters;

therefore, it is recommended that at least two methods be used at any site during the early stages of a project.

Terzaghi's rock mass classification

The earliest reference to the use of rock mass classification for the design of tunnel support is in a paper by Terzaghi (1946) in which the rock loads, carried by steel sets, are estimated based on a descriptive classification. While no useful purpose would be served by including details of Terzaghi's classification in this discussion on the design of support, it is interesting to examine the rock mass descriptions included in his original paper, because he draws attention to those characteristics that dominate rock mass behaviour, particularly in situations where gravity constitutes the dominant driving force. The clear and concise definitions and the practical comments included in these descriptions are good examples of the type of engineering geology information which is most useful for engineering design.

Terzaghi's descriptions (quoted directly from his paper) are:

- *Intact* rock contains neither joints nor hair cracks. Hence, if it breaks, it breaks across sound rock. Because of the damage to the rock due to blasting, spalls may drop off the roof several hours or days after blasting. This is known as a *spalling* condition. Hard, intact rock may also be encountered in the *popping* condition involving the spontaneous and violent detachment of rock slabs from the sides or roof.
- *Stratified* rock consists of individual strata with little or no resistance against separation along the boundaries between the strata. The strata may or may not be weakened by transverse joints. In such rock the spalling condition is quite common.
- *Moderately jointed* rock contains joints and hair cracks, but the blocks between joints are locally grown together or so intimately interlocked that vertical walls do not require lateral support. In rocks of this type, both spalling and popping conditions may be encountered.
- *Blocky and seamy* rock consists of chemically intact or almost intact rock fragments which are entirely separated from each other and imperfectly interlocked. In such rock, vertical walls may require lateral support.
- *Crushed* but chemically intact rock has the character of crusher run. If most or all the fragments are as small as fine sand grains and no re-cementation has taken place, crushed rock below the water table exhibits the properties of a water-bearing sand.
- *Squeezing* rock slowly advances into the tunnel without perceptible volume increase. A prerequisite for squeeze is a high percentage of microscopic and sub-microscopic particles of micaceous minerals or clay minerals with a low swelling capacity.
- *Swelling* rock advances into the tunnel chiefly on account of expansion. The capacity to swell seems to be limited to those rocks that contain clay minerals such as montmorillonite, with a high swelling capacity.

Classifications involving stand-up time

Lauffer (1958) proposed that the stand-up time for an unsupported span is related to the quality of the rock mass in which the span is excavated. In a tunnel, the unsupported span

is defined as the span of the tunnel or the distance between the face and the nearest support, if this is greater than the tunnel span. Lauffer's original classification has since been modified by several authors, notably Pacher et al (1974), and now forms part of the general tunnelling approach known as the New Austrian Tunnelling Method.

The significance of the stand-up time concept is that an increase in the span of the tunnel leads to a significant reduction in the time available for the installation of support. For example, a small pilot tunnel may be successfully constructed with minimal support, while a larger span tunnel in the same rock mass may not be stable without the immediate installation of substantial support.

The New Austrian Tunnelling Method includes several techniques for safe tunnelling in rock conditions in which the stand-up time is limited before failure occurs. These techniques include the use of smaller headings and benching or the use of multiple drifts to form a reinforced ring inside which the bulk of the tunnel can be excavated. These techniques are applicable in soft rocks such as shales, phyllites and mudstones in which the squeezing and swelling problems, described by Terzaghi (see previous section), are likely to occur. The techniques are also applicable when tunnelling in excessively broken rock, but great care should be taken in attempting to apply these techniques to excavations in hard rocks in which different failure mechanisms occur.

In designing support for hard rock excavations, it is prudent to assume that the stability of the rock mass surrounding the excavation is not time dependent. Hence, if a structurally defined wedge is exposed in the roof of an excavation, it will fall as soon as the rock supporting it, is removed. This can occur at the time of the blast or during the subsequent scaling operation. If it is required to keep such a wedge in place, or to enhance the margin of safety, it is essential that the support be installed as early as possible, preferably before the rock supporting the full wedge is removed. On the other hand, in a highly stressed rock, failure will generally be induced by some change in the stress field surrounding the excavation. The failure may occur gradually and manifest itself as spalling or slabbing or it may occur suddenly in the form of a rock burst. In either case, the support design must consider the change in the stress field rather than the ‘stand-up’ time of the excavation.

Rock quality designation index (RQD)

The Rock Quality Designation index (*RQD*) was developed by Deere (Deere et al 1967) to provide a quantitative estimate of rock mass quality from drill core logs. RQD is defined as the percentage of intact core pieces longer than 100 mm (4 inches) in the total length of core. The core should be at least NW size (54.7 mm or 2.15 inches in diameter) and should be drilled with a double-tube core barrel. The correct procedures for measurement of the length of core pieces and the calculation of *RQD* are summarised in Figure 1.

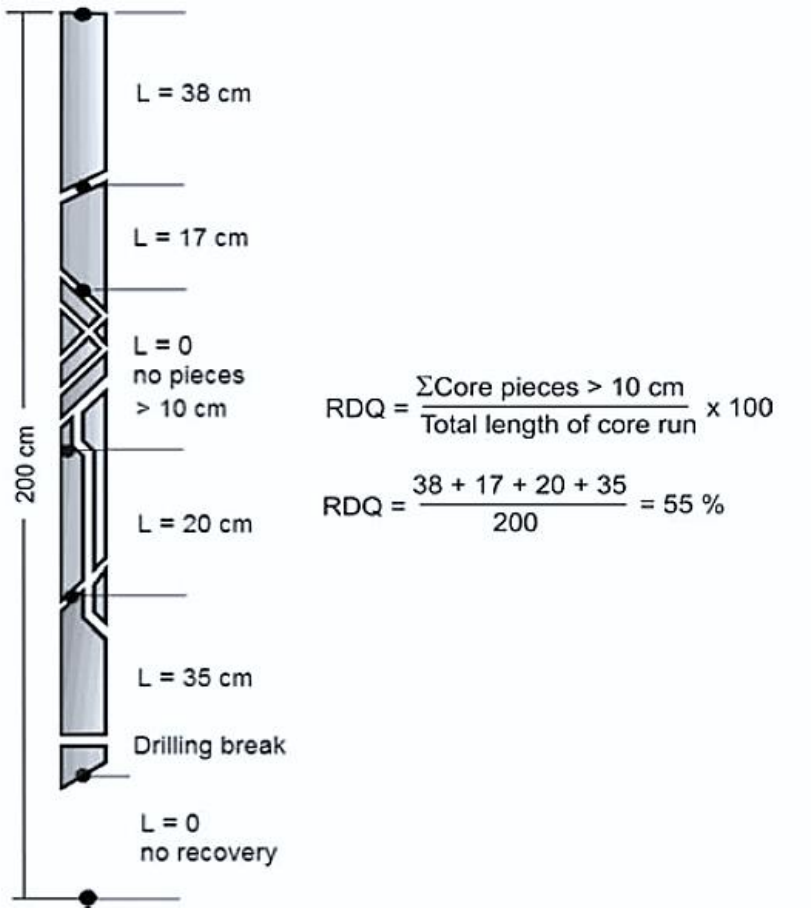

Figure 1: Procedure for measurement and calculation of *RQD* (After Deere, 1989).

Palmström (1982) suggested that, when no core is available, but discontinuity traces are visible in surface exposures or exploration adits, the *RQD* may be estimated from the number of discontinuities per unit volume. The suggested relationship for clay-free rock masses is:

$$RQD = 115 - 3.3\ J_V \qquad (1)$$

where J_V is the sum of the number of joints per unit length for all joint (discontinuity) sets known as the volumetric joint count.

RQD is a directionally dependent parameter, and its value may change significantly, depending upon the borehole orientation. The use of the volumetric joint count can be quite useful in reducing this directional dependence.

RQD is intended to represent the rock mass quality in situ. When using diamond drill core, care must be taken to ensure that fractures, which have been caused by handling or the drilling process, are identified and ignored when determining the value of *RQD*.

When using Palmström's relationship for exposure mapping, blast induced fractures should not be included when estimating J_V.

Deere's *RQD* was widely used, particularly in North America, after its introduction. Cording and Deere (1972), Merritt (1972) and Deere and Deere (1988) attempted to relate *RQD* to Terzaghi's rock load factors and to rockbolt requirements in tunnels. In the context of this discussion, the most important use of *RQD* is as a component of the *RMR* and *Q* rock mass classifications covered later in this chapter.

Rock Structure Rating (RSR)

Wickham et al (1972) described a quantitative method for describing the quality of a rock mass and for selecting appropriate support on the basis of their Rock Structure Rating (*RSR*) classification. Most of the case histories, used in the development of this system, were for relatively small tunnels supported by means of steel sets, although historically this system was the first to make reference to shotcrete support. In spite of this limitation, it is worth examining the *RSR* system in some detail since it demonstrates the logic involved in developing a quasi-quantitative rock mass classification system.

The significance of the *RSR* system, in the context of this discussion, is that it introduced the concept of rating each of the components listed below to arrive at a numerical value of $RSR = A + B + C$.

1. *Parameter A, Geology:* General appraisal of geological structure on the basis of:
    a. Rock type origin (igneous, metamorphic, sedimentary)
    b. Rock hardness (hard, medium, soft, decomposed)
    c. Geologic structure (massive, slightly faulted/folded, moderately faulted/folded, intensely faulted/folded).
2. *Parameter B, Geometry*: Effect of discontinuity pattern with respect to the direction of the tunnel drive on the basis of:
    a. Joint spacing
    b. Joint orientation (strike and dip)
    c. Direction of tunnel drive.
3. *Parameter C*: Effect of groundwater inflow and joint condition on the basis of:
    a. Overall rock mass quality on the basis of A and B combined
    b. Joint condition (good, fair, poor)
    c. Amount of water inflow (in gallons per minute per 1000 feet of tunnel).

Note that the *RSR* classification used Imperial units and that these units have been retained in this discussion.

Three tables from the Wickham et al (1972) paper are reproduced in Tables 1, 2 and 3. These tables can be used to evaluate the rating of each of these parameters to arrive at the *RSR* value (maximum $RSR = 100$).

Table 1: Rock Structure Rating: Parameter A: General area geology

	Basic Rock Type				Geological Structure			
	Hard	Mediu	Soft	Decompose				
Igneous	1	2	3	4		Slightly	Moderatel	Intensivel
Metamorp	1	2	3	4		Folded or	Folded or	Folded or
Sedimentar	2	3	4	4	Massive	Faulted	Faulted	Faulted
Type 1					30	22	15	9
Type 2					27	20	13	8
Type 3					24	18	12	7
Type 4					19	15	10	6

Table 2: Rock Structure Rating: Parameter *B*: Joint pattern, direction of drive

	Strike ⊥ to Axis					Strike || to Axis		
	Direction of Drive					Direction of Drive		
	Bot	With Dip		Against Dip		Either direction		
	Dip of Prominent Joints [a]					Dip of Prominent Joints		
Average joint spacing	Flat	Dippin	Vertica	Dippin	Vertica	Flat	Dipping	Vertica
1. Very closely jointed, < 2	9	11	13	10	12	9	9	7
2. Closely jointed, 2-6 in	13	16	19	15	17	14	14	11
3. Moderately jointed, 6-	23	24	28	19	22	23	23	19
4. Moderate to blocky, 1-2	30	32	36	25	28	30	28	24
5. Blocky to massive, 2-4 ft	36	38	40	33	35	36	24	28
6. Massive, > 4 ft	40	43	45	37	40	40	38	34

Table 3: Rock Structure Rating: Parameter *C*: Groundwater, joint condition

	Sum of Parameters *A* + *B*					
	13 - 44			45 - 75		
	Joint Condition [b]					
Anticipated water inflow gpm/1000 ft of tunnel	Good	Fair	Poor	Good	Fair	Poor
None	22	18	12	25	22	18
Slight, < 200 gpm	19	15	9	23	19	14
Moderate, 200-1000	15	22	7	21	16	12
Heavy, > 1000 gp	10	8	6	18	14	10

[a] Dip: flat: 0-20°; dipping: 20-50°; and vertical: 50-90°

[b] Joint condition: good = tight or cemented; fair = slightly weathered or altered; poor = severely weathered, altered, or open

For example, a hard metamorphic rock which is slightly folded or faulted has a rating of A = 22 (from Table 1). The rock mass is moderately jointed with joints striking perpendicular to the tunnel axis which is being driven east-west and dipping at between 20° and 50°.

Table 2 gives the rating for B = 24 for driving with dip (defined below).

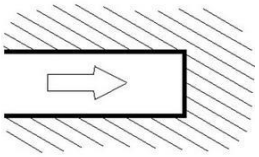

Drive with dip

The value of $A + B$ = 46 and this means that, for joints of fair condition (slightly weathered and altered) and a moderate water inflow of between 200 and 1,000 gallons per minute, Table 3 gives the rating for C = 16. Hence, the final value of the rock structure rating $RSR = A + B + C$ = 62.

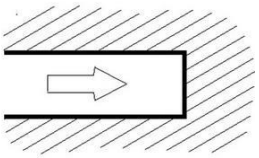

Drive against dip

A typical set of prediction curves for a 24-foot diameter tunnel are given in Figure 2 which shows that, for the *RSR* value of 62 derived above, the predicted support would be 2 inches of shotcrete and 1 inch diameter rockbolts spaced at 5-foot centres. As indicated in the figure, steel sets would be spaced at more than 7 feet apart and would not be considered a practical solution for the support of this tunnel.

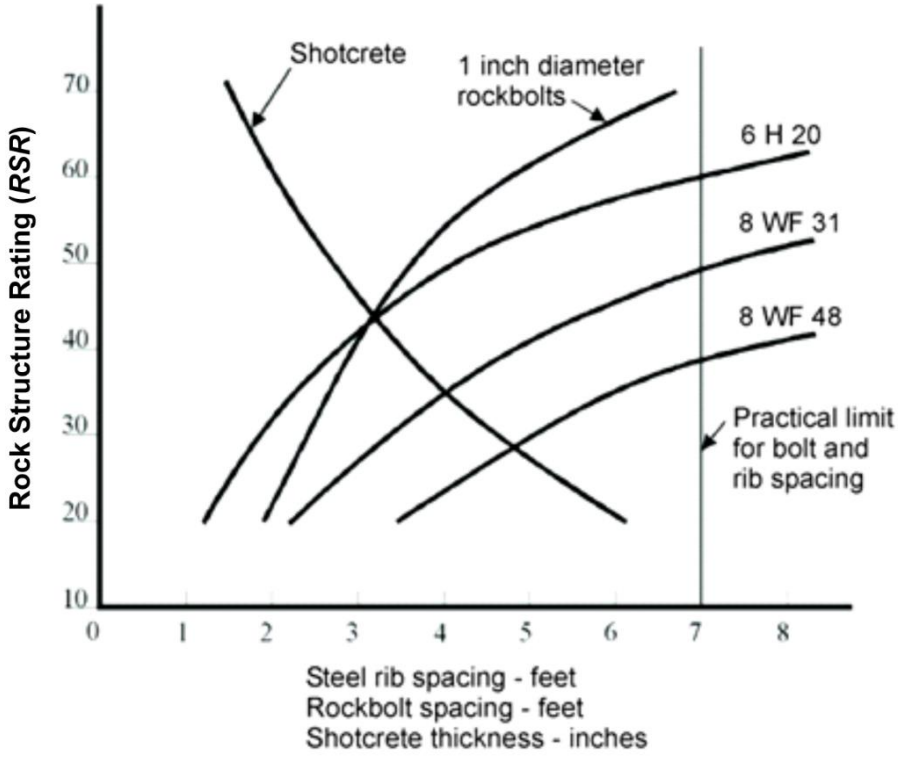

Figure 2: *RSR* support estimates for a 24 ft. (7.3 m) diameter circular tunnel. Note that rockbolts and shotcrete are generally used together. (After Wickham et al 1972).

For the same size tunnel in a rock mass with *RSR* = 30, the support could be provided by 8 WF 31 steel sets (8-inch deep wide flange I section weighing 31 lb per foot) spaced 3 feet apart, or by 5 inches of shotcrete and 1 inch diameter rockbolts spaced at 2.5 feet centres. In this case it is probable that the steel set solution would be cheaper and more effective than the use of rockbolts and shotcrete.

Although the *RSR* classification system is not widely used today, Wickham et al's work played a significant role in the development of the classification schemes discussed in the remaining sections of this chapter.

Geomechanics Classification - RMR

Bieniawski (1976) published the details of a rock mass classification called the Geomechanics Classification or the Rock Mass Rating (*RMR*) system. Over the years, this system has been successively refined as more case records have been examined and the reader should be aware that Bieniawski has made significant changes in the ratings assigned to different parameters. The discussion which follows is based upon the 1989 version of the classification (Bieniawski, 1989). Both this version and the 1976 version deal with estimating the strength of rock masses. The following six parameters are used to classify a rock mass using the *RMR* system:

1. Uniaxial compressive strength of rock material
2. Rock Quality Designation (*RQD*)
3. Spacing of discontinuities
4. Condition of discontinuities
5. Groundwater conditions
6. Orientation of discontinuities.

In applying this classification system, the rock mass is divided into a number of structural regions and each region is classified separately. The boundaries of the structural regions usually coincide with a major structural feature such as a fault or with a change in rock type. In some cases, significant changes in discontinuity spacing or characteristics, within the same rock type, may necessitate the division of the rock mass into a number of small structural regions.

The Rock Mass Rating system is presented in Table 4, giving the ratings for each of the six parameters listed above. These ratings are summed to give a value of *RMR*. The following example illustrates the use of these tables to arrive at an *RMR* value.

A tunnel is to be driven through slightly weathered granite with a dominant joint set dipping at 60^{o} against the direction of the drive. Index testing and logging of diamond drilled core give typical Point-load strength index values of 8 MPa and average *RQD* values of 70%. The slightly rough and slightly weathered joints with a separation of < 1 mm, are spaced at 300 mm. Tunnelling conditions are anticipated to be wet.

Table 4: Rock Mass Rating System (After Bieniawski 1989).

A. CLASSIFICATION PARAMETERS AND THEIR RATINGS									
Parameter			Range of values						
1	Strength of intact rock material	Point-load strength index	>10 MPa	4 - 10 MPa	2 - 4 MPa	1 - 2 MPa	For this low range - uniaxial compressive test is preferred		
		Uniaxial comp. strength	>250 MPa	100 - 250 MPa	50 - 100 MPa	25 - 50 MPa	5 - 25 MPa	1 - 5 MPa	< 1 MPa
	Rating		15	12	7	4	2	1	0
2	Drill core *Quality RQD*		90% - 100%	75% - 90%	50% - 75%	25% - 50%	< 25%		
	Rating		20	17	13	8	3		
3	Spacing of		> 2 m	0.6 - 2 . m	200 - 600 mm	60 - 200 mm	< 60 mm		
	Rating		20	15	10	8	5		
4	Condition of discontinuities (See E)		Very rough surfaces Not continuous No separation Unweathered wall rock	Slightly rough surfaces Separation < 1 mm Slightly weathered walls	Slightly rough surfaces Separation < 1 mm Highly weathered walls	Slickensided surfaces or Gouge < 5 mm thick or Separation 1-5 mm Continuous	Soft gouge >5 mm thick or Separation > 5 mm Continuous		
	Rating		30	25	20	10	0		
5	Ground water	Inflow per 10 m tunnel length (l/m)	None	< 10	10 - 25	25 - 125	> 125		
		(Joint water press)/ (Major principal σ)	0	< 0.1	0.1, - 0.2	0.2 - 0.5	> 0.5		
		General conditions	Completely dry	Damp	Wet	Dripping	Flowing		
	Rating		15	10	7	4	0		

B. RATING ADJUSTMENT FOR DISCONTINUITY ORIENTATIONS (See F)						
Strike and dip orientations		Very favourable	Favourable	Fair	Unfavourable	Very Unfavourable
Ratings	Tunnels & mines	0	-2	-5	-10	-12
	Foundations	0	-2	-7	-15	-25
	Slopes	0	-5	-25	-50	

C. ROCK MASS CLASSES DETERMINED FROM TOTAL RATINGS						
Rating	100 ← 81	80 ← 61	60 ← 41	40 ← 21	< 21	
Class number	I	II	III	IV	V	
Description	Very good rock	Good rock	Fair rock	Poor rock	Very poor rock	

D. MEANING OF ROCK CLASSES					
Class number	I	II	III	IV	V
Average stand-up time	20 yrs for 15 m span	1 year for 10 m span	1 week for 5 m span	10 hrs for 2.5 m span	30 min for 1 m span
Cohesion of rock mass (kPa)	> 400	300 - 400	200 - 300	100 - 200	< 100
Friction angle of rock mass (deg)	> 45	35 - 45	25 - 35	15 - 25	< 15

E. GUIDELINES FOR CLASSIFICATION OF DISCONTINUITY conditions					
Discontinuity length (persistence)	< 1 m	1 - 3 m	3 - 10 m	10 - 20 m	> 20 m
Rating	6	4	2	1	0
Separation (aperture)	None	< 0.1 mm	0.1 - 1.0 mm	1 - 5 mm	> 5 mm
Rating	6	5	4	1	0
Roughness	Very rough	Rough	Slightly rough	Smooth	Slickensided
Rating	6	5	3	1	0
Infilling (gouge)	None	Hard filling < 5 mm	Hard filling > 5 mm	Soft filling < 5 mm	Soft filling > 5 mm
Rating	6	4	2	2	0
Weathering	Unweathered	Slightly weathered	Moderately weathered	Highly weathered	Decomposed
Ratings	6	5	3	1	0

F. EFFECT OF DISCONTINUITY STRIKE AND DIP ORIENTATION IN TUNNELLING**			
Strike perpendicular to tunnel axis		Strike parallel to tunnel axis	
Drive with dip - Dip 45 - 90°	Drive with dip - Dip 20 - 45°	Dip 45 - 90°	Dip 20 - 45°
Very favourable	Favourable	Very unfavourable	Fair
Drive against dip - Dip 45-90°	Drive against dip - Dip 20-45°	Dip 0-20 - Irrespective of strike°	
Fair	Unfavourable	Fair	

* Some conditions are mutually exclusive. For example, if infilling is present, the roughness of the surface will be overshadowed by the influence of the gouge. In such cases use A.4 directly.
** Modified after Wickham et al (1972).

The *RMR* value for the example under consideration is determined as follows:

Table	*Item*	*Value*	*Rating*
4: A.1	Point load index	8 MPa	12
4: A.2	*RQD*	70%	13
4: A.3	Spacing of discontinuities	300 mm	10
4: E.4	Condition of discontinuities	Note 1	22
4: A.5	Groundwater	Wet	7
4: B	Adjustment for joint orientation	Note 2	-5
		Total	59

Note 1. For slightly rough and altered discontinuity surfaces with a separation of < 1 mm, Table 4.A.4 gives a rating of 25. When more detailed information is available, Table 4.E can be used to obtain a more refined rating. Hence, in this case, the rating is the sum of: 4 (1-3 m discontinuity length), 4 (separation 0.1-1.0 mm), 3 (slightly rough), 6 (no infilling) and 5 (slightly weathered) = 22.

Note 2. Table 4.F gives a description of 'Fair' for the conditions assumed where the tunnel is to be driven against the dip of a set of joints dipping at 60^{o}. Using this description for 'Tunnels and Mines' in Table 4.B gives an adjustment rating of -5.

Bieniawski (1989) published a set of guidelines for the selection of support in tunnels in rock for which the value of *RMR* has been determined. These guidelines are reproduced in Table 4. Note that these guidelines have been published for a 10 m span horseshoe shaped tunnel, constructed using drill and blast methods, in a rock mass subjected to a vertical stress < 25 MPa (equivalent to a depth below surface of <900 m).

For the case considered earlier, with *RMR* = 59, Table 4 suggests that a tunnel could be excavated by top heading and bench, with a 1.5 to 3 m advance in the top heading. Support should be installed after each blast and the support should be placed at a maximum distance of 10 m from the face. Systematic rock bolting, using 4 m long 20 mm diameter fully grouted bolts, spaced at 1.5 to 2 m in the crown and walls, is recommended. Wire mesh, with 50 to 100 mm of shotcrete for the crown and 30 mm of shotcrete for the walls, is recommended.

The value of *RMR* of 59 indicates that the rock mass is on the boundary between the 'Fair rock' and 'Good rock' categories. In the initial stages of design and construction, it is advisable to utilise the support suggested for fair rock. If the construction is progressing well with no stability problems, and the support is performing very well, then it should be possible to gradually reduce the support requirements to those indicated for a good rock mass. In addition, if the excavation is required to be stable for a short amount of time, then it is advisable to try the less expensive and extensive support suggested for good rock. However, if the rock mass surrounding the excavation is expected to undergo large mining induced stress changes, then more substantial support appropriate for fair rock should be

installed. This example indicates that a great deal of judgement is needed in the application of rock mass classification to support design.

Table 5: Guidelines for excavation and support of 10 m span rock tunnels in accordance with the *RMR* system (After Bieniawski 1989).

Rock mass class	Excavation	Rock bolts (20 mm diameter, fully grouted)	Shotcrete	Steel sets
I - Very good rock *RMR*: 81-100	Full face, 3 m advance.	Generally no support required except spot bolting.		
II - Good rock *RMR*: 61-80	Full face , 1-1.5 m advance. Complete support 20 m from face.	Locally, bolts in crown 3 m long, spaced 2.5 m with occasional wire mesh.	50 mm in crown where required.	None.
III - Fair rock *RMR*: 41-60	Top heading and bench 1.5-3 m advance in top heading. Commence support after each blast. Complete support 10 m from face.	Systematic bolts 4 m long, spaced 1.5 - 2 m in crown and walls with wire mesh in crown.	50-100 mm in crown and 30 mm in sides.	None.
IV - Poor rock *RMR*: 21-40	Top heading and bench 1.0-1.5 m advance in top heading. Install support concurrently with excavation, 10 m from face.	Systematic bolts 4-5 m long, spaced 1-1.5 m in crown and walls with wire mesh.	100-150 mm in crown and 100 mm in sides.	Light to medium ribs spaced 1.5 m where required.
V – Very poor rock *RMR*: < 20	Multiple drifts 0.5-1.5 m advance in top heading. Install support concurrently with excavation. Shotcrete as soon as possible after blasting.	Systematic bolts 5-6 m long, spaced 1-1.5 m in crown and walls with wire mesh. Bolt invert.	150-200 mm in crown, 150 mm in sides, and 50 mm on face.	Medium to heavy ribs spaced 0.75 m with steel lagging and forepoling if required. Close invert.

It should be noted that Table 5 has not had a major revision since 1973. In many mining and civil engineering applications, steel fibre reinforced shotcrete may be considered in place of wire mesh and shotcrete.

Modifications to *RMR* for mining

Bieniawski's Rock Mass Rating (*RMR*) system was originally based upon case histories drawn from civil engineering. Consequently, the mining industry tended to regard the classification as somewhat conservative and several modifications have been proposed in order to make the classification more relevant to mining applications. A comprehensive summary of these modifications was compiled by Bieniawski (1989).

Laubscher (1977, 1984), Laubscher and Taylor (1976) and Laubscher and Page (1990) have described a Modified Rock Mass Rating (*MRMR*) system for mining. This system takes the basic *RMR* value, as defined by Bieniawski, and adjusts it to account for in situ and induced stresses, stress changes and the effects of blasting and weathering. A set of support recommendations is associated with the resulting *MRMR* value. In using Laubscher's *MRMR* system it should be borne in mind that many of the case histories upon which it is based are derived from caving operations. Originally, block caving in asbestos

mines in Africa formed the basis for the modifications but, subsequently, other case histories from around the world have been added to the database.

Cummings et al (1982) and Kendorski et al (1983) have also modified Bieniawski's RMR classification to produce the *MBR* (modified basic *RMR*) system for mining. This system was developed for block caving operations in the USA. It involves the use of different ratings for the original parameters used to determine the value of *RMR* and the subsequent adjustment of the resulting *MBR* value to allow for blast damage, induced stresses, structural features, distance from the cave front and size of the caving block. Support recommendations are presented for isolated or development drifts as well as for the final support of intersections and drifts.

Rock Tunnelling Quality Index, *Q*

Based on an evaluation of a large number of case histories of underground excavations, Barton et al (1974) of the Norwegian Geotechnical Institute proposed a Tunnelling Quality Index (*Q*) for the determination of rock mass characteristics and tunnel support requirements. The numerical value of the index *Q* varies on a logarithmic scale from 0.001 to a maximum of 1,000 and is defined by:

$$Q = \frac{RQD}{J_n} \times \frac{J_r}{J_a} \times \frac{J_w}{SRF} \qquad (2)$$

where RQD is the Rock Quality Designation
J_n is the joint set number
J_r is the joint roughness number
J_a is the joint alteration number
J_w is the joint water reduction factor
SRF is the stress reduction factor

In explaining the meaning of the parameters used to determine the value of *Q*, Barton et al (1974) offer the following comments:

> *The first quotient (RQD*/J_n), representing the structure of the rock mass, is a crude measure of the block or particle size, with the two extreme values (100/0.5 and 10/20) differing by a factor of 400. If the quotient is interpreted in units of centimetres, the extreme 'particle sizes' of 200 to 0.5 cm are seen to be crude but fairly realistic approximations. Probably the largest blocks should be several times this size and the smallest fragments less than half the size. (Clay particles are of course excluded).
>
> The second quotient (J_r/J_a) represents the roughness and frictional characteristics of the joint walls or filling materials. This quotient is weighted in favour of rough, unaltered joints in direct contact. It is to be expected that such surfaces will be close to peak strength, that they will dilate strongly when sheared, and, they will therefore be, especially favourable to tunnel stability.
>
> When rock joints have thin clay mineral coatings and fillings, the strength is reduced significantly. Nevertheless, rock wall contact after small shear displacements have

occurred may be a very important factor for preserving the excavation from ultimate failure.

Where no rock wall contact exists, the conditions are extremely unfavourable to tunnel stability. The 'friction angles' (given in Table 6) are a little below the residual strength values for most clays and are possibly downgraded by the fact that these clay bands or fillings may tend to consolidate during shear, at least if normal consolidation or if softening and swelling has occurred. The swelling pressure of montmorillonite may also be a factor here.

The third quotient (J_w/SRF) consists of two stress parameters. *SRF* is a measure of: 1) loosening load in the case of an excavation through shear zones and clay bearing rock, 2) rock stress in competent rock, and 3) squeezing loads in plastic incompetent rocks. It can be regarded as a total stress parameter. The parameter J_w is a measure of water pressure, which has an adverse effect on the shear strength of joints due to a reduction in effective normal stress. Water may, in addition, cause softening and possible out-wash in the case of clay-filled joints. It has proved impossible to combine these two parameters in terms of inter-block effective stress, because paradoxically a high value of effective normal stress may sometimes signify less stable conditions than a low value, despite the higher shear strength. The quotient (J_w/SRF) is a complicated empirical factor describing the 'active stress'.

It appears that the rock tunnelling quality *Q* can now be considered to be a function of only three parameters which are crude measures of:

1. Block size	(*RQD/Jn*)
2. Inter-block shear strength	(*Jr/ Ja*)
3. Active stress	(*Jw/SRF*)

Undoubtedly, there are several other parameters which could be added to improve the accuracy of the classification system. One of these would be the joint orientation. Although many case records include the necessary information on structural orientation in relation to excavation axis, it was not found to be the important general parameter that might be expected. Part of the reason for this may be that the orientations of many types of excavations can be, and normally are, adjusted to avoid the maximum effect of unfavourably oriented major joints. However, this choice is not available in the case of tunnels, and more than half the case records were in this category. The parameters *Jn*, *Jr* and *Ja* appear to play a more important role than orientation, because the number of joint sets determines the degree of freedom for block movement (if any), and the frictional and dilatational characteristics can vary more than the down-dip gravitational component of unfavourably oriented joints. If joint orientations had been included, the classification would have been less general, and its essential simplicity lost.

Table 6 (After Barton et al 1974) gives the classification of individual parameters used to obtain the Tunnelling Quality Index *Q* for a rock mass.

The use of Table 6 is illustrated in the following example involving a 15 m span crusher chamber for an underground mine to be excavated in a norite at a depth of 2,100 m below

surface. The rock mass contains two sets of joints controlling stability. These joints are undulating, rough and unweathered with very minor surface staining. *RQD* values range from 85% to 95% and laboratory tests on core samples of intact rock give an average uniaxial compressive strength of 170 MPa. The principal stress directions are approximately vertical and horizontal. The magnitude of the horizontal principal stress is approximately 1.5 times that of the vertical principal stress. The rock mass is locally damp, but there is no evidence of flowing water.

The numerical value of *RQD* is used directly in the calculation of *Q* and, for this rock mass, an average value of 90 will be used. Table 6.2 shows that, for two joint sets, the joint set number, *Jn* = 4. For rough or irregular joints which are undulating, Table 6.3 gives a joint roughness number of *Jr* = 3. Table 6.4 gives the joint alteration number, *Ja* = 1.0, for unaltered joint walls with surface staining only. Table 6.5 shows that, for an excavation with minor inflow, the joint water reduction factor, *Jw* = 1.0. For a depth below surface of 2,100 m the overburden stress will be approximately 57 MPa and, in this case, the major principal stress σ_1 = 85 MPa. Since the uniaxial compressive strength of the norite is approximately 170 MPa, this gives a ratio of $\sigma_c / \sigma_1 = 2$. Table 6.6 shows that, for competent rock with rock stress problems, this value of σ_c / σ_1 can be expected to produce heavy rock burst conditions and that the value of *SRF* should lie between 10 and 20. A value of *SRF* = 15 will be assumed for this calculation. Using these values gives:

$$Q = (90/40) * (3/1) * (1/15) = 4.5$$

In relating the value of the index *Q* to the stability and support requirements of underground excavations, Barton et al (1974) defined an additional parameter which they called the Equivalent Dimension, *De*, of the excavation. This dimension is obtained by dividing the span, diameter or wall height of the excavation by a quantity called the Excavation Support Ratio, *ESR*. Hence:

$$De = \text{(Excavation span, diameter, or height (m))} / \text{Excavation Support Ratio ESR}$$

The value of *ESR* is related to the intended use of the excavation and to the degree of security which is demanded of the support system installed to maintain the stability of the excavation. Barton et al (1974) suggest the following values:

Excavation category		*ESR*
A	Temporary mine openings.	3-5
B	Permanent mine openings, water tunnels for hydro power (excluding high pressure penstocks), pilot tunnels, drifts and headings for large excavations.	1.6
C	Storage rooms, water treatment plants, minor road and railway tunnels, surge chambers, access tunnels.	1.3
D	Power stations, major road and railway tunnels, civil defence chambers, portal intersections.	1.0
E	Underground nuclear power stations, railway stations, sports and public facilities, factories.	0.8

Table 6: Classification of individual parameters used in the Tunnelling Quality Index *Q*

DESCRIPTION	VALUE	NOTES
1. ROCK QUALITY DESIGNATION	***RQD***	
A. Very poor	0 - 25	1. Where *RQD* is reported or measured as ≤ 10 (including 0),
B. Poor	25 - 50	a nominal value of 10 is used to evaluate *Q*.
C. Fair	50 - 75	
D. Good	75 - 90	2. *RQD* intervals of 5, i.e. 100, 95, 90 etc. are sufficiently
E. Excellent	90 - 100	accurate.
2. JOINT SET NUMBER	J_n	
A. Massive, no or few joints	0.5 - 1.0	
B. One joint set	2	
C. One joint set plus random	3	
D. Two joint sets	4	
E. Two joint sets plus random	6	
F. Three joint sets	9	1. For intersections use ($3.0 \times J_n$)
G. Three joint sets plus random	12	
H. Four or more joint sets, random,	15	2. For portals use ($2.0 \times J_n$)
heavily jointed, 'sugar cube', etc.		
J. Crushed rock, earthlike	20	
3. JOINT ROUGHNESS NUMBER	J_r	
a. Rock wall contact		
b. Rock wall contact before 10 cm shear		
A. Discontinuous joints	4	
B. Rough and irregular, undulating	3	
C. Smooth undulating	2	
D. Slickensided undulating	1.5	1. Add 1.0 if the mean spacing of the relevant joint set is
E. Rough or irregular, planar	1.5	greater than 3 m.
F. Smooth, planar	1.0	
G. Slickensided, planar	0.5	2. J_r = 0.5 can be used for planar, slickensided joints having
c. No rock wall contact when sheared		lineations, provided that the lineations are oriented for
H. Zones containing clay minerals thick	1.0	minimum strength.
enough to prevent rock wall contact	(nominal)	
J. Sandy, gravely or crushed zone thick	1.0	
enough to prevent rock wall contact	(nominal)	
4. JOINT ALTERATION NUMBER	J_a	ϕr degrees (approx.)
a. Rock wall contact		
A. Tightly healed, hard, non-softening,	0.75	1. Values of ϕr, the residual friction angle,
impermeable filling		are intended as an approximate guide
B. Unaltered joint walls, surface staining only	1.0	25 - 35 to the mineralogical properties of the
C. Slightly altered joint walls, non-softening	2.0	25 - 30 alteration products, if present.
mineral coatings, sandy particles, clay-free		
disintegrated rock, etc.		
D. Silty-, or sandy-clay coatings, small clay-	3.0	20 - 25
fraction (non-softening)		
E. Softening or low-friction clay mineral coatings,	4.0	8 - 16
i.e. kaolinite, mica. Also chlorite, talc, gypsum		
and graphite etc., and small quantities of swelling		
clays. (Discontinuous coatings, 1 - 2 mm or less)		

Table 6: (cont'd.) Classification of individual parameters used in the Tunnelling Quality Index *Q* (After Barton et al 1974).

4, JOINT ALTERATION NUMBER	J_a	ϕr degrees (approx.)	
b. Rock wall contact before 10 cm shear			
F. Sandy particles, clay-free, disintegrating rock etc.	4.0	25 - 30	
G. Strongly over-consolidated, non-softening clay mineral fillings (continuous < 5 mm thick)	6.0	16 - 24	
H. Medium or low over-consolidation, softening clay mineral fillings (continuous < 5 mm thick)	8.0	12 - 16	
J. Swelling clay fillings, i.e. montmorillonite, (continuous < 5 mm thick). Values of J_a depend on percent of swelling clay-size particles, and access to water.	8.0 - 12.0	6 - 12	
c. No rock wall contact when sheared			
K. Zones or bands of disintegrated or crushed	6.0		
L. rock and clay (see G, H and J for clay	8.0		
M. conditions)	8.0 - 12.0	6 - 24	
N. Zones or bands of silty- or sandy-clay, small clay fraction, non-softening	5.0		
O. Thick continuous zones or bands of clay	10.0 - 13.0		
P. & R. (see G.H and J for clay conditions)	6.0 - 24.0		
5. JOINT WATER REDUCTION	J_W	approx. water pressure (kgf/cm^2)	
A. Dry excavation or minor inflow i.e. < 5 l/m locally	1.0	< 1.0	
B. Medium inflow or pressure, occasional outwash of joint fillings	0.66	1.0 - 2.5	
C. Large inflow or high pressure in competent rock with unfilled joints	0.5	2.5 - 10.0	1. Factors C to F are crude estimates; increase J_W if drainage installed.
D. Large inflow or high pressure	0.33	2.5 - 10.0	
E. Exceptionally high inflow or pressure at blasting, decaying with time	0.2 - 0.1	> 10	2. Special problems caused by ice formation are not considered.
F. Exceptionally high inflow or pressure	0.1 - 0.05	> 10	
6. STRESS REDUCTION FACTOR		***SRF***	
a. Weakness zones intersecting excavation, which may cause loosening of rock mass when tunnel is excavated			
A. Multiple occurrences of weakness zones containing clay or chemically disintegrated rock, very loose surrounding rock any depth)		10.0	1. Reduce these values of *SRF* by 25 - 50% but only if the relevant shear zones influence do not intersect the excavation
B. Single weakness zones containing clay, or chemically disintegrated rock (excavation depth < 50 m)		5.0	
C. Single weakness zones containing clay, or chemically disintegrated rock (excavation depth > 50 m)		2.5	
D. Multiple shear zones in competent rock (clay free), loose surrounding rock (any depth)		7.5	
E. Single shear zone in competent rock (clay free). (depth of excavation < 50 m)		5.0	
F. Single shear zone in competent rock (clay free). (depth of excavation > 50 m)		2.5	
G. Loose open joints, heavily jointed or 'sugar cube', (any depth)		5.0	

Table 6: (cont'd.) Classification of individual parameters in the Tunnelling Quality Index *Q* (After Barton et al 1974).

DESCRIPTION	VALUE			NOTES
6. STRESS REDUCTION FACTOR			***SRF***	
b. Competent rock, rock stress problems				
	σ_c/σ_1	$\sigma_t\sigma_1$		2. For strongly anisotropic virgin stress field
H. Low stress, near surface	> 200	> 13	2.5	(if measured): when $5 \leq \sigma_1/\sigma_3 \leq 10$, reduce σ_c
J. Medium stress	200 - 10	13 - 0.66	1.0	to $0.8\sigma_c$ and σ_t to $0.8\sigma_t$. When σ_1/σ_3 > 10,
K. High stress, very tight structure	10 - 5	0.66 - 0.33	0.5 - 2	reduce σ_c and σ_t to $0.6\sigma_c$ and $0.6\sigma_t$, where
(usually favourable to stability, may				σ_c = unconfined compressive strength, and
be unfavourable to wall stability)				σ_t = tensile strength (point load) and σ_1 and
L. Mild rockburst (massive rock)	5 - 2.5	0.33 - 0.16	5 - 10	σ_3 are the major and minor principal stresses.
M. Heavy rockburst (massive rock)	< 2.5	< 0.16	10 - 20	3. Few case records available where depth of
c. Squeezing rock, plastic flow of incompetent rock				crown below surface is less than span width.
under influence of high rock pressure				Suggest *SRF* increase from 2.5 to 5 for such
N. Mild squeezing rock pressure			5 - 10	cases (see H).
O. Heavy squeezing rock pressure			10 - 20	
d. Swelling rock, chemical swelling activity depending on presence of water				
P. Mild swelling rock pressure			5 - 10	
R. Heavy swelling rock pressure			10 - 15	

ADDITIONAL NOTES ON THE USE OF THESE TABLES

When making estimates of the rock mass Quality (*Q*), the following guidelines should be followed in addition to the notes listed in the tables:

1. When borehole core is unavailable, *RQD* can be estimated from the number of joints per unit volume, in which the number of joints per metre for each joint set are added. A simple relationship can be used to convert this number to *RQD* for the case of clay free rock masses: $RQD = 115 - 3.3\ J_v$ (approx.), where J_v = total number of joints per m^3 ($0 < RQD < 100$ for $35 > J_v > 4.5$).
2. The parameter J_n representing the number of joint sets will often be affected by foliation, schistosity, slaty cleavage or bedding etc. If strongly developed, these parallel 'joints' should obviously be counted as a complete joint set. However, if there are few 'joints' visible, or if only occasional breaks in the core are due to these features, then it will be more appropriate to count them as 'random' joints when evaluating J_n.
3. The parameters J_r and J_a (representing shear strength) should be relevant to the weakest significant joint set or clay filled discontinuity in the given zone. However, if the joint set or discontinuity with the minimum value of J_r/J_a is favourably oriented for stability, then a second, less favourably oriented joint set or discontinuity may sometimes be more significant, and its higher value of J_r/J_a should be used when evaluating *Q*. The value of J_r/J_a should in fact relate to the surface most likely to allow failure to initiate.
4. When a rock mass contains clay, the factor *SRF* appropriate to loosening loads should be evaluated. In such cases the strength of the intact rock is of little interest. However, when jointing is minimal and clay is completely absent, the strength of the intact rock may become the weakest link, and the stability will then depend on the ratio rock-stress/rock-strength. A strongly anisotropic stress field is unfavourable for stability and is roughly accounted for as in note 2 in the table for stress reduction factor evaluation.
5. The compressive and tensile strengths (σ_c and σ_t) of the intact rock should be evaluated in the saturated condition if this is appropriate to the present and future in situ conditions. A very conservative estimate of the strength should be made for those rocks that deteriorate when exposed to moist or saturated conditions.

The crusher station discussed earlier falls into the category of permanent mine openings and is assigned an excavation support ratio *ESR* = 1.6. Hence, for an excavation span of 15 m, the equivalent dimension, *De* = 15/1.6 = 9.4.

The equivalent dimension, *De*, plotted against the value of *Q*, is used to define a number of support categories in a chart published in the original paper by Barton et al (1974). This chart has recently been updated by Grimstad and Barton (1993) to reflect the increasing use of steel fibre reinforced shotcrete in underground excavation support. Figure 3 is reproduced from this updated chart.

From Figure 3, a value of *De* of 9.4 and a value of *Q* of 4.5 places this crusher excavation in category (4) which requires a pattern of rockbolts (spaced at 2.3 m) and 40 to 50 mm of unreinforced shotcrete.

Because of the mild to heavy rock burst conditions which are anticipated, it may be prudent to de-stress the rock in the walls of this crusher chamber. This is achieved by using relatively heavy production blasting to excavate the chamber and omitting the smooth blasting usually used to trim the final walls of an excavation such as an underground powerhouse at shallower depth. Caution is recommended in the use of de-stress blasting and, for critical applications, it may be advisable to seek the advice of a blasting specialist before embarking on this course of action.

Løset (1992) suggests that, for rocks with $4 < Q < 30$, blasting damage will result in the creation of new 'joints' with a consequent local reduction in the value of *Q* for the rock surrounding the excavation. He suggests that this can be accounted for by reducing the *RQD* value for the blast damaged zone.

Assuming that the *RQD* value for the de-stressed rock around the crusher chamber drops to 50 %, the resulting value of *Q* = 2.9. From Figure 3, this value of *Q*, for an equivalent dimension, *De* of 9.4, places the excavation just inside category (5) which requires rockbolts, at approximately 2 m spacing, and a 50 mm thick layer of steel fibre reinforced shotcrete.

Barton et al (1980) provide additional information on rockbolt length, maximum unsupported spans and roof support pressures to supplement the support recommendations published in the original 1974 paper.

The length L of rockbolts can be estimated from the excavation width B and the Excavation Support Ratio ESR:

$$L = 2 + \frac{0.15B}{ESR} \tag{3}$$

The maximum unsupported span can be estimated from:

$$\textit{Maximum span (unsupported)} = 2\,ESR\,Q^{0.4} \tag{4}$$

Based upon analyses of case records, Grimstad and Barton (1993) suggest that the relationship between the value of Q and the permanent roof support pressure P_{roof} is estimated from:

$$P_{roof} = \frac{2\sqrt{Jn}\, Q^{-\frac{1}{3}}}{3Jr} \tag{5}$$

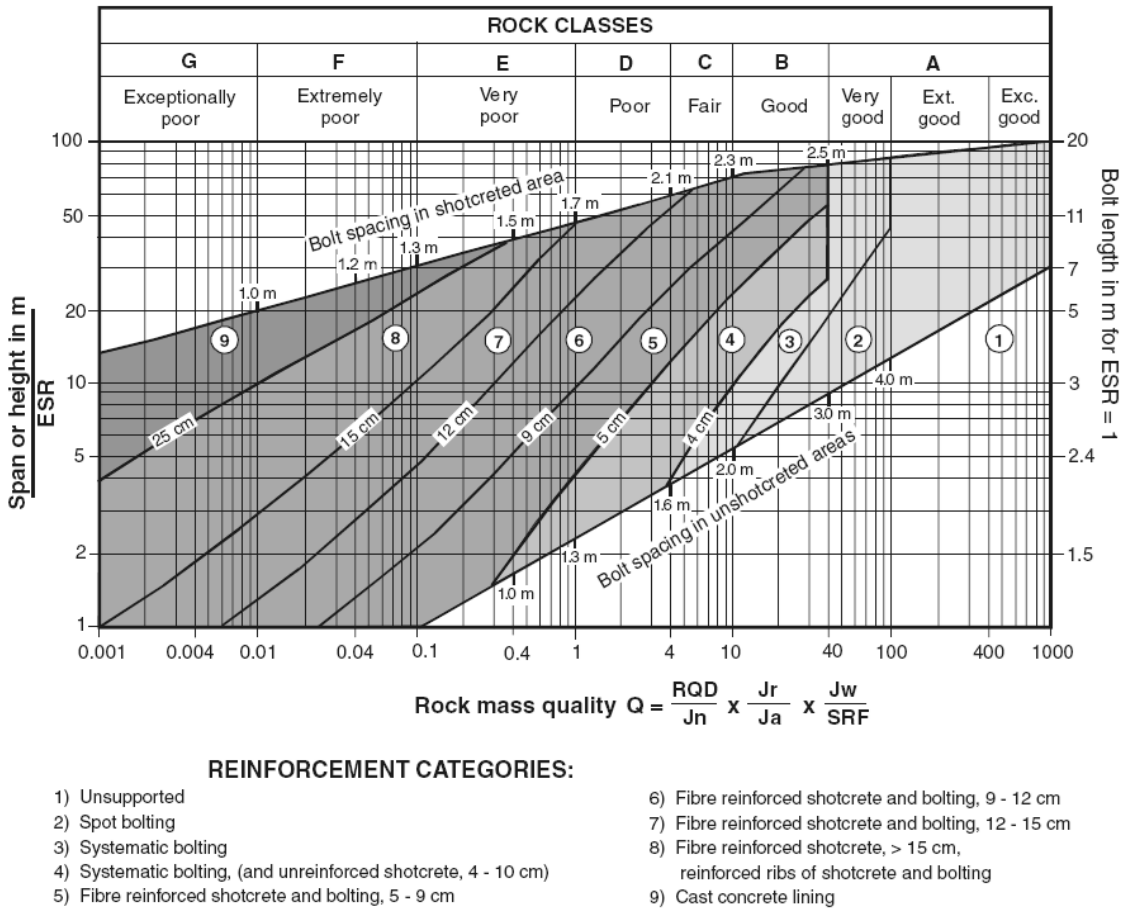

Figure 3: Estimated support categories based on the tunnelling quality index Q (After Grimstad and Barton, 1993, reproduced from Palmstrom and Broch, 2006).

Using rock mass classification systems

The two most widely used rock mass classifications are Bieniawski's *RMR* (1976, 1989) and Barton et al's *Q* (1974). Both methods incorporate geological, geometric and design/engineering parameters in arriving at a quantitative value of their rock mass quality. The similarities between *RMR* and *Q* stem from the use of identical, or very similar,

parameters in calculating the final rock mass quality rating. The differences between the systems lie in the different weightings given to similar parameters and in the use of distinct parameters in one or the other scheme.

RMR uses compressive strength directly while *Q* only considers strength as it relates to in situ stress in competent rock. Both schemes deal with the geology and geometry of the rock mass, but in slightly different ways. Both consider groundwater, and both include some component of rock material strength. Some estimate of orientation can be incorporated into *Q* using a guideline presented by Barton et al (1974): …'the parameters *Jr* and *Ja* should ... relate to the surface most likely to allow failure to initiate.' The greatest difference between the two systems is the lack of a stress parameter in the *RMR* system.

When using either of these methods, two approaches can be taken. One is to evaluate the rock mass specifically for the parameters included in the classification methods; the other is to accurately characterise the rock mass and then attribute parameter ratings at a later time. The latter method is recommended since it gives a full and complete description of the rock mass which can easily be translated into either classification index. If rating values alone had been recorded during mapping, it would be almost impossible to carry out verification studies.

In many cases, it is appropriate to give a range of values to each parameter in a rock mass classification and to evaluate the significance of the final result. An example of this approach is given in Figure 4 which is reproduced from field notes prepared by Dr. N. Barton on a project. In this particular case, the rock mass is dry and is subjected to 'medium' stress conditions (Table 6.6.K) and hence $Jw = 1.0$ and SRF = 1.0. Histograms showing the variations in *RQD*, *Jn*, *Jr* and *Ja*, along the exploration adit mapped, are presented in this figure. The average value of $Q = 8.9$ and the approximate range of Q is $1.7 < Q < 20$. The average value of *Q* can be used in choosing a basic support system while the range gives an indication of the possible adjustments which will be required to meet different conditions encountered during construction.

A further example of this approach is given in a paper by Barton et al (1992) concerned with the design of a 62 m span underground sports hall in jointed gneiss. Histograms of all the input parameters for the *Q* system are presented and analysed in order to determine the weighted average value of *Q*.

Carter (1992) has adopted a similar approach, but extended his analysis to include the derivation of a probability distribution function and the calculation of a probability of failure in a discussion on the stability of surface crown pillars in abandoned metal mines.

Throughout this chapter it has been suggested that the user of a rock mass classification scheme should check that the latest version is being used. It is also worth repeating that the use of two rock mass classification schemes side by side is advisable.

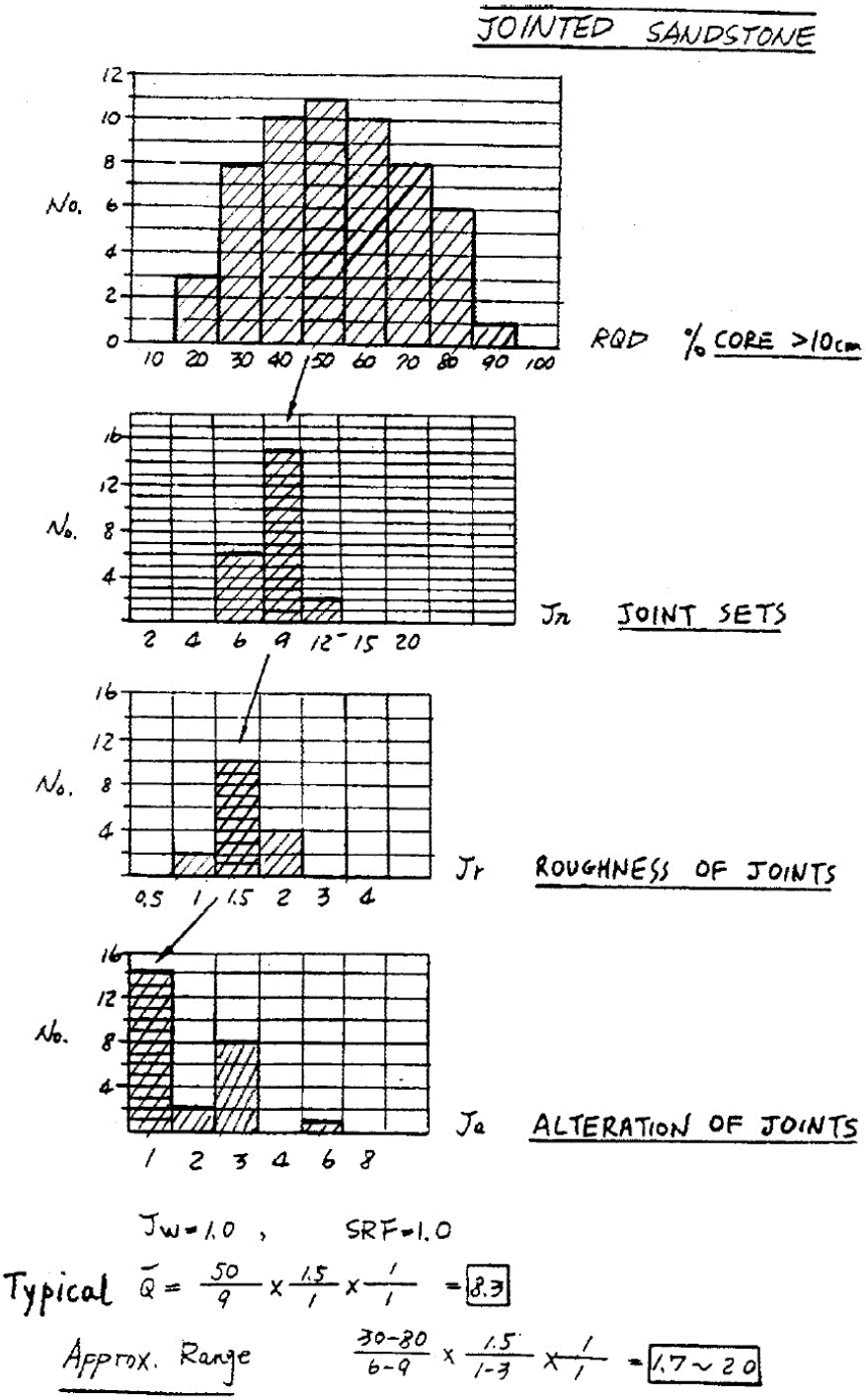

Figure 4: Histograms showing variations in *RQD*, *Jn*, *Jr* and *Ja* for a dry jointed sandstone under 'medium' stress conditions, reproduced from field notes prepared by Dr. N. Barton.

References

Barton, N., By, T.L., Chryssanthakis, L., Tunbridge, L., Kristiansen, J., Løset, F., Bhasin, R.K., Westerdahl, H. and Vik, G. 1992. Comparison of prediction and performance for a 62 m span sports hall in jointed gneiss. *Proc. 4th. int. rock mechanics and rock engineering conf.*, Torino. Paper 17.

Barton, N., Løset, F., Lien, R. and Lunde, J. 1980. Application of the Q-system in design decisions. In *Subsurface space,* (ed. M. Bergman) **2,** 553-561. New York: Pergamon.

Barton, N.R., Lien, R. and Lunde, J. 1974. Engineering classification of rock masses for the design of tunnel support. *Rock Mech.* **6**(4), 189-239.

Bieniawski, Z.T. 1973. Engineering classification of jointed rock masses. *Trans S. Afr. Inst. Civ. Engrs* **15**, 335-344.

Bieniawski, Z.T. 1976. Rock mass classification in rock engineering. In *Exploration for rock engineering, proc. of the symp*., (ed. Z.T. Bieniawski) **1**, 97-106. Cape Town: Balkema.

Bieniawski, Z.T. 1989. *Engineering rock mass classifications.* New York: Wiley.

Carter, T.G. 1992. A new approach to surface crown pillar design. *Proc. 16th. Canadian Rock Mechanics Symposium, Sudbury*, 75-83.

Carter, T.G. 1992. Prediction and uncertainties in geological engineering and rock mass characterization assessments. *Proc. 4th. int. rock mechanics and rock engineering conf.*, Torino. Paper 1.

Cording, E.J. and Deere, D.U. 1972. Rock tunnel supports and field measurements. *Proc. North American rapid excav. tunneling conf.*, Chicago, (eds. K.S. Lane and L.A. Garfield) **1**, 601-622. New York: Soc. Min. Engrs, Am. Inst. Min. Metall. Petrolm Engrs.

Cummings, R.A., Kendorski, F.S. and Bieniawski, Z.T. 1982. *Caving rock mass classification and support estimation*. U.S. Bureau of Mines Contract Report #J0100103. Chicago: Engineers International Inc.

Deere, D.U. 1989. *Rock quality designation (RQD) after 20 years*. U.S. Army Corps Engrs Contract Report GL-89-1. Vicksburg, MS: Waterways Experimental Station.

Deere, D.U. and Deere, D.W. 1988. The rock quality designation (RQD) index in practice. In *Rock classification systems for engineering purposes*, (ed. L. Kirkaldie), ASTM Special Publication 984, 91-101. Philadelphia: Am. Soc. Test. Mat.

Deere, D.U., Hendron, A.J., Patton, F.D. and Cording, E.J. 1967. Design of surface and near surface construction in rock. In *Failure and breakage of rock, proc. 8th U.S. symp. rock mech*., (ed. C. Fairhurst), 237-302. New York: Soc. Min. Engrs, Am. Inst. Min. Metall. Petrolm Engrs.

Grimstad, E. and Barton, N. 1993. Updating the Q-System for NMT. *Proc. int. symp. on sprayed concrete - modern use of wet mix sprayed concrete for underground support*, Fagernes. 46-66. Oslo: Norwegian Concrete Assn.

Kendorski, F., Cummings, R., Bieniawski, Z.T. and Skinner, E. 1983. Rock mass classification for block caving mine drift support. *Proc. 5th congr. Int. Soc. Rock Mech.*, Melbourne, B51-B63. Rotterdam: Balkema.

Laubscher, D.H. 1977. Geomechanics classification of jointed rock masses - mining applications. *Trans. Instn Min. Metall.* **86**, A1-8.

Laubscher, D.H. 1984. Design aspects and effectiveness of support systems in different mining conditions. *Trans Instn Min. Metall.* **93**, A70 - A82.

Laubscher, D.H. and Taylor, H.W. 1976. The importance of geomechanics classification of jointed rock masses in mining operations. In *Exploration for rock engineering*, (ed. Z.T. Bieniawski) **1**, 119-128. Cape Town: Balkema.

Laubscher, D.M. and Page, C.H. 1990. The design of rock support in high stress or weak rock environments. *Proc. 92nd Can. Inst. Min. Metall. AGM*, Ottawa, Paper # 91.

Lauffer, H. 1958. Gebirgsklassifizierung für den Stollenbau. *Geol. Bauwesen* **24**(1), 46-51.

Løset, F. 1992. Support needs compared at the Svartisen Road Tunnel. *Tunnels and Tunnelling*, June.

Merritt, A.H. 1972. Geologic prediction for underground excavations. *Proc. North American. rapid excav. tunneling conf.*, Chicago, (eds K.S. Lane and L.A. Garfield) **1,** 115-132. New York: Soc. Min. Engrs, Am. Inst. Min. Metall. Petrolm Engrs.

Pacher, F., Rabcewicz, L. and Golser, J. 1974. Zum der seitigen Stand der Gebirgsklassifizierung in Stollen-und Tunnelbau. *Proc. XXII Geomech. colloq.*, Salzburg, 51-58.

Palmström, A. 1982. The volumetric joint count - a useful and simple measure of the degree of rock jointing. *Proc. 4th congr. Int. Assn Engng Geol.*, Delhi **5**, 221-228.

Palmstrom, A. and Broch, E. 2006. Use and misuse of rock mass classification systems with particular reference to the Q-system. *Tunnels and Underground Space Technology*, **21**, 575-593.

Ritter, W. 1879. *Die Statik der Tunnelgewölbe.* Berlin: Springer.

Terzaghi, K. 1946. Rock defects and loads on tunnel supports. In *Rock tunneling with steel supports*, (eds. R. V. Proctor and T. L. White) **1**, 17-99. Youngstown, OH: Commercial Shearing and Stamping Company.

Wickham, G.E., Tiedemann, H.R. and Skinner, E.H. 1972. Support determination based on geologic predictions. In *Proc. North American rapid excav. tunneling conf.*, Chicago, (eds K.S. Lane and L.A. Garfield), 43-64. New York: Soc. Min. Engrs, Am. Inst. Min. Metall. Petrolm Engrs.

13. Tunnels in weak rock

Introduction

Tunnelling in weak rock presents some special challenges to the geotechnical engineer since misjudgements in the design of support systems can lead to very costly failures. To understand the issues involved in the process of designing support for this type of tunnel it is necessary to examine some very basic concepts of how a rock mass surrounding a tunnel deforms and how the support systems act to control this deformation. Once these basic concepts have been explored, examples of practical support designs for different conditions will be considered.

Deformation around an advancing tunnel

Figure 1 shows the results of a three-dimensional finite element analysis of the deformation of the rock mass surrounding a circular tunnel advancing through a weak rock mass subjected to equal stresses in all directions. The plot shows displacement vectors in the rock mass as well as the shape of the deformed tunnel profile. Figure 2 gives a graphical summary of the most important features of this analysis.

Deformation of the rock mass starts about one-half a tunnel diameter ahead of the advancing face and reaches its maximum value about one- and one-half diameters behind the face. At the face position about one-third of the total radial closure of the tunnel has already occurred and the tunnel face deforms inwards as illustrated in Figures 1 and 2. Whether or not these deformations induce stability problems in the tunnel depends upon the ratio of rock mass strength to the in-situ stress level, as will be demonstrated in the following pages.

Note that it is assumed that the deformation process described occurs immediately upon excavation of the face. This is a reasonable approximation for most tunnels in rock. The effects of time dependent deformations upon the performance of the tunnel and the design of the support system will be not be discussed in this chapter.

Tunnel deformation analysis

In order to explore the concepts of rock support interaction in a form which can readily be understood, a very simple analytical model will be utilised. This model involves a circular tunnel subjected to a hydrostatic stress field in which the horizontal and vertical stresses are equal.

For the sake of simplicity this analysis is based on the Mohr-Coulomb failure criterion which gives a very simple solution for the progressive failure of the rock mass surrounding the tunnel.

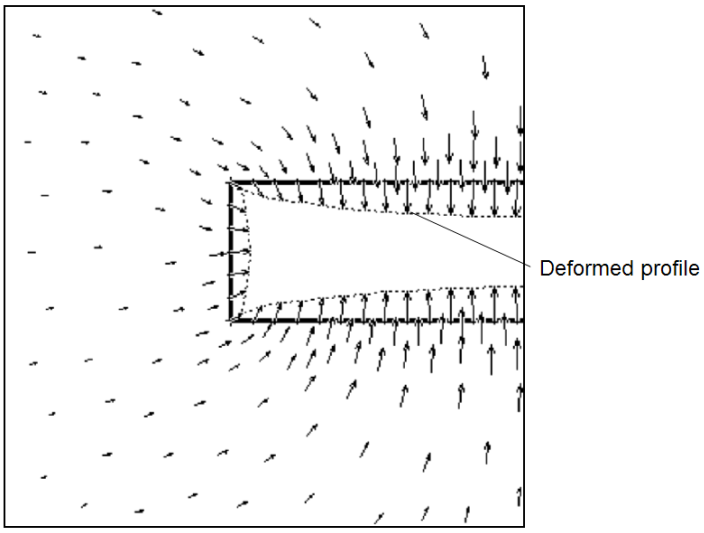

Figure 1: Vertical section through a three-dimensional finite element model of the failure and deformation of the rock mass surrounding the face of an advancing circular tunnel. The plot shows displacement vectors as well as the shape of the deformed tunnel profile.

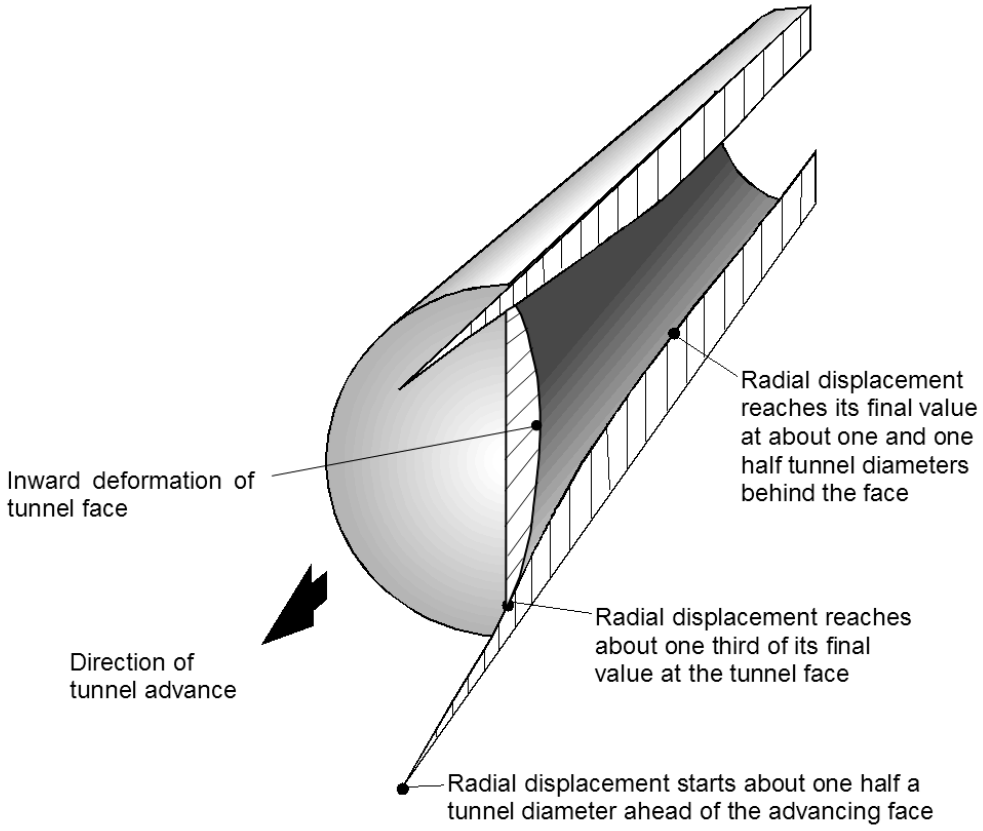

Figure 2: Pattern of deformation in the rock mass surrounding an advancing tunnel.

In this analysis it is assumed that the surrounding heavily jointed rock mass behaves as an elastic-perfectly plastic material in which failure involving slip along intersecting discontinuities is assumed to occur with zero plastic volume change (Duncan Fama, 1993). Support is modelled as an equivalent internal pressure and, although this is an idealised model, it provides useful insights on how support operates.

Definition of failure criterion

It is assumed that the onset of plastic failure, for different values of the effective confining stress $\sigma_3^{'}$, is defined by the Mohr-Coulomb criterion and expressed as:

$$\sigma_1^{'} = \sigma_{cm} + k\sigma_3^{'} \tag{1}$$

The uniaxial compressive strength of the rock mass σ_{cm} is defined by:

$$\sigma_{cm} = \frac{2c^{'}\cos\phi^{'}}{(1-\sin\phi^{'})} \tag{2}$$

and the slope k of the $\sigma_1^{'}$ versus $\sigma_3^{'}$ line as:

$$k = \frac{(1+\sin\phi^{'})}{(1-\sin\phi^{'})} \tag{3}$$

where $\sigma_1^{'}$ is the axial stress at which failure occurs

$\sigma_3^{'}$ is the confining stress

$c^{'}$ is the cohesive strength and

$\phi^{'}$ is the angle of friction of the rock mass

Analysis of tunnel behaviour

Assume that a circular tunnel of radius r_o is subjected to hydrostatic stresses p_o and a uniform internal support pressure p_i as illustrated in Figure 3. Failure of the rock mass surrounding the tunnel occurs when the internal pressure provided by the tunnel lining is less than a critical support pressure p_{cr}, which is defined by:

$$p_{cr} = \frac{2p_o - \sigma_{cm}}{1+k} \tag{4}$$

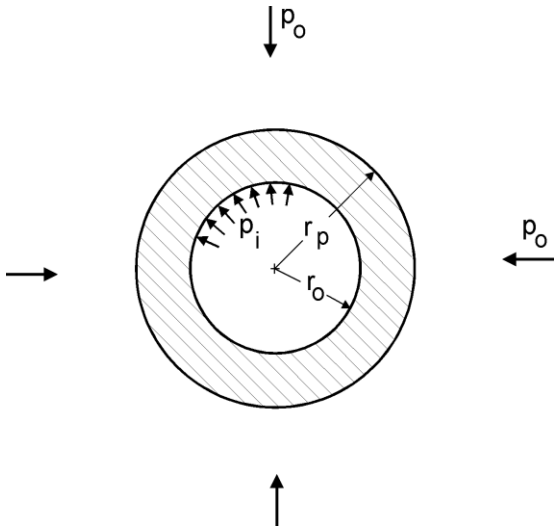

Figure 3: Plastic zone surrounding a circular tunnel.

If the internal support pressure p_i is greater than the critical support pressure p_{cr}, no failure occurs, the behaviour of the rock mass surrounding the tunnel is elastic and the inward radial elastic displacement of the tunnel wall is given by:

$$u_{ie} = \frac{r_o(1+\nu)}{E_m}(p_o - p_i) \tag{5}$$

where E_m is the Young's modulus or deformation modulus and
ν is the Poisson's ratio.

When the internal support pressure p_i is less than the critical support pressure p_{cr}, failure occurs and the radius r_p of the plastic zone around the tunnel is given by:

$$r_p = r_o\left[\frac{2(p_o(k-1)+\sigma_{cm})}{(1+k)((k-1)p_i+\sigma_{cm})}\right]^{\frac{1}{(k-1)}} \tag{6}$$

For plastic failure, the total inward radial displacement of the walls of the tunnel is:

$$u_{ip} = \frac{r_o(1+\nu)}{E}\left[2(1-\nu)(p_o - p_{cr})\left(\frac{r_p}{r_o}\right)^2 - (1-2\nu)(p_o - p_i)\right] \tag{7}$$

A spreadsheet for the determination of the strength and deformation characteristics of the rock mass and the behaviour of the rock mass surrounding the tunnel is given in Figure 4.

Input:

sigci =	10	MPa	mi =	10		GSI =	25	
mu =	0.30		ro =	3.0	m	po =	2.0	Mpa
pi =	0.0	MPa	pi/po =	0.00				

Output:

mb =	0.69		s =	0.0000		a =	0.525	
k =	2.44		phi =	24.72	degrees	coh =	0.22	MPa
sigcm =	0.69	MPa	E =	749.9	MPa	pcr =	0.96	MPa
rp =	6.43	m	ui =	0.0306	m	ui=	30.5957	mm

sigcm/po	0.3468	rp/ro = 2.14	ui/ro = 0.0102

Calculation:

									Sums
sig3	1E-10	0.36	0.71	1.1	1.43	1.79	2.14	2.50	10.00
sig1	0.00	1.78	2.77	3.61	4.38	5.11	5.80	6.46	29.92
sig3sig1	0.00	0.64	1.98	3.87	6.26	9.12	12.43	16.16	50
sig3sq	0.00	0.13	0.51	1.15	2.04	3.19	4.59	6.25	18

Cell formulae:

```
   mb = mi*EXP((GSI-100)/28)
    s = IF(GSI>25,EXP((GSI-100)/9),0)
    a = IF(GSI>25,0.5,0.65-GSI/200)
 sig3 = Start at 1E-10 (to avoid zero errors) and increment in 7 steps of  sigci/28 to 0.25*sigci
 sig1 = sig3+sigci*(((mb*sig3)/sigci)+s)^a
    k = (sumsig3sig1 - (sumsig3*sumsig1)/8)/(sumsig3sq-(sumsig3^2)/8)
  phi = ASIN((k-1)/(k+1))*180/PI()
  coh = (sigcm*(1-SIN(phi*PI()/180)))/(2*COS(phi*PI()/180))
sigcm = sumsig1/8 - k*sumsig3/8
    E = IF(sigci>100,1000*10^((GSI-10)/40),SQRT(sigci/100)*1000*10^((GSI-10)/40))
  pcr = (2*po-sigcm)/(k+1)
   rp = IF(pi<pcr,ro*(2*(po*(k-1)+sigcm)/((1+k)*((k-1)*pi+sigcm)))^(1/(k-1)),ro)
   ui = IF(rp>ro,ro*((1+mu)/E)*(2*(1-mu)*(po-pcr)*((rp/ro)^2)-(1-2*mu)*(po-pi)),ro*(1+mu)*(po-pi)/E)
```

Figure 4: Spreadsheet for the calculation of rock mass characteristics and the behaviour of the rock mass surrounding a circular tunnel in a hydrostatic stress field.

A more elaborate analysis of the same problem, using the Hoek-Brown failure criterion, has been published by Carranza-Torres and Fairhurst (1999) and Carranza-Torres (2004). The details of these analyses are beyond the scope of this discussion but the results have been incorporated into a program called RocSupport[1] and are used in the following discussion.

Dimensionless plots of tunnel deformation

A useful means of studying general behavioural trends is to create dimensionless plots from the results of parametric studies. One such dimensionless plot is presented in Figure 5. This plot was constructed from the results of a Monte Carlo analysis in which the input parameters for rock mass strength and tunnel deformation were varied at random in 2000 iterations. It is remarkable that, in spite of the very wide range of conditions included in these analyses, the results follow a very similar trend and that it is possible to fit curves which give a very good indication of the average trend.

[1] Available from www.rocscience.com

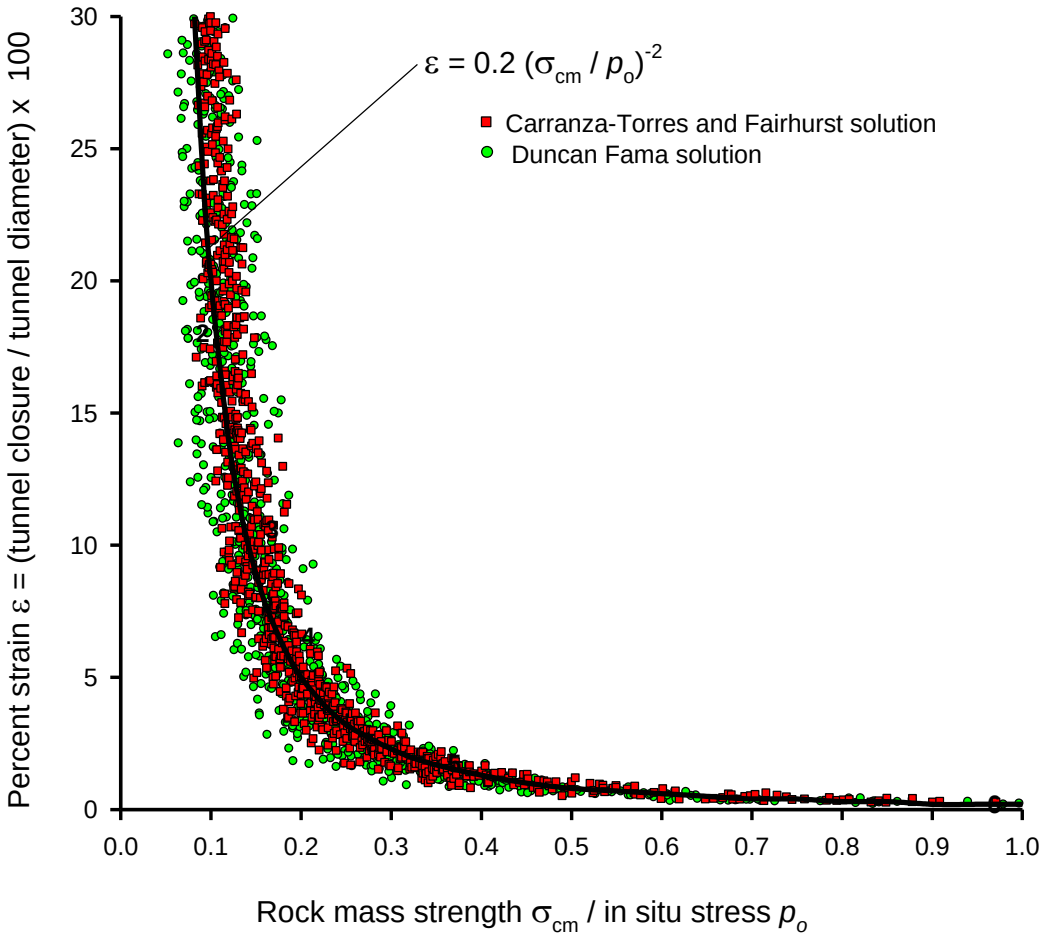

Figure 5: Tunnel deformation versus ratio of rock mass strength to in situ stress based on a Monte-Carlo analysis which included a wide range of input parameters [2].

Figure 5 is a plot of the ratio of tunnel wall displacement to tunnel radius against the ratio of rock mass strength to in-situ stress. Once the rock mass strength falls below 20% of the in-situ stress level, deformations increase substantially and, unless these deformations are controlled, collapse of the tunnel is likely to occur.

Based on field observations and measurements, Sakurai (1983) suggested that tunnel strain levels in excess of approximately 1% are associated with the onset of tunnel instability and with difficulties in providing adequate support. Field observations by Chern et al (1998), plotted in Figure 6, confirm Sakurai's proposal.

[2] Using the program @RISK in conjunction with a Microsoft Excel spreadsheet for estimating rock mass strength and tunnel behaviour (equations 4 to 7). Uniform distributions were sampled for the following input parameters, the two figures in brackets define the minimum and maximum values used: Intact rock strength σ_{ci} (1,30 MPa), Hoek-Brown constant m_i (5,12), Geological Strength Index GSI (10,35), In situ stress (2, 20 MPa), Tunnel radius (2, 8 m).

Note that some tunnels which suffered strains as high as 5% did not exhibit stability problems. All the tunnels marked as having stability problems were successfully completed but the construction problems increased significantly with increasing strain levels. Hence, the 1% limit proposed by Sakurai is only an indication of increasing difficulty and it should not be assumed that sufficient support should be installed to limit the tunnel strain to 1%. In fact, in some cases, it is desirable to allow the tunnel to undergo strains of as much as 5% before activating the support.

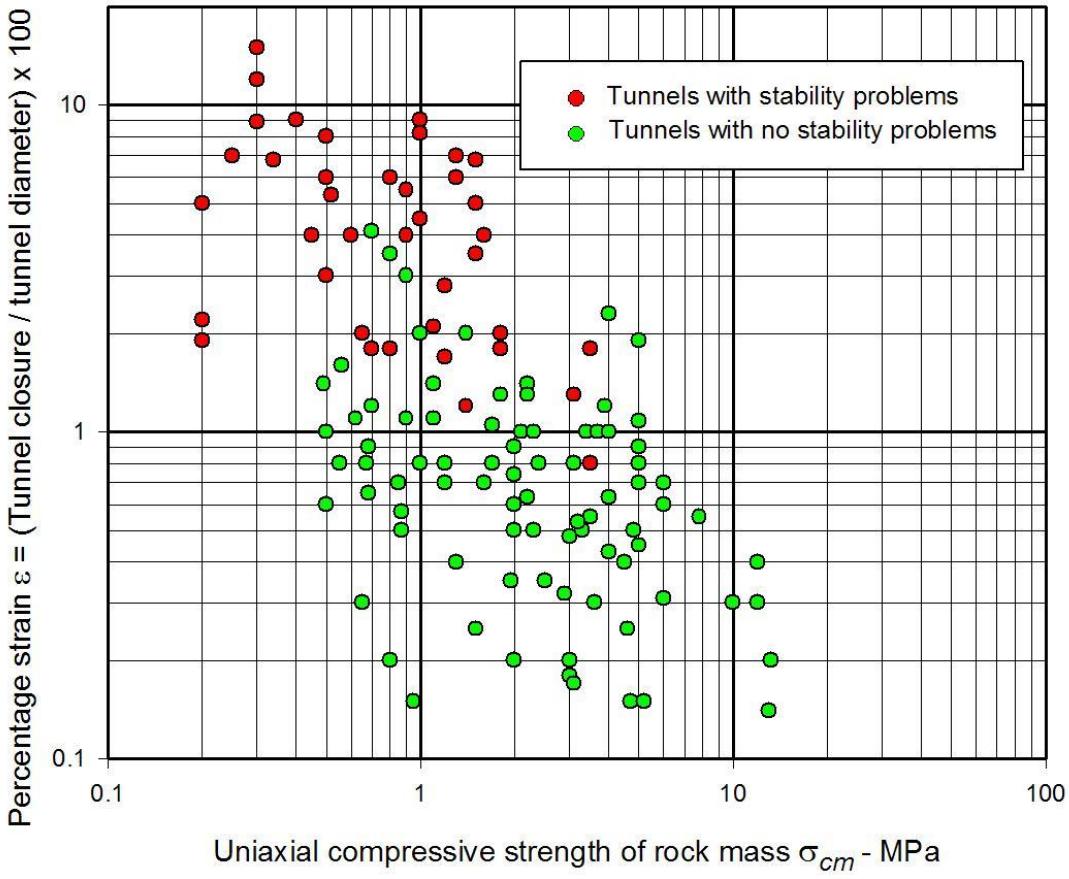

Figure 6: Field observations by Chern et al (1998) from the Second Freeway, Pinglin and New Tienlun headrace tunnels in Taiwan.

Figures 5 is for the condition of zero support pressure ($p_i = 0$). Similar analyses were run for a range of support pressures versus in situ stress ratios (p_i/p_o) and a statistical curve fitting process was used to determine the best fit curves for the generated data for each p_i/p_o value. The resulting curve for tunnel displacement for different support pressures is given in Figure 7.

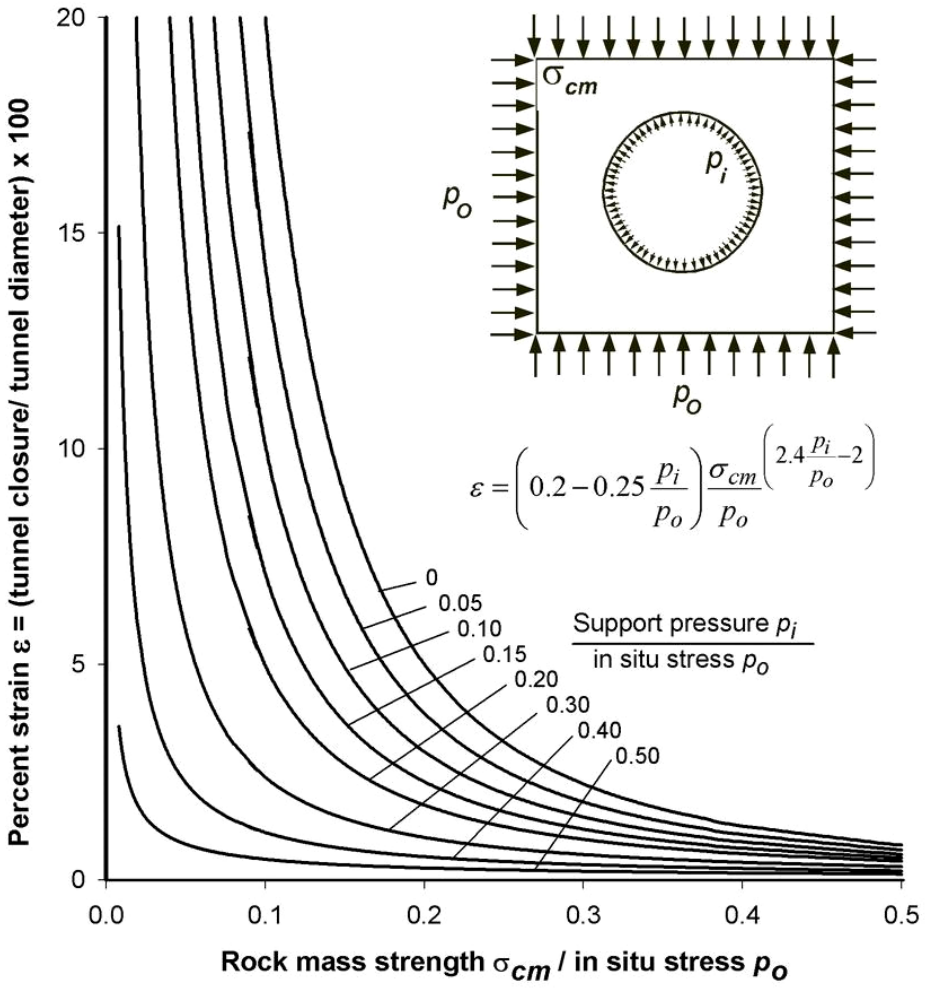

Figure 7: Ratio of tunnel deformation to tunnel radius versus the ratio of rock mass strength to in situ stress for different support pressures.

The series of curves shown in Figures 7 are defined by the equation:

$$\varepsilon\% = \frac{ui}{ro} \times 100 = \left(0.2 - 0.25\frac{p_i}{p_o}\right)\frac{\sigma_{cm}}{p_o}\left(2.4\frac{p_i}{p_o} - 2\right) \qquad (8)$$

where rp = Plastic zone radius
u_i = Tunnel sidewall deformation
r_o = Original tunnel radius in metres
pi = Internal support pressure
p_o = In situ stress = depth below surface × unit weight of rock mass
σ_{cm}= Rock mass strength = $2c' \cos\phi' / (1 - \sin\phi')$

A similar analysis was carried out to determine the size of the plastic zone surrounding the tunnel which is defined by:

$$\frac{rp}{ro} = \left(1.25 - 0.625\frac{p_i}{p_o}\right)\frac{\sigma_{cm}}{p_o}^{\left(\frac{p_i}{p_o} - 0.57\right)} \tag{9}$$

Estimates of support capacity

Hoek and Brown (1980a) and Brady and Brown (1985) have published equations which can be used to calculate the capacity of mechanically anchored rockbolts, shotcrete or concrete linings, or steel sets for a circular tunnel. No useful purpose would be served by reproducing these equations here, but they have been used to estimate the values plotted in Figure 8 (from Hoek, 1998).

Figure 8 shows maximum support pressures and maximum elastic displacements, p_{sm} and u_{sm}, for different support systems installed in circular tunnels of different diameters. Note that, in all cases, the support is assumed to act over the entire surface of the tunnel walls. In other words, the shotcrete and concrete linings are closed rings, the steel sets are complete circles and the mechanically anchored rockbolts are installed in a regular pattern that completely surrounds the tunnel.

Because this model assumes perfect symmetry under hydrostatic loading of circular tunnels, no bending moments are induced in the support. In reality, there will always be some asymmetric loading, particularly for steel sets and shotcrete placed on rough rock surfaces. Hence, induced bending will result in support capacities that are lower than those given in Figure 8. Furthermore, the effect of not closing the support ring, as is frequently the case, leads to a drastic reduction in the capacity and stiffness of steel sets and concrete or shotcrete linings.

Practical example

In order to illustrate the application of the concepts presented in this chapter, the following practical example is considered.

A 4 m span drainage tunnel is to be driven in the rock mass behind the slope of an open pit mine. The tunnel is at a depth of approximately 150 m below surface and the general rock is a granodiorite of fair quality. A zone of heavily altered porphyry associated with a fault has to be crossed by the tunnel and the properties of this zone, which has been exposed in the open pit, are known to be very poor. Mine management has requested an initial estimate of the behaviour of the tunnel and of the probable support requirements. The following example presents one approach to this problem, using some of the techniques described earlier in this chapter and then expanding them to allow a more realistic analysis of tunnel support behaviour.

Support type	Flange width - mm	Section depth - mm	Weight – kg/m	Curve number	Maximum support pressure p_{imax} (MPa) for a tunnel of diameter D (metres) and a set spacing of s (metres)
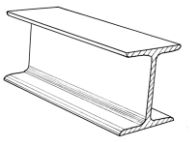 Wide flange rib	305	305	97	1	$p_{i\max} = 19.9D^{-1.23}/s$
	203	203	67	2	$p_{i\max} = 13.2D^{-1.3}/s$
	150	150	32	3	$p_{i\max} = 7.0D^{-1.4}/s$
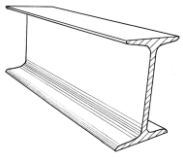 I section rib	203	254	82	4	$p_{i\max} = 17.6D^{-1.29}/s$
	152	203	52	5	$p_{i\max} = 11.1D^{-1.33}/s$
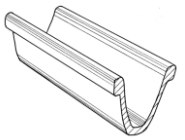 TH section rib	171	138	38	6	$p_{i\max} = 15.5D^{-1.24}/s$
	124	108	21	7	$p_{i\max} = 8.8D^{-1.27}/s$
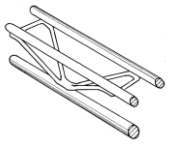 3 bar lattice girder	220	190	19	8	$p_{i\max} = 8.6D^{-1.03}/s$
	140	130	18		
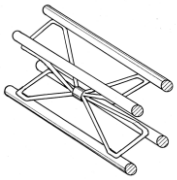 4 bar lattice girder	220	280	29	9	$p_{i\max} = 18.3D^{-1.02}/s$
	140	200	26		
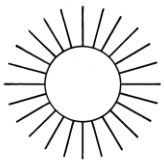 Rockbolts or cables spaced on a grid of s x s metres	34 mm rockbolt			10	$p_{i\max} = 0.354/s^2$
	25 mm rockbolt			11	$p_{i\max} = 0.267/s^2$
	19 mm rockbolt			12	$p_{i\max} = 0.184/s^2$
	17 mm rockbolt			13	$p_{i\max} = 0.10/s^2$
	SS39 Split set			14	$p_{i\max} = 0.05/s^2$
	EXX Swellex			15	$p_{i\max} = 0.11/s^2$
	20mm rebar			16	$p_{i\max} = 0.17/s^2$
	22mm fibreglass			17	$p_{i\max} = 0.26/s^2$
	Plain cable			18	$p_{i\max} = 0.15/s^2$
	Birdcage cable			19	$p_{i\max} = 0.30/s^2$

Support type	Thickness - mm	Age - days	UCS - MPa	Curve number	Maximum support pressure p_{imax} (MPa) for a tunnel of diameter D (metres)
 Concrete or shotcrete lining	1m	28	35	20	$p_{i\max} = 57.8D^{-0.92}$
	300	28	35	21	$p_{i\max} = 19.1D^{-0.92}$
	150	28	35	22	$p_{i\max} = 10.6D^{-0.97}$
	100	28	35	23	$p_{i\max} = 7.3D^{-0.98}$
	50	28	35	24	$p_{i\max} = 3.8D^{-0.99}$
	50	3	11	25	$p_{i\max} = 1.1D^{-0.97}$
	50	0.5	6	26	$p_{i\max} = 0.6D^{-1.0}$

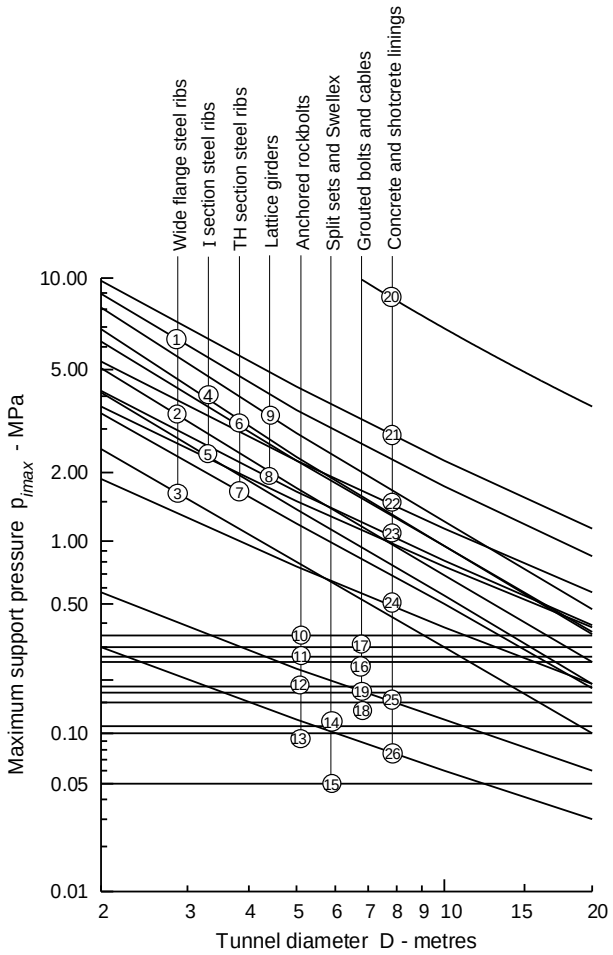

Figure 8: Approximate maximum capacities for different support systems installed in circular tunnels. Note that steel sets and rockbolts are all spaced at 1 m.

Estimate of rock mass properties

Figures 5 and 7 show that a crude estimate of the behaviour of the tunnel can be made if the ratio of rock mass strength to in situ stress is available. For the purpose of this analysis the in-situ stress is estimated from the depth below surface and the unit weight of the rock. For a depth of 150 m and a unit weight of 0.027 MN/m^3, the vertical in situ stress is approximately 4 MPa. The fault material is considered incapable of sustaining high differential stress levels and it is assumed that the horizontal and vertical stresses are equal within the fault zone.

In the case of the granodiorite, the laboratory uniaxial compressive strength is approximately 100 MPa. However, for the fault material, specimens can easily be broken by hand as shown in Figure 11. The laboratory uniaxial compressive strength of this material is estimated at approximately 10 MPa.

Based upon observations in the open pit mine slopes and utilizing the procedures described in the chapter on 'Rock mass properties', the granodiorite is estimated to have a GSI value of approximately 55. The fault zone, shown in Figure 9, has been assigned GSI = 15.

Figure 9: Heavily altered porphyry can easily be broken by hand.

The program RocLab[3] implements the methodology described in the chapter on 'Rock mass properties' and, in particular, the equations given in the 2002 version of the Hoek-Brown failure criterion (Hoek et al, 2002). This program has been used to calculate the global rock mass strength σ_{cm} for the granodiorite and the fault zone. The results are presented below:

Material	σ_{ci} - MPa	GSI	m_i	σ_{cm}	σ_{cm}/po
Granodiotite	100	55	30	33	8.25
Fault	10	15	8	0.6	0.15

Support requirements

Figures 5 and 6 show that, for the granodiorite with a ratio of rock mass strength to in situ stress of 8.25, the size of the plastic zone and the induced deformations will be negligible. This conclusion is confirmed by the appearance of an old drainage tunnel that has stood for several decades without any form of support. Based upon this evaluation, it was decided that no permanent support was required for the tunnel in the fair quality granodiorite. Spot bolts and shotcrete were installed for safety where the rock mass was more heavily jointed. The final appearance of the tunnel in granodiorite is shown in Figure 10.

Figure 10: Appearance of the drainage tunnel in fair quality granodiorite in which no permanent support was required. Spot bolts and shotcrete were installed for safety in jointed areas. The concrete lined drainage channel is shown in the centre of the tunnel floor.

[3] This program can be downloaded (free) from www.rocscience.com.

In the case of the altered porphyry and fault material, the ratio of rock mass strength to in situ stress is 0.15. From Equation 9 the radius of plastic zone for a 2 m radius tunnel in this material is approximately 7.4 m without support. The tunnel wall deformation is approximately 0.18 m which translates into a tunnel strain of (0.18/2) *100 = 9%.

Based on the observations by Sakurai (1983) and Chern et al (1998), the predicted strain of 9% for the mine drainage tunnel discussed earlier is clearly unacceptable and substantial support is required in order to prevent convergence and possible collapse of this section. Since this is a drainage tunnel, the final size is not a major issue and a significant amount of closure can be tolerated.

An approach that is frequently attempted, in such cases, is to install sufficient support behind the face of the tunnel to limit the strain to an acceptable level. Assuming a practical limit of 2% strain (from Figure 6), equation 8 and Figure 7 show that, for $\sigma_{cm}/p_o = 0.15$, an internal support pressure of approximately $p_i/p_o = 0.25$ is required to support the tunnel. For $p_o = 4$ MPa this means a support pressure $p_i = 1$ MPa.

Figure 8 shows that, for a 4 m diameter tunnel, a support in excess of 1 MPa can only be provided by a passive system of steel, sets, lattice girders, shotcrete or concrete lining or by some combination of these systems. These systems have to be installed in a fully closed ring (generally in a circular tunnel) in order to act as a load bearing structure. Rockbolts or cables, even assuming that they could be anchored in the fault material, cannot provide this level of equivalent support.

There are several problems associated with the installation of heavy passive support in this particular tunnel. These are:

1. The remainder of the drainage tunnel is horseshoe shaped as shown in Figure 10. Changing the section to circular for a relative short section of fault zone is not a very attractive proposition because of the limitations this would impose on transportation of equipment and materials through the zone.
2. The use of heavy steel sets creates practical problems in terms of bending the sets into the appropriate shape. A practical rule of thumb is that an H or I section can only be bent to a radius of approximately 14 times the depth of the section. Figure 11 which shows a heavy H section set being bent and there is significant buckling of the inside flange of the set.
3. The use of shotcrete or concrete lining is limited by the fact that it takes time for these materials to harden and to achieve the required strength required to provide adequate support. The use of accelerators or of thick linings can partially overcome these problems, but may introduce another set of practical problems.

The practical solution adopted in the actual case upon which this example is based was to use sliding joint top hat section sets. These sets, as delivered to site, are shown in Figure 12 which illustrates how the sections fit into each other. The assembly of these sets to form a sliding joint is illustrated in Figure 14 and the installation of the sets in the tunnel is illustrated in Figure 15.

Figure 12: Buckling of an H section steel set being bent to a small radius. Temporary stiffeners have been tack welded into the section to minimise buckling but a considerable amount of work is required to straighten the flanges after these stiffeners have been removed.

Figure 13 Top hat section steel sets delivered to site ready to be transported underground.

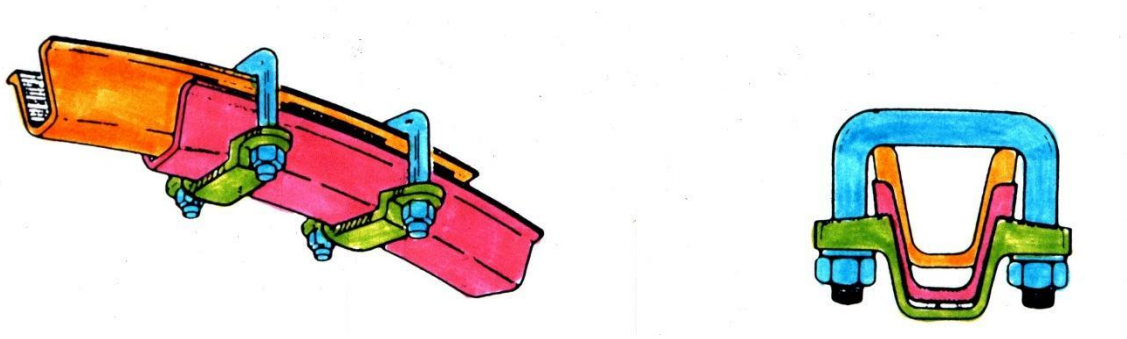

Figure 14 Assembly of a sliding joint in a top hat section steel set.

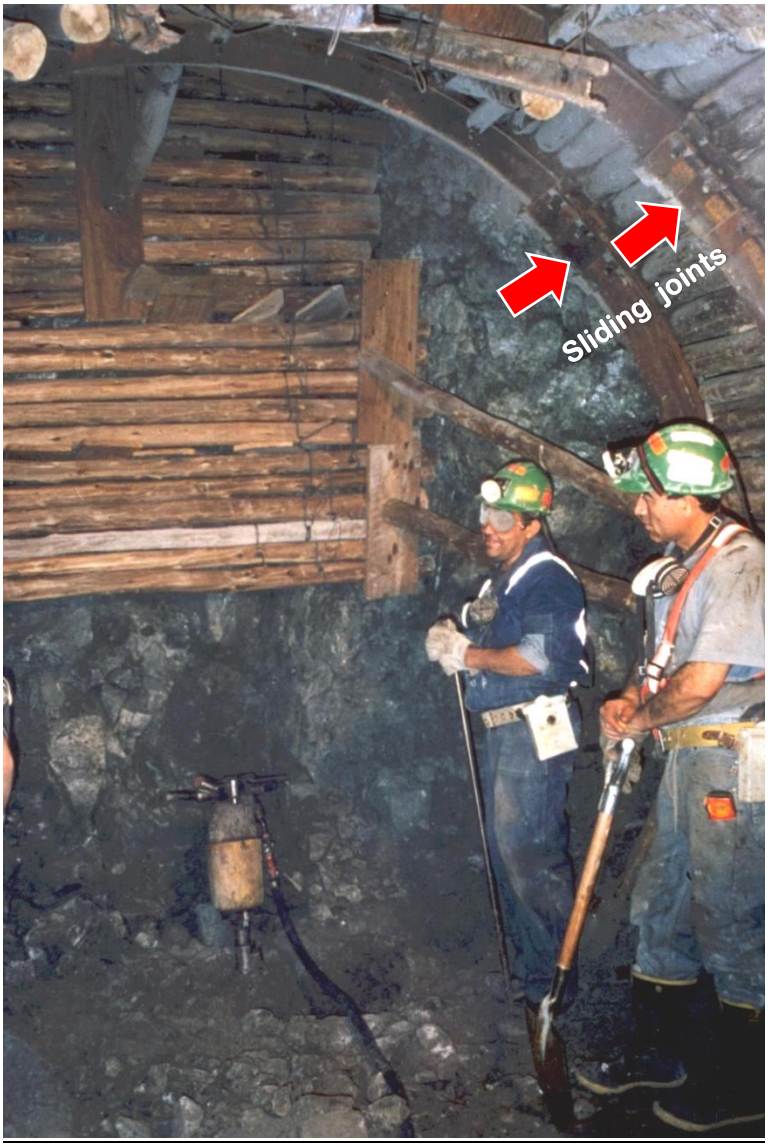

Figure 15: Installation of sliding joint top hat section steel sets immediately behind the face of a tunnel being advanced through very poor quality rock.

The sets are installed immediately behind the advancing face which, in a rock mass such as that considered here, is usually excavated by hand. The clamps holding the joints are tightened to control the frictional force in the joints which slide progressively as the face is advanced and the rock load is applied to the sets.

The use of sliding joints in steel sets allows very much lighter section sets to be used than would be the case for sets with rigid joints. These sets provide immediate protection for the workers behind the face but they permit significant deformation of the tunnel to take place as the face is advanced. In most cases, a positive stop is welded onto the sets so that, after a pre-determined amount of deformation has occurred, the joint locks and the set becomes rigid. A trial-and-error process has to be used to find the amount of deformation that can be permitted before the set locks. Too little deformation will result in obvious buckling of the set while too much deformation will result in loosening of the surrounding rock mass.

In the case of the tunnel illustrated in Figure 15, lagging behind the sets consists of wooden poles of approximately 100 mm diameter. A variety of materials can be used for lagging but wood, in the form of planks or poles, is still the most common material used in mining. In addition to the lagging, a timber mat has been propped against the face to improve the stability of the face. This is an important practical precaution since instability of the tunnel face can result in progressive ravelling ahead of the steel sets and, in some cases, collapse of the tunnel.

The way in which sliding joints work is illustrated diagrammatically in Figure 16.

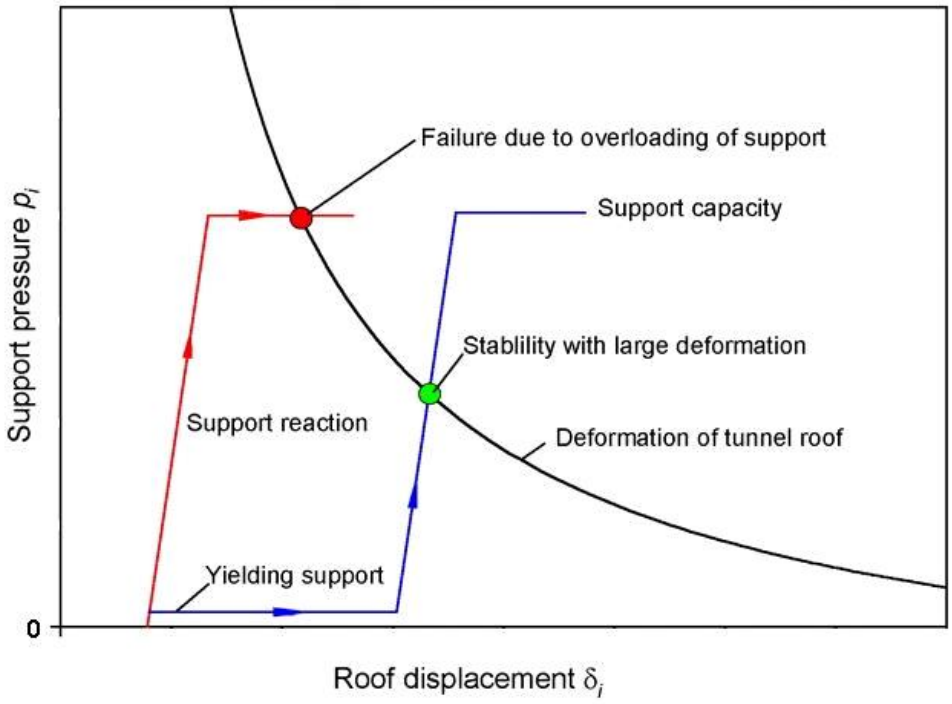

Figure 16: Delay in the activation of passive support by the use of sliding joints.

Figure 16 shows that passive support in the form of steel sets, lattice girders, shotcrete or concrete linings can fail if installed too close to the face. This is because the support pressure required to achieve stability is larger than the capacity of the support system. As the displacements in the tunnel increase as the face moves away from the section under consideration, the support pressure required to achieve equilibrium decreases as illustrated by the curve in Figure 16. Delaying the activation of the support system, using sliding joints, can stabilize the tunnel at support pressures within the capacity of the support.

Many systems have been used to introduce these yielding elements into tunnels with squeezing problems. An example is the use of sliding joints in steel sets as shown in Figure 16. Another system is to use "stress controllers" in which controlled buckling of an inner steel tube provides the yielding required and the system locks and becomes more rigid when a pre-determined deformation has occurred. This system, developed by Professor Wulf Schubert (Schubert, 1996) at the University of Graz in Austria, is illustrated in Figures 17 and 18.

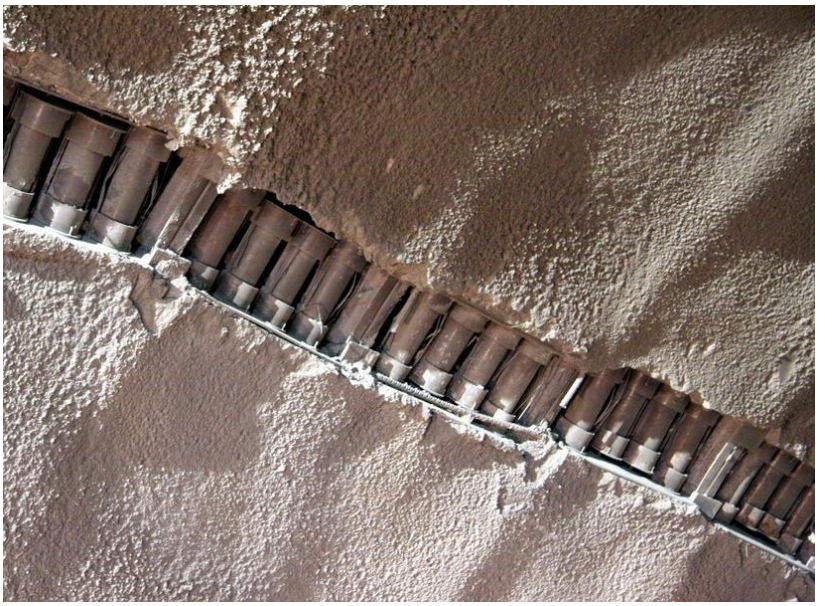

Figure 17: A row of stress controllers installed in a slot in the shotcrete lining in a tunnel

Figure 18: Section through a stress controller showing the buckling inner tube. After Schubert, 1996.

As an alternative to supporting the face, as illustrated in Figure 15, spiles or forepoles can be used to create an umbrella of reinforced rock ahead of the advancing face. Figure 19 illustrate the general principles of the technique. In the example illustrated, spiling is being used to advance a 7 m span, 3 m high tunnel top heading through a clay-rich fault zone material in a tunnel in India. The spiles, consisting of 25 mm steel bars, were driven in by means of a heavy sledgehammer.

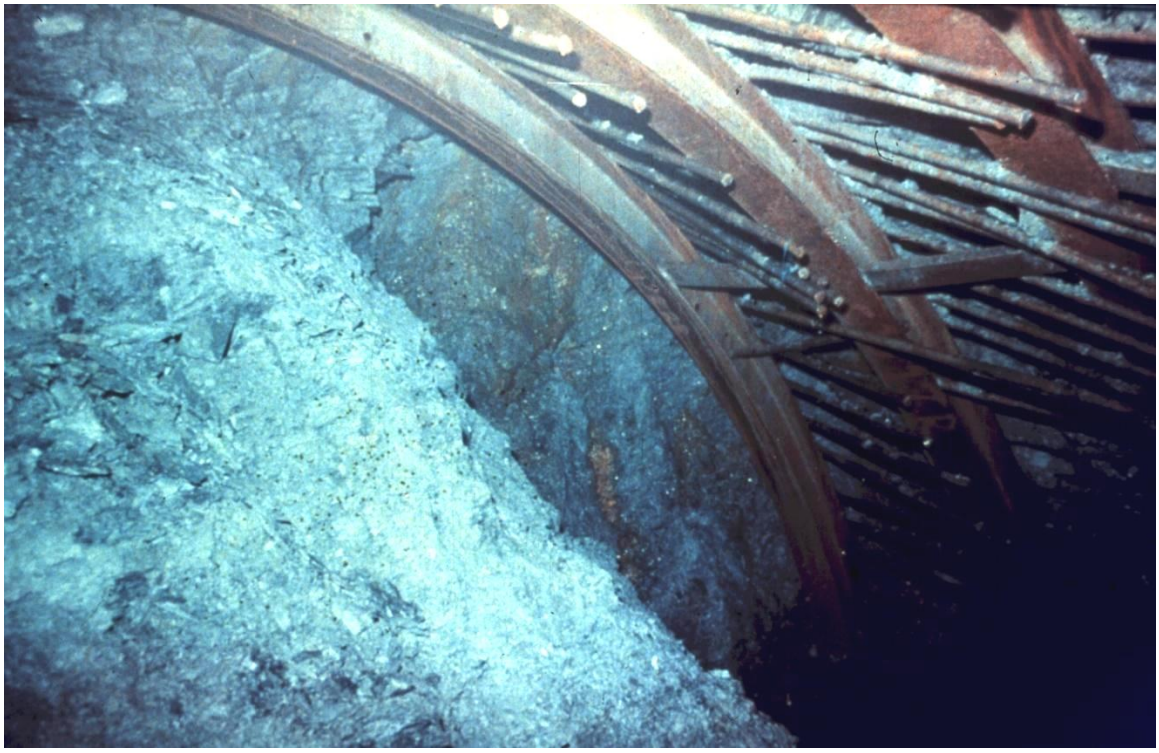

Figure 19: Spiling in very poor quality clay-rich fault zone material.

Figure 20 shows a more elaborate system used in large span tunnels in poor quality rock masses. This system relies on grouted fiberglass dowels, which can be cut relatively easily, to stabilize the face ahead of the tunnel and grouted forepoles to provide a protective umbrella over the face. These forepoles consist of 75 to 140 mm diameter steel pipes through which grout is injected. In order for the forepoles to work effectively the rock mass should behave in a frictional manner so that arches or bridges can form between individual forepoles. The technique is not very effective in fault gouge material containing a siginifcant proportion of clay unless the forepole spacing is very close. The forepoles are installed by means of a special drilling machine as illustrated in Figure 21.

While these forepole umbrella systems can add significantly to the cost of driving tunnels and can also result in very slow advance rates, they have been used very successfully in driving many transportation tunnels in Europe (Carrieri et al, 1991).

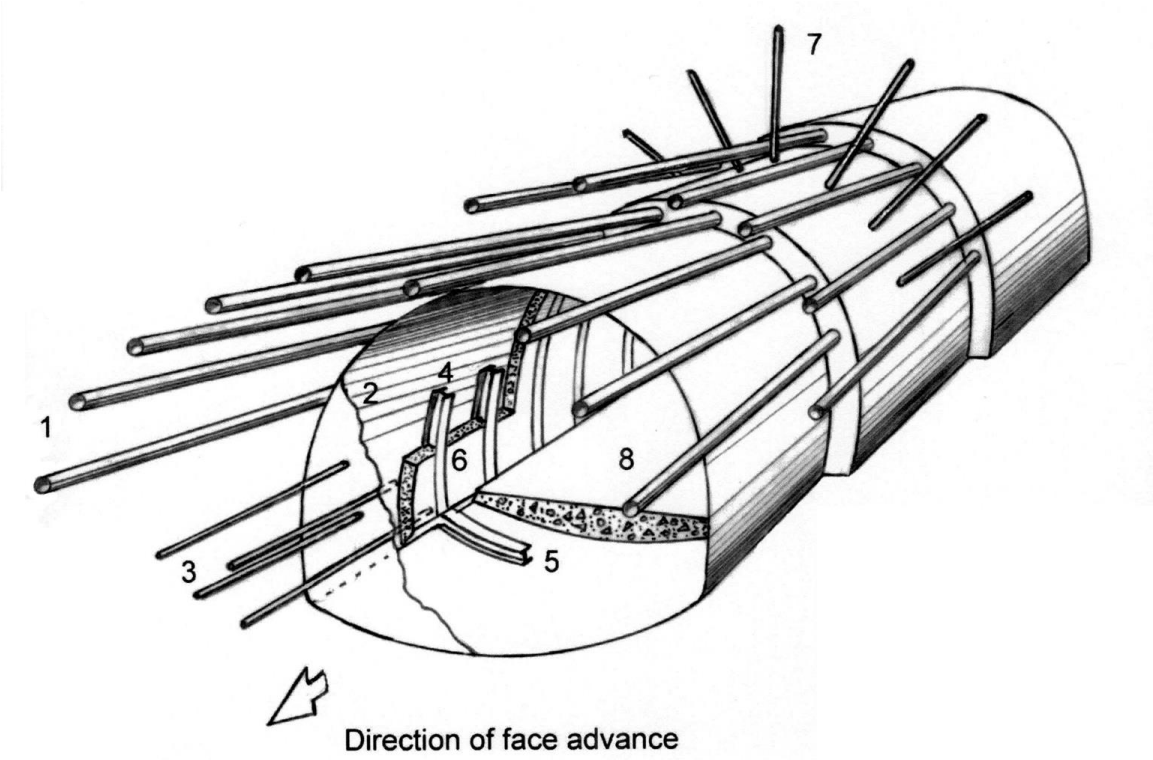

1 Forepoles – typically 75- or 114-mm diameter pipes, 12 m long installed every 8 m along the tunnel to create a 4 m overlap between successive forepole umbrellas.

2 Shotcrete – applied immediately behind the face and to the face, in cases where face stability is a problem. Typically, this initial shotcrete layer is 25 to 50 mm thick.

3 Grouted fiberglass dowels – Installed midway between forepole umbrella installation steps to reinforce the rock immediately ahead of the face. These dowels are usually 6 to 12 m long and are spaced on a 1 m x 1 m grid.

4 Steel sets – installed as close to the face as possible and designed to support the forepole umbrella and the stresses acting on the tunnel.

5 Invert struts – installed to control floor heave and to provide a footing for the steel sets.

6 Shotcrete – typically steel fibre reinforced shotcrete applied as soon as possible to embed the steel sets to improve their lateral stability and also to create a structural lining.

7 Rockbolts as required. In very poor-quality rock, it may be necessary to use self-drilling rockbolts in which a disposable bit is used and is grouted into place with the bolt.

8 Invert lining – either shotcrete or concrete can be used, depending upon the end use of the tunnel.

Figure 20: Full face 10 m span tunnel excavation through weak rock under the protection of a forepole umbrella. The final concrete lining is not included in this figure.

Figure 21: Installation of 12 m long 75 mm diameter pipe forepoles in an 11 m span tunnel top heading in a fault zone.

References

Brady, B.H.G. and Brown, E.T. 1985. *Rock mechanics for underground mining*. London: Allen and Unwin.

Carranza-Torres, C. and Fairhurst, C. 1999. The elasto-plastic response of underground excavations in rock masses that satisfy the Hoek-Brown failure criterion. *Int. J. Rock Mech. Min. Sci.* **36**(6), 777–809.

Carranza-Torres, C. 2004. Elasto-plastic solution of tunnel problems using the generalized form of the Hoek-Brown failure criterion. In proc. ISRM SINOROCK2004 symposium China, (Eds. J.A. Hudson and F. Xia-Ting). *Int. J. Rock Mech. Min. Sci.* **41**(3), 480–481.

Carranza-Torres, C. 2004. Some Comments on the Application of the Hoek-Brown Failure Criterion for Intact Rock and Rock Masses to the Solution of Tunnel and Slope Problems. In *MIR 2004 – X conference on rock and engineering mechanic,* Torino, (eds. G. Barla and M. Barla). Chapter 10, 285–326. Pàtron Editore. Bologna: Pàtron Editore.

Chern, J.C., Yu, C.W., and Shiao, F.Y. 1998. Tunnelling in squeezing ground and support estimation. *Proc. reg. symp. sedimentary rock engineering,* Taipei, 192-202.

Duncan Fama, M.E. 1993. Numerical modelling of yield zones in weak rocks. In *Comprehensive rock engineering*, (ed. J.A. Hudson) **2**, 49-75. Oxford: Pergamon.

Hoek, E. and Brown, E.T. 1980. *Underground excavations in rock*. London: Instn Min. Metall.

Hoek, E. and Brown, E.T. 1997. Practical estimates of rock mass strength. *Int. J. Rock Mech. & Mining Sci. & Geomech. Abstr.* **34**(8), 1165-1186.

Hoek, E. 1998. Tunnel support in weak rock, keynote address, *Symp. On sedimentary rock engineering*. Taipei, Taiwan, 20-22.

Hoek, E., Carranza-Torres, C.T., Corkum, B. Hoek-Brown failure criterion-2002 edition. In P*roceedings of the Fifth North American Rock Mechanics Symp.*, Toronto, Canada, **1**: 267–73.

Carrieri, G., Grasso, P., Mahtab, A. and Pelizza, S. 1991. Ten years of experience in the use of umbrella-arch for tunnelling. *Proc. SIG Conf. On Soil and Rock Improvement*, Milano **1**, 99-111.

Sakurai, S. 1983. Displacement measurements associated with the design of underground openings. *Proc. Int. Symp. Field Measurements in Geomechanics,* Zurich, **2,** 1163-1178.

Schubert, W. 1996. Dealing with squeezing conditions in Alpine tunnels. *Rock Mech. Rock Engng.* **29**(3), 145-153.

14. Design of large underground caverns – a case history based on the Mingtan Pumped Storage Project in Taiwan

Introduction

Large underground caverns are used for a variety of purposes in civil engineering. These include caverns housing turbines, electrical generators and transformers in hydroelectric projects, caverns for storing liquid or gaseous fuels, underground warehouses, and underground sports facilities. Because of the high capital costs and the risks associated with public access to these facilities, care must be taken in the design of the caverns to ensure that potential risks are kept to an absolute minimum while, at the same time, providing cost effective and practical engineering solutions. An example of a large underground hydroelectric complex in Taiwan will be used to illustrate the design and process for this type of civil engineering facility and for permanent mining structures such as underground crusher stations.

The Mingtan Pumped Storage Project is located at the geographic centre of Taiwan as illustrated in Figure 1. It utilises the existing Sun Moon Lake as its upper reservoir. The lower reservoir was created by a 60 m high concrete gravity dam on the Shuili River. As illustrated in Figure 2, a pair of 3 km long, 7.5 m diameter headrace tunnels bring the water from the Sun Moon Lake to the surge shafts. From there, inclined steel-lined penstocks convey the water to six reversible pump-turbines, which are housed in a 22 m wide x 46 m high x 158 m long underground power cavern. The transformers are in a parallel 13 m wide x 20 m high x 170 m long cavern. The powerhouse and transformer complex has been excavated in the left bank of the Shuili River at a depth of approximately 300 m below surface. The total generating capacity of the scheme is 1600 megawatts.

The project is owned and operated by the Taiwan Power Company and the engineering design was carried out by Sinotech Engineering Consultants, Inc. Many of the details given below are from papers by Cheng and Liu (1993) and Hoek and Moy (1993).

Geological setting

Taiwan is in the Cenozoic Orogenic belt, at the link between the Ryuku Island Arc to the north and the Philippines Orogeny to the south. It is situated on a convergent and compressive boundary between the Erasian Plate and the Philippines Sea Plate. The frequent occurrence of earthquakes on the island indicates that Taiwan is located in a belt of young tectonic activity. The mountain ranges extend generally in a north-south direction with the highest peak rising more than 3000 m above sea level. North-south striking thrust faults extend over the entire length of the island.

The Central Range, which forms the backbone of the island, consists of Tertiary sub metamorphic rocks distributed over the western flank and crest, and pre-Tertiary metamorphic rocks distributed over the eastern flank. The Western Foothills are composed of Neogeny clastic sediments in alternating beds of sandstone, siltstone and shale interspersed with limestone and tuff.

The sub metamorphic rocks of the western Central Range (sandstones and argillite) and the sandstones and siltstones of the Western Foothills exhibit tight asymmetric synclines and anticlines, and extensive thrust faulting. The entire area of the project is located between two major north-south faults of this type, namely the Shuilikeng (or Chuchih) fault passing close to the lower reservoir damsite and the Lishan fault running through to the east of the Sun Moon Lake, the upper reservoir of the project.

The power cavern complex is in sandstone, sandstone with siltstone interbeds and several siltstone beds belonging to the Waichecheng Series. The sandstones are fine grained to conglomeratic and sometimes quartzitic. In general, they are strong to very strong although they are slightly to moderately weathered. Locally, softer zones of highly weathered or altered material are encountered. The siltstones are moderately strong and almost always sheared. Occasionally, massive sandstone beds occur with a thickness of up to 7 m. The general appearance of the rock mass in an exploration adit is shown in Figure 3.

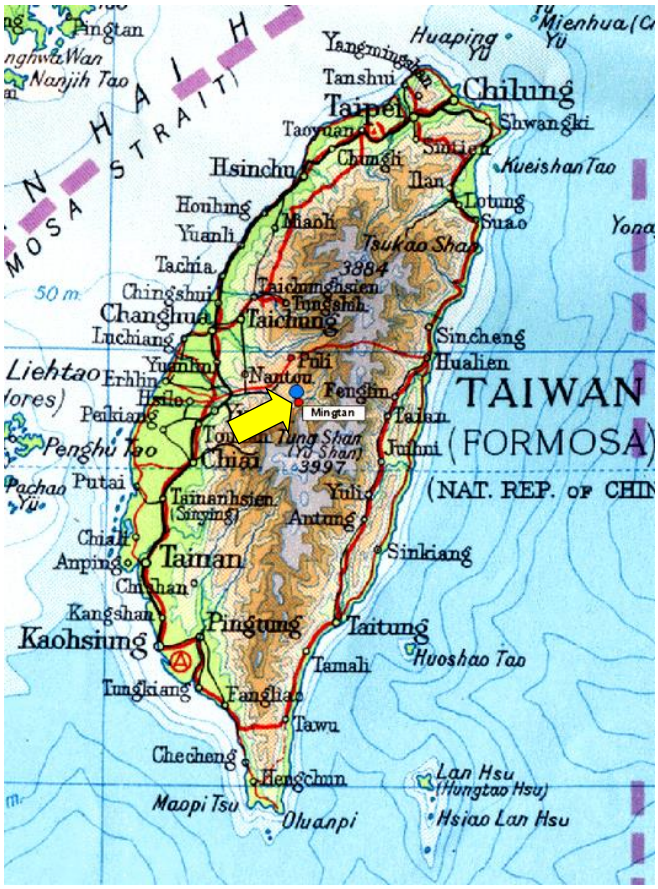

Figure 1: Map of the island of Taiwan with the location of the Mingtan Pumped Storage Project in the centre of the country (yellow arrow).

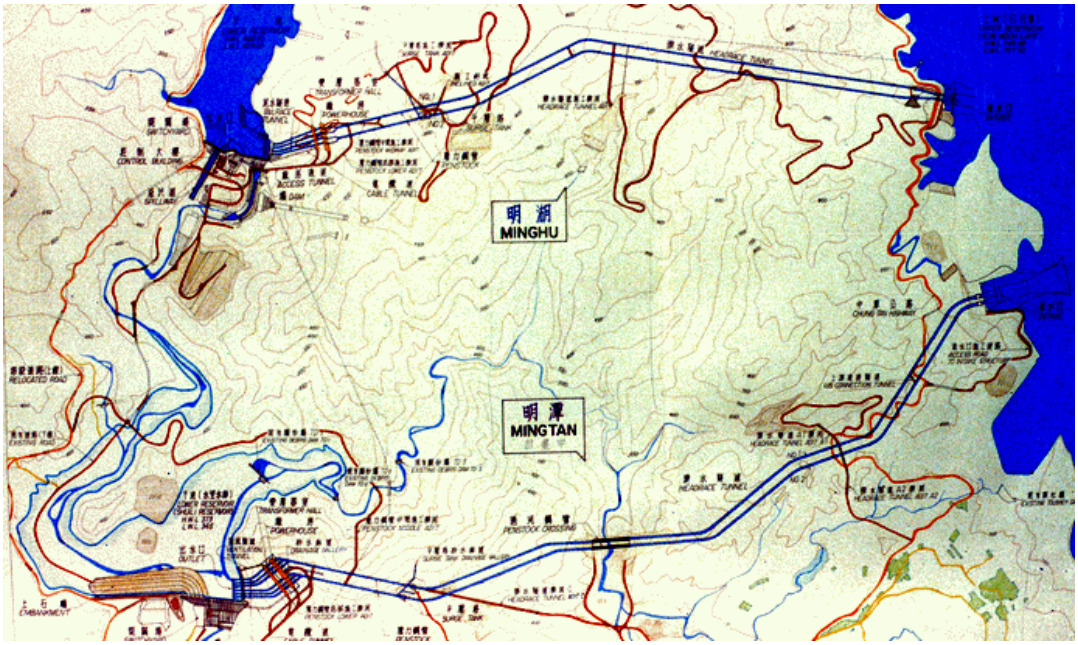

Figure 2: Plan showing the layout of the Minghu Pumped Storage Project (top) and Mingtan Pumped Storage Project (bottom).

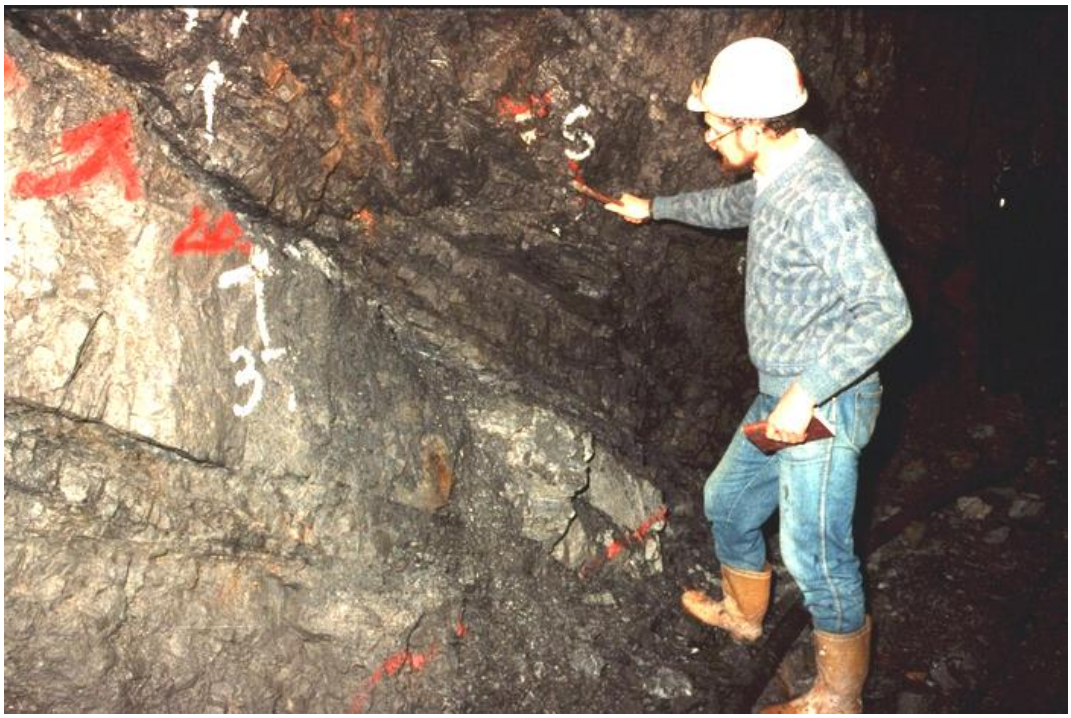

Figure 3: Sandstone and siltstone sequence exposed in and underground exploration adit. A thick bed of massive sandstone can be seen in the centre of the photograph and this is sandwiched between bedded sandstones and siltstones of moderate quality. The contact surfaces between these different beds are frequently heavily sheared.

Structural Geology

The attitude of the bedding planes is uniform throughout the powerhouse area, with a strike and dip of N39°E/34°SE as shown in Figure 4. The bedding is generally tight and spaced from a few centimetres to more than 2 m. Some planes contain a thin layer of clay of about 5 mm thickness.

Eight shear zones (sometimes also referred to as faults) were encountered in the cavern area. All these features are parallel to the bedding planes, occurring in the relatively soft siltstone or interbedded sandstone and siltstone layers. These shear zones are composed of multiple clay seams and shattered, softened, or decomposed rock.

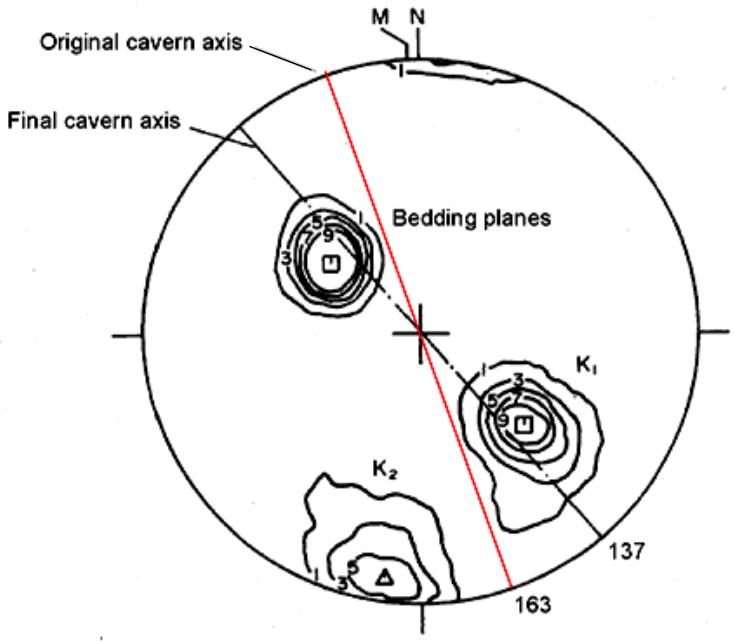

Figure 4: Attitude of bedding planes and joint sets K1 and K2. (based on 2257 measurements)

The original orientation of the power cavern complex, shown in Figure 4, was chosen to keep the penstocks and tailrace tunnels in a straight line. Because of concerns about the formation of wedges in the roof, sidewalls and end walls of the underground caverns, the underground complex was rotated by 26° so that the strike of the bedding planes is almost exactly perpendicular to the cavern axis. While this involved the introduction of curvature in the water transmission tunnels, this curvature was acceptable in view of the improved stability conditions associated with the new alignment.

A geological plan of the powerhouse area is shown in Figure 5 and an isometric drawing of the underground complex is reproduced in Figure 6.

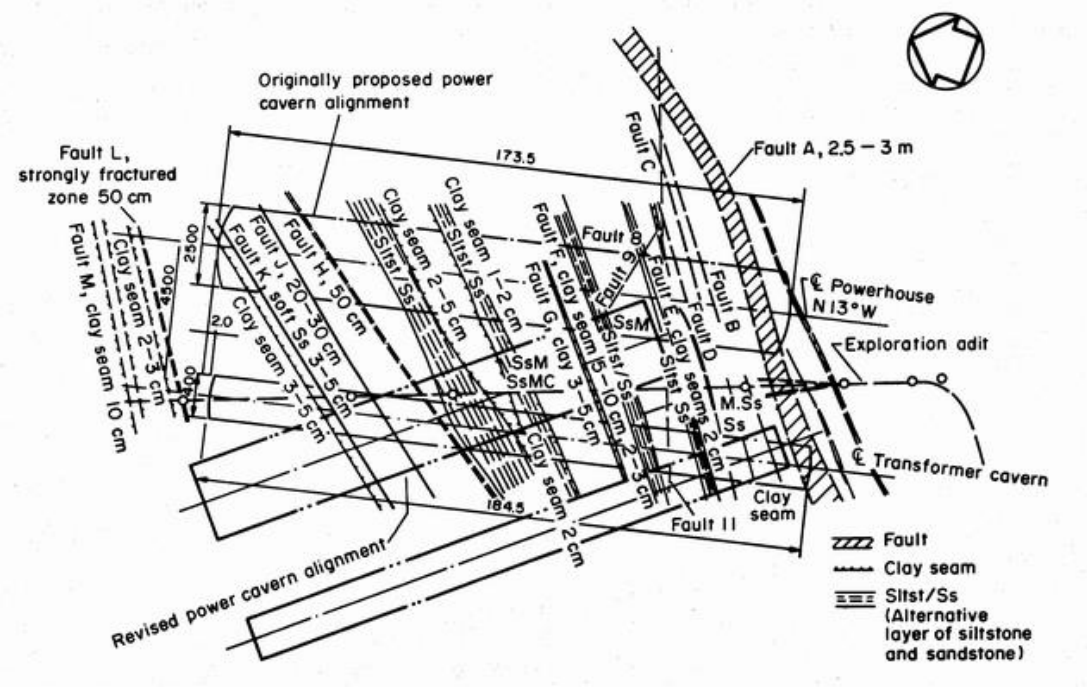

Figure 5: Geological plan of the cavern area showing the original and revised cavern orientations.

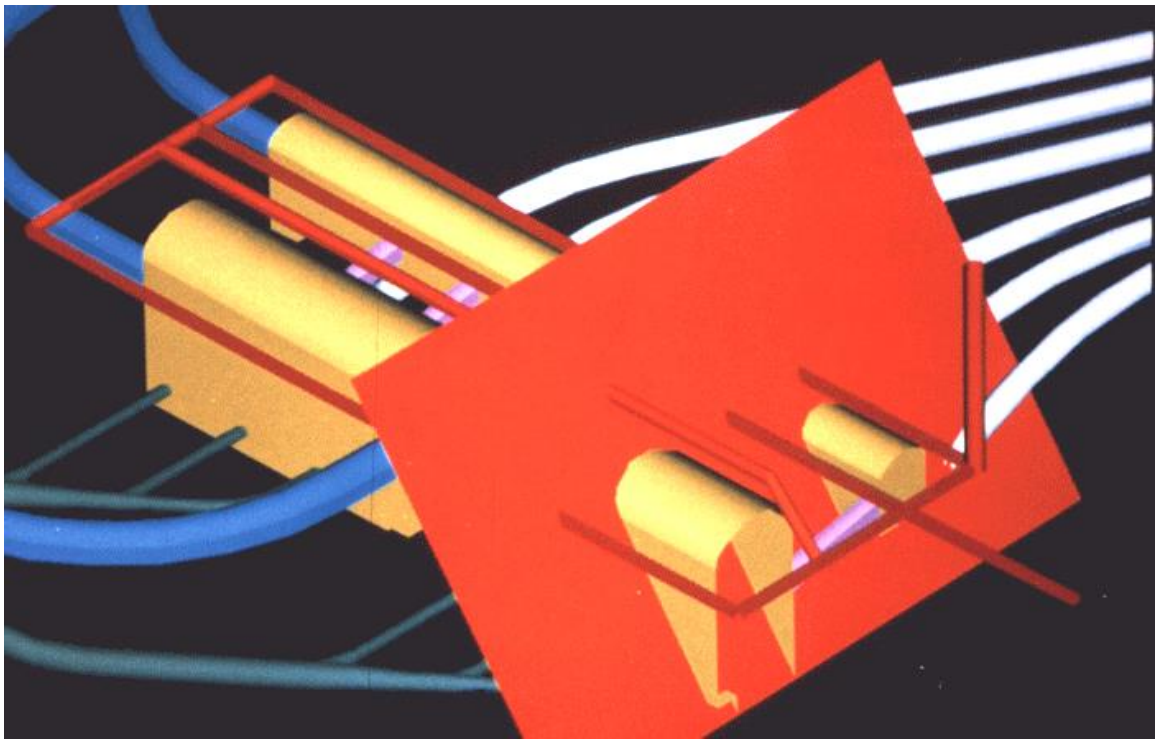

Figure 6: Isometric drawing of the underground complex in relation to the bedding plane orientation (a typical bedding plane is shown in red).

Rock mass properties

Laboratory and in situ tests were carried out in the 1970s for both the Minghu and Mingtan Projects (see Figure 2). The Minghu project was completed in the early 1980s. Detailed design of the Mingtan project commenced in 1982.

The rock mass in the powerhouse area was divided into three types: jointed sandstone, bedded sandstone and faults. The rock mass classifications for these three rock types are given in Table 1. The properties of the intact rock components are listed in Table 2 and the measured in situ deformation modulus values for the rock mass are listed in Table 3. A typical field plate loading test is illustrated in Figure 7.

Table 1: Rock mass classifications for the rock mass in the powerhouse area

Rock type	*RMR*	*Q*	*Rock quality*
Jointed sandstone	63 – 75	12 – 39	Good
Bedded sandstone	56 – 60	7 – 13	Fair to good
Faults or shear zones	10 - 33	0.1 – 1.1	Very poor to poor

Table 2: Intact rock properties from laboratory tests

	Uniaxial compressive Strength MPa		*Modulus of elasticity GPa*	
Rock type	*Range*	*Average*	*Range*	*Average*
Sandstone	101-219	166	14.3-29.3	22.3
Siltstone	22-95	41	6.7-16.2	10.6
Interbedded sandstone and siltstone	34-97	66	10.1-17.9	12.8
Coarse grained sandstone	49-123	72		

Table 3: Deformation modulus of rock masses

	Deformation modulus - GPa	
Rock type	*Flat jack tests*	*Plate loading tests*
Sandstone	2.7 – 2.9 ↧	3.2 – 5.1 ↧
	2.2 – 5.6 ⇆	2.3 – 5.0 ⇆
Siltstone	3.3 – 12.4 ↧	
	5.7 – 14.8 ⇆	
Interbedded sandstone and siltstone	2.2 ↧	2.8 ↧
	10.9 ⇆	3.0 ⇆

↧ Normal to bedding, ⇆ parallel to bedding.

Figure 7: A plate loading test to determine the in-situ deformation modulus of the rock mass exposed in an exploration adit.

On the basis of the rock mass classifications and the laboratory and field tests listed in Tables 1 to 3, the following estimates of the rock mass properties were made using the Hoek-Brown criterion. (Hoek and Brown, 1980, 1988)

Table 4: Estimated rock mass properties – based on laboratory and field tests

Rock type	*RMR*	σ_{ci} *MPa*	m_b	*s*	*c* *MPa*	ϕ *degrees*	E^1 *GPa*
Jointed sandstone	63 – 75	100	4.3	0.02	3.8	50	2.7-5.6
Bedded sandstone	56 – 60	100	1.5	0.002	3.3	45	3.3-15
Faults or shear zones	10 - 33	46	0.64	0.0002	0.2	40	2

[1] From in situ test results

In situ stresses

In situ stress measurements were carried out in an exploration adit using overcoring on a Stress Tensor Tube developed by Rocha et al (1974). The results of these stress measurements are given in Table 5.

Table 5: Measured in situ stresses

Principal stresses	*Stress directions*	
MPa	*Bearing (degrees)*	*Plunge (degrees)*
7.1	340	40
3.9	240	10
2.9	140	50

In transforming these stresses onto a plane corresponding to a cross-section of the cavern, a vertical stress of approximately 5.0 MPa is calculated and the ratio of horizontal to vertical stress is found to be approximately 0.9. This compares with the measured ratio of horizontal to vertical stress of 1.4 for the Minghu power cavern which is located approximately three kilometres away and which was completed in the early 1980s. In applying these results to the analysis of the Mingtan power cavern, a range of horizontal to vertical in situ stress ratios of 0.8 to 1.5 were used to cover the uncertainty associated with the measured value. A further discussion on the interpretation of these in situ stress measurements can be found in Wittke (1990, page 935).

Choice of power cavern shape

The Minghu power cavern was designed by a Japanese consulting group who followed traditional methods involving the use of a cast-in-place concrete arch for supporting the cavern roof. During construction of this cavern very high stresses were induced in both the concrete and the reinforcing steel because of the response of the stiff concrete arch to deformations in the relatively deformable rock mass.

Since the designers of the Mingtan project did not want the same problems to occur in this project, three different cavern shapes were investigated. These cavern shapes were:

a. A mushroom shaped cavern with a concrete arch, like the Minghu cavern
b. A conventional horseshoe shaped cavern with vertical sidewalls and
c. An elliptical cavern designed for optimal stress distribution in the surrounding rock mass.

The mushroom shaped cavern was included for reference purposes since the behaviour of the Minghu cavern had been well documented. The conventional horseshoe shaped cavern was the preferred choice in terms of ease of construction but the elliptical cavern, proposed by a German consulting group, was also analysed. The results of analyses of these three cavern shapes are presented in Figures 8, 9 and 10.

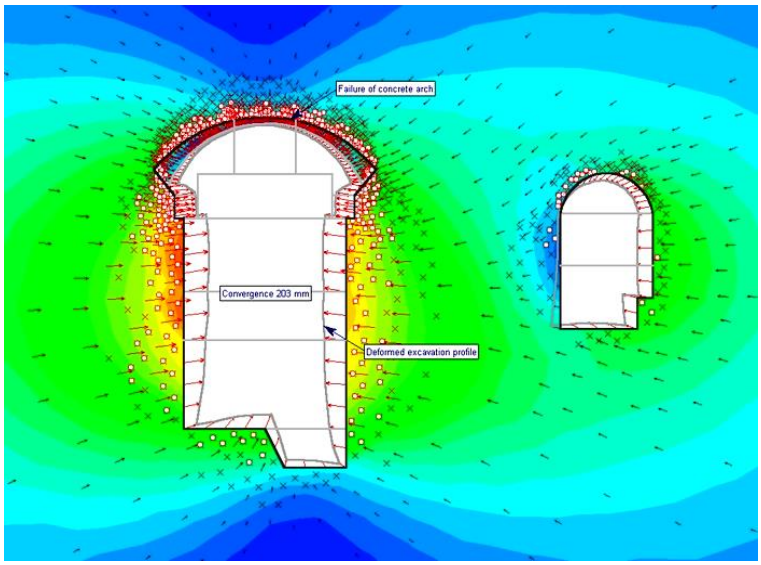

Figure 8: Deformation and failure of the rock mass surrounding a mushroom shaped cavern with a concrete roof arch. Failure of the concrete arch means that this design is not acceptable.

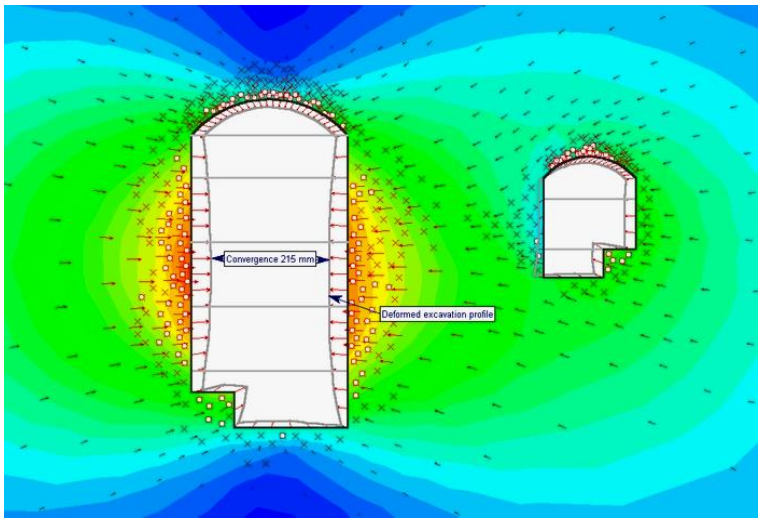

Figure 9: Deformation and failure of the rock mass around an unsupported horseshoe shaped cavern. Failure of the rock mass in the roof and sidewalls is such that extensive support will be required.

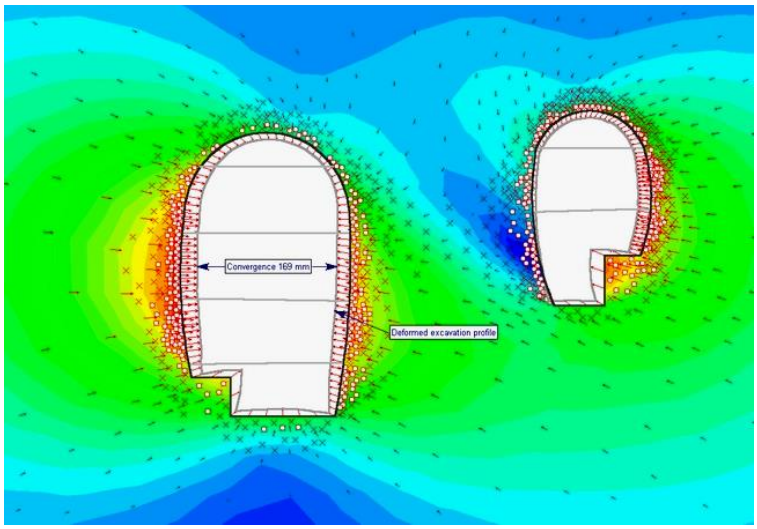

Figure 10: Deformation and failure of the rock mass surrounding an unsupported elliptical cavern. Failure of the rock mass in the roof and sidewalls is such that extensive support will be required, although less than for the horseshoe shaped cavern.

The comparative studies illustrated in Figures 8, 9 and 10, showed that the mushroom shaped cavern with the concrete roof arch was not an acceptable design. The analysis indicated that even more extensive overstressing of the concrete arch would occur than had been the case in the Minghu cavern. The best stress distribution was given by the elliptical cavern, but it was judged that the amount of support required to stabilise this and the horseshoe shaped cavern would not be significantly different. Consequently, the conventional horseshoe shaped vertical cavern was chosen for the final shape. It was considered that this would make for the simplest construction procedure and that the overall underground complex would incur lower costs than an elliptical cavern.

Distance between caverns

The analyses presented in Figures 8, 9 and 10 show the typical deformation pattern in which the smaller transformer gallery tends to be drawn towards the larger machine hall. This is not a problem when the pillar between these two caverns is sufficiently large but, if the pillar is too small, overstressing of the pillar can occur.

A study was carried out in which the width of the pillar between the transformer gallery and the machine hall was varied. The results of this study showed that the optimum pillar width is obtained when the distance between the two caverns is approximately equal to the height of the larger of the two caverns. This finding is generally applicable when designing caverns in weak rock masses.

Seam treatment in the cavern roof

The final layout of the Mingtan powerhouse and transformer caverns is illustrated in Figure 11. The project was constructed in two phases such that preparatory works were carried out in a preliminary contract, while the bulk of the construction was carried out in the main contract. This arrangement provided the opportunity for stabilization of the cavern roof to be carried out during the preliminary contract.

As pointed out earlier and as illustrated in Figure 5, the powerhouse cavern crosses eight faults or shear zones. The influence of these faults on the stability of the cavern was of major concern and it was decided that pre-treatment of the cavern roof was necessary in order to ensure that the main contract could proceed without severe problems due to roof instability. This pre-treatment consisted of removal and replacement of the clay seams in the faults to the maximum extent possible, followed by reinforcement of the rock mass in the roof by means of grouted cables.

The treatment of the faults involved high pressure washing of the clay seams and backfilling the voids with non-shrinking concrete. This technique was developed for the treatment of similar faults in the foundation of the Feitsui arch dam near Taipei (Cheng, 1987). Figure 12 shows the arrangement of longitudinal working galleries and cross-cuts used to access the clay seams. It was found that the clay washing, and replacement could be carried out to a depth of about 4 m. The thickest and weakest fault (Fault H in Figure 5) was manually excavated and backfilled to a similar depth.

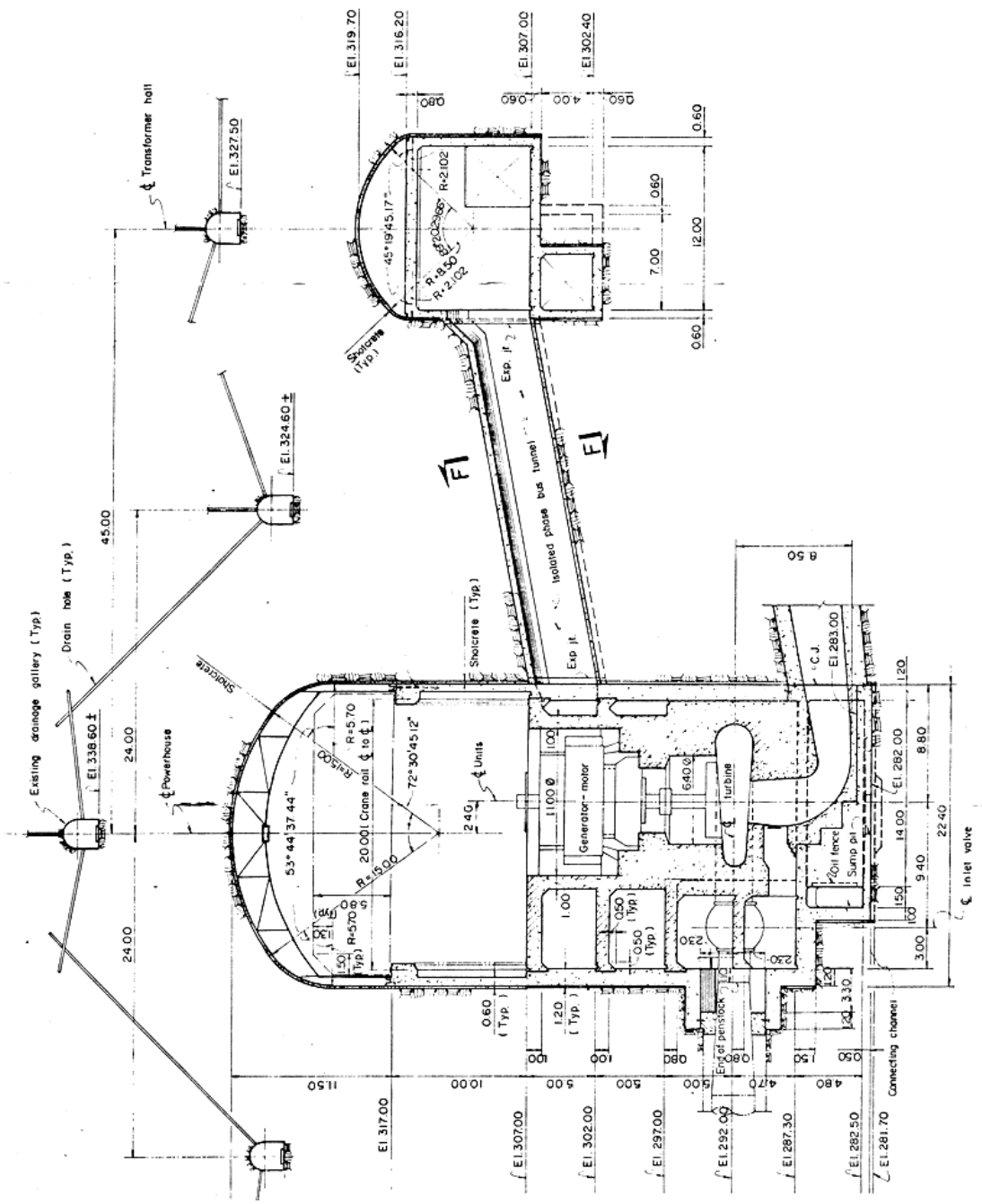

Figure 11: Final layout of the Mingtan powerhouse cavern and transformer gallery.

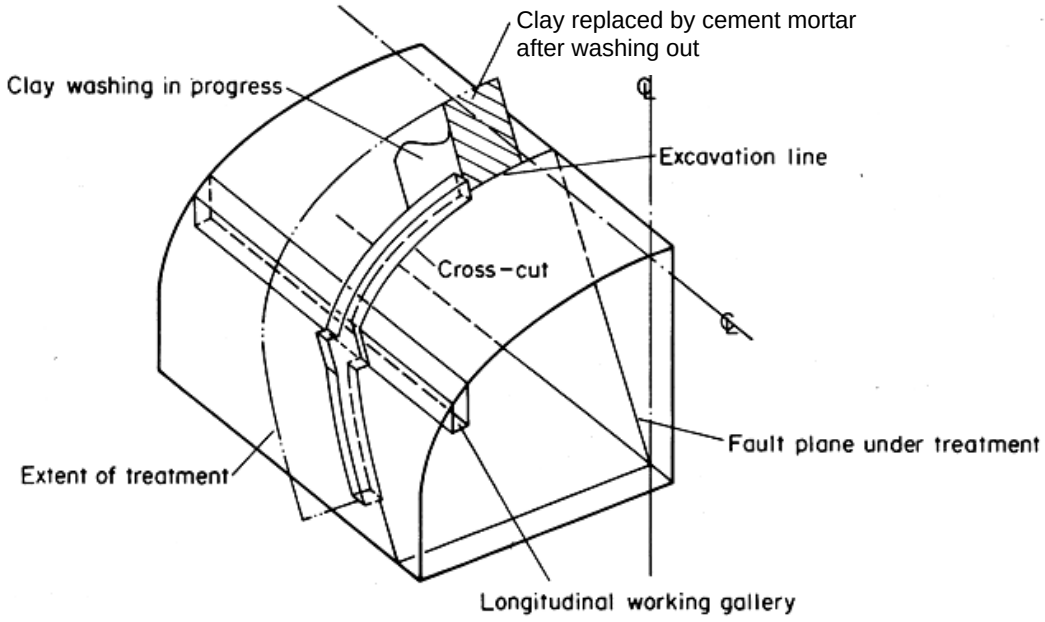

Figure 12: Washing and replacement of clay seams in the faults encountered in the roof and upper sidewalls of the Mingtan power cavern. This treatment was carried out from two longitudinal working galleries before excavation of the cavern commenced in the main contract.

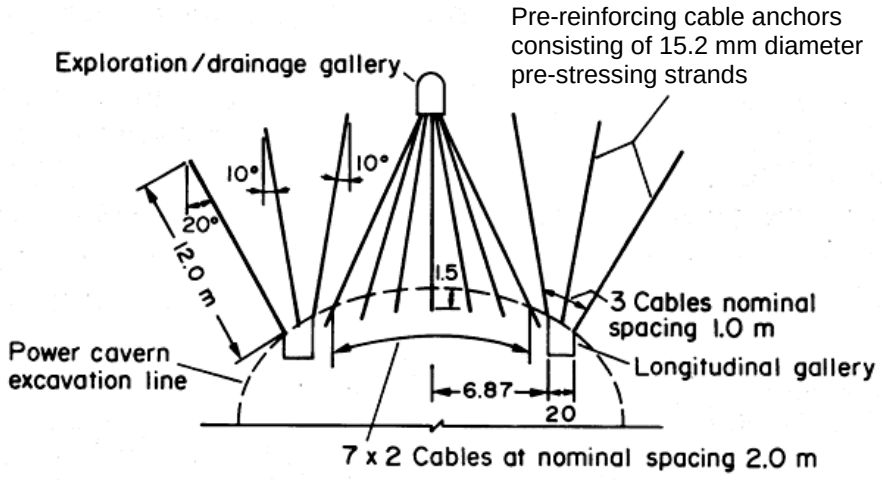

Figure 13: Pre-reinforcement of the power cavern roof by means of grouted untensioned cables placed from the longitudinal working galleries and from an existing exploration and drainage gallery above the roof.

Once the seam treatment in the roof had been completed, a series of untensioned grouted cables were installed as illustrated in Figure 13. Since these cables were installed before excavation of the cavern commenced, tensioning of the reinforcement was not necessary since the cables would be loaded by deformation induced by the cavern excavation. A load of a few tons was used to straighten the cables before they were fully grouted in place. As the lower ends of the cables installed downwards from the drainage gallery were exposed in the roof of the cavern, these ends were cleaned, and an anchor system was installed before the excess cables lengths were cut off.

The installation of the cables from one of the longitudinal working galleries is illustrated in Figure 14.

Figure 14: Untensioned grouted cables installed from the longitudinal working galleries to pre-reinforce the rock mass above the power cavern roof.

Choice of cavern roof and sidewall reinforcement

In contrast to the Minghu powerhouse cavern in which the roof is supported by a stiff concrete arch, the Mingtan cavern is supported by "active" support consisting of cables, rockbolts and shotcrete. A precedent for the design of this support is the experience from existing caverns, plotted in Figures 15 and 16.

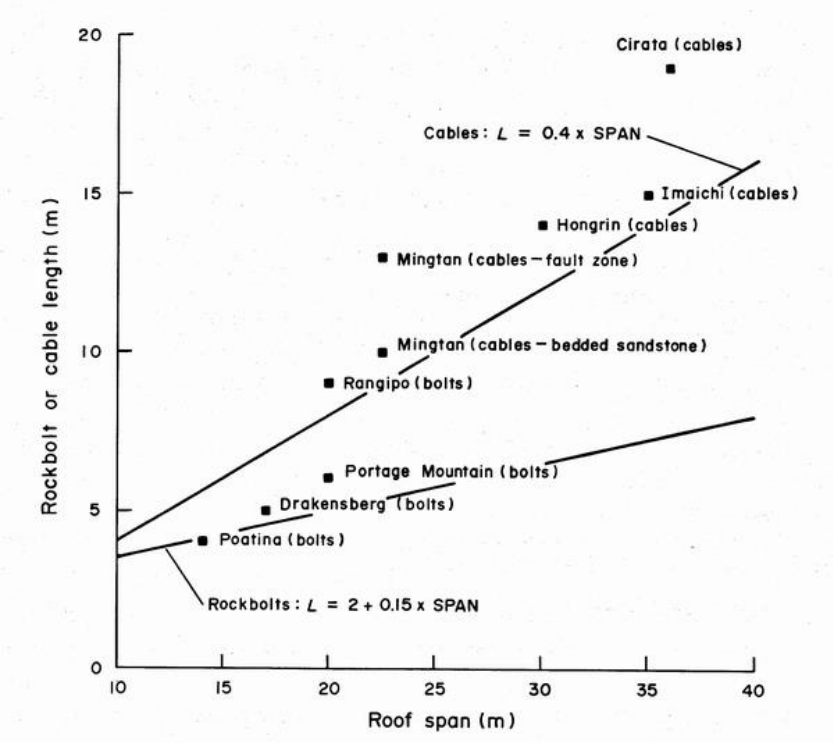

Figure 15: Precedents for rockbolt and cable lengths for different cavern roof spans.

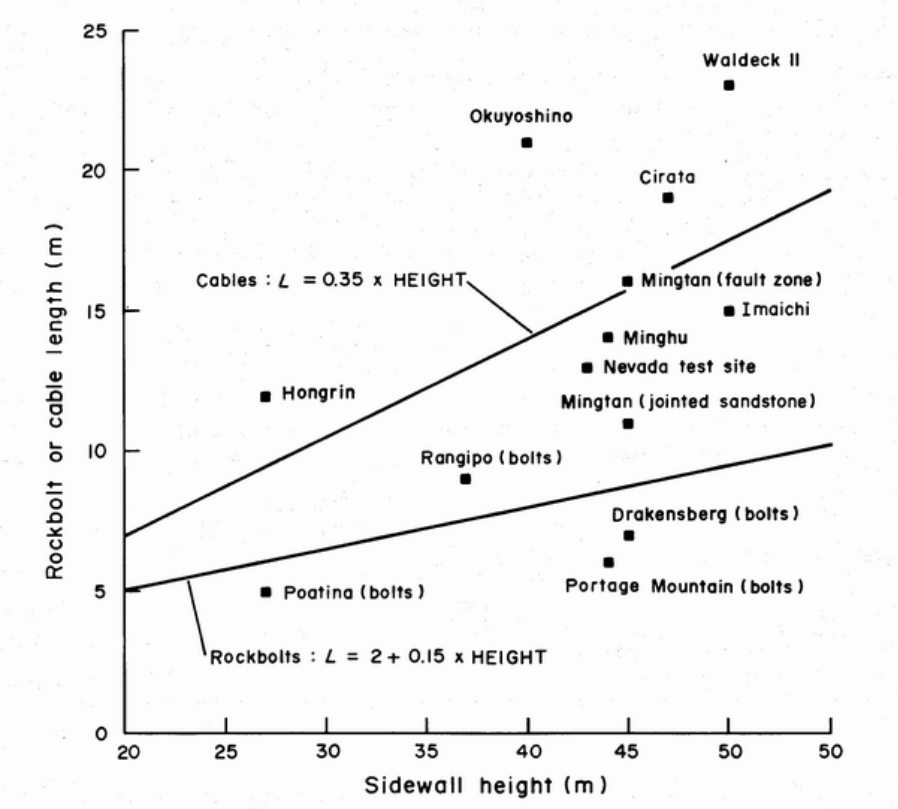

Figure 16: Precedents for rockbolt and cable lengths for different cavern sidewall heights.

Early in the design process it was decided to use cables rather than rockbolts as the primary support system. As can be seen from Figures 15 and 16, the chosen cable lengths were between 10 and 12 m for the roof and 10 and 15 m for the sidewalls of the cavern, depending upon the material in which the cables were anchored. These cable lengths were confirmed and refined by means of the numerical analyses described later.

While shotcrete played an important role in maintaining the integrity of the exposed rock in the cavern roof and sidewalls, its contribution was ignored in designing the overall support system. The decision to ignore the contribution of shotcrete was made on the basis that shotcrete had not been used in any previous cavern construction in Taiwan and it was felt that this lack of experience could lead to shotcrete of uncertain quality and reliability. In fact, this is a prudent step in any cavern design where there is doubt about the control of construction quality. Shotcrete is particularly vulnerable to deficiencies in the skill of the operators. It is not wise to rely on its support effectiveness where construction quality is questionable.

Interactive design using numerical analysis

The main contract for the construction of the Mingtan underground complex was an Owner-Engineer-Contractor Target Price contract in which the Engineer played a very active role during construction. The good-for-construction drawings indicated the construction sequence, the lengths of cables and rockbolts and the thickness of the shotcrete, but included considerable latitude for these items to be varied during construction, depending upon the measured performance of the support elements.

Seven instrumentation stations were set up along the axis of the cavern. These consisted of grouted rod extensometers in the roof and sidewalls as well as cable anchor load cells on selected cables that were left ungrouted. The roof extensometers, illustrated in Figure 17, played a critical role in the interactive design process since these were installed before excavation of the cavern commenced and they provided a calibration of the assumed rock mass properties used in the numerical models.

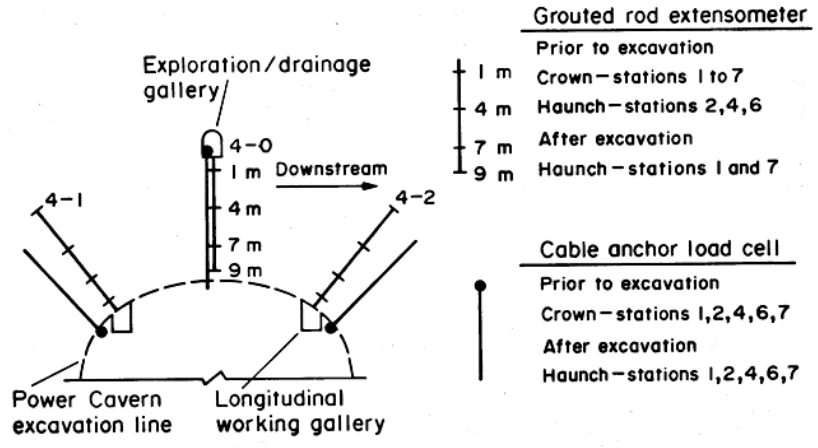

Figure 17: Typical instrumentation array installed in the cavern roof before excavation of the cavern commenced.

The two-dimensional finite difference Itasca program FLAC was the primary tool used for back-analysis of the measured response of the rock mass above the roof of the cavern and for analysis of the remaining support system.

When construction of the cavern commenced, the deformations in the roof were measured by means of the extensometers illustrated in Figure 17. These deformations were compared with those predicted by the numerical modelling. It was found that the deformations in the immediate vicinity of the roof were significantly greater than predicted. Therefore, it was necessary to reduce the modulus of the rock mass in this region by a factor of almost 2 in order to bring the predicted and measured values into coincidence. It was concluded that this modulus reduction was due to blast damage and, for the remaining numerical models, a 2 m thick zone of "blast damaged" rock was wrapped around each excavation stage.

The properties of the rock mass and blast damaged zone, derived from back analysis of the cavern arch excavation, are listed in Table 6. Comparing these properties with those listed in Table 4 shows a reasonable agreement although the cohesive strengths are generally lower than those predicted from the laboratory tests.

Table 6: Rock mass properties derived from back-analysis of cavern arch excavation

Rock type	*c* *MPa*	*ϕ* *degrees*	*E* *GPa*
Jointed sandstone	1.0	50	6.0
Bedded sandstone	0.8	45	4.5
Faults or shear zones	0.15	30	2.0
Blast damage zone	0.2	45	2.5

The appearance of the initial blast results in the first section of the cavern to be excavated is illustrated in Figure 18. The dipping bedded sandstone made it very difficult to achieve an accurate excavation profile and that loosening of the rock mass immediately behind this profile is inevitable. Figure 19 shows that, as experience was gained, the appearance of the cavern improved significantly.

Typical numerical modelling details are illustrated in Figures 20 and 21. In this case the model has been re-created using the RocScience program Phase2 rather than FLAC which was used for the original analysis. This model was excavated in six stages and the cable reinforcement was installed in each stage to simulate the actual construction sequence. This model shows that the rock mass failure (denoted by the × symbol for shear and the o symbol for tension) are generally well contained by the envelope of the reinforcing cables. The deformation of the cavern boundary is evenly distributed around the cavern perimeter thereby satisfying one of the key criteria for acceptability of the performance of the support system.

Figure 18: Blast damage in the first section of the cavern arch to be excavated.

Figure 19: Completed excavation of the cavern arch.

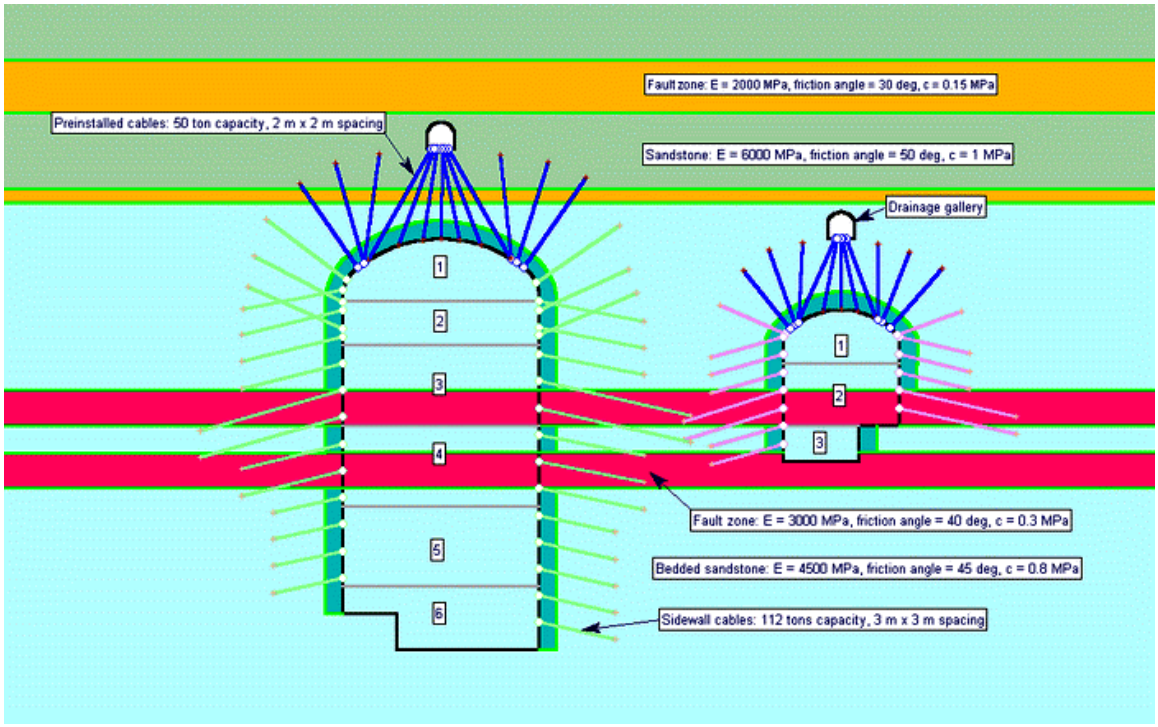

Figure 20: Numerical model showing distribution of material and layout of reinforcement in the rock mass surrounding the caverns.

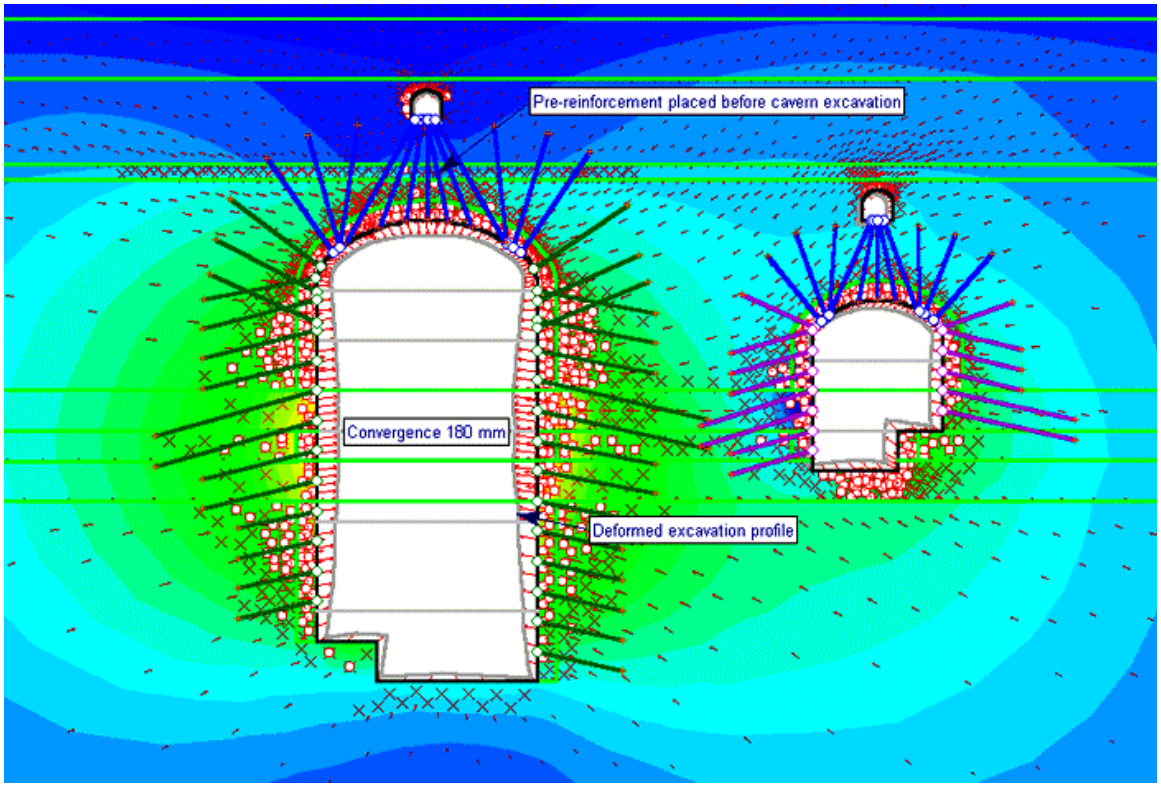

Figure 21: Typical results from numerical modelling showing rock mass failure and deformation of the cavern boundaries.

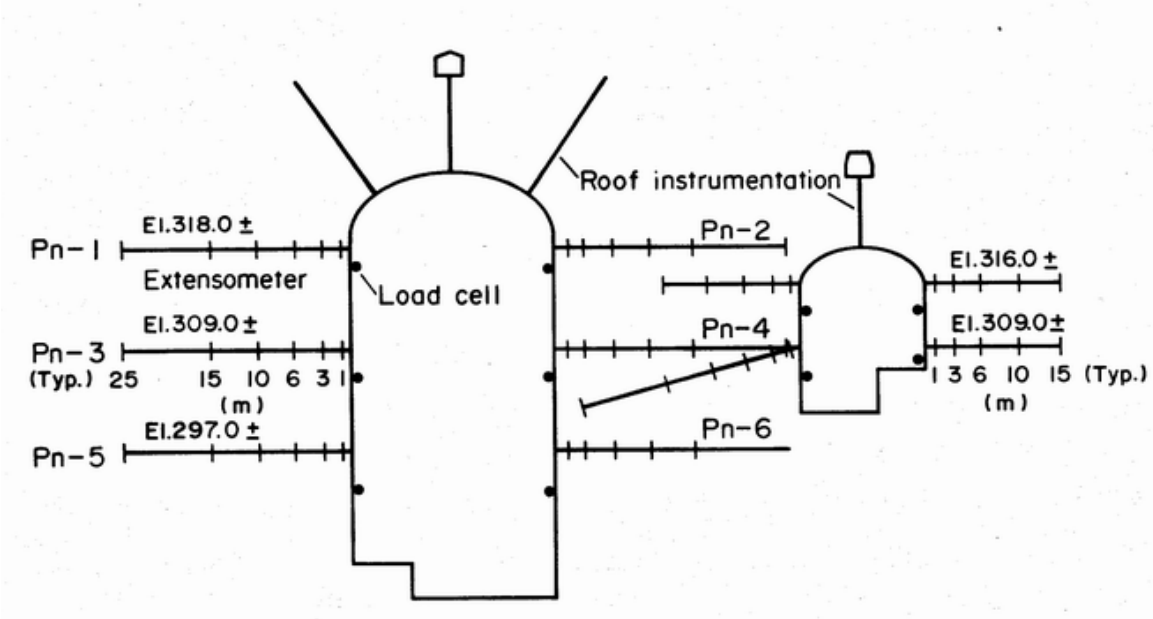

Figure 22: Typical layout of sidewall extensometers for the Mingtan underground complex.

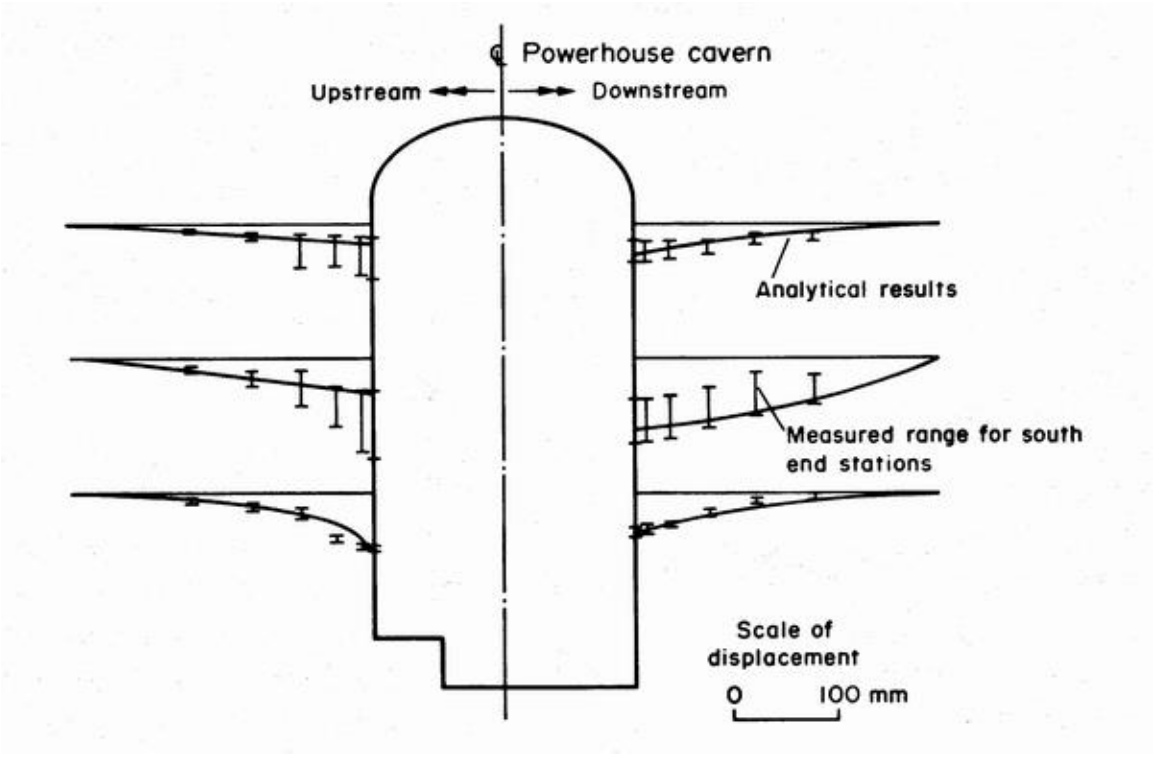

Figure 23: Comparison between predicted and measured deformations in the Mingtan power cavern sidewalls.

The layout of the extensometers in the cavern sidewalls is illustrated in Figure 22 while Figure 23 shows a comparison between the measured and predicted sidewall deformations. In general, the agreement between the measured and predicted deformations for all seven measuring stations along the cavern was very good. The use of the numerical model proved to be a very powerful tool in ongoing refinement of the cavern support design as construction progressed.

Details of the cables installed in the roof and sidewalls of the Mingtan powerhouse cavern are given in Figure 24.

Temporary crane beam design

A critical factor in the design of any large cavern is the availability of cranes to assist in the various stages of construction. When the cavern roof is supported by means of rockbolts or cables and shotcrete, it is particularly important to maintain access to the roof at all stages. This is necessary because the shotcrete tends to crack due to deformation induced by downward excavation of the cavern. In addition, damage to the rockbolts or cables needs to be repaired, as well, it is sometimes necessary to install additional reinforcement to deal with unanticipated problems.

In the case of the Mingtan Cavern, extensometer measurements in one part of the cavern roof indicated that excessive movements were occurring. Close inspection of this area revealed that a set of intersecting discontinuities had released a wedge of rock which was not adequately supported. Because this problem was detected in good time, it was remedied by the installation of additional cables in the area. The availability of a crane at this stage of construction was important since it enabled continuous inspection and repair of the cavern roof.

There are various approaches to the provision of cranes in large caverns. In some cases, the temporary construction crane is supported on light rails which are rockbolted to the cavern sidewalls. This was the case for the Mingtan Cavern. The temporary crane rails are shown in Figure 25 which is a view of the cavern from the temporary crane platform. As shown in Figure 11, the permanent crane is supported on rails carried on concrete columns.

Another approach is to combine permanent and temporary crane beams into a single system. This was done for the Drakensberg Pumped Storage Project in South Africa where heavy cast-in–place concrete beams were anchored to the cavern walls as illustrated in Figure 26. These provided support for both the temporary construction crane, illustrated in Figure 27, and for the main cavern crane.

Figure 28 shows the crane beam suspended from the curved sidewalls of an elliptical power cavern in the Singkarak hydroelectric project in Indonesia. A different approach is illustrated in Figure 29 which shows the crane beams for the temporary construction crane in the Thissavros project in Greece. These beams were later supported on concrete columns to provide support for the much heavier main crane.

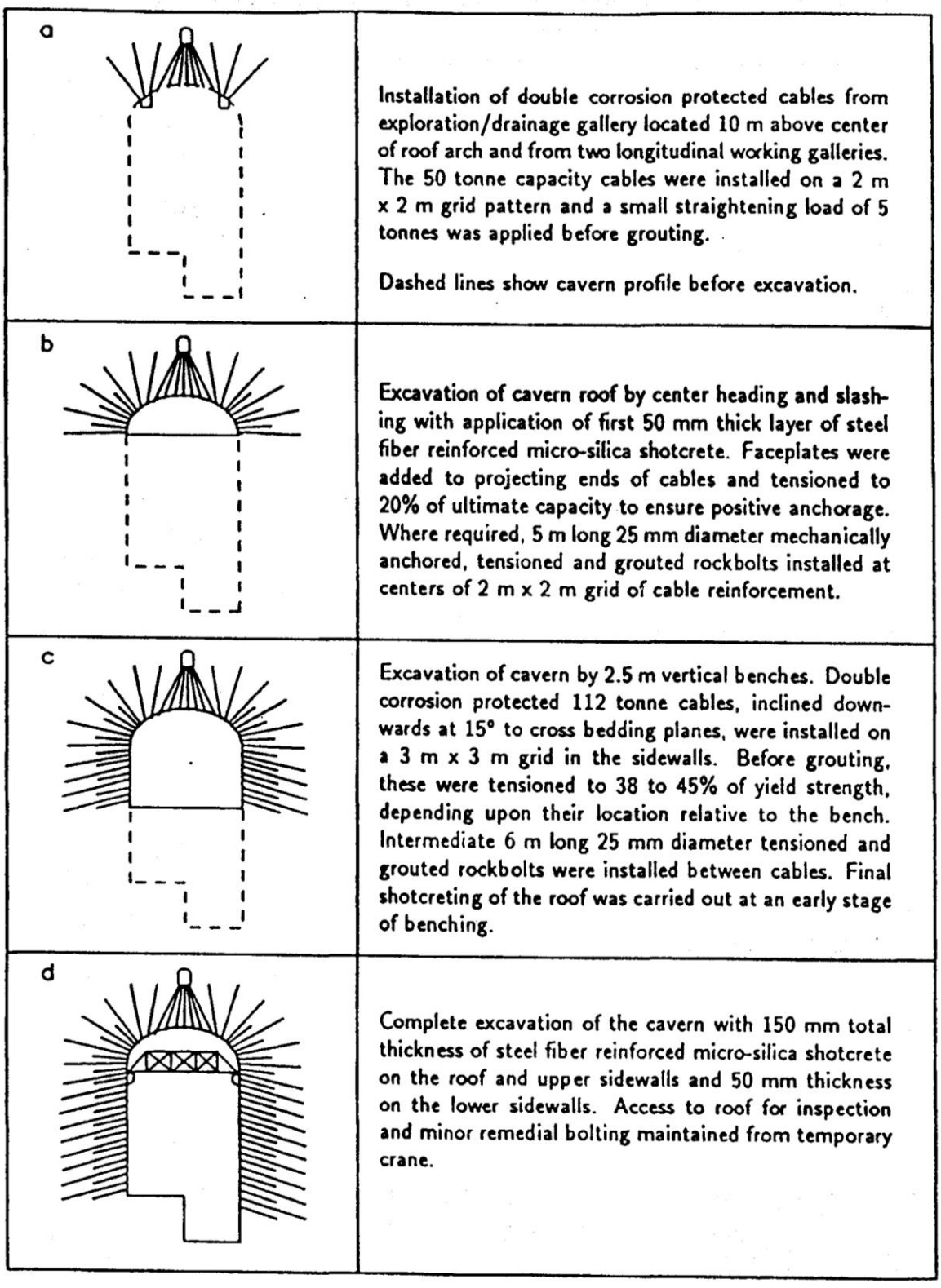

Figure 24: Details of cable support installed in the Mingtan power cavern.

Figure 25: View of the Mingtan cavern from the platform of a temporary construction crane supported on rails bolted to the cavern walls.

Figure 26: Cast in place concrete crane beam being anchored to the sidewall of the power cavern of the Drakensberg Pumped Storage Project in South Africa.

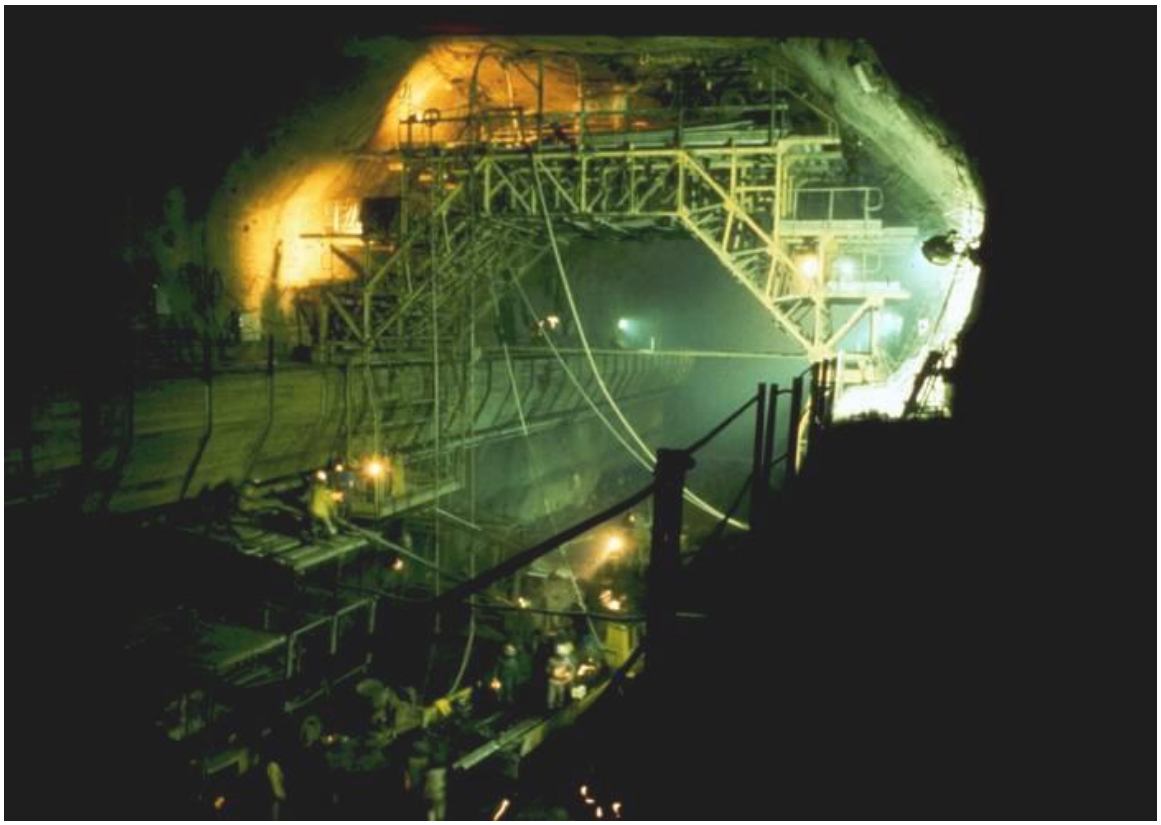

Figure 27: Temporary construction crane running on the main crane beams of the Drakensberg power cavern.

Figure 28: Crane beam anchored to the curved wall of the elliptical power cavern of the Singkarak hydroelectric project in Indonesia.

Figure 29: Crane beams rock bolted to the walls of the power cavern of the Thissavros hydroelectric project in Greece. These rails provided support for the temporary construction crane shown in the photograph. The stubs projecting from the bottom of the beams were later attached to concrete columns that provided support for the main crane.

Need for three-dimensional numerical modelling

The design of the Mingtan underground complex was carried out with the aid of two-dimensional numerical models. A few three-dimensional model analyses were carried out but these were of limited value in this project. On the other hand, in some projects it is important to use three-dimensional models to study critical elements of the design. In particular, the bus tunnels, linking the powerhouse and the transformer caverns and the draft tubes at the base of the power cavern, can create critical construction problems in weak or heavily structured rock masses.

Figure 30 shows a three-dimensional model of the underground complex of the Nathpa Jhakri hydroelectric project in India. This model was created using the program 3DEC and was used to investigate the overall stability of the cavern complex in a rock mass in which the properties varied significantly along the length of the complex.

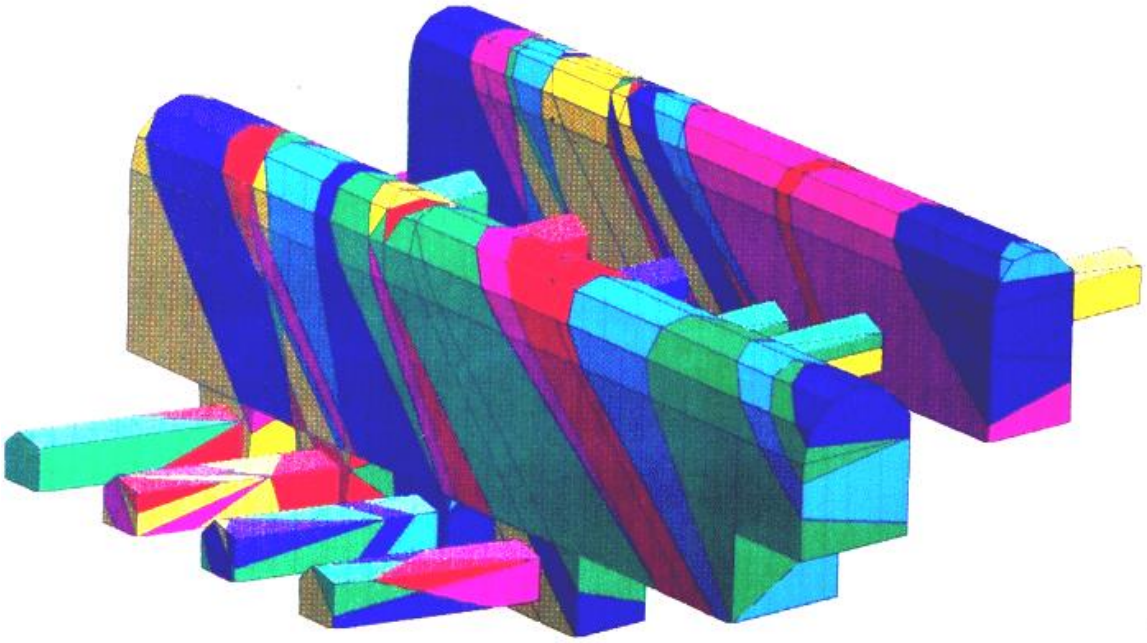

Figure 30: Three-dimensional 3DEC model of the Nathpa Jhakri underground caverns in India. Different colours in the model denote different rock mass properties. The complexity of the intersections of the four draft tubes and the lower part of the cavern can be seen in this illustration. This model study was carried out by Dr B. Dasgupta.

Long-term performance

While the Mingtan support system described earlier performed very well during construction, there was some concern about its long-term performance and its response to possible creep movements in the rock mass. Consequently, monitoring of many of the instrument arrays was continued for several years after construction.

The early part of the monitoring record for the roof and haunch extensometers in the Mingtan power cavern is shown in Figure 31. These curves show rapid response of the extensometers to excavation of the top heading and upper benches. This is followed by stabilisation of the deformations as the cavern is benched down to its lowest elevation.

In the ten years since the project was completed and put into operation, ongoing measurements of some of these instruments has shown that long-term movement of the rock mass is negligible. This confirms typical observations in most rock masses, other than rheological material such as salt and potash, in which excavations, that have been fully stabilised, do not exhibit time dependent behaviour.

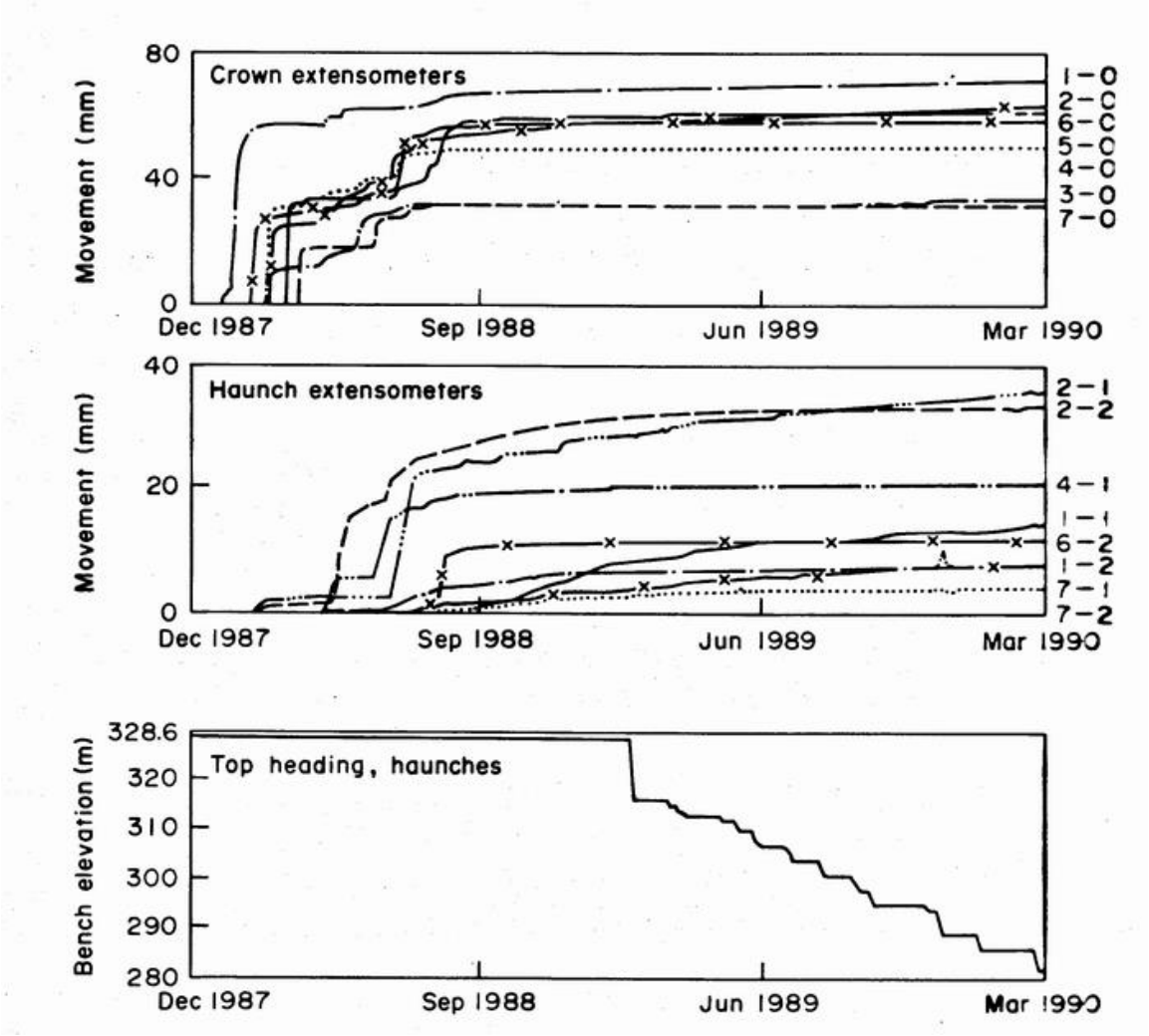

Figure 31: Response of crown and haunch extensometers in the seven monitoring sections along the length of the Mingtan power cavern.

The ultimate test – earthquake loading

A Richter magnitude 7.6 earthquake occurred very close to the Sun Moon Lake in the central mountains of Taiwan on September 21, 1999. The epicentre of this earthquake has been placed at approximately 15 km from the Mingtan Project, as illustrated in Figure 32.

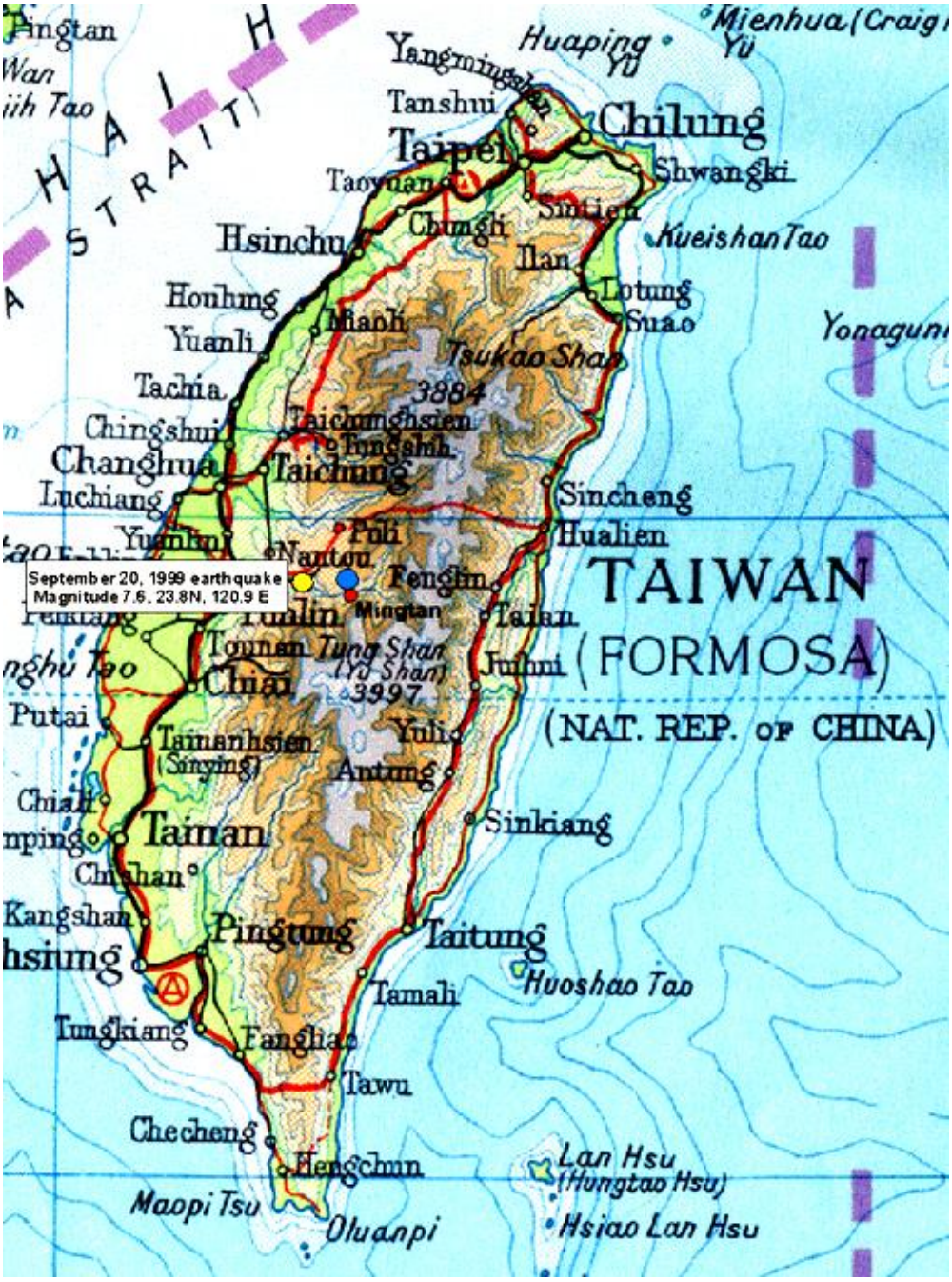

Figure 32: Location of the September 21, 1999 Richter magnitude 7.6 earthquake in relation to the Mingtan project.

In accordance with normal underground cavern design procedures, no allowance had been made for earthquake loading in the design of the Mingtan underground complex. Hence the loading imposed by the large earthquake of September 21, 1999, represented an ultimate test of the validity of this design approach. Incidentally, it was reported that 98% of the buildings were structurally damaged in the town of Puli, close to the earthquake epicentre.

Soon after the earthquake, the Sun Moon Lake area was visited by a team organised by University of California, Berkeley, and funded by the US National Science Foundation. Dr Mike McRae of Jacobs Associates, consulting engineers in El Segundo, California, was a member of this team and his comments on the visit are as follows[2]:

"We visited Mingtan and Minghu and both facilities exhibited only minor damage. Minghu exhibited some hairline cracks in the sidewalls of the main chamber and several new leaks had developed in the upstream wall of the powerhouse, the largest (about 10 gpm) being in the area of the penstock intersection closest to the control room. Some localised spalling in the granite tiles in the floor of the powerhouse had also occurred. It was also reported to us that the inflows into the drainage gallery had increased.

The results of the instrumentation at Mingtan indicates 5 mm of additional crown displacement following the earthquake and an increase in the water inflow from 0.027 m^3/sec to 0.05 m^3/sec. During our inspection of the roof of the powerplant we observed some very localised cracking in the shotcrete with the cracks being up to 12 mm wide and up to 2.5 m long. It appears that seismically induced movements in the localized blocks were responsible for the cracking. No significant leaks were observed in the crown. Some minor cracks were also observed in the wall near the control room."

Acknowledgements

The permission of the Taiwan Power Company and of Sinotech Engineering Consultants Inc., to use the material presented in these notes, is gratefully acknowledged.

References

Cheng, Y. 1987. New development in seam treatment of Feitsui arch dam foundation. *Proc. 6th cong. ISRM, Montreal*, 319-326.

Cheng, Y. and Liu, S.C. 1990. Power caverns of the Mingtan Pumped Storage Project, Taiwan. In *Comprehensive Rock Engineering* (ed. J.A. Hudson) **5**, 111-132. Oxford: Pergamon.

[2] Fax from Mike McRae to Evert Hoek, 14 October 1999.

Hoek, E and Brown E.T. 1988. The Hoek-Brown failure criterion - a 1988 update. *Proc. 15th Canadian Rock Mech. Symp*. (ed. J.H. Curran). Toronto: 31-38. Civil Engineering Dept., University of Toronto.

Hoek, E. and Brown E.T. 1980. *Underground Excavations in Rock*. London: Instn Min.Metall.

Hoek, E. and Moy, D. 1993. Design of large powerhouse caverns in weak rock. In *Comprehensive rock engineering*, (ed. J.A. Hudson) **5**, 85-110. Oxford: Pergamon.

Rocha, M., Silvério, A., Pedro, J.O. and Delgado, J.S. 1974. A new development of the LNEC stress tensor gauge. *Proc. 3rd ISRM congress, Denver*. **1**.

Wittke, W. 1990. *Rock Mechanics – Theory and Applications with Case Histories.* Berlin: Springer-Verlag.

15. The Rio Grande project - Argentina

Introduction

The Rio Grande Pumped Storage Project is located on the Rio Grande River near the town of Santa Rosa de Calamucita in the Province of Cordoba in Argentina. It has an installed capacity of 1000 MW and provides electrical storage facilities for the power grid and, in particular, for a nuclear power plant about 50 km away from Rio Grande.

The project is owned by Agua y Energia Electrica, one of the principal Argentinean electrical utility organisations. Preliminary feasibility studies were carried out by the owner, followed by detailed design studies by Studio G. Pietrangeli of Rome. The scheme was partly financed by Italy and some of the construction was done by Condote de Agua, an Italian contractor. I was involved as a senior consultant with Golder Associates, who were involved in the design and supervision of support installed to control the stability of most of the major underground excavations.

The main underground facilities are located in massive gneiss of very good quality. The upper reservoir is impounded behind a rockfill dam and water is fed directly from the intakes down twin penstocks which then bifurcate to feed into the four pump-turbines. These turbines, together with valves and the control equipment, are housed in a large underground cavern with a span of 25 m and a height of 44 m.

Draft tubes from the turbines feed into twin tunnels which, with a down-stream surge shaft, form the surge control system for this project. The twin tunnels join just downstream of the surge tank and discharge into a single tailrace tunnel with a span of 12 m and height of 18 m. This tailrace tunnel is about 6 km long, constructed by a full-face drill-and-blast top heading, with a span of 12 m and height of 8 m, followed by a 10 m benching operation. A view of the top heading is given in Figure 1.

Tailrace tunnel support

Because of the excellent quality of the gneiss, most of the underground excavations did not require support. Minimal provision for support was made in the contract documents. Assessment of underground stability and installation of support, where required, was done on a ‘design-as-you-go’ basis which proved to be very effective and economical. Reports from site, many years after the start of construction and commissioning of the plant, show that there were no problems with rockfalls or underground instability.

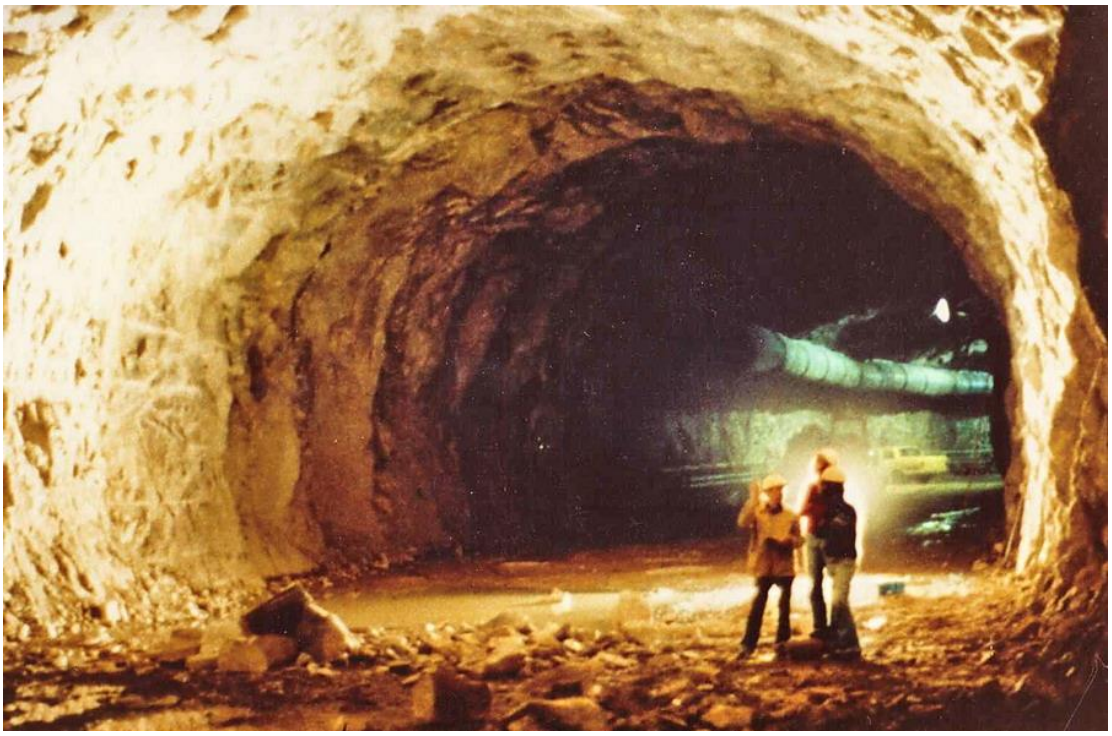

Figure 1: The 12 m span 8 m high top heading for the tailrace tunnel was constructed by full-face drill-and-blast and, because of the excellent quality of the massive gneiss, was largely unsupported.

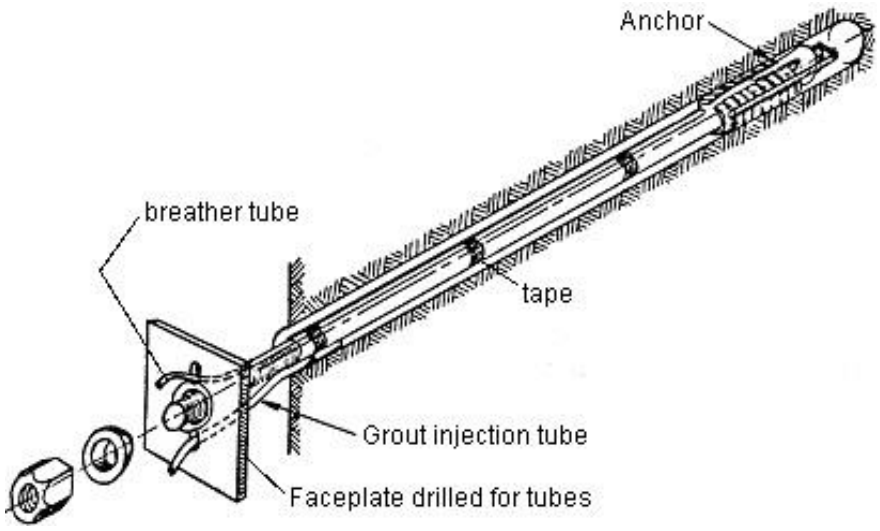

Figure 2: Mechanically anchored rockbolts of the type used on the Rio Grande project. These bolts were tensioned to 70% of their yield load upon installation and then, at a later stage, were re-tensioned and fully grouted.

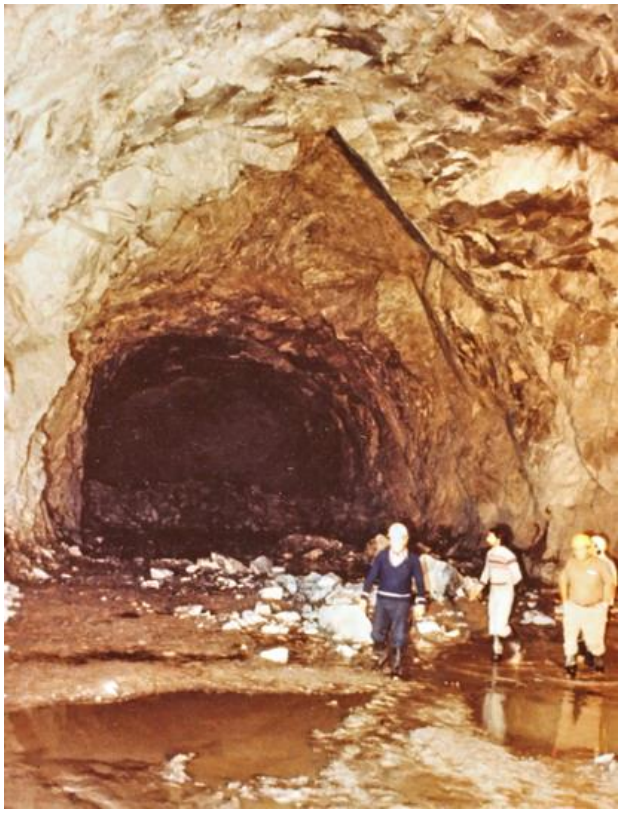

Figure 3: A wedge failure in the roof of the top heading of the Rio Grande tailrace tunnel.

Decisions on support were made on the basis of inspection of the excavated faces by a resident team of geotechnical engineers. Where the appearance of the face indicated that a zone of heavily jointed rock, usually associated with faulting, was being entered, the top heading was reduced to a 6 m span by 8 m high pilot tunnel to limit the volume of unstable rock which could be released from the roof. This pilot tunnel was large enough to accommodate the seven-boom jumbo, as illustrated in Figure 4, but small enough to limit the size of roof falls to manageable proportions. Bolting from inside the pilot heading was used to pre-support the potentially unstable wedges and blocks in the roof.

In the case of the tailrace tunnel, which is a large excavation, the support comprised mechanically anchored and cement grouted rockbolts as illustrated in Figure 2, with mesh reinforced shotcrete where required. These bolts were generally installed to control the type of wedge failure illustrated in Figure 3. In the case of particularly large wedges, calculations of the factor of safety and support requirements were carried out on a programmable calculator, using an early version of the program UnWedge.

Figure 4: A 6 m wide heading driven ahead of the tunnel face to permit pre-reinforcement of potentially unstable wedges in the roof. The seven-boom jumbo is seen working in the heading.

Support for power cavern

A cross-section of the power cavern is given in Figure 5. This figure includes the five main excavation stages for the cavern. Careful mapping of significant structural features in the roof and walls of the central access drive at the top of the cavern provided information for estimating potentially unstable blocks and wedges which could form in the roof of the cavern. Figure 6 illustrates a number of such wedges in one section of the cavern roof. At each stage of the cavern excavation, long rockbolts (up to 10 m length) were installed to stabilise wedges or blocks which had been determined as being potentially unstable.

Because gneiss has usually undergone some tectonic deformation during its geological history, projection of structural features from visible exposures tends to be an imprecise process. Consequently, the potentially unstable blocks and wedges had to be reassessed after each excavation step revealed new information. The structural plan illustrated in

Figure 6 had to be modified many times during excavation and it shows the final plan prepared after the full cavern roof had been exposed.

A general view of the cavern excavation is given in Figure 7. This photograph was taken when the bulk of the cavern had been completed and only a few benches in the bottom of the cavern remained to be excavated. The enlarged top of the cavern is to accommodate the overhanging crane that is supported on columns from the cavern floor. An alternative design for this cavern would have been to support the crane on concrete beams anchored to the walls as is commonly done in good quality rock.

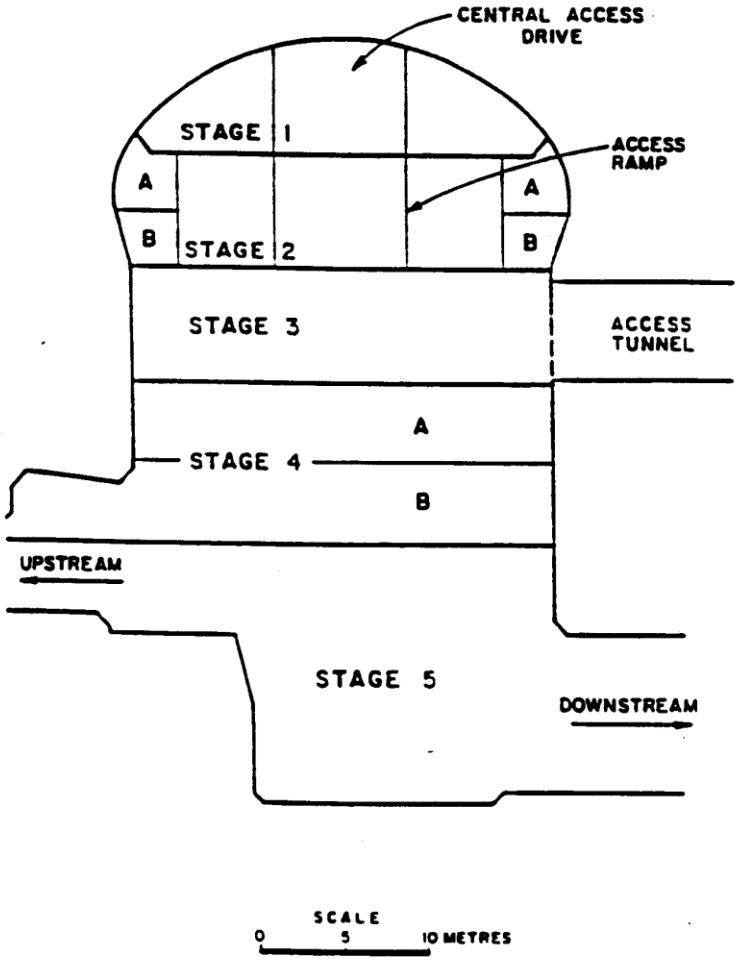

Figure 5: Cavern profile and excavation stages.

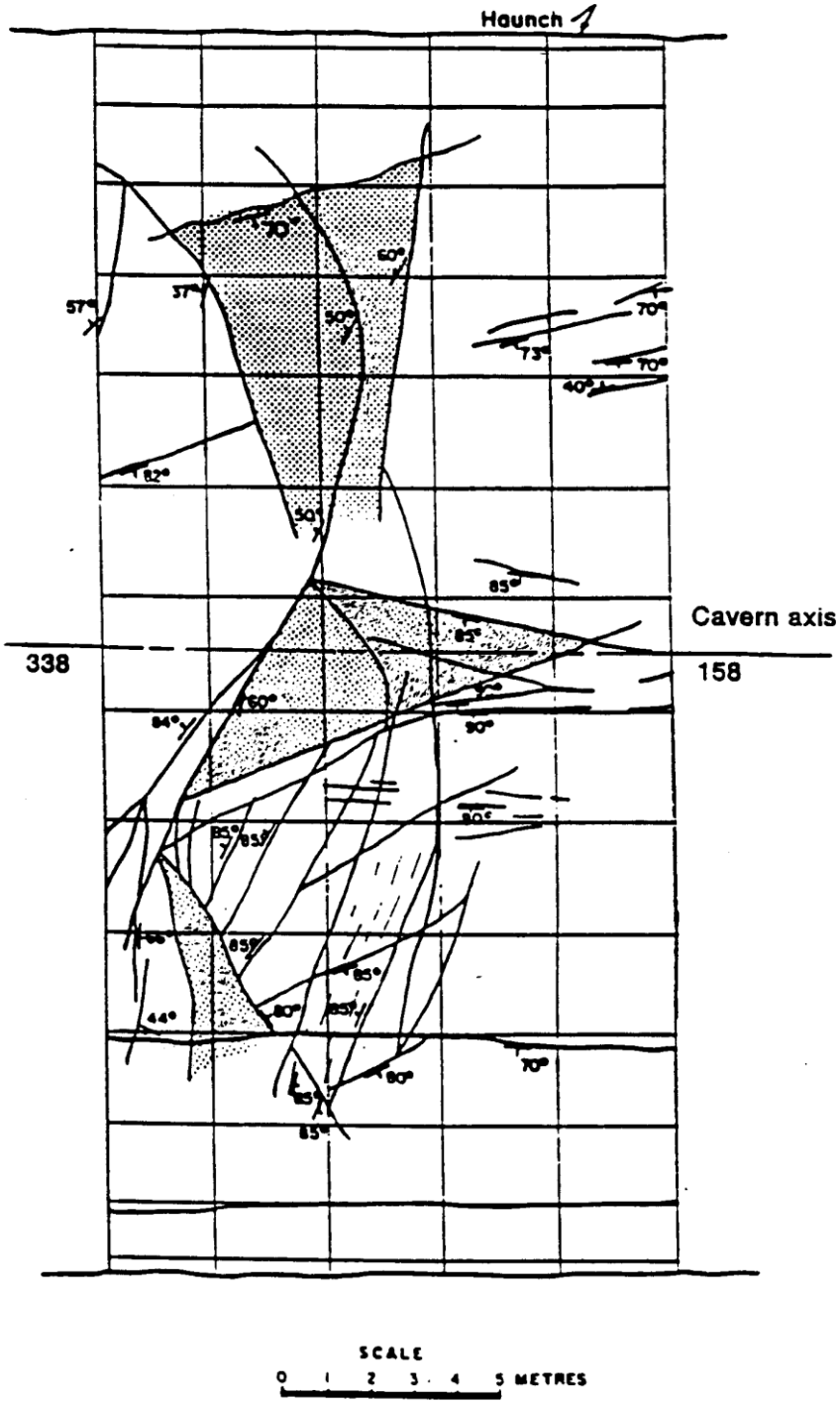

Figure 6: A plan of the traces of geological features mapped in part of the cavern roof. The shaded areas represent potentially unstable wedges requiring reinforcement.

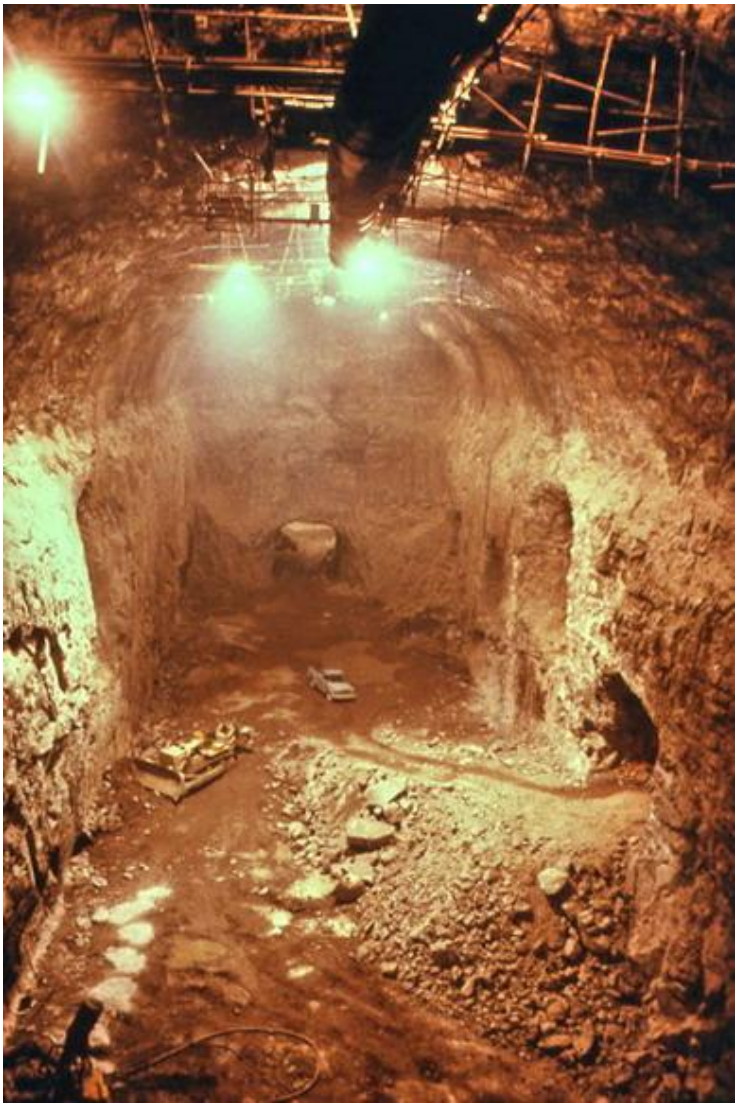

Figure 7: A view of the 25 m span Rio Grande power cavern during excavation of the lower benches.

Discussion of support design and costs

Apart from rockbolts installed to control isolated, structurally controlled, blocks and wedges in the roof and sidewalls and some areas of closely jointed rock which were shotcreted, the cavern was unsupported. While this was successful for this particular project, it is not the approach which should generally be used for a critical excavation such as an underground powerhouse.

The damage resulting from even a small rockfall in such a cavern is out of all proportion to the savings achieved by eliminating pattern rock bolting and full shotcrete lining. Hence, in addition to the rockbolts installed to control structural instability, as described earlier, I would recommend a normal pattern of 25 mm diameter, 5 m long bolts (20% of the excavation span) on a 2.5 m grid. In addition, I would recommend the placement of 50 mm of fibre-reinforced micro-silica shotcrete over the entire roof and upper sidewalls of the cavern. Based on current north American costs, this additional support, involving approximately 600 rockbolts and about 300 m^3 of shotcrete, would have cost approximately US $200,000. In terms of the overall project cost and the increased long-term security in the cavern, this would normally be regarded as a good investment.

In contrast, consider the 6 km long tailrace tunnel in which the consequences of a small rockfall are minimal. Assume that a pattern of 4 m long bolts on a 2 m grid (say 10 bolts per section) and a 50 mm shotcrete thickness had been specified for the roof and upper sidewalls of the tailrace tunnel. This would involve 30,000 bolts and 5,400 m^3 of shotcrete at a total cost approaching US $5 million. This example illustrates the need to give careful consideration to the function and risks associated with each underground excavation before deciding upon the support system to be used.

Analysis using UnWedge program

UnWedge[1] is a user-friendly micro-computer program which can be used to analyse the geometry and stability of wedges defined by intersecting structural discontinuities in the rock mass surrounding an underground excavation. The analysis is based upon the assumption that the wedges, defined by three intersecting discontinuities, are subjected to gravitational loading only. In other words, the stress field in the rock mass surrounding the excavation is not taken into account. While this assumption leads to some inaccuracy in the analysis, it generally leads to a lower factor of safety than that which would occur if the in-situ stresses were taken into account.

The application of the program UnWedge to the analysis of a potentially unstable wedge in the Rio Grande cavern is illustrated in the following discussion.

Input Data

The dips and dip directions of a number of planes can be entered directly into the table which appears when the ‘Input data’ option is chosen or this information can be entered in the form of a DIPS file. Once the data has been read into the program, the great circles representing the discontinuities are displayed on the screen as illustrated in Figure 8 and the user is prompted to select the three joint planes to be included in the analysis. Alternatively, the program can be instructed to compute the three most critical planes –

[1] Available from www.rocscience.com

those giving the largest wedges with the lowest factors of safety. Once the information on these planes has been entered, the unit weight of the rock and the shear strengths of the joints are entered. Finally, the water pressure acting on the joint surface is entered. In most cases, the default water pressure of 0 will be chosen, but the user may check the sensitivity of the wedge to pore water pressure by entering appropriate values.

In the case of the rock mass surrounding the Rio Grande Cavern, the dips and dip directions of the following three sets of joints are included in Figure 8:

1 88/225 shear joint set
2 85/264 shear joint set
3 50/345 tension joint set
Cavern axis: trend 158, plunge 0

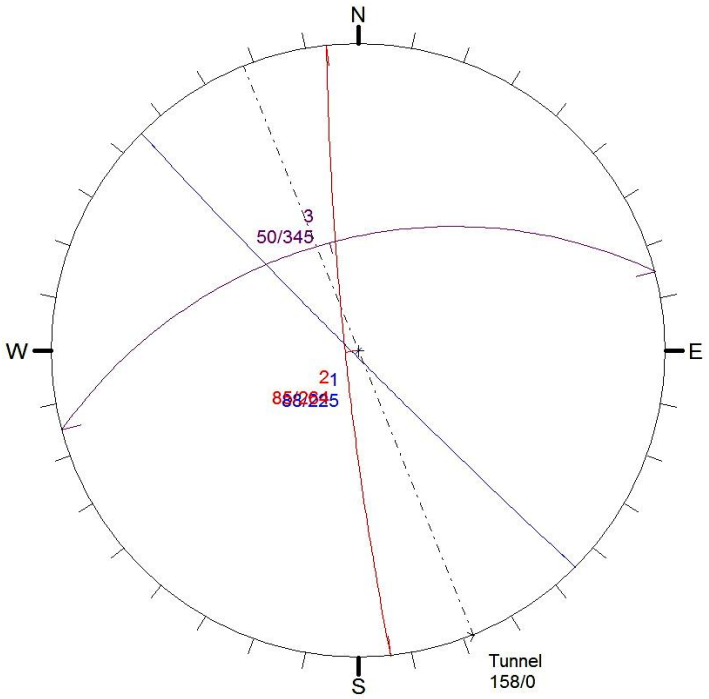

Figure 8: Great circles representing four joint sets which occur in the rock mass surrounding the Rio Grande cavern - imported as a DIPS file.

Input of excavation cross-section

In setting up this analysis, the co-ordinates shown in Figure 9 were used to define the cavern profile. These co-ordinates must be entered sequentially and must form a closed

figure. The profile is formed from straight line and arc segments. A sufficient number of co-ordinates should be entered to ensure that a smooth profile is generated.

Determination of wedge geometry

Depending upon the shape of the cross-section, a maximum of six wedges can be formed with three intersecting joint planes. Selecting the '3D wedge view" option gives a number of views showing the shape and size of these wedges. The two wedges formed on the cavern end walls can be viewed by activating the 'End wedges' option.

Figure 10 shows the wedges formed in the case of the Rio Grande power cavern for the three joint planes defined in Figure 8. The weight of each of these wedges, the failure mode and the calculated factor of safety are shown in the figure. Obviously, the most dangerous wedge in this situation is the wedge formed in the roof while the wedge formed in the floor is stable and need not be considered further in this analysis.

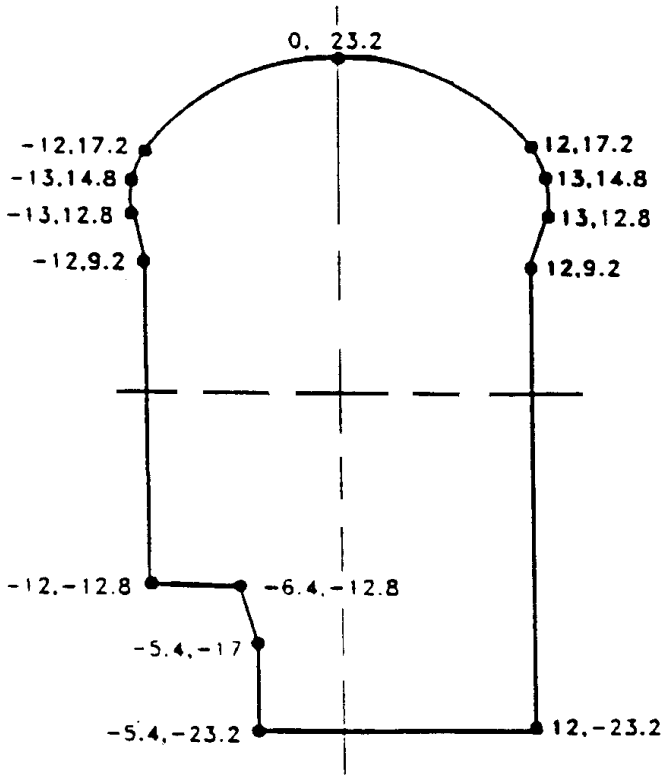

Figure 9: Co-ordinates used to define the profile of the cavern.

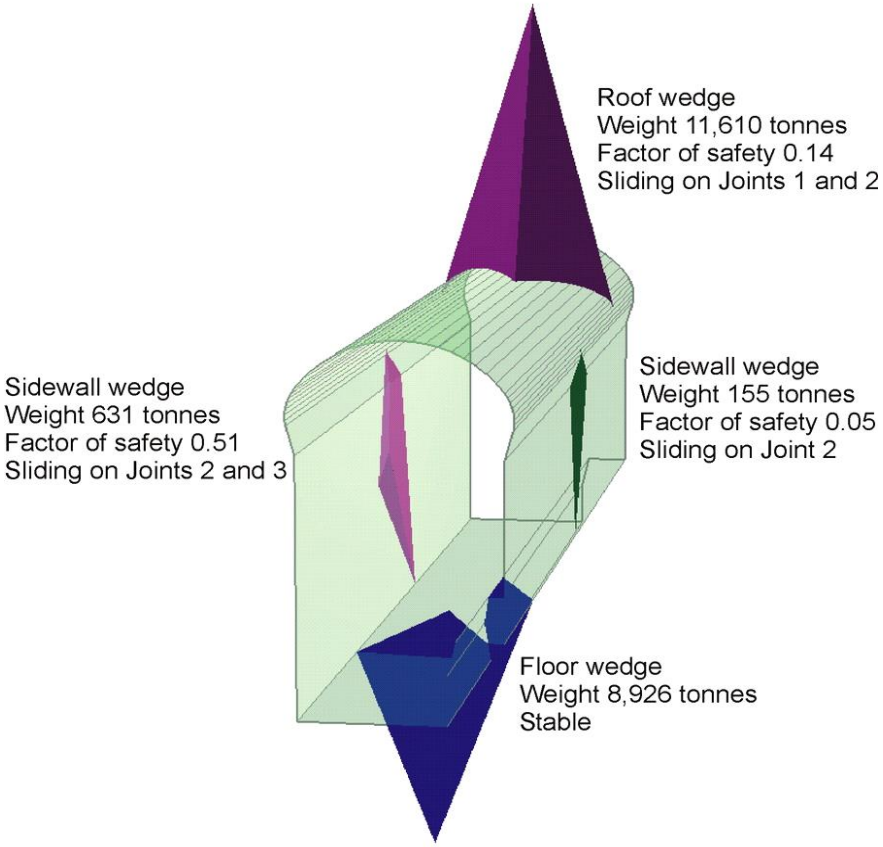

Figure 10: Perspective view of the wedges formed in the rock mass surrounding the Rio Grande power cavern.

Sizing or wedges

The program UnWedge automatically determines the largest wedge that can occur in the rock mass adjacent to the excavation profile. In the case of the roof wedge, shown in Figure 10, the wedge extends over the full 25 m span of the cavern and weighs 11,610 tonnes. While, in exceptional circumstances, such wedges may occur, the limited extent of joints in many rock masses will restrict the size of the wedges to much smaller dimensions than those determined by UnWedge for the large excavations.

As illustrated in Figure 6, the trace length of joint number 3 (50/345) in the upper roof wedge is approximately 6 m. When the 'Scale wedges' is chosen, the user can define the size of the wedge in terms of the area of the face on the excavation surface, the volume of the wedge, the height of the apex of the wedge, the length of one of the joint traces or the persistence of one of the joints. In this case a trace length of 6 m is entered for joint

number 3, defined by 50/345, and the resulting wedge is illustrated in Figure 11. This wedge weighs 220 tonnes and will require about seven 50 tonne capacity fully grouted cables to give a factor of safety of about 1.5 which is considered appropriate for a cavern of this type.

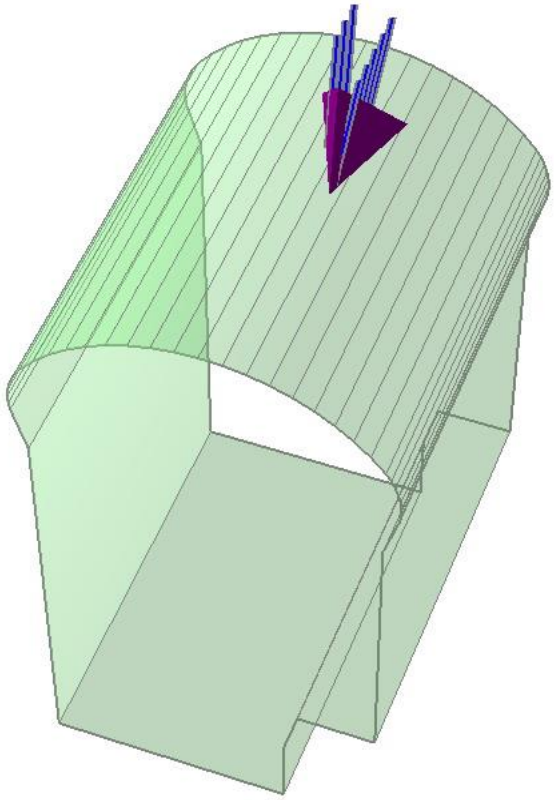

Figure 11: Perspective view of roof wedge in the Rig Grande cavern roof. The size of this wedge has been defined by setting the trace length of the 50/345 joint to 6 m. Eight 10 m long 50 tonne capacity grouted anchors give a factor of safety of 1.6.

UnWedge allows the user to add a layer of shotcrete and calculates the factor of safety increase as a result of such an addition. Since the shotcrete can only be added once the surface of the wedge is fully exposed, it is not taken into account in calculating the support required to stabilise the wedge. The increase in safety factor, which occurs after the shotcrete has set, can be regarded as a long-term bonus and it does allow the user to choose a slightly lower factor of safety for the immediate support of the wedge.

Conclusion

The power and transformer caverns, as well as the 12 m span 18 m high tailrace tunnel, were successfully excavated and supported using the rock bolt support discussed in this chapter. Construction commenced in 1976. The plant entered commercial operation in 1986 and the project is still in operation.

While there is little unusual in the overall design and operation of this project, the construction in the late 1970s and early 1980s was in the relatively early days of computer aided support design of underground excavations. These notes on practical rock engineering do not cover the long and complicated history of this subject since that is not their purpose. However, an interesting paper by Arturo Amos entitled, “The Rio Grande Pumped Storage Complex, Cordoba Province – A Case Study of Excavations in Contrasting Rock Anisotropy”, was published in a volume entitled, Surface and Underground Case Histories, edited by E. Hoek, which was the fifth of five volumes which make up the collection entitled, Comprehensive Rock Engineering, of which John A. Hudson was the editor in chief. This paper gives a comprehensive discussion of the project that provides historical and factual details for anyone interested in the history, geology, design and construction details.

16. Rockbolts and cables

Introduction

Rockbolts and dowels have been used for many years for the support of underground excavations and a wide variety of bolt and dowel types have been developed to meet different needs which arise in mining and civil engineering.

Rockbolts generally consist of plain steel rods with a mechanical or chemical anchor at one end and a face plate and nut at the other. They are always tensioned after installation. For short term applications the bolts are generally left ungrouted. For more permanent applications or in rock in which corrosive groundwater is present, the space between the bolt and the rock can be filled with cement or resin grout.

Dowels or anchor bars generally consist of deformed steel bars which are grouted into the rock. Tensioning is not possible and the load in the dowels is generated by movements in the rock mass. In order to be effective, dowels have to be installed before significant movement in the rock mass has taken place. Figure 1 illustrates a number of typical rockbolt and dowel applications that can be used to control different types of failure that occur in rock masses around underground openings.

The move towards larger underground excavations in both mining and civil engineering has resulted in the gradual development of cable reinforcement technology to take on the support duties which exceed the capacity of traditional rockbolts and dowels. Some of the hardware issues that are critical in the successful application of cables in underground excavations are reviewed in this chapter.

Rockbolts

Mechanically anchored rockbolts

Expansion shell rockbolt anchors come in a wide variety of styles, but the basic principle of operation is the same in all of these anchors. As shown in Figure 2, the components of a typical expansion shell anchor are a tapered cone with an internal thread and a pair of wedges held in place by a bail. The cone is screwed onto the threaded end of the bolt and the entire assembly is inserted into the hole that has been drilled to receive the rockbolt. The length of the hole should be at least 100 mm longer than the bolt. Otherwise the bail will be dislodged by being forced against the end of the hole. Once the assembly is in place, a sharp pull on the end of the bolt will seat the anchor. Tightening the bolt will force the cone further into the wedge thereby increasing the anchor force.

	Low stress levels	High stress levels
Massive rock	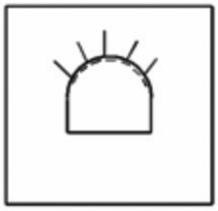 Massive rock subjected to low in situ stress levels. No permanent support. Light support may be required for construction safety.	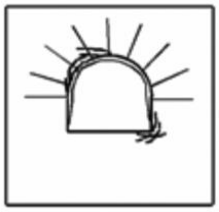 Massive rock subjected to high in situ stress levels. Pattern rockbolts or dowels with mesh or shotcrete to inhibit fracturing and to keep broken rock in place.
Jointed rock	 Massive rock with relatively few discontinuities subjected to low in situ stress conditions. 'Spot' bolts located to prevent failure of individual blocks and wedges. Bolts must be tensioned.	 Massive rock with relatively few discontinuities subjected to high in situ stress conditions. Heavy bolts or dowels, inclined to cross rock structure, with mesh or steel fibre reinforced shotcrete on roof and sidewalls.
Heavily jointed rock	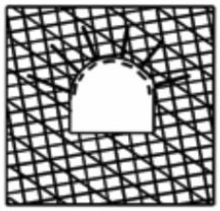 Heavily jointed rock subjected to low in situ stress conditions. Light pattern bolts with mesh and/or shotcrete will control ravelling of near surface rock pieces.	 Heavily jointed rock subjected to high in situ stress conditions. Heavy rockbolt or dowel pattern with steel fibre reinforced shotcrete. In extreme cases, steel sets with sliding joints may be required. Invert struts or concrete floor slabs may be required to control floor heave.

Figure 1: Typical rockbolt and dowel applications to control different types of rock mass failure during tunnel driving.

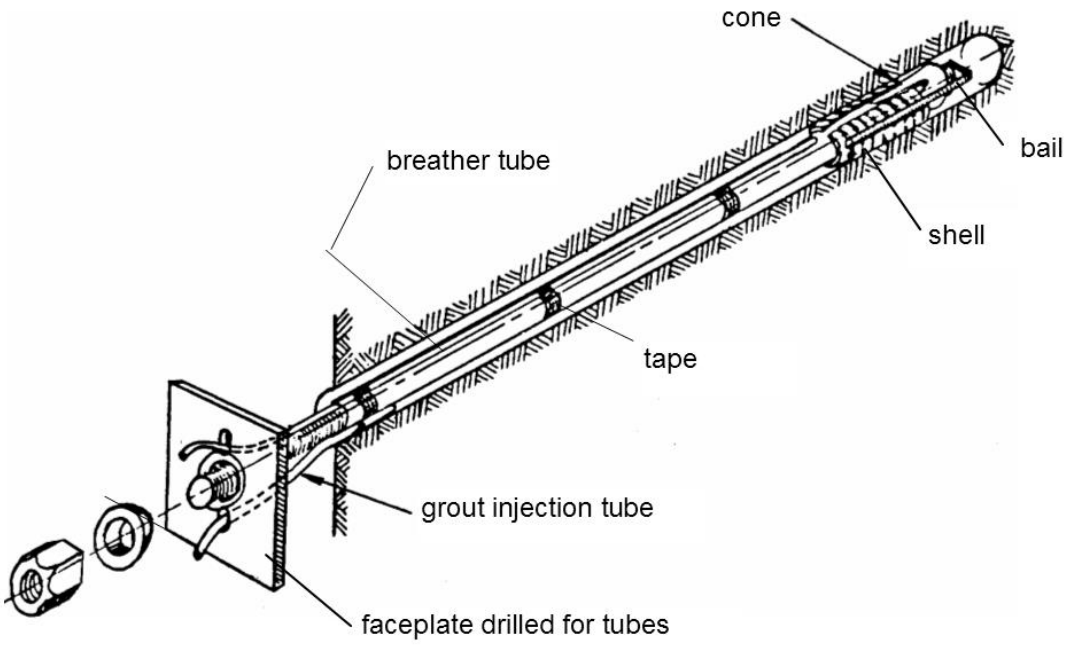

Figure 2: Components of a mechanically anchored rockbolt with provision for grouting.

These expansion shell anchors work well in hard rock, but they are not very effective in closely jointed rocks and in soft rocks, because of deformation and failure of the rock in contact with the wedge grips. In such rocks, the use of resin cartridge anchors, described later in this chapter, is recommended.

At the other end of the rockbolt from the anchor, a fixed head or threaded end and nut system can be used. In either case, some form of faceplate is required to distribute the load from the bolt onto the rock face. In addition, a tapered washer or conical seat is needed to compensate for the fact that the rock face is very seldom at right angles to the bolt. A wide variety of faceplates and tapered or domed washers are available from rockbolt suppliers.

In general, threads on rockbolts should be as coarse as possible and should be rolled rather than cut. A fine thread is easily damaged and will cause installation problems in a typical underground environment. A cut thread weakens the bolt and it is not unusual to see bolts with cut threads that have failed at the first thread at the back of the nut. Unfortunately, rolled thread bolts are more expensive to manufacture and the added cost tends to limit their application to situations where high strength bolts are required.

Tensioning of rockbolts is important to ensure that all of the components are in contact and that a positive force is applied to the rock. In the case of light 'safety' bolts, the amount of tension applied is not critical and tightening the nut with a conventional

wrench or with a pneumatic torque wrench is adequate. Where the bolts are required to carry a significant load, it is generally recommended that a tension of approximately 70% of the capacity of the bolt be installed initially. This provides a known load with a reserve in case of additional load being induced by displacements in the rock mass.

One of the primary causes of rockbolt failure is rusting or corrosion. This can be counteracted by filling the gap between the bolt and the drillhole wall with grout. While this is not required in temporary support applications, grouting should be considered where the ground-water is likely to induce corrosion or where the bolts are required to perform a 'permanent' support function.

The traditional method of grouting uphole rockbolts is to use a short grout tube to feed the grout into the hole and a smaller diameter breather tube, extending to the end of the hole, to bleed the air from the hole. The breather tube is generally taped to the bolt shank. This tends to cause problems because the tube and its attachments can be damaged during transportation or insertion into the hole. In addition, the faceplate has to be drilled to accommodate the two tubes, as illustrated in Figure 2. Sealing the system for grout injection can be a problem.

Many of these difficulties are overcome by using a hollow core bolt. While more expensive than conventional bolts, these hollow bolts make the grouting process much more reliable and should be considered wherever permanent rockbolt installations are required. The grout should be injected through a short grout tube inserted into the collar of the hole and the central hole in the bolt should be used as a breather tube. When installing these bolts in down holes, the grout should be fed through the bolt to the end of the hole and the short tube used as a breather tube.

Since the primary purpose of grouting mechanically anchored bolts is to prevent corrosion and to lock the mechanical anchor in place, the strength requirement for the grout is not as important as it is in the case of grouted dowels or cables (to be discussed later). The grout should be readily pumpable without being too fluid and a typical water/cement ratio of 0.4 to 0.5 is a good starting point for a grout mix for this application. It is most important to ensure that the annular space between the bolt and the drillhole wall is completely filled with grout. Pumping should be continued until there is a clear indication that the air has stopped bleeding through the breather tube or that grout is seen to return through this tube.

Resin anchored rockbolts

Mechanically anchored rockbolts have a tendency to work loose when subjected to vibrations due to nearby blasting or when anchored in weak rock. Consequently, for applications where it is essential that the support load be maintained, the use of resin anchors should be considered.

A typical resin product is made up of two component cartridges containing a resin and a catalyst in separate compartments, as shown in Figure 3. The cartridges are pushed to the end of the drillhole ahead of the bolt rod that is then spun into the resin cartridges by the drill. The plastic sheath of the cartridges is broken and the resin and catalyst are mixed by this spinning action. Setting of the resin occurs within a few minutes (depending upon the specifications of the resin mix) and a very strong anchor is created.

This type of anchor will work in most rocks, including the weak shales and mudstones in which expansion shell anchors are not suitable. For 'permanent' applications, consideration should be given to the use of fully resin-grouted rockbolts, illustrated in Figure 4. In these applications, several slow-setting resin cartridges are inserted into the drillhole behind the fast-setting anchor cartridges.

Figure 3: Two-component resin cartridge used for anchoring and grouting rockbolts.

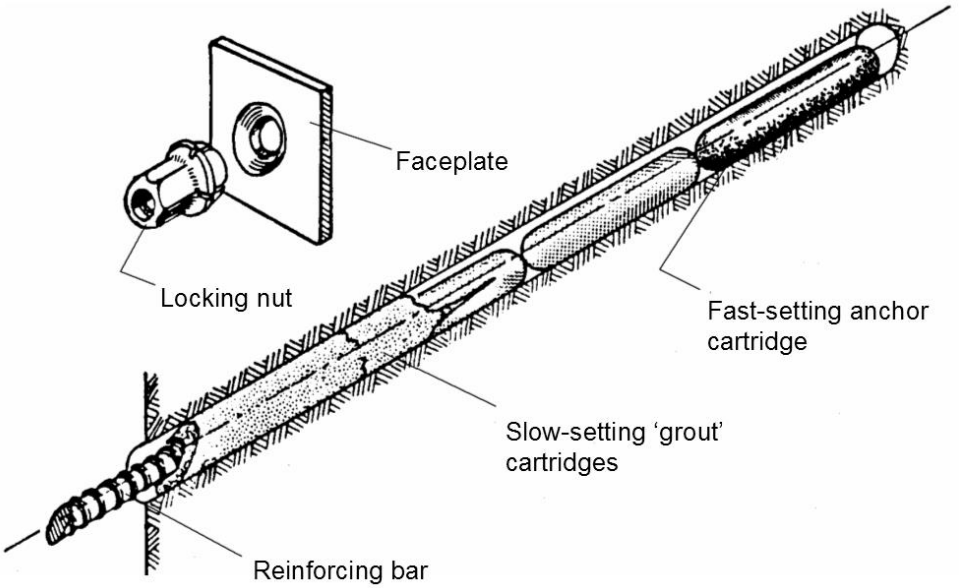

Figure 4: Typical set-up for creating a resin anchored and grouted rockbolt. Resin grouting involves placing slow-setting resin cartridges behind the fast-setting anchor cartridges and spinning the bolt rod through them all to mix the resin and catalyst. The bolt is tensioned after the fast-setting anchor resin has set and the slow-setting resin sets later to grout the rod in place.

Spinning the bolt rod through all of these cartridges initiates the chemical reaction in all of the resins but, because the slow-setting 'grout' cartridges are timed to set in up to 30 minutes, the bolt can be tensioned within two or three minutes of installation (after the fast anchor resin has set). This tension is then locked in by the later-setting grout cartridges and the resulting installation is a fully tensioned, fully grouted rockbolt.

The high unit cost of resin cartridges is offset by the speed of installation. The process described above results in a completely tensioned and grouted rockbolt installation in one operation, something that cannot be matched by any other system currently on the market. However, there are potential problems with resins.

Most resin/catalyst systems have a limited shelf life which, depending upon storage temperatures and conditions, may be as short as six months. Purchase of the resin cartridges should be limited to the quantities to be used within the shelf life. Care should be taken to store the boxes under conditions that conform to the manufacturer's recommendations. In critical applications, it is good practice to test the activity of the resin by sacrificing one cartridge from each box, before the contents are used underground. This can be done by breaking the compartment separating the resin and catalyst by hand and, after mixing the components, measuring the set time to check whether this is within the manufacturer's specifications.

Breaking the plastic sheath of the cartridges and mixing the resins effectively can also present practical problems. Cutting the end of the bolt rod at an angle to form a sharp tapered point will help in this process, but the user should also be prepared to do some experimentation to achieve the best results. Note that the length of time, or the number of rotations for spinning the resins, is limited. Once the setting process has been initiated, the structure of the resin can be damaged and the overall installation weakened by additional spinning. Most manufacturers supply instructions on the number of rotations or the length of time for spinning.

In some weak argillaceous rocks, the drillhole surfaces become clay-coated during drilling. This causes slipping of the resin cartridges during rotation, resulting in incomplete mixing and an unsatisfactory bond. In highly fractured rock masses, the resin may seep into the surrounding rock before setting, leaving voids in the resin column surrounding the rockbolt. In such cases, the use of cement grouting rather than resin grouting may provide a more effective solution.

There is some uncertainty about the long-term corrosion protection offered by resin grouts. For temporary applications, these concerns are probably not an issue because of the limited design life for most rockbolt installations. However, where very long service life is required, cement grouted bolts may provide better long-term protection.

Dowels

Grouted dowels

When conditions are such that installation of support can be carried out very close to an advancing face, or in anticipation of stress changes that will occur at a later excavation stage, dowels can be used in place of rockbolts. The essential difference between these systems is that tensioned rockbolts apply a positive force to the rock, while dowels depend upon movement in the rock to activate the reinforcing action. Mining draw points, which are mined before the overlying stopes are blasted, are good examples of excavations where untensioned grouted dowels will work well.

The simplest form of dowel in use today is the cement grouted dowel as illustrated in Figure 5. A thick grout (typically a 0.3 to 0.35 water/cement ratio grout) is pumped into the hole by inserting the grout tube to the end of the hole and slowly withdrawing the tube as the grout is pumped in. Provided that a sufficiently viscous grout is used, it will not run out of the hole. The dowel is pushed into the hole about halfway and then given a slight bend before pushing it fully into the hole. This bend will serve to keep the dowel firmly lodged in the hole while the grout sets. Once the grout has set, a face plate and nut can be fitted onto the end of the dowel and pulled up tight. Placing this faceplate is important since, if the dowel is called on to react to displacements in the rock mass, the rock close to the borehole collar will tend to pull away from the dowel unless restrained by a faceplate.

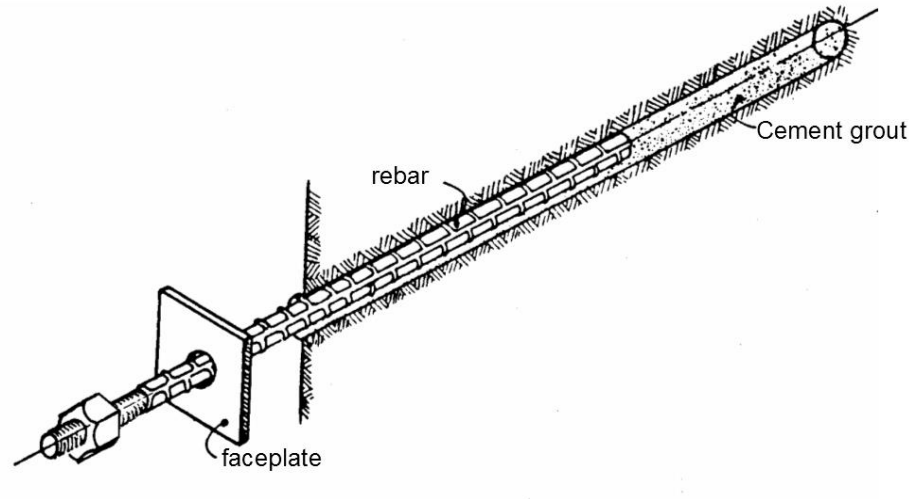

Figure 5: Grouted dowel using a deformed bar inserted into a grout-filled hole.

In mining draw points and ore-passes, the flow of broken rock can cause serious abrasion and impact problems. The projecting ends of grouted rebars can obstruct the flow of the rock. Alternatively, the rebar can be bent, broken or ripped out of the rock mass. In such cases, grouted flexible cable, illustrated in Figure 6, can be used in place of the more rigid rebar. This will allow great flexibility with impact and abrasion resistance.

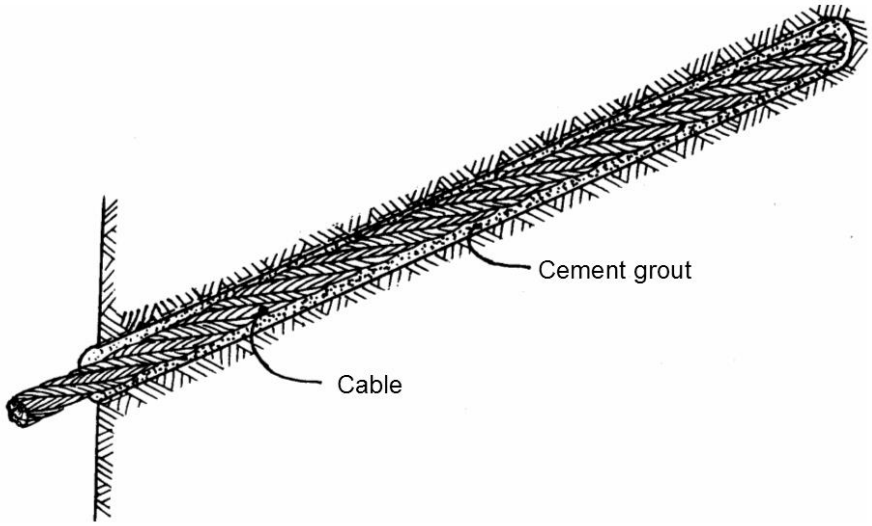

Figure 6: Grouted cables can be used in place of rebar when more flexible support is required or where impact and abrasion can cause problems with rigid support.

Older type grouted dowels such as the Scandinavian 'perfobolt' or dowels, where the grout is injected after the rod has been inserted, tend not to be used any more. The installation is more complex and time consuming and the end product does not perform any better than the simple grouted dowel described earlier.

Friction dowels or 'Split Set' stabilisers

Split Set stabilisers were originally developed by Scott (1976, 1983) and are manufactured and distributed by several manufactures that can be found by searching for “split sets” or “friction stabilizers” on the Internet. The system, illustrated in Figure 7, consists of a slotted high strength steel tube and a face plate. It is installed by pushing it into a slightly undersized hole and the radial spring force generated, by the compression of the C shaped tube, provides the frictional anchorage along the entire length of the hole. A list of typical Split Set stabiliser dimensions and capacities is given in Table 1.

Because the system is quick and simple to install, it has gained acceptance by miners throughout the world. The device is particularly useful in mild rockburst environments because it will slip rather than rupture and, when used with mesh, will retain the broken rock generated by a mild burst. Provided that the demand imposed on Split Sets stabilisers does not exceed their capacity, the system works well and can be considered for many mining applications. They are seldom used in civil engineering applications.

Corrosion remains one of the prime problems with Split Set stabilisers since protection of the outer surface of the dowel is not feasible. Galvanising the tube helps to reduce corrosion, but is probably not a preventative measure which can be relied upon for long term applications in aggressive environments.

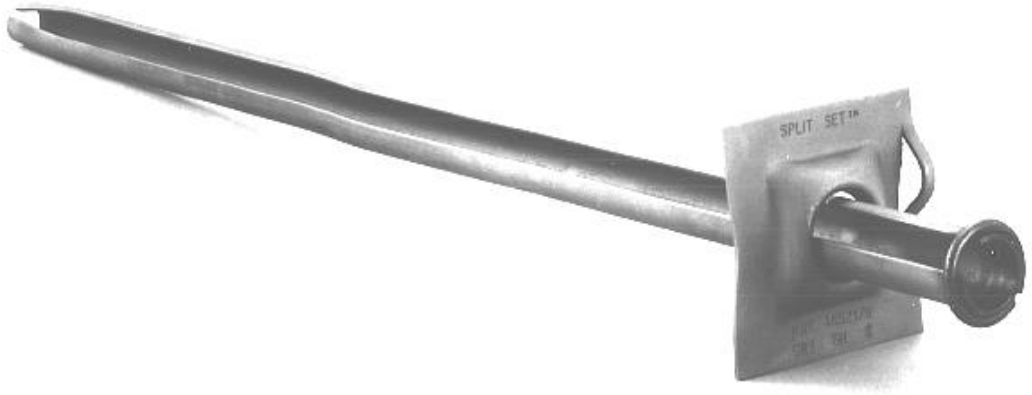

Figure 7: Split Set stabiliser. Ingersoll-Rand photograph.

Table 1: Split Set specifications (After Split Set Division, Ingersoll-Rand Company).

Split Set stabiliser model	*SS-33*	*SS-39*	*SS-46*
Recommended nominal bit size	31 to 33 mm	35 to 38 mm	41 to 45 mm
Breaking capacity, average	10.9 tonnes	12.7 tonnes	16.3 tonnes
minimum	7.3 tonnes	9.1 tonnes	13.6 tonnes
Recommended initial anchorage (tonnes)	2.7 to 5.4	2.7 to 5.4	4.5 to 8..2
Tube lengths	0.9 to 2.4 m	0.9 to 3.0 m	0.9 to 3.6 m
Nominal outer diameter of tube	33 mm	39 mm	46 mm
Domed plate sizes	150x150 mm	150x150 mm	150x150 mm
	125x125 mm	125x125 mm	
Galvanised system available	yes	yes	yes
Stainless steel model available	no	yes	no

'Swellex' dowels

Developed and marketed by Atlas Copco, the 'Swellex' system is illustrated in Figure 8. The dowel, which may be up to 12 m long, consists of a 42 mm diameter tube which is folded during manufacture to create a 25 to 28 mm diameter unit which can be inserted into a 32 to 39 mm diameter hole. No pushing force is required during insertion. The dowel is activated by injection of high-pressure water (approximately 30 MPa or 4,300 psi) which inflates the folded tube into intimate contact with the walls of the borehole.

During 1993, the original Swellex dowel was replaced by the EXL Swellex which is manufactured from a high strength, but ductile, steel. This steel allows significant displacement without loss of capacity. Stillborg (1994), carried out a series of tests in which bolts and dowels were installed across a simulated 'joint' and subjected to tensile loading. In the EXL Swellex dowel tests, opening of the joint concentrates loading onto the portion of the dowel crossing the joint, causing a reduction in diameter and a progressive 'de-bonding' of the dowel away from the joint. The ductile characteristic of the steel allows the de-bonded section to deform under constant load until, eventually, failure occurs when the total displacement reaches about 140 mm at a constant load of approximately 11 tonnes. These tests are described in greater detail later in this Chapter.

Corrosion of Swellex dowels is a matter of concern since the outer surface of the tube is in direct contact with the rock. Atlas Copco has worked with coating manufacturers to overcome this problem and claims to have developed effective corrosion resistant coatings.

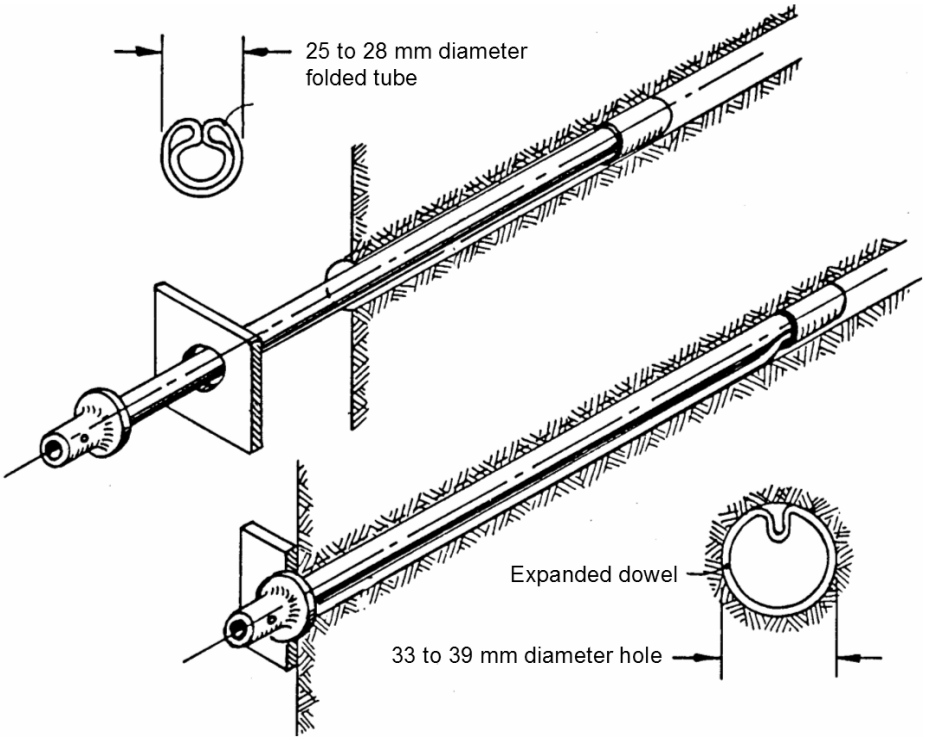

Figure 8: Atlas Copco ‘Swellex’ dowel.

Speed of installation is the principal advantage of the Swellex system as compared with conventional rockbolts and cement grouted dowels. In fact, the total installation cost of Swellex dowels or Spilt Set stabilisers tends to be less than that of alternative reinforcement systems, when installation time is considered. Both systems are ideal for use with automated rock bolters.

Load-deformation characteristics

Stillborg (1994) carried out several tests on rockbolts and dowels installed across a simulated 'joint', using two blocks of high strength reinforced concrete. This type of test gives a more accurate representation of conditions encountered underground than does a standard 'pull-out' test. The rockbolts and dowels tested were installed in percussion drilled holes using the installation techniques used in a normal underground mining operation. The installed support systems were then tested by pulling the two blocks of concrete apart at a fixed rate and measuring the displacement across the simulated 'joint'.

The results of Stillborg's tests are summarised in Figure 9 which gives load deformation curves for all the bolts and dowels tested. The configuration used in each test and the results obtained are summarised on the next page:

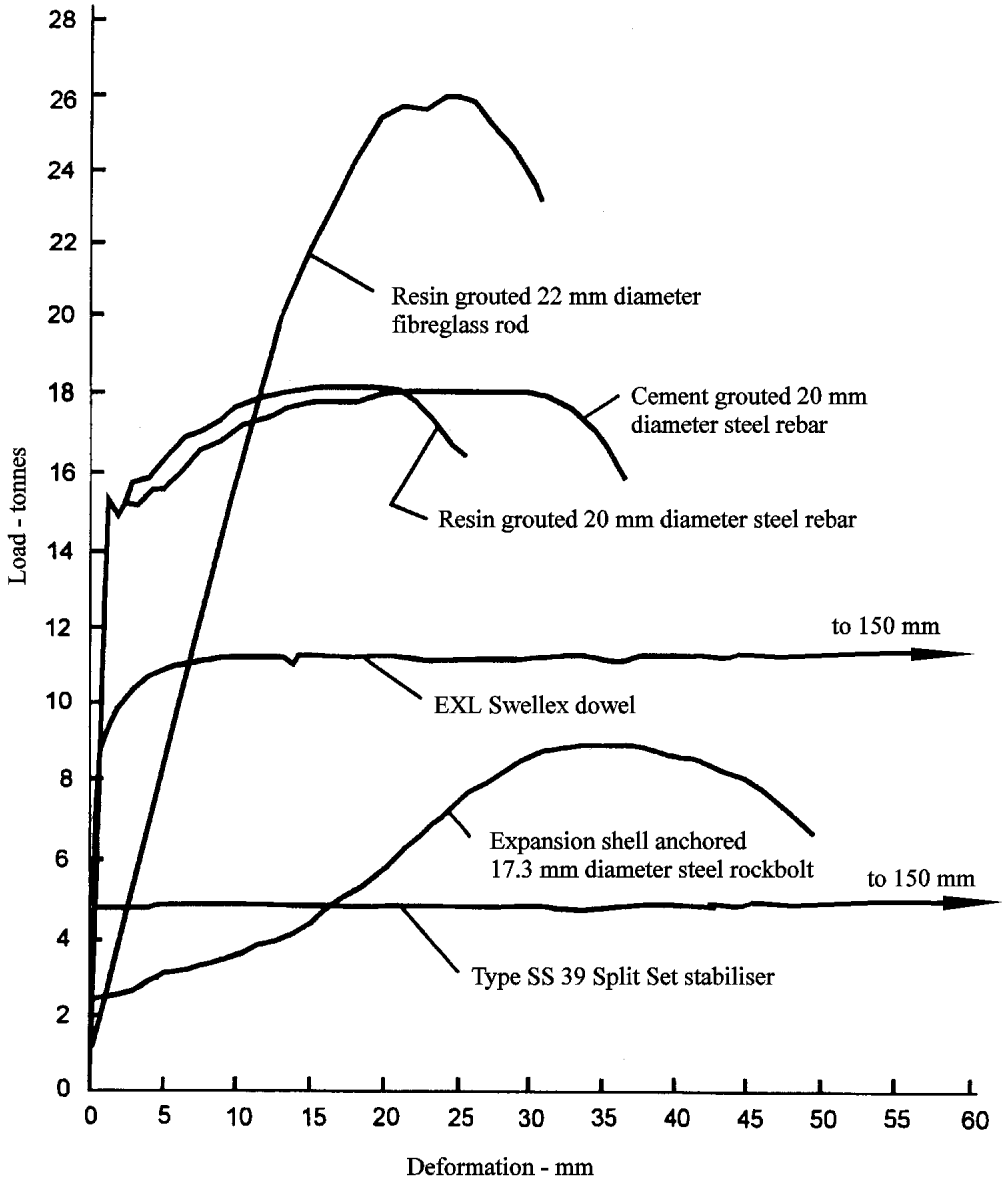

Figure 9: Load-deformation results obtained by Stillborg in tests carried out at Luleå University in Sweden. High strength reinforced concrete with a uniaxial compressive strength of 60 MPa was used for the test blocks. Holes were drilled with a percussion rig to simulate in situ rock conditions.

1. Expansion shell anchored rockbolt

Steel rod diameter: 17.28 mm

Ultimate tensile strength of bolt shank: approximately 12.7 tonnes

Expansion shell anchor: Bail type three wedge anchor

At the pre-load of 2.25 tonnes, no deformation of the face plate

At a load of 4 tonnes, the face plate has deformed 9.5 mm and is completely flat, the bolt shank has deformed an additional 3.5 mm giving a total deformation of 13 mm at 4 tonnes load

Failure initiates at a load of 8 tonnes and a deformation of 25 mm with progressive failure of the expansion shell anchor in which the cone is pulled through the wedge

Maximum load is 9 tonnes at a deformation of 35 mm.

2. Cement grouted steel rebar

Steel bar diameter: 20 mm

Ultimate tensile strength of steel rebar: 18 tonnes

Faceplate: flat plate

Borehole diameter: 32 mm

Cement grout: 0.35 water/cement ratio grout cured for 11 days

At a load of 15 tonnes and an elastic deformation of about 1.5 mm, a sudden load drop is characteristic of hot rolled rebar steel

Maximum load is 18 tonnes at a deformation of 30 mm.

3. Resin grouted steel rebar

Steel rebar diameter: 20 mm

Ultimate tensile strength of steel rebar: 18 tonnes

Faceplate: flat plate

Borehole diameter: 32 mm

Resin grout: Five 580 mm long, 27 mm diameter polyester resin cartridges. Curing time 60 minutes. Mixed by rotating rebar through cartridges in the borehole.

At a load of 15 tonnes and an elastic deformation of about 1.5 mm, a sudden load drop is characteristic of hot rolled rebar steel

Maximum load is 18 tonnes at a deformation of 20 mm

The resin is stronger than the cement grout and local fracturing and bond failure in and near the joint is limited as compared with the cement grouted rebar, leading to a reduced ultimate displacement at rebar failure.

4. Resin grouted fibreglass rod

Fibreglass rod diameter: 22 mm

Ultimate tensile strength of fibreglass rod: 35 tonnes

Faceplate: special design by H. Weidmann AG. Switzerland (see margin drawing - after Stillborg)

Borehole diameter: 32 mm

Resin grout: Five 580 mm long, 27 mm diameter polyester resin cartridges. Curing time 60 minutes. Mixed by rotating fibreglass rod through cartridges in the borehole

At approximately 1.5 tonnes load, failure of the fibreglass/resin interface initiates and starts progressing along the rod. As bond failure progresses, the fiberglass rod deforms over a progressively longer 'free' length

General bond failure occurs at a load of approximately 26 tonnes and a deformation of 25 mm

The ultimate capacity of this assembly is determined by the bond strength between the resin and the fibreglass rod and by the relatively low frictional resistance of the fibreglass.

5. Split Set stabiliser, type SS 39

Tube diameter: 39 mm

Ultimate tensile strength of steel tube: 11 tonnes

Faceplate: special design by manufacturer (see Figure 8)

Borehole diameter: 37 mm

Dowel starts to slide at approximately 5 tonnes and maintains this load for the duration of the test which, in this case, was to a total displacement of 150 mm.

6. EXL Swellex dowel

Tube diameter: 26 mm before expansion

Ultimate tensile strength of steel tube: 11.5 tonnes (before expansion)

Type of face plate: Domed plate

Borehole diameter: 37 mm

Pump pressure for expansion of dowel: 30 MPa

At 5 tonnes load the dowel starts to deform locally at the joint and, at the same time, 'bond' failure occurs at the joint and progresses outward from the joint as the load is increased. General 'bond' failure occurs at 11.5 tonnes at a deformation of approximately 10 mm. The dowel starts to slide at this load and maintains the load for the duration of the test which, in this case, was to 150 mm.

Cables

A comprehensive review of cable support in underground mining has been given in a book by Hutchinson and Diederichs (1996). This book is recommended for the selection and installation of cable support for either mining or civil engineering applications.

Some of the main cable types used by mining were summarised by Windsor (1992) and are illustrated in Figure 10.

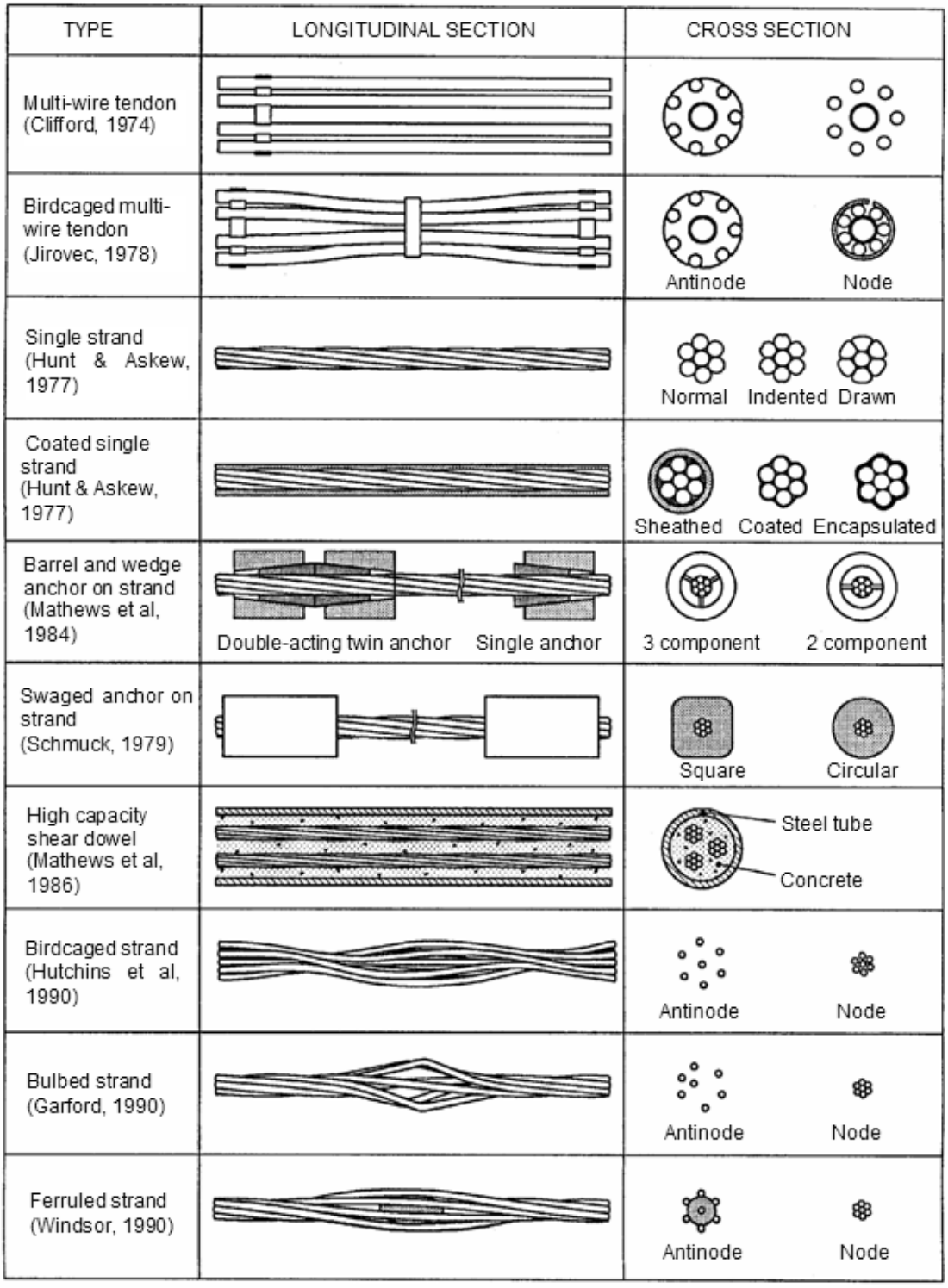

Figure 10: Summary of the development of cable reinforcing systems for underground mining (Windsor, 1992).

Bond strength

The forces and displacements associated with a stressed cable grouted into a borehole in rock are illustrated in Figure 11.

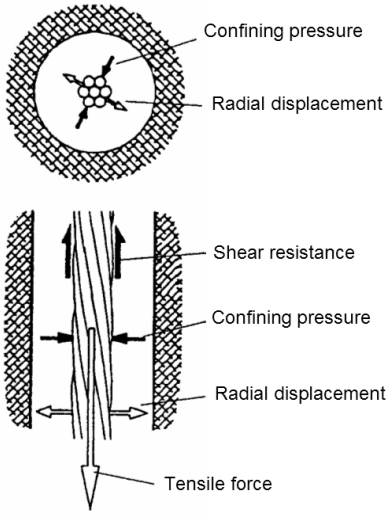

Figure 11: Forces and displacements associated with a stressed cable grouted into a borehole in rock.

As the cable pulls out from the grout, the resultant interference of the spiral steel wires with their associated grout imprints or flutes causes radial displacement or dilation of the interface between the grout and the cable. The radial dilation induces a confining pressure that is proportional to the combined stiffness of the grout and the rock surrounding the borehole. The shear stress, which resists sliding of the cable, is a product of the confining pressure and the coefficient of friction between the steel wires and the grout. Shear strength, therefore, increases with higher grout strength, increases in the grout and the rock stiffness, and increases in the confining stresses in the rock after installation of the cable. Conversely, decrease in shear strength can be expected if any of these factors decrease or if the grout crushes.

Theoretical models of the behaviour of this rock/grout/cable system have been developed by Yazici and Kaiser (1992), Kaiser et al (1992), Hyett et al (1992). The second of these models has been incorporated into the RocScience programs RS2 and RS3.

Grouts and grouting

The question of grout quality has always been a matter of concern in reinforcement systems for underground construction. One of the critical factors in this matter has been the evolution of grout pumps capable of pumping grouts with a low enough water/cement ratio (by weight) to achieve adequate strengths. Fortunately, this problem has now been overcome because there is a range of grout pumps on the market which will pump very viscous grouts and will operate reliably under typical underground conditions.

The results of a comprehensive testing programme on Portland cement grouts have been summarised by Hyett et al (1992). Figures 12 and 13 are based upon this summary. Figure 12 shows the decrease in both 28-day uniaxial compressive strength and deformation modulus with increasing water/cement ratio. Figure 13 gives Mohr failure envelopes for three water/cement ratios. These results show that the properties of grouts with water/cement ratios of 0.35 to 0.4 are significantly better than those with ratios in excess of 0.5. However, Hyett et al found that the scatter in test results increased markedly for water/cement ratios less than 0.35. The implication is that the ideal water/cement ratio for use with cable reinforcement lies in the range of 0.35 to 0.4.

The characteristics of grouts with different water/cement ratios are described as follows (after Hyett et al 1992):

w/c ratio	*Characteristics at end of grout hose*	*Characteristics when handled*
< 0.30	Dry, stiff sausage structure.	Sausage fractures when bent. Grout too dry to stick to hand. Can be rolled into balls.
0.30	Moist sausage structure. 'Melts' slightly with time.	Sausage is fully flexible. Grout will stick to hand. Easily rolled into wet, soft balls.
0.35	Wet sausage structure. Structure 'melts' away with time.	Grout sticks readily to hand. Hangs from hand when upturned.
0.4	Sausage structure lost immediately. Flows viscously under its own weight to form pancake.	Grout readily sticks to hand but can be shaken free.
0.5	Grout flows readily and splashes on impact with ground.	Grout will drip from hand - no shaking required.

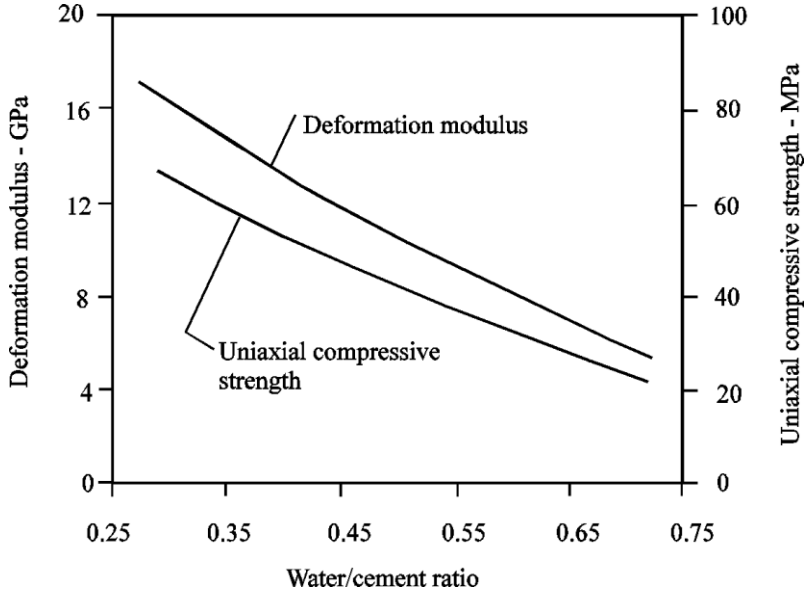

Figure 12: Relationship between the water/cement ratio and the average uniaxial compressive strength and deformation modulus for grouts tested at 28 days.

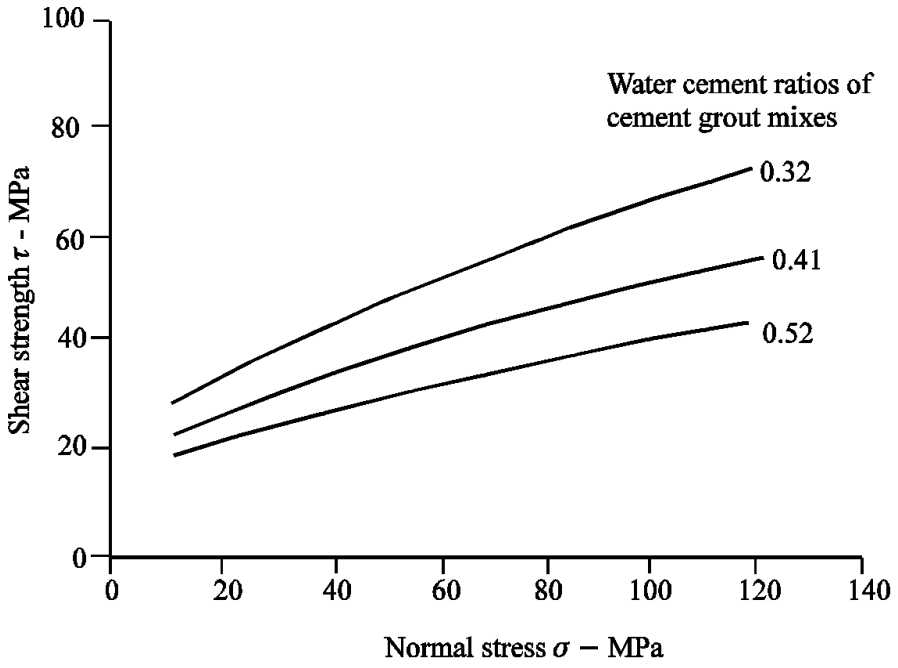

w/c ratio	σ_c *MPa*	*constant m*	*constant s*	*Friction angle* $\phi°$	*Cohesion c MPa*
0.32	78	3.05	1	24	25
0.41	54	2.14	1	20	19
0.52	38	1.67	1	17	14

Figure 13: Mohr failure envelopes for the peak strength of grouts with different water/cement ratios, tested at 28 days.

Cable installation

The left-hand drawing in Figure 14 shows the traditional method of grouting a cable in an up hole. This method will be called the 'breather tube method'. The grout, usually having a water/cement ratio ≥ 0.4, is injected into the bottom of the hole through a large diameter tube, typically 19 mm diameter. The air is bled through a smaller diameter tube taped onto the cable, which extends to the end of the hole. Both tubes and the cable are sealed into the bottom of the hole by means of a plug of cotton waste or of quick setting mortar. As shown, the direction of grout travel is upwards in the hole, which tends to favour a grout column that is devoid of air gaps since any slump in the grout tends to fill these gaps.

Apart from the difficulty of sealing the collar of the hole, the main problem with this system is that it is difficult to detect when the hole is full of grout. Typically, the hole is judged to be full when air ceases to flow from the bleed tube. This may occur prematurely if air is vented into an open joint along the hole. In addition, a void the size of the bleed tube is likely to be left in the grout column. Therefore, it is preferable to stop grouting the borehole only when grout returns along the bleed tube. However, a viscous grout will not flow down a 9 mm bleed tube and so a larger tube is required.

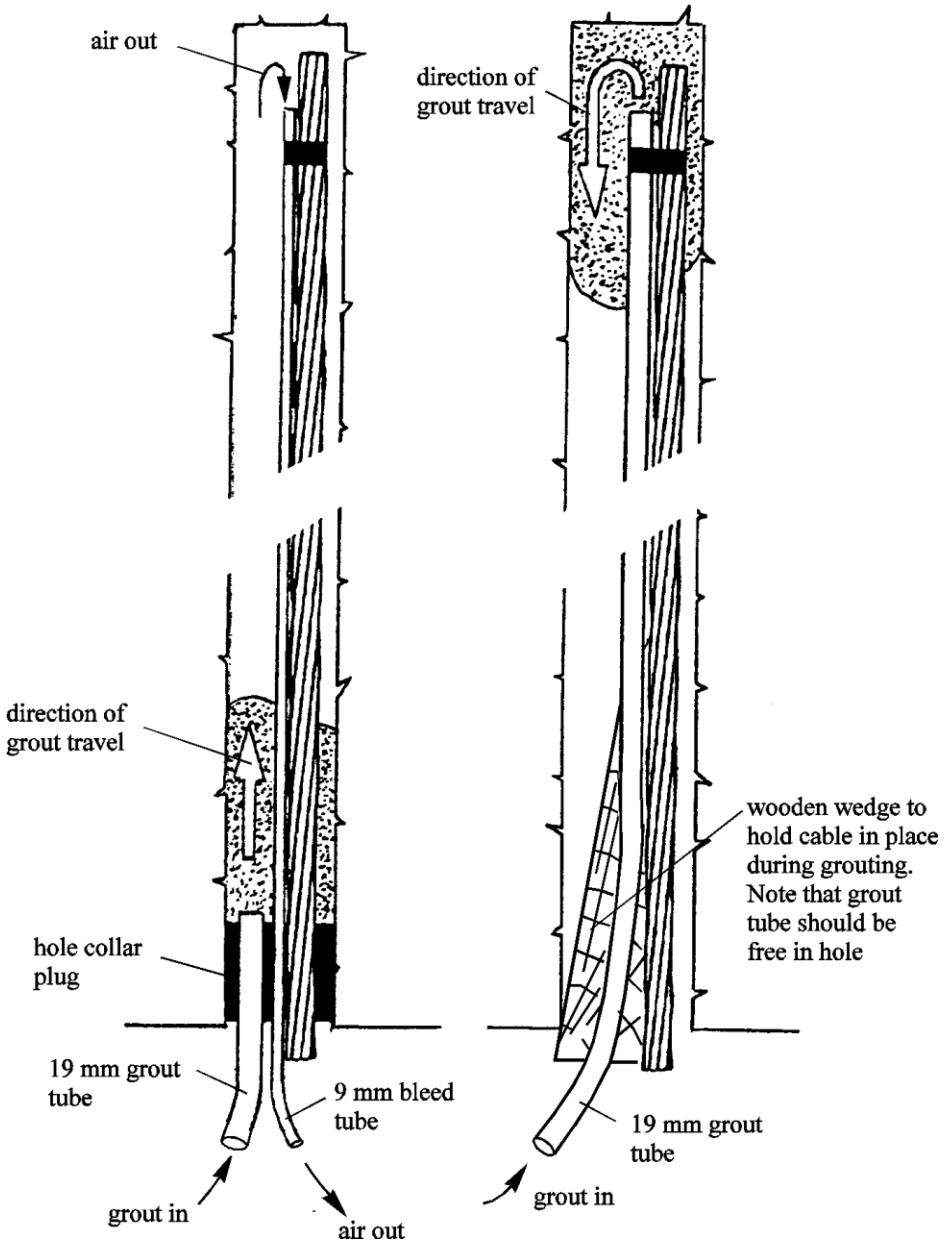

Figure 14: Alternative methods for grouting cables in up holes.

An alternative method, called the ‘grout tube method’ is illustrated in the right-hand drawing in Figure 14. In this case a large diameter grout injection tube extends to the end of the hole and is taped onto the cable. The cable and tube are held in place in the hole by a wooden wedge inserted into the hole collar. Note that care must be taken to avoid compressing the grout tube between the wedge and the cable. Grout is injected to the top of the hole and is pumped down the hole until it appears at the hole collar. If a watery grout appears first at the collar of the hole, grout pumping is continued until a consistently thick grout is observed.

Provided that a very viscous mix is used (0.3 to 0.35 water/cement ratio), the grout will have to be pumped into the hole and there is little danger of slump voids being formed. However, a higher water/cement ratio mix will almost certainly result in air voids in the grout column because of slumping of the grout. The principal advantage of this method is that it is obvious when the hole is full of grout and this, together with the smaller number of components required, makes the method attractive when compared with the traditional method for grouting plain strand cables. In addition, the thicker grout used in this method is not likely to flow into fractures in the rock, preferring instead the path of least flow resistance towards the borehole collar.

The procedure used for grouting down holes is similar to the grout tube method, described above, without the wooden wedge in the borehole collar. The grout tube may be taped to the cable or retracted slowly from the bottom of the hole as grouting progresses. It is important to ensure that the withdrawal rate does not exceed the rate of filling the hole, so that air voids are not introduced. This is achieved by applying, by hand, a slight downward force to resist the upward force applied to the tube by the rising grout column. Grout of any consistency is suitable for this method but the best range for plain strand cables is between 0.3 and 0.4 water/cement ratio.

Modified cables, such as birdcage, ferruled or bulbed strand, should be grouted using a 0.4 water/cement ratio mix to ensure that the grout is fluid enough to fill the cage structure of these cables. Therefore, the breather tube method must be used for these types of cables, since the grout flow characteristics required by the grout tube method is limited to grouts in the range of 0.3 to 0.35 water/cement ratio.

One of the most critical components in a cable installation is the grout column. Every possible care must be taken to ensure that the column contains as few air voids as possible. In the breather tube method, a large diameter breather tube will allow the return of grout as well as air. When using the grout tube method in up holes, a 0.3 to 0.35 water/cement ration grout will ensure that pumping is required to cause the grout column to flow, which will avoid slumping of the grout in the borehole. A grout with a water/cement ratio of less than 0.3 should be avoided, since it will tend to form encapsulated air voids as it flows around the cable.

A hollow cable, illustrated in Figure 15, introduced by Atlas Copco, and this could reduce some of the grouting problems discussed above.

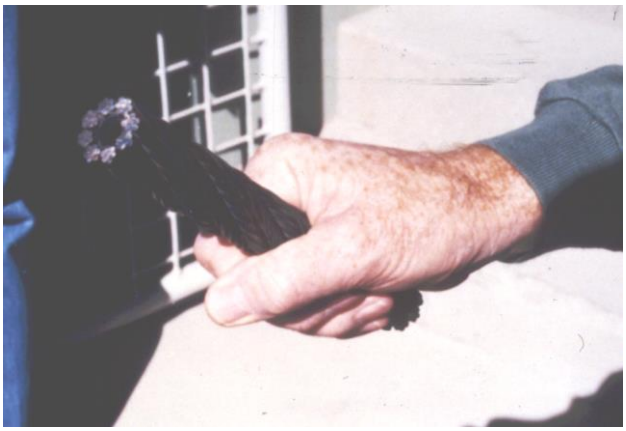

Figure 15: Hollow cable by Atlas Copco.

Cables for slope reinforcement

Most of the applications described in this chapter have been related to underground excavations. However, under certain circumstances, it may also be necessary to reinforce slopes and foundations and cables which have proved to be very effective in such applications.

Figure 16 illustrates a unit set up for drilling 140 m long 50 mm diameter holes for the installation of cables, illustrated in Figure 17, in a slope.

Figure 16: Drilling machine for the installation of 40 m long reinforcing cables in 150 mm diameter holes in a dam excavation.

Figure 17: 40 m long multi-strand cables with a capacity of 200 tons each being prepared for installation in a dam excavation.

These cables were installed to stabilise the slopes of a dam foundation in gneiss. Sheet jointing parallel to the surface of the steep slopes would have resulted in large scale slope instability if the excavation, which undercut these sheet joints, had not been reinforced.

The cables illustrated have an ultimate capacity of 312 tons and a working load of 200 tons. The cables were fully grouted after tensioning. The cost of materials and installation for these cables was approximately US$ 500 per metre.

References

Hutchinson, D.J. and Diederichs, M.S. 1996. *Cablebolting in underground mines.* Vancouver: Bitech.

Hyett, A.J., Bawden, W.F. and Coulson, A.L. 1992. Physical and mechanical properties of normal Portland cement pertaining to fully grouted cable bolts. In *Rock support in mining and underground construction, proc. int. symp. rock support,* Sudbury, (eds. P.K. Kaiser and D.R. McCreath), 341-348. Rotterdam: Balkema.

Kaiser, P.K., Yazici, S. and Nosé, J. 1992. Effect of stress change on the bond strength of fully grouted cables. *Int. J. Rock Mech.. Min. Sci. Geomech. Abstr.* **29**(3), 293-306.

Scott, J.J. 1976. Friction rock stabilizers - a new rock reinforcement method. In *Monograph on rock mechanics applications in mining,* (eds W.S. Brown, S.J. Green and W.A. Hustrulid), 242-249. New York: Soc. Min. Engrs, Am. Inst. Min. Metall. Petrolm Engrs.

Scott, J.J. 1983. Friction rock stabilizer impact upon anchor design and ground control practices. In *Rock bolting: theory and application in underground construction*, (ed. O. Stephansson), 407-418. Rotterdam: Balkema.

Stillborg, B. 1994. *Professional users handbook for rock bolting,* 2nd edn. Clausthal-Zellerfeld: Trans Tech Publications.

Windsor, C.R. 1992. Cable bolting for underground and surface excavations. In *Rock support in mining and underground construction, proc. int. symp. on rock support*, Sudbury, (eds. P.K. Kaiser and D.R. McCreath), 349-376. Rotterdam: Balkema.

Yazici, S. and Kaiser, P.K. 1992. Bond strength of grouted cable bolts. *Int J. Rock Mech. Min. Sci. & Geomech. Abstr*. **29**(3), 279-292.

17. Model to demonstrate how rockbolts work

In the 1960, I visited the laboratories of the Snowy Mountains Authority in Cooma, Australia and was shown a model used by Mr Tom Lang to demonstrate how rockbolts work. He had used many innovative rock engineering concepts in the design of the caverns and tunnels of the Snowy Mountains Project and this model was one of his educational tools. I was so impressed by this model that I used a version of it when teaching a graduate course on rock engineering at the University of Toronto. As one of their projects the students would assemble this model from scratch and so discover for themselves how the rockbolts work. The series of photographs included in this document were taken during one such project. The model in these photographs was based on a version of Tom Lang's model constructed by the U.S. Army Corps of Engineers Waterways Experiment Station in Vicksburg, Mississippi.

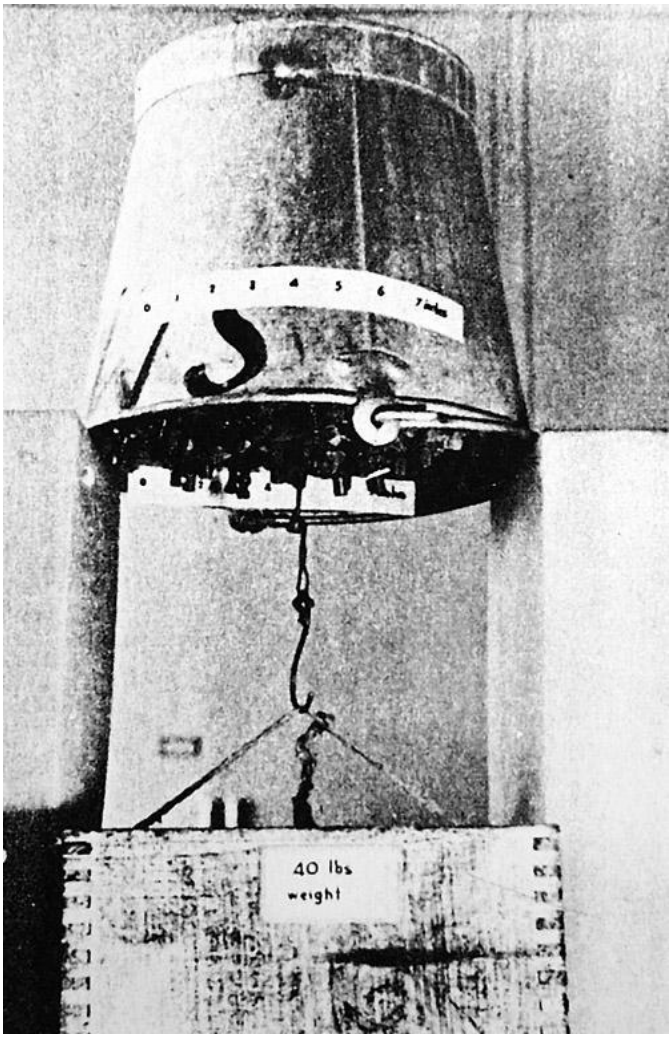

Figure 1: The rockbolt model in Tom Lang's office in Cooma, Australia. The inverted galvanized bucket contained gravel which was held together by means of a pattern of miniature rockbolts. In addition to binding the gravel together and creating sufficient friction to hold it in the bucket, a 40 lb (18 kg) weight was suspended from a small beam attached to the rockbolts.

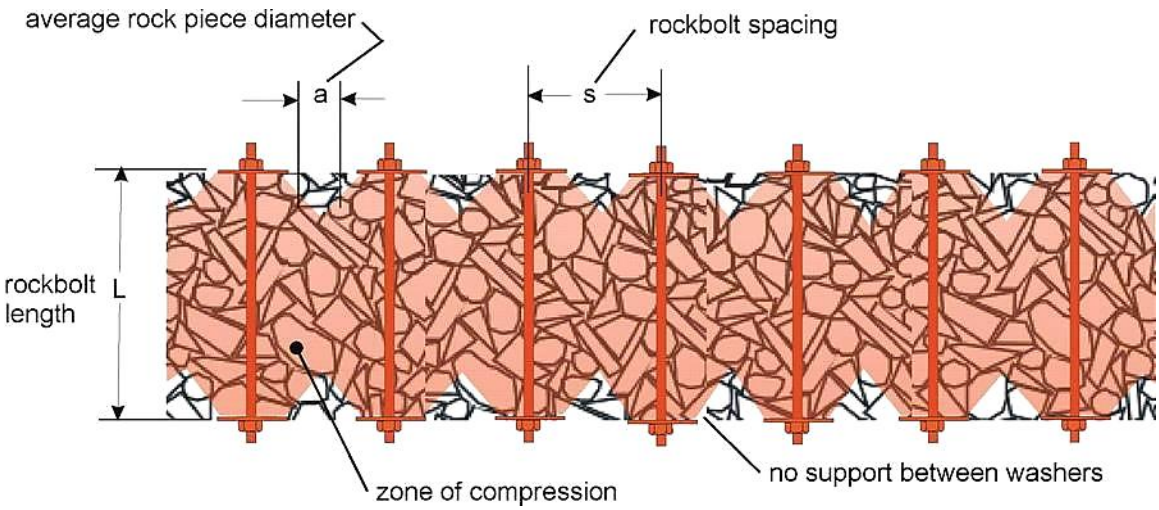

Figure 2: Tom Lang's explanation of how rockbolts work. A zone of compression is induced in the region shown in red it provides effective reinforcement to the rock mass when the rockbolt spacing s is less than 3 times the average rock piece diameter a. The rockbolt length L should be approximately 2s. Note there is no support between the washers (unless mesh or shotcrete is applied) and the rock pieces will fall out of these zones on the underside of the beam.

Figure 3: The empty frame of the rockbolt plate model.

Figure 4: Miniature rockbolts ready for installation.

Figure 5: Uniformly sized clean gravel for the plate.

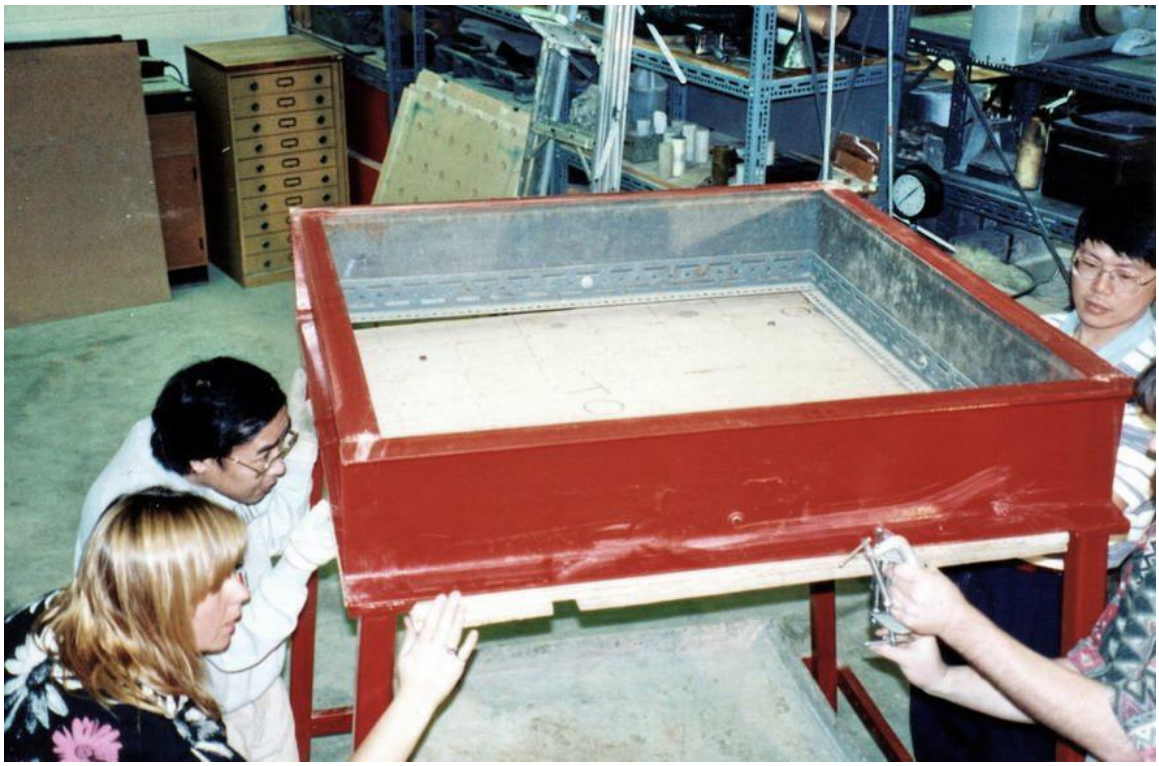

Figure 6: Attachment of the temporary base to the model frame.

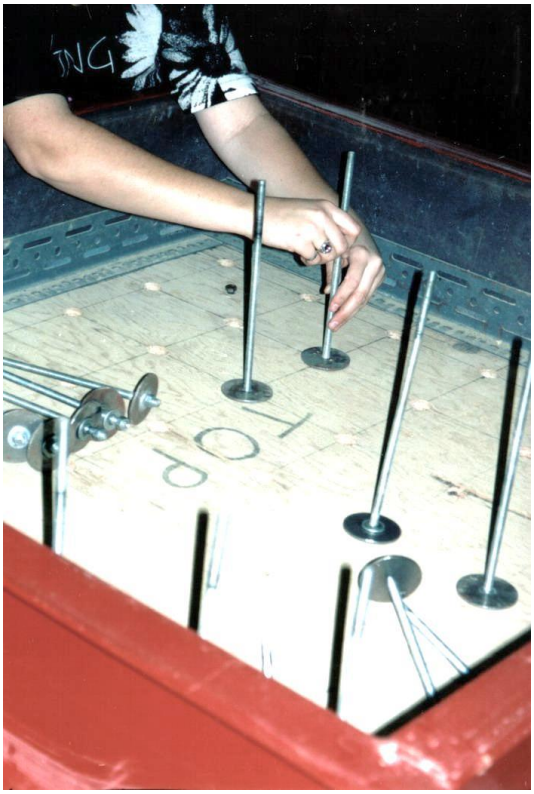

Figure 7: Positioning the rockbolts in holes drilled into the temporary base.

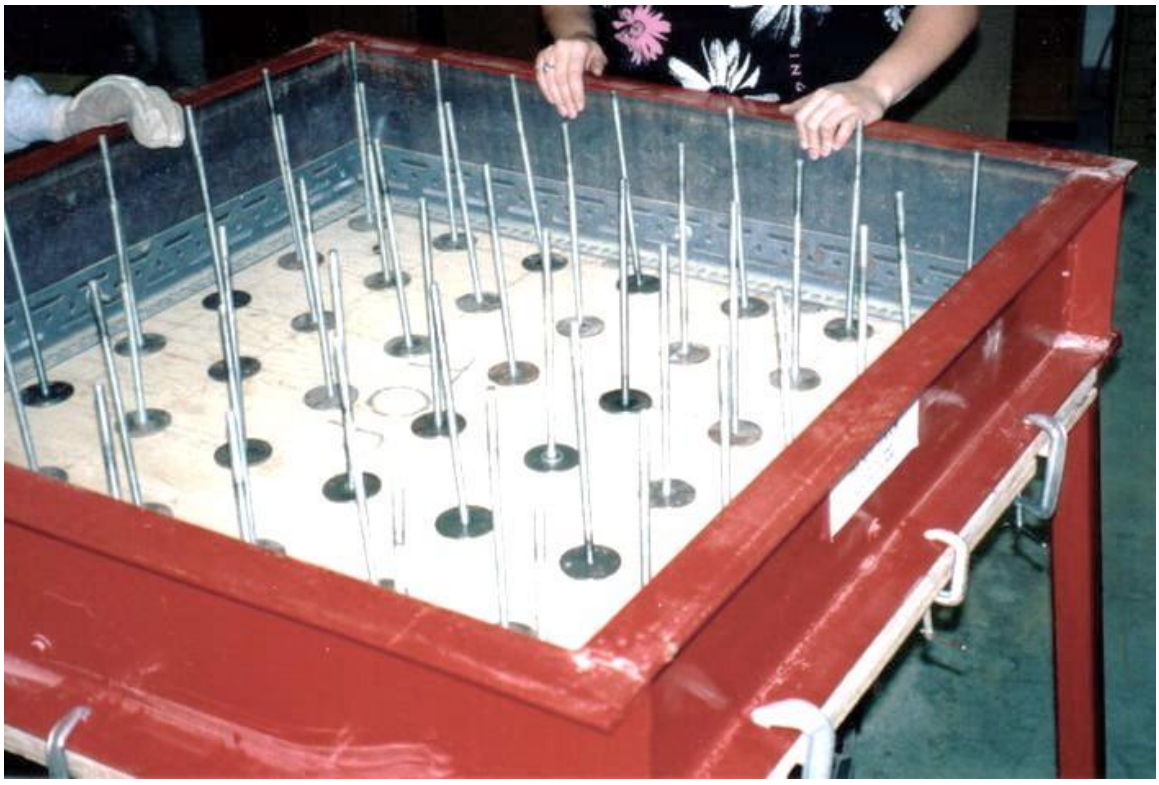

Figure 8: The rockbolts in position ready for the gravel to be placed.

Figure 9: Placing the gravel in the frame.

Figure 10: “Mechanical compacting” of the gravel.

Figure 11: Washers and nuts placed on the rockbolts and tightened.

Figure 12: Holding the bottom nut during bolt tightening.

Figure 13: The temporary base removed from the self-supporting rock plate.

Figure 14: The load-carrying capacity of the bolted gravel plate.

18. Shotcrete support

Introduction

The use of shotcrete for the support of underground excavations was pioneered by the civil engineering industry. Reviews of the development of shotcrete technology have been presented by Rose (1985), Morgan (1993) and Franzén (1992). Rabcewicz (1969) was largely responsible for the introduction of the use of shotcrete for tunnel support in the 1930s, and for the development of the New Austrian Tunnelling Method for excavating in weak ground.

In recent years the mining industry has become a major user of shotcrete for underground support. It can be expected to make its own contributions to this field as it has in other areas of underground support. The simultaneous working of multiple headings, difficulty of access and unusual loading conditions are some of the problems which are peculiar to underground mining and which require new and innovative applications of shotcrete technology.

An important area of shotcrete application in underground mining is in the support of 'permanent' openings such as ramps, haulages, shaft stations and crusher chambers. Rehabilitation of conventional rockbolt and mesh support can be very disruptive and expensive. Increasing numbers of these excavations are being shotcreted immediately after excavation. The incorporation of steel fibre reinforcement into the shotcrete is an important factor in this escalating use, since it minimises the labour-intensive process of mesh installation.

Trials and observations suggest that shotcrete can provide effective support in mild rockburst conditions (McCreath and Kaiser, 1992, Langille and Burtney, 1992).

Shotcrete technology

Shotcrete is the generic name for cement, sand and fine aggregate concretes which are applied pneumatically and compacted dynamically under high velocity.

Dry mix shotcrete

As illustrated in Figure 1, the dry shotcrete components, which may be slightly pre-dampened to reduce dust, are fed into a hopper with continuous agitation. Compressed air is introduced through a rotating barrel or feed bowl to convey the materials in a continuous stream through the delivery hose. Water is added to the mix at the nozzle.

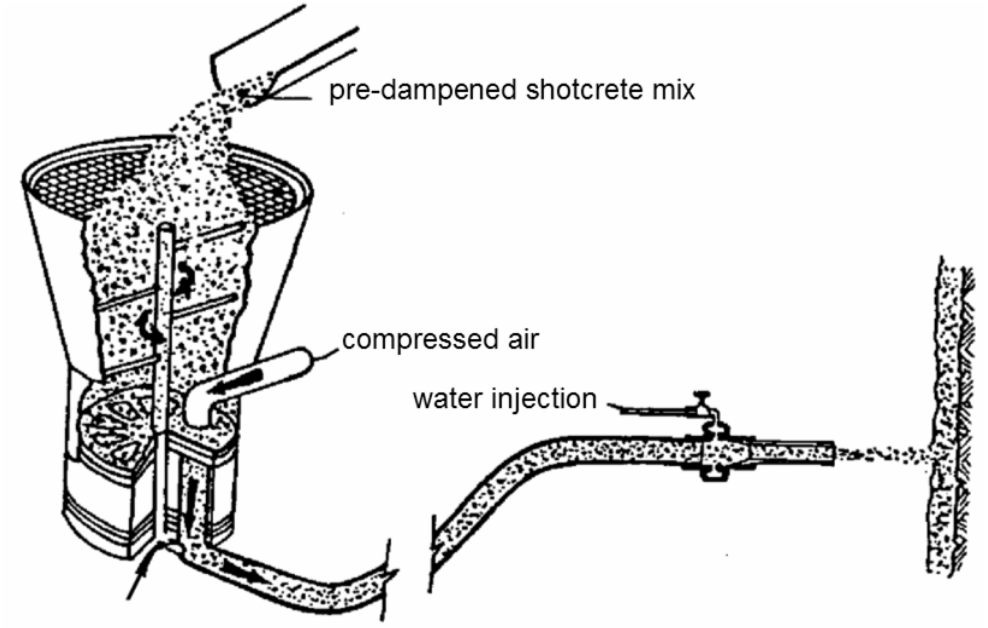

Figure 1: Simplified sketch of a typical dry mix shotcrete system. After Mahar et al (1975).

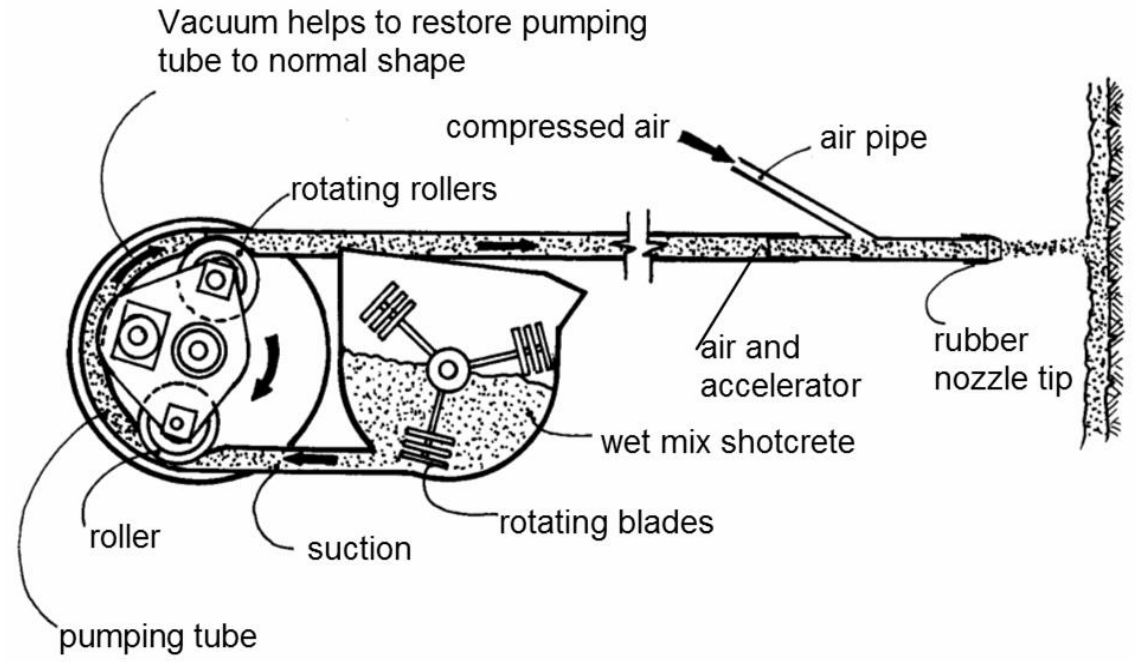

Figure 2: One typical type of wet mix shotcrete machine. After Mahar et al (1975).

Wet mix shotcrete

In this case the shotcrete components and the water are mixed (usually in a truck mounted mixer) before delivery into a positive displacement pumping unit, which then delivers the mix hydraulically to the nozzle where air is added to project the material onto the rock surface.

The final product of either the dry or wet shotcrete process is very similar. The dry mix system tends to be more widely used in mining, because of inaccessibility for large transit mix trucks and because it generally uses smaller and more compact equipment which can be moved around relatively easily in an underground mine environment. The wet mix system is ideal for high production applications in mining and civil engineering where a deep shaft or long tunnel is being driven and where access allows the application equipment and delivery trucks to operate on a more or less continuous basis. Decisions to use the dry or wet mix shotcrete process are usually made on a site-by-site basis.

Steel fibre reinforced micro silica shotcrete

Of the many developments in shotcrete technology, two of the most significant were the introduction of silica fume, used as a cementitious admixture, and steel or polypropylene fibre reinforcement.

Silica fume or micro silica is a by-product of the ferro silicon metal industry and is an extremely fine pozzolan. Pozzolans are cementitious materials which react with the calcium hydroxide produced during cement hydration. Silica fume, added in quantities of 8 to 13% by weight of cement, can allow shotcrete to achieve compressive strengths which are double or triple the value of plain shotcrete mixes. The result is an extremely strong, impermeable and durable shotcrete. Other benefits include reduced rebound, improved flexural strength, improved bond with the rock mass and the ability to place layers of up to 200 mm thick in a single pass because of the shotcrete's 'stickiness'. However, when using wet mix shotcrete, this stickiness decreases the workability of the material and superplasticizers are required to restore this workability.

Steel fibre reinforced shotcrete was introduced in the 1970s and has since gained world-wide acceptance as a replacement for traditional wire mesh reinforced plain shotcrete. The main role that reinforcement plays in shotcrete is to impart ductility to an otherwise brittle material. As pointed out earlier, rock support is only called upon to carry significant loads once the rock surrounding an underground excavation deforms. This means that unevenly distributed non-elastic deformations of significant magnitude may overload and lead to failure of the support system, unless that system has sufficient ductility to accommodate these deformations.

Typical steel fibre reinforced silica fume shotcrete mix designs are summarised in Table 1. These mixes can be used as a starting point when embarking on a shotcrete project, but it may be necessary to seek expert assistance to 'fine tune' the mix designs to suit site specific requirements. For many dry mix applications, it may be advantageous to purchase pre-mixed shotcrete in bags of up to 1,500 kg capacity, as illustrated in Figure 3.

Table 1: Typical steel fibre reinforced silica fume shotcrete mix designs (After Wood, 1992)

Components	Dry mix		Wet mix	
	kg./m^3	% dry materials	kg./m^3	% wet materials
Cement	420	19.0	420	18.1
Silica fume additive	50	2.2	40	1.7
Blended aggregate	1,670	75.5	1,600	68.9
Steel fibres	60	2.7	60	2.6
Accelerator	13	0.6	13	0.6
Superplasticizer	-	-	6 litres	0.3
Water reducer	-	-	2 litres	0.1
Air entraining admixture	-	-		if required
Water	controlled at nozzle		180	7.7
Total	2,213	100	2,321	100

Figure 3: Bagged pre-mixed dry shotcrete components being delivered into a hopper feeding a screw conveyor, fitted with a pre-dampener, which discharges into the hopper of a shotcrete machine.

Figure 4 shows the steel fibre types which are available on the North American market. In addition to their use in shotcrete, these fibres are also widely used in concrete floor slabs for buildings, in airport runways and in similar concrete applications.

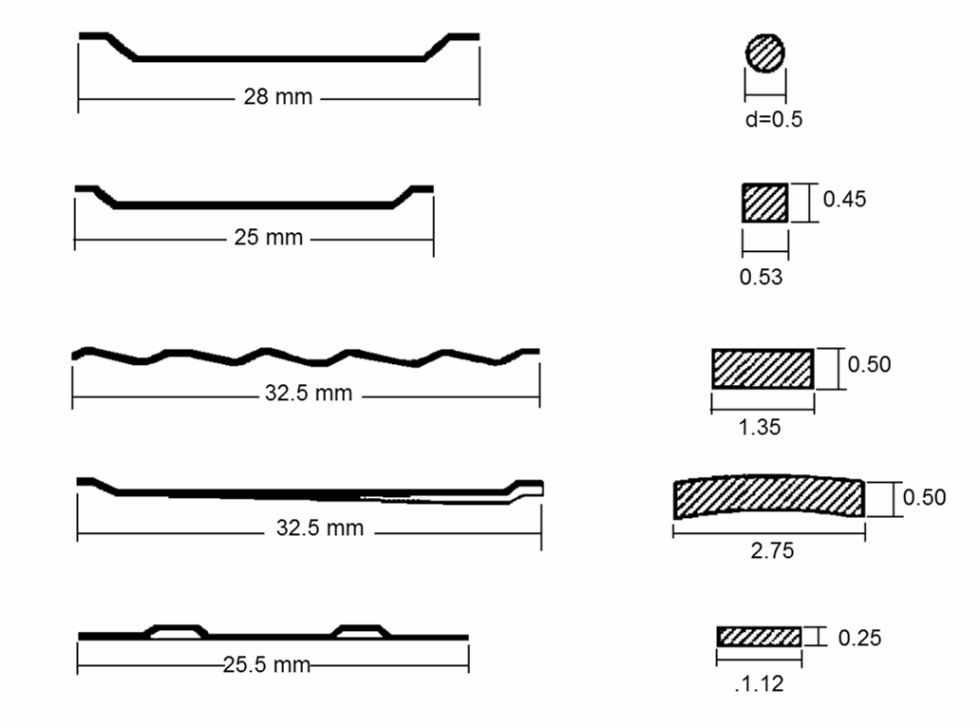

Figure 4. Steel fibre types available on the North American market. After Wood et al (1993). (Note: all dimensions are in mm).

Wood et al (1993) have reported the results of a comprehensive comparative study in which all the fibres shown in Figure 4 were used to reinforce shotcrete samples which were then subjected to a range of tests. Plain and fibre reinforced silica fume shotcrete samples were prepared by shooting onto vertical panels, using both wet and dry mix processes. The fibre reinforced samples all contained the same steel fibre dosage of 60 kg/m^3 (see Table 1). All the samples were cured under controlled relative humidity conditions and all were tested seven days after shooting.

These tests showed that the addition of steel fibres to silica fume shotcrete enhances both the compressive and flexural strength of the hardened shotcrete by up to 20%. A significant increase in ductility was also obtained in all the tests on fibre reinforced samples, compared with plain samples. While different fibres gave different degrees of improvement, all of the fibres tested were found to exceed the levels of performance commonly specified in

North America (i.e., 7-day compressive strength of 30 MPa for dry mix, 25 MPa for wet mix and 7-day flexural strength of 4 MPa).

Kompen (1989) carried out bending tests on slabs of unreinforced shotcrete and shotcrete reinforced with 'Dramix'[1] steel fibres, shown in Figure 5. The shotcrete had an unconfined compressive strength, determined from tests on cubes, of 50 MPa. The results of these tests are reproduced in Figure 6. The peak strength of these slabs increased by approximately 85% and 185% for 1.0 and 1.5 volume % of fibres, respectively. The ductility of the fibre reinforced slabs increased by approximately 20 and 30 times for the 1.0 and 1.5 volume % of fibres, respectively.

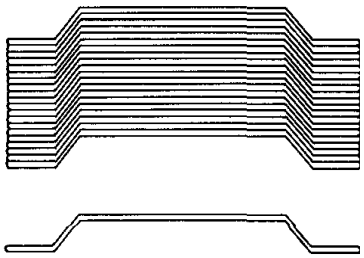

Figure 5: 'Dramix' steel fibres used in slab bending tests by Kompen (1989). The fibres are glued together in bundles with a water-soluble glue to facilitate handling and homogeneous distribution of the fibres in the shotcrete.

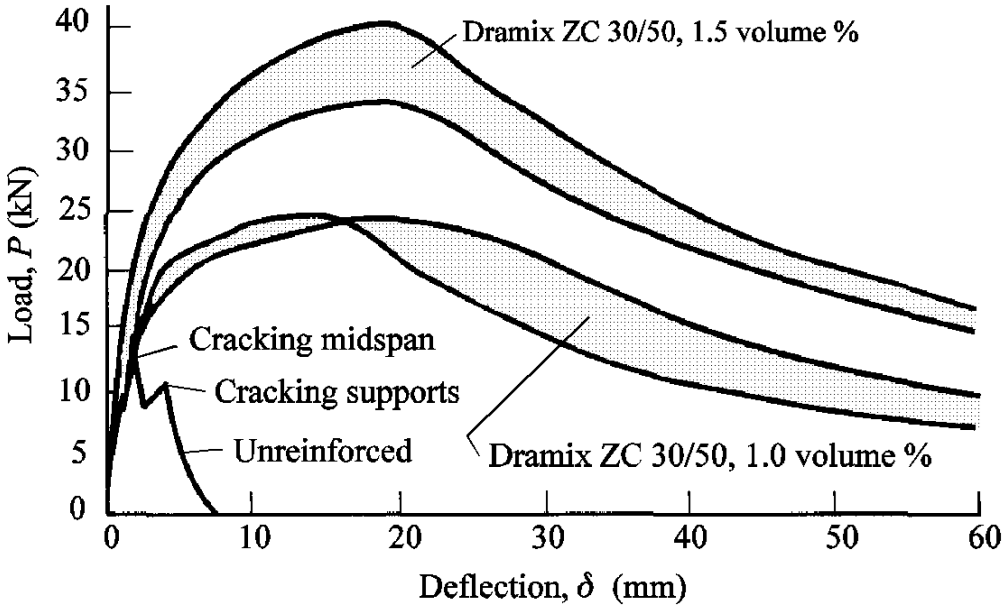

Figure 6: Load deflection curves for unreinforced and steel fibre reinforced shotcrete slabs tested in bending. After Kompen (1989).

[1] Manufactured by N.V. Bekaert S.A., B-8550 Zwevegem, Belgium.

In recent years there has been a move towards using fibres other than steel for reinforcing shotcrete. Morgan et al (1989) have reported on the comparative performance of polypropylene and steel fibre reinforced shotcrete and Papworth (2002) discussed a number of other non-metallic fibres that have been used successfully for shotcrete reinforcement. The interested reader can find a large number of papers on recent development in this field on the Internet by searching for "fibre reinforced shotcrete".

Mesh reinforced shotcrete

While steel fibre reinforced shotcrete has been widely accepted in both civil and mining engineering, mesh reinforced shotcrete is still widely used and is preferred in some applications. In very poor quality, loose rock masses, where adhesion of the shotcrete to the rock surface is poor, the mesh provides a significant amount of reinforcement, even without shotcrete. Therefore, when stabilising slopes in very poor-quality rock masses or when building bulkheads for underground fill, weldmesh is frequently used to stabilise the surface or to provide reinforcement. In such cases, plain shotcrete is applied later to provide additional support and to protect the mesh against corrosion.

Kirsten (1992, 1993) carried out a comprehensive set of bending tests on both mesh and fibre reinforced shotcrete slabs. The loads versus deflection curves that he obtained were similar to those reported by Kompen, reproduced in Figure 6. He found that the load carrying capacity of the mesh and fibre reinforced shotcrete samples were not significantly different, but that the mesh reinforced samples were superior in bending with both point loads and uniformly distributed loads. He concluded that this was due to the more favourable location of the mesh reinforcement in the slabs subjected to bending.

Kirsten also concluded that the quality control, required to obtain a consistent dosage and uniform distribution of fibres in shotcrete, is more easily achieved in civil engineering than in mining applications. This is a reflection of the multiple working headings and the difficulties of access that are common problems associated with many mines. Under these circumstances, more reliable reinforcement will be obtained with mesh reinforced rather than fibre reinforced shotcrete. However, in large mines, in which many of the 'permanent' openings are similar to those on large civil engineering sites, these problems of quality control should not arise.

Chainlink mesh, used in many underground mining excavations to support loose rock, is not usually suitable for shotcrete reinforcement. This is because penetration of the shotcrete is inhibited by the twisted joints as illustrated in Figure 7. This allows air cavities to form behind the mesh and these may allow water to enter and cause corrosion of the mesh.

On the other hand, weldmesh, tightly pinned against the rock face as illustrated in Figure 8, is generally ideal for shotcrete applications. Typically, the weldmesh should be made from 4 mm diameter wire welded into a 100 mm x 100 mm grid. This type of mesh is

strong enough for most underground applications and the sheets are light enough to be handled by one man.

Figure 8: Welded wire mesh, firmly attached to the rock surface, provides excellent reinforcement for shotcrete.

Figure 7: Chainlink mesh, while very strong and flexible, is not ideal for shotcrete application because it is difficult for the shotcrete to penetrate the mesh.

Shotcrete applications

The quality of the final product is closely related to the application procedures used. These procedures include: surface preparation, nozzling technique, lighting, ventilation, communications, and crew training.

Shotcrete should not be applied directly to a dry, dusty or frozen rock surface. The work area is usually sprayed with an air-water jet to remove loose rock and dust from the surface to be shot. The damp rock will create a good surface on which to bond the initial layer of shotcrete paste. The nozzleman commonly starts low on the wall and moves the nozzle in small circles working his way up towards the back or roof. Care must be taken to avoid applying fresh materials on top of rebound or over sprayed shotcrete. It is essential that the air supply is consistent and has sufficient capacity to ensure the delivery of a steady stream of high velocity shotcrete to the rock face. Shooting distances are ideally about 1 to 1.5 metres. Holding the nozzle further from the rock face will result in a lower velocity flow of materials which leads to poor compaction and a higher proportion of rebound.

A well-trained operator can produce excellent quality shotcrete manually, when the work area is well-lit and well-ventilated, and when the crew members are in good communication with each other using prescribed hand signals or voice activated FM radio headsets. However, this is a very tiring and uncomfortable job, especially for overhead shooting, and compact robotic systems are increasingly being used to permit the operator to control the nozzle remotely. Typical robotic spray booms are illustrated in Figures 9, 10 and 11.

Figure 9: A truck mounted shotcrete robot being used in a large civil engineering tunnel. Note that the nozzle is approximately one metre from the rock surface.

Figure 10: Compact trailer-mounted robot unit for remote controlled shotcrete application.

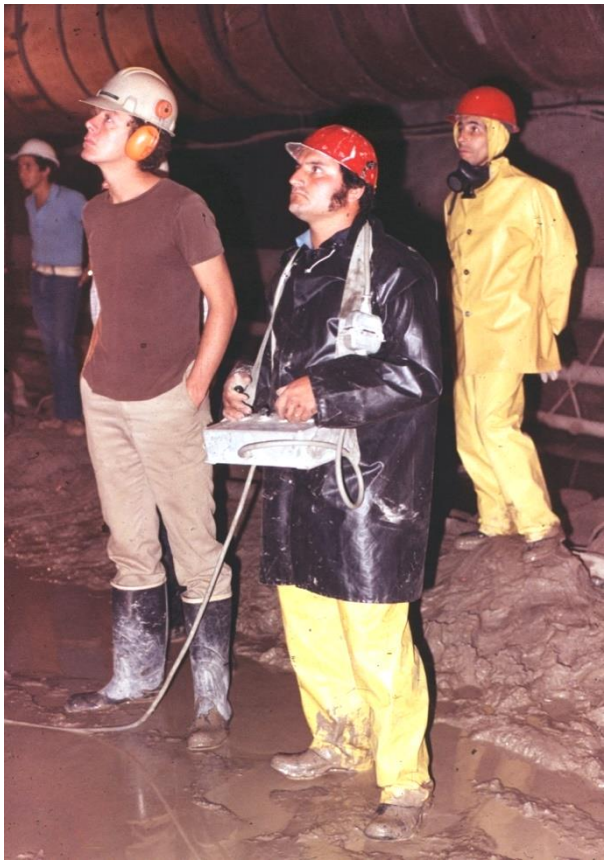

Figure 11: Shotcrete operator using a remotely controlled unit to apply shotcrete to a rock face in a large civil engineering excavation.

Figure 12: Plastic pipes used to provide drainage for a shotcrete layer applied to a rock mass with water-bearing joints.

When shotcrete is applied to rock masses with well-defined water-bearing joints, it is important to provide drainage through the shotcrete layer in order to relieve high water pressures. Drain holes, fitted with plastic pipes as illustrated in Figure 12, are commonly used for this purpose. Where the water inflow is not restricted to a few specific features, a porous fibre mat can be attached to the rock surface before the shotcrete layer is applied. When practical to do so, the water from these drains should be collected and directed into a drainage ditch or sump.

Design of shotcrete support

The design of shotcrete support for underground excavations is a very imprecise process. However, one observation, which is commonly made by practical engineers with years of experience in using shotcrete underground, is that it almost always performs better than anticipated. There are many examples (very few of which are documented) where shotcrete has been used as a last act of desperation in an effort to stabilise the failing rock around a tunnel and, to most people's surprise, it has worked.

The complex interaction between the failing rock mass around an underground opening, and a layer of shotcrete of varying thickness with properties which change as it hardens, defies most attempts at theoretical analysis. It is only in recent years, with the development of powerful numerical tools, that it has been possible to contemplate realistic analyses, which will explore the possible support-interaction behaviour of shotcrete. A clear understanding of shotcrete behaviour will require many more years of experience in the use of and in the interpretation of the results obtained from these programs. It is also important to recognise that shotcrete is very seldom used alone and its use in combination with rockbolts, cable bolts, lattice girders or steel sets further complicates the problem of analysing its contribution to support.

Current shotcrete support 'design' methodology relies very heavily upon rules of thumb and precedent experience. Wickham et al (1972) related the thickness of a shotcrete tunnel lining to their Rock Structure Rating (*RSR*). Bieniawski (1989) gave recommendations on shotcrete thicknesses (in conjunction with rockbolts or steel sets) for different Rock Mass Ratings (*RMR*) for a 10 m span opening. Grimstad and Barton (1993) have published an updated relating different support systems, including shotcrete and fibre reinforced shotcrete, to the Tunnelling Quality Index *Q*. Vandewalle (1993) collected various rules of thumb from a variety of sources and included them in his monograph.

Table 2 is a compilation of current shotcrete practice, combining all of these empirical rules and adding in my own practical experience. The reader is warned that this table can only be used as an approximate guide when deciding upon the type and thickness of shotcrete to be applied in a specific application. Modifications will almost certainly be required to deal with local variations in rock conditions and shotcrete quality.

Table 2: Summary of recommended shotcrete applications in underground mining for different rock mass conditions.

Rock mass description	*Rock mass behaviour*	*Support requirements*	*Shotcrete application*
Massive metamorphic or igneous rock. Low stress conditions.	No spalling, slabbing or failure.	None.	None.
Massive sedimentary rock. Low stress conditions.	Surfaces of some shales, siltstones, or claystones may slake as a result of moisture content change.	Sealing surface to prevent slaking.	Apply 25 mm thickness of plain shotcrete to permanent surfaces as soon as possible after excavation. Repair shotcrete damage due to blasting.

Massive rock with single wide fault or shear zone.	Fault gouge may be weak and erodible and may cause stability problems in adjacent jointed rock.	Provision of support and surface sealing in vicinity of weak fault of shear zone.	Remove weak material to a depth equal to width of fault or shear zone and grout rebar into adjacent sound rock. Weldmesh can be used if required to provide temporary rockfall support. Fill void with plain shotcrete. Extend steel fibre reinforced shotcrete laterally for at least width of gouge zone.
Massive metamorphic or igneous rock. High stress conditions.	Surface slabbing, spalling and possible rockburst damage.	Retention of broken rock and control of rock mass dilation.	Apply 50 mm shotcrete over weldmesh anchored behind bolt faceplates, or apply 50 mm of steel fibre reinforced shotcrete on rock and install rockbolts with faceplates; then apply second 25 mm shotcrete layer. Extend shotcrete application down sidewalls where required.
Massive sedimentary rock. High stress conditions.	Surface slabbing, spalling and possible squeezing in shales and soft rocks.	Retention of broken rock and control of squeezing.	Apply 75 mm layer of fibre reinforced shotcrete directly on clean rock. Rockbolts or dowels are also needed for additional support.
Metamorphic or igneous rock with a few widely spaced joints. Low stress conditions.	Potential for wedges or blocks to fall or slide due to gravity loading.	Provision of support in addition to that available from rockbolts or cables.	Apply 50 mm of steel fibre reinforced shotcrete to rock surfaces on which joint traces are exposed.
Sedimentary rock with a few widely spaced bedding planes and joints. Low stress conditions.	Potential for wedges or blocks to fall or slide due to gravity loading. Bedding plane exposures may deteriorate in time.	Provision of support in addition to that available from rockbolts or cables. Sealing of weak bedding plane exposures.	Apply 50 mm of steel fibre reinforced shotcrete on rock surface on which discontinuity traces are exposed, with particular attention to bedding plane traces.
Jointed metamorphic or igneous rock. High stress conditions.	Combined structural and stress-controlled failures around opening boundary.	Retention of broken rock and control of rock mass dilation.	Apply 75 mm plain shotcrete over weldmesh anchored behind bolt faceplates or apply 75 mm of steel fibre reinforced shotcrete on rock, install rockbolts with faceplates and then apply second 25 mm shotcrete layer Thicker shotcrete layers may be required at high stress concentrations.
Bedded and jointed weak sedimentary rock. High stress conditions.	Slabbing, spalling and possibly squeezing.	Control of rock mass failure and squeezing.	Apply 75 mm of steel fibre reinforced shotcrete to clean rock surfaces as soon as possible, install rockbolts, with faceplates, through shotcrete, apply second 75 mm shotcrete layer.
Highly jointed metamorphic or igneous rock. Low stress conditions.	Ravelling of small wedges and blocks defined by intersecting joints.	Prevention of progressive ravelling.	Apply 50 mm of steel fibre reinforced shotcrete on clean rock surface in roof of excavation. Rockbolts or dowels may be needed for additional support for large blocks.
Highly jointed and bedded sedimentary rock. Low stress conditions.	Bed separation in wide span excavations and ravelling of bedding traces in inclined faces.	Control of bed separation and ravelling.	Rockbolts or dowels required to control bed separation. Apply 75 mm of fibre reinforced shotcrete to bedding plane traces before bolting.

Heavily jointed igneous or metamorphic rock, conglomerates or cemented rockfill. High stress conditions.	Squeezing and 'plastic' flow of rock mass around opening.	Control of rock mass failure and dilation.	Apply 100 mm of steel fibre reinforced shotcrete as soon as possible and install rockbolts, with face-plates, through shotcrete. Apply additional 50 mm of shotcrete if required. Extend support down sidewalls if necessary.
Heavily jointed sedimentary rock with clay coated surfaces. High stress conditions.	Squeezing and 'plastic' flow of rock mass around opening. Clay rich rocks may swell.	Control of rock mass failure and dilation.	Apply 50 mm of steel fibre reinforced shotcrete as soon as possible, install lattice girders or light steel sets, with invert struts where required, then more steel fibre reinforced shotcrete to cover sets or girders. Forepoling or spiling may be required to stabilise face ahead of excavation. Gaps may be left in final shotcrete to allow for movement resulting from squeezing or swelling. Gap should be closed once opening is stable.
Mild rockburst conditions in massive rock subjected to high stress conditions.	Spalling, slabbing and mild rockbursts.	Retention of broken rock and control of failure propagation.	Apply 50 to 100 mm of shotcrete over mesh or cable lacing which is firmly attached to the rock surface by means of yielding rockbolts or cable bolts.

References

Bieniawski Z.T. 1989. *Engineering Rock Mass Classifications*. New York: Wiley. 251 pages.

Franzén, T. 1992. Shotcrete for underground support - a state of the art report with focus on steel fibre reinforcement. In *Rock support in mining and underground construction, proc. int. symp. rock support,* Sudbury, (eds P.K. Kaiser and D.R. McCreath), 91-104. Rotterdam: Balkema.

Grimstad, E. and Barton, N. 1993. Updating the Q-System for NMT. *Proc. int. symp. on sprayed concrete - modern use of wet mix sprayed concrete for underground support*, Fagernes, (eds Kompen, Opsahl and Berg). Oslo: Norwegian Concrete Assn.

Kirsten, H.A.D. 1992. Comparative efficiency and ultimate strength of mesh- and fibre-reinforced shotcrete as determined from full-scale bending tests. *J. S. Afr. Inst. Min. Metall*. Nov., 303-322.

Kirsten, H.A.D. 1993. Equivalence of mesh- and fibre-reinforced shotcrete at large deflections. *Can. Geotech. J.* **30**, 418-440.

Kompen, R. 1989. Wet process steel fibre reinforced shotcrete for rock support and fire protection, Norwegian practice and experience. In *Proc. underground city conf.*, Munich, (ed. D. Morfeldt), 228-237.

Langille, C.C. and Burtney, M.W. 1992. Effectiveness of shotcrete and mesh support in low energy rockburst conditions at INCO's Creighton mine. In *Rock support in mining and underground construction, proc. int. symp. rock support,* Sudbury, (eds. P.K. Kaiser and D.R. McCreath), 633-638. Rotterdam: Balkema.

Mahar, J.W., Parker, H.W. and Wuellner, W.W. 1975. *Shotcrete practice in underground construction*. US Dept. Transportation Report FRA-OR&D 75-90. Springfield, VA: Nat. Tech. Info. Service.

McCreath, D.R. and Kaiser, P.K. 1992. Evaluation of current support practices in burst-prone ground and preliminary guidelines for Canadian hardrock mines. In *Rock support in mining and underground construction, proc. int. symp. rock support*, Sudbury, (eds P.K. Kaiser and D.R. McCreath), 611-619. Rotterdam: Balkema.

Morgan, D.R. 1993. Advances in shotcrete technology for support of underground openings in Canada. In *Shotcrete for underground support V, proc. engineering foundation conf.*, Uppsala, (eds J.C. Sharp and T. Franzen), 358-382. New York: Am. Soc. Civ. Engrs.

Morgan, D. R., McAskill, N., Richardson, B. W., and Zellers, R. C. 1989. "A Comparative evaluation of plain, polypropylene fiber, steel fiber and wire mesh reinforced shotcretes," *Transportation Research Record, No. 1226, Concrete and Concrete Construction*, 78-87. Washington, DC: Transportation Research Board, National Research, Council.

Papworth, F. 2002. Design guidelines for the use of fiber-reinforced shotcrete for ground support. *American Shotcrete Assn Shotcrete Magazine*, Spring.

Rabcewicz, L. 1969. Stability of tunnels under rock load. *Water Power* **21**(6-8) 225-229, 266-273, 297-304.

Rose, D. 1985. Steel fibre reinforced shotcrete for tunnel linings: the state of the art. *Proc. North American rapid excav. tunneling conf.* **1**, 392-412. New York: Soc. Min. Engrs, Am. Inst. Min. Metall. Petrolm Engrs.

Vandewalle, M. 1993. *Dramix: Tunnelling the world.* 3rd edn. Zwevegem, Belgium: N.V. Bekaert S.A.

Wickham, G.E., Tiedemann, H.R. and Skinner, E.H. 1972. Support determination based on geologic predictions. In *Proc. North American rapid excav. tunneling conf.*, Chicago, (eds. K.S. Lane and L.A. Garfield), 43-64. New York: Soc. Min. Engrs, Am. Inst. Min. Metall. Petrolm Engrs.

Wood, D.F. 1992. Specification and application of fibre reinforced shotcrete. In *Rock support in mining and underground construction, proc. int. symp. on rock support*, Sudbury, (eds. P.K. Kaiser and D.R. McCreath), 149-156. Rotterdam: Balkema.

Wood, D.F., Banthia, N. and Trottier, J-F. 1993. A comparative study of different steel fibres in shotcrete. In *Shotcrete for underground support VI*, Niagara Falls, 57-66. New York: Am. Soc. Civ. Engrs.

19. Tensile failure and spalling

Introduction

The purpose of this chapter is to summarize the combinations of in situ stress and rock properties that can lead to tensile failure, spalling and one type of rockbursting in intact or sparsely jointed massive rock surrounding tunnels and boreholes. Generally, tensile failure occurs at much lower stress levels than spalling. It occurs first and progresses until the cracks have reached a stable configuration. As the stress levels increase, spalling can be initiated. This also progresses in a stepwise manner until a stable configuration is reached and the spalls stop. At much higher stress levels, cracks remote from the excavation boundary can interact with the tensile cracks and spalls to create a large-scale shear fracture. This can collapse the tunnel with the release of a significant amount of energy which may be one of the mechanisms responsible for the violent failures known as rockbursts.

Numerous papers on each or on all these failure mechanisms have been published. Several of these will be referred to in this chapter. While the general conclusions reached are similar, a wide range of different opinions on details of the failure mechanisms are presented. In the discussion which follows, a set of mechanisms will be presented which appear to fit numerous practical observations that I have made over the years. I make no claim that these mechanisms are more logical or correct than alternative mechanisms proposed, but they do provide credible explanations for understanding these failure processes.

Failure initiation and propagation in intact rock surrounding a tunnel

Figure 1 illustrates the in-situ stresses and the induced stresses around the boundary of a circular excavation such as a tunnel or borehole in intact or sparsely jointed massive rock. In this case, it has been assumed that the maximum principal stress P acts in a horizontal direction and that the minor principal stress kP has a much lower magnitude. If the value of $k < 0.33$, then tensile stress zones will be induced in the excavation sidewalls as illustrated. When the tensile stresses on the boundary exceed the tensile strength of the rock, horizontal cracks will develop in the rock. There may be several parallel cracks, with very small opening widths, as illustrated in the right-hand sidewall of the lower figure, or there may be a single wider crack as shown in the left-hand sidewall. These tensile cracks propagate a limited distance before stopping and becoming completely stable. They have no significant influence on the development of spalling which occurs at higher stress levels. The distance to which single cracks will propagate was determined by Hoek (1965) in glass and rock plate models, as illustrated in Figures 2 and 3. The development of spalling in the roof and floor of the circular excavation is illustrated in the lower drawing in Figure 1.

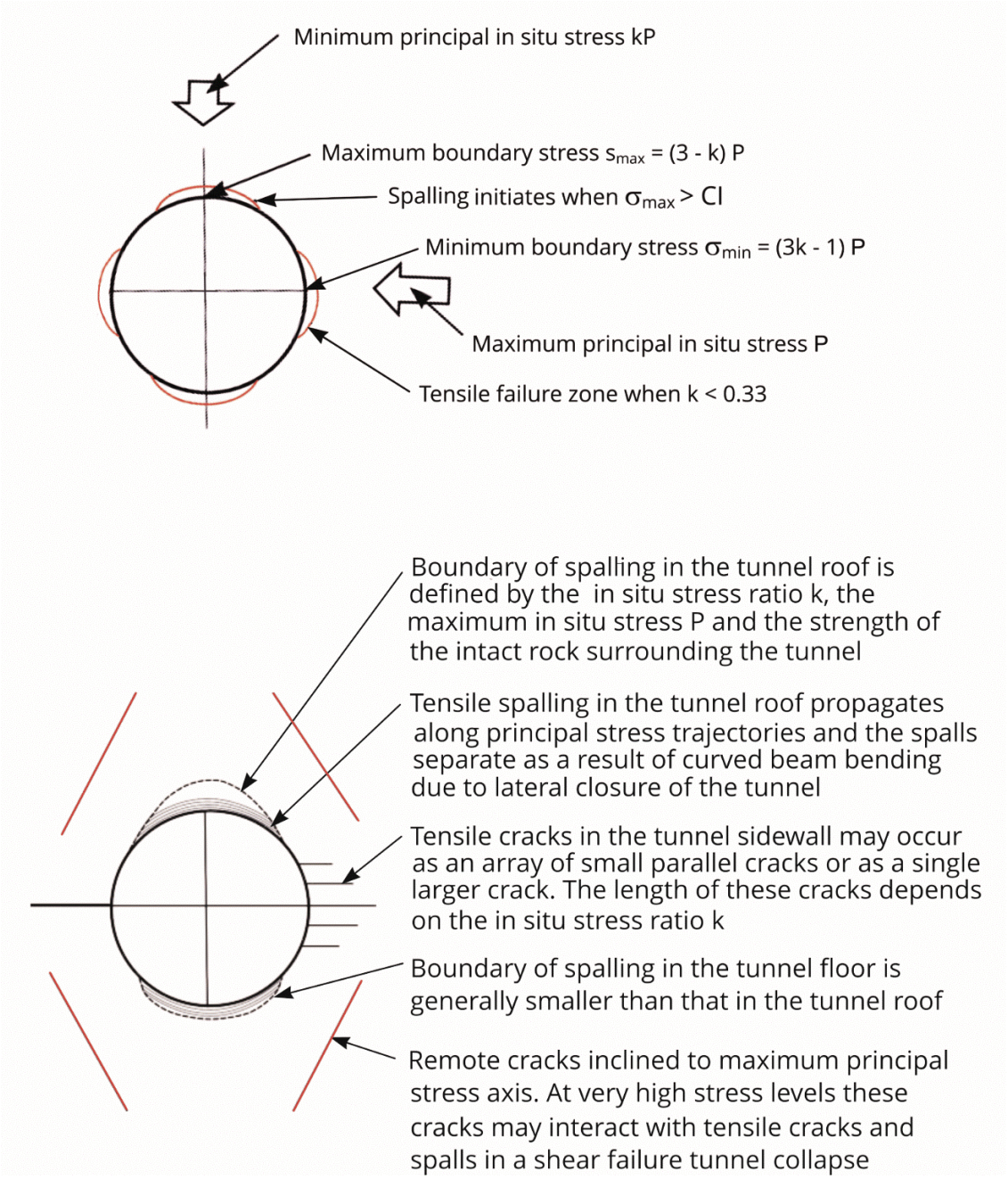

Figure 1: Stress conditions and resulting failure types in highly stressed intact or sparsely jointed massive rock surrounding a circular tunnel or borehole.

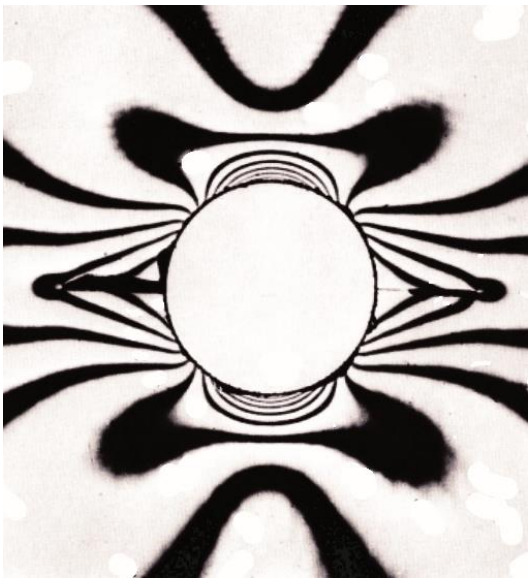

Figure 2: Photoelastic pattern in a glass plate model showing the distribution of ($\sigma_1 - \sigma_3$) contours and the formation of tensile cracks in the sidewalls.

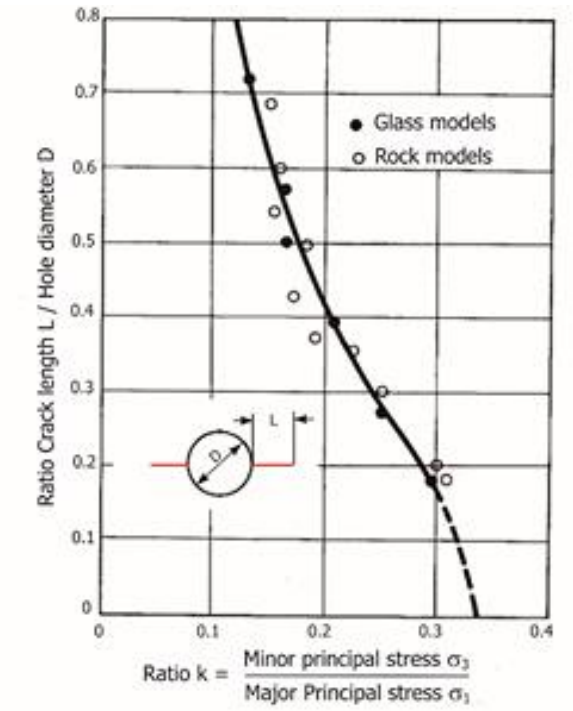

Figure 3: Length of stable cracks in glass and rock models tested by Hoek (1965).

Spalling initiates when the boundary stress exceeds the crack initiation stress CI in the roof and floor of the tunnel, as shown in Figure 1. Nicksair and Martin (2013) showed that tensile crack initiation (CI) in various rocks can initiate at approximately 45% of the uniaxial compressive strength (UCS) of the intact rock, as shown in Figure 4. This crack initiation is a pre-requisite for spalling. It is necessary to establish the in-situ stress conditions that can cause the initiation of these cracks when a tunnel is excavated in an intact or sparsely jointed rock mass.

Figure 5: Spalling in the sidewalls of a machine bored mine shaft in massive rock.

A typical spall from the walls of a machine bored shaft or tunnel in highly stressed massive rock is illustrated in Figure 5. These spalls initiate on the tunnel boundary, at points of maximum compressive stress which are defined by the normal to the maximum principal stress direction. As shown in Figure 1, the maximum boundary stress at these locations is σ_{1max} = (3 – k) P, where k is the ratio of minor to major principal stresses (σ_3/σ_1) and P is the magnitude of the major in situ principal stress. As discussed above, spalling initiates when the maximum boundary stress exceeds the crack initiation strength CI. This results in the spalling initiation relationship:

$$CI = (3 - k)P \tag{1}$$

Observation of spalling in the field show that, in massive intact rock, the spalls occur as thin plates such as that illustrated in Figure 6. As shown in the close-up photograph reproduced in Figure 7, the appearance of the spall surface suggests that it has occurred because of pure tensile failure, with no signs of slickensides which are normally associated with shear failure. This, in turn, suggests that the spalling is controlled by tensile failure rather than by shearing, which is the default failure mode assumed in many numerical programs used for shaft and tunnel failure analysis.

Figure 6: Plate-like spall from a tunnel in massive granite.

Figure 7: Spalls showing tensile failure surfaces with no signs of slickensides associated with shearing.

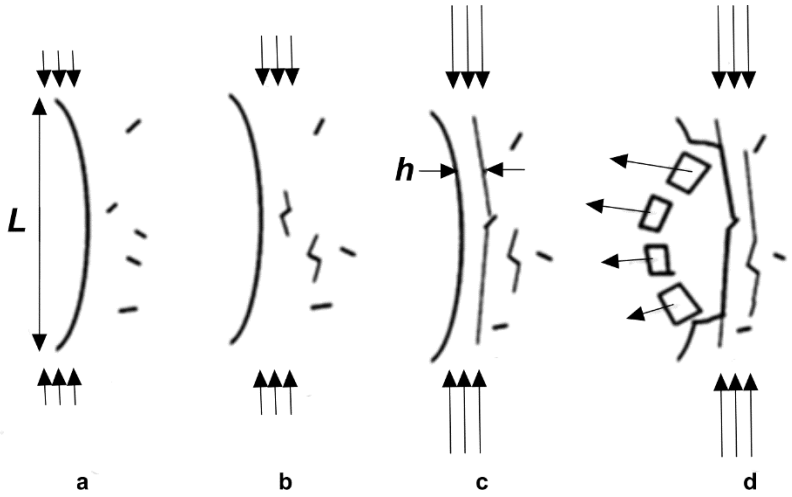

a. Existing microcracks in the rock adjacent to the excavation boundary
b. Propagation of wing cracks from isolated microcracks as stress increases
c. Propagation of wing cracks from microcrack close to excavation boundary due to lack of confinement
d. Buckling failure of spall adjacent to excavation boundary and creation of a new spall due to lateral stress relief

Figure 8: Simplified illustration of the mechanism of spall formation, from Dyskin and Germanovich, 1993.

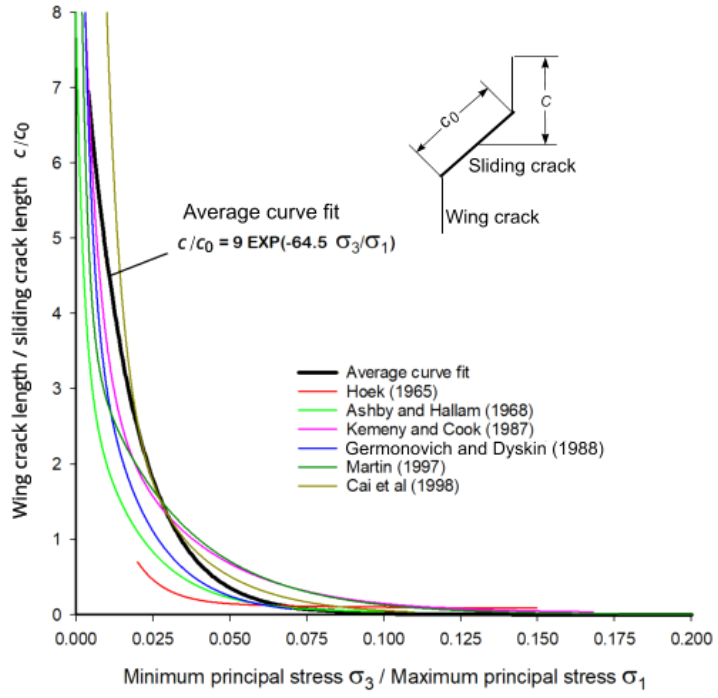

Figure 9: Vertical wing crack length from critically inclined Griffith cracks for different ratios of minor to major principal stress.

Figure 8 shows the mechanism of spalling proposed by Dyskin and Germanovich (1993). This involves the propagation of wing cracks formed at the tips of existing microcracks in the rock, which, as shown by several authors in Figure 9, depends upon the reduction of the ratio of the minor to major principal stresses. As this ratio decreases close to zero at the excavation boundary, the wing crack length increases to the full extent of the overstressed section of the boundary and thin plates are formed. As shown in Figures 6 and 7, these plates are typically 1 to 2 cm thick in 4 to 5 m diameter tunnels.

As suggested in Figure 8, once a slender slab has developed in the wall of an excavation, any additional loading will apply an axial load to this plate. This will result in bending failure of the plate and a creation of a new excavation boundary behind which a new spall will fall. The process tends to be self-propagating until conditions are reached which make it difficult or impossible for new spalls to develop.

The most important of these conditions is the overall shape of the complete set of spalls in relation to the ratio of the maximum stress in the tunnel wall to the uniaxial compressive strength of the surrounding rock. Diederichs et al (2010) have summarized in situ observations of the depth of spalling for circular tunnels in the plot reproduced in Figure 10. This plot shows that the spalling depth is controlled by the ratio of the maximum stress on the tunnel boundary to the uniaxial compressive strength (UCS) or the crack initiation stress (CI).

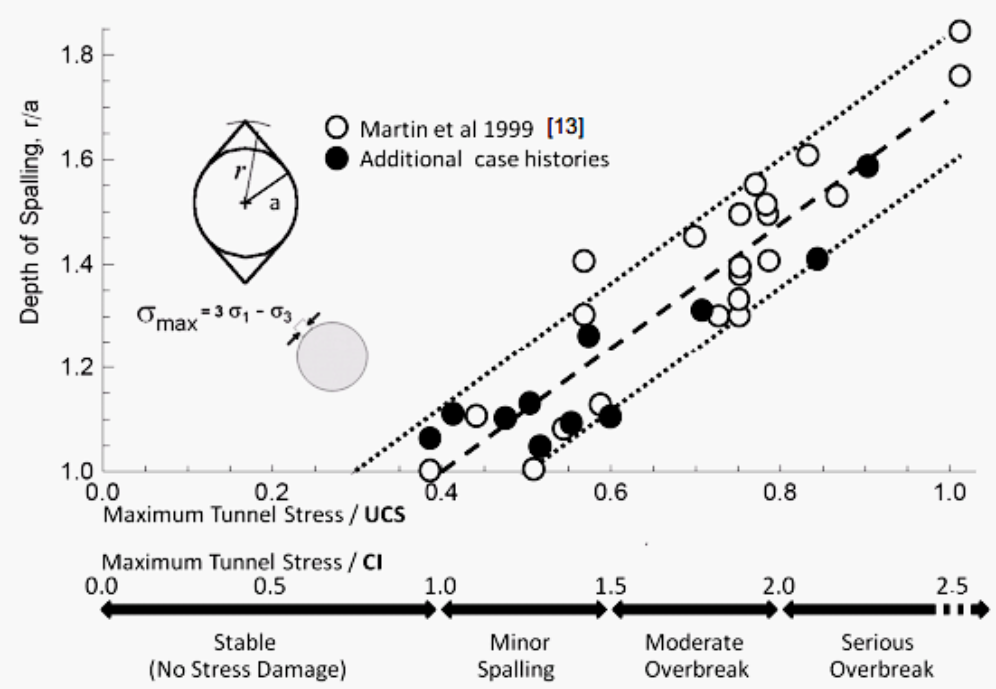

Figure 10: Plot of measured depth of spalling for a circular tunnel by Diederichs et al. (2010).

Progressive spalling in the AECL URL Mine-by test tunnel

A classic case of progressive spalling is the Mine-by Test Tunnel in the Atomic Energy of Canada Ltd. Underground Research Laboratory (URL) at Pinawa, Manitoba, Canada. The layout of the URL is shown in Figure 11. The final spall boundaries in this tunnel are illustrated in Figure 12. These spalls have been studied in detail by numerous authors including Martin et al (1996), Martin (1997), Diederichs et al (2004) and Diederichs (2007).

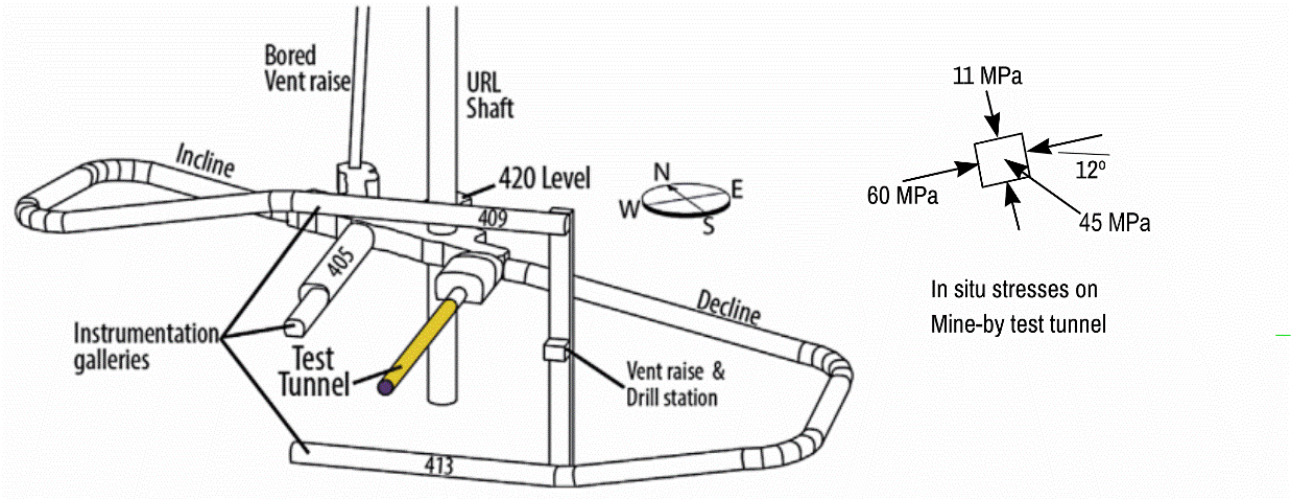

Figure 11: AECL URL Mine-by Test Tunnel excavated in Lac du Bonnet granite at a depth of 420 m below surface. Modified from Martin and Read (1996).

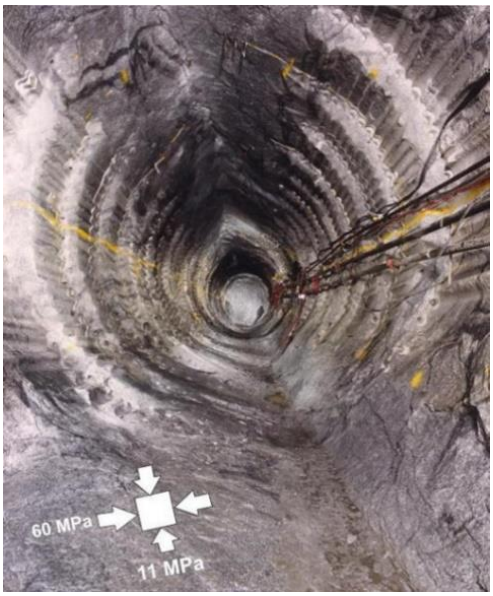

Figure 12: Spalling in the roof and floor of the Mine-by Test Tunnel. Note that the final roof and floor profiles shown here were only exposed after completion of the tunnel and excavation and scaling of the spalled material which remained attached to the boundary.

(Photograph provided by Professor C.D Martin)

During the excavation of the URL Mine-by tunnel, instruments for monitoring acoustic emission (AE) and micro seismic (MS) events were installed in the rock mass surrounding the tunnel. Read and Martin (1996) describe the results of these measurements. One of their plots is reproduced in Figure 13, showing spalling in the roof and floor. Acoustic emissions were measured in the tensile stress zones in the tunnel sidewalls, but no identifiable tensile cracks were found in these regions. It was assumed that these acoustic emissions were due to the formation of numerous parallel tensile cracks, the apertures of which were too small to detect visually.

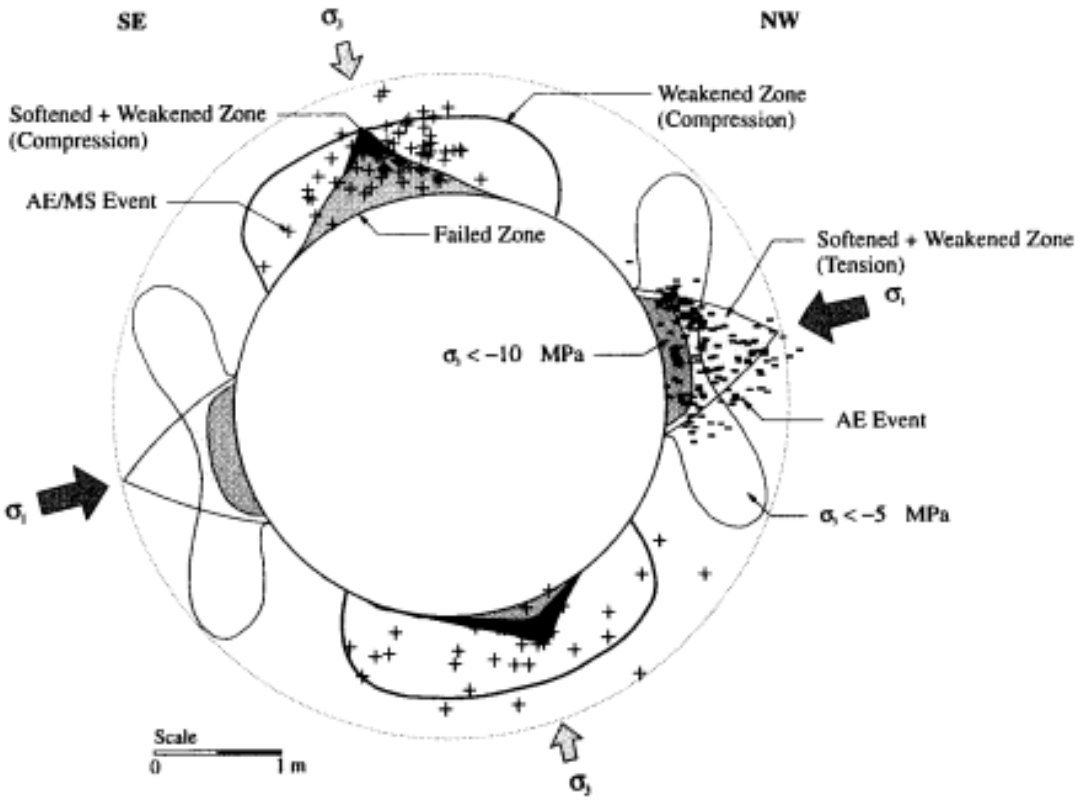

Figure 13: Excavation induced damage around the URL Mine-by tunnel. From Read and Martin (1996).

The URL was excavated in massive Lac du Bonnet granite, the mechanical properties of which were determined by Lau and Gorski (1992) in the CANMET laboratories in Ottawa, Ontario, Canada. The definition of the stresses at crack initiation, strain localization and peak strength plotted in Figure 14 are based on a modified figure from Martin and Christiansson (2009). Figure 15 shows the principal stress plots for crack initiation, onset of strain localization and peak strength for these tests.

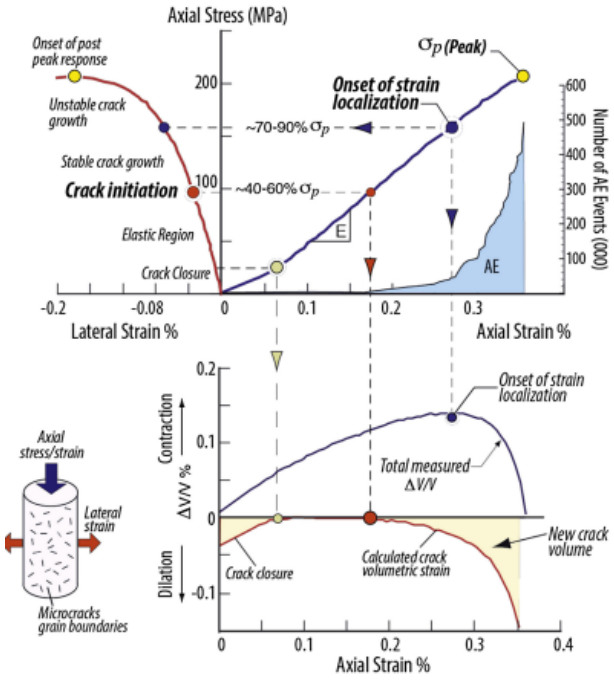

Figure 14: Stages in the progressive failure of intact specimens of Lac du Bonnet granite. Modified from Martin and Christiansson (2009).

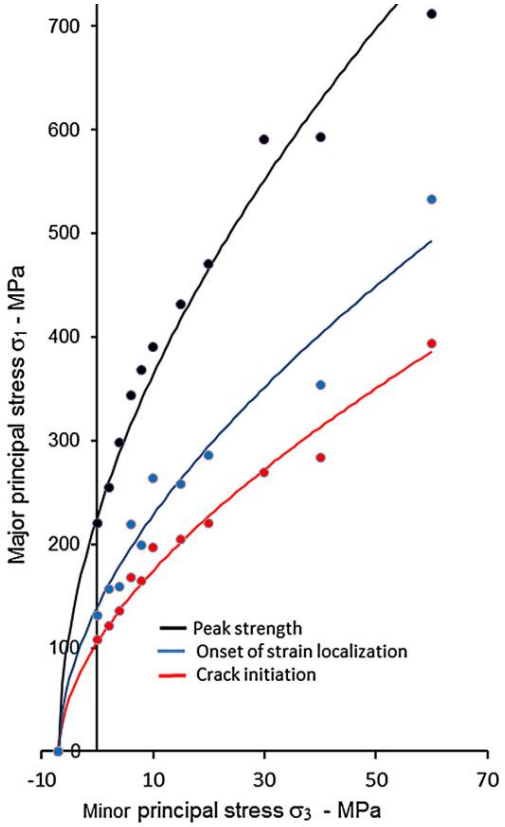

Figure 15: Tensile crack initiation, strain localization and peak strength for Lac du Bonnet granite from tests by Lau and Gorski (1992).

The transition from failure initiation to shear failure of the intact rock has been discussed extensively by Diederichs et al (2004), Diederichs (2007), Kaiser et al (2000), Kaiser (2006), Kaiser et al (2015), Bewick et al (2015) and Perras and Diederichs (2016). Several of these discussions have referred to research on the propagation of wing cracks from inclined Griffith cracks, summarized in Figure 9. The curves in Figure 9 show that the ratio of the length of the tensile wing cracks to the initiating defect, such as a grain boundary, decreases exponentially from a ratio of $\sigma_3/\sigma_1 = 0$ to almost zero at $\sigma_3/\sigma_1 > 0.1$. Note that some of these curves are based on the initiating defect being represented by an open elliptical crack (Hoek, Ashby and Hallam, Germanovich and Dyskin, Cai et al) while the curves published by Kemeny and Cook and by Martin are for closed sliding cracks, such as grain boundaries.

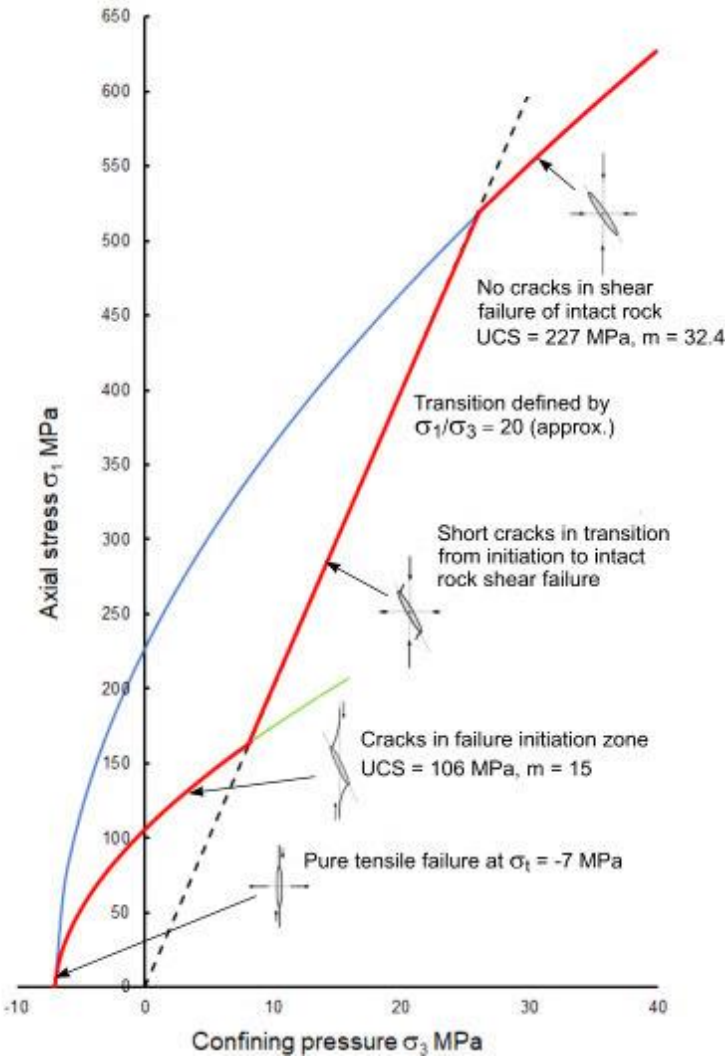

Figure 16: Composite failure curve for spalling of Lac du Bonnet Granite from Pinawa, Manitoba, Canada.

Figure 16 presents a composite failure curve, for intact and undamaged Lac du Bonnet granite, constructed using Hoek-Brown failure envelopes based on the triaxial test data shown in Figure 11. The envelope for fracture initiation is defined by the equation $\sigma_1 = \sigma_3 + CI\ (m.\ \sigma_3 + 1)\ ^{0.5}$, with CI = 106 MPa and m = 15. The equation for the intact granite is $\sigma_1 = \sigma_3 + UCS\ (m.\ \sigma_3 + 1)\ ^{0.5}$ where UCS = 227 MPa and m = 32.4. A uniaxial tensile strength $\sigma_t = -7$ MPa is based on direct tensile tests performed by Lau and Gorski (1992).

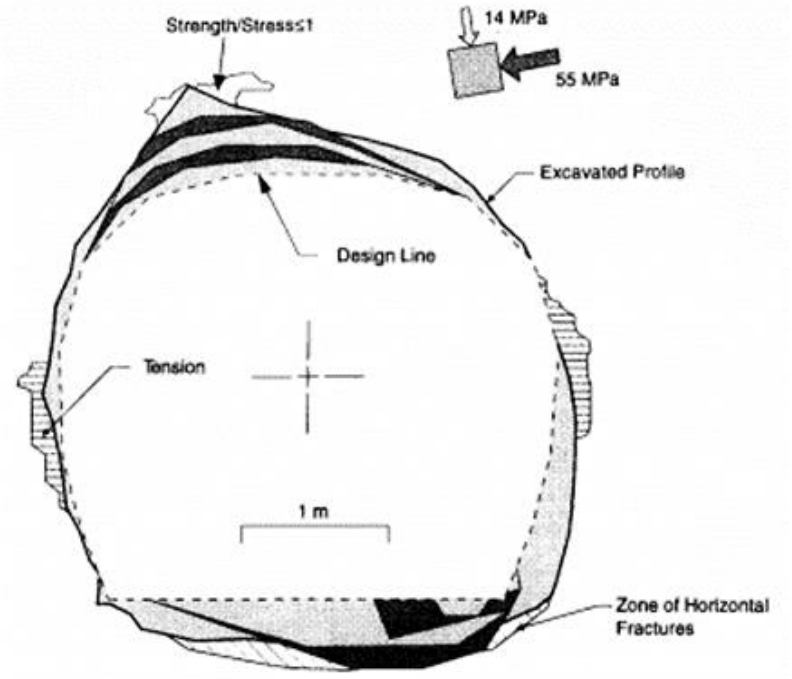

Figure 17: Numerical simulation of the slabbing process using elastic analyses and an elastic-brittle constitutive model. From Read and Martin (1996).

Observation of spalling in tunnels shows that this is a stepwise process in which each spall changes the boundary of the excavation and the surrounding stress field, resulting in the initiation of the next spall, as shown in Figure 17. The following quotation is from Martin (1997):

"In an attempt to simulate the slabbing process observed *in situ*, Read (1991) developed a routine within FLAC to conduct an iterative elastic analysis with explicit checks for tensile, compressive (shear) and slabbing failure based on a Hoek-Brown failure criterion with σ_c = 100, m = 12 and s = 1. A unidirectional tensile cutoff criterion was used in the case of tensile failure, which resulted in minor stress redistribution in the sidewalls of the tunnel. As in the previous analysis, compressive failure was noted close to the tunnel boundary in the roof and floor regions of the tunnel. Using a confining stress criterion in combination with a buckling criterion as a basis for removing elements

at the free boundary, i.e., where the confinement was zero, Read (1991) found that the zone of removed material grew progressively, and was similar in shape to that observed *in situ.* He concluded that this type of modelling predicted responses for the instrumentation that were significantly different from those predicted by closed-form solutions for a circular hole in an infinite elastic medium. He also found that the shape of the predicted V-shaped notch was very dependent on the element removal scheme. Without the buckling constraint on the element removal scheme, Read (1991) found that the depth of the V-shaped notch approached *2a* where *a* is the radius of the tunnel. However, with the buckling constraint, the depth of the V-shaped notch was reduced to *1.5a*."

At the time of Read's analysis in 1991, the concept of failure initiation at 45% of the uniaxial compressive strength of the intact rock had not been recognized. Hence, despite the promising results obtain by Read, his method was not adequate, and needs to be modified to incorporate the three-stage failure criterion shown in Figure 15. The step-by-step elastic analysis that I have carried out, using the RocScience finite element program RS2, is described below. Note that this analysis has been carried out on an idealized circular tunnel instead of the surveyed tunnel shape used by Read and Martin (1966).

Tensile failure in the tunnel sidewalls

As a tunnel is advanced through a stressed rock mass, the stresses on the tunnel boundary increase as the support provided by the rock mass ahead of the face decreases with distance from the face. The first boundary stress to exceed the available rock strength is in the tunnel sidewalls where the Strength Factor is 0.26 (σ_t = -7 MPa, σ_{min} = -27 MPa). No tensile cracks were observed in the tunnel sidewalls, so it was assumed that several parallel cracks, each with a very small aperture, occurred in the tensile stress zone. The propagation of these parallel tensile cracks is illustrated in Figure 18. The maximum depth of this cracked zone is 0.5 m, in the sidewalls of the 3.5 m diameter tunnel.

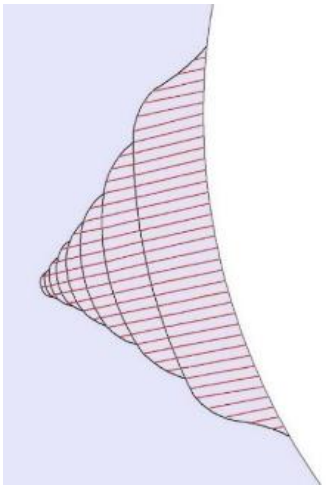

Figure 18: Progressive propagation of parallel tensile cracks in the sidewall of the Mine-by tunnel.

Progressive spalling in the tunnel roof

The zone of potential failure initiation, defined by a Hoek-Brown failure curve with CI = 106 MPa and m = 15, is contained within the $\sigma_1/\sigma_3 = 20$ contours in Figure 16. Spalling failure can occur within this zone, with the spalls commencing at the tunnel boundary where the Strength Factor is 0.67 ($CI/\sigma_{max} = 106/169$), in the roof and floor. Typically, these initial spalls are about 3 cm thick plates, as illustrated in Figure 6.

As the spalls progress it becomes increasing difficult for the failed material to fall away from the tunnel roof. In extreme situations, such as those illustrated in Figure 19, the spalls are confined and can only be dislodged by scaling using heavy mechanical equipment. The confined spalled material left in place, after the main spall has fallen away or been removed, is critical in defining the changed boundary shape used in the analysis of the next spall.

Figure 19: Confined spalls in the sharp corner of a square tunnel in a South African deep level gold mine. Depending on the changes in boundary shape, because of previous spalls, new spalls may find it difficult or impossible to escape from this confinement.

Photograph from the collection of the late Professor R.A.L. Black of the Royal School of Mines, Imperial College, London.

Read (1991) used a buckling criterion to estimate the constraint imposed on the slabs formed during the tunnel spalling process. I have experimented with numerous processes to investigate this constraint, including buckling of curved plates and Voronoi joint models, but while these studies have been very interesting, they did not produced results which were practical to implement in the modelling process discussed in this document.

The method finally adopted for the definition of the zone of spalled material that is free to fall is illustrated in Figure 20. This starts with the definition of the zone in which fracture initiation can initiate, defined by the $\sigma_1/\sigma_3 = 20$ contours, as shown in Figures 16. Within this zone, The Strength Factor contours are calculated, using the Hoek-Brown failure criterion with CI = 106 MPa and m = 15.

For $\sigma_1/\sigma_3 = 20$ and Strength Factors = 1.0 (light grey zone in Figure 20), fracture initiation can occur, but conditions for the development of spalling are not satisfied. Micro-seismic and acoustic emission events are likely to occur in this zone, as suggested in Figure 20.

For $\sigma_1/\sigma_3 = 20$ and Strength Factors < 1.0 (green zone in Figure 15), spalling can develop, but it is probable that some of this material will remain confined and will not be free to fall.

For Strength Factors < 0.93 (defined by the tangent point to the $\sigma_1/\sigma_3 = 20$ contour and shown as the red zone in Figure 20), the spalls are fully developed and free to fall from the roof of the excavation.

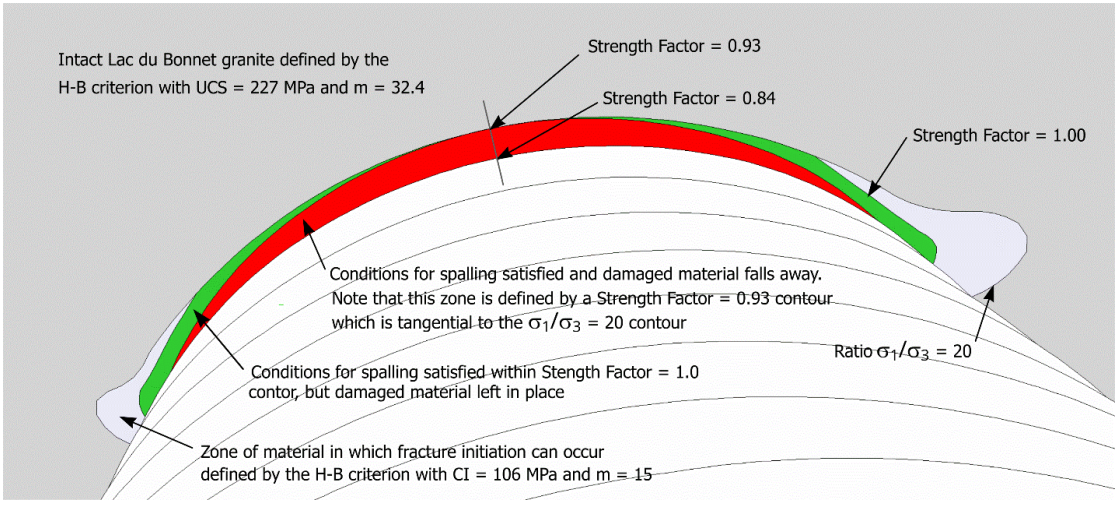

Figure 20: Definition of the 8th spalling zone in the roof of the Mine-by tunnel.

Note that, in the floor of the tunnel, the first spall is identical to that in the roof, as shown in Figure 1. However, since this spall is generally covered by roadbed material and, as in the case of the Mine-by tunnel, it was only excavated after completion of the tunnel, the final shape of the floor spall zone is quite different from the roof spall.

The results of the complete spalling analysis for the roof of the Mine-by tunnel are presented in Figure 21, which includes the measured principal stress values at the peak of each of the 24 spalls. This analysis can be considered to produce an ideal collection of spalls in a completely homogeneous, isotropic intact rock. These conditions are

seldom found in actual tunnels. It is interesting to compare the shape and depth of the 24th spall in Figure 21 with the surveyed shapes of the actual spalls in the Mine-by tunnel, shown in Figure 22.

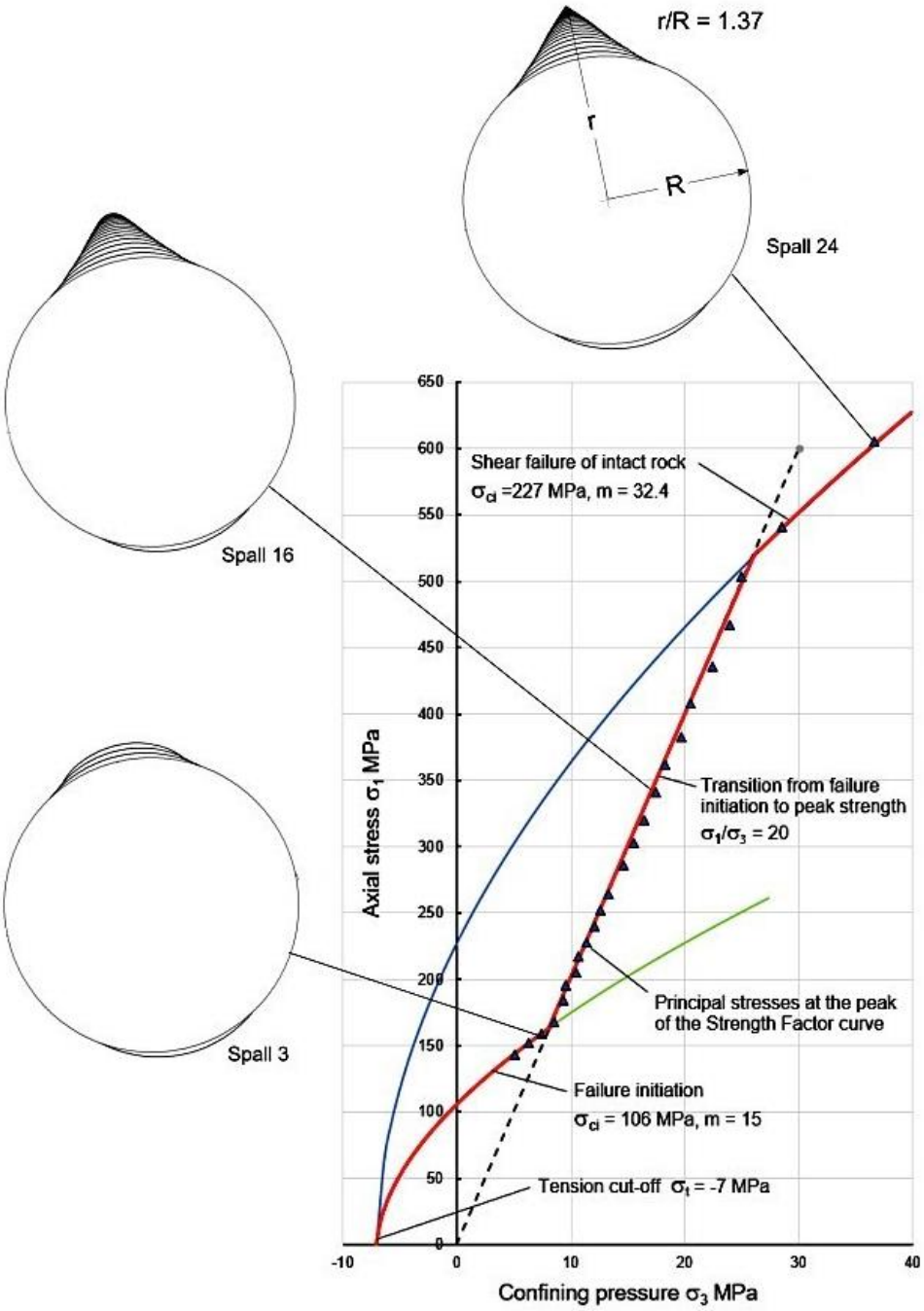

Figure 21: Composite failure curve for spalling of Lac du Bonnet Granite in the URL Mine-by tunnel, with predicted spalls and maximum stress values for each spall.

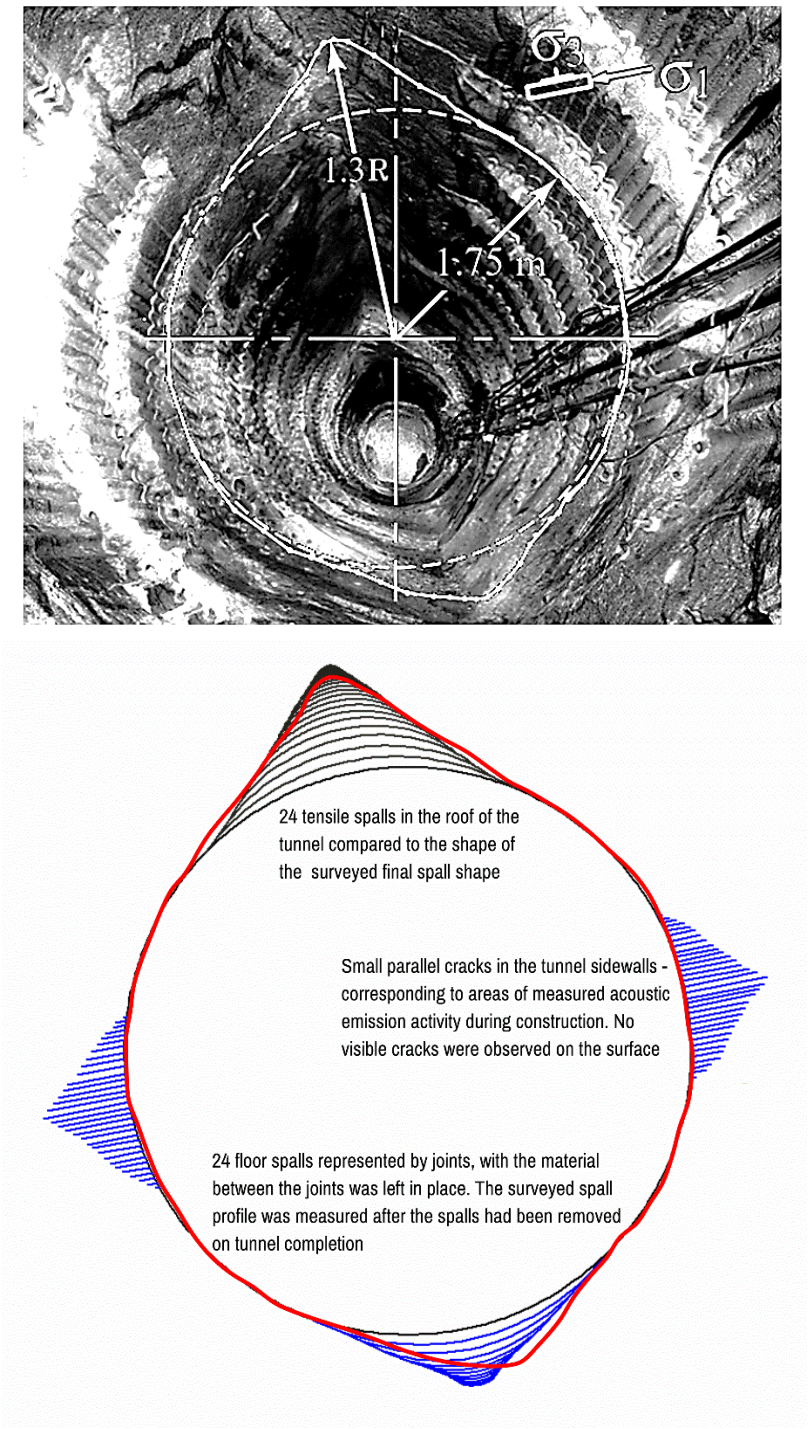

Figure 22: Comparison between surveyed (red) and predicted spalls in the URL Mine-by tunnel.

The value of this analysis lies not in its absolute accuracy, but rather in the fact that it follows a simple logical process that can be applied to any situation in which spalling can occur in brittle materials such as rock and concrete.

A major limitation of the analysis presented in this document is that it was performed using the RocScience finite element program RS2 which requires information to be transferred between the modeler and the interpreter for each spall. While this is analysis provides a wealth of interesting and useful information, it is extremely time-consuming and, therefore, of limited use as a practical engineering design tool. However, if this analysis could be carried out in a program, such as a boundary element program, which included both calculation and interpretation on the same screen, the usefulness would be considerably enhanced.

Tensile failure and progressive spalling in a model

Hoek (1965) investigated tensile failure and progressive spalling in rock plate models cut from blocks of a very uniform fine-grained Granite Aplite. This rock was known to be a potential source of severe rockbursting in very deep level mines and this was a main reason for its choice as a test material. Triaxial tests on 25 mm diameter core specimens of this rock were carried in the rock mechanics laboratory in the South African Council for Scientific and Industrial Research (CSIR) and in the laboratory operated by Professor W.F. Brace in the Department of Earth and Planetary Science at the Massachusetts Institute of Technology (MIT) in the USA. The results of these tests, summarized in Figure 23, show that the rock has a uniaxial compressive strength of σ_{ci} = 600.4 MPa, a Hoek-Brown constant m_i = 18.8 and a tensile strength σ_t = -22.2 MPa.

Before moving on to a discussion on spalling failures, tensile failures, which tend to develop in excavation boundaries at a much lower stress level, will be discussed. This question was studied on physical models with both glass and rock as the model materials as shown in Figures 24. The equipment used to carry out these studies is discussed in the Appendix 1.

The results of these studies are summarized in Figure 23. These cracks can only initiate at ratios of lateral to vertical stress (k) of less than 0.33 and the length of the cracks increases rapidly for $k < 0.1$. The main conclusion from these studies was that the development and propagation of a tensile crack has a negligible influence upon the initiation and propagation of spalling in the excavation boundaries at 90° to the tensile cracks. Consequently, in the following study of spalling, tensile cracks have been inserted into the numerical model to coincide with the length of the observed cracks in the rock plate model and, thereafter, the influence of the tensile cracks has been ignored.

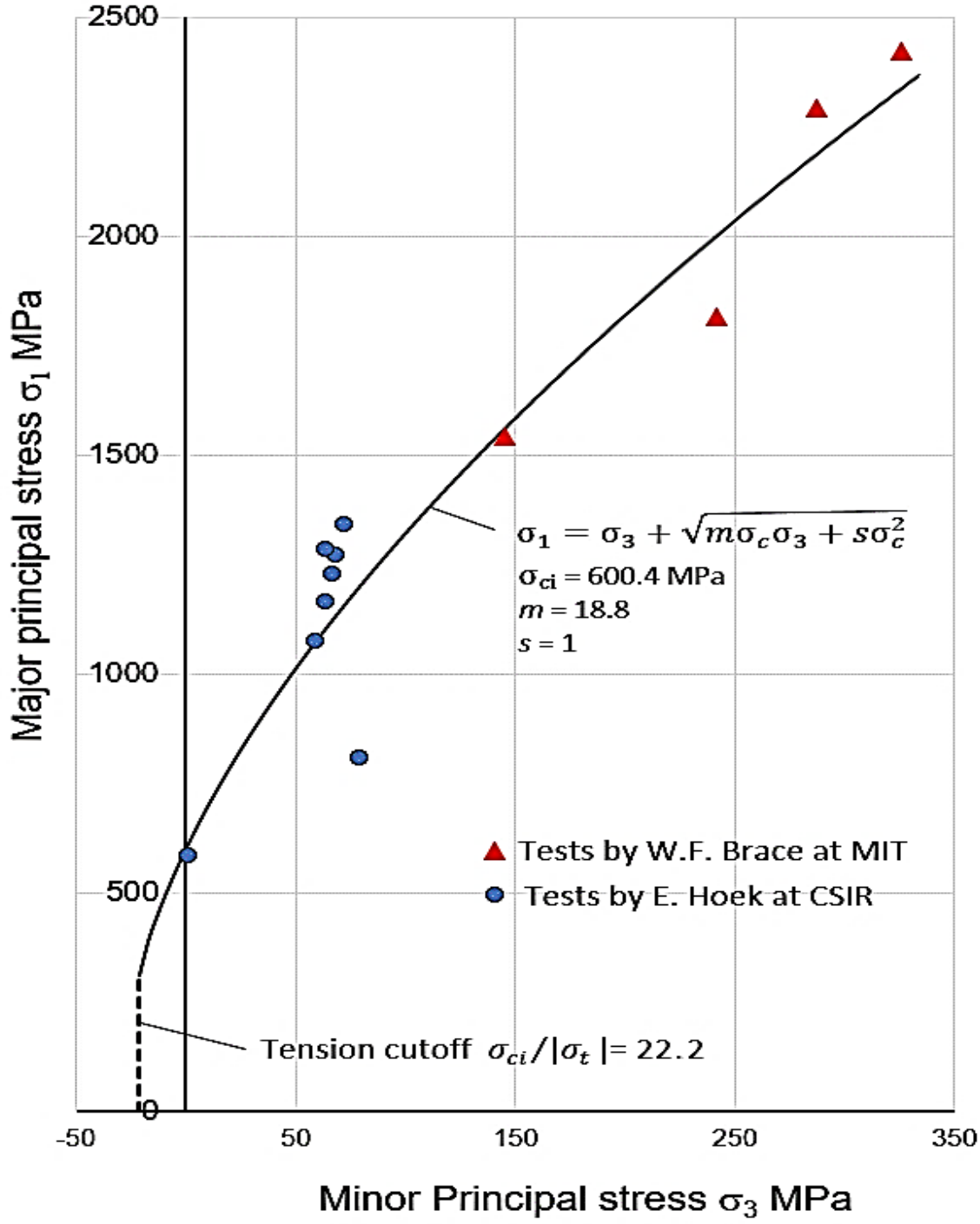

Figure 23: Results of triaxial tests on Granite Aplite. (After Hoek and Brown, 2018).

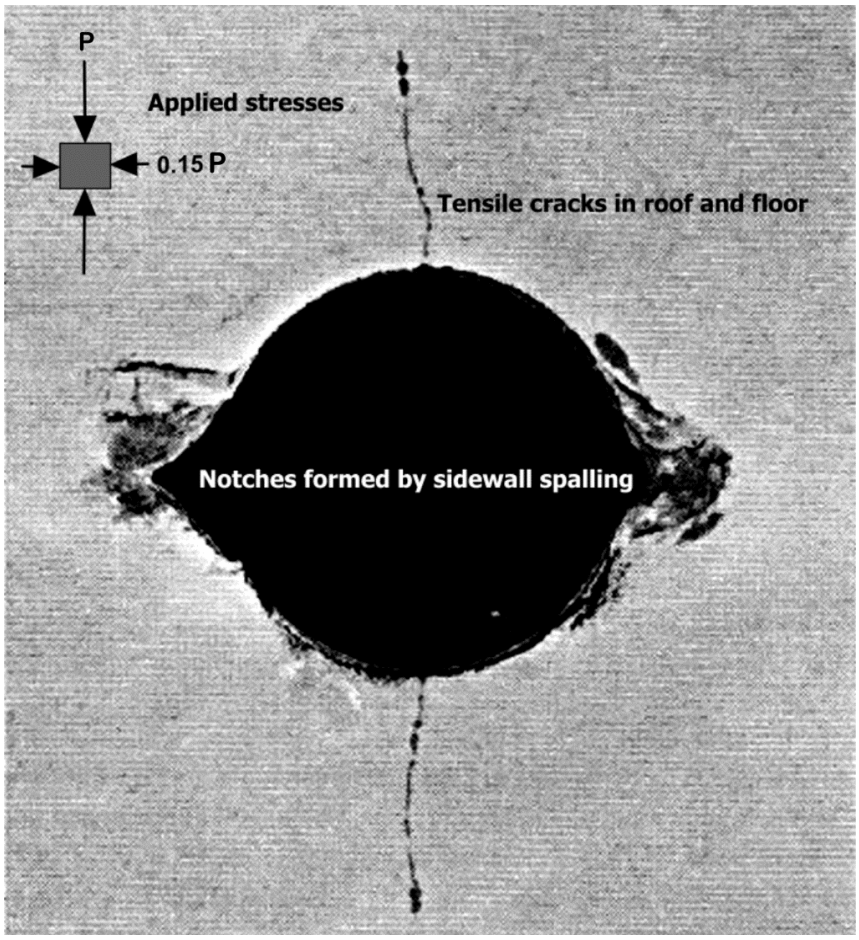

Figure 24: Development of tensile cracks in the roof and floor and spalling in the sidewalls of a 2.54 cm diameter hole in the rock plate model. Because of the lack of confinement normal to the faces of the model, some spalling occurred in the plane of the model. Despite this, the spall profile is clearly defined in the left-hand sidewall.

Initiation and propagation of spalling

No tests on fracture initiation were carried out on the Granite Aplite core in 1963 and hence, to construct a composite failure curve, it has been assumed that fracture initiation occurred at CI = 0.45 x σ_{ci} = 270.2 MPa. The tensile strength σ_t = -22 MPa is assumed to remain unaltered and the Hoek-Brown constant mi = 15 is estimated based on the Lac du Bonnet example. The transition from spalling initiation to intact rock failure has been assumed to occur at σ_1/σ_3 = 20. The resulting composite curve is shown in Figure 25.

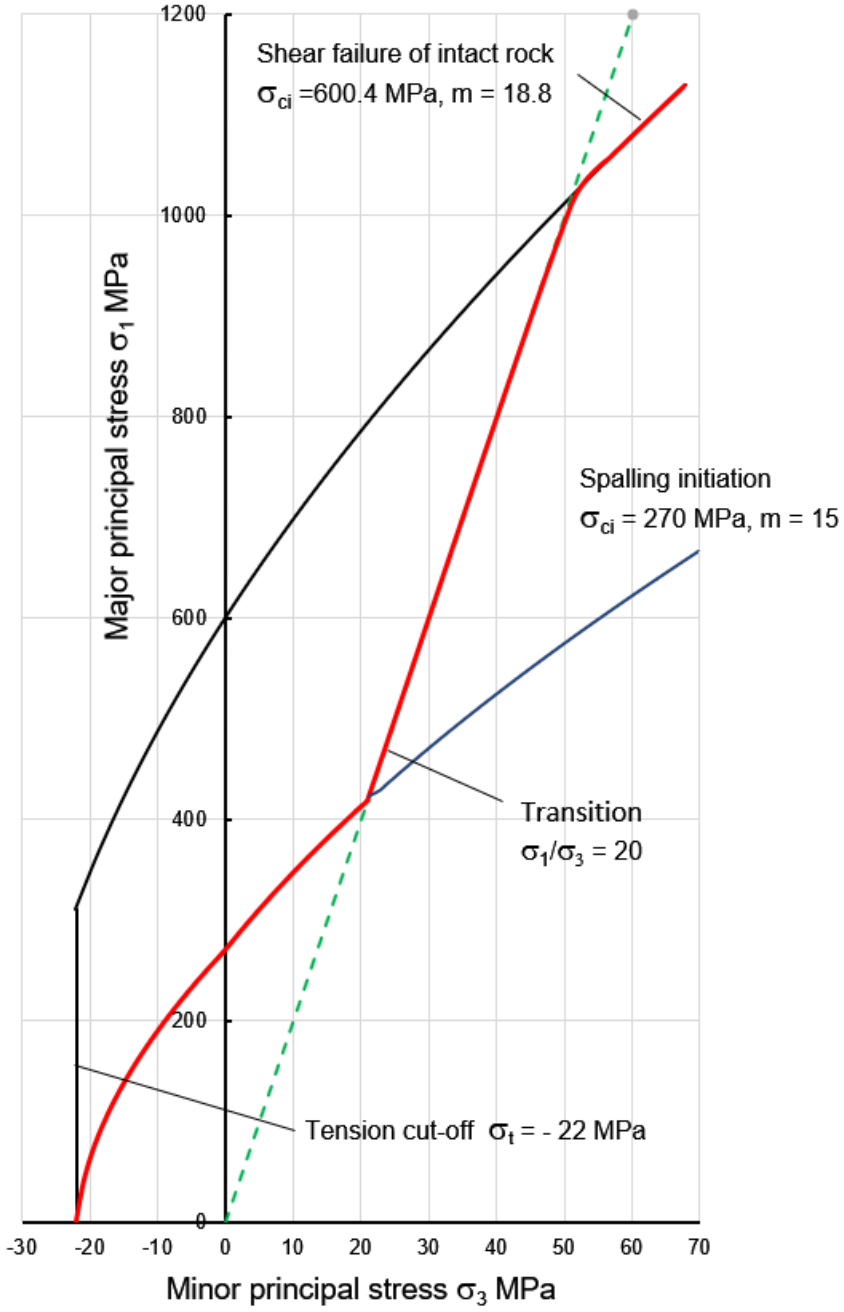

Figure 25: Composite failure curve for spalling of Granite Aplite.

Tensile cracks, in the roof and floor of the hole, initiated at an applied vertical stress of P = 61.5 MPa. This gives a tangential stress of $\sigma_\theta = P\,(3k - 1) = -33.8$ MPa. This is significantly higher than the -22.2 MPa given in Figure 23 and the difference is attributed to the epoxy resin photoelastic layer bonded to the model surface.

Based on the interpretation plotted in Figure 25, spalling in the excavation sidewalls can be expected to initiate at an applied vertical stress of $\sigma_v = 270.2/(3 - k) = 95.4$ MPa. Unfortunately, in the photographic records available to me it is impossible to detect this spalling initiation. The only reliable information is that reproduced in Figure 24 which shows that the sidewall spall is complete at an applied vertical stress of P = 175 MPa and a lateral stress of Q = 26.3 MPa. These stresses have been used in the following numerical analysis, recalling that spalling initiation would have occurred at a much lower stress level.

In the study of tensile failure and spalling, shown in Figure 24, a 15.2 cm square by 0.63 cm thick rock plate model was subjected to gradual increments of uniformly distributed vertical and lateral stresses in the equipment described in Appendix 1. A constant ratio of lateral and vertical stresses of k = 0.15 was used throughout the test.

Analysis of progressive spalling

A numerical model, representing the physical model illustrated in Figure 24, was constructed in the RocScience program RS2 and used to model the sequential spalling sequence.

Definition of the conditions for spalling are shown in Figure 25. For low stress conditions, spalling can initiate when the ratio of the induced principal stresses σ_1/σ_3 exceed the Strength Factor defined by the Hoek-Brown criterion with CI = 270 MPa and mi = 15. As the levels of the induced principal stresses increase, the transition defined by the ratio $\sigma_3/\sigma_1 = 0.05$, is reached and the extent of spalling is limited by this line. At even higher stress levels, the transition curve will encounter the intact rock strength curve, defined by the Hoek-Brown criterion with UCS = 600.4 MPa and mi = 18.8, and spalling will occur in the intact rock.

Figure 26 shows the zone in which conditions for spalling are satisfied for the first spall in the RS2 model. This zone encompasses damaged material that can fall away as a spall and damaged material that remains is held in place by the geometry of the ends of the potential spall zone.

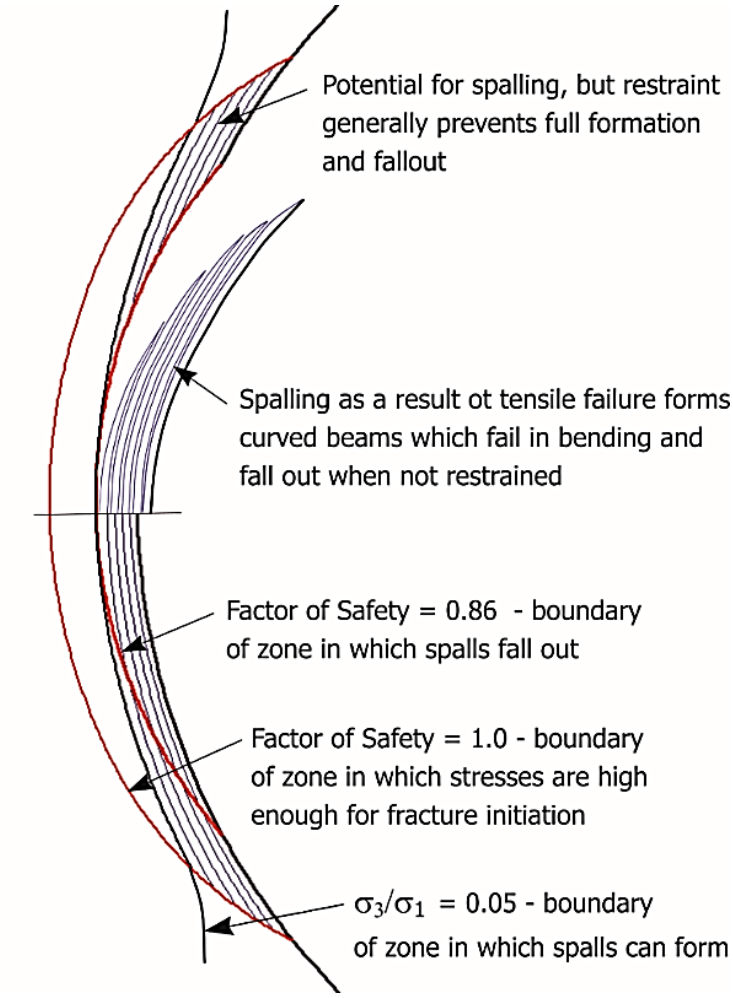

Figure 26: Definition of conditions for spalling and of the spall that falls away from the excavation sidewalls.

The successive spalls illustrated in Figure 26 were calculated by running 30 models in which the new geometry, created by removing the spall in each model, was the starting point for the next model. This proved to be a very robust procedure in which errors made in entering a spall were generally corrected by the following spall.

In developing this procedure, the major issue was to differentiate between damaged material that could fall away as a spall and damaged material that would be left in place. The final choice, defined in Figure 26, was based on my observations in many underground excavations, in which spalling was encountered, as well as numerical experiments in which details of the spalling process were simulated in numerical models.

Figure 27 shows excellent agreement between the predicted and measured spall profiles for this example.

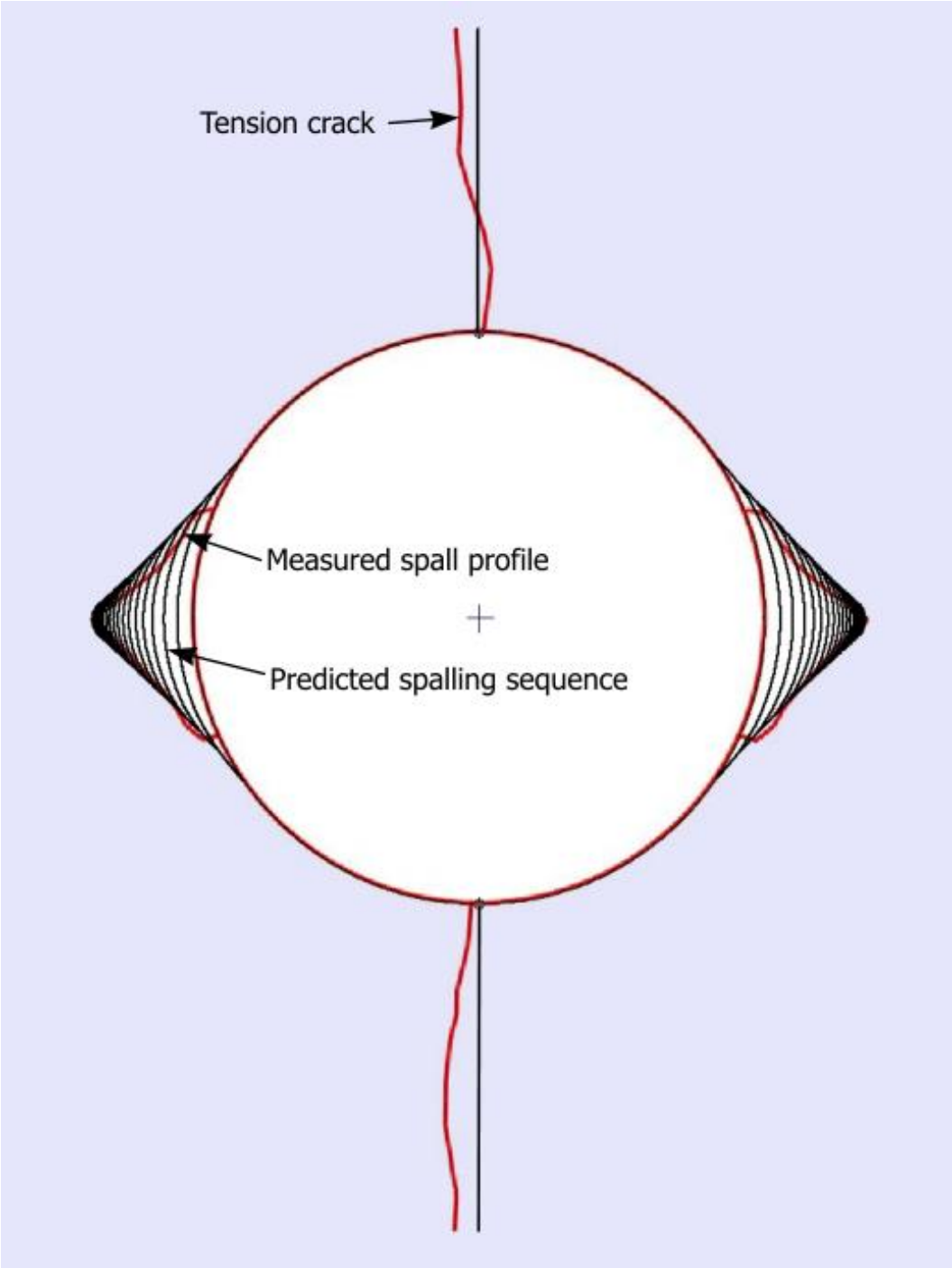

Figure 27: Comparison between predicted spalling sequence and profile and the measured profile in the model illustrated in Figure 22.

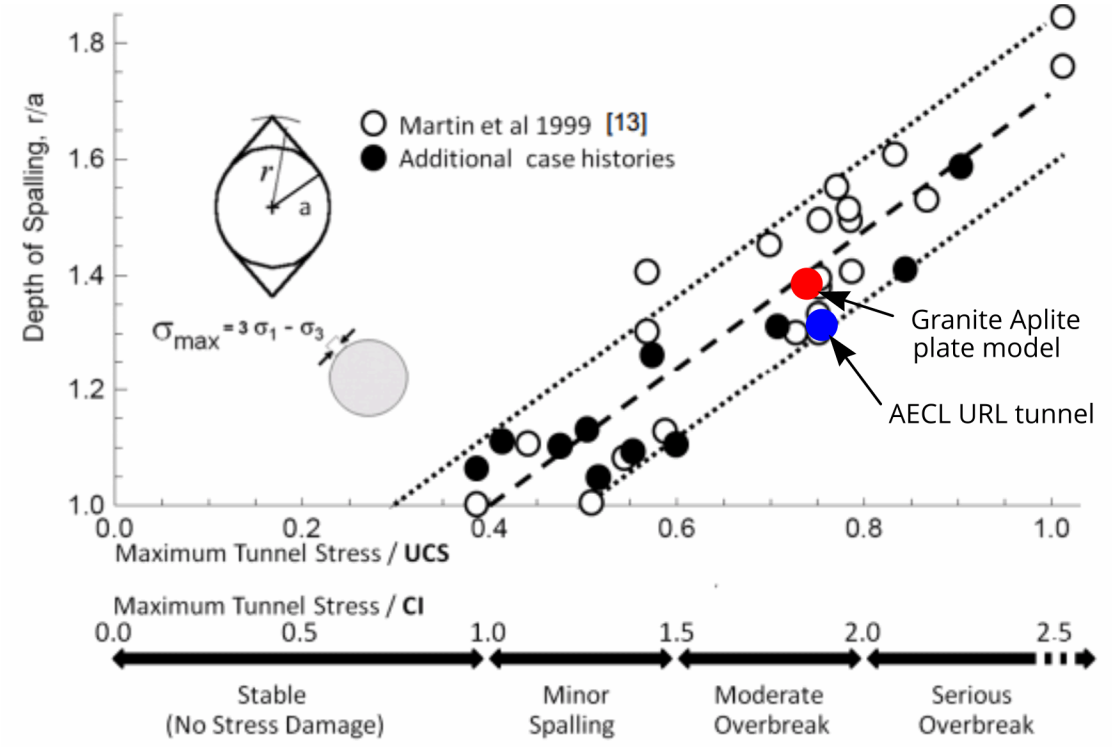

Figure 28: Plot of Figure 10 including AECL URL tunnel and Granite Aplite plate model results.

Progression from spalling into shear failure

In discussing the progression from tensile to shear failure in some circumstances, Shen and Barton (2018) offer the following comments

> "We believe that tunnel spalling is a result of tensile fracturing due to excessive extensional strain caused by the uniaxial/biaxial compression stress state as the tunnel wall is approached. Tensile fracturing and spalling may be the start of a failure process at the early stage, but it is unlikely to be the root cause of massive failure. Further away from the wall/roof of an underground excavation, the confining stress (σ3) will be higher, and the major principal stress will be lower due to the moderation of stress concentration with distance from the opening. Hence, tensile fracturing conditions may not be met anymore. In this region, shear fracturing driven by high shear stress will be dominant. In other words, massive shear failures, not tensile failures, are needed to explain the observations at higher stress levels."

Figure 29: Results of a rockburst in a South African gold mine at a depth of approximately 3000 m below surface. This photograph was taken in the early 1960s and was included in a collection belonging to Professor R.A.L. Black of the Royal School of Mines in London.

The photograph reproduced in Figure 29 shows the remnants of an underground mine excavation in South Africa after a major rockburst. These events are extremely dangerous and practically impossible to predict.

As shown in Figure 30, the rock plate model shown in Figure 24 was loaded to failure. I do not have detailed information on the spalling and shear failure beyond the load used for the analysis shown in Figure 24, but I do have the set of reflected light photoelastic photographs shown. These indicate the growth of cracks parallel to the major principal stress trajectories in the rock remote from the excavation boundary and the eventual failure of the surrounding rock.

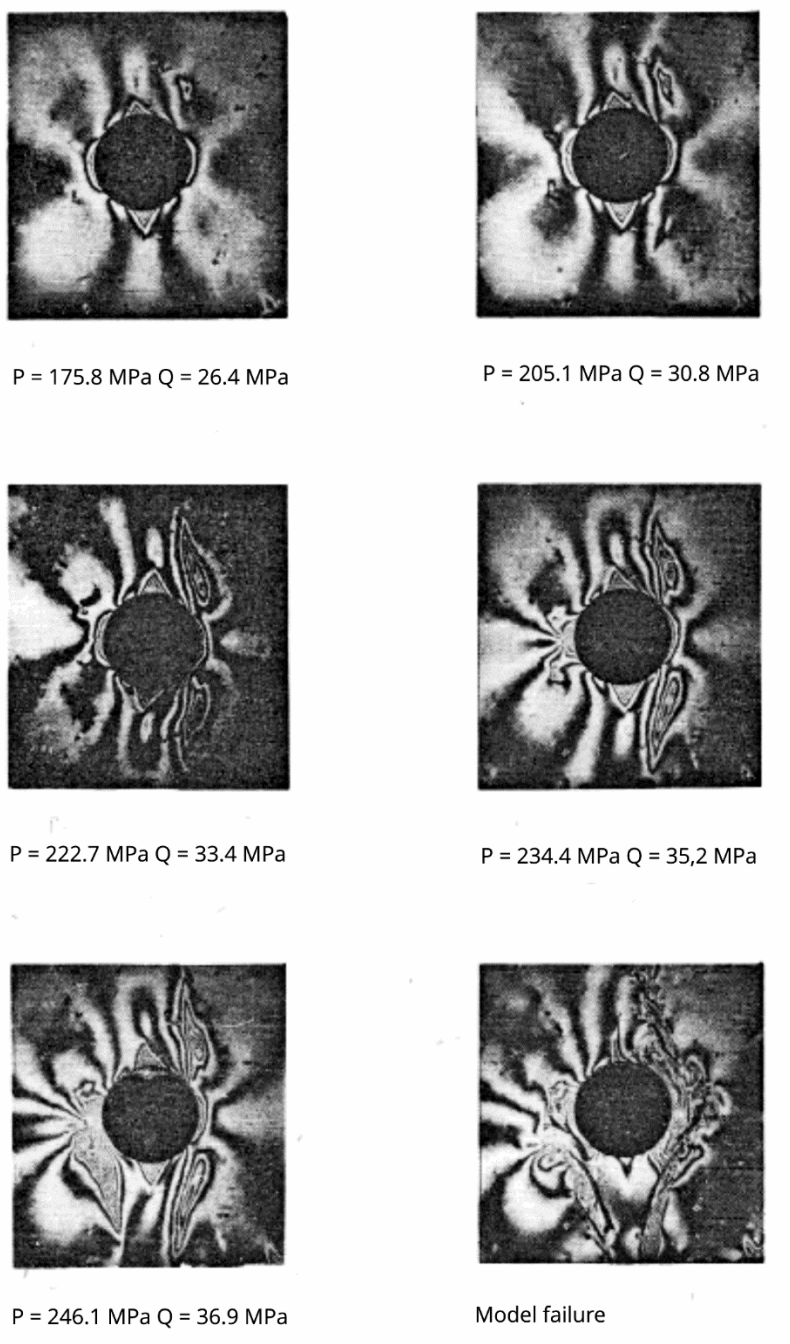

Figure 30: Reflected light photoelastic patterns captured by means of a high-speed flash unit during the loading to failure of a rock plate model. An epoxy resin layer had been bonded onto the rock surface by means of a reflective epoxy cement.

List of references

Ashby MF, Hallam D. 1986. The failure of brittle solids containing small cracks under compressive stress. *Acta Metallurgica*. 34(3):497-510.

Bewick, R.P., Amman, F., Kaiser, P.K and Martin C.D. 2015. Interpretation of UCS test results for engineering design. *Proc. 13th International ISRM Congress*, Montreal.

Cai M and Kaiser PK. 2014. In-situ rock spalling strength near excavation boundaries. *Rock Mech. Rock Eng*., 47:659-675.

Cai M, Kaiser PK, Martin CD. 1998. A tensile model for the interpretation of micro-seismic events near underground openings. *Pure and Applied Geophysics*. 153: 67-92.

Cain, S and Diederichs, M.S. 2016. The impact of tunnel shape and profile details on brittle damage development. Proc. Tunneling Association of Canada Annual Conference, Ottawa, 2016.

Dyskin, A.V and Germanovich, L.N. 1993. Model of crack growth in microcracked rock. *Int. J. Rock Mech. Min. Sci. and Geomech. Abstr.* 30(7):820.

Diederichs, MS, Carter, T. Martin, CD. 2010. Practical Rock Spall Prediction in Tunnel. In Proceedings of World Tunneling Congress 2010 - Vancouver. 8 pages.

Diederichs, M. S. 2007. Mechanistic interpretation and practical application of damage and spalling prediction criteria for deep tunnelling. *Can. Geotech. J.*, **44**, 1082-1116.

Diederichs, M.S., Kaiser, P.K. and Eberhardt, E. 2004. Damage initiation and propagation in hard rock tunnelling and the influence of near-face stress rotation. *International Journal of Rock Mechanics & Mining Sciences*, 41: 785-812.

Germanovich, J.N. and Dyskin, A.V. 1988. A model of brittle failure for material with cracks in uniaxial loading. *Mechanics of Solids* 23(2):111-112.

Hoek E. 1965 Rock fracture under static stress conditions. Pretoria, *South Africa: Council for Scientific and Industrial Research Report MEG 383*. Also available at a PhD thesis from https://www.rocscience.com/learning/hoek-s-corner/publications.

Hoek, E. and Bieniawski, Z.T. 1965. Brittle rock fracture propagation in rock under compression. *International Journal of Fracture Mechanics*, **1**(3), 137-155.

Hoek, E. and Martin, D. 2014. Fracture initiation and propagation in intact rock – A review. *Journal of Rock Mechanics and Geotechnical Engineering*, **6**(4), 287–300.

Kaiser, P.K., Diederichs, M.S., Martin, C.D., Sharp, J. and Steiner, W. 2000. Underground works in hard rock tunnelling and mining. *GeoEng2000*, Technomic Publ. Co., 841-926.

Kaiser, P.K. 2006. Rock mechanics considerations for construction of deep tunnels in brittle rock. Keynote paper presented at the Asia Rock Mechanics Symposium in Singapore, 2006.

Kaiser, P.K. Bewick, R.P. and Amann, F. 2015. Overcoming challenges of rock mass characterization for underground construction in deep mines. *Proc. 13th International ISRM Congress*, Montreal.

Kemeny, J.M. and Cook, N.G.W. 1987. Crack models for the failure of rock under compression. In: Desai CS, Krempl E, Kiousis PD, Kundu T, editors. *Proceedings of the 2nd international conference constitutive laws for engineering materials, theory and applications*, vol. 1. London: Elsevier Science Publishing Co. 879-887.

Lau J.S.O and Gorski B. 1992. Uniaxial and triaxial compression tests on URL rock samples from boreholes 207-045-GC3 and 209-069-PH3. *CANMET Divisional Report MRL 92 e 025 (TR)*; 1992. p. 46.

Martin C.D. and Read R.S. 1996. AECL's Mine-by experiment: a test tunnel in brittle rock. In: Aubertin M, Hassani F, Mitri H, editors. *Proceedings of the 2nd North American rock mechanics symposium*, vol. 1. Rotterdam: A.A. Balkema; 1996. pp. 13-24.

Martin, C.D, Kaiser, P.K. and Alcott, J.M, 1996. Predicting the depth of stress-induced failure around underground openings. *In Proc. 49th Canadian Geotechnical Conference*, St. John's, C-CORE, Vol. 1, 105-114.

Martin, C.D. 1997. The 17th Canadian Geotechnical Colloquium: The effect of cohesion loss and stress path on brittle rock strength. *Canadian Geotechnical Journal*, 34 (5): 698-725.

Martin, C.D., Kaiser, P.K., and McCreath, D.R. 1999. Hoek-Brown parameters for predicting the depth of brittle failure around tunnels. Canadian Geotechnical Journal, 36 (1): 136-151.

Martin, C.D, Christiansson, R. 2009. Estimating the potential for spalling around a deep nuclear waste repository in crystalline rock. *International Journal of Rock Mechanics and Mining Sciences* 46(2): 219 -228.

Nicksiar, M. and Martin, C,D. 2013. Crack initiation stress in low porosity crystalline and sedimentary rocks. *Engineering Geology* 2013; 154: 64-76.

Ramsey, J. Chester, F. 2004. Hybrid fracture and the transition from extension fracture to shear fracture. N*ature* 2004.

Read, R.S. (1991). Mine-by Experiment - prediction of excavation-induced rock mass response. Technical Memorandum URL-EXP-022-M048, Atomic Energy of Canada Limited.

Read, R.S. and Martin C.D. 1996. Technical Summary of AECL's Mine-by Experiment Phase 1: Excavation Response. AECL-11311, COG-95-171.

Perras, M.A. and Diederichs, M.S. 2016. Predicting excavation zone depths in brittle rocks. *J Rock Mechanics and Geotechnical Engineering*, 2016, 60-74.

Shen, B. and Barton, N. 2018. Rock fracturing mechanisms around underground opening, *Geomechanics and Engineering*, Vol.16, No. 1, 2018, 35-47.

Stacey, T.S. 1981. A Simple Extension Strain Criterion for Fracture of Brittle Rock. Int. ,1. *Rock Mech. Min. Sci. & Geomech*. Abstr. Vol. 18. pp. 469-474.

Appendix 1 – Equipment for loading glass and rock models

Figure A1: Biaxial loading frame for loading 15 cm square glass or rock plate models with uniformly distributed vertical and lateral loads, described in Hoek, 1965. The equipment was constructed and used in the Mechanical Engineering Research Institute of the South African Council for Scientific and Industrial Research.

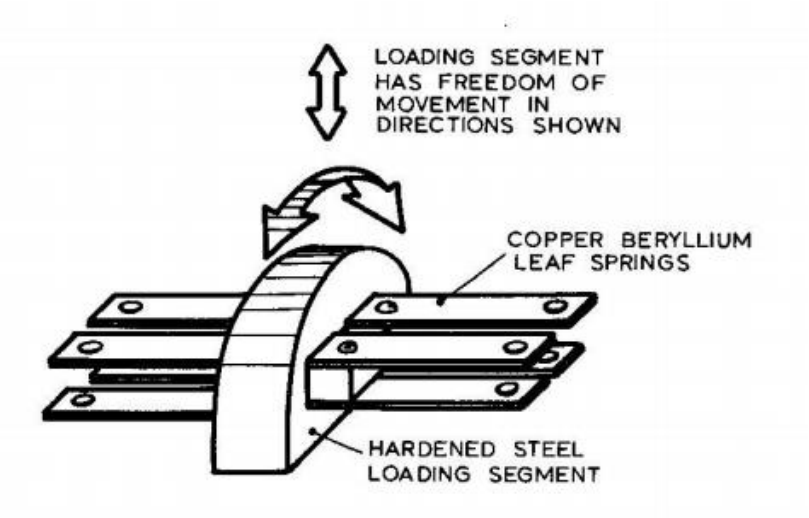

Figure A2: Detail of a loading element for distributing the loads onto the model boundaries.

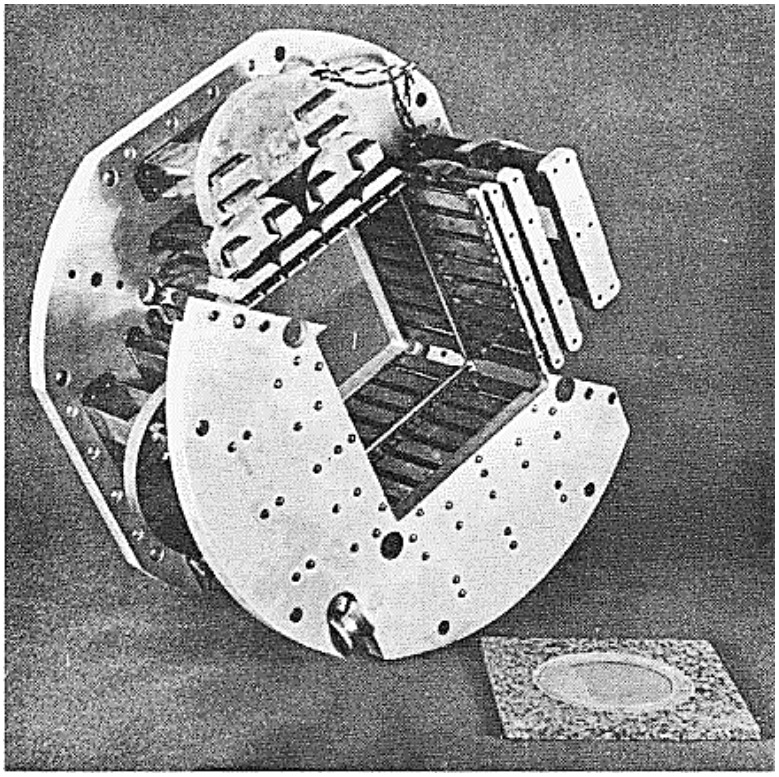

Figure A3: Assembled loading structure for application of uniformly distributed loading to the model plate boundaries.

20. Analysis of rockfall hazards

Introduction

Rockfalls are a major hazard in rock cuts for highways and railways in mountainous terrain. While rockfalls do not pose the same level of economic risk as large scale failures which can, and do, close major transportation routes for days at a time, the number of people killed by rockfalls tends to be of the same order as people killed by all other forms of rock slope instability. Badger and Lowell (1992) summarised the experience of the Washington State Department of Highways. They stated that 'A significant number of accidents and nearly a half dozen fatalities have occurred because of rockfalls in the last 30 years … [and] … 45 percent of all unstable slope problems are rock fall related'. Hungr and Evans (1989) note that, in Canada, there have been 13 rockfall deaths in the past 87 years. Almost all of these deaths have been on the mountain highways of British Columbia.

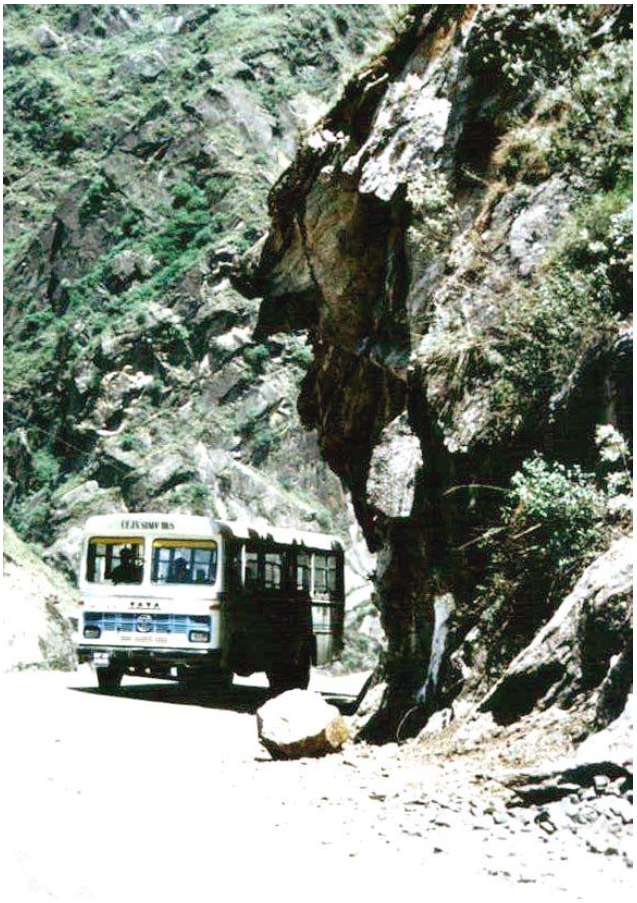

Figure 1: A rock slope on a mountain highway. Rockfalls are a major hazard on such highways.

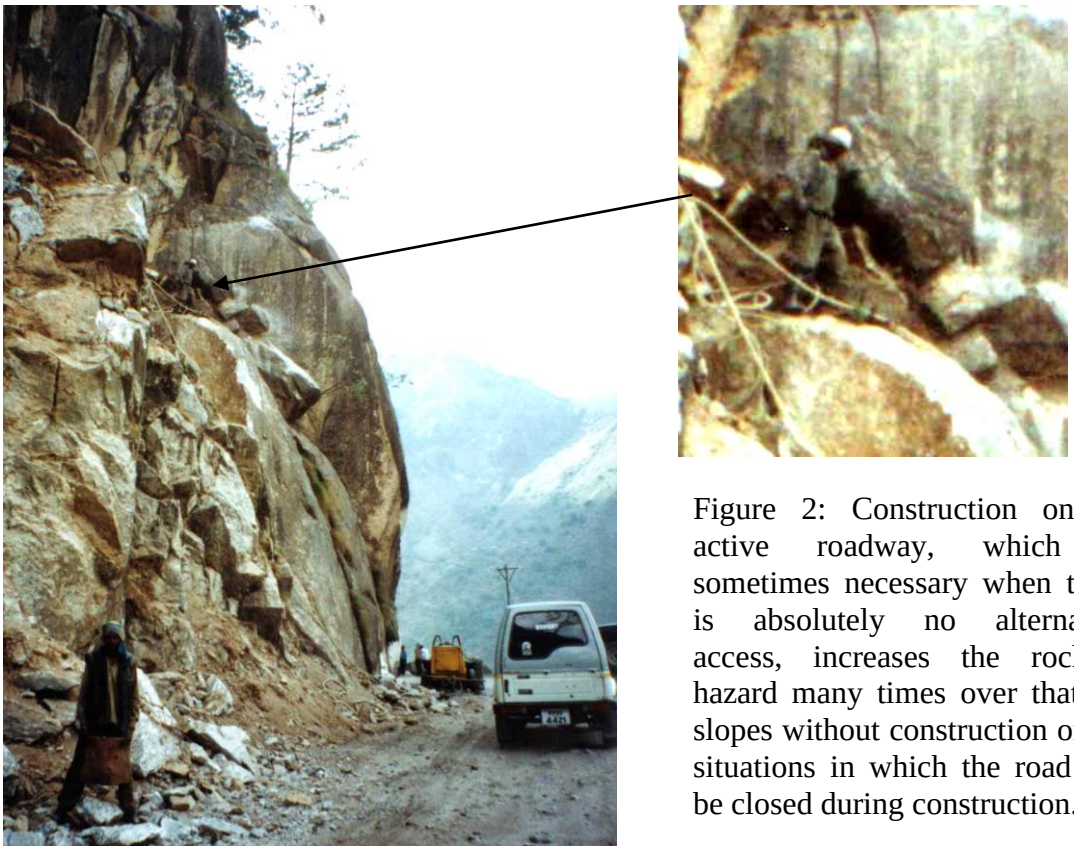

Figure 2: Construction on an active roadway, which is sometimes necessary when there is absolutely no alternative access, increases the rockfall hazard many times over that for slopes without construction or for situations in which the road can be closed during construction.

Mechanics of rockfalls

Rockfalls are generally initiated by some climatic or biological event that causes a change in the forces acting on a rock. These events may include pore pressure increases due to rainfall infiltration, erosion of surrounding material during heavy rain storms, freeze-thaw processes in cold climates, chemical degradation or weathering of the rock, root growth or leverage by roots moving in high winds. In an active construction environment, the potential for mechanical initiation of a rockfall will probably be one or two orders of magnitude higher than the climatic and biological initiating events described above.

Once movement of a rock perched on the top of a slope has been initiated, the most important factor controlling its fall trajectory is the geometry of the slope. In particular, dip slope faces, such as those created by the sheet joints in granites, are important because they impart a horizontal component to the path taken by a rock after it bounces on the slope or rolls off the slope. The most dangerous of these surfaces act as 'ski-jumps' and impart a high horizontal velocity to the falling rock, causing it to bounce a long way out from the toe of the slope.

Clean faces of hard unweathered rock are the most dangerous because they do not retard the movement of the falling or rolling rock to any significant degree. On the other hand, surfaces covered in talus material, scree or gravel absorb a considerable amount of the energy of the falling rock and, in many cases, will stop it completely.

This retarding capacity of the surface material is expressed mathematically by a term called the *coefficient of restitution*. The value of this coefficient depends upon the nature of the materials that form the impact surface. Clean surfaces of hard rock have high coefficients of restitution while soil, gravel and completely decomposed granite have low coefficients of restitution. This is why gravel layers are placed on catch benches in order to prevent further bouncing of falling rocks.

Other factors such as the size and shape of the rock boulders, the coefficients of friction of the rock surfaces and whether or not the rock breaks into smaller pieces on impact are all of lesser significance than the slope geometry and the coefficients of restitution described above. Consequently, relative crude rockfall simulation models are capable of producing reasonably accurate predictions of rockfall trajectories. Obviously more refined models will produce better results, provided that realistic input information is available. Some of the more recent rockfall models are those of Bozzolo et al (1988), Hungr and Evans (1989), Spang and Rautenstrauch (1988) and Azzoni et al (1995).

Most of these rockfall models include a Monte Carlo simulation technique to vary the parameters included in the analysis. This technique is similar to the random process of throwing dice - one for each parameter being considered. The program Rocfall[1] is a program that can be used for rockfall analyses using a number of probabilistic options. Figure 3 shows a single rockfall trajectory while Figure 4 shows the trajectories for 100 rockfalls using the Monte Carlo simulation process.

Possible measures which could be taken to reduce rockfall hazards

Identification of potential rockfall problems

It is neither possible nor practical to detect all potential rockfall hazards by any techniques currently in use in rock engineering. In some cases, for example, when dealing with boulders on the top of slopes, the rockfall hazards are obvious. However, the most dangerous types of rock failure occur when a block is suddenly released from an apparently sound face by relatively small deformations in the surrounding rock mass. This can occur when the forces acting across discontinuity planes, which isolate a block from its neighbours, change as a result of water pressures in the discontinuities or a reduction of the shear strength of these planes because of long term deterioration due to weathering. This release of ‘keyblocks’ can sometimes precipitate rockfalls of significant size or, in extreme cases, large scale slope failures.

[1] Available from www.rocscience.com

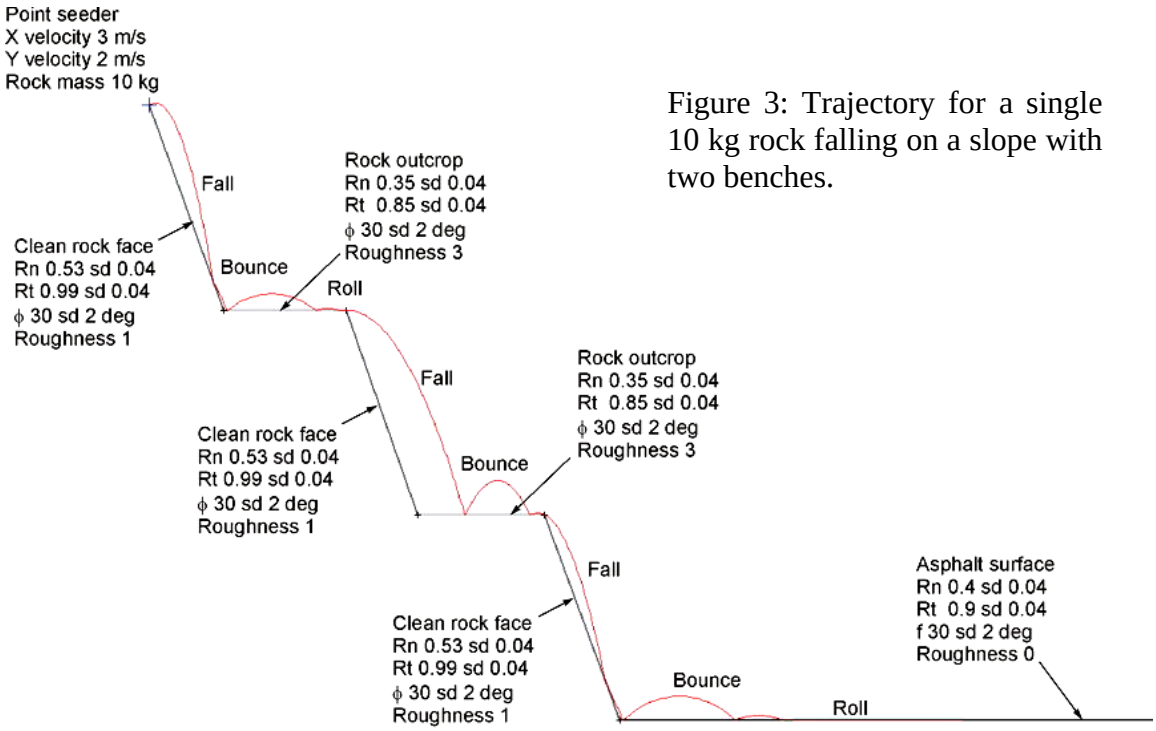

Figure 3: Trajectory for a single 10 kg rock falling on a slope with two benches.

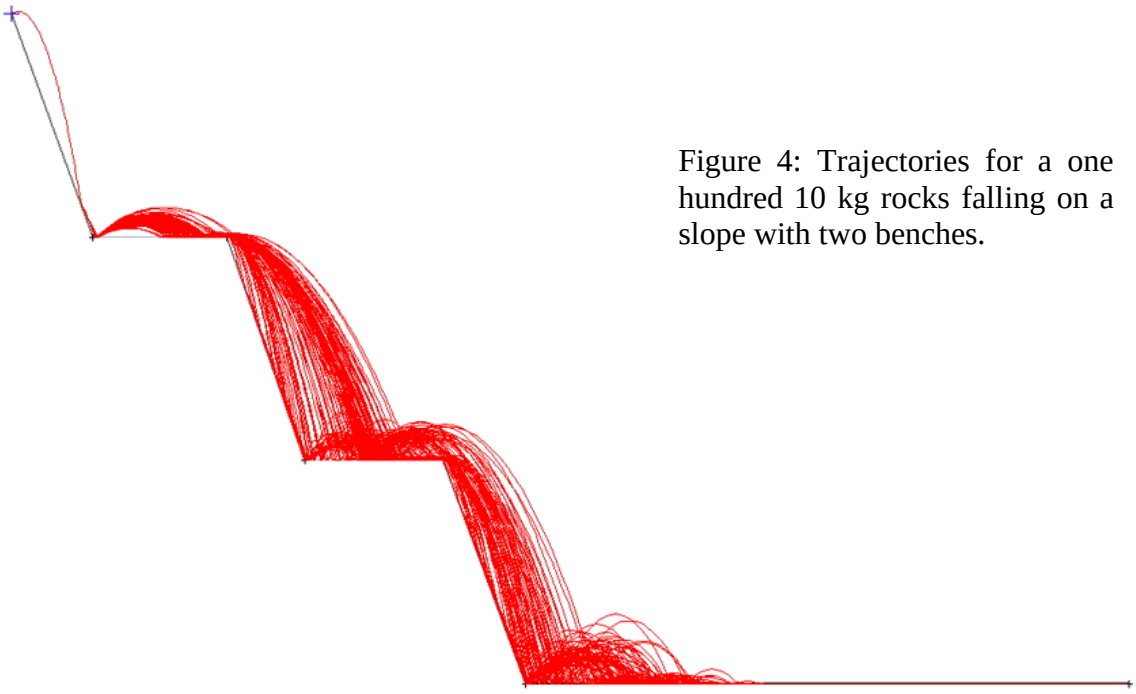

Figure 4: Trajectories for a one hundred 10 kg rocks falling on a slope with two benches.

While it is not suggested that rock faces should not be carefully inspected for potential rockfall problems, it should not be assumed that all rockfall hazards will be detected by such inspections.

Reduction of energy levels associated with excavation

Traditional excavation methods for hard rock slopes involve the use of explosives. Even when very carefully planned controlled blasts are carried out, high intensity short duration forces act on the rock mass. Blocks and wedges which are at risk can be dislodged by these forces. Hence, an obvious method for reducing rockfall hazards is to eliminate excavation by blasting or by any other method, such as ripping, which imposes concentrated, short duration forces or vibrations on the rock mass. Mechanical and hand excavation methods can be used and, where massive rock has to be broken, chemical expanding rock breaking agents may be appropriate.

Physical restraint of rockfalls

If it is accepted that it is not possible to detect or to prevent all rockfalls, then methods for restraining those rockfalls, which do occur, must be considered. These methods are illustrated in Figure 5.

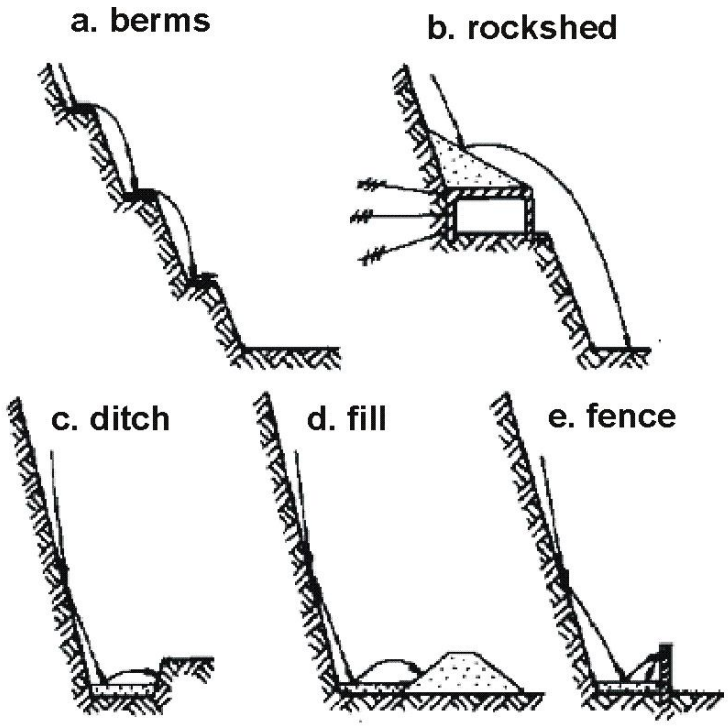

Figure 5: Possible measures to reduce the damage due to rockfalls. After Spang (1987).

Berms are a very effective means of catching rockfalls and are frequently used on permanent slopes. However, berms can only be excavated from the top downwards and they are of limited use in minimising the risk of rockfalls during construction.

Rocksheds or avalanche shelters are widely used on steep slopes above narrow railways or roadways. An effective shelter requires a steeply sloping roof covering a relatively narrow span. In the case of a wide multi-lane highway, it may not be possible to design a rockshed structure with sufficient strength to withstand large rockfalls. It is generally advisable to place a fill of gravel or soil on top of the rockshed in order to act as both a retarder and a deflector for rockfalls.

Rock traps work well in catching rockfalls provided that there is sufficient room at the toe of the slope to accommodate these rock traps. In the case of very narrow roadways at the toe of steep slopes, there may not be sufficient room to accommodate rock traps. This restriction also applies to earth or rock fills and to gabion walls or massive concrete walls.

Catch fences or barrier fences in common use are estimated to have an energy absorption capacity[2] of 100 kNm. This is equivalent to a 250 kg rock moving at approximately 20 metres per second. More robust barrier fences, such as those used in the European Alps[3], have an energy absorbing capacity of up to 2500 kNm which means that they could stop a 6250 kg boulder moving at approximately 20 metres per second. Details of a typical high capacity net are illustrated in Figure 6.

Another restraint system which merits further consideration is the use of *mesh draped* over the face. This type of restraint is commonly used for permanent slopes and is illustrated in Figure 7. The mesh is draped over the rock face and attached at several locations along the slope. The purpose of the mesh is not to stop rockfalls, but to trap the falling rock between the mesh and the rock face and so to reduce the horizontal velocity component which causes the rock to bounce out onto the roadway below.

Probably the most effective permanent rockfall protective system for most highways is the construction of a catch ditch at the toe of the slope. The base of this ditch should be covered by a layer of gravel to absorb the energy of falling rocks and a sturdy barrier fence should be placed between the ditch and the roadway. The location of the barrier fence can be estimated by means of a rockfall analysis such as that used to calculate the trajectories presented in Figure 3. The criterion for the minimum distance between the toe of the slope and the rock fence is that no rocks can be allowed to strike the fence before their kinetic energy has been diminished by the first impact on the gravel layer in the rock trap.

---

[2] The kinetic energy of a falling body is given by 0.5 x mass x velocity^2.

[3] Wire mesh fence which incorporates cables and energy absorbing slipping joints is manufactured by Geobrugg Protective Systems, CH-8590 Romanshorn, Switzerland, Fax +41 71466 81 50.

a: Anchor grouted into rock with cables attached.

b: Geobrugg ring net shown restraining a boulder. These nets can be designed with energy absorbing capacities of up to 2500 kNm which is equivalent to a 6 tonne boulder moving at 20 m per second.

c: Geobrugg energy absorbing ring. When subjected to impact loading the ring deforms plastically and absorbs the energy of the boulder

Figure 6: Details of a rockfall net system manufactured by Geobrugg of Switzerland.

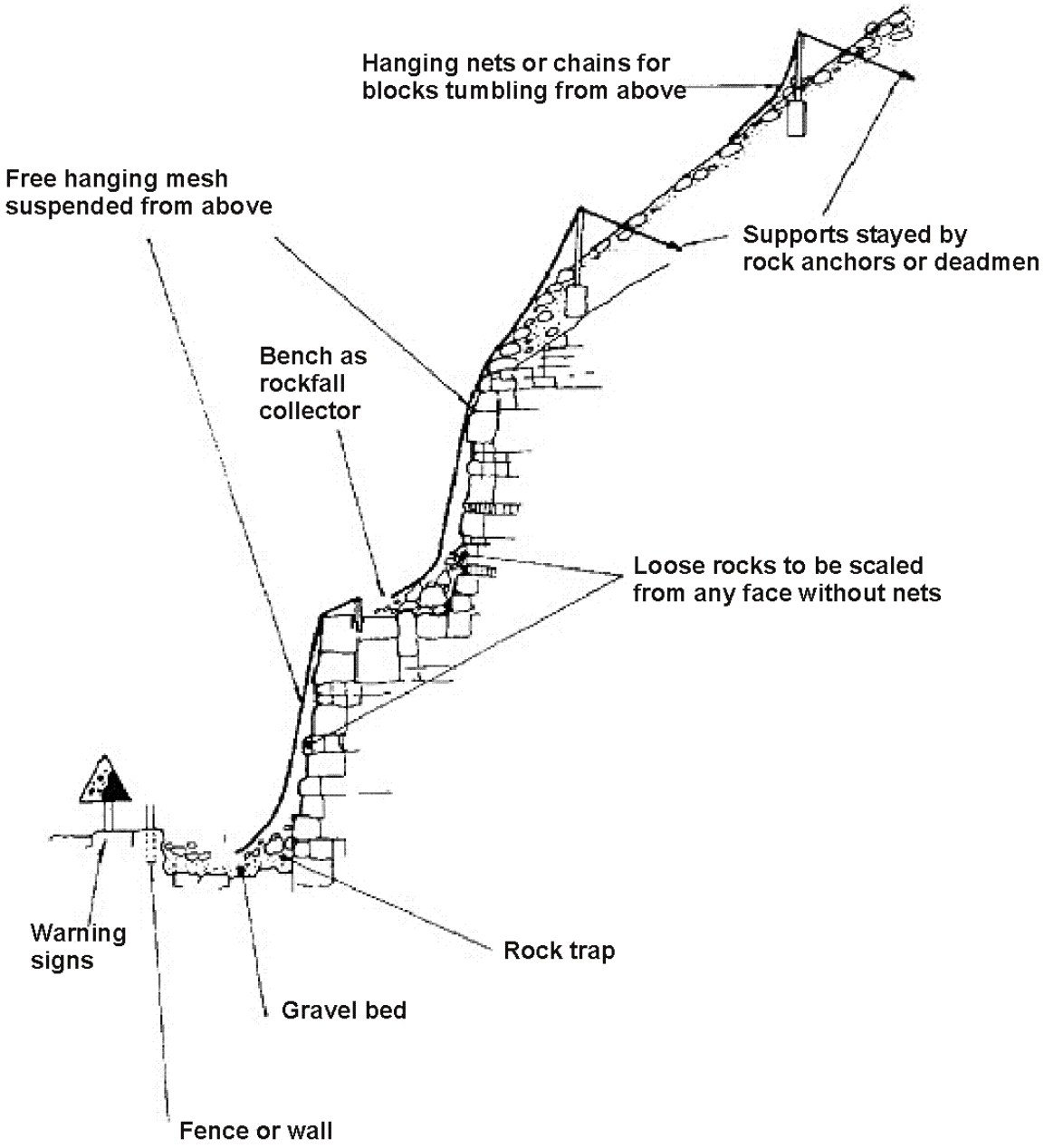

Figure 7: Rockfall control measures. After Fookes and Sweeney (1976).

A simple design chart for ditch design, based upon work by Ritchie (1963), is reproduced in Figure 8.

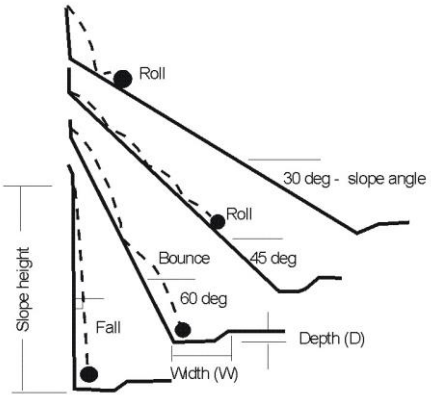

Rock falls on slopes

Figures taken from FHWA Manual 'Rock Slopes' November 1991. USDOT Chapter 12 Page 19.

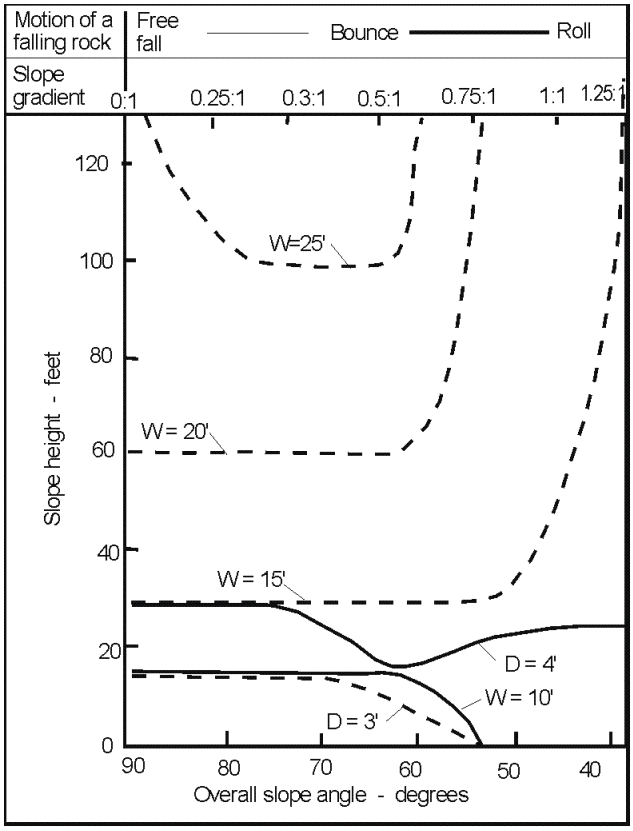

Ditch Design Chart

Figure 8: Rockfall ditch design chart based upon work by Ritchie (1963).

Rockfall Hazard Rating System

Highway and railway construction in mountainous regions presents a special challenge to geologists and geotechnical engineers. This is because the extended length of these projects makes it difficult to obtain sufficient information to permit stability assessments to be carried out for each of the slopes along the route. This means that, except for sections which are identified as particularly critical, most highway slopes tend to be designed on the basis of rather rudimentary geotechnical analyses. Those analyses which are carried out are almost always concerned with the overall stability of the slopes against major sliding or toppling failures which could jeopardise the operation of the highway or railway. It is very rare to find a detailed analysis of rockfall hazards except in heavily populated regions in highly developed countries such as Switzerland.

In recognition of the seriousness of this problem and of the difficulty of carrying out detailed investigations and analyses on the hundreds of kilometres of mountain highway in the western United States and Canada, highway and railway departments have worked on classification schemes which can be carried out by visual inspection and simple calculations. The purpose of these classifications is to identify slopes which are particularly hazardous and which require urgent remedial work or further detailed study.

In terms of rockfall hazard assessment, one of the most widely accepted[4] is the Rockfall Hazard Rating System (RHRS) developed by the Oregon State Highway Division (Pierson et al. 1990). Table 1 gives a summary of the scores for different categories included in the classification while Figure 9 shows a graph which can be used for more refined estimates of category scores.

The curve shown in Figure 9 is calculated from the equation $y = 3^x$ where, in this case, x = (Slope height- feet)/25. Similar curves for other category scores can be calculated from the following values of the exponent x.

Slope height	x = slope height (feet) / 25
Average vehicle risk	x = % time / 25
Sight distance	x = (120 - % Decision sight distance) / 20
Roadway width	x = (52 - Roadway width (feet)) / 8
Block size	x = Block size (feet)
Volume	x = Volume (cu.ft.) / 3

[4] This system has been adopted by the States of Oregon, Washington, New Mexico and Idaho and, in slightly modified form, by California, Colorado and British Columbia.

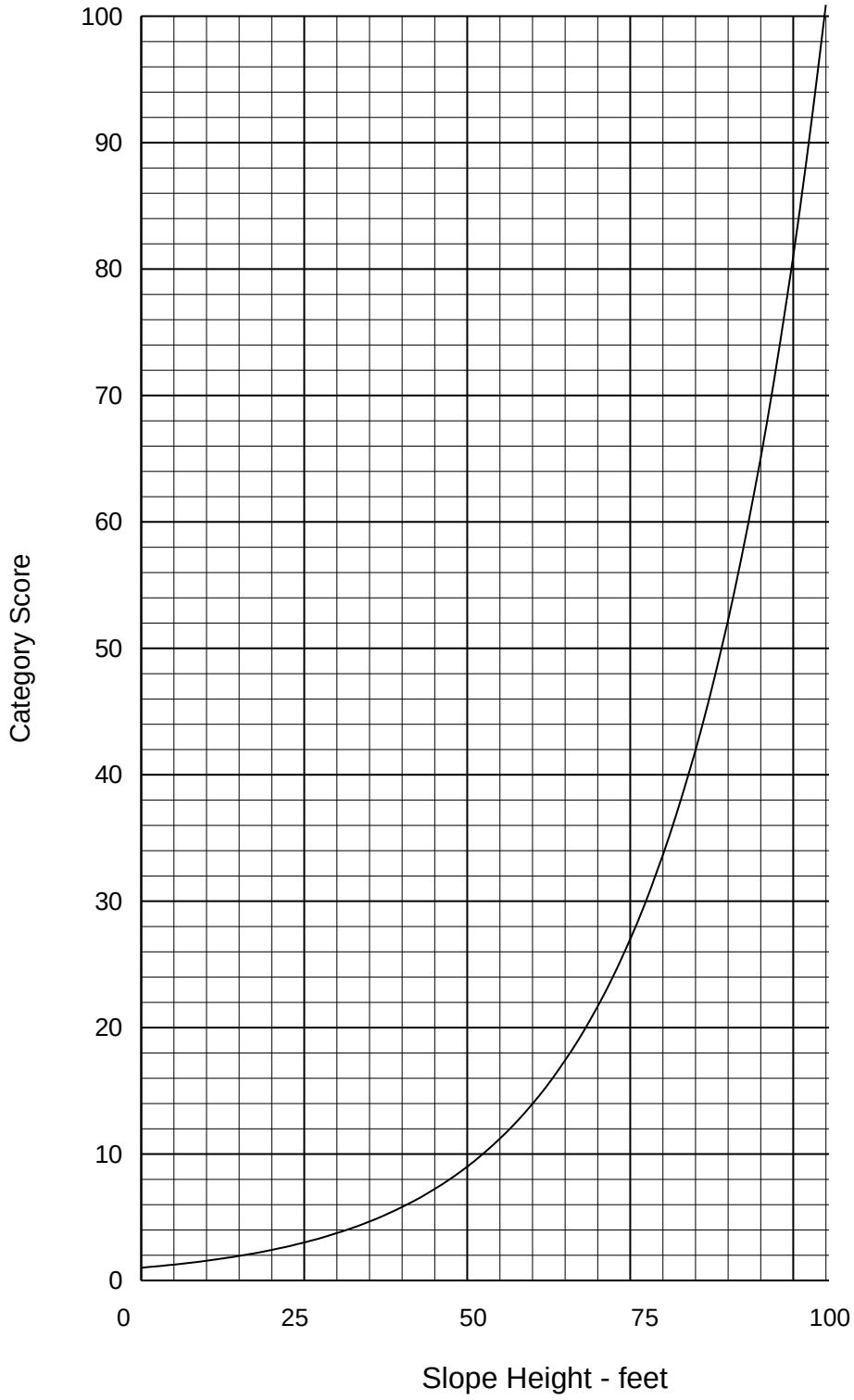

Figure 9: Category score graph for slope height.

Table 1: Rockfall Hazard Rating System.

CATEGORY			RATING CRITERIA AND SCORE			
			POINTS 3	POINTS 9	POINTS 27	POINTS 81
SLOPE HEIGHT			25 FT	50 FT	75 FT	100 FT
DITCH EFFECTIVENESS			Good catchment	Moderate catchment	Limited catchment	No catchment
AVERAGE VEHICLE RISK			25% of the time	50% of the time	75% of the time	100% of the time
PERCENT OF DECISION SIGHT DISTANCE			Adequate site distance, 100% of low design value	Moderate sight distance, 80% of low design value	Limited site distance, 60% of low design value	Very limited sight distance, 40% of low design value
ROADWAY WIDTH INCLUDING PAVED SHOULDERS			44 feet	36 feet	28 feet	20 feet
GEOLOGIC CHARACTER	CASE 1	STRUCTURAL CONDITION	Discontinuous joints, favorable orientation	Discontinuous joints, random orientation	Discontinuous joints, adverse orientation	Continuous joints, adverse orientation
		ROCK FRICTION	Rough, irregular	Undulating	Planar	Clay infilling or slickensided
	CASE 2	STRUCTURAL CONDITION	Few differential erosion features	Occasional erosion features	Many erosion features	Major erosion features
		DIFFERENCE IN EROSION RATES	Small difference	Moderate difference	Large difference	Extreme difference
BLOCK SIZE ——— QUANTITY OF ROCKFALL/EVENT			1 FT ——— 3 cubic yards	2 FT ——— 6 cubic yards	3 FT ——— 9 cubic yards	4 FT ——— 12 cubic yards
CLIMATE AND PRESENCE OF WATER ON SLOPE			Low to moderate precipitation; no freezing periods, no water on slope	Moderate precipitation or short freezing periods or intermittent water on slope	High precipitation or long freezing periods or continual water on slope	High precipitation and long freezing periods or continual water on slope and long freezing periods
ROCKFALL HISTORY			Few falls	Occasional falls	Many falls	Constant falls

Slope Height

This item represents the vertical height of the slope not the slope distance. Rocks on high slopes have more potential energy than rocks on lower slopes, thus they present a greater hazard and receive a higher rating. Measurement is to the highest point from which rockfall is expected. If rocks are coming from the natural slope above the cut, use the cut

height plus the additional slope height (vertical distance). A good approximation of vertical slope height can be obtained using the relationships shown below.

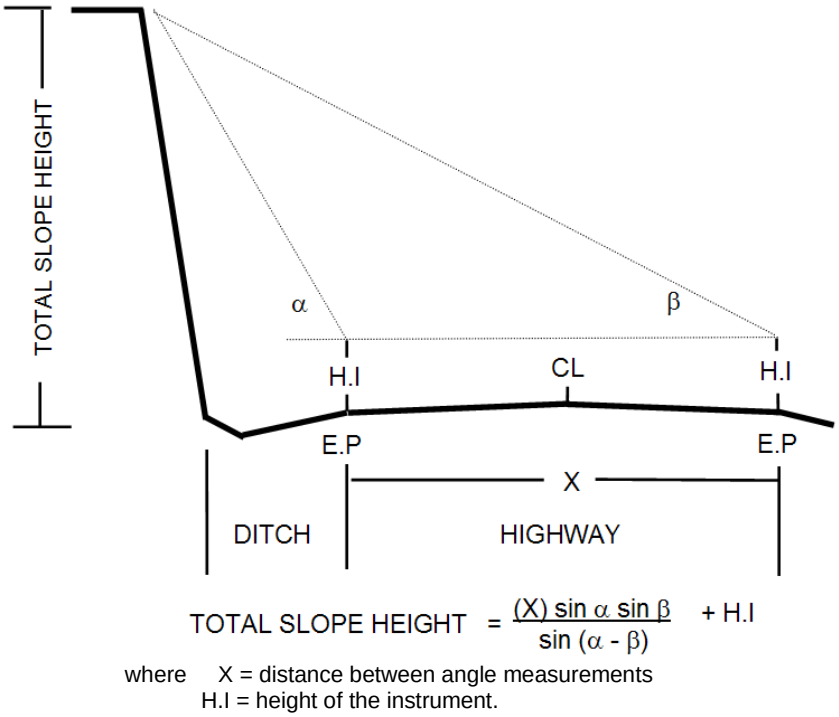

Figure 10: Measurement of slope height.

Ditch Effectiveness

The effectiveness of a ditch is measured by its ability to prevent falling rock from reaching the roadway. In estimating the ditch effectiveness, the rater should consider several factors, such as: 1) slope height and angle; 2) ditch width, depth and shape; 3) anticipated block size and quantity of rockfall; 4) impact of slope irregularities (launching features) on falling rocks. It's especially important for the rater to evaluate the impact of slope irregularities because a launching feature can negate the benefits expected from a fallout area. The rater should first evaluate whether any of the irregularities, natural or man-made, on a slope will launch falling rocks onto the paved roadway. Then, based on the number and size of the launching features, estimate what portion of the falling rocks will be affected. Valuable information on ditch performance can be obtained from maintenance personnel. Rating points should be assigned as follows:

3 points	*Good Catchment*. All or nearly all of falling rocks are retained in the catch ditch.
9 points	*Moderate Catchment*. Falling rocks occasionally reach the roadway.
27 points	*Limited Catchment*. Falling rocks frequently reach the roadway.
81 points	*No Catchment*. No ditch or ditch is totally ineffective. All or nearly all falling rocks reach the roadway.

Reference should also be made to Figure 8 in evaluating ditch effectiveness.

Average Vehicle Risk (AVR)

This category measures the percentage of time that a vehicle will be present in the rockfall hazard zone. The percentage is obtained by using a formula (shown below) based on slope length, average daily traffic (ADT) and the posted speed limit at the site. A rating of 100% means that on average a car can be expected to be within the hazard section 100% of the time. Care should be taken to measure only the length of a slope where rockfall is a problem. Over estimated lengths will strongly skew the formula results. Where high ADT's or longer slope lengths exist values greater than 100% will result. When this occurs it means that at any particular time more than one car is present within the measured section. The formula used is:

$$\frac{\text{ADT (cars/hour)} \times \text{Slope Length (miles)} \times 100\%}{\text{Posted Speed Limit (miles per hour)}} = \text{AVR}$$

Percent of Decision Sight Distance

The decision sight distance (DSD) is used to determine the length of roadway in feet a driver must have to make a complex or instantaneous decision. The DSD is critical when obstacles on the road are difficult to perceive, or when unexpected or unusual manoeuvres are required. Sight distance is the shortest distance along a roadway that an object of specified height is continuously visible to the driver.

Throughout a rockfall section the sight distance can change appreciably. Horizontal and vertical highway curves along with obstructions such as rock outcrops and roadside vegetation can severely limit a driver's ability to notice a rock in the road. To determine where these impacts are most severe, first drive through the rockfall section from both directions. Decide which direction has the shortest line of sight. Both horizontal and vertical sight distances should be evaluated. Normally an object will be most obscured when it is located just beyond the sharpest part of a curve. Place a six-inch object in that position on the fogline or on the edge of pavement if there is no fogline. The rater then

walks along the fogline (edge of pavement) in the opposite direction of traffic flow, measuring the distance it takes for the object to disappear when your eye height is 3.5 ft above the road surface. This is the measured sight distance. The decision sight distance can be determined by the table below. The distances listed represent the low design value. The posted speed limit through the rockfall section should be used.

Posted Speed Limit (mph)	Decision Sight Distance (ft)
30	450
40	600
50	750
60	1,000
70	1.100

These two values can be substituted into the formula below to calculate the 'Percent of Decision Sight Distance.'

$$\frac{\text{Actual Site Distance}\quad(\qquad)}{\text{Decision Site Distance}\quad(} \times 100\% = \_\_\_\_\_\%$$

Roadway Width

This dimension is measured perpendicular to the highway centreline from edge of pavement to edge of pavement. This measurement represents the available manoeuvring room to avoid a rockfall. This measurement should be the minimum width when the roadway width is not consistent.

Geologic Character

The geologic conditions of the slope are evaluated with this category. Case 1 is for slopes where joints, bedding planes, or other discontinuities, are the dominant structural feature of a rock slope. Case 2 is for slopes where differential erosion or oversteepened slopes is the dominant condition that controls rockfall. The rater should use whichever case best fits the slope when doing the evaluation. If both situations are present, both are scored but only the worst case (highest score) is used in the rating.

Case 1

Structural Condition Adverse joint orientation, as it is used here, involves considering such things as rock friction angle, joint filling, and hydrostatic head if water is present. Adverse joints are those that cause block, wedge or toppling failures. 'Continuous' refers to joints greater than 10 feet in length.

3 points *Discontinuous Joints, Favourable Orientation* Jointed rock with no adversely oriented joints, bedding planes, etc.

9 points *Discontinuous Joints, Random Orientation* Rock slopes with randomly oriented joints creating a three-dimensional pattern. This type of pattern is likely to have some scattered blocks with adversely oriented joints but no dominant adverse joint pattern is present.

27 points *Discontinuous Joints, Adverse Orientation* Rock slope exhibits a prominent joint pattern, bedding plane, or other discontinuity, with an adverse orientation. These features have less than 10 feet of continuous length.

81 points *Continuous Joints, Adverse Orientation* Rock slope exhibits a dominant joint pattern, bedding plane, or other discontinuity, with an adverse orientation and a length of greater than 10 feet.

Rock Friction This parameter directly affects the potential for a block to move relative to another. Friction along a joint, bedding plane or other discontinuity is governed by the macro and micro roughness of a surface. Macro roughness is the degree of undulation of the joint. Micro roughness is the texture of the surface of the joint. In areas where joints contain highly weathered or hydrothermally altered products, where movement has occurred causing slickensides or fault gouge to form, where open joints dominate the slope, or where joints are water filled, the rockfall potential is greater. Noting the failure angles from previous rockfalls on a slope can aid in estimating general rock friction along discontinuities.

3 points *Rough, Irregular* The surfaces of the joints are rough and the joint planes are irregular enough to cause interlocking. This macro and micro roughness provides an optimal friction situation.

9 points *Undulating* Also macro and micro rough but without the interlocking ability.

27 points *Planar* Macro smooth and micro rough joint surfaces. Surface contains no undulations. Friction is derived strictly from the roughness of the rock surface.

81 points *Clay Infilling or Slickensided* Low friction materials, such as clay and weathered rock, separate the rock surfaces negating any micro or macro roughness of the joint planes. These infilling materials have much lower friction angles than a rock on rock contact. Slickensided joints also have a very low friction angle and belong in this category.

Case 2

Structural Condition This case is used for slopes where differential erosion or oversteepening is the dominant condition that leads to rockfall. Erosion features include oversteepened slopes, unsupported rock units or exposed resistant rocks on a slope that may eventually lead to a rockfall event. Rockfall is caused by a loss of support either locally or throughout the slope. Common slopes that are susceptible to this condition are: layered units containing easily weathered rock that erodes undermining more durable rock; talus slopes; highly variable units such as conglomerates, mudflows, etc. that weather causing resistant rocks and blocks to fall, and rock/soil slopes that weather allowing rocks to fall as the soil matrix material is eroded.

3 points	*Few Differential Erosion Features* Minor differential erosion features that are not distributed throughout the slope.
9 points	*Occasional Erosion Features* Minor differential erosion features that are widely distributed throughout the slope.
27 points	*Many Erosion Features* Differential erosion features are large and numerous throughout the slope.
81 points	*Major Erosion Features* Severe cases such as dangerous erosion-created overhangs; or significantly oversteepened soil/rock slopes or talus slopes.

Difference in Erosion Rates The Rate of Erosion on a Case 2 slope directly relates to the potential for a future rockfall event. As erosion progresses, unsupported or oversteepened slope conditions develop. The impact of the common physical and chemical erosion processes as well as the effects of man's actions should be considered. The degree of hazard caused by erosion and thus the score given this category, should reflect how quickly erosion is occurring; the size of rocks, blocks, or units being exposed; the frequency of rockfall events; and the amount of material released during an event.

3 points	*Small Difference* The difference in erosion rates is such that erosion features develop over many years. Slopes that are near equilibrium with their environment are covered by this category.
9 points	*Moderate Difference* The difference in erosion rates is such that erosion features develop over a few years.
27 points	*Large Difference* The difference in erosion rates is such that erosion features develop annually.
81 points	*Extreme Difference* The difference in erosion rates is such that erosion features develop rapidly.

Block Size or Quantity of Rockfall Per Event

This measurement should be representative of whichever type of rockfall event is most likely to occur. If individual blocks are typical of the rockfall, the block size should be used for scoring. If a mass of blocks tends to be the dominant type of rockfall, the quantity per event should be used. This can be determined from the maintenance history or estimated from observed conditions when no history is available. This measurement will also be beneficial in determining remedial measures.

Climate and Presence of Water on Slope

Water and freeze/thaw cycles both contribute to the weathering and movement of rock materials. If water is known to flow continually or intermittently from the slope, it is rated accordingly. Areas receiving less than 20 inches per year are 'low precipitation areas.' Areas receiving more than 50 inches per year are considered 'high precipitation areas.' The impact of freeze/thaw cycles can be interpreted from knowledge of the freezing conditions and its effects at the site.
The rater should note that the 27-point category is for sites with long freezing periods or water problems such as high precipitation or continually flowing water. The 81-point category is reserved for sites that have both long freezing periods and one of the two extreme water conditions.

Rockfall History

This information is best obtained from the maintenance person responsible for the slope in question. It directly represents the known rockfall activity at the site. There may be no history available at newly constructed sites or where poor documentation practices have been followed and a turnover of personnel has occurred. In these cases, the maintenance cost at a particular site may be the only information that reflects the rockfall activity at that site. This information is an important check on the potential for future rockfalls. If the score you give a section does not compare with the rockfall history, a review should be performed. As a better database of rockfall occurrences is developed, more accurate conclusions for the rockfall potential can be made.

3 points	*Few Falls* - Rockfalls have occurred several times according to historical information but it is not a persistent problem. If rockfall only occurs a few times a year or less, or only during severe storms this category should be used. This category is also used if no rockfall history data is available.
9 points	*Occasional Falls* - Rockfall occurs regularly. Rockfall can be expected several times per year and during most storms.

27 points	*Many Falls* - Typically rockfall occurs frequently during a certain season, such as the winter or spring wet period, or the winter freeze-thaw, etc. This category is for sites where frequent rockfalls occur during a certain season and is not a significant problem during the rest of the year. This category may also be used where severe rockfall events have occurred.
81 points	*Constant Falls* - Rockfalls occur frequently throughout the year. This category is also for sites where severe rockfall events are common.

In addition to scoring the above categories, the rating team should gather enough field information to recommend which rockfall remedial measure is best suited to the rockfall problem. Both total fixes and hazard reduction approaches should be considered. A preliminary cost estimate should be prepared.

Risk analysis of rockfalls on highways

The analysis of the risk of damage to vehicles or the death of vehicle occupants as a result of rockfalls on highways has not received very extensive coverage in the geotechnical literature. Papers which deal directly with the probability of a slope failure event and the resulting death, injury or damage have been published by Hunt (1984), Fell (1994), Morgan (1991), Morgan et al (1992) and Varnes (1984). Most of these papers deal with landslides rather than with rockfalls. An excellent study of risk analysis applied to rockfalls on highways is contained in an MSc thesis by Christopher M. Bunce (1994), submitted to the Department of Civil Engineering at the University of Alberta. This thesis reviews risk assessment methodology and then applies this methodology to a specific case in which a rockfall killed a passenger and injured the driver of a vehicle.

RHRS rating for Argillite Cut

Bunce carried out a study using the Rockfall Hazard Rating System for the Argillite Cut in which the rockfall occurred. A summary of his ratings for the section in which the rockfall happened and for the entire cut is presented in Table 2. The ratings which he obtained were 394 for the rockfall section and 493 for the entire cut. Note that this highway has been upgraded and the Argillite Cut no longer exists. However, Bunce's work still provides a good case history for the application of the Rockfall Hazard Rating System.

The RHRS system does not include recommendations on actions to be taken for different ratings. This is because decisions on remedial action for a specific slope depend upon many factors such as the budget allocation for highway work which cannot be taken into account in the ratings. However, in personal discussions with Mr Lawrence Pierson, the

principal author of the RHRS, I was informed that in the State of Oregon, slopes with a rating of less than 300 are assigned a very low priority while slopes with a rating in excess of 500 are identified for urgent remedial action.

Figure 11: The Argillite Cut on Highway 99 in British Columbia, Canada.

Risk analysis for Argillite Cut

Bunce (1994) presented several approaches for the estimation of the annual probability of a fatality occurring because of a rockfall in the Argillite Cut. Some of these approaches are relatively sophisticated and I must question whether this level of sophistication is consistent with the quality of the input information which is available on highway projects.

Table 2: RHRS ratings for Argillite Cut on Highway 99 in British Columbia (after Bunce, 1994).

	Section where rockfall occurred		Rating for entire cut	
Parameter	Value	Rating	Value	Rating
Slope height	36	100	35	100
Ditch effectiveness	Limited	27	Limited	27
Average vehicle risk	7	1	225	100
Sight distance	42	73	42	73
Roadway width	9.5	17	9.5	17
Geological structure	Very adverse	81	Adverse	60
Rock friction	Planar	27	Planar	27
Block size	0.3 m	3	1 m	35
Climate and water	High precip.	27	High precip.	27
Rockfall history	Many falls	40	Many falls	27
Total score		394		493

One approach which I consider to be compatible with the rockfall problem and with quality of input information available is the event tree analysis. This technique is best explained by means of the practical example of the analysis for the Argillite Cut, shown in Figure 12. I have modified the event tree presented by Bunce (1994) to make it simpler to follow.

In the event tree analysis, a probability of occurrence is assigned to each event in a sequence which could lead to a rockfall fatality. For example, in Figure 12; it is assumed that it rains 33% of the time, that rockfalls occur on 5% of rainy days, that vehicles are impacted by 2% of these rockfalls, that 50% of these impacts are significant, i.e. they would result in at least one fatality. Hence, the annual probability of fatality resulting from a vehicle being hit by a rockfall triggered by rain is given by (0.333 * 0.05 * 0.02 * 0.5) = $1.67*10^{-4}$.

The event tree has been extended to consider the annual probability of occurrence of one, two and three or more fatalities in a single accident. These probabilities are shown in the final column of Figure 12. Since there would be at least one fatality in any of these accidents, the total probability of occurrence of a single fatality is $(8.33 + 5.56 + 2.78)*10^{-5} = 1.7 * 10^{-4}$, as calculated above. The total probability of at least two fatalities is $(5.56 + 2.78) * 10^{-5} = 8.34 * 10^{-5}$ while the probability of three or more fatalities remains at $2.78 * 10^{-5}$ as shown in Figure 12.

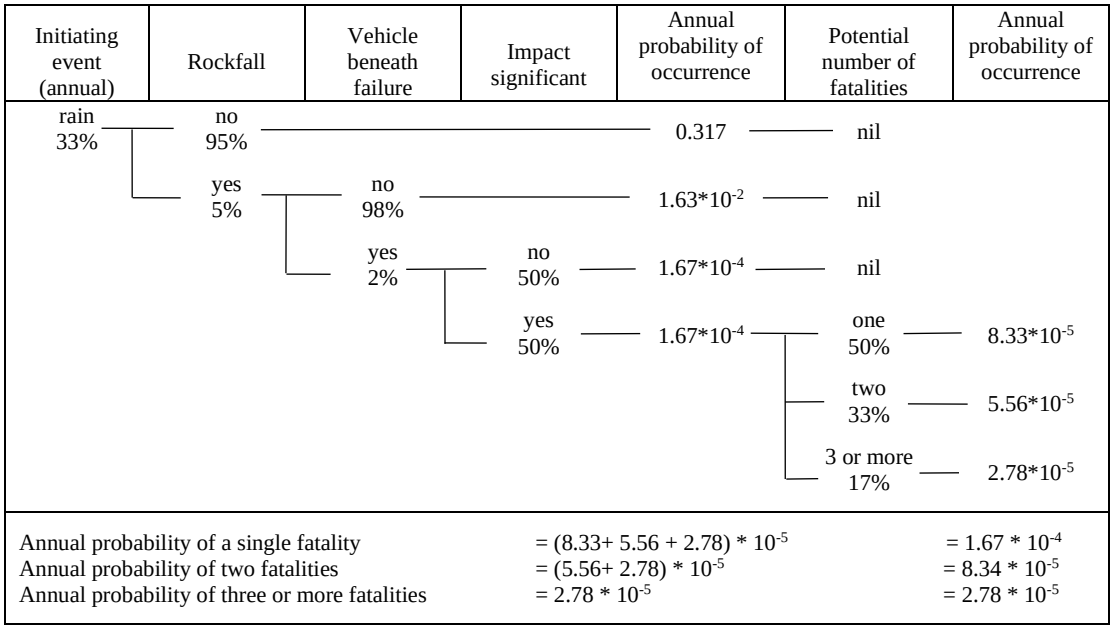

Figure 12: Event tree analysis of rockfalls in the Argillite Cut in British Columbia.

Suppose that it is required to carry out construction work on the slopes of a cut and that it is required to maintain traffic flow during this construction. It is assumed that the construction work lasts for 6 months (50% of a year) and that rockfalls are initiated 20% of the working time, i.e., on 36 days. Using the Argillite cut as an example, all other factors in the event tree remain the same as those assumed in Figure 12. The results of this analysis are presented in Figure 13 which shows that there is an almost ten-fold increase in the risk of fatalities from rockfalls as a result of the ongoing construction activities.

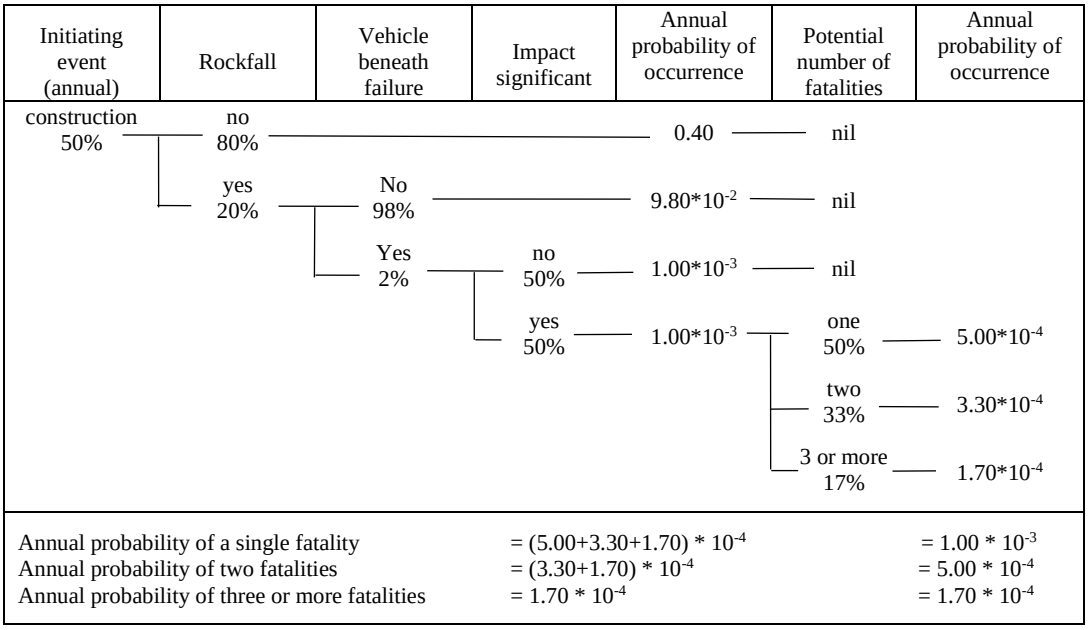

Figure 13: Event tree for a hypothetical example in which construction activities on the Argillite Cut are carried out for a period of six months while the highway is kept open.

Comparison between assessed risk and acceptable risk

The estimated annual probabilities of fatalities from rockfalls, discussed in the previous sections, have little meaning unless they are compared with acceptable risk guidelines used on other major civil engineering construction projects.

One of the earliest attempts to develop an acceptable risk criterion was published by Whitman (1984). This paper was very speculative and was published in order to provide a basis for discussion on this important topic. In the time since this paper was published a great deal of work has been done to refine the concepts of acceptable risk and there are now more reliable acceptability criteria than those suggested by Whitman.

Figure 14, based on a graph published by Nielsen, Hartford and MacDonald (1994), summarises published and proposed guidelines for tolerable risk. The line marked 'Proposed BC Hydro Societal Risk' is particularly interesting since this defines an annual probability of occurrence of fatalities due to dam failures as 0.001 lives per year or 1 fatality per 1000 years. A great deal of effort has gone into defining this line and I consider it to be directly applicable to rock slopes on highways which, like dams, must be classed as major civil engineering structures for which the risks to the public must be reduced to acceptable levels.

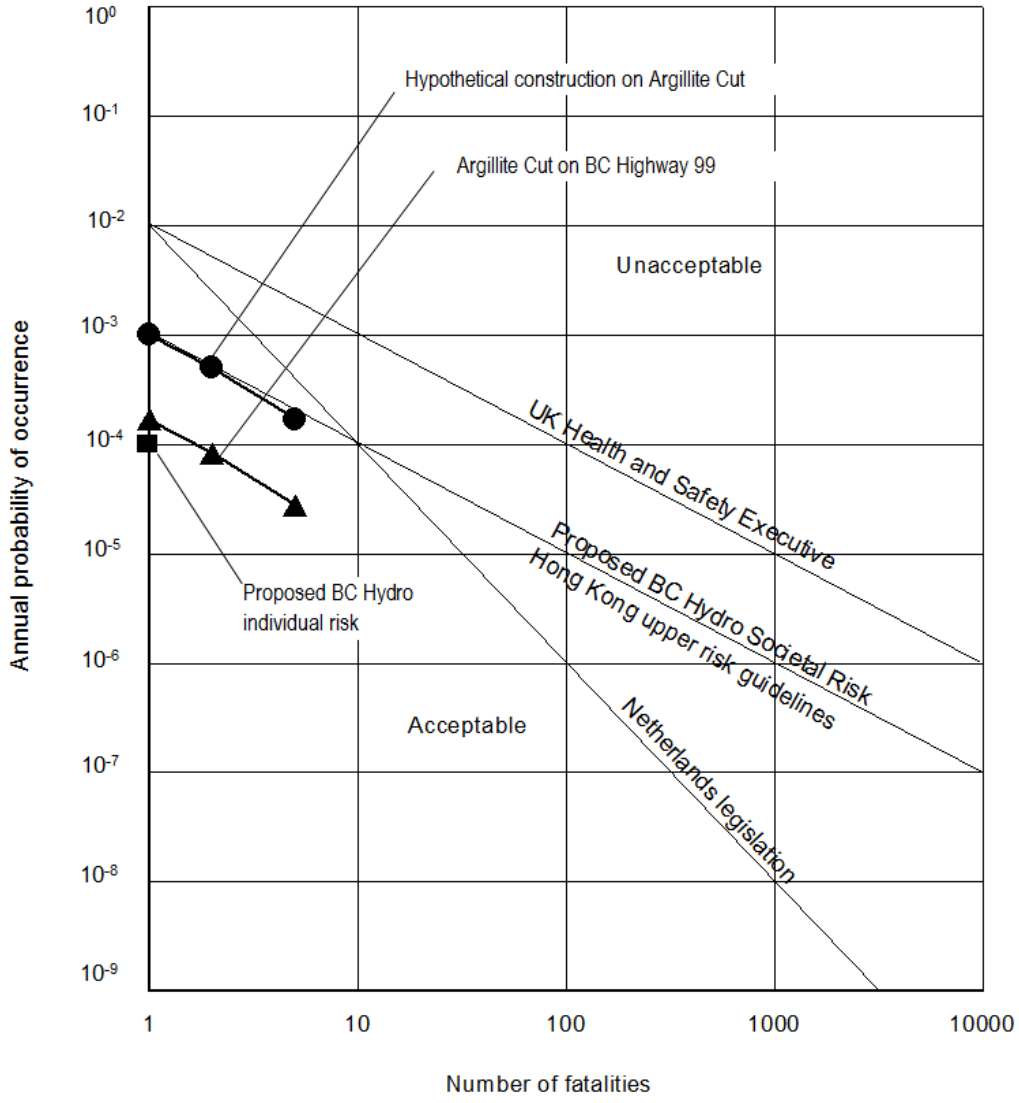

Figure 14: Comparison between risks of fatalities due to rockfalls with published and proposed acceptable risk criteria.

Another point to be noted in Figure 14 is that marked 'Proposed BC Hydro Individual risk'. This annual probability of fatalities of 10^{-4} (1 in 10,000) is based upon the concept that the risk to an individual from a dam failure should not exceed the individual 'natural death' risk run by the safest population group (10 to 14 year old children). Consensus is also developing that the annual probability of fatality of 10^{-4} defines the boundary between voluntary (restricted access to site personnel) and involuntary (public access) risk (Nielsen, Hartford and MacDonald, 1994).

On Figure 14, I have plotted the estimated annual probabilities of fatalities from rockfalls on the Argillite Cut on BC Highway 99, with and without construction. These plots show that the estimated risk for these slopes, without construction, is significantly lower than the 0.001 lives per year line. The estimated risk for the Argillite Cut slopes during active construction is approximately ten times higher and is marginally higher than the 0.001 lives per year criterion. Given the fact that courts tend to be unsympathetic to engineers who knowingly put the public at risk, it would be unwise to proceed with construction while attempting to keep the traffic flowing. A more prudent course of action would be to close the highway during periods of active construction on the slopes, even if this meant having to deal with the anger of frustrated motorists.

Conclusions

The Rockfall Hazard Rating System and the Event Tree risk assessments, discussed on the previous pages, are very crude tools which can only be regarded as semi-quantitative. However, the trends indicated by these tools together with common sense engineering judgement, give a reasonable assessment of the relative hazards due to rockfalls from cut slopes adjacent to highways and railways.

References

Azzoni, A., La Barbera, G. and Zaninetti, A. 1995. Analysis and prediction of rockfalls using a mathematical model. *Int. J. Rock Mech. Min. Sci. and Geomech. Abstracts.* . **32,** (7) 709-724.

Badger, T.C. and Lowell, S. 1992. Rockfall Control Washington State. In *Rockfall Prediction and Control and Landslide Case Histories, Transportation Research Record,* National Research Council, Washington, No 1342, 14-19.

Bozzolo, D., Pamini, R. and Hutter, K. 1988. Rockfall analysis - a mathematical model and its test with field data. *Proc. 5th Intl symposium on Landslides, Lusanne.* July 1988, **1**, 555-560.

Bunce, C.M. 1994. Risk Analysis for Rock Fall on Highways. *MSc thesis submitted to the Department of Civil Engineering, University of Alberta, Canada.* 129 pages.

Fell, R. 1994. Landslide risk assessment and acceptable risk. *Can. Geotech. J.* **31**, 261-272.

Fookes, P.G. and Sweeney, M. 1976. Stabilisation and control of local rockfalls and degrading of slopes. *Quart. J. Engng Geol.* **9**,37-55.

Hoek, E. 1986. Rockfall: a computer program for predicting rockfall trajectories. Unpublished internal notes, Golder Associates, Vancouver.

Hungr, O. and Evans, S.G. 1989. Engineering aspects of rockfall hazard in Canada. Geological Survey of Canada, Open File 2061, 102 pages.

Hunt, R.E. 1984. Slope failure risk mapping for highways: Methodology and case history. In *Rockfall prediction and Control and Landslide Case Histories.* Transportation Research Record, National Research Council, Washington, No. 1343. 42-51.

Morgan, G.C. 1991. Qualification of risks from slope hazards. In *Landslide Hazards in the Canadian Cordillera.* Geological Association of Canada, Special Publication.

Morgan, G.C., Rawlings, G.E. and Sobkowicz, J.C. 1992. Evaluation of total risk to communities from large debris flows. *Geotechnical and Natural Hazards,* Vancouver Geotechnical Society and Canadian Geotechnical Society, Vancouver, BC, Canada, May 6-9, 1992, 225—236.

Nielsen, N.M., Hartford, D.N.D. and MacDonald. 1994. Selection of tolerable risk criteria for dam safety decision making. *Proc. 1994 Canadian Dam Safety Conference, Winnipeg, Manitoba.* Vancouver: BiTech Publishers, 355-369.

Pierson, L.A., Davis, S.A. and Van Vickle, R. 1990. Rockfall Hazard Rating System Implementation Manual. Federal Highway Administration (FHWA) Report FHWA-OR—EG-90-01. FHWA, U.S. Department of Transportation.

Ritchie, A.M., 1963. The evaluation of rockfall and its control. *Highway Record.* **17**.

Spang, R.M. and Rautenstrauch, R.W. 1988. Empirical and mathematical approaches to rockfall prediction and their practical applications. *Proc. 5th Int. Symp. on Landslides, Lusanne*. **2**,1237-1243.

Varnes, D.J. 1984. Landslide hazard zonation: a review of principles and practice. *Natural Hazards 3.* UNESCO, Paris, 63 pages.

Whitman. R.V. 1984. Evaluating calculated risk in geotechnical engineering. *J. Geotech. Eng, ASCE* **110(**2), 145-186.

21. Blasting damage in rock

Introduction

The development of rock mechanics as a practical engineering tool in both underground and surface mining has followed a rather erratic path. Only the most naively optimistic amongst us would claim that the end of the road has been reached and that the subject has matured into a fully developed applied science. On the other hand, there have been some real advances which only the most cynical would discount.

One of the results of the erratic evolutionary path has been the emergence of different rates of advance of different branches of the subject of rock mechanics. Leading the field are subjects such as the mechanics of slope instability, the monitoring of movement in surface and underground excavations and the analysis of induced stresses around underground excavations. Trailing the field are subjects such as the rational design of tunnel support, the movement of groundwater through jointed rock masses and the measurement of in situ stresses. Bringing up the rear are those areas of application where rock mechanics has to interact with other disciplines and one of these areas involves the influence of blasting upon the stability of rock excavations.

Historical perspective

By far the most common technique of rock excavation is that of drilling and blasting. From the earliest days of blasting with black powder, there have been steady developments in explosives, detonating and delaying techniques and in our understanding of the mechanics of rock breakage by explosives.

It is not the development in blasting technology that is of interest in this discussion. It is the application of this technology to the creation of excavations in rock and the influence of the excavation techniques upon the stability of the remaining rock.

As is frequently the case in engineering, subjects that develop as separate disciplines tend to develop in isolation. Hence, a handful of highly skilled and dedicated researchers, frequently working in association with explosives manufacturers, have developed techniques for producing optimum fragmentation and minimising damage in blasts. At the other end of the spectrum are miners who have learned their blasting skills by traditional apprenticeship methods, and who are either not familiar with the specialist blasting control techniques or are not convinced that the results obtained from the use of these techniques justify the effort and expense. At fault in this system are owners and managers who are more concerned with cost than with safety and design or planning

engineers who see both sides but are not prepared to get involved because they view blasting as a black art with the added threat of severe legal penalties for errors.
The need to change the present system is not widely recognised because the impact of blasting damage upon the stability of structures in rock is not widely recognised or understood. It is the author's aim, in the remainder of this chapter, to explore this subject and to identify the causes of blast damage and to suggest possible improvements in the system.

A discussion on the influence of excavation processes upon the stability of rock structures would not be complete without a discussion on machine excavation. The ultimate in excavation techniques, which leave the rock as undisturbed as possible, is the full-face tunnelling machine. Partial face machines or roadheaders, when used correctly, will also inflict very little damage on the rock. The characteristics of tunnelling machines will not be discussed here but comparisons will be drawn between the amount of damage caused by these machines and by blasting.

Blasting damage

It appears to me, a casual reader of theoretical papers on blasting, that the precise nature of the mechanism of rock fragmentation as a result of detonation of an explosive charge is not fully understood. However, from a practical point of view, it seems reasonable to accept that both the dynamic stresses induced by the detonation and the expanding gases produced by the explosion play important roles in the fragmentation process.

Duvall and Fogelson (1962), Langefors and Khilstrom (1973) and others, have published blast damage criteria for buildings and other surface structures. Almost all of these criteria relate blast damage to peak particle velocity resulting from the dynamic stresses induced by the explosion. While it is generally recognised that gas pressure assists in the rock fragmentation process, there has been little attempt to quantify this damage.

Work on the strength of jointed rock masses suggests that this strength is influenced by the degree of interlocking between individual rock blocks separated by discontinuities such as bedding planes and joints. For all practical purposes, the tensile strength of these discontinuities can be taken as zero, and a small amount of opening or shear displacement will result in a dramatic drop in the interlocking of the individual blocks. It is easy to visualise how the high-pressure gases expanding outwards from an explosion will jet into these discontinuities and cause a breakdown of this important block interlocking. Obviously, the amount of damage or strength reduction will vary with distance from the explosive charge, and also with the in-situ stresses which have to be overcome by the high pressure gases before loosening of the rock can take place. Consequently, the extent of the gas pressure induced damage can be expected to decrease with depth below surface, and surface structures such as slopes will be very susceptible to gas pressure induced blast damage.

An additional cause of blast damage is that of fracturing induced by release of load (Hagan, 1982). This mechanism is best explained by the analogy of dropping a heavy steel plate onto a pile of rubber mats. These rubber mats are compressed until the momentum of the falling steel plate has been exhausted. The highly compressed rubber mats then accelerate the plate in the opposite direction and, in ejecting it vertically upwards, separate from each other. Such separation between adjacent layers explains the tension fractures frequently observed in open pit and strip mine operations where poor blasting practices encourage pit wall instability. McIntyre and Hagan (1976) report vertical cracks parallel to and up to 55 m behind newly created open pit mine faces where large multi-row blasts have been used.

Whether or not one agrees with the postulated mechanism of release of load fracturing, the fact that cracks can be induced at very considerable distance from the point of detonation of an explosive must be a cause for serious concern. Obviously, these fractures, whatever their cause, will have a major disruptive effect upon the integrity of the rock mass and this, in turn, will cause a reduction in overall stability.

Hoek (1975) has argued that blasting will not induce deep seated instability in large open pit mine slopes. This is because the failure surface can be several hundred metres below the surface in a very large slope, and also because this failure surface will generally not be aligned in the same direction as blast induced fractures. Hence, unless a slope is already very close to the point of failure, and the blast is simply the last straw that breaks the camel's back, blasting will not generally induce major deep-seated instability.

On the other hand, near surface damage to the rock mass can seriously reduce the stability of the individual benches which make up the slope and which carry the haul roads. Consequently, in a badly blasted slope, the overall slope may be reasonably stable, but the face may resemble a rubble pile.

In a tunnel or other large underground excavation, the problem is rather different. The stability of the underground structure is very much dependent upon the integrity of the rock immediately surrounding the excavation. In particular, the tendency for roof falls is directly related to the interlocking of the immediate roof strata. Since blast damage can easily extend several metres into the rock which has been poorly blasted, the halo of loosened rock can give rise to serious instability problems in the rock surrounding the underground openings.

Damage control

The ultimate in damage control is machine excavation. Anyone who has visited an underground metal mine and looked up a bored raise will have been impressed by the lack of disturbance to the rock and the stability of the excavation. Even when the stresses in the rock surrounding the raise are high enough to induce fracturing in the walls, the

damage is usually limited to less than half a metre in depth, and the overall stability of the raise is seldom jeopardised.

Full-face and roadheader type tunnelling machines are becoming more and more common, particularly for civil engineering tunnelling. These machines have been developed to the point where advance rates and overall costs are generally comparable or better than the best drill and blast excavation methods. The lack of disturbance to the rock and the decrease in the amount of support required are major advantages in the use of tunnelling machines.

For surface excavations, there are a few cases in which machine excavation can be used to great advantage. In the Bougainville open pit copper mine in Papua New Guinea, trials were carried out on dozer cutting of the final pit wall faces. The final blastholes were placed about 19 m from the ultimate bench crest position. The remaining rock was then ripped using a D-10 dozer, and the final 55 degree face was trimmed with the dozer blade. The rock is a very heavily jointed andesite, and the results of the dozer cutting were remarkable when compared with the bench faces created by the normal open pit blasting techniques.

The machine excavation techniques described above are not widely applicable in underground mining situations, and consideration must therefore be given to what can be done about controlling damage in normal drill and blast operations.

A common misconception is that the only step required to control blasting damage is to introduce pre-splitting or smooth blasting techniques. These blasting methods, which involve the simultaneous detonation of a row of closely spaced, lightly charged holes, are designed to create a clean separation surface between the rock to be blasted and the rock which is to remain. When correctly performed, these blasts can produce very clean faces with a minimum of overbreak and disturbance. However, controlling blasting damage starts long before the introduction of pre-splitting or smooth blasting.

As pointed out earlier, a poorly designed blast can induce cracks several metres behind the last row of blastholes. Clearly, if such damage has already been inflicted on the rock, it is far too late to attempt to remedy the situation by using smooth blasting to trim the last few metres of excavation. On the other hand, if the entire blast has been correctly designed and executed, smooth blasting can be very beneficial in trimming the final excavation face.

Figure 1 illustrates a comparison between the results achieved by a normal blast and a face created by presplit blasting in jointed gneiss. It is evident that, in spite of the fairly large geological structures visible in the face, a good clean face has been achieved by the pre-split. It is also not difficult to imagine that the pre-split face is more stable than the section which has been blasted without special attention to the final wall condition.

The correct design of a blast starts with the very first hole to be detonated. In the case of a tunnel blast, the first requirement is to create a void into which rock broken by the blast can expand. This is generally achieved by a wedge or burn cut which is designed to create a clean void and to eject the rock originally contained in this void clear of the tunnel face.

Figure 1: Comparison between the results achieved by pre-split blasting (on the left) and normal bulk blasting for a surface excavation in gneiss.

In today's drill and blast tunnelling in which multi-boom drilling machines are used, the most convenient method for creating the initial void is the burn cut. This involves drilling a pattern of carefully spaced parallel holes which are then charged with powerful explosive and detonated sequentially using millisecond delays. A detailed discussion on the design of burn cuts is given by Hagan (1980).

Once a void has been created for the full length of the intended blast depth or `pull', the next step is to break the rock progressively into this void. This is generally achieved by sequentially detonating carefully spaced parallel holes, using one-half second delays. The purpose of using such long delays is to ensure that the rock broken by each successive blasthole has sufficient time to detach from the surrounding rock and to be ejected into the tunnel, leaving the necessary void into which the next blast will break.

A final step is to use a smooth blast in which lightly charged perimeter holes are detonated simultaneously in order to peel off the remaining half to one metre of rock, leaving a clean excavation surface.

The details of such a tunnel blast are given in Figure 2. The development of the burn cut is illustrated in Figure 3 and the sequence of detonation and fracture of the remainder of the blast is shown in Figure 4. The results achieved are illustrated in a photograph reproduced in Figure 5. In this particular project, a significant reduction in the amount of support installed in the tunnel was achieved as a result of the implementation of the blasting design shown in Figure 2.

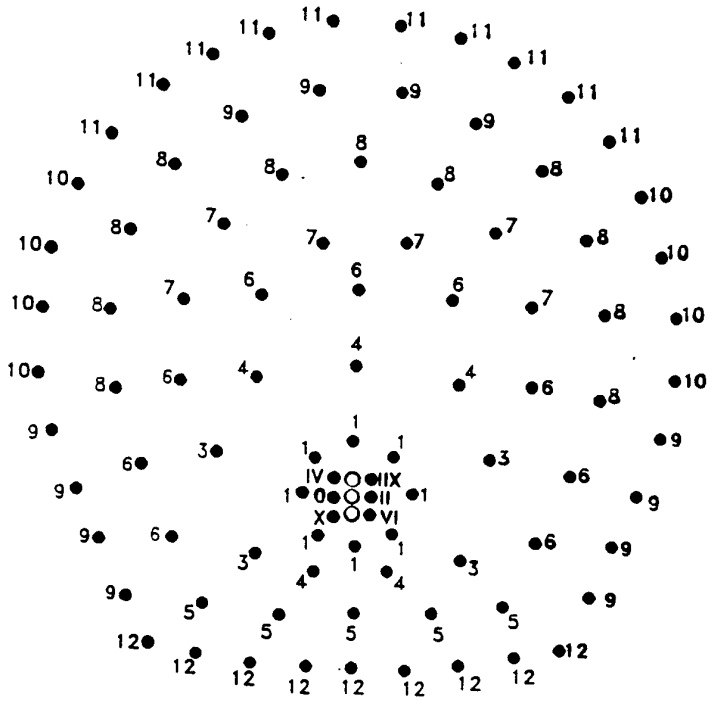

Holes	no	Dia mm	Explosives	Total wt. kg	Detonators
Burn	14	45	Gelamex 80, 18 sticks/hole	57	Millisec
Lifters	9	45	Gelamex 80, 16 sticks/hole	33	Half-sec
Perimeter	26	45	Gurit, 7 sticks/hole and Gelamex 80, 1 stick/hole	26	Half-sec
Others	44	45	Gelamex 80, 13 sticks/hole	130	Half-sec
Relief	3	75	No charge		
Total	96			246	

Figure 2: Blasthole pattern and charge details used by Balfour Beatty - Nuttall on the Victoria hydroelectric project in Sri Lanka. Roman numerals refer to the detonation sequence of millisecond delays in the burn cut, while Arabic numerals refer to the half-second delays in the remainder of the blast.

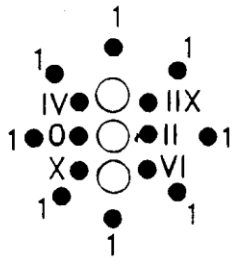

Layout of holes

Milliscond delay VI

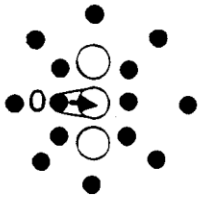

Millisecond delay 0

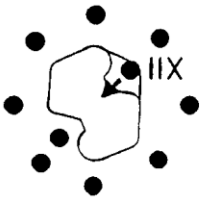

Millisecond delay IIX

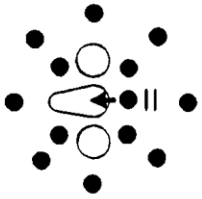

Millisecond delay II

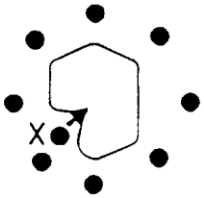

Millisecond delay X

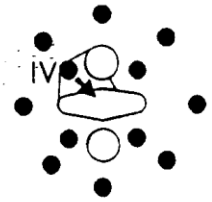

Millisecond delay IV

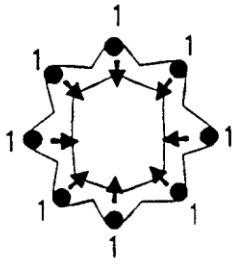

Half-second delay 1

Figure 3 Development of a burn cut using millisecond delays.

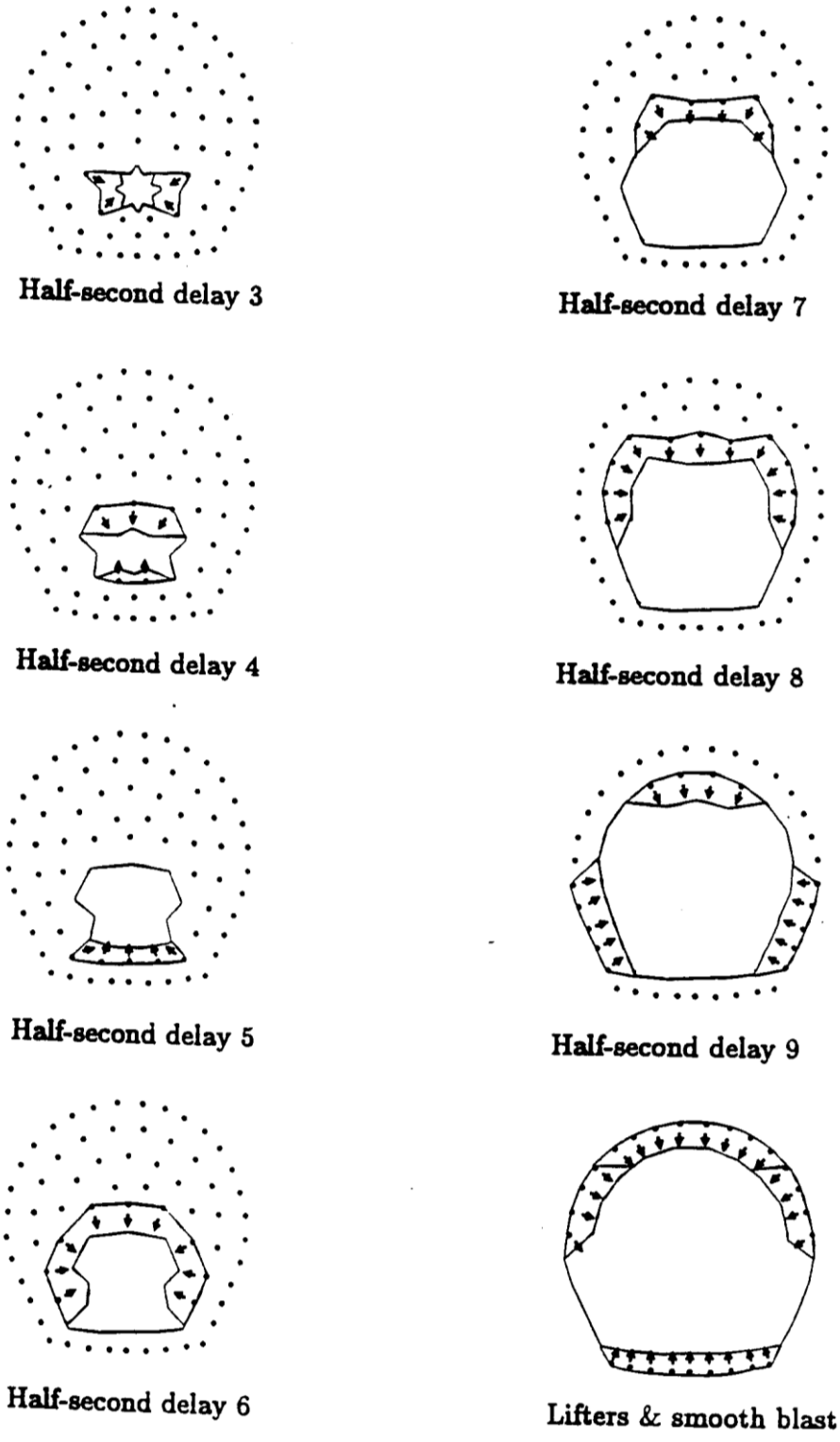

Figure 4: Use of half-second delays in the main blast and smooth blasting of the perimeter of a tunnel.

Figure 5: Results achieved using well designed and carefully controlled blasting in a 19 foot diameter tunnel in gneiss in the Victoria hydroelectric project in Sri Lanka. Note that no support is required in this tunnel as a result of the minimal damage inflicted on the rock. Photograph reproduced with permission from the British Overseas Development Administration and from Balfour Beatty - Nuttall.

A final point on blasting in underground excavations is that it is seldom practical to use pre-split blasting, except in the case of a benching operation. In a pre-split blast, the closely spaced parallel holes (similar to those numbered 9, 10 and 11 in Figure 2) are detonated before the main blast instead of after, as in the case of a smooth blast. Since a pre-split blast carried out under these circumstances has to take place in almost completely undisturbed rock which may also be subjected to relatively high induced stresses, the chances of creating a clean break line are not very good. The cracks, which should run cleanly from one hole to the next, will frequently veer off in the direction of some pre-existing weakness such as foliation. For these reasons, smooth blasting is preferred to pre-split blasting for tunnelling operations.

In the case of rock slopes such as those in open pit mines, the tendency today is to use large diameter blastholes on a relatively large spacing. These holes are generally detonated using millisecond delays which are designed to give row by row blasting.

Unfortunately, scatter in the delay times of the most commonly used open pit blasting systems can sometimes cause the blastholes to fire out of sequence, and this can produce poor fragmentation as well as severe damage to the rock which is to remain to form stable slopes.

Downhole delay systems which can reduce the problems associated with the detonation of charges in large diameter blastholes are available, but open pit blasting engineers are reluctant to use them because of the added complications of laying out the blasting pattern, and also because of a fear of cut-offs due to failure of the ground caused by the earlier firing blastholes. There is clearly a need for further development of the technology and the practical application of bench blasting detonation delaying, particularly for the large blasts which are required in open pit mining operations.

Blasting design and control

While there is room for improvement in the actual techniques used in blasting, many of the existing techniques, if correctly applied, could be used to reduce blasting damage in both surface and underground rock excavation. As pointed out earlier, poor communications and reluctance to become involved on the part of most engineers, means that good blasting practices are generally not used on mining and civil engineering projects.

What can be done to improve the situation? In the writer's opinion, the most critical need is for a major improvement in communications. Currently available, written information on control of blasting damage is either grossly inadequate, as in the case of blasting handbooks published by explosives manufacturers, or it is hidden in technical journals or texts which are not read by practical blasting engineers. Ideally, what is required is a clear, concise book, which sets out the principles of blasting design and control in unambiguous, non- mathematical language. Failing this, a series of articles, in similarly plain language, published in trade journals, would help a great deal.

In addition to the gradual improvement in the understanding of the causes and control of blast damage which will be achieved by the improvement in communications, there is also a need for more urgent action on the part of engineers involved in rock excavation projects. Such engineers, who should at least be aware of the damage being inflicted by poor blasting, should take a much stronger line with owners, managers, contractors and blasting foremen. While these engineers may not feel themselves to be competent to redesign the blasts, they may be able to persuade the other parties to seek the advice of a blasting specialist. Explosives manufacturers can usually supply such specialist services or can recommend individuals who will assist in improving the blast design. Incidentally, in addition to reducing the blasting damage, a well-designed blast is generally more efficient and may provide improved fragmentation and better muck-pile conditions at the same cost.

Conclusion

Needless damage is being caused to both tunnels and surface excavation by poor blasting. This damage results in a decrease in stability which, in turn, adds to the costs of a project by the requirement of greater volumes of excavation or increased rock support.

Tools and techniques are available to minimise this damage, but these are not being applied very widely in neither the mining nor civil engineering industries because of a lack of awareness of the benefits to be gained, and a fear of the costs involved in applying controlled blasting techniques. There is an urgent need for improved communications between the blasting specialists who are competent to design optimum blasting systems and the owners, managers and blasting foremen who are responsible for the execution of these designs.

Research organisations involved in work on blasting should also recognise the current lack of effective communications and, in addition to their work in improving blasting techniques, they should be more willing to participate in field-oriented programs in co-operation with industry. Not only will organisations gain invaluable practical knowledge but, by working side-by-side with other engineers, they will do a great deal to improve the general awareness of what can be achieved by good blasting practices.

References

Duvall, W.I. and Fogelson, D.E. 1962. Review of criteria for estimating damage to residences from blasting vibrations. *U.S. Bur. Mines Rep. Invest.* 5986. 19 pages.

Hagan, T.N. 1980. Understanding the burn cut - a key to greater advance rates. *Trans. Instn. Min. Metall. (Sect. A: Min. Industry*) , **89**, A30-36.

Hagan, T.N. 1982. Controlling blast-induced cracking around large caverns. *Proc. ISRM symp., rock mechanics related to caverns and pressure shafts*, Aachen, West Germany.

Hoek, E. 1975. Influence of drilling and blasting on the stability of slopes in open pit mines and quarries. *Proc. Atlas Copco Bench Drilling Days symp*., Stockholm, Sweden.

Langefors, U. and Khilstrom, B. 1973. *The modern technique of rock blasting*. 2nd edn. New York: Wiley. 405 pages.

McIntyre, J.S. and Hagan, T.N. 1976. The design of overburden blasts to promote highwall stability at a large strip mine. *Proc. 11th Canadian rock mech. symp.* , Vancouver.